

Novel Pharmacological Approaches to Target Mitochondrial Metabolism and DNA Damage Response in Colorectal Cancer and their Synergism with Established Chemotherapeutics

Vom Fachbereich Chemie der Rheinland-Pfälzischen Technischen Universität Kaiserslautern-Landau zur Verleihung des akademischen Grades „Doktor der Naturwissenschaften“ genehmigte Dissertation

DE-386

Dissertation



vorgelegt von

Philipp Demuth

geboren in Hachenburg

Betreuer: Prof. Dr. Jörg Fahrer

Kaiserslautern, 19.12.2024

Der experimentelle Teil dieser Arbeit wurde in der Zeit von Januar 2020 bis März 2023 am Fachbereich Chemie, Fachrichtung Lebensmittelchemie und Toxikologie der Rheinland-Pfälzischen Technischen Universität Kaiserslautern-Landau in der Arbeitsgruppe von Prof. Dr. Jörg Fahrer durchgeführt.

Promotionskommission

Vorsitzender: Prof. Dr. Georg Manolikakes

Berichtersteller 1: Prof. Dr. Jörg Fahrer

Berichterstellerin 2: Prof. Dr. Zuzana Storchová

Prüferin: Dr. Tina Kostka

Eidesstattliche Erklärung

Hiermit erkläre ich, Philipp Demuth, dass ich die vorliegende Dissertation mit dem Titel „*Novel Pharmacological Approaches to Target Mitochondrial Metabolism and DNA Damage Response in Colorectal Cancer and their Synergism with Established Chemotherapeutics*“ selbstständig verfasst und nur die in der Arbeit angegebenen Quellen und Hilfsmittel genutzt habe. Alle Ergebnisse anderer Personen wurden entsprechend gekennzeichnet. Teile dieser Arbeit wurden bereits in Publikationen, Vorträgen oder Postern veröffentlicht. Die vorliegende Dissertation habe ich weder im Ganzen noch in Teilen als Prüfungsarbeit bei einem anderen Fachbereich eingereicht und kein anderes Promotionsverfahren bei einer anderen Hochschule beantragt oder eröffnet. Die geltende Promotionsordnung des Fachbereichs Chemie der Rheinland-Pfälzischen Technischen Universität Kaiserslautern-Landau vom 10.12.2019 ist mir bekannt.

Mannheim, den

Philipp Demuth

Zusammenfassung

Das kolorektale Karzinom (KRK) stellt weltweit eine der am häufigsten diagnostizierten Tumorerkrankungen dar und tritt insbesondere in der Gruppe der jungen Erwachsenen mit einer steigenden Inzidenz auf. Fortschreitende Entwicklungen in der Tumorforschung haben in den vergangenen Jahren zu neuen Behandlungsansätzen geführt, beispielsweise auf dem Gebiet der Immuntherapeutika. Dennoch basiert das Behandlungsregime seit über 50 Jahren auf der zytostatischen Verbindung 5-Fluoruracil (5-FU) und ihren Derivaten, die in Kombination mit den Substanzen Leucovorin (LV), Oxaliplatin (OXA) und Irinotecan (IT) eingesetzt werden. Die antitumorigene Wirkung etablierter chemotherapeutischer Ansätze beruht auf der Induktion von DNA-Schäden, welche insbesondere in Geweben mit einer hohen Proliferationsrate, wie etwa Tumoren, zu Zelltod führen. Aktuelle Ansätze in der Wirkstoffforschung adressieren hingegen spezifische Veränderungen im Tumormetabolismus sowie von DNA-Reparaturmechanismen als mögliche Ziele in der Behandlung des KRK.

Die Untersuchung der antineoplastischen Wirksamkeit neuentwickelter Substanzen, vermittelt durch die Inhibierung der DNA-Reparatur, die Disruption des mitochondrialen Metabolismus und die Induktion von DNA-Schäden, stellte den Fokus dieser Arbeit dar. Hierzu wurde das Potential von Substanzen für die Therapie des KRK untersucht, welche bereits klinische Anwendung für die Behandlung anderer Tumorerkrankungen finden, wie der metabolische Inhibitor Devimistat und die Poly-(ADP-Ribose)-Polymerase (PARP)-Inhibitoren Olaparib und Veliparib. Daneben wurde die biologische Aktivität von neuen chemischen Verbindungen analysiert, welche natürlichen Ursprungs sind (aus marinen Schwämmen isolierte Merosesquiterpene) oder als potenzielle PARP-Inhibitoren chemisch synthetisiert wurden. Als Modell für die vielfältigen molekularen Subtypen des KRK kamen KRK-Zelllinien mit unterschiedlichem Mutationsstatus zur Anwendung. Zur Aufklärung des pharmakologischen Wirkmechanismus wurden zudem genetische *knockdown* Versuche durchgeführt oder isogene *knockout* Zelllinien eingesetzt. Des Weiteren wurden intestinale Tumororganoide und Organoide murinen Ursprungs sowie Kurzzeitkulturen aus KRK-Patienten verwendet, um die Tumorspezifität der beobachteten Effekte zu untersuchen. Eine Reihe von Methoden, wie beispielsweise Durchflusszytometrie, konfokale Mikroskopie, Genexpressionsanalysen und Western-Blot, wurde eingesetzt, um die zugrundeliegenden Zelltodmechanismen aufzuklären. Zur Identifizierung potenzieller Synergismen wurde die Zytotoxizität des mitochondrialen Disruptors Devimistat sowie von PARP-Inhibitoren in Kombination mit den etablierten Chemotherapeutika 5-FU, OXA und IT in verschiedenen KRK-Zelllinien quantifiziert. Abschließend wurde Devimistat als Einzelbehandlung oder in Kombination mit IT in einem murinen Xenograft-Tumormodell eingesetzt, um die therapeutische Wirksamkeit *in vivo* zu bewerten.

In unserer ersten Studie zum metabolischen Inhibitor Devimistat konnten wir demonstrieren, dass die Substanz unabhängig von genetischen oder epigenetischen Aberrationen zu tumorspezifischer Zytotoxizität in KRK-Zelllinien und murinen Tumororganoiden führt. Eine verminderte Sauerstoffverbrauchsrate, eine verringerte mitochondriale Aktivität und die Bildung reaktiver Sauerstoffspezies wurden als zugrundeliegende Mechanismen identifiziert, welche zu p53-unabhängigem Zelltod in KRK-Zellen führen. Combeneft-Modellierung und Chou-Talalay-Analyse zeigten eine synergistische Wirkung von Devimistat in Kombination mit den Chemotherapeutika IT und 5-FU. Die Herabregulierung antiapoptotischer Bcl-2 Proteine und die posttranslationale Akkumulation des proapoptotischen Proteins Bim konnten mithilfe von Genexpressions- und Western-Blot-Analysen sowie genetischen *knockdown*-Experimenten als ursächlich für den beobachteten Synergismus mit IT und 5-FU bestimmt werden. Die antitumorogene Wirksamkeit und synergistische Aktivität in Kombination mit IT wurden unter der Verwendung humaner KRK-Zellen in einem Xenograft-Mausmodell bestätigt.

In unserer zweiten Studie untersuchten wir die Aktivität von 11 verschiedenen Merosesquiterpenen in drei KRK-Zelllinien mit unterschiedlichem Mutationsstatus und identifizierten die höchste Zytotoxizität für die Substanzen Ilimaquinone (IQ), Dactylospontriol (DS) und Smenospongine (SP). Mechanistisch induzieren alle drei Substanzen unabhängig vom p53-Status der untersuchten Zelllinie DNA-Strangbrüche und eine heraufregulierte DNA-Schadensantwort, welche zu Zellzyklusarrest und Aktivierung der mitochondrialen Apoptose führte. Des Weiteren zeigten die untersuchten Merosesquiterpene deutliche Zytotoxizität in murinen Tumororganoiden, was auf eine potenzielle Anwendbarkeit in *in vivo* Studien zur Behandlung des KRK hinweist.

In unserer dritten Studie untersuchten wir die Applikation etablierter und neuentwickelter PARP-Inhibitoren für die Behandlung von KRK-Zellen mit Defizienzen hinsichtlich verschiedener DNA-Reparaturproteine. Hierzu wurden die zwei neuartigen Substanzen X17613 und X17618 basierend auf einem *in silico* und *in vitro* Screening identifiziert, welche in submikromolaren Konzentrationen die Aktivität von PARP-1 inhibieren. Im Gegensatz zu den klinisch eingesetzten Inhibitoren Olaparib und Veliparib zeigten die beiden neuen Substanzen keine Zytotoxizität in KRK-Zelllinienpaaren mit profizientem und defizientem PARP-1-Status. Entsprechend wurde durch X17613 und X17618 weder eine Induktion des DNA-Schadensmarkers γ H2AX hervorgerufen noch die Dissoziation von PARP-1 von der DNA verhindert, ein Mechanismus der als *PARP-trapping* bezeichnet wird. In einer KRK-Zelllinie, die durch eine BRCA2 (*breast cancer type 2 susceptibility protein*)-Defizienz keine DNA-Reparatur mittels homologer Rekombination durchführen kann, führte X17613 zu einer erhöhten Sensitivität gegenüber IT.

Zusammengefasst untersuchte diese Arbeit das Potential neuartiger pharmakologischer Therapieansätze in der Behandlung des KRK. Dies beinhaltete die Verwendung des mitochondrialen Disruptors Devimistat in Kombination mit etablierten Chemotherapeutika, die Untersuchung des zytotoxischen Potentials von marinen Merosesquiterpenen und die Identifikation neuer PARP-Inhibitoren anhand eines *in silico* und *in vitro* Screenings. Unsere Ergebnisse geben einen Einblick in die zugrundeliegenden Toxizitätsmechanismen, den potenziellen Synergismus mit klinisch angewandten Substanzen und den Einfluss bekannter KRK-Mutationen auf die Sensitivität, um eine weitere Entwicklung dieser möglichen Therapieansätze zu unterstützen.

Abstract

Colorectal cancer (CRC) is one of the most frequently diagnosed malignant diseases worldwide and occurs at an alarmingly increasing rate especially in young adults. Ongoing progress in the field of cancer pharmacology has provided new treatment options in recent years, particularly in the form of immunotherapy. Yet, standard chemotherapy has been based on cytostatic agent 5-fluorouracil (5-FU) for over five decades with the more recent addition of leucovorin (LV), oxaliplatin (OXA) and irinotecan (IT). Established chemotherapeutic approaches mainly rely on the induction of DNA damage, which particularly affects rapidly growing cancer cells. The altered tumor metabolism and the DNA repair machinery have more recently been identified as potential drug targets in CRC.

The assessment of novel anticancer drugs for CRC with a focus on induction of DNA damage, inhibition of DNA repair and disruption of mitochondrial metabolism as potential mechanisms constituted the objective of this work. For this purpose, this PhD thesis aimed to evaluate the applicability of antitumor agents which are already clinically used in the treatment of other cancer entities, including the metabolic inhibitor devimistat and the poly (ADP-ribose)-polymerase inhibitors (PARPi) olaparib and veliparib. In addition, the biological activity of novel chemical compounds for CRC treatment was analyzed. The investigated substances were either derived from natural sources (merosesquiterpenes isolated from marine sponges) or chemically synthesized as potential PARPi. CRC cell lines with varying mutational status were applied as surrogates representing the diversity of this disease and experiments with transient genetic knockdown or isogenic knockout cell lines were performed to further detail the pharmacological mode of action of the tested compounds. In addition, murine intestinal tumor organoids and primary organoids as well as patient-derived short-term cultures were used to elucidate the tumor cell specificity of the observed effects. An array of methods was utilized to investigate the underlying cell death mechanisms, including flow cytometry, confocal microscopy, western blot and gene expression analysis. The cytotoxicity of the mitochondrial disruptor devimistat and of PARPi in combination with established CRC chemotherapeutic 5-FU, OXA and IT was analyzed in CRC cell lines to identify a potential synergy. Finally, devimistat was applied either as monotherapy or in combination with IT in a murine xenograft model to evaluate the therapeutic efficacy *in vivo*.

At first, the tumor cell specific cytotoxicity of the metabolic inhibition by devimistat was revealed, independent of genetic and epigenetic alterations in CRC cell lines and murine tumor organoids. A reduced oxygen consumption rate (OCR), attenuated mitochondrial activity and induction of reactive oxygen species (ROS) were identified as underlying mechanisms, resulting in p53-independent induction of CRC cell death. Synergistic anticancer activity was achieved by combination treatment with the chemotherapeutic agents IT and 5-FU, as

demonstrated by a Combeneft-model and Chou-Talalay analyses. Mechanistically, synergism was based on downregulation of antiapoptotic Bcl-2 proteins and posttranslational accumulation of the proapoptotic protein Bim, as demonstrated by transient genetic knockout experiments. Antitumor efficacy and synergistic activity with IT were confirmed by applying human CRC cells in a xenograft mouse model.

In the second study, a compound library comprised of 11 merosesquiterpenes isolated from marine sponges was analyzed and ilimaquinone (IQ), dactylosporin (DS) and smenospongine (SP) were identified as the most cytotoxic compounds in a panel of three human CRC cell lines. On the mechanistic level, all three compounds induced DNA strand breaks and upregulated the DNA damage response (DDR) irrespective of the mutational status of p53, resulting in cell cycle arrest and activation of the mitochondrial apoptosis pathway. Furthermore, merosesquiterpenes induced pronounced cytotoxicity in murine intestinal tumor organoids, underlining their potential in CRC treatment.

In the third study, the applicability of established and novel PARPi in the treatment of DNA repair deficient and proficient CRC was investigated. Therefore, the two novel compounds X17613 and X17618, which inhibit PARP-1 activity in sub-micromolar concentrations, were identified based on an *in silico* and *in vitro* screening of a library of novel 3,4-bifunctionalized and -bridged indole compounds. In contrast to clinically applied PARPi olaparib and veliparib, both compounds showed no cytotoxicity in PARP-1-deficient and -proficient CRC cell line pairs. In accordance, absence of γ H2AX formation and low PARP-1 trapping activity compared to olaparib were identified after treatment with X17613 and X17618. In the last step, sensitization of BRCA2 (breast cancer type 2 susceptibility protein)-deficient CRC cells to IT was demonstrated for X17613.

In conclusion, our research assessed the potential of novel therapeutic approaches for CRC treatment, including mitochondrial disruption by the clinically applied metabolic inhibitor devimistat, inhibition of DNA repair by novel PARP-1 inhibitors and DNA damage induction by marine sponge toxins. Our results provide insight into the underlying molecular mechanisms, the potential synergistic activity with clinically applied drugs and the impact of common CRC mutations on sensitivity to guide further development of new therapeutic approaches.

Table of Contents

Zusammenfassung.....	I
Abstract.....	IV
Table of Contents.....	VI
List of Abbreviations.....	XI
List of Figures.....	IX
List of Tables.....	X
1. Background.....	1
1.1. Colorectal Cancer.....	1
1.1.1. Etiology, staging and statistics of CRC.....	1
1.1.2. Chemotherapy of CRC.....	7
1.1.3. Metastasis of CRC.....	19
1.2. The Altered Metabolism of Tumor Cells.....	23
1.2.1. The deregulated of metabolism as a hallmark of cancer.....	24
1.2.2. Mechanisms of metabolic alterations.....	27
1.2.3. The altered tumor metabolism as a target in CRC.....	35
1.2.4. The metabolic inhibitor devimistat.....	37
1.3. PARP-1 as a Target in CRC Tumor Therapy.....	42
1.3.1. PARP-1 in health and disease.....	42
1.3.2. Targeting PARP-1 in tumor therapy.....	47
2. Objectives.....	57
3. Cumulative Part: Publications.....	59
3.1. The Mitochondrial Disruptor Devimistat (CPI-613) Synergizes with Genotoxic Anticancer Drugs in Colorectal Cancer Therapy in a Bim-Dependent Manner.....	59
3.2. Natural Meroterpenes Activate the DNA Damage Response via DNA Strand Break Formation and Trigger Apoptotic Cell Death in p53-Wild-Type and Mutant Colorectal Cancer.....	84
3.3. Targeting PARP-1 and DNA Damage Response Defects in Colorectal Cancer Chemotherapy with Established and Novel PARP Inhibitors.....	123

4.	Summary of Results	161
4.1.	Publication I: The Mitochondrial Disruptor Devimistat (CPI-613) Synergizes with Genotoxic Anticancer Drugs in Colorectal Cancer Therapy in a Bim-Dependent Manner	161
4.2.	Publication II: Natural Merosesquiterpenes Activate the DNA Damage Response via DNA Strand Break Formation and Trigger Apoptotic Cell Death in p53-Wild-Type and Mutant Colorectal Cancer.....	163
4.3.	Publication III: Targeting PARP-1 and DNA Damage Response Defects in Colorectal Cancer Chemotherapy with Established and Novel PARP Inhibitors....	164
5.	Summarizing Discussion	166
5.1.	Publication I: The Mitochondrial Disruptor Devimistat (CPI-613) Synergizes with Genotoxic Anticancer Drugs in Colorectal Cancer Therapy in a Bim-Dependent Manner	166
5.1.1.	Devimistat targets the mitochondria of CRC cells.....	167
5.1.2.	Devimistat induces selective cell death in CRC cells and organoids.....	168
5.1.3.	Synergism of devimistat with genotoxic chemotherapeutics	170
5.2.	Publication II: Natural Merosesquiterpenes Activate the DNA Damage Response via DNA Strand Break Formation and Trigger Apoptotic Cell Death in p53-Wild-Type and Mutant Colorectal Cancer.....	175
5.2.1.	Cell death induction by merosesquiterpenes in CRC cells.....	175
5.2.2.	The Role of p53 for the cell death induction by merosesquiterpenes.....	177
5.3.	Publication III: Targeting PARP-1 and DNA Damage Response Defects in Colorectal Cancer Chemotherapy with Established and Novel PARP Inhibitors....	181
5.3.1.	Identification of novel PARP inhibitors for CRC treatment by <i>in silico</i> and <i>in vitro</i> testing.....	182
5.3.2.	Role of PARP-1 expression for activity of PARPi monotreatment.....	183
5.3.3.	Cytotoxicity of PARPi as monotreatment and in combination with chemotherapeutic drugs in CRC.....	184
5.3.4.	Combining devimistat and PARPi in CRC treatment.....	187
6.	Conclusion and Outlook	189
6.1.	Conclusion.....	189

Table of Contents

6.2. Outlook: Metabolic Inhibition by Devimistat Modulates Intracellular Signaling Pathways Associated with Metastasis and Metabolism.....191

7. References.....200

8. Acknowledgements237

9. Curriculum Vitae.....239

10. Publications.....240

11. Conference Attendances.....241

List of Figures

Figure 1: Genetic alterations during the etiology of CRC.	5
Figure 2: Mechanism of action, cellular uptake and metabolism of the chemotherapeutic drugs irinotecan, oxaliplatin and capecitabine.	15
Figure 3: Mechanisms of targeted therapy approaches applied in CRC treatment.....	17
Figure 4: The metastatic cascade of colorectal cancer and associated signaling pathways.	21
Figure 5: Effects of tumor suppressor activity and oncogenic signaling on the metabolic reprogramming of CRC.	29
Figure 6: The modulation of pathways associated with CRC metastasis by TCA cycle metabolites.....	35
Figure 7: Metabolic inhibitors applied in the treatment of solid tumors in clinical trials.	36
Figure 8: Enzymatic mechanism of PARP-1, its role in DNA repair and the effect of pharmacological PARP-1 inhibition.....	45
Figure 9: Overview of clinically approved PARP inhibitors and their corresponding field of application.	49
Figure 10: The mechanism of synthetic lethality induced by the application of PARP-1 inhibitors in HR-deficient cancer cells.	51
Figure 11: Mechanistic overview summarizing the synergism of devimistat with anticancer drugs IT and 5-FU in colorectal cancer cells.	174
Figure 12: Mechanistic model of the merosesquiterpene-induced cell death pathway.	179
Figure 13: Devimistat attenuates the migration of tumor cells and is equally active in primary tumor- and metastasis-derived cell lines.	192
Figure 14: Devimistat downregulates the nuclear translocation of pSmad2 and the expression of EMT transcription factor ZEB1.....	193
Figure 15: Gene set enrichment and differential expression analysis based on proteomic changes in response to devimistat treatment.....	196

List of Tables

Table 1: Overview of the consensus molecular subtypes of CRC.....	3
Table 2: TNM system for staging of CRC.	7
Table 3: Overview of clinical trials applying PARPi in CRC treatment.....	55

List of Abbreviations

A

AA6	S-2-[(2,6-dichlorobenzoyl) amino] succinic acid
ABC	ATP-binding cassette
ACAT	acetyl-coenzyme A acetyltransferase
ACSS	acetyl-CoA synthetase short-chain family member
ACC	acetyl-CoA carboxylase
ACLY	ATP-citrate lyase
ACOX	acetyl-CoA oxidase
AIF	apoptosis-inducing factor
AKI	acute kidney injury
AML	acute myeloid leukemia
AMPK	5' adenosine monophosphate-activated protein kinase
AOM	azoxymethane
APC	adenomatous polyposis coli
APS	ammonium persulphate
ARID	AT-rich interactive domain-containing protein
ASCO	American Society of Clinical Oncology
ASCT	alanine/serine/cysteine amino acid transporter
ATP	adenosine triphosphate
ATM	ataxia-telangiectasia mutated
ATR	ataxia-telangiectasia and Rad3-related protein
AUC	area under the curve

B

BCKDC	branched-chain α -ketoacid dehydrogenase complex
BER	base excision repair
BRAF	v-Raf murine sarcoma viral oncogene homolog B1
BRCA	breast cancer susceptibility protein
BSA	bovine serum albumin
BW	body weight

C

C	cytosine
Cad	cadherin
CAD	carbamoyl-phosphate synthetase
CAF	cancer associated fibroblasts
CAPOX	capecitabine + oxaliplatin
CCCP	carbonyl cyanide m-chlorophenyl hydrazone
CCS	clear cell sarcoma
CD	cluster of differentiation
CDA	cytidine deaminase
CDK	cyclin dependent kinase
CES	carboxylesterase
CH2THF	5,10-methylenetetrahydrofolat
Chk	checkpoint kinase
CHOP	C/EBP homologous protein
CI	combination index
CIMP	CpC-island methylated phenotype
CIN	chromosomal instability
CMS	consensus molecular subtypes
CNT	concentrative nucleoside transporters
COX	cytochrome c oxidase subunit
CPT	carnitine palmitoyltransferase
CRC	colorectal cancer
CSC	cancer stem cell
CTC	circulating tumor cell
CTLA	cytotoxic T-lymphocyte-associated protein

List of Abbreviations

D

D2HG	D-2-hydroxyglutarate
DAG	diacylglycerol
DACH	1,2-diaminocyclohexane
DCA	dichloroacetate
DCK	deoxycytidine kinase
DDR	DNA damage response
DHFU	dihydrofluorouracil
DLC	dynein light chain
DMSO	dimethyl sulphoxide
DNA	deoxyribonucleic acid
dNTP	deoxynucleotide
DPD	dihydropyrimidine dehydrogenase
DPV	differential pulse voltammetry
DR	death receptor
DS	dactylospontriol
DSB	double-strand break
dTMP	thymidine monophosphate
DTT	dithiothreitol
dTTP	thymidine triphosphate
dUMP	deoxyuridine monophosphate
dUTP	deoxyuridine triphosphate
DYRK	dual specificity tyrosine-phosphorylation-regulated kinase

E

4EBP	eIF4E binding protein
ECM	extracellular matrix
EGF	endothelial growth factor
EGFR	epidermal growth factor receptor
EMA	European Medicines Agency
EMT	epithelial-to-mesenchymal transition
ENT	equilibrative nucleoside transporters
ErbB	erythroblastosis oncogene B
ERCC	excision repair cross-complementing
ERK	extracellular signal-regulated kinase
EtOH	ethanol
EWL	Ewing sarcoma

F

FADH ₂	flavin adenine dinucleotide
FACS	fluorescence-activated cell sorting
FAP	familial adenomatous polyposis
FCCP	carbonyl cyanide-p-trifluoromethoxy phenyl hydrazone
FCS	fetal calf serum
FDA	(US) Food and Drug Administration
FdUMP	fluorodeoxyuridine monophosphate
FdUTP	fluorodeoxyuridine triphosphate
FGF	fibroblast growth factor
FH	fumarate hydratase
FOLFIRI	5-fluorouracil + folinic acid + irinotecan
FOLFOX	5-fluorouracil + folinic acid + oxaliplatin
FOLFOXIRI	5-fluorouracil + folinic acid + oxaliplatin + irinotecan
FP	fluoropyrimidine
FPG	formamidopyrimidine DNA glycosylase
FUS	fused in sarcoma
FUTP	fluorouridine triphosphate
5-FU	5-fluorouracil

List of Abbreviations

G

G	guanine
G6PD	glucose-6-phosphate dehydrogenase
GARP	glycoprotein A repetitions predominant
GI	gastrointestinal
GLDH	glutamate dehydrogenase
GLS	glutaminase
GLUT	glucose transporter
GPT	glutamate pyruvate transaminase
GSH	glutathione
GST	glutathione-S transferase
GTP	guanosine triphosphate
GUS	glucuronidase

H

H ₂ DCFDA	2',7'-Dichlorofluorescein diacetate
H6PD	hexose-6-phosphate dehydrogenase
HAT	histone acetyltransferase
HCEC	human colon epithelial cells
hCTR	human copper transporter
HDAC	histone deacetylase
HE	hematoxylin and eosin
hENT	human equilibrative nucleoside transporter
HEPES	4-(2-hydroxyethyl)-1-piperazineethanesulphonic acid
HIF	hypoxia-inducible factor
HK	hexokinase
HNPCC	hereditary nonpolyposis colorectal cancer
HNSCC	head and neck squamous cell carcinoma
HPF	histone PARylation Factor
HR	homologous recombination
HRD	homologous recombination deficiency
HRP	horseradish peroxidase

I

IBD	inflammatory bowel disease
IC ₅₀	inhibitory concentration, 50%
IDH	isocitrate dehydrogenase
IgG	immunoglobulin G
IL	interleukin
i.p.	intraperitoneal
IP3	inositol triphosphate
IQ	ilimaquinone
IROX	irinotecan + oxaliplatin
IT	irinotecan
i.v.	intravenous

J

JAK	Janus kinase
JNK	Jun kinase

K

KGDH	α -ketoglutarate dehydrogenase complex
KRAS	Kirsten rat sarcoma

L

LA	α -lipoic acid
LDH	lactate dehydrogenase
LOH	loss of heterozygosity

List of Abbreviations

M

mCRC	metastatic colorectal cancer
MCT	monocarboxylate transporter
MEK	mitogen-activated protein kinase kinase
MET	mesenchymal-to-epithelial transition
MED	mediator of RNA polymerase II transcription
miRNA	micro RNA
MLH1	MutL protein homolog
MLL	mixed-lineage leukemia
MMEJ	microhomology-mediated end joining
MMP	matrix-metalloproteases
MMR	mismatch repair
MMS	methyl methane sulfonate
MOM	mitochondrial outer membrane
MOMP	mitochondrial outer membrane permeabilization
MPC	mitochondrial pyruvate carrier
MRE	meiotic recombination homolog
MRP	multidrug resistance associated proteins
MSH	MutS protein homolog
MSI	microsatellite instable
MSS	microsatellite stable
mt	mutant
MTD	maximum tolerated dose
mtDNA	mitochondrial DNA
mTOR	mammalian target of rapamycin
mTORC	mTOR complex

N

NAC	<i>N</i> -acetylcysteine
NAD	nicotinamide adenine dinucleotide
NADPH	nicotinamide adenine dinucleotide phosphate
NAT	<i>N</i> -acetyl transferase
ncRNA	ncRNAs
NCT	National Clinical Trial number
NEAA	non-essential amino acids
NER	nucleotide excision repair
NGS	next generation sequencing
NHEJ	non-homologous end joining
NQO	NAD(P)H-quinone oxidoreductase

O

OCR	oxygen consumption rate
OLA	olaparib
OPRT	orotate phosphoribosyl transferase
OS	overall survival
OXA	oxaliplatin
OXPPOS	oxidative phosphorylation

P

PAR	poly (ADP-ribose)
PARP	poly (ADP-ribose) polymerase
PBS	phosphate buffered saline
PC	pyruvate carboxylase
PCCA	propionyl-CoA carboxylase
PCK	phosphoenolpyruvate carboxykinase
PD	programmed death receptor
PDAC	pancreatic ductal adenocarcinoma
PDGF	platelet-derived growth factor
PDH	pyruvate dehydrogenase complex
PD-L	programmed death receptor-ligand
PDK	pyruvate dehydrogenase kinase
PDP	pyruvate dehydrogenase phosphatase

List of Abbreviations

PDX	patient-derived xenograft
PEG	prostaglandin
PFK	phosphofructokinase
PFS	progression free survival
PGC	peroxisome proliferator-activated receptor gamma coactivator
PHD	prolyl hydroxylase
PI	propidium iodide
PI3K	phosphoinositide 3-kinase
PIK3CA	phosphatidylinositol-4,5-bisphosphate 3-kinase, catalytic subunit alpha
PIM	serine/threonine-protein kinase pim
PIP2	phosphatidylinositol-phosphate
PKM	pyruvate kinase
PMS	postmeiotic segregation increased
Pol	DNA polymerase
PPT	palmitoyl-protein thioesterase
PPP	pentose phosphate pathway
PRPS	phosphoribosyl-pyrophosphate synthetase
PTEN	phosphatase and tensin homolog
PTIP	PAX-interacting protein 1
PTS1R	peroxisomal targeting signal 1 receptor

Q

qPCR	quantitative real-time polymerase chain reaction
------	--

R

RAD	radiation sensitive protein
Raf	rapidly Accelerated Fibrosarcoma
Ras	rat sarcoma virus
Rb	retinoblastoma protein
RNA	ribonucleic acid
ROS	reactive oxygen species
Rot	rotenone
RPA	replication protein A
rpm	rounds per minute
RT	room temperature
RTK	receptor tyrosine kinases

S

S6K1	p70S6 kinase
SCID	severe combined immunodeficient
SCNA	somatic copy number alterations
SCO	synthesis of cytochrome C oxidase
SDH	succinate dehydrogenase
SDS	sodium dodecyl sulphate
SDS-PAGE	sodium dodecyl sulphate polyacrylamide gel electrophoresis
SEM	standard error of the mean
SIRT	sirtuin
SLC	solute carrier transporter
Smad	mothers against decapentaplegic homolog
SN-38	7-ethyl-10-hydroxy-camptothecin
SP	smenospongine
SSB	single strand break
STAT3	signal transducer and activator of transcription 3
SUCNR1	succinate receptor 1

T

TAF	TATA-binding protein-associated factor
tBOOH	tert-butyl hydroperoxide
TCA	tricarboxylic acid cycle
TEMED	tetramethyl ethylenediamine
TET	ten-eleven translocation
TFAM	mitochondrial transcription factor A

List of Abbreviations

TGF	transforming growth factor
TGFBR	TGF- β receptor
TIS	translocated in sarcoma
TME	tumor microenvironment
TNM	tumor, node, metastasis
TOP	topoisomerase
TOPBP	topoisomerase II binding protein
TP	thymidine phosphorylase
TRAIL	TNF-related apoptosis-inducing ligand
TRF	telomeric repeat-binding factor
T _{reg}	regulatory T cell
TS	thymidylate synthase
U	
UGT	uridine 5'-diphospho-glucuronosyltransferase
UICC	Union of international cancer control
ULK	Unc-51-like autophagy-activating kinase
UNG	uracil-DNA glycosylase
UPR	unfolded protein response
V	
VEGF	vascular endothelial growth factor
VEL	veliparib
VM	valinomycin
W	
WT	wild-type
X	
XPF	xeroderma pigmentosum group F
XRCC	X-ray repair cross-complementing protein
Z	
ZEB	zinc finger E-box-binding homeobox
z-VAD-FMK	carbobenzoxy-valyl-alanyl-aspartyl-[O-methyl]-fluoromethylketone
$\Delta\Psi_m$	mitochondrial membrane potential
γ H2AX	phosphorylated H2A histone family member X

1. Background

1.1. Colorectal Cancer

With over 1.9 million new cases worldwide and approximately 900,000 deaths in 2020, colorectal cancer (CRC) emerged as the second leading cause of cancer-related deaths worldwide, confronting the health care systems with the need for new therapeutic approaches to target this disease (Sung et al., 2021). Despite ongoing progress in multiple disciplines of cancer treatment, including radiation, surgery and chemotherapy, the 5-year survival rate of metastatic CRC is still low, with only 14% (Siegel et al., 2020). A matter of particular importance is the increasing incidence among patients under 50 years, highlighting the insufficient understanding with regards to the interplay of genetic susceptibilities and environmental risk factors (Stoffel and Murphy, 2020): Predispositions encompass the occurrence of inflammatory bowel disease (IBD) including Crohn's disease or ulcerative colitis as pre-existing conditions as well as genetic disorders like Lynch syndrome or the familial adenomatous polyposis (FAP) syndrome (Valle et al., 2019). Worldwide, the incidence of CRC correlates with the developmental index and shows a higher frequency in first world countries, reflecting the impact of lifestyle risk factors like an increased intake of animal-source foods, excess weight and decreased physical activity (Siegel et al., 2020; Sung et al., 2021).

1.1.1. Etiology, staging and statistics of CRC

The colorectal tumorigenesis has been identified as a multistep process: In general, a mutation of colonic epithelial cells leads to the development of aberrant crypt foci resulting in an adenomatous polyp, a benign tumor restricted in size. Additional genetic and epigenetic alterations, for example loss-of-function mutations of tumor suppressors, gain-of-function mutations of oncogenes and DNA hypermethylation lead to the promotion of tumor growth and the development of a malignant tumor or carcinoma. Over time, this tumor accumulates additional mutations and might finally be enabled to metastasize to distant organs, as outlined in Figure 1 (L. H. Nguyen et al., 2020; Vogelstein et al., 1988). The adenoma-carcinoma model, first proposed 35 years ago by Vogelstein et al. was subsequently supplemented by additional models of CRC tumor development, termed the serrated pathway (Yamane et al., 2014) and inflammatory pathway, which differ in their molecular mechanisms and account for approximately 10-15% of CRC cases (Keum and Giovannucci, 2019). The concept of increasing malignancy during the process of carcinogenesis is progressively overhauled: A more recently proposed model for CRC development revealed that a set of intermixed

subclones arises already in the initiation phase of CRC tumor development, indicating that highly aggressive tumor cells may be present early in oncogenesis and subsequently increase in proportion (Sottoriva et al., 2015).

In general, the development of CRC can be divided into the phases of initiation, promotion and progression: The initiation step commonly involves inactivation of tumor suppressors, typically due to mutations occurring spontaneously or in response to environmental and dietary carcinogens. The promotion phase is characterized by clonal expansion of altered cells, caused by suppressed cell death and upregulated proliferation. Finally, during the progression phase a benign, preneoplastic lesion develops to an invasive tumor, accompanied by activation of oncogenes and loss of additional tumor suppressors (Luebeck and Moolgavkar, 2002).

In CRC, a frequently occurring event in initiation is the inactivation of the tumor suppressor Adenomatous polyposis coli (*APC*) gene, leading to accumulation of β -catenin and dysregulation of the Wnt-signaling pathway. This occurs either due to germline mutations, which cause a hereditary predisposition to CRC termed familial adenomatous polyposis (FAP), or due to somatic *APC* mutations, found in 80% of CRC tumors (Zhang and Shay, 2017). Furthermore, functional impairment of the DNA mismatch repair (MMR) pathway because of epigenetic regulation as well as sporadic (Koopman et al., 2009) or germline (Liu et al., 1996) mutations including the MMR proteins MLH1 and MSH2 represents an important CRC risk factor (Hewish et al., 2010). The promotion phase of CRC commonly involves mutations of the GTPase RAS: Expression of mutated *KRAS*-G12D, -G12V and -G13D genes occurs in 40% of overall CRC cases and 77% of metastatic CRC (mCRC) cases, causing permanent activation of the RAS signaling pathway (Neumann et al., 2009; Vaughn et al., 2011).

Furthermore, oncogenic mutations of *BRAF* gene expressed as *BRAF*-V600E appear in 10% of CRC cases (Sanz-Garcia et al., 2017). While the occurrence of mutated *KRAS* and *BRAF* has been considered mutually exclusive in CRC, the application of next generation sequencing (NGS) in a cohort of 820 CRC patients revealed rare concomitant alterations with an incidence of 0.5% (Deshwar et al., 2018). Mutations of the tumor suppressor gene *TP53* are frequently observed in CRC and a polymorphism of the gene has been associated with increased CRC risk (Gemignani et al., 2004; Iacopetta, 2003). Functional alterations of the transforming growth factor β (TGF- β) pathway regularly occur during colorectal carcinogenesis. Mutations of the TGF- β receptor II (TGFBR2) or the transcription factor Smad4 (small mothers against decapentaplegic homolog 4) impair the tumor-suppressive function of the corresponding pathway, while still enabling

induction of epithelial-to-mesenchymal transition. This dual role of TGF- β signaling in tumor cells is further discussed in Chapter 1.1.4.1.

In addition, somatic copy number alterations (SCNA) cause the loss or gain of DNA sections with a size of over 1 kb through non-allelic homologous recombination (HR), thereby leading to the amplification of oncogenes or attenuation of tumor suppressors (Wang et al., 2016b). CRC is a heterogeneous disease with varying outcomes and marked differences in drug sensitivity. Guinney et al. summarized the consensus molecular subtypes (CMS) of colorectal cancer in a classification system. Based on gene expression analysis, four groups with characteristic molecular features were differentiated, which predetermine progression, prognosis and treatment-response as outlined in Table 1 (Guinney et al., 2015; Thanki et al., 2017).

Table 1: Overview of the consensus molecular subtypes of CRC. According to Guinney et al., four different subtypes can be differentiated based on genomic and epigenetic alterations, which manifest in clinical implications, including prognosis and location (Guinney et al., 2015; Thanki et al., 2017).

Subtype Alternate name	CMS1	CMS2 (Canonical)	CMS3 (Metabolic)	CMS4 (Mesenchymal)
Incidence	14%	37%	13%	23%
Genomic alteration	MSI hypermutation	SCNA high	-	SCNA high
Epigenetic alterations	CIMP high	-	CIMP low	-
Characteristics	Immune infiltration and activation	Epithelial, Wnt and MYC activation	Epithelial, metabolic deregulation	TGF- β activation, stromal infiltration angiogenesis
Associated mutations	<i>ATM, BRAF, TGFB2, PTEN</i>	<i>APC, KRAS, TP53, PIK3CA</i>	<i>APC, KRAS, TP53, PIK3CA</i>	<i>APC, KRAS, TP53, PIK3CA</i>
Prognosis	Worse survival after relapse	-	-	Worse relapse free- and overall survival
Location	Proximal	Distal	Mixed	Distal

In addition to mutations that drive colorectal carcinogenesis, epigenetic alterations are commonly occurring in CRC. Modifications of histones and the DNA are among the most important changes, which are frequently dysregulated as part of the pathophysiological process of CRC initiation and progression (Jung et al., 2020). One of the best characterized epigenetic alterations in humans is DNA methylation at the C5 position of cytosine. Catalyzed by DNA methyltransferases, this modification typically occurs at CpG-dinucleotides which show a high abundance in many gene promotor regions (Jones and Baylin, 2007; Yagi et al., 2010). In CRC cells, transcriptional repression is often facilitated by CpG-hypermethylation in the promotor region of tumor suppressor genes, including *CDKN2A* (Bihl et al., 2012), *MLH1* (Cunningham et al., 1998) and *APC* (Liang et al., 2017). DNA methylation profiles of a subset of CRC tumors with distinct molecular features are characterized by a CpG island methylator phenotype (CIMP) (Puccini et al., 2017).

Histone modifications, especially methylation and acetylation, depict another mechanism by which gene expression is regularly altered in CRC (Jung et al., 2020). In non-dividing cells, DNA is tightly associated with histones, protein octamers composed of two pairs of each of the four core histone proteins Histone 2A (H2A), H2B, H3 and H4. Post-translational modification of the core histone proteins regulates the histone-DNA interaction and can modulate the association with binding proteins. Enzymatic activity of histone acetyltransferases (HATs) and histone deacetylases (HDACs) can alter gene expression of tumor suppressors and proto-oncogenes and hence is considered a component of CRC tumorigenesis (Gargalionis et al., 2012). Besides, non-coding RNAs (ncRNAs) like micro RNAs (miRNAs) regulate gene expression by interacting with mRNA transcripts and thereby modulate many CRC-associated pathways (Jia et al., 2022).

Nearly one third of all CRC cases is associated with inherited genetic alterations (Grady, 2003). The Lynch syndrome, also referred to as hereditary nonpolyposis colorectal cancer (HNPCC), constitutes one of the most common genetic predispositions and is associated with a 50-80% lifetime risk of the development of colon cancer, accounting for 2-4% of all CRC cases. The condition is inherited in an autosomal dominant fashion and typically leads to an early onset of CRC development, characterized by poor differentiation and proximal tumor localization (Jasperson et al., 2010). Mechanistically, germline mutations in a class of genes responsible for DNA mismatch repair (MMR), including *MLH1*, *MSH2*, *MSH6*, and *PMS2*, result in an elevated rate of single nucleotide mutations and microsatellite instability (MSI) (Jasperson et al., 2010).

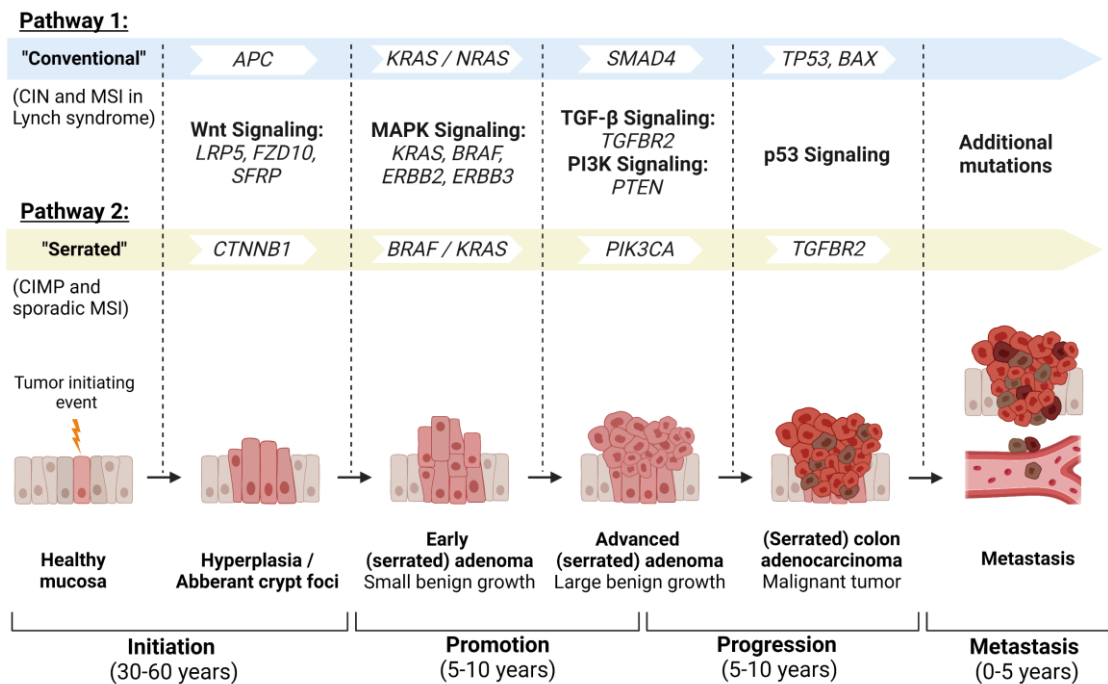


Figure 1: Genetic alterations during the etiology of CRC. The conventional and the serrated pathway can be differentiated as the two main, discrete sequences of malignant transformation from healthy colon to colorectal cancer which together account for approximately 90% of CRC cases (Kim and Bodmer, 2022). Sequence specific and shared activations of oncogenes and inactivation of tumor suppressors occur in the different stages of CRC pathways, which involve initiation, promotion, progression and metastasis of the primary tumor (Kuipers et al., 2015). CIN, chromosomal instability; CTNNB1, catenin- β 1; MAPK, mitogen-activated protein kinase; PI3K, phosphatidylinositol 3-kinase; PIK3CA, phosphatidylinositol-4,5-bisphosphate 3-kinase; PTEN, phosphatase and tensin homologue (Created with BioRender)

As the second most frequent inherited form of CRC, familial adenomatous polyposis (FAP) is characterized by the formation of multiple adenomas in the colorectum at a young age and inevitable cancer development if left untreated (Leoz et al., 2015). FAP is caused by germline mutations of the tumor suppressor gene *APC*, an antagonist of the canonical Wnt signaling pathway. *APC* induces phosphorylation and ubiquitination of cytoplasmic β -catenin, leading to its proteolytic degradation. In the absence of functional *APC*, cytoplasmic β -catenin accumulates, enters the nucleus and binds to transcription factors of the TCF/LEF family to induce expression of a specific set of genes to promote proliferation and survival at the expense of differentiation (Hankey et al., 2018).

In addition, several categories of potentially more common but less penetrant genetic causes for CRC susceptibility have been identified based on population studies. This includes variants and polymorphisms, as for example of *TGFR1*6A*, *HRAS1-VNTR*

and *APC-I1307K*, of genes encoding for the glutathione-S transferases mu (*GSTM1*), theta (*GSTT1*), and pi (*GSTP1*) and of genes encoding for the *N*-acetyl transferases 1 and 2 (*NAT1*, *NAT2*) (Jasperson et al., 2010).

As opposed to inherited CRC, the likelihood and frequency of spontaneous mutations that lead to the development of sporadic CRC are often subject to dietary and lifestyle choices (Gay et al., 2012; Naguib et al., 2010). Thus far, a variety of environmental risk factors have been connected to the development of sporadic CRC, including obesity, smoking, alcohol-consumption and lack of physical activity (Durko and Malecka-Panas, 2014). The nutritional profile linked to CRC is characterized by a fiber-deficient, fat-rich, high calory diet lacking fruits and vegetables (Durko and Malecka-Panas, 2014). Additionally, high intake of processed and red meat represents a risk factor (Seiwert et al., 2020). In a large population-based case control study, comparing 4,092 individuals with CRC to 3,032 without CRC, it was estimated that at least 45% of CRC could be prevented by adopting healthy life style behaviors, regardless of potential genetic predispositions (Carr et al., 2018).

Clinical staging represents a critical tool in the clinical management of CRC. The Union of international cancer control (UICC) publishes the “TNM Classification of Malignant Tumors” as a globally accepted framework for the classification of cancer extent and spread. The TNM system differentiates between the T category, which describes tumor size and site, the N category, which describes lymph node involvement and the M category, which describes the occurrence of distant metastatic spread (Compton and Greene, 2004). Based on pathological and clinical approaches, a tumor stage from I to IV is derived, which helps to guide chemotherapy, facilitates preoperative patient management, and serves as a predictor of prognosis and survival (Table 2).

Based on the records of 164,996 CRC patients, an overall survival rate of 63.0% was observed that decreased with age and revealed to be significantly higher in women compared to men in patients under 75 years (Majek et al., 2012). Striking differences of survival were identified between the stages of CRC: While for patients with localized tumors a relative survival of 89.5% was determined, a drop to 65.4% for regional and 14.9% for distant colorectal cancer metastasis underlines the urgency of an early diagnosis (Majek et al., 2012).

Table 2: TNM system for staging of CRC. A CRC stage from I to IV can be derived depending on the size and site of the primary tumor, the involvement of regional lymph nodes and the occurrence of distant metastases (Compton and Greene, 2004).

Stage	T: Primary tumor	N: Regional lymph nodes	M: Distant metastasis
I	T1	N0	M0
	T2	N0	M0
IIA	T3	N0	M0
IIB	T4	N0	M0
IIIA	T1	N1	M0
	T2	N1	M0
IIIB	T3	N1	M0
	T4	N1	M0
IIIC	any	N2	M0
IV	any	any	M1

1.1.2. Chemotherapy of CRC

In general, the clinical treatment of malignant diseases is guided by standard protocols. In the following, the clinical practice guidelines of the ESMO (European Society For Medical Oncology) and the ASCO (American Society of Clinical Oncology) for treatment of localized and metastatic CRC are summarized (Argilés et al., 2020; Cervantes et al., 2023; Morris et al., 2023). Depending on the mutational status of the tumor, the stage of the disease and the age of the patient, several overarching approaches are applied to clinically treat CRC: In stage 0 and stage I CRC, the cancer cells have not spread outside the colon wall itself. Full surgical resurrection of the tumor is possible and paired with a tight follow-up, without the need for adjuvant chemotherapy. Depending on the cancer localization and differentiation grade, local colectomy and surgical resurrection of nearby lymph nodes can be advisable (Argilés et al., 2020).

During treatment of stage II CRC, decision-making is frequently based on the MSS/MSI status: While MSI-high patients do not benefit from adjuvant chemotherapy, fluoropyrimidine monotreatment plus leucovorine can be conducted in MSS patients. Additional factors that might indicate application of adjuvant chemotherapy include tumor outgrowth into blood and lymph vessels, perforation of the colon wall and poor histological differentiation grade (Argilés et al., 2020). The decision-making process for

the therapeutic approach of the first line treatment is generally based on the patient's age and general state of health. Generally, fluoropyrimidines, which are considered the backbone of adjuvant CRC chemotherapy, reduce the risk of death in stage II colon cancer by an absolute 3-5% and in stage III disease by 10-15%, with a further 4-5% improvement with the application of oxaliplatin-containing combinations (Argilés et al., 2020).

In stage III CRC patients, adjuvant chemotherapy is generally conducted independent of the molecular subtype. A combination of fluoropyrimidines and oxaliplatin is considered the standard of care in stage III, with a significant improvement of DFS over fluoropyrimidine monotherapy, as demonstrated in three landmark clinical trials (André et al., 2009; Haller et al., 2011; Kuebler et al., 2007). When choosing a regimen for the adjuvant chemotherapy of stage III CRC, the treatment duration has to be considered: Both, leucovorin/5-fluorouracil/oxaliplatin (FOLFOX) for 6 months and capecitabine plus oxaliplatin (CAPOX) for 3 months can be recommended (Grothey et al., 2018).

Stage IV CRC, also referred to as mCRC, has spread from the colon to distant tissues and organs and is therefore in most cases unlikely to be cured by surgery. For first line treatment of patients with initially unresectable MSS or proficient mismatch repair (pMMR) mCRC, doublet (folinic acid, FU, IT or OXA) or triplet (folinic acid, FU, IT and OXA) are recommended (Morris et al., 2023) as reviewed in the treatment guidelines for colorectal cancer of the American Society of Clinical Oncology (ASCO). In patients with MSI-high or MMR-deficient mCRC, the monoclonal programmed death receptor 1 (PD-1) antibody pembrolizumab should be offered as first line treatment. By blocking the PD-1 ligand (PD-L1) mediated T cell evasion of cancer cells, PD-1 antibodies enhance the immune suppression of CRC, in particular if a high mutational burden is present (Le Dung et al., 2015). Mechanistically, neo-antigens derived from tumor-related mutations likely attract T cell infiltration, resulting in an improved therapeutic outcome (McGranahan et al., 2016). Application of anti-EGFR therapy in combination with doublet chemotherapy is indicated in patients with MSS or pMMR left-sided, RAS wild-type mCRC. Patients with previously treated *BRAF*-V600E mutant mCRC can benefit from cotreatment with monoclonal EGFR antibody cetuximab and the *BRAF*-inhibitor encorafenib. Mutations of *BRAF*, a serine/threonine kinase of the EGFR-signaling pathway, are found in 5-10% of mCRC cases and cause constitutive activation of downstream kinases, as further outlined in Chapter 1.1.2.4. (Morris et al., 2023). For the treatment of patients with *RAS*-mutant, right-sided disease, FOLFOXIRI in combination with antibodies against the vascular endothelial growth factor A (VEGF-A) should be considered, as for example bevacizumab, but application of the regimen is often limited by chemotherapy tolerability (Cervantes et al., 2023).

If initial treatment does not suspend disease progression or needs to be discontinued due to toxicity, additional treatment options are selected for second line treatment, depending on the drugs applied in the first line (Vogel et al., 2017). Following failure of 5-FU single agent treatment, regimens include FOLFOX, FOLFIRI and IROX, which showed superior efficacy compared to FOLFIRI (Guglielmi and Sobrero, 2007). If IT was applied as first line treatment, FOLFOX is usually used in the second line, with the addition of bevacizumab yielding improved outcome (Giantonio et al., 2007). Arnold et al. analyzed treatment options beyond the second line in a systematic review of 938 references and included 68 references for quality synthesis: Improvement in overall survival is most likely achieved by a combination of the nucleoside analogue trifluridine and thymidine phosphorylase inhibitor tipiracil or by applying the receptor tyrosine kinase inhibitor regorafenib (Arnold et al., 2018).

Depending on the applied chemotherapy, several severe side effects may occur and tight management is crucial, underlining the necessity to consider age, comorbidities and disease state in the treatment plan (Eng, 2009). In contrast to neoadjuvant chemotherapy, which is applied prior to the surgical resection of the tumor, adjuvant chemotherapy is conducted subsequently to reduce the risk of disease reoccurrence (Grothey et al., 2018). While application of adjuvant chemotherapy is clearly indicated in stage III and stage IV CRC, a risk-benefit analysis based on histological and molecular markers can be conducted for stage II CRC to guide decisions on an individual basis (Kannarkatt et al., 2017). Neoadjuvant chemotherapy is implemented in the therapy of several malignant diseases, including breast and pancreatic cancer but a general benefit for the treatment of CRC remains elusive (Glynn-Jones et al., 2012; Schrag et al., 2014). For the specific treatment of locally advanced rectal cancer, the application of neoadjuvant FOLFIRINOX significantly improved disease-free survival and is better tolerated than adjuvant chemotherapy (Conroy et al., 2021).

As outlined above, different cytostatic agents are routinely combined in specific treatment regimen in the therapy of CRC. Typically, these involve the antimetabolite 5-fluorouracil (5-FU), the topoisomerase I (TOP1) inhibitor irinotecan (IT) and the cross-linking agent oxaliplatin (OXA) as backbone therapy. Since these cytostatic drugs constitute the most frequently applied chemotherapeutics in CRC (Morris et al., 2023), the following chapter focuses on IT, 5-FU and OXA or the corresponding prodrugs, respectively. The chemical structures, most relevant cellular targets and known uptake mechanisms are outlined in Figure 2.

1.1.2.1. Irinotecan

Irinotecan is a derivative of the naturally occurring substance camptothecin, which was discovered in 1966 by M. E. Wall and M. C. Wani in a screening for novel anticancer drugs. Like its mother compound, irinotecan inhibits the enzyme TOP1, thereby inducing cytotoxicity in a large variety of tumor cells. Uniquely among camptothecins, irinotecan is a prodrug that is metabolically activated by a carboxylesterase (CES), particularly CES2 followed by CES1, to 7-ethyl-10-hydroxy-camptothecin (SN-38). As the major metabolite, SN-38 has a 100-1,000-fold higher potency than IT and is therefore responsible for the majority of biological effects observed due to irinotecan treatment, although only 2-3% of IT are activated (Mathijssen et al., 2001). Detoxification occurs predominantly in the liver due to glucuronidation by uridine 5'-diphosphoglucuronosyltransferase (UGT) 1A1, leading to the formation of the inactive metabolite SN-38 glucuronide (SN-38G). Activity of bacterial β -glucuronidase (GUS) in the gastrointestinal tract (GI) tract was identified as an important determinant of IT-induced GI tract damage and resultant diarrhea (Bhatt et al., 2020). In addition, metabolic inactivation of IT can be catalyzed by CYP3A4/5 (Fujita et al., 2015). Polymorphism of UGT1A1 such as UGT1A1*6 and UGT1A1*28 can result in severe toxicity of IT treatment due to an attenuated drug metabolism (Minami et al., 2007). Besides drug metabolizing enzymes, transporters expressed in the human liver are involved in the pharmacokinetics of IT: Biliary excretion is facilitated by ATP-binding cassette (ABC) transporter, subfamily C, member 2 (ABCC2), ABC transporter, subfamily G, member 2 (ABCG2) and ABC transporter, subfamily B, member 1 (ABCB1) (Chu et al., 1998).

The mechanism of DNA damage induction by camptothecin and its analogues appears to depend entirely on a reversible stabilization of the TOP1 cleavage complex (TOP1CC), resulting in the inhibition of DNA religation and thereby induction of DNA single-strand breaks (Thomas and Pommier, 2019). The prolonged attenuation of DNA synthesis leads to the replication-dependent formation of DNA double-strand breaks, subsequent S/G₂ cell cycle arrest and finally cell death. Several DNA repair proteins are involved in the resolution of IT-induced DNA damage. PARP-1 limits the toxicity of TOP1 inhibitors by promoting replication fork reversal to allow for religation and repair of the TOP1CC (Das et al., 2014; Ray Chaudhuri et al., 2012). ATR and its corresponding downstream kinase Chk1 can induce transient arrest of fork progression to allow for repair of broken replication forks, thereby attenuating cytotoxicity induced by TOP1 inhibitors (Jossé et al., 2014). Overexpression of XRCC1, which plays a critical role as a scaffolding protein in the base excision repair pathway, results in resistance against camptothecin cytotoxicity in cancer cells (Park et al., 2002).

IT has been applied in the treatment of solid tumors, including pancreatic, colorectal and lung cancer for over three decades. As described above, IT is frequently utilized as a second line chemotherapeutic drug for treatment of advanced CRC, when the first line treatment consisting of 5-FU and OXA failed, and in the first line treatment of mCRC. Several phase-II and phase-III clinical trials revealed that inclusion of IT in chemotherapy regimen improved 1-year survival rate and overall quality of life and prolonged pain-free, progression-free and overall survival (Fujita et al., 2015). Standard administration of IT is carried out by clinical i.v. infusion. Around 15-20% of patients receiving IT monotherapy develop severe side effects which include diarrhea, febrile neutropenia, anemia, and thrombocytopenia, resulting in a reduced quality of life and dose-limiting toxicities (Thomas and Pommier, 2019). Cotreatment with additional anticancer drugs, including 5-FU and OXA can further increase the frequency and severity of side effects (de With et al., 2023).

1.1.2.2. 5-Fluorouracil

The compound 5-fluorouracil (5-FU) is derived by the substitution of hydrogen to fluorine in the C5 position of uracil, one of the four nucleobases in the nucleic acid RNA. As one of the earliest anticancer drugs, 5-FU was first synthesized in 1957 by Heidelberger and colleagues, after an increased uptake of uracil by tumors had previously been discovered (Heidelberger et al., 1957). 5-FU is frequently applied in the treatment of different solid malignancies, including head and neck, pancreatic, stomach, esophageal and breast cancer (Vodenkova et al., 2020). In the context of CRC, 5-FU was incorporated in treatment regimen nearly 30 years ago and is nowadays standardly applied in combination with leucovorin (LV). As an inhibitor of thymidylate synthase (TS), LV enhances the efficacy of 5-FU treatment, thereby increasing patient survival and therapy response rates (Thirion et al., 2004). Despite ongoing progression in the development of novel therapeutic approaches, 5-FU still represents a mainstay of chemotherapy combination regimens in CRC treatment (Vodenkova et al., 2020).

The antitumorigenic effects of 5-FU are induced by several mechanisms. Inhibition of TS results in a depletion of the intracellular deoxynucleotide pool, which is required for DNA synthesis and repair. Applying 5,10-methylenetetrahydrofolat (CH₂THF) as a methyl donor, TS catalyzes the methylation of deoxyuridine monophosphate (dUMP) to thymidine monophosphate (dTMP). Fluorodeoxyuridine monophosphate (FdUMP), which is endogenously generated from 5-FU, competitively blocks the nucleotide binding position of TS and thereby prevents binding of dUMP. As a result, formation of dTMP is impeded, leading to thymidine depletion induced cytotoxicity particularly in rapidly proliferating cells. Furthermore, the enzyme orotic acid phosphoribosyl transferase

(OPRT) catalyzes the formation of 5-fluorouridine triphosphate (FUTP) utilizing phosphoribosyl pyrophosphate (PRPP) as a cosubstrate. The incorporation of FUTP attenuates RNA synthesis, disrupts the processing of rRNAs, tRNAs and snRNAs and reduces protein biosynthesis, which has been identified as the main contributor for 5-FU mediated cytotoxicity (Pettersen et al., 2011). Additionally, the induction of DNA strand breaks has been described due to the incorporation of 5-FU (Longley et al., 2003). The MMR pathway drives the cytotoxic activity of 5-FU in tumor cells (Iwaizumi et al., 2011), rendering the MMR status an important predeterminant for the corresponding therapeutic response (Sargent et al., 2010). The repair of 5-FU-DNA adducts is predominantly executed by base excision repair (BER), initiated by uracil-N DNA glycosylases (UNG) (Pettersen et al., 2011). Induction of thymine to guanine point mutations as a consequence of 5-FU treatment has been identified by tumor whole genome sequencing in CRC and might be linked to the occurrence of secondary malignancies (Christensen et al., 2019).

After administration by infusion, around 20% of 5-FU is directly excreted via urine. A high proportion of 5-FU is metabolically inactivated by dihydropyrimidine dehydrogenase (DPD) to dihydrofluorouracil (DHFU) in the liver. Accordingly, it has been demonstrated that only 3% of the applied 5-FU dose is responsible for cytotoxic activity in malignant tissue as well as side effects in several organs (Diasio and Harris, 1989). Therefore, usage of oral 5-FU was dissipated early, and subsequent pharmacological research focused on the application of 5-FU as a prodrug to increase its bioavailability, leading to the development of the compound capecitabine. Following its rapid absorption through the gastrointestinal wall, capecitabine is rapidly converted to 5'-deoxy-5-fluorouridine by carboxylesterases (CES) and cytidine deaminases (CDA) in the liver which is subsequently metabolized to 5-FU by thymidine phosphorylases (TP) (Vodenkova et al., 2020). Cellular uptake of 5-FU is mainly facilitated by concentrative nucleoside transporters (CNTs/SLC28s) and equilibrative nucleoside transporters (ENTs/SLC29s), which enable bidirectional transport and thereby attenuate 5-FU efficacy in CRC. (Hruba et al., 2023; Phua et al., 2013). In addition, the active 5-FU metabolite FdUMP is actively excreted by cancer cells via the efflux pump MRP8 (ABCC11), thereby conferring resistance to treatment with this nucleotide analogue (Oguri et al., 2007).

While 5-FU is generally considered a comparably safe chemotherapeutic agent, several types of adverse side effects and toxic events were described in CRC patients: Besides general symptoms like fever, fatigue, mucositis, diarrhea and vomiting, hematological effects can occur and include thrombocytopenia, leukopenia and anemia (Latchman et al., 2014; Zhang et al., 2018). Among the dose-limiting toxicities observed after treatment with 5-FU and its prodrug, capecitabine, are hematological symptoms (e.g. neutropenia,

hyperbilirubinemia) as well as gastrointestinal (e.g. diarrhea, stomatitis) and skin conditions (e.g. hand-foot syndrome) (Kline et al., 2014; Walko and Lindley, 2005). Complete or partial deficiency in DPD is observed in 0.1-3% of the general population and has been identified as an important determinant of susceptibility to severe 5-FU-induced toxicity (Bocci et al., 2006).

1.1.2.3. Oxaliplatin

Oxaliplatin consists of a central platinum atom surrounded by a 1,2-diaminocyclohexane (DACH) group and a bidentate oxalate ligand. Different stereochemical isomers of the complex exist, with the *trans*-1-(R,R)-DACH-Pt isomer, referred to as oxaliplatin, exhibiting the highest cytotoxicity (Lévi et al., 2000). Oxaliplatin constitutes a further step in drug development emerging from first- and second-generation platinum compounds like cisplatin and carboplatin and demonstrates improved antitumor activity (Cvitkovic, 1998; Rottenberg et al., 2021). While CRC exhibits a primary resistance against cisplatin and carboplatin, attributable to an intrinsically high expression of cytoplasmic efflux transporters and upregulated DNA adduct repair mechanisms, OXA revealed to be highly antitumorigenic in clinical studies, as reviewed by Grothey and Goldberg (Grothey and Goldberg, 2004).

Intravenous administration of OXA is followed by a short initial distribution phase and subsequent drug removal over a time course of 48 h, mainly via renal clearance. In urine, around 20 platinum species were identified after administration, with the main constituents being glutathione (GSH)-DACH-Pt and different creatinine derivatives (Kweekel et al., 2005). While passive diffusion was considered the main contributor to cellular OXA uptake, evidence about the role of active cellular transport systems emerged in recent years: Transporters involved in the sequestration and intrusion of copper, including human copper transporter 1 (hCTR1), participate in OXA uptake (Buß et al., 2018; Howell et al., 2010), while increased expression levels of the copper efflux transporter ATP7B have been linked with poor outcome in CRC patients receiving oxaliplatin-based therapy (Martinez-Balibrea et al., 2009). The role of members of the solute carrier (SLC) transporters, including organic cation transporters (OCT) 1, OCT2 and OCT3, and of members of the ABC family of efflux transporters, including multidrug-resistance associated proteins (MRP) 1 and MRP4, for the sensitivity of CRC towards OXA remains elusive (Martinez-Balibrea et al., 2015). Contrasting, MRP2 expression has been linked to FOLFOX therapy outcome in CRC and was identified as a limiting factor for oxaliplatin accumulation in CRC cells (Myint et al., 2019). In corresponding *in vitro* experiments, the cytotoxic response was restored by MRP2 inhibition, underlining the significance of MRP2 expression for sensitivity to OXA treatment (Myint et al., 2019).

As a prodrug, OXA is activated by non-enzymatic hydrolysis and displacement of the oxalate group to monochloro-, dichloro- and diaquo-compounds. Following its cellular uptake, rapid binding of OXA to nucleophilic molecules occurs, including amino- and sulfur groups in DNA, RNA and proteins. In addition, passive and GST-mediated glutathione-adduct formation inactivates OXA and facilitates its efflux (Fronik et al., 2022). Correspondingly, the main contributors to cytotoxicity of OXA in tumor cells are induction of intrastrand DNA crosslinks, especially between two adjacent guanine-residues or guanine- and adenine-residues as well as Pt-DNA adducts and DNA protein crosslinks, which block DNA replication and transcription (Graham et al., 2000; Rottenberg et al., 2021).

In contrast to cisplatin adducts, the MMR does not recognize and repair OXA-adducts, rendering MMR-defective CRC cells sensitive towards OXA-treatment (Martin et al., 2008). *In vitro* studies revealed the NER as the main oxaliplatin-induced DNA damage repair system and showed a comparable role of the NER for DNA damage induced by cisplatin and OXA. In accordance, genetic knockdown of the endonuclease ERCC1 (excision repair cross-complementing 1) or its interaction partner XPF (xeroderma pigmentosum group F) result in higher sensitivity towards OXA treatment *in vitro* (Hatch et al., 2014). While the mutational status of *TP53* was unable to predict sensitivity towards OXA in a panel of 30 cell lines, cDNA microarray data of 9216 transcripts revealed correlation with expression of DNA repair and apoptosis related genes, including *ERCC1* (Arango et al., 2004). Clinically, increased *ERCC1* expression of CRC tumors measured by quantitative real-time polymerase chain reaction (qPCR) was a predictor of reduced OXA-treatment efficacy, as reviewed by Bohanes and colleagues (Bohanes et al., 2011).

The molecular mechanism of OXA-induced cell death in CRC cell lines is characterized by induction of G₂/M arrest and activation of the intrinsic apoptosis pathway, including mitochondrial Bax translocation, cytochrome c release and caspase-3 cleavage (Arango et al., 2004). In parallel, development of OXA-resistance in CRC cell lines was caused by frameshift mutations in the *BAX* gene, resulting in complete loss of *BAX* transcription (Gourdier et al., 2002). In general, addition of OXA to CRC chemotherapy is considered safe but several adverse effects have been described, including significantly higher incidence of grade III and IV neutropenia and an increase of diarrhea and stomatitis (Haller, 2000). In contrast to other chemotherapeutics applied in CRC treatment, neurosensory symptoms frequently occur in response to OXA treatment and can culminate in dose-limiting neurotoxicity (Beijers et al., 2014).

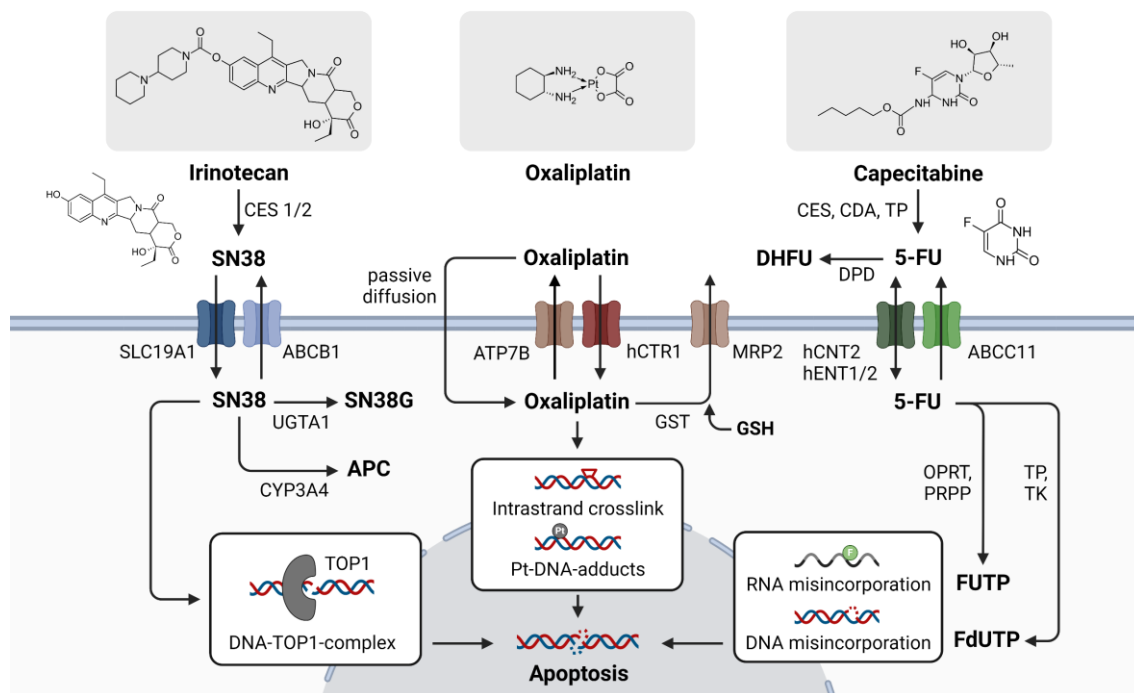


Figure 2: Mechanism of action, cellular uptake and metabolism of the chemotherapeutic drugs irinotecan, oxaliplatin and capecitabine. Following administration, irinotecan and capecitabine require conversion to their respective active metabolites SN-38 and 5-FU. Several drug transporters have been identified which are responsible for specific cellular uptake of the compounds or facilitate their excretion, thereby enabling chemoresistance. While the mode of action for IT, OXA and 5-FU is predominantly based on the induction of DNA damage, the corresponding mechanisms differ, as depicted in the schematic model. (Created with BioRender)

1.1.2.4. Targeted therapy of CRC

In recent years, various novel approaches for CRC treatment were clinically approved. Besides small molecule kinase inhibitors, which are applied to attenuate the activity of several cancer specific signaling cascades, antibodies targeting receptors responsible for tumor cell growth are used as a treatment option especially in mCRC (Xie et al., 2020), as summarized in Figure 3. Upregulation of the epidermal growth factor receptor (EGFR) has been observed in 60-80% of CRC cases and is associated with poor overall survival, thereby rendering it a frequently utilized therapeutic target (Cunningham et al., 2004). The EGFR belongs to the family of erythroblastosis oncogene B (ErbB) receptor tyrosine kinases, which upon ligand binding mediate downstream activation of several intracellular signaling pathways, including JAK (Janus kinase)/STAT3 (Signal transducer and activator of transcription 3), PI3K/AKT and RAS/RAF/MEK/ERK, to induce migration, proliferation, survival and cellular growth (Roskoski, 2019a). The clinically approved murine-human chimeric immunoglobulin G (IgG) antibody cetuximab specifically binds the external domain of the EGFR, inducing degradation and internalization of the receptor (Cunningham et al., 2004). Proceeding its approval for IT-insensitive mCRC by

the United States Food and Drug Administration (FDA) in 2004 (Xie et al., 2020), cetuximab was revealed to significantly improve overall- and progression free survival in patients with CRC that did not respond to treatment with IT, 5-FU or OXA (Jonker et al., 2007). The more recently developed, fully humanized antibody panitumumab circumnavigates hypersensitivity reactions associated with the application of murine-human chimeric antibodies (Yarom and Jonker, 2011). Unlike cetuximab, panitumumab does not trigger antibody-dependent cell-mediated cytotoxicity but still improves clinical outcomes in CRC due to a higher potency in the recruitment of myeloid effector cells (García-Foncillas et al., 2019; Rösner et al., 2019).

The formation of new blood vessels, termed angiogenesis, depicts another critical step in tumor initiation, growth and metastasis. While angiogenesis is finely tuned by several intra- and intercellular signaling pathways, the growth factor VEGF-A was identified as a major contributor to its tumor-promoting effects. Upon binding of VEGF-A to the VEGF receptor 2 (VEGFR2), the RAS/RAF/ERK/MAPK and PI3K/AKT pathways are activated to induce epithelial cell growth and promote cell survival (Goel and Mercurio, 2013). High serum levels of circulating VEGF have been associated with poor survival in CRC and were identified as predictors of liver and lung metastasis (Lopez et al., 2019). Targeted therapy of angiogenesis was first established as a valuable approach for CRC treatment when humanized monoclonal IgG antibody bevacizumab that specifically binds VEGF-A was revealed to improve progression-free survival (PFS) and overall survival (OS) of metastatic CRC in combination with IT, 5-FU and leucovorin in the AVF2107 clinical trial and was subsequently approved by the FDA (Hurwitz et al., 2004). Ramucirumab constitutes a more recently FDA-approved fully humanized monoclonal IgG antibody targeted at VEGFR2 that significantly improved PFS in combination with FOLFIRI (Tabernero et al., 2015).

Furthermore, small molecule inhibitors of dysregulated growth signaling pathways are successfully applied in the treatment of CRC. The multi-kinase inhibitor regorafenib blocks several protein kinases involved in the progression of CRC, including VEGF, RAF and FGFR. Application of regorafenib revealed to provide survival benefits for patients with treatment-refractory metastatic CRC and thus received treatment approval by the FDA (Arai et al., 2019; Grothey et al., 2013). Encorafenib, a potent inhibitor of RAF kinases, attenuates ERK phosphorylation, thereby inhibiting CRC cell growth with limited induction of apoptosis (Jenkins et al., 2024). The application of encorafenib in combination with cetuximab has been approved as the new standard of care in previously treated *BRAF*-V600E-mutant metastatic colorectal cancer, leading to improved OS, ORR and PFS (Kopetz et al., 2019; Tabernero et al., 2021).

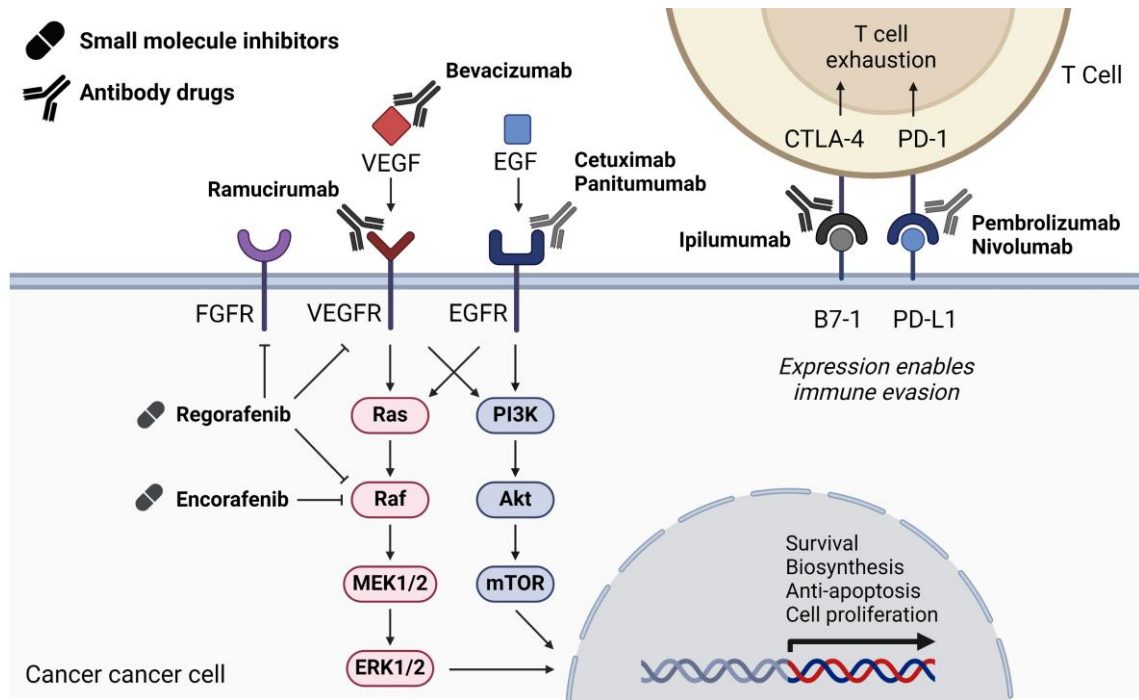


Figure 3: Mechanisms of targeted therapy approaches applied in CRC treatment. Small molecule inhibitors and antibody drugs are differentiated as indicated. While circulating growth factors (e.g. VEGF) and the corresponding receptors (e.g. VEGFR and EGFR) are targeted by monoclonal antibodies, small molecule kinase inhibitors are applied to attenuate the downstream signaling. In addition, immune-checkpoint receptors programmed cell death protein 1 (PD-1) and cytotoxic T-lymphocyte-associated Protein 4 (CTLA-4) are routinely targeted by applying monoclonal antibodies to impede immune evasion of cancer cells. (Created with BioRender)

Beyond the targeted therapeutic interference with intracellular pathways mediating growth and proliferation, novel approaches aim to improve the immunorecognition of cancer cells. In CRC, overexpression of the transmembrane proteins B7-1 and PD-L1 on the cellular surface enables the interaction with the corresponding immune-checkpoint receptors cytotoxic T-lymphocyte-associated protein 4 (CTLA-4) and PD-1 on the T cell surface, thereby attenuating T cell signaling and anti-tumorigenic immune response by a mechanism referred to as T cell exhaustion (Xie et al., 2020). The first FDA-approved immune checkpoint inhibitor is ipilimumab, which targets CTLA-4 and was initially applied in melanoma treatment. In 2018 it received approval for the therapy of refractory mCRC in a doublet regimen with nivolumab (Lenz et al., 2018). Pembrolizumab, a monoclonal antibody against PD-1, was revealed to prolong PFS and reduce side effects in combination with 5-FU in the treatment of MSI-high and MMR-deficient mCRC (André et al., 2020). Only a small portion of CRC patients respond to the therapy with immune checkpoint inhibitors. In particular, MSI-high cancers with high mutational burden and MMR-deficiency showed an improved response rate (Xie et al., 2020).

1.1.2.5. Merosesquiterpenes as novel anticancer compounds

Historically, natural compounds found in plants, fungi or microorganisms provided an important source of pharmacologically active agents, either directly or after subsequent structural modifications. The secondary metabolism of these stationary life forms evolved to overcome environmental needs and challenges, resulting in a large variety of bioactive compounds, some of which were identified as exerting antitumorigenic activity. Prominent examples include vincristine, camptothecin and etoposide, which can be found in plant species, as well as bleomycin and daunorubicin, naturally synthesized by bacteria (Demain and Vaishnav, 2011). As shown by the chemotherapeutic drugs eribulin, cytarabine and vidarabine, chemical compounds synthesized by marine sponges can serve as lead structures for the development of novel anticancer agents (Mayer et al., 2010). Despite ongoing advances in rational drug design, high throughput screening of natural compound libraries is still applied in the pharmaceutical industry as a reliable source of potential new drug candidates (David et al., 2015).

In the 50-year period from 1963 to 2013, nearly 25,000 novel marine compounds were identified and reported in literature, with 33% contributed by the phylum of *porifera*, also referred to as marine sponges (Blunt et al., 2015). A large variety of chemical compounds are biosynthesized by marine sponges, many of which exhibit pharmacological activity, including alkaloids, terpenoids, lipids and macrolides (Essack et al., 2011). Among them, merosesquiterpenes are a group of biological compounds, structurally characterized by a sesquiterpene unit joined with a quinone or phenolic moiety (Alvarez-Manzaneda et al., 2011).

Corresponding natural substances can be found in sponges as well as plants and fungi. They exhibit a wide structural diversity with mixed biosynthetic origins (Fuloria et al., 2022). Among this group, the most potent biological activities are frequently reported for bicyclic terpene moieties, also referred to as drimanes (Carrasco et al., 2014). While the plethora of pharmacological effects observed for sesquiterpenes include anti-inflammatory, anti-bacterial, anti-viral, anti-oxidant and anti-diabetic activity, this chapter will focus on the anti-cancer activity (Tian et al., 2023).

A particularly well studied member of the class of merosesquiterpenes is ilimaquinone (IQ). Several studies revealed growth inhibition and cytotoxicity in pancreatic, liver, lung and prostate cancer cells *in vitro* (Lu et al., 2007). In CRC cells, induction of TRAIL-dependent cell death was observed in response to IQ treatment, characterized by ROS-dependent upregulation of death receptor 4 and 5 (DR4 and DR5) expression (Do et al., 2014). Pyruvate dehydrogenase kinase (PDK), the negative regulator of PDH, was identified as a potential target. By interfering with the ATP-binding pocket of the enzyme,

IQ leads to generation of ROS and depolarization of the mitochondrial membrane, thereby inducing apoptotic cell death in several cancer cell lines (Kwak et al., 2020). Furthermore, IQ-dependent accumulation and Ser15-phosphorylation of p53 as well as caspase-3 cleavage and apoptotic cell death were observed in CRC cell lines (Lee et al., 2015). Tumor suppressor p53-dependent induction of apoptosis by IQ was also revealed in oral squamous cell carcinoma (Lin et al., 2020). In a screening of 296 natural compounds regarding their cytotoxicity and potential to activate DDR, IQ was identified to induce histone 2AX phosphorylation (γ H2AX) and DNA strand break formation in pancreatic cancer cells (van Stuijvenberg et al., 2020).

Among the group of merosesquiterpenes, smenospongine (SP) represents a less studied compound. Investigation in breast cancer cell lines revealed activation of 5' adenosine monophosphate-activated protein kinase (AMPK) and p38 signaling, thereby inducing cell cycle arrest and activation of the intrinsic apoptosis pathway (Tang et al., 2018). In the human leukemia cell lines HL60 and U937, SP induced dose dependent activation of apoptosis and G₁ cell cycle arrest. Increased expression of p21 and phosphorylation of the retinoblastoma protein (Rb) were observed and occurred independent of p21-promotor activation, as demonstrated by luciferase transporter gene transfection (Kong et al., 2008).

1.1.3. Metastasis of CRC

Metastasis, which describes the dissemination of malignant cells from an initial primary tumor site to secondary sites, often occurs in the final stages of tumor progression and represents the main contributor to mortality in CRC (Cervantes et al., 2023). While, in general, the primary tumor can be managed by surgical excision, the spreading of malignant cells to distant organs, such as liver, lung and brain, results in a dismal prognosis (Fidler, 2003; Langley and Fidler, 2011). Although preventive measures evolved in recent years, the proportion of CRC patients that exhibit metastases at diagnosis (20%) has been stable in the last two decades (van der Geest et al., 2015). Analysis of 49,096 CRC patients revealed the liver to be the most common site of metastasis for both colon (70%) and rectal (70%) cancer. A more frequent metastatic colonization of thoracic organs was observed by rectal cancer (47%) compared to colon cancer (32%) (Riihimäki et al., 2016).

Typically, the development of metastases follows the metastatic cascade, as outlined in Figure 4 (Obenauf and Massagué, 2015): The process of epithelial-to-mesenchymal transition (EMT), which is frequently induced by oncogenic activation of the TGF- β signaling pathway in CRC (Calon et al., 2012), plays a fundamental role in the early steps

of tumor invasion: Cancer cells obtain a mesenchymal phenotype, which includes loss of intercellular adhesion and polarization as well as an increase of motility and invasiveness, as further discussed in Chapter 1.1.4.1. (Thiery et al., 2009). During local invasion, tumor cells utilize proteases (e.g. MMPs) to break down the extracellular matrix and leave the confined primary tumor into the adjacent parenchyma. An invasive front at the edge of the tumor develops, where close interaction with the tumor microenvironment further facilitates growth signaling and immunosuppression (Joyce and Pollard, 2009). Small GTPases of the Rho-family including RhoA, which control intracellular actin dynamics and thereby cell motility, are an important driver of tumor cell migration and invasion (Crosas-Molist et al., 2022).

Single tumor cells or tumor cell clusters invade the blood or lymphatic circulation, where interaction with non-malignant cells may enhance survival. Anoikis, an apoptosis mechanism induced by the detachment from the extracellular matrix, is evaded by NF- κ B signaling in CRC cells (Yoo et al., 2015). Furthermore, circulating tumor cells are exposed to increased levels of oxidative stress, which leads to stabilization of HIF1 α to further drive metastasis and tumor cell survival (Nagaraju et al., 2015). In distant organs, cancer cells, which become trapped in narrow capillaries, penetrate the microvascular wall utilizing MMPs to extravasate into the tissue (Nguyen et al., 2009). In addition, the protein ANGPTL4 (angiopoietin-like 4) has been shown to promote CRC metastasis by increasing vascular permeability and venous invasion (Nakayama et al., 2011). While only a fractional amount of tumor cells entering the circulation and reaching a colonization site survive, few cells may be sufficient to enable the growth of a metastasis (Nguyen et al., 2009).

1.1.3.1. The role of epithelial-to-mesenchymal transition

Epithelial-to-mesenchymal transition (EMT) is a fundamental biological process that occurs during numerous steps of embryonic development and is responsible for wound healing in adult organisms. During the malignant progression of various tumor diseases, EMT depicts an important regulator of tumor cell metastasis. In general, epithelial cells, which are characterized by a high intracellular adhesion, a non-migratory phenotype and apical-basal polarity, begin to migrate as single cells which display a dorsal-ventral polarity. This process is accompanied by loss of cell adhesion markers (e.g. E-cadherin), redistribution of actin fibers and increased expression of matrix-metalloproteases (MMPs). Several pathways, including the EGF, FGF, TGF- β and Wnt-signaling pathways are involved in the induction of EMT to different degrees, depending on cell type and tissue (Thiery et al., 2009).

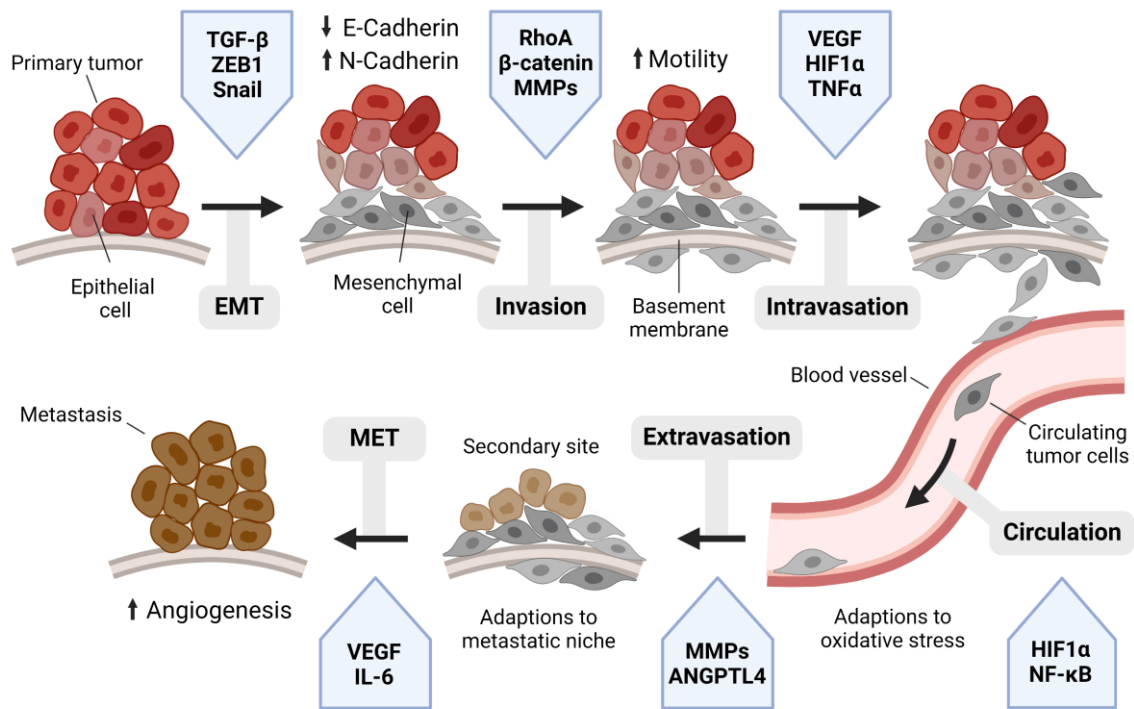


Figure 4: The metastatic cascade of colorectal cancer and associated signaling pathways.

The process of tumor metastasis can be subdivided into several steps, starting with phenotypic alterations during EMT, the subsequent invasion through physiological barriers and intravasation into the circulation, leading to spread of circulating tumor cells to distant organs, where extravasation and metastasis formation occur. The different steps of the metastatic cascade are driven by several signaling pathways which are activated by oncogenes, environmental stimuli or cytokines secreted in the TME (Zhou et al., 2022). (Created with BioRender)

The TGF- β pathway upregulates EMT in different settings, including tumor metastasis: In mammalian epithelial cells, three isoforms of TGF- β are expressed, encoded by the genes *TGFB1*, *TGFB2*, *TGFB3*, depending on tissue type and developmental context. While TGF- β 1 is expressed in most tissues and its role in cancer well studied, only specific organs exhibit expression of the isoforms TGF- β 2 (heart and eye) and TGF- β 3 (developing lung) (Wakefield and Hill, 2013). The cytokine TGF- β binds to the corresponding TGF- β receptor (TGFB β R) 2, leading to recruitment and phosphorylation of TGFB β R1, thereby inducing its kinase activity. Active TGFB β R1 phosphorylates the transcription factors Smad2 and Smad3, which heterodimerize with Smad4. This Smad complex enters the nucleus, where it acts as a transcription factor to induce the expression of TGF- β responsive target genes in a cell- and tissue-specific context, including Zinc finger E-box-binding homeobox 1 (*ZEB1*), *SNAIL 1/2* and *TWIST* (Massagué, 2012). Additionally, other Smad and non-Smad signaling pathways are induced by active TGFB β R1 and TGFB β R2, resulting in a complex network which regulates various cellular processes including proliferation and differentiation (Lampropoulos et al., 2012).

TGF- β functions as a tumor suppressor in early phases of colorectal carcinogenesis and mutations of associated pathways are known to occur in the process of malignant transformation. Accordingly, TGF- β has been observed to induce cell cycle arrest and cell death in early steps of tumorigenesis (Xu and Pasche, 2007). Other studies revealed that most CRC cells do not completely downregulate TGF- β signaling (Zavadil and Böttinger, 2005). Instead, several late-stage cancer types, redirect TGF- β signaling to facilitate increased malignancy by inducing EMT, while remaining insensitive regarding its growth inhibiting effects (Hao et al., 2019). Alterations of Smad2 and Smad3 phosphorylation sites have been identified to play an important role for the change of TGF- β -induced signal transduction during CRC progression (Matsuzaki et al., 2009). Among the molecular alterations taking place during the malignant transformation of CRC, outlined in Chapter 1.1.1., TGFBR2 and Smad4 mutations are frequently observed. In particular loss of Smad3 has been associated with metastatic CRC (Zhu et al., 1998).

Despite its growth inhibiting effects in isolated CRC cells, increased TGF- β concentrations were observed in CRC patients who exhibited liver metastases (Tsushima et al., 2001). When discussing the effects of TGF- β on tumor metastasis, it is important to consider the complex interactions in the tumor microenvironment (TME) rather than only its effects on isolated cells (Bellomo et al., 2016). TGF- β -dependent signaling between cancer associated fibroblasts (CAFs) and CRC cells has been revealed as crucial for the induction of metastasis and is associated with poor prognosis (Calon et al., 2015). Correspondingly, metastasis and chemoresistance induced by TGF- β in CRC were revealed to be mediated by Interleukin-11 (IL-11) which promotes the recruitment of immune suppressive CAFs (Calon et al., 2012). Excretion of TGF- β by tumor-associated macrophages has been described to induce HIF1 α -dependent invasion of CRC cells *in vitro* (C. Liu et al., 2021). In addition, loss of *MED12*, a negative regulator of TGFBR2, was shown to be associated with chemotherapy resistance in CRC patients by inducing an EMT-like phenotype (Huang et al., 2014). TGF- β expression has been linked to certain molecular subtypes of CRC. A positive correlation between MSS status and activity of the TGF- β pathway was observed (Pino et al., 2010). In certain, *BRAF*-mutated types of serrated CRC, TGF- β signaling was correlated with poor prognosis (Fessler et al., 2016).

Several approaches have been established to target TGF- β dependent signaling in CRC. The small molecule drug galunisertib inhibits kinase activity of TGFBR1, thereby impairing phosphorylation of Smad2 and downregulating the canonical TGF- β signaling pathways. Galunisertib was shown to decrease growth of breast, prostate and colon cancer *in vivo* (Herbertz et al., 2015). LY2109761, a dual kinase inhibitor of TGFBR1 and

TGFBR2 was shown to attenuate liver metastasis and prolong survival *in vivo* by targeting Smad- and non-Smad-dependent EMT in colon and pancreatic cancer (Melisi et al., 2008; Zhang et al., 2009). In line with these observations, *in vivo* findings confirmed the effects of LY2109761 on metastasis of breast and prostate cancer in a xenograft mouse model (Ganapathy et al., 2010; Wan et al., 2012). First phase II clinical trials of LY2157299 (galunisertib) in combination with radiochemotherapy in CRC have been finished recently and revealed a marked increase in therapy response (Yamazaki et al., 2022).

A clinical study of TGFBR1-inhibitor vactosertib in cotreatment with pembrolizumab is currently executed in MSS mCRC (NCT03724851) and first results indicated a favorable safety profile and a promising efficacy (T. W. Kim et al., 2021). Regulatory T cells (T_{reg}) can attenuate the activity of nearby immune cells by activating latent TGF- β 1 via the transmembrane protein GARP (glycoprotein A repetitions predominant) (Liénart et al., 2018; Salem et al., 2019). In order to target the tumor promoting and suppressing dual role of TGF- β signaling in a more targeted way, de Streel et al. developed and applied antibodies against complexes of GARP and TGF- β 1 in an *in vivo* xenograft mouse model using CT26 colon carcinoma cells to restore T cell-mediated anti-tumor immunity (de Streel et al., 2020).

1.2. The Altered Metabolism of Tumor Cells

First described by Otto Warburg, the metabolic adaptations of tumor cells have been known for nearly 100 years. Nevertheless, a thorough understanding of the underlying processes only emerged recently with the advent of high content biomolecular methods such as transcriptome and metabolome analysis (Stine et al., 2022). During the malignant transformation of healthy cells and in the course of tumor development, metabolic alterations occur as a consequence of oncogenic signaling or in response to alterations of the tumor microenvironment (Martínez-Reyes and Chandel, 2021). In the last decade, five core elements of metabolic alterations in tumors have been differentiated (Danzi et al., 2023):

- I) The unregulated acquisition of extracellular nutrients enabling cellular proliferation and survival even under nutrient deprivation and their utilization in core metabolic pathways, including glycolysis, the pentose-phosphate pathway (PPP) and the TCA cycle (Seyfried et al., 2020).
- II) An increased nitrogen-demand to supply biosynthetic pathways for cellular biomolecules including nucleotides, amino acids, glutathione and polyamines (Kodama et al., 2020).

- III) The modulation of gene expression mediated by metabolites or metabolic enzymes including acetylation, phosphorylation and succinylation.
- IV) A dependence on antioxidants (e.g. GSH, NADPH) and antioxidant enzymes (e.g. catalase, superoxide dismutase) to mitigate the effects of ROS which acts as a pro-growth signal to sustain tumor initiation, progression, metastasis and angiogenesis (Panieri and Santoro, 2016).
- V) An accumulation of oncometabolites (e.g. succinate, fumarate, and 2-hydroxyglutarate) compared to non-malignant tissue due to loss- or gain-of-function mutations of respective enzymes (Yang et al., 2013).

The different aspects of the deregulated metabolism in cancer, including the central role of the TCA cycle, the metabolic regulation by tumor suppressors and oncogenes, and the effects of oncometabolites, are further delineated in the following chapters.

1.2.1. The deregulated of metabolism as a hallmark of cancer

The metabolic alterations which occur during the malignant transformation of tumor cells are considered as a hallmark of cancer (Hanahan, 2022). Several aspects of the carcinogenesis process result in changes of the cellular metabolic phenotype, including rewiring in the TME, loss of tumor suppressor genes and mutations of metabolic enzymes. Nevertheless, to which extend the deregulation of cellular energetics occurs directly in response to oncogenic signaling and thereby enables increased proliferation and provision of biosynthetic substrates is not yet fully understood (Martínez-Reyes and Chandel, 2021). Based on additional evidence regarding this question, the concept of metabolic reprogramming emerged in the last decade. Tumor-associated metabolic alterations are initiated by oncogenes and are not only the result of mutations, damaged mitochondria or adaptations to changing environmental conditions (Ward and Thompson, 2012). In addition, deregulated intracellular concentrations of metabolites like fumarate, succinate or α -ketoglutarate can impair cellular feedback mechanisms resulting in an oncogenic activity (Fu et al., 2022; Martínez-Reyes and Chandel, 2020).

The metabolic phenotype of tumor cells changes during the process of carcinogenesis influenced by specific microenvironmental conditions. During tumor-growth, oxygen supply is limited by diffusion early on, resulting in hypoxia and upregulation of glycolysis. As a key regulator of this adaption, hypoxia-inducible transcription factor 1 α (HIF1 α) mediates a shift towards glycolysis by inducing expression of glycolytic enzymes and glucose transporter 1 (GLUT1) while inhibiting mitochondrial metabolism due to activation of pyruvate dehydrogenase kinase (PDK), as further outlined in Chapter 1.2.2.1. (Marin-Hernandez et al., 2009; Papandreou et al., 2006). In CRC, HIF1 α induces

expression of angiogenic growth factors VEGF and platelet-derived growth factor β (PDGF β), which stimulate angiogenesis to provide the tumor with oxygen and nutrients (Cao et al., 2009; Manzat Saplacan et al., 2017) and positively correlate with advanced TNM-stage, vascular invasion and consequently poor survival (Rasheed et al., 2009).

Another important determinant for the metabolic status in CRC is the mitochondrial pyruvate carrier (MPC), which consists of the subunits MPC1 and MPC2. This transporter, which facilitates the mitochondrial uptake of pyruvate to enable its catabolism in the TCA cycle, is frequently deleted or downregulated in CRC tissue and its absence correlates with poor prognosis (Schell et al., 2014). Re-expression of MPC in CRC cells reverses the Warburg-effect and restores oxidative metabolism, resulting in reduced xenograft-tumor growth *in vivo* (Schell et al., 2014). In line with these findings, Cuezva and colleagues showed that a high bioenergetic mitochondrial index compared to the cellular glycolytic potential provides a positive prognostic value regarding the progression of CRC (Cuezva et al., 2002).

The diversity of metabolic phenotypes reported among CRC is a consequence of the distinctive mutations of tumor suppressors and oncogenes in tumors, as further discussed in Chapter 1.2.2. During malignant transformation, a reduced mtDNA copy number was revealed in carcinoma tissue of CRC patients compared to non-malignant adenoma. In addition, mtDNA copy number was identified to be significantly lower in MSS and *BRAF*-mutated tumors, while being higher in *KRAS*-mutated tumors (van Osch et al., 2015). In support of this observation, analysis of ATP-dependent respiration rate and mitochondrial outer membrane (MOM) permeability in patient-derived tumor specimen linked *KRAS*-mutations to an oxidative phenotype and *BRAF* mutations to glycolysis (Rebane-Klemm et al., 2020). However, the Warburg-subtype, indicated by somatic mutations of the genes *RAS*, *BRAF*, *PI3KCA*, and *MET* (MNNG HOS transforming gene) encoding for a receptor tyrosine kinase, did not affect survival within mutational subgroups in a cohort of 2,344 patients in contrast to the MMR status (Offermans et al., 2023).

1.2.1.1. The tricarboxylic acid cycle

The tricarboxylic acid (TCA) cycle functions as the main hub for a plethora of metabolic processes and is highly conserved in aerobic organisms. Briefly, acetyl-CoA is oxidized in a series of chemical reactions to generate the reduction equivalents NADH and FADH₂, which are utilized during oxidative phosphorylation to generate ATP. Intermediates of the TCA cycle do not only serve metabolic functions but are also involved in cellular signaling, thereby enabling metabolic dysregulations to promote cancer development and progression (Eniafe and Jiang, 2021).

A pronounced deregulation of the TCA cycle was reported for human colon carcinoma tissue in several studies. Downregulation of TCA cycle intermediates, including fumarate, malate, succinate and oxalate, accompanied by upregulated purine, pyrimidine and amino acid concentrations as well as fatty acid synthesis could be observed in comparison to healthy colon tissue (Denkert et al., 2008; Mal et al., 2012; Ong et al., 2010). In CRC, the molecular consequence of attenuated α -ketoglutarate (α KG) levels is well examined. Impairment of mitochondrial respiration by silencing mitochondrial transcription factor A (TFAM), a key transcription factor for mitochondrial DNA (mtDNA) replication and gene transcription, led to accumulation of α KG and impairment of HIF1 α and Wnt/ β -catenin signaling. Knockout of prolyl hydroxylase domain protein 2 (PHD2), an α KG-dependent dioxygenase, rescued HIF1 α and Wnt/ β -catenin protein expression, revealing the role of α KG as a signaling molecule during tumorigenesis (Wen et al., 2019). Correspondingly, α KG has been shown to drive differentiation *in vivo* and in CRC tumoroids by inducing hypomethylation of DNA and histone H3K4me3, which leads to downregulation of Wnt-target genes (Tran et al., 2020).

Cancer cells rely on intermediates of the TCA cycle for biosynthetic reactions, epigenetic remodeling and oncogenic signaling. Since a continuous withdrawal of metabolites would lead to the break-down of the TCA cycle, anaplerotic reactions represent a fundamental part of this metabolic network (Inigo et al., 2021). The deamination of glutamine to glutamate by glutaminase (GLS) and the subsequent generation of α KG by glutamate dehydrogenase (GLDH), termed glutaminolysis, represents an integral anaplerotic pathway. Upregulation of GLS and GLDH expression have been observed in human CRC tumor specimen and were linked to poor disease progression and metastasis (Huang et al., 2014; Liu et al., 2015; Song et al., 2017). Glutamine was identified as a critical anaplerotic substrate based on which colon cancer cells replenish the TCA cycle *in vivo* (Zhao et al., 2019).

A higher dependency on glutamine was observed in CRC tumors with mutations of the *PIK3CA* gene (Zhao et al., 2019). Correspondingly, *PIK3CA* mutations were shown to upregulate glutamate pyruvate transaminase 2 (GPT2) expression in CRC, which converts glutamine to α KG for TCA cycle anaplerosis (Hao et al., 2016). Overexpression of GLDH1 and reduced expression of mitochondrial aspartate/glutamate carrier 2 (SLC25A13) corresponded to poor prognosis and tumor aggressiveness in CRC (Miyao et al., 2016). The additional impact of TCA cycle metabolites on the process of cancer metastasis and EMT, two important drivers of malignancy in CRC, is detailed in Chapter 1.2.2.2.

1.2.1.2. Oxidative phosphorylation

The oxidative phosphorylation (OXPHOS) constitutes the final metabolic pathway, in which the molecular electron donors NADH and FADH₂ that are a product of glycolysis and TCA cycle are applied to generate an electrical potential across the inner mitochondrial membrane and thereby enable ATP synthesis. A deregulation of OXPHOS is regularly observed in different types of cancer. While in some cases upregulation of several respiration-chain complexes and mitochondrial respiration occurs, other tumors exhibit a downregulated OXPHOS (Gaude and Frezza, 2016).

Based on the metabolic phenotype of the tumor, the deregulation may not only result in excessive aerobic glycolysis but can also manifest as an upregulated OXPHOS, illustrated for CRC by several studies. CRC tissue samples derived from MSS tumors exhibited an upregulated copy number of mtDNA, positively correlating with tumor stage (Feng et al., 2011). In accordance, increased mtDNA copy number was associated with a reduction of apoptosis and a higher proliferation in MSS CRC cell lines, dependent on upregulated OXPHOS (Sun et al., 2018). Induction of OXPHOS with a concurrent unchanged glycolytic activity was identified in biopsies obtained from CRC tumor tissue in comparison to surrounding non-malignant tissue (Chekulayev et al., 2015).

Several studies revealed an association of an upregulated OXPHOS with the development of chemoresistance. In a xenograft mouse model, 5-FU treatment was reported to select for CRC cells which underwent metabolic reprogramming to OXPHOS to meet their energetic needs (Denise et al., 2015). Vellinga and colleagues revealed that chemotherapeutic intervention with 5-FU and OXA in CRC patients led to upregulated OXPHOS in corresponding liver metastases, resulting in chemoresistance. Treatment of associated patient-derived colonosphere cultures induced an upregulated expression of respiratory chain enzymes, increased mitochondrial biomass and higher oxygen consumption rate mediated by the histone deacetylase sirtuin-1 (SIRT1) and its substrate, the peroxisome proliferator-activated receptor coactivator PGC1 α , indicating a clinical relevance (Vellinga et al., 2015).

1.2.2. Mechanisms of metabolic alterations

In non-malignant cells, proliferation, differentiation and the balance between survival and death are tightly regulated by specific signaling pathways, which also control metabolic processes (Shortt and Johnstone, 2012). As described in the preceding chapter, neoplastic transformation depends on the induction of proliferative stimuli (e.g. oncogenes) and the disruption of mechanisms that avoid uncontrolled proliferation (e.g. tumor suppressors).

The altered metabolism of tumors was long considered a passive consequence of dysfunctional mitochondria. Recent studies revealed that the metabolic changes of malignant cells occur in response to deregulated signaling, thereby facilitating cell growth and supplying biosynthetic pathways to provide a selective advantage over untransformed cells (Brown et al., 2018; Martínez-Reyes and Chandel, 2020). Transcriptional regulators and kinases, which are frequently associated with alterations of the metabolic phenotype in CRC includes oncogenes HIF1 α , MYC, PI3K, AKT, mTOR and KRAS as well as the tumor suppressor p53 (Tarrado-Castellarnau et al., 2016). In addition, oncometabolites and TCA cycle intermediates have been identified as critical signaling molecules, which omit further influence on CRC metabolism.

1.2.2.1. The role of oncogenes and tumor suppressors

MYC: Acting as a proto-oncogene, deregulated expression of the transcription factor MYC has been observed in over 20% of cancer entities (Dang et al., 2006). In CRC, inactivating mutations of the *APC* gene or activating mutations of β -catenin result in the transcription factor-dependent upregulation of MYC expression (He et al., 1998). As an important regulator of cellular proliferation and differentiation, an increase of MYC was observed during adenoma as well as carcinoma stage of CRC and identified as a main contributor to the metabolic reprogramming of CRC (Satoh et al., 2017). A MYC-induced upregulation of 231 genes has been observed in CRC, which encode for enzymes and transporters involved in glycolysis, glutaminolysis and carbon metabolism (Satoh et al., 2017). In detail, MYC-dependent metabolic modulation in CRC included downregulation of catabolic genes engaged in fatty acid β -oxidation (e.g. carnitine palmitoyltransferase, *CPT2*) and upregulation of anabolic genes responsible for *de novo* synthesis of pyrimidines (e.g. carbamoyl-phosphate synthetase, *CAD*), purines (e.g. phosphoribosyl-pyrophosphate synthetase, *PRPS2*) and fatty acids (e.g. palmitoyl-protein thioesterase 1, *PPT1*) (Satoh et al., 2017). Additionally, MYC induced expression of glycolytic genes (e.g. *LDHA*) and transcriptionally repressed genes associated with the TCA cycle (e.g. *IDH3A*), thereby promoting a shift towards glycolysis (Tang et al., 2019). MYC was observed to downregulate miR-23, a suppressor of the enzyme GLS, resulting in enhanced glutamine metabolism (Gao et al., 2009). Accordingly, glutaminolysis is induced by upregulation of *GLS* and *ASCT1* (ASC amino acid transporter 1) gene expression in CRC, which is facilitated by MYC (Xu et al., 2015).

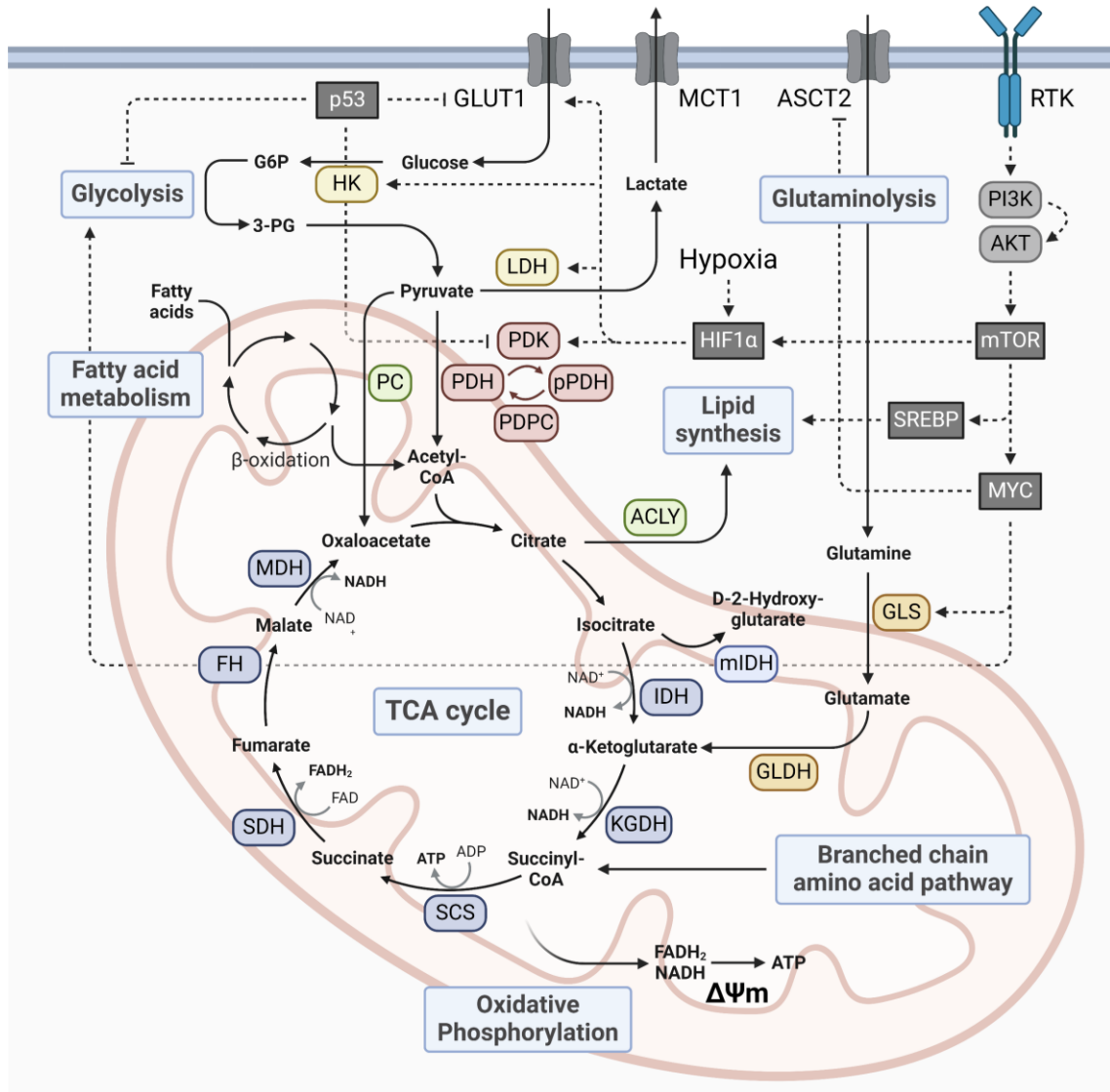


Figure 5: Effects of tumor suppressor activity and oncogenic signaling on the metabolic reprogramming of CRC. A multitude of metabolic pathways evolve around the TCA cycle, including anabolic (e.g. lipid synthesis) and catabolic (e.g. glycolysis) processes. In addition, anaplerotic reactions (e.g. glutaminolysis) are necessary to replenish intermediates, which are repurposed for biosynthetic processes (Neitzel et al., 2020). ACLY, ATP citrate lyase; FH, Fumarate hydratase; MDH, Malate dehydrogenase; SCS, Succinyl coenzyme A synthetase; SDH, Succinate dehydrogenase; SREBP, Sterol regulatory element-binding protein; PDPC, pyruvate dehydrogenase phosphatase; PDK, pyruvate dehydrogenase; $\Delta\Psi_m$, mitochondrial membrane potential. (Created with BioRender)

HIF1 α : As a heterodimeric transcription factor, HIF1 consists of the constitutively expressed subunit HIF1 β and the subunit HIF1 α , which is post-transcriptionally controlled by the cellular oxygen state (Nagaraju et al., 2015). Under normoxia, degradation of HIF1 α by the 26s proteasome is controlled by hydroxylation of two proline residues, catalyzed by the enzyme prolyl hydroxylase 1 (PHD1). Hypoxic conditions result in a downregulated activity of PHD1, leading to HIF1 α stabilization and subsequent

transcription of target genes (Erez et al., 2003). In cancer cells, stabilization of HIF1 α under normoxic conditions can be induced by deregulated signaling pathways, as described for the PI3K/AKT/mTOR axis, and is associated with malignant progression (Agani and Jiang, 2013). Opposed to healthy mucosa, HIF1 α upregulation was observed in 55% of CRC tumor specimens and positively correlated with tumor stage and an aggressive histological and clinical behavior (Cao et al., 2009). In accordance, loss of PHD1 was detected in 71% of CRC patients and associated with advanced tumor stage and short overall survival (Melling et al., 2023). Mechanistically, HIF1 α regulated expression is enabled by hypoxia-responsive element promotor regions found in genes associated with metabolism and angiogenesis, including *VEGF*, cytochrome c oxidase subunit 2 (*COX2*) and *GLUT1* (Nagaraju et al., 2015). Vascularization and angiogenesis of CRC tumors is associated with HIF1 α -dependent VEGF expression (Forsythe et al., 1996; Goel and Mercurio, 2013) and COX2 overexpression, leading to enhanced prostaglandin E2 (PEG2) levels (Tsuji et al., 1998).

KRAS: Mutations of *KRAS* are observed in 40% of CRC tumors and frequently result in reduced treatment response and poor clinical outcome (Vaughn et al., 2011). As an integral part of the MAPK/ERK pathway, the small GTPase KRAS regulates cellular processes involved in migration, proliferation, differentiation and apoptosis. In addition, alterations of the metabolic phenotype in malignant cells have been described as a consequence of deregulated MAPK and PI3K signaling pathways driven by KRAS (Kerk et al., 2021). Enhanced glucose uptake and a thereby increased glycolytic flux constitute the central mechanisms of KRAS-induced metabolic alterations in tumors. In CRC cells exhibiting mutations of *KRAS*, upregulated expression of glucose transporters (GLUT) enables a more efficient uptake of glucose (Iwamoto et al., 2014). In addition, key enzymes of glycolytic pathways are either activated or transcriptionally upregulated by KRAS-signaling, allowing for an enhanced synthesis of amino acids and nucleotides (Amendola et al., 2019; Hutton et al., 2016). Mutated *KRAS* promotes the reduction of pyruvate to lactate and facilitates subsequent cellular clearance via the TME by upregulated expression of lactate transporters, which helps to avoid lactate accumulation (H. Liu et al., 2021). The TCA cycle of *KRAS*-mutated tumor cells is characterized by an increased carbon flux and the utilization of intermediates for anabolic synthesis, which is supplied by glutamine in anaplerotic reactions (Gaglio et al., 2011). In CRC, a positive feedback mechanism was reported for KRAS and HIF1 α (Chun et al., 2010). While hypoxia upregulates KRAS expression in several CRC cell lines (Zeng et al., 2010), KRAS reciprocally stabilizes HIF1 α , enabling increased cellular survival under hypoxic conditions (Kikuchi et al., 2009).

PI3K-AKT-mTOR: Activated by receptor tyrosine kinases (RTK) or G-protein coupled receptors in response to various growth factors (e.g. EGF) or oncogenes (e.g. KRAS), phosphatidylinositol 3-kinases (PI3Ks) enable downstream cellular growth signal transduction in CRC (Danielsen et al., 2015). Active PI3K catalyzes the phosphorylation of phosphatidylinositol-4,5-bisphosphate (PIP₂) to the second messenger phosphatidylinositol-3,4,5-trisphosphate (PIP₃), which activates the downstream effector serine/threonine kinase AKT and subsequently mammalian target of rapamycin (mTOR), thereby facilitating cellular proliferation (Fruman et al., 2017). The isoform AKT1 stimulates several pathways in cellular metabolism, including glycolysis (Li et al., 2019) and OXPHOS (Huang et al., 2019), by direct phosphorylation or transcriptional induction. In addition to its direct involvement in metabolic reprogramming, deregulated AKT activates mTOR, which subsequently forms the mTOR complex 1 (mTORC1). By phosphorylating eIF4E binding protein (4EBP) and p70S6 kinase 1 (S6K1), mTORC1 directly promotes mRNA translation and thus cellular protein synthesis, resulting in an increased cellular proliferation (Saxton and Sabatini, 2017).

p53: Best known for its integral role in the regulation of DNA repair and cell cycle progression, mutations of the tumor suppressor gene *TP53*, either associated with a loss or gain of function, have been described for about 60% of CRC tumors (Olivier et al., 2010). In addition, several mechanisms of the metabolic reprogramming in CRC tumors are associated with mutations of p53, including aerobic glycolysis, TCA cycle and the PPP (J. Zhang et al., 2023). In a pivotal study, Li et al. revealed that not the canonical p53 activity (e.g. apoptosis, cell cycle and senescence) but metabolic control depicts the major tumor suppressive mechanism of p53 in an *in vivo* mouse lymphoma model (Li et al., 2012). Accordingly, p53 was shown to regulate central aspects of metabolism. Glycolysis is repressed by wild-type p53 via transcriptional downregulation of glucose transporter gene expression (*GLUT1*, *GLUT12*) (Zawacka-Pankau et al., 2011), whereas mutant p53 can facilitate their translocation to the plasma membrane (C. Zhang et al., 2013). Wild-type p53 represses aerobic glycolysis by downregulating expression of the monocarboxylate transporter 1 (MCT1), thereby inhibiting the extracellular transport of lactate (Boidot et al., 2012). Under physiological conditions, wild-type p53 promotes OXPHOS by downregulating expression of PDK2 (Contractor and Harris, 2012) and inducing parkin, a key regulator of mitochondrial homeostasis (Zhang et al., 2011), as well as SCO2 (synthesis of cytochrome C oxidase 2), an integral factor of the electron transport chain (Matoba et al., 2006).

1.2.2.2. Oncometabolites

While serving a fundamental role in the provision of energy equivalents and providing building blocks for biosynthetic reactions, the TCA cycle is also a source of several signaling molecules. Intermediates like fumarate, succinate, α KG and citrate regulate the function of a plethora of enzymes, which are involved in epigenetic regulation or function as transcription factors (Martínez-Reyes and Chandel, 2020). At the same time, mutations that may occur in certain enzymes of the TCA cycle can lead to the generation of oncometabolites (Fu et al., 2022). One of the most significant oncometabolites is D-2-hydroxygutarate (D2HG), a molecule that leads to the deregulation of multiple cellular processes including metabolism, proliferation and differentiation (Cairns and Mak, 2013). It is formed in several tumor entities due to a gain of function mutation of the enzyme IDH1/2. While wild-type IDH1/2 converts isocitrate to α KG and CO_2 in an oxidative decarboxylation, mutant IDH1/2 catalyzes the conversion of α KG to D2HG (Waitkus et al., 2018). As a competitive inhibitor of ten-eleven translocases (TET), D2HG disrupts the stepwise demethylation, which is normally catalyzed by these enzymes, and thereby induces hypermethylation of histones and DNA to promote tumorigenesis, as shown in Figure 6.

Gain of function mutations of IDH1/2 leading to generation of 2HG are rare in CRC, occurring in 0.9% of cases, and are observed more frequently in *BRAF*-V600E-mutated CRCs, with an incidence of 3.0% (Huang et al., 2021). Notably, a recent study described elevated levels of D2HG in CRC cell lines in the absence of mutant *IDH1* or *IDH2* (Atalay and Kayali, 2022). Accumulation of D2HG has been associated with tumor progression in colitis-associated CRC *in vivo* (Han et al., 2018). HIF1 α dependent downregulation of the enzyme D2HG-Dehydrogenase (D2HGDH), which catalyzes elimination of D2HG, was subsequently identified in mucosal biopsies of ulcerative colitis patients that developed CRC (Han et al., 2018). L2HG has been recently reported to activate the mTOR pathway, thereby inducing expression of ATF4 and improving the survival of CRC tumor cells (Tabata et al., 2023). Furthermore, several metabolic intermediates covalently modify proteins via lysine acetylation including crotonylation, lactylation, succinylation, propionylation, butyrylation, malonylation, glutarylation, 2-hydroxy-isobutyrylation and β -hydroxybutyrylation, thereby regulating gene expression and intracellular signaling pathways (Fu et al., 2022). A significantly upregulated crotonylation of α -enolase (ENO1) has been reported in human CRC tissue and was mechanistically linked to enhanced growth, migration and invasion as well as a reduced sensitivity towards glucose deprivation *in vitro* (Hou et al., 2021). Succinylation of citrate synthase (CS), which catalyzes the rate-limiting first step of the TCA cycle, significantly decreases its enzymatic activity, thereby suppressing colon cancer proliferation and

migration (Ren et al., 2020). In summary, the available studies highlight that in CRC, occurrence of mutated enzymes IDH1 and IDH2 and subsequent accumulation of the oncometabolite 2HG is rare. Nevertheless, tumor-promoting effects of deregulated TCA cycle intermediates are frequently observed and associated with an altered protein expression and activity due to epigenetic regulation or posttranslational modification (Martínez-Reyes and Chandel, 2020).

1.2.2.3. Metabolic alterations during metastasis

Metabolic alterations can be a direct consequence of the phenotypic changes during the process of EMT or can occur in response to alterations of the cellular energy supply during metastasis. In general, tumor cells display metabolic plasticity, which describes the ability to utilize one metabolite during different steps of the metabolic cascade. Furthermore, nutrient flexibility may enable reliance on multiple metabolites during a specific step. Differentiation of these two phenomena helps to dissect the targetability of tumor metabolism during metastasis (Bergers and Fendt, 2021).

Adaptations of the tumor metabolism arise in different steps of the metastatic cascade. In CRC, the process of EMT leads to alterations of tumor metabolism but in parallel, metabolites or oncometabolites act as signaling molecules, modulating EMT and driving the early steps of metastatic progression (Wei et al., 2020). Metabolic changes allow circulating tumor cells (CTCs) to withstand the environmental stressors occurring during circulation, including oxidative stress and shear forces (Bergers and Fendt, 2021). Recently published studies detailed approaches to target EMT by applying metabolic inhibitors (Ramesh et al., 2020; Wei et al., 2020). In addition, several metabolites and intermediates of the TCA cycle have been described to modulate EMT and metastasis:

- I) D-2-hydroxyglutarate: Produced by the mutant enzymes IDH1 and IDH2, D-2-hydroxyglutarate (D2HG) constitutes a potential oncometabolite in CRC that induces EMT and distant metastases. D2HG leads to increased trimethylation of Histone H3 lysine 4 in the promotor of the *ZEB1* gene, thereby elevating transcription of this EMT master regulator (Colvin et al., 2016). In accordance, downregulation of antimetastatic miR200 microRNAs and upregulation of ZEB1 protein expression have been observed in CRC cells in response to D2HG (Grassian et al., 2012).
- II) Succinate: Mutations of the genes encoding for the succinate dehydrogenase (SDH) subunits (*SDHA* and *SDHB*) which are associated with different hereditary cancer entities including CRC result in accumulation of succinate in the mitochondrial matrix, from where it is transported to the cytoplasm and excreted

in the extracellular milieu (D. Zhang et al., 2013). While high intracellular succinate levels can result in HIF1 α stabilization due to inhibition of prolyl hydroxylases (PHD), extracellular secretion of succinate by malignant cells can enhance cancer cell migration and facilitate metastasis by inducing succinate receptor-1 (SUCNR1)-mediated ERK1/2 and STAT3 signaling and subsequent transcriptional activation of VEGF (Kuo et al., 2022). Knockdown of SDHB has been described to induce EMT in CRC cells mediated by activation of the SNAIL1-Smad3/4 axis (Wang et al., 2016a).

- III) Fumarate: Accumulation of fumarate due to loss of fumarate hydratase in renal cancer was observed to inhibit α KG dependent dioxygenases, so called TETs. This caused reduced demethylation in the regulatory region of the antimetastatic miRNA cluster miRNA200 and upregulation of the expression of EMT-inducing transcription factors (Sciacovelli et al., 2016). A pronounced downregulation of FH expression has been observed in human CRC samples and was associated with accumulation of fumarate compared to corresponding healthy tissue, leading to stabilization of HIF1 α (Hu et al., 2013).
- IV) α -Ketoglutarate: In breast cancer, α KG was shown to inhibit EMT by enhancing expression of tumor suppressors SDH and fumarate hydratase (FH), which reduced intracellular concentration of the oncometabolites succinate and fumarate, thereby stabilizing PHD2 and decreasing HIF1 α protein levels (Tseng et al., 2018). Inhibition of KGDH led to downregulation of EMT and reduced tumor cell invasion in breast cancer cells *in vivo* and *in vitro*. The underlying mechanism involved accumulation of α KG, activation of TETs, upregulation of anti-metastatic miRNA200 and downregulation of the ZEB1/MMP3 axis (Atlante et al., 2018).
- V) β -hydroxybutyrate: As recently published by Mao et al., upregulated serum levels of β -hydroxybutyrate in CRC patients induce acetyl-coenzyme A acetyltransferase 1 (ACAT1) leading to downstream IDH1 acetylation, thereby facilitating CRC proliferation and metastasis (Mao et al., 2023).
- VI) Acetyl-CoA: In breast cancer, acetyl-CoA dependent acetylation of Smad2 due to attenuated acetyl-CoA carboxylase (ACC) 1 activity was described to induce EMT and metastasis *in vivo* (Garcia et al., 2017). Furthermore, promotion of CRC metastasis by HOX (Homeobox) 13A was shown to be mediated by ATP-citrate lyase (ACLY), an enzyme that catalyzes the conversion of citrate to acetyl-CoA and oxaloacetate (Qiao et al., 2021). Abnormal expression of ACLY is associated with the migration and invasion ability of CRC cells and contributes to drug resistance of metastatic CRC (Li et al., 2024).

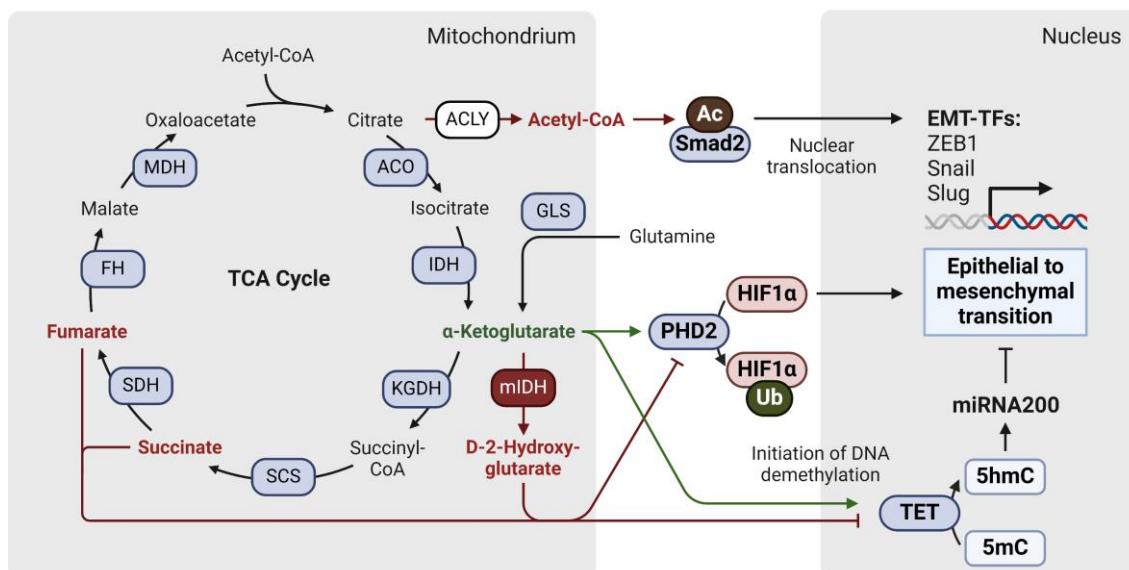


Figure 6: The modulation of pathways associated with CRC metastasis by TCA cycle metabolites. TCA cycle intermediate α KG functions as a cosubstrate of TETs, which induce expression of the antimetastatic miRNA200 by catalyzing the demethylation of its promoter, and of PHD2, which ubiquitinates HIF1 α . The oncometabolite D2HG as well as the intermediates succinate and fumarate attenuate activity of TETs and of PHD2, thereby promoting EMT and in consequence metastasis of CRC. (Created with BioRender)

1.2.3. The altered tumor metabolism as a target in CRC

The use of cytostatic drugs, which is still the standard of care for the treatment of most malignant diseases, is regularly accompanied by severe side effects and the development of resistances, as outlined in Chapter 1.1.2. Confronted with the need for new therapeutic approaches, the altered metabolism of cancer cells was identified as a potential vulnerability that may be exploited by applying novel small molecule inhibitors (Luengo et al., 2017; Stine et al., 2022). Nevertheless, the diversity and plasticity of the tumor metabolism complicates its utilization as a therapeutic target. Attempts aimed at the deregulated aerobic glycolysis as the most obvious metabolic alteration in tumors by applying inhibitors of GLUT1/2/3 (e.g. WZB-117), HK2 (e.g. FV-429) and LDHA (e.g. FX-11) showed limited preclinical effectivity (Yu et al., 2016) and no compound has reached market authorization to date (Stine et al., 2022).

Nevertheless, several metabolic inhibitors have reached clinical testing so far including drugs that target glutaminolysis (CB-839 & IPN60090) and the intracellular utilization of glutamine (DRP-104), the lipid synthesis (TVB-2640), the OXPHOS (IM156 & IACS-010759) and the MCT1-dependent excretion of lactate produced during aerobic glycolysis (AZD-3965) (Stine et al., 2022). Furthermore, compounds which inhibit the

enzymes IDH1 (Ivosidenib) or IDH2 (Enasidenib) and thereby attenuate generation of the oncometabolite 2HG in patients with specific mutations of *IDH1* and *IDH2* genes are already clinically applied in the treatment of acute myeloid leukemia (AML) and cholangiocarcinoma, as summarized in Figure 7 (Pirozzi and Yan, 2021).

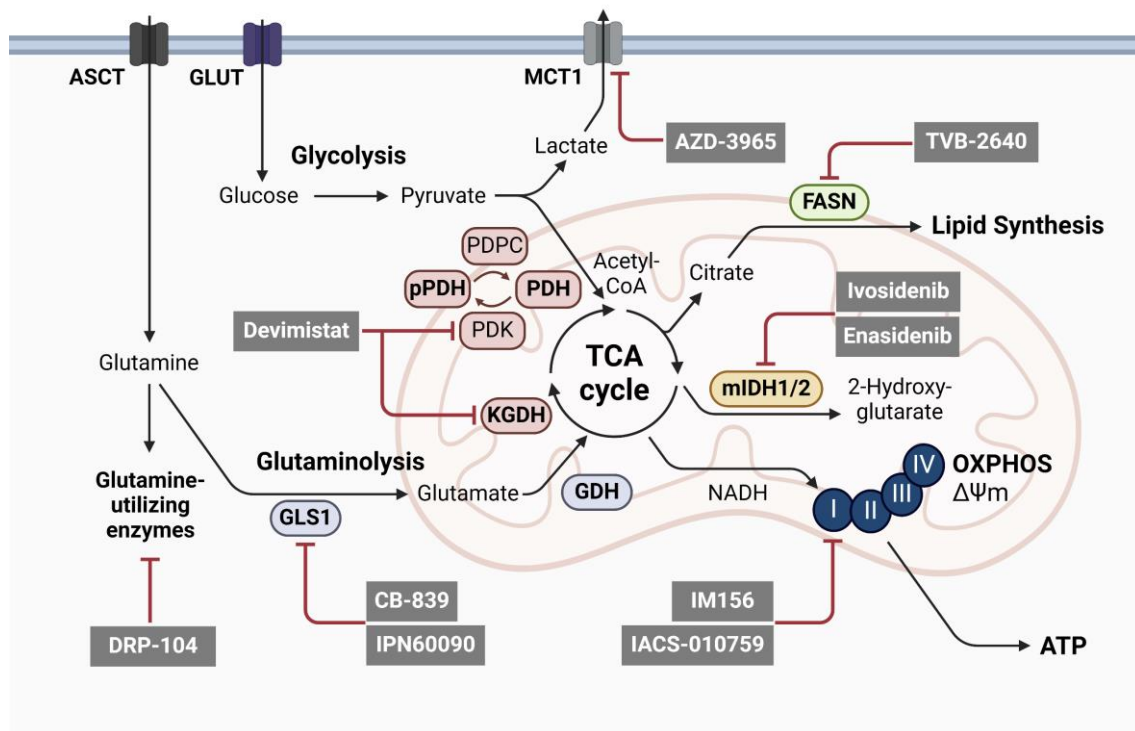


Figure 7: Metabolic inhibitors applied in the treatment of solid tumors in clinical trials. Several approaches which focused on the altered metabolism of tumor cells have reached clinical application so far. Metabolic processes which have been targeted include glutaminolysis, oxidative phosphorylation, lipid synthesis, aerobic glycolysis and the TCA cycle. (Created with BioRender)

The TCA cycle, which is the central hub of anabolic and catabolic reactions and frequently altered due to oncogenic signaling, mutations or oncometabolites, has been identified as a promising target in cancer therapy (Neitzel et al., 2020). Therefore, pharmacological inhibition of enzymes associated with the TCA cycle could provide a promising strategy for cancer treatment, either as a single-agent regimen or in combination with conventional chemo- or radiotherapy (Anderson et al., 2018). Thus, the lipolate devimistat has been developed to attenuate the activity of the TCA cycle enzymes pyruvate dehydrogenase (PDH) and α -ketoglutarate dehydrogenase (KGDH) and is currently applied in clinical studies for CRC treatment.

1.2.4. The metabolic inhibitor devimistat

Devimistat, a derivative of the coenzyme α -lipoic acid (LA), was developed by Rafael Pharmaceuticals Inc. (formerly known as Cornerstone Pharmaceuticals Inc.) under the abbreviation CPI-613 as a tumor-specific antimitochondrial drug with a novel mode of action (Zachar et al., 2011). As a first-in-class agent, devimistat targets the mitochondria of tumor cells to enable a potential broad-spectrum efficacy in the treatment of a variety of cancer entities, including hematological malignancies as well as solid tumors (Stuart et al., 2014). Chemically, two benzyl groups are covalently attached to the sulfur atoms of LA, rendering this compound redox-inactive. Devimistat is derived from its mother compound by applying a two-step synthetic procedure as detailed by Gibson and colleagues (Gibson et al., 2011).

1.2.4.1. Mechanism of action

As a mimic of the coenzyme LA, devimistat targets the altered metabolism of tumor cells. In opposition to existing small-molecule inhibitors of the tumor metabolism, devimistat has a dual mode of action by impairing the function of PDH and KGDH (Stuart et al., 2014; Zachar et al., 2011). The underlying mechanism differs for the two enzymes: Due to devimistat-activity, PDH is downregulated by activation of its regulator PDH-kinase (PDK), leading to a reduction of its enzymatic activity. Under physiological conditions, activity of the enzyme PDH is tightly regulated. Devimistat-induced hyperphosphorylation of its E1 α subunit results in permanent inactivation of the enzyme, thereby blocking the utilization of pyruvate derived from glycolysis in the TCA cycle. Impairment of the mitochondrial carbon flow by devimistat was shown to result in cancer cell death, while coadministration of acetate as an alternative to acetyl-CoA prevented these effects (Pardee et al., 2014). An alternative mechanism was described for the devimistat-induced inhibition of KGDH. In contrast to PDH, no phosphorylation is involved in the regulation of KGDH activity. Instead, oxidative stress has been described to reversibly inactivate KGDH by glutathionylation of its E2 lipoate residues (Applegate et al., 2008). Devimistat causes hyperstimulation of the endogenous redox-mechanism responsible for the regulation of KGDH-activity in a tumor cell specific manner. A ROS-burst dependent on the catalytic E3 subunit of the KGDH-complex impairs its autoregulatory function, rendering the enzyme dysfunctional (Stuart et al., 2014).

1.2.4.2. Biokinetics

Several studies investigated the pharmacokinetics of devimistat by applying preclinical *in vitro* and *in vivo* models or as part of clinical studies. Lee and colleagues investigated the metabolism of devimistat *in vitro* by applying human and rat liver S9-mixes. After its

oxidation during phase I metabolism, mainly catalyzed by CYP2C8 and CYP3A4/5, subsequent phase II O-glucuronidation at the terminal carboxyl group of devimistat can occur (Lee et al., 2011). Solely in human S9, a sulfoxide metabolite is generated based on the devimistat-glucuronide metabolite. Biotransformation of devimistat leads to detoxification of the compound, as revealed by cytotoxicity studies of its metabolites in lung and ovarian cancer cells (Lee et al., 2011). Based on administration of [¹⁴C]-labeled devimistat in rats, β-oxidation was identified as the main pathway of elimination, with the majority of metabolites excreted via feces (59%) and urine (22%) (Reddy et al., 2022). After intravenous administration of the maximum tolerable dose (2940 mg/m²) in patients with hematologic malignancies, plasma concentrations of around 40 μM were measured. A triphasic elimination pattern with a first half-life ($t_{1/2}$) of about 1.34 h was observed for devimistat (Pardee et al., 2014). An additional study revealed the active metabolite, CPI-2850 (4,6-bis-benzylsulphanyloctanoic acid) rapidly emerged as the major circulating species over time. Secondary peaks during the elimination phase of devimistat ($t_{1/2} \approx 2$ h) and CPI-2850 ($t_{1/2} \approx 54$ h) are indicative of enterohepatic circulation (Alistar et al., 2017).

1.2.4.3. Antitumor effects *in vitro*

Developed as a dual function inhibitor that simultaneously targets two metabolic enzymes, devimistat represents a first-in-class anticancer drug and its effects have hence been assessed in a plethora of *in vitro* studies. Applying a panel of tumor cell lines, with origin in bone, breast, colorectal, kidney, lung, muscle, ovarian, pancreatic, prostate and urine cancer, EC₅₀ values between 100-280 μM were detected in a first cytotoxicity screening (Zachar et al., 2011). Comparison of lung (H460), breast (SKBR-3) and kidney (ACHN) cancer cell lines with primary cells of the corresponding organs revealed significantly higher cytotoxicity in malignantly transformed cells (Zachar et al., 2011). After devimistat treatment, downregulation of cyclins D3, E1, E2, F, A2, B1 and cyclin dependent kinase (CDK) 2 gene expression was induced in BxPC-3 pancreatic cancer cells but not in non-transformed NIH-3T3 mouse fibroblast cells, indicating a tumor specific mode of action (Lee et al., 2014). Induction of cell death via several mechanisms was described in response to devimistat treatment. Morphological changes indicative of apoptotic cell death were observed, including membrane blebbing and nuclear subinclusions, accompanied by cleavage of PARP-1 and caspase-3 (Zachar et al., 2011). Correspondingly, apoptotic and necrotic cell death in response to devimistat treatment were identified by Annexin-V/PI costaining. Application of pan-caspase inhibitor carbobenzoxy-valyl-alanyl-aspartyl-[O-methyl]-fluoromethylketone (z-VAD-FMK) did not result in a decline of apoptotic cell death, suggesting the occurrence of

additional cell death mechanisms in response to devimistat (Zachar et al., 2011). In prostate cancer cell lines, devimistat treatment induced cell death due to p53-independent accumulation of Noxa and a decrease of MCL1, a mitochondrial inhibitor of apoptosis that neutralizes Bak/Bax and sequesters Bim (Arai et al., 2020).

The mitochondria as a crucial target of devimistat have been further assessed within several studies. Chronic treatment of cancer cell lines with devimistat over 7 days induced attenuation of the mitochondrial membrane potential but did not result in a reduction of mitochondrial size or number (Mordhorst et al., 2019). Short term treatment led to a substantial and initially reversible reduction of ATP levels, which however finally caused cancer cell death (Zachar et al., 2011). Correspondingly, in pancreatic cancer cells morphologic alterations of mitochondria, including a disrupted cristae morphology and reduced cristae junctions, were observed by transmission electron microscopy after devimistat treatment (Gao et al., 2020). In a novel approach, Koo and colleagues recently applied differential pulse voltammetry (DPV) to measure extracellular electrochemical signals in cervical cancer cells after devimistat treatment and detected changes at low concentrations of 2 μ M after comparably short treatment duration of 1 h (Koo et al., 2023). Hala et al. used embryo-larval zebrafish as a model to study the metabolic effects of devimistat *in vivo*: The oxygen consumption rate (OCR) after devimistat treatment for 5 days was significantly reduced to 22% of the solvent control and recovered up to day 20 (Hala et al., 2021). In accordance, a significantly decreased OCR was observed in biliary tract cancer cell lines in response to devimistat treatment (Mohan et al., 2023).

A potential resistance mechanism against the mitochondrial effects of devimistat was recently observed by Rivas et al. By surpassing the TCA cycle, fatty acid β -oxidation of intracellular lipid stores directly supplies the mitochondrial electron transport system after devimistat treatment in carcinoma cells. Application of the receptor tyrosine kinase (RTK) inhibitor crizotinib abrogates peroxisomal lipid β -oxidation, thereby sensitizing resistant pancreatic ductal adenocarcinoma (PDAC) tumors against devimistat *in vivo* (Rivas et al., 2022). In addition, by utilizing etomoxir, an inhibitor of mitochondrial fatty acid import, and thioridazine, an inhibitor of peroxisomal fatty acid β -oxidation, sensitivity towards devimistat could be restored (Rivas et al., 2022). In pancreatic cancer cells, activation of the AMPK-ACC axis induced by devimistat treatment was found to inhibit lipid metabolism and thereby induce ROS-mediated apoptosis (Gao et al., 2020).

Glutamine metabolism as a potential route of devimistat-resistance was assessed in head and neck squamous cell carcinoma (HNSCC)-cells. Glutaminase 1 (GLS1) was upregulated due to devimistat treatment and promoted glutaminolysis as a compensatory route to facilitate cancer cell survival. Applying the GLS1 inhibitor CB-839

impaired the glutamine-dependency of HNSCC and led to synergistic anticancer effect in combination with devimistat (Lang et al., 2021). Correspondingly, transcriptome analysis showed deregulation of several metabolic pathways, including upregulation of glutamine-to-glutamate conversion and downregulation of fatty acid β -oxidation (Hala et al., 2021). Lactate frequently accumulates in the tumor microenvironment as a critical byproduct of the altered tumor metabolism. Devimistat was found to synergize with inhibitors of lactate metabolism *in vitro*, but a orthotopic pancreatic cancer mouse model failed to reproduce the tumor growth inhibiting effects, presumably due to an insufficient lactate inhibitor efficacy (Kumstel et al., 2022). In a different study, devimistat abrogated the protective effects lactate exerted in an acidic environment on tumor growth of pancreatic cancer cells (Koncošová et al., 2021).

Formation of autolysosomes in response to devimistat treatment and modulation of metabolism were observed in porcine fibroblasts and discussed as a mechanism that enabled the cells to maintain viability (Mordhorst et al., 2019). In line with these findings, Gao and colleagues reported activation of autophagy via the AMPK-ULK1 (Unc-51-like autophagy-activating kinase) signaling pathway in pancreatic cancer cells *in vitro*, indicated by a decrease of p62, accumulation of LC3B-II and an increase of double membraned vacuoles (Gao et al., 2020). Activation of AMPK signaling in response to devimistat was also observed in AML cells, underlining the significance of autophagy (Pardee et al., 2018a). Investigation of the effects of devimistat in clear cell sarcoma (CCS) cells revealed a significant increase of cell death due to blocking of devimistat-induced autolysosome formation by chloroquine cotreatment (Egawa et al., 2018). Devimistat may provide a therapeutic opportunity for treatment-enriched ovarian cancer by specifically targeting the cancer stem cell (CSC) population. Following metabolic inhibition, frequency of CD (cluster of differentiation) 133+ and CD117+ OvCa cells was reduced and CSC associated properties, including tumorigenicity and sphere forming capacity, were impeded (Bellio et al., 2019).

Devimistat has already been applied in several clinical trials in combination with established cancer therapy, as further outlined in Chapter 1.2.4.5., but to date few studies have investigated the underlying molecular mechanisms for solid tumors. In preclinical experiments devimistat significantly reduced OCR and synergized with cisplatin and gemcitabine in two cell line models of advanced biliary tract cancer (Mohan et al., 2023). Investigation of combining devimistat treatment with radiation in PDAC cell lines revealed reduced proliferation, enhanced cell death and alterations of key mitochondrial metabolites, indicating a radio-sensitizing activity (Khan et al., 2023).

1.2.4.4. *In vivo* studies

Several *in vivo* studies have been conducted using devimistat, either to study the underlying mechanisms of its antitumorigenic activity or to provide safety information prior to clinical testing. A frequently applied approach in current cancer research is the xenograft mouse model, which allows the usage of human cancer cell lines or patient-derived cells in an *in vivo* setting (Kung, 2007). Estimation of the general tolerability of devimistat *in vivo* revealed 100 mg/kg as the maximum tolerated dose (MTD) in CD1-nu/nu mice (Zachar et al., 2011). The anti-cancer efficacy of devimistat was assessed using the pancreatic ductal adenocarcinoma cell line 6606PDA injected into the pancreas of C57BL6/J mice. Administration of devimistat in a dose of 10 mg/kg BW five times per week did not impair tumor growth rate. Reduction of animal weight compared to the control group was reported at the end of treatment, indicating a too high dose (Kumstel et al., 2022). In contrast, Lee et al. reported prolonged survival and tumor growth inhibition in a xenograft model of pancreatic carcinoma cell line BxPC-3 in CD1-nu/nu mice after treatment with 25 mg/kg BW devimistat once per week (Lee et al., 2014). Utilizing a metastasis model of clear cell sarcoma with human skeletal muscle myoblast (HS-MM) cells in severe combined immunodeficient (SCID) mice, application of devimistat (25 mg/kg BW) combined with chloroquine (50 mg/kg BW) two times per week resulted in a decreased rate of mesenteric metastasis (Egawa et al., 2018).

1.2.4.5. Clinical trials

Thus far, more than 30 studies have assessed the applicability of devimistat in the treatment of hematological malignancies and solid tumors either as monotherapy or in combination with established chemotherapeutic drugs under the developmental designation CPI-613. Devimistat received orphan drug status by the European Medicines Agency (EMA) for the treatment of pancreatic cancer and AML. The FDA granted devimistat an orphan drug status for patients with pancreatic and biliary cancer, AML, peripheral T cell and Burkitt's lymphoma, myelodysplastic syndrome and soft tissue sarcoma. However, an open center phase III trial (NCT03504410) regarding the applicability of devimistat in combination with cytarabine and mitoxantrone for the treatment of AML (Pardee et al., 2018a), termed ARMADA 2000, was terminated due to lack of efficacy. As reported recently, no improvement of remission rates and overall survival could be demonstrated (Pardee et al., 2024). In parallel, an open-label randomized phase III trial (NCT03504423) of devimistat in combination with modified FOLFIRINOX compared to FOLFIRINOX for the treatment of metastatic pancreas adenocarcinoma termed AVENGER 500, was conducted (Philip et al., 2019). In total, 528 patients who had not previously received any treatment were enrolled and overall

survival (OS), progression-free survival (PFS), duration of response, and overall response rate were assessed as secondary endpoints. As indicated by an OS of 11.7 months for FOLFIRINOX compared to 11.1 months for modified FOLFIRINOX in combination with devimistat, no statistically significant therapy improvement occurred. A first phase I clinical trial (NCT02232152) regarding the application of devimistat in combination with 5-FU for the therapy of previously treated colorectal cancer has been conducted (Rocha Lima et al., 2019). A durable, stable disease, describing neither growth nor shrinkage of tumor size, was reported at the MTD of 2250 mg/m², indicating antitumor activity (Rocha Lima et al., 2019). A phase I trial (NCT05070104) for devimistat in combination with modified FOLFIRINOX plus Bevacizumab for the treatment of mCRC was planned but has recently been withdrawn.

Among the clinical studies conducted so far, few adverse effects of devimistat were described. The general side effects comprised fatigue, headache, nausea, vomiting, diarrhea and in consequence electrolyte imbalance (Alistar et al., 2017). Serious adverse events observed included thrombocytopenia, anemia, neutropenia and lymphopenia as well as hyperglycemia, hypokalemia and hypoalbuminemia (Alistar et al., 2017). A more specific adverse event described by Anderson et al. after devimistat treatment is reversible acute kidney injury (AKI) observed especially in older patients after a latent time. Metabolic inhibition and induction of ROS presumably caused injury of the metabolically highly active renal epithelium, resulting in AKI (Anderson et al., 2019).

1.3. PARP-1 as a Target in CRC Tumor Therapy

The preservation of genomic integrity is fundamentally important for the maintenance of cellular homeostasis and survival. Various intracellular signaling pathways, summarized as the DNA damage response (DDR), assure the efficient repair of double-strand breaks (DSB) as one the most harmful forms of DNA alterations (Ceccaldi et al., 2016). Beside an endogenous generation, caused by DNA replication errors or metabolic ROS formation, DSBs can be induced by exogenous sources, including ionizing radiation and genotoxic compounds (Cannan and Pederson, 2016). The rapid recognition of DNA strand breaks and the subsequent recruitment of DDR factors are realized by several cellular sensors, which include the enzyme poly-(ADP-Ribose) polymerase-1 (PARP-1) as an important mediator.

1.3.1. PARP-1 in health and disease

PARP-1 plays a critical role in the recognition and regulation of the DNA damage repair. By catalyzing the attachment of poly ADP-ribose (PAR) to intracellular protein acceptors,

PARP-1 facilitates the recruitment of DNA repair mediators and decompaction of chromatin, enabling a higher repair efficiency. Thereby, PARylation processes are involved in several DDR pathways, including DNA mismatch repair (MMR), single strand break repair (SSBR), nucleotide excision repair (NER), homologous recombination (HR) and non-homologous end joining (NHEJ) (Ray Chaudhuri and Nussenzweig, 2017). For this reason, PARP-1 inhibition has been clinically exploited in the therapy of several cancer subtypes, including DNA repair-deficient ovarian, breast and prostate cancer. Growing evidence indicates beneficial outcome for the application of PARP inhibitors (PARPi) in combination with conventional chemotherapy even in the absence of DNA repair deficiencies (Matulonis and Monk, 2017).

1.3.1.1. Structure, mechanism and role in DNA repair

The family of PARP enzymes catalyzes the NAD⁺-dependent attachment of ADP-ribose polymers to acceptor proteins and thereby modulates a multitude of cellular signaling pathways (Gibson and Kraus, 2012; Jubin et al., 2016). Currently, 17 homologues of PARP are known in humans, differing regarding their function and structure, with PARP-1 accounting for 80-90% of total cellular PARylation (Jubin et al., 2016). Structurally, PARP-1 consists of three domains responsible for N-terminal DNA binding, auto-modification and catalytic activity: The DNA binding domain contains three zinc finger motifs and a nuclear localization sequence (Langelier et al., 2010). The auto-modification domain includes a breast cancer type 1 susceptibility protein (BRCA1) C terminus motif and facilitates protein-protein interaction. In the catalytic domain of the C-terminus, the PARP-signature motif (PSM) can be found: six β -strands and one α -helix that include a donor site for nicotinamide and an acceptor site for adenosine to transfer ADP residues from NAD⁺ to target sites (Kinoshita et al., 2004).

PARP-1 is predominantly activated by damaged DNA, particularly DNA strand breaks, (Kun et al., 2002; Zandarashvili et al., 2020) and further induction of its enzymatic activity can occur in response to several cellular stimuli, including abnormal DNA structures, nucleosomes and a variety of protein-binding partners (Lonskaya et al., 2005). Furthermore, induction by kinase cascades represents a DNA damage independent route of PARP-1 modulation. For instance, catalytic activity of PARP-1 is enhanced by pERK1/2-induced phosphorylation dependent or independent of DNA damage (Kauppinen et al., 2006). Upon its activation, PARP-1 rapidly interacts with the DNA damage site to initiate recruitment of DNA repair complexes within seconds, thereby acting as a first line sensor of the DDR (Ray Chaudhuri and Nussenzweig, 2017; Satoh and Lindahl, 1992).

On a molecular level, zinc finger domains F1 and F2 of PARP-1 recognize distinct structures which only occur in damaged DNA, including exposed nucleic bases and the phosphate backbone (Langelier et al., 2011). Interaction with a DNA break results in an allosteric switch that destabilizes the helical domain blocking the NAD⁺ binding site, causing a relief of the enzymatic auto-inhibition and leading to a 1000-fold induction of PARP-1 activity (Langelier et al., 2018). In addition, various signaling factors present at the DNA damage site further modulate PARP-1 activity. The Ku70-Ku80 heterodimer, a component of the non-homologous end joining (NHEJ) repair pathway, competes with PARP-1 in a cell cycle dependent manner, with Ku70-Ku80 being preferentially recruited in the G₁/S phase and PARP-1 in the S/G₂ phase (Yang et al., 2018). In order to prevent activation of DDR on telomeric DNA strand ends, activity of PARP-1 is attenuated by telomeric repeat-binding factor 2 (TRF2) (Schmutz et al., 2017).

PARP-1 functions as a first responder to facilitate DNA repair. By utilizing intracellular NAD⁺ pools, PARP-1 synthesizes poly-ADP ribose (PAR) attached to various target proteins near the damage site to initiate binding of repair complexes. PARylation of histones results in the decompaction of chromatin structures, allowing for a better accessibility of the damaged DNA for repair enzymes (Pandey and Black, 2021). Histone PARylation Factor 1 (HPF1) modulates the catalytic activity of PARP-1 and switches its substrate specificity from modifying Asp/Glu residues to Ser residues, thereby limiting auto-PARylation and promoting PARylation of histones and downstream modulators of DNA repair (Gibbs-Seymour et al., 2016).

In detail, substrate modification by PARP-1 involves addition of ADP-ribose to the carboxyl group of target proteins via ester linkage. Subsequent linear PAR chain elongation through synthesis of 2',1"-O-glycosidic ribose-ribose bonds and additional branching via 2',1" ribose-ribose bonds results in the formation of large PAR polymers (Pandey and Black, 2021). The precise role of PAR in DDR signaling is gradually becoming understood and includes assembly of the proteins FUS/TIS (fused in sarcoma/translocated in sarcoma), EWL (Ewing sarcoma) and TAF15 (TATA-binding protein-associated factor) to reorganize the soluble nuclear space around the DNA damage site (Altmeyer et al., 2015). In addition, PAR polymers provide a binding site for various DNA repair proteins which contain PAR-binding motifs, thereby allowing for the efficient recruitment of the DDR machinery (Liu et al., 2017).

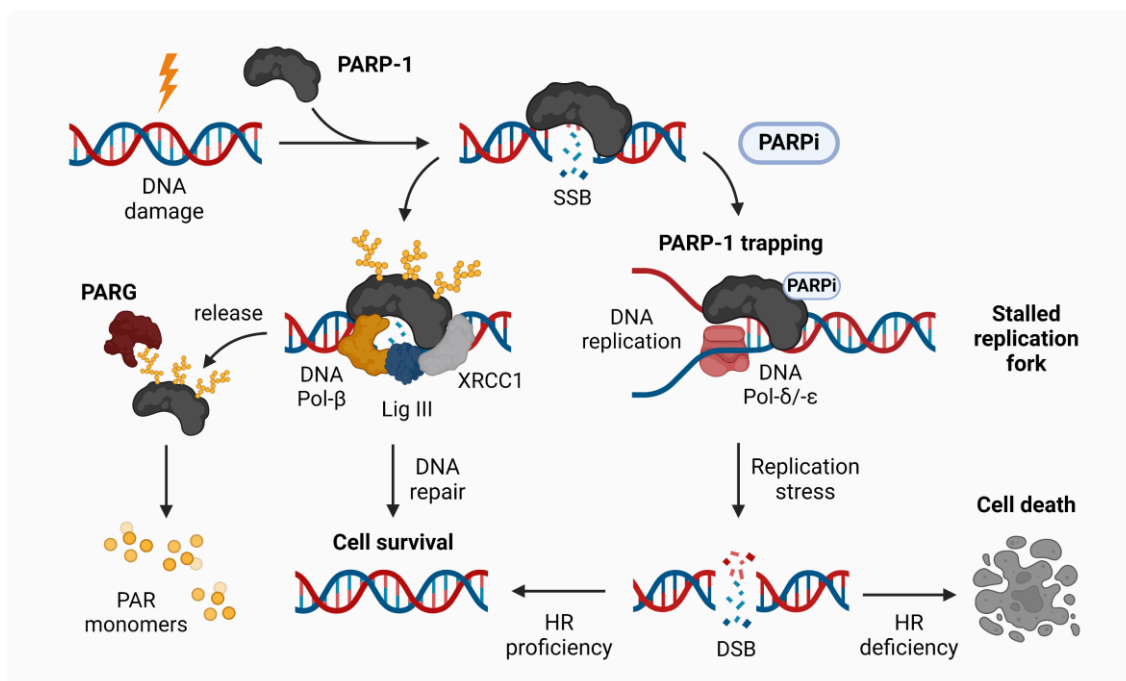


Figure 8: Enzymatic mechanism of PARP-1, its role in DNA repair and the effect of pharmacological PARP-1 inhibition. PARP-1 rapidly detects and binds DNA single strand breaks (SSB), catalyzing ADP-ribosylation of histones and several DNA repair factors. Auto-ribosylation of PARP-1 results in the dissociation of PARP-1 from damaged DNA followed by its regeneration by poly (ADP-ribose) glycohydrolase (PARG). Binding of PARPi not only impairs the PARylation of protein acceptors but also auto-ribosylation, thereby attenuating the dissociation of PARP-1, which results in the trapping of PARP. DNA replication in the presence of trapped PARP-1 leads to the generation of blocked and unresolved replication forks and finally induction of DSBs. (Created with BioRender)

PARP-1 itself constitutes a major acceptor of PAR polymers, in a process referred to as auto-PARylation. As precise and sensitive modulation of PARP-1 activity is critical for its function, PARP-1 hyperactivation is associated with several pathological conditions, including inflammation and cancer (Dörsam et al., 2018; Liu et al., 2016). The auto-modification with negatively-charged PAR leads to the repulsion of PARP-1 from the DNA and its dissociation within minutes of its initial binding (Ray Chaudhuri and Nussenzweig, 2017). Additionally, PARP-1 auto-PARylation facilitates binding of the DNA repair protein XRCC1 that acts as a scaffold for the recruitment of enzymes DNA polymerase beta (Pol-β) to fill DNA gaps and Ligase IIIα to ligate DNA nicks (Pandey and Black, 2021). An integral part of the PARylation homeostasis is the removal of PAR residues from substrates by PAR hydrolyzing enzymes. With its endoglycosidase and exoglycosidase activity, poly (ADP-ribose) glycohydrolase (PARG) hydrolyzes the ribosyl-ribosyl bonds in PAR polymers (Barkauskaite et al., 2013). Despite its lower intracellular abundance compared to PARP-1, PARG is critical for functional DNA repair and genomic stability (Koh et al., 2004; Min et al., 2010).

Besides its important role for DNA repair and survival, deregulated PARP-1 signaling can also have detrimental consequences. Overactivation of PARP-1 was shown to induce a caspase-independent mode of cell death. This process, termed parthanatos, is characterized by PAR-induced nuclear translocation of the mitochondrial-associated apoptosis-inducing factor (AIF), causing chromatin condensation and DNA fragmentation (Fatokun et al., 2014). Consequently, inhibition of PARP-1 has been discussed as an approach to target cell death in neurodegenerative and myocardial diseases (Kaundal et al., 2006; Ordog et al., 2021). The important role of PARP-1 for malignant diseases is extensively discussed in the following chapter with a focus on CRC.

1.3.1.2. The role of PARP-1 in cancer

In contrast to most other known DNA repair enzymes, increased expression of PARP-1 is frequently observed in several types of cancer compared with their histologically normal counterparts, including breast, uterine, lung, and ovarian cancers (Ossovskaya et al., 2010). While in general, PARP-1 expression revealed to be high in a majority of CRC tumors, around 26% showed low and 6% no expression of the enzyme (Sulzyc-Bielicka et al., 2012). A similar pattern was also observed in breast tumors (Domagala et al., 2011). Low PARP-1 expression as an indicator of poor prognosis was described for gastric (Park et al., 2022), pancreatic (Klauschen et al., 2012) and breast tumors (Aiad et al., 2015) and assumed to occur due to an increase of genomic instability in the absence of PARP-1. In contrast, high PARP-1 expression was linked to poor prognosis in ovarian (Molnár et al., 2020), gastric (Liu et al., 2016) and prostate cancer (Acar et al., 2021).

Dörsam and colleagues investigated the dual role of PARP-1 in CRC: In early phases of carcinogenesis, PARP-1 can protect against DNA alkylation-induced CRC development by facilitating DNA repair. During disease progression, PARP-1 overexpression was observed in human CRC, indicative of a tumor-promoting role. Inflammation-driven tumor growth and induction of the IL6-STAT3-cyclin D1 axis was revealed as a mechanism of PARP-1-induced cancer progression (Dörsam et al., 2018). Analysis of 60 stage II and III colon cancer cases of patients who underwent resection and adjuvant chemotherapy revealed high nuclear expression of PARP-1 in 63.3% of tumors that correlated with disease progression and the occurrence of lymph node metastases (Abdelrahman et al., 2020). Accordingly, increased PARP-1 levels were found in CRC tumor specimen compared to healthy and benign adenoma tissue (Dörsam et al., 2018; Dziaman et al., 2014).

Deregulated expression of PARP-1 in certain types of cancer can directly modulate the activity of certain DNA repair pathways. In healthy cells, microhomology-mediated end joining (MMEJ), an error-prone DNA repair pathway of double-strand breaks, forms a backup pathway of HR and NHEJ and contributes to the stability of repetitive DNA (Sfeir and Symington, 2015). As a mutagenic DNA repair pathway, MMEJ is intrinsically error prone and associated with the generation of insertions and deletions, thereby contributing to genomic instability, a hallmark of cancer (Patterson-Fortin and D'Andrea, 2020). Different HR factors, including BRCA1, BRCA2 and RPA (replication protein A) have been demonstrated to downregulate MMEJ in non-malignant human cells (Ahrabi et al., 2016). In consequence, upregulation of MMEJ frequently occurs in tumor entities which exhibit deficiencies of the HR DNA repair pathway, including breast, ovarian and prostate cancer (Ceccaldi et al., 2015).

As a critical factor of the MMEJ pathway, PARP-1 competes with Ku70-Ku80 for the binding to DSBs and facilitates recruitment of MMEJ-specific DNA polymerase theta (Pol- θ) (Sharma et al., 2015). Upregulation of PARP-1 levels in tumors has been associated with an increase of MMEJ (Muvarak et al., 2015). MMEJ has recently been demonstrated to enable chemoresistance by promoting reversion mutations of the HR factor BRCA (Lukashchuk et al., 2022). As an integral component of DNA repair, expression of PARP-1 correlates with sensitivity to anti-cancer treatment that relies on the induction of DNA damage. Higher activity or upregulated expression of PARP-1 have been shown to facilitate resistance against chemotherapeutic drugs (Michels et al., 2013; Wu et al., 2013; Xu et al., 2019). In parallel, a high PARP-1 level caused resistance of nasopharyngeal carcinoma cells against radiation therapy *in vitro* and *in vivo* due to upregulated DNA repair (Chow et al., 2013).

1.3.2. Targeting PARP-1 in tumor therapy

The involvement of PARP enzymes in the detection and repair of DNA damage led to the development of specific PARP inhibitors (PARPi) as targeted therapeutics for malignant diseases (Lord and Ashworth, 2008). First approaches applied 3-aminobenzamide to reveal a potentiated sensitivity against DNA damage inducing compounds by inhibited PARylation (Durkacz et al., 1980), resulting in the targeted search for more potent and selective PARPi (Curtin and Szabo, 2020). Following extensive chemical screening and preclinical research, a novel generation of PARPi was developed and finally clinically applied (Rouleau et al., 2010). The observation that a marked inhibition of DNA repair only occurs when PARP-1 activity is downregulated by at least 90% further underlined the requirement of sufficient potency and specificity (Rouleau et al., 2010; Satoh and Lindahl, 1992). While all clinically applied PARPi share

a characteristic benzamide moiety as a key feature necessary for binding to the catalytic center of PARP-1, they differ in size and flexibility, which results in different PARP trapping potencies and binding affinities, as summarized in Figure 9 (D.-S. Kim et al., 2021).

Consequently, marked differences were observed for the substrate selectivity of PARPi: At higher concentrations, all clinically applied PARPi show promiscuity among the different members of the PARP family, with the highest selectivity for PARP-1 and PARP-2 observed for veliparib and niraparib (Thorsell et al., 2017). In addition, several off-target kinases, including tankyrase 1/2, the dual specificity tyrosine-phosphorylation-regulated kinase 1A (DYRK1A), the serine/threonine-protein kinase pim-3 (PIM3), hexose-6-phosphate dehydrogenase (H6PD) and deoxycytidine kinase (DCK), have been identified with IC_{50} values in the sub-micromolar range, which might account for the characteristic patterns of clinical side effects observed for PARPi (Antolin et al., 2020; Knezevic et al., 2016).

PARP-1 trapping mainly occurs in response to its enzymatic inhibition. The enzyme-inhibitor complex remains attached to the DNA, resulting in the formation of DNA double-strand breaks during replication (Pommier et al., 2016). PARP-1 inhibitors differ in their capability to induce PARP-1 trapping. While a linear correlation between the potency to inhibit PARP-1 and to trap the PARP-1-DNA complex has been observed (Hopkins et al., 2015), the ability to induce PARP-1 trapping was subsequently identified as an independent property of PARPi. Recently, the molecular correlation between the inhibitor mode of action and the PARP-1 trapping profile was elucidated and three different types of PARPi were differentiated (Zandarashvili et al., 2020). While type II PARPi (e.g. olaparib) do not affect allostery, type I PARPi alter allostery to retain PARP on the DNA (e.g. EB-48) and type III PARPi alter allostery to release PARP from the DNA (veliparib). Nevertheless, catalytic inhibition by all three types blocks the auto-modification dependent release of PARP-1 from the DNA (Zandarashvili et al., 2020). Xue and colleagues quantified the retention potencies of commonly applied and novel PARPi considering the influence of frequently observed PARP-1 mutations associated with PARPi-resistance. First, PARPi compete with NAD^+ at its binding site to inhibit catalytic activity followed by allosteric modulation, which changes DNA retention of PARP-1 (Xue et al., 2022). While the retention potency of clinically relevant PARPi is predominantly determined by the initial step, their distinct induction of allosteric changes can be abrogated by structural PARP-1 mutations (Xue et al., 2022).

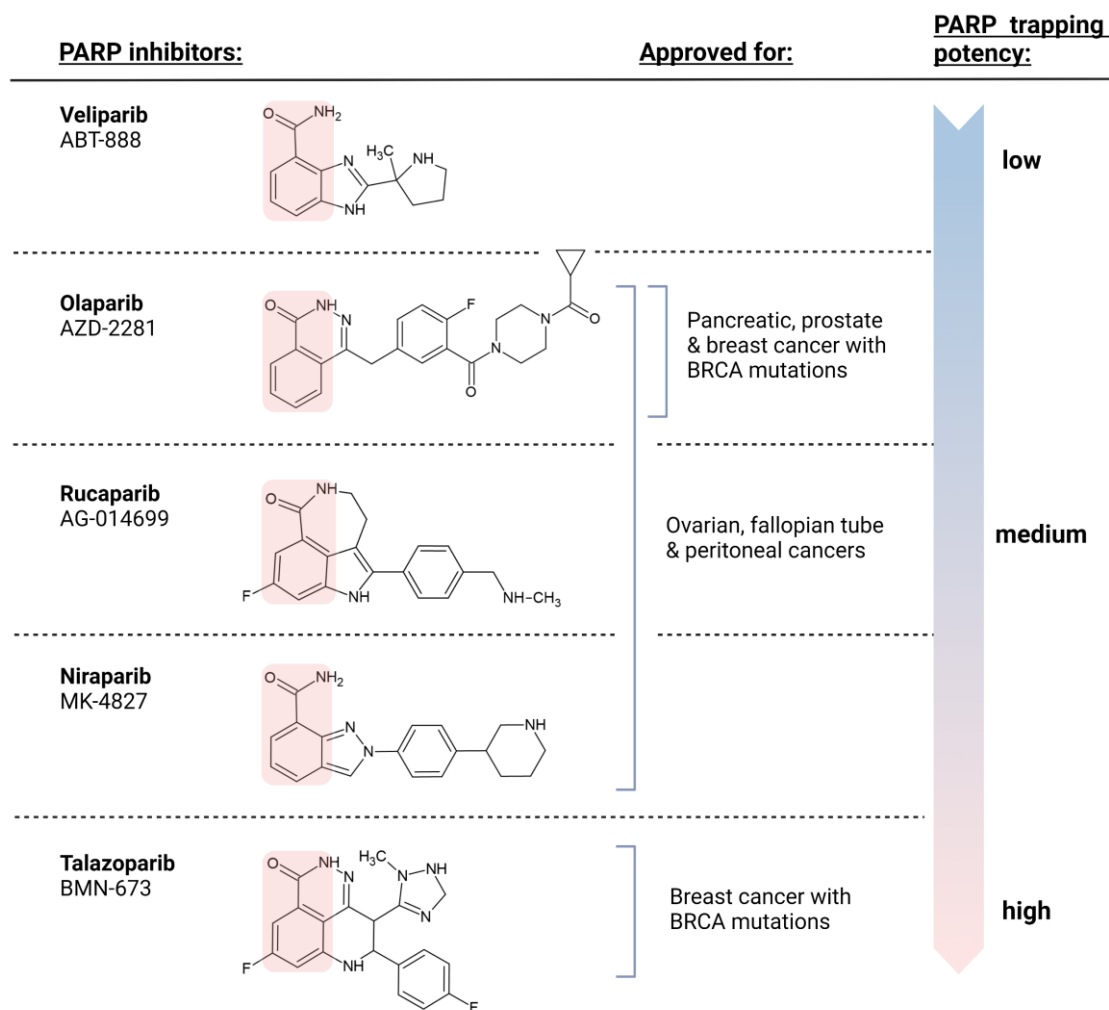


Figure 9: Overview of clinically approved PARP inhibitors and their corresponding field of application. Thus far, five different PARPi have been clinically approved with a focus on different cancer entities. The biologically relevant benzamide moiety, highlighted in red, functions as an analogue of NAD⁺ and is shared by all structures. PARPi differ regarding their PARP trapping potency and are tiered accordingly (Thomas et al., 2018). (Created with BioRender)

Two distinct approaches in the application of PARPi can be differentiated, which consequently determine their required characteristics during drug development. On the one hand, PARPi are applied as monotherapy to target malignant cells with genetic alterations that result in a dependence on functional PARP-1 for DNA repair and survival, following the concept of synthetic lethality. On the other hand, PARPi can be combined with DNA damaging agents or radiation therapy to improve therapeutic efficacy in a synergistic manner (Plummer et al., 2008). The two approaches and the required characteristics of the applied PARPi are further discussed in the following chapters.

1.3.2.1. The concept of synthetic lethality

The role of PARP-1 in malignant diseases can only be understood in the context of deregulated or mutated DNA repair pathways. Homologous recombination (HR), an essential pathway for the highly accurate repair of DNA double-strand breaks, is enabled by the interplay of several proteins, including BRCA1/2, ATM (Ataxia-telangiectasia mutated), RAD51 (radiation sensitive protein 51) and MRE11 (meiotic recombination 11 homolog) (Hoppe et al., 2018). Deficiencies of the HR pathway, caused by the genetic or epigenetic inactivation of respective genes, are commonly observed in several tumor entities and associated with an increased level of genomic alterations (Lord and Ashworth, 2016). Since HR is responsible for the resolution of interstrand crosslinks, cells with mutations of corresponding genes are highly sensitive to platinum-based cytostatic drugs and other agents that cause DNA crosslinks (Turner et al., 2004). Furthermore, HR-deficient cells heavily rely on PARP-1 dependent DNA repair, which has led to the development of clinically applicable PARP-1 inhibitors that target this susceptibility (Mateo et al., 2019).

As the most frequently observed HR deficiency, monoallelic germline mutations of *BRCA1/2* genes are associated with a higher risk for cancer development in affected individuals (L. Nguyen et al., 2020). Their role for the early onset of ovarian and breast cancer was discovered in the early 1990s and their identification was subsequently applied as a potential biomarker for cancer susceptibility (Hall et al., 1990; Hoppe et al., 2018). Cancer development in *BRCA1/2* mutation carriers generally follows the “two-hit” hypothesis, as tumorigenesis requires the somatic inactivation of the remaining functional *BRCA* allele, either due to mutation or epigenetic inactivation (Stoppa-Lyonnet, 2016). Mechanistically, BRCA1/2 proteins constitute key components during the process of HR and therefore have a fundamental role in the repair of DNA DSBs (Venkitaraman, 2001). As described above, healthy cells heavily rely on the HR pathway to resolve DNA strand breaks and are therefore hardly affected by PARPi. In contrast, cells deficient in BRCA1/2 are incapable of HR and in consequence DNA SSBs remain unrepaired, accumulate and finally lead to cell death when PARP-1 is inhibited, as shown in Figure 10 (Bryant et al., 2005). This mechanism does not only apply to *BRCA1/2* deficiencies, but has also been observed for mutations of other HR proteins, which cause a higher susceptibility towards PARP-1 inhibition (D.-S. Kim et al., 2021). Based on this concept, termed synthetic lethality, specific PARP-1 inhibitors were developed over a decade ago and first applied as single agent treatment for cancers defective in *BRCA1/2*, therefore unable to repair DSBs by HR. Promising clinical data was followed by a fast approval and a subsequent development of additional PARPi for different tumor types, which is still ongoing (Mateo et al., 2019).

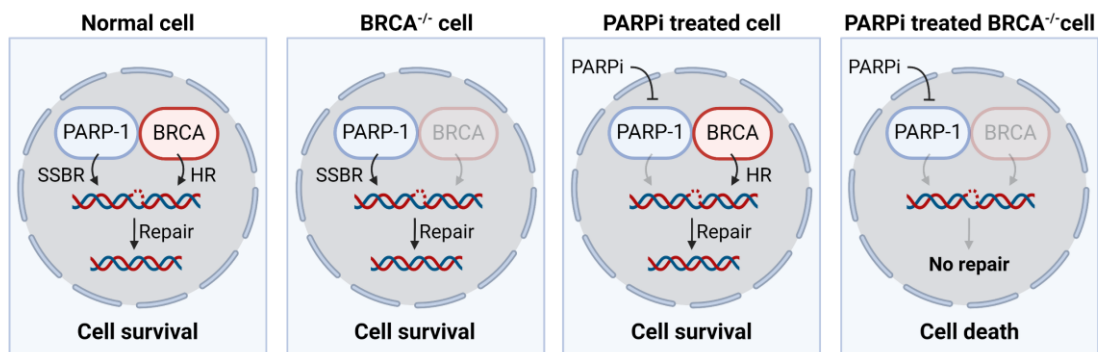


Figure 10: The mechanism of synthetic lethality induced by the application of PARP-1 inhibitors in HR-deficient cancer cells. In healthy cells, DNA damage in the form of single strand breaks is repaired via the PARP-dependent SSBR (Abbotts and Wilson, 2017) or via HR, which requires functional BRCA1/2. Cells deficient in functional BRCA1/2, frequently associated with several types of cancer, rely on SSBR and therefore PARP-1 for repair of damaged DNA. Application of PARPi has little effect on healthy cells since HR can still serve as an alternative DNA repair pathway. Cells deficient in BRCA1/2 are highly sensitive against PARP-1 inhibition, as damaged DNA cannot be repaired. (Created with BioRender)

Furthermore, PARP trapping has been identified as the main mechanism of PARPi induced attenuation of DNA repair (Pommier et al., 2016). Binding of PARPi prevents the auto-modification of PARP, thereby impeding its release from the DNA which results in stalled replication forks and the subsequent formation of DNA DSBs. Cells deficient in the HR DNA repair pathway are unable to resolve DNA DSBs, which leads to the activation of cell death programs (Lord and Ashworth, 2017). Besides the well-studied role for breast and ovarian cancer, *BRCA1* mutations were shown to be associated with a five-fold higher incidence of CRC in women younger than 50 years. No such correlation was found for *BRCA2* mutations and older women (Sopik et al., 2015). Mutations of *BRCA1/2* genes might also occur during tumor progression, but sensitivity towards PARPi was only found in carriers of hereditary mutations of *BRCA1/2* genes (Jonsson et al., 2019). In accordance with these findings, a recently published study by Bhamidipati et al. analyzed 1760 cancer patients with somatic *BRCA1/2* gene alterations, of which 189 (11%) had a CRC diagnosis, and revealed cooccurrence of pathogenic DNA polymerase epsilon (Pol-ε) mutations but could not show additional benefit of PARPi treatment (Bhamidipati et al., 2024).

Despite the therapeutic advances achieved by PARP-1 inhibitors, cancer cells adapt to drug treatment and a majority will develop resistances (Dias et al., 2021). So far, three main survival mechanisms of tumors treated with PARPi were identified: Restoration of HR, restoration of replication fork stability and drug target related resistance. Clinically documented reversion mutations or epigenetic alterations can restore function of

BRCA1/2 and thereby HR (Sakai et al., 2008). This process is often facilitated by the high genomic instability observed in *BRCA1/2*-deficient cancer cells. Loss of PAX-interacting protein 1 (PTIP), an MLL (mixed-lineage leukemia) 3/4 complex protein, was found to protect *BRCA1/2*-deficient cells from PARPi by attenuating the recruitment of the MRE11 nuclease to stalled replication forks that protects nascent DNA strands from degradation (Ray Chaudhuri et al., 2016). Furthermore, mutations of PARP itself can confer resistance against the effects of PARPi. In talazoparib treated ovarian cancer cells, deletions of nucleotides encoding for DNA-contacting amino-acid residues K119 and S120 within the second zinc finger domain were identified, which leads to the impairment of DNA binding and avoidance of cytotoxic PARP-1 trapping (Pettitt et al., 2018). As recently demonstrated, mutations of the catalytic core of PARP-1 alter how different PARPi affect its allostery to favor a pro-release state and attenuate the inhibitor's PARP trapping capacity (Xue et al., 2022). Several approaches are currently discussed to tackle the resistance to PARPi. The protein ATR (ataxia telangiectasia and Rad3-related), a serine/threonine-protein kinase, enables HR and protection of replication forks in *BRCA1/2*-deficient cells by facilitating RAD51 loading onto DSBs and stalled replication forks (Yazinski et al., 2017). Hence, combination therapy with PARP and ATR inhibitors could represent a potential method to overcome this resistance mechanism (Kim et al., 2020, 2017).

Besides *BRCA1/2* deficiency, synthetic lethality by PARP inhibition may arise due to mutations of other proteins involved in the HR pathway, leading to HR deficiency (HRD). A large-scale study investigated HR genes in 52,426 tumors across 21 cancer lineages by next-generation sequencing. The overall frequency of HR-DDR mutations was 17.4%, with *ARID1A* (AT-rich interactive domain-containing protein) as the most frequently mutated gene (7.2%), followed by *BRCA2* (3.0%), *BRCA1* (2.8%), *ATM* (1.3%), *ATR* (1.3%), and *CHEK2* (1.3%). For CRC, a frequency of 15.0% was observed, with 3.1% of CRC bearing multiple HR-DDR mutations (Heeke et al., 2018). In line with these results, an analysis of 9,321 CRC patients by Arai et al. revealed mutations of DDR in 13.8% of tumors with enrichment in MSI-high tumors (76.4%) as well as in the right-sided *RAS*-WT, *BRAF*-mutant, and CMS1 subgroups (Arai et al., 2021).

Functional HR deficiency is associated with loss of heterozygosity (LOH) of intermediate size regions, caused by defective repair of sister chromatids during mitosis (Abkevich et al., 2012). Compared to MSI-high tumors, more cases of MSS cancers showed a high LOH (16.2% vs 9.5%), indicating that HRD cases in MSS tumors more frequently impair HR function (Lee and Kopetz, 2022). In a recently published work, Lee and colleagues proposed a newly developed assay to quantify real-time HR activity in tumor cells rather than gene expression analysis to identify tumors susceptible towards PARPi treatment

(Lee et al., 2023). When applying the assay to patient-derived tumor specimen, marked differences in the sensitivity towards PARPi were identified. While CRC and triple-negative breast cancer cells were highly sensitive towards inhibition of PARP, exhibiting IC_{50} values in the picomolar range, ovarian cancer cells were more resistant, showing IC_{50} values that ranged from nanomolar to micromolar concentrations (Lee et al., 2023).

1.3.2.2. Synergism with chemotherapeutic drugs

The application of PARP-1 inhibitors beyond the concept of synthetic lethality has been a focus of several studies (Matulonis and Monk, 2017; Vitiello et al., 2018). Synergy of PARP-1 inhibitors with established chemotherapeutics could improve the therapeutic efficacy or allow the application of lower doses, thereby reducing side effects of conventional drugs (McQuade et al., 2018). Furthermore, hyperactivation and upregulation of PARP-1 in response to chemotherapy has been shown in several types of cancer, serving as a resistance mechanism due to the induction of DNA damage repair (Kim et al., 2020; Mariano et al., 2015; Michels et al., 2013).

Several preclinical studies have evaluated the potential benefit of PARPi in combination with cytostatic agents for the treatment of CRC and dissected the impact of different molecular subtypes. Screening of the synergistic effects exerted by PARPi and chemotherapeutic drugs IT, 5-FU and OXA in CRC cell lines revealed the highest activity for the combination of rucaparib with IT (Augustine et al., 2019). Wang et al. showed increased sensitivity towards olaparib in *ATM*-deficient CRC cells as demonstrated by the application of *ATM*-deficient cell lines, *ATM* inhibitors and transient knockdown (Wang et al., 2017). In accordance, combination of PARPi ABT-888 (veliparib) and ATR inhibition at non-toxic doses synergistically enhanced SN-38-mediated cytotoxicity in several CRC cell lines (Abu-Sanad et al., 2015).

Microsatellite instability occurs in about 15% of CRC cases and is associated with mutations of DNA mismatch repair genes, such as *MRE11* (Vilar et al., 2011). Mutations of *MRE11* as well as its genetic knockdown were accompanied by an increased sensitivity towards PARP-1 inhibition by veliparib *in vitro* (Vilar et al., 2011). As recently shown, *MRE11* homolog A (*MRE11A*) is significantly overexpressed in CRC tumor specimen compared to healthy tissues and high levels corresponded with poor overall survival, rendering it a potential biomarker to select CRC patients for treatment options targeting HR deficiency including PARPi (Azambuja et al., 2023). In contrast, no difference for the MSS/MSI status regarding the sensitivity towards PARP inhibition *in vitro* and *in vivo* was detected in CRC cells in a different study (Genther Williams et al., 2015). Nevertheless, potentiating effects in combination with SN-38, the active metabolite of IT, were observed regardless of the molecular status (Genther Williams et

al., 2015). A recently published study by Paul et al. showed that veliparib potentiated cytotoxicity of 5-FU in MMR-proficient CRC cells by attenuating the MMR pathway *in vitro* and *in vivo* (Paul et al., 2023). Following veliparib cotreatment, elevated DNA damage, induction of the mitochondrial apoptosis pathway and downregulation of MMR pathway-related proteins MSH2 (MutS homolog 2), MLH1 (MutL homolog 1), the mismatch repair endonuclease PMS2 (postmeiotic segregation increased 2), and Pol- δ were observed, indicating potential applicability in CRC chemotherapy regimen (Paul et al., 2023). Niraparib monotreatment or the combination with IT, 5-FU and OXA were analyzed in a panel of 8 KRAS- or BRAF-mutated CRC cell lines from all four CMS clusters. Niraparib showed the strongest synergism with IT, independent of molecular subtype (Vitiello et al., 2018).

Smeby and colleagues further dissected the underlying molecular determinants of the susceptibility to PARP inhibition in CRC. By correlating the sensitivity towards PARP inhibition (olaparib, talazoparib, niraparib, rucaparib) in 93 CRC cell lines with the molecular status, biomarkers related to deficient HR were identified as non-predictive (Smeby et al., 2020). Instead, *TP53* wild-type status was identified to correlate with PARPi sensitivity, possibly due to the regulation of RAD51-repression (Smeby et al., 2020). Accordingly, potentiation of SN-38 cytotoxicity by olaparib cotreatment was revealed to be further upregulated by transient knockdown of RAD51 (Tahara et al., 2014). These diverse and in part conflicting results underline the significance of the applied PARPi, the mechanism of the chemotherapeutic drug and the mutational status of the used CRC cell line for the occurrence of a synergistic activity.

Aside from chemotherapy, studies revealed beneficial effects of PARP-1 inhibition in combination with radiotherapy. In a CRC mouse model, concurrent veliparib treatment and radiation significantly enhanced the effects of anti-PD-1-mediated survival and tumor growth inhibition (Seyedin et al., 2020). Loss of the DNA damage repair protein XRCC2 sensitizes CRC cells to radiation in combination with PARP-1 inhibition by olaparib *in vitro* and in a xenograft mouse model (Qin et al., 2022).

1.3.2.3. Clinical trials of PARP inhibitors in CRC

First PARPi were clinically approved for the treatment of breast and ovarian cancers over 10 years ago. To date, 11 clinical trials have been registered for the application of PARPi in the treatment of CRC, either as monotherapy or in combination with additional chemotherapeutics (Table 3). In CRC patients, monotreatment with olaparib after failure of standard systemic chemotherapy showed no partial or complete response, regardless of MSS status. The authors concluded that future studies should focus on the combinations of PARPi with radiotherapy or chemotherapy with DNA damage inducing

drugs (Leichman et al., 2016). A first phase I trial applying combination treatment with IT and olaparib in the treatment of CRC reported lack of antitumor efficacy. Intermittent administration of olaparib was necessary to avoid drug-induced toxicity, which was not considered tolerable (Chen et al., 2016). First phase II clinical trials of veliparib in combination with the FOLFIRI chemotherapy regimen revealed significant improvement of the treatment outcome. Additionally, an increase of hematological adverse events was observed in response to veliparib cotreatment, including anemia and neutropenia (Gorbunova et al., 2019).

In summary, application of existing PARPi in CRC treatment has not been able to improve therapy outcome. Nevertheless, the studies conducted so far repurposed the PARPi veliparib and olaparib, which were initially developed for application in the context of BRCA1/2 mutations. Only recently, the determinants of the synergy between PARPi and DNA damage inducing drugs have been understood and yet have to be applied for the development of PARPi specifically intended for this purpose. Clinical studies which applied PARPi in the context of CRC treatment are summarized in Table 3.

Table 3: Overview of clinical trials applying PARPi in CRC treatment. The information has been retrieved from the database www.clinicaltrials.gov in July 2024. “Terminated” indicates that the study was stopped early with or without renewal while “Completed” indicates that the study ended normally.

Cancer type	Drug(s)	Phase	Status	Reference
Solid tumors	HS-10502	I	Not yet recruiting (2023-2026)	NCT05740956
Advanced solid tumors and colorectal cancer	M9466 FOLFIRI	I	Not yet recruiting (2024-2026)	NCT06509906
Metastatic colorectal or gastroesophageal cancer	Talazoparib Trifluridine + Tipiracil	I	Recruiting (2021-2027)	NCT04511039
Colorectal cancer	Irinotecan Olaparib	I	Completed (2008-2015)	NCT00535353
Solid tumors	Veliparib FOLFIRI Paclitaxel + Carboplatin	I	Completed (2013-2016)	NCT02033551
Pancreatic, colorectal or biliary cancer	Rucaparib FOLFIRI	I/II	Not yet recruiting (2018-2025)	NCT03337087

Background

Advanced solid tumors	Durvalumab Olaparib Cediranib	I/II	Recruiting (2015-2025)	NCT02484404
Advanced solid malignancies	AZD5305 Paclitaxel Carboplatin	I/II	Recruiting (2020-2026)	NCT04644068
Solid tumors	CB-839 Talazoparib	I/II	Terminated (2019-2020)	NCT03875313
Metastatic colorectal cancer	Niraparib	II	Withdrawn (2023)	NCT05412706
Colorectal cancer (MMR-D/MSI-H)	Niraparib Dostarlimab	II	Not yet recruiting (2024-2017)	NCT06365970
Advanced or metastatic colorectal cancer	Niraparib Panitumumab	II	Not yet recruiting (2019-2024)	NCT03983993
Colorectal cancer (HRD)	Fluzoparib Irinotecan	II	Not yet recruiting (2023)	NCT05732129
Colorectal cancer (HRD)	Olaparib Pembrolizumab	II	Recruiting (2022-2025)	NCT05201612
Metastatic colorectal cancer	Veliparib FOLFIRI Bevacizumab	II	Completed (2014-2017)	NCT02305758
Colorectal cancer	Temozolomide ABT-888	II	Completed (2009-2013)	NCT01051596
Colorectal cancer (MSI)	Olaparib	II	Completed (2009-2012)	NCT00912743
MGMT-hypermethylated colorectal cancer	Olaparib Temozolomide	II	Completed (2020-2023)	NCT04166435
Metastatic colorectal cancer	Olaparib Bevacizumab	III	Completed (2020-2023)	NCT04456699

2. Objectives

The current standard-of-care for patients with CRC includes cytostatic drugs (IT, 5-FU and OXA) as well as monoclonal antibodies targeted against growth factors (e.g. bevacizumab), growth factor receptors (e.g. cetuximab) and immune receptors (pembrolizumab). Ongoing progress in molecular cancer diagnostics not only has helped to understand the mechanisms of carcinogenesis but has also been crucial in identifying new targets in this complex disease. Therefore, novel chemotherapeutic compounds emerged in the recent years, improving the prognosis of several types of cancer. The assessment of new pharmacological approaches in CRC chemotherapy represents the overarching scope of this PhD thesis. Therefore, three pivotal points should be addressed in this work:

- I. The deregulated metabolism of tumor cells as a target in CRC allowing for a tumor specific mechanism of action that complements established chemotherapy based on DNA damage inducing cytostatic drugs. While mitochondrial alterations of cancer have been studied in depth, only recently devimistat received clinical approval as one of the first drugs targeting the deregulated TCA cycle of tumor cells (Philip et al., 2019; Rocha Lima et al., 2019). Our first publication aimed to assess the potential of devimistat as a building block in CRC treatment, either as monotherapy or in combination with established chemotherapy. Therefore, the following questions were addressed:
 - What impact does the molecular subtype of CRC cell lines have on their sensitivity towards devimistat and is the cytotoxicity cancer cell specific?
 - Can mitochondrial disruption be confirmed as the underlying mechanism of cytotoxicity for CRC cell lines and which cell death pathways are triggered?
 - Does devimistat act synergistically with established chemotherapeutic drugs and can the corresponding molecular mechanism be identified?
 - Can the effects observed for mono- and cotreatment be transferred to an animal model to assess the therapeutic efficacy *in vivo*?
- II. The pharmacological induction of DNA damage and ROS to specifically target rapidly dividing tumor cells is a common approach in chemotherapy. In the treatment of CRC, the range of clinically applied cytostatic drugs is limited and the development of chemoresistance frequently impedes therapy outcome. Biologically active compounds found in nature with distinct mechanisms of action

could complement the existing pharmacological options in CRC therapy. Thus, our second publication focused on the following questions:

- Can novel compounds with anticancer activity in CRC cell lines be identified in a screening of 11 merosesquiterpenes isolated from marine sponges?
- What is the mode of action of the most active merosesquiterpenes in CRC cell lines with regards to induction of DNA damage, production of ROS and activation of the mitochondrial apoptosis pathway?
- What impact does the cellular p53 status have on cell death induction triggered by merosesquiterpenes?
- Can the observed results for anticancer activity be confirmed in murine tumor organoids?

III. The DNA damage repair machinery of CRC cells enables chemoresistance against routinely applied cytostatic agents and assures proliferation despite extensive genetic and epigenetic alterations. Inhibitors of the DNA repair enzyme PARP-1 have been clinically applied in the treatment of specific cancer entities exhibiting mutations of BRCA1/2 for over 10 years, including breast, ovarian and prostate cancer. Only recently, PARP-1 emerged as a potential target in tumor subtypes with mutational alterations beyond BRCA1/2. In our third publication, the applicability of novel PARP-1 inhibitors for CRC therapy should be evaluated and therefore the following questions were addressed:

- Can novel PARP-1 inhibitors be identified based on *in silico* and *in vitro* screening of a library of novel 3,4-bifunctionalized and -bridged indole compounds?
- How does HR deficiency affect the cytotoxicity of novel and established PARP-1 inhibitors in CRC cell lines and does the combination with genotoxic anticancer drugs improve anticancer activity?
- How does the PARP-1 trapping capacity of novel and established PARP-1 inhibitors relate to their cytotoxicity as monotherapy and in combination with genotoxic anticancer drugs?

In summary, this work aimed to assess novel chemotherapeutic approaches for CRC treatment with an emphasis on the investigation of underlying molecular mechanisms, considering the impact of mutations commonly observed in CRC.

3. Cumulative Part: Publications

3.1. The Mitochondrial Disruptor Devimistat (CPI-613) Synergizes with Genotoxic Anticancer Drugs in Colorectal Cancer Therapy in a Bim-Dependent Manner

Publication I

Carina Arnold*, Philipp Demuth*, Nina Seiwert, Simon Wittmann, Kerstin Boengler, Birgit Rasenberger, Markus Christmann, Magdalena Huber, Thomas Brunner, Michael Linnebacher, Jörg Fahrer

*Contributed equally to this work

In a short preamble I would like to expand on the funding and the collaborations which made the following publication possible as well as my participation in it. This publication, in which I have a shared first authorship, was created in collaboration with 10 coauthors. The project was funded by the Wilhelm Sander Foundation and conducted within their scopes, which is the development of novel therapeutic approaches for cancer treatment. During the creation of the publication, I took part in the formal analysis, validation, investigation and methodology as well as the writing of the original draft and its subsequent review and editing. I conducted the experiments on the activity of devimistat in murine primary and tumor organoids, the induction of ROS and the quantification of vital mitochondria. In addition, I performed the experiments regarding the role of Bim for the synergism of devimistat with IT and 5-FU, which included cell culture, western blot analysis, siRNA mediated Bim knockdown and analysis of tumor lysates. The gene expression analysis of cell death markers by qPCR was conducted by the Department of Toxicology at the University Medical Center in Mainz, Germany.

This publication appeared in the peer-reviewed journal *Molecular Cancer Therapeutics* (Volume 21) in January 2022.

Arnold, C., Demuth, P., Seiwert, N., Wittmann, S., Boengler, K., Rasenberger, B., Christmann, M., Huber, M., Brunner, T., Linnebacher, M., Fahrer, J., 2022. The Mitochondrial Disruptor Devimistat (CPI-613) Synergizes with Genotoxic Anticancer Drugs in Colorectal Cancer Therapy in a Bim-Dependent Manner. *Mol Cancer Ther* 21, 100–112.

DOI: <https://doi.org/10.1158/1535-7163.MCT-21-0393>

The Mitochondrial Disruptor Devimistat (CPI-613) Synergizes with Genotoxic Anticancer Drugs in Colorectal Cancer Therapy in a Bim-Dependent Manner



Carina Arnold^{1,2,3}, Philipp Demuth¹, Nina Seiwert^{1,2,3}, Simon Wittmann¹, Kerstin Boengler⁴, Birgit Rasenberger³, Markus Christmann³, Magdalena Huber⁵, Thomas Brunner⁶, Michael Linnebacher⁷, and Jörg Fahrner^{1,2,3}

ABSTRACT

Colorectal cancer is one of the most frequent tumor entities, with an increasing incidence and mortality in younger adults in Europe and the United States. Five-year survival rates for advanced colorectal cancer are still low, highlighting the need for novel targets in colorectal cancer therapy. Here, we investigated the therapeutic potential of the compound devimistat (CPI-613) that targets altered mitochondrial cancer cell metabolism and its synergism with the antineoplastic drugs 5-fluorouracil (5-FU) and irinotecan (IT) in colorectal cancer. Devimistat exerted a comparable cytotoxicity in a panel of established colorectal cancer cell lines and patient-derived short-term cultures independent of their genetic and epigenetic status, whereas human colonic epithelial cells were more resistant, indicating tumor selectivity. These findings were corroborated in intestinal organoid and tumoroid models. Mechanistically, devimistat disrupted mitochondrial membrane potential and severely

impaired mitochondrial respiration, resulting in colorectal cancer cell death induction independent of p53. Combination treatment of devimistat with 5-FU or IT demonstrated synergistic cell killing in colorectal cancer cells as shown by Combeneft modeling and Chou–Talalay analysis. Increased cell death induction was revealed as a major mechanism involving downregulation of antiapoptotic genes and accumulation of proapoptotic Bim, which was confirmed by its genetic knockdown. In human colorectal cancer xenograft mouse models, devimistat showed antitumor activity and synergized with IT, resulting in prolonged survival and enhanced therapeutic efficacy. In human tumor xenografts, devimistat prevented IT-triggered p53 stabilization and caused synergistic Bim induction. Taken together, our study revealed devimistat as a promising candidate in colorectal cancer therapy by synergizing with established antineoplastic drugs *in vitro* and *in vivo*.

Introduction

Colorectal cancer is among the most prevalent types of cancer worldwide and exhibits an increasing incidence and mortality rate in low- and middle-income countries (1). Not only are elderly age groups affected, but also an elevated number of cases is observed in young adults (2). Several risk factors are associated with colorectal cancer including nutrition (3), lack of physical activity (4), as well as genetic predisposition (5). The treatment of colorectal cancer includes surgical resection of the primary tumor, generally in combination with che-

motherapy and radiation, depending on the stage and localization of the disease (6). Drugs usually applied are the antimetabolite 5-fluorouracil (5-FU) and folic acid (leucovorin) combined with another DNA-damaging agent [irinotecan (IT) or oxaliplatin] used in a specific regimen (FOLFOX or FOLFIRI; ref. 6). Additionally, highly specific treatment with antiangiogenic drugs (e.g., bevacizumab) or epidermal growth factor receptor inhibitors (e.g., cetuximab) emerged in the last decade as targeted options for first- or second-line therapy of colorectal cancer, respectively (7).

More recently, a new class of anticancer drugs was developed, derived from the endogenous enzymatic cofactor α -lipoic acid (LA), which plays a crucial role in mitochondrial energy production and was shown to have cytotoxic effects in several types of cancer cells (8). Devimistat (CPI-613) is a derivative of LA, containing two benzyl rings covalently bound to the sulfur atoms of LA, rendering it non-redox active (9). Devimistat acts as an inhibitor of the mitochondrial enzymes pyruvate dehydrogenase (PDH) and α -ketoglutarate dehydrogenase (KGDH), thereby interfering with the altered energy metabolism of tumor cells (10). The mechanism of enzymatic inhibition differs between both enzymes: PDH activity is impaired indirectly due to induction of its negative regulator pyruvate dehydrogenase kinase, whereas the enzyme KGDH is inactivated by a devimistat-induced reactive oxygen species (ROS) burst (9, 11).

The cytotoxic activity of devimistat has been demonstrated in various cancer cell lines, including mainly pancreatic, kidney, lung, breast, ovarian, and prostate cancer cells, whereas moderate impact on untransformed cells was observed (9, 11, 12). The underlying mechanism of cytotoxicity included induction of apoptosis as well as caspase-independent cell death pathways, as revealed in pancreatic and lung cancer cells (11, 12). As an inhibitor of mitochondrial key enzymes, devimistat was found to target the altered energy metabolism

¹Division of Food Chemistry and Toxicology, Department of Chemistry, Technical University of Kaiserslautern, Kaiserslautern, Germany. ²Rudolf Buchheim Institute of Pharmacology, Justus Liebig University Giessen, Giessen, Germany. ³Department of Toxicology, University Medical Center, Mainz, Germany. ⁴Institute for Physiology, Faculty of Medicine, Justus Liebig University Giessen, Giessen, Germany. ⁵Institute for Medical Microbiology and Hospital Hygiene, University of Marburg, Marburg, Germany. ⁶Biochemical Pharmacology, Department of Biology, University of Konstanz, Konstanz, Germany. ⁷Department of General Surgery, Molecular Oncology and Immunotherapy, Rostock University Medical Center, Rostock, Germany.

Note: Supplementary data for this article are available at Molecular Cancer Therapeutics Online (<http://mct.aacrjournals.org/>).

C. Arnold and P. Demuth contributed equally to this work.

Corresponding Author: Jörg Fahrner, Division of Food Chemistry and Toxicology, Department of Chemistry, Technical University of Kaiserslautern, Erwin-Schroedinger-Str. 52, D-67663 Kaiserslautern, Germany. Phone: 49-631/2052974; E-mail: fahrner@chemie.uni-kl.de

Mol Cancer Ther 2022;21:100–12

doi: 10.1158/1535-7163.MCT-21-0393

©2021 American Association for Cancer Research

of tumor cells: low serum and glucose conditions as well as carnosine, an inhibitor of glycolytic ATP production, synergistically enhanced the cytotoxicity of devimistat (9, 13). Several years ago, devimistat entered clinical testing and progressed especially for the treatment of acute myeloid leukemia and pancreatic cancer (14, 15). Clinical studies demonstrated beneficial effects by combining devimistat with standard chemotherapeutics such as antimetabolites, indicated by an increased overall and progression-free survival, patient performance, and response rate (14–17). Yet, the underlying mechanisms of this interplay are only partially understood.

In our study, we aimed to analyze the potential synergistic effects of devimistat with 5-FU and IT in the treatment of colorectal cancer *in vitro* and *in vivo*. To this end, we screened a panel of established human colorectal cancer cell lines including patient-derived short-term cultures and normal human colonic epithelial cells (HCEC) for their sensitivity toward devimistat and the chemotherapeutics 5-FU and IT. Tumor selectivity of devimistat was further addressed using murine intestinal organoids and intestinal tumoroids. The mode of action of devimistat in colorectal cancer cells was detailed by cell death measurements, assessment of mitochondrial function, and genotoxicity studies. The potential synergism of devimistat with chemotherapeutics was then investigated in colorectal cancer cells using Combeneft modeling and Chou–Talalay analysis. Underlying mechanisms such as apoptosis, cell-cycle regulation, and genotoxicity were analyzed by various methods such as qPCR, western blot detection, flow cytometry, and genetic knockdown experiments. Finally, these findings were translated into two xenograft mouse models and supported by tumor xenograft analysis.

Materials and Methods

Cell culture

Cell lines were cultured under sterile conditions at 37°C and 5% CO₂ in humidified atmosphere. The human colorectal cancer cell lines included HCT116-p53^{+/+}, HCT116-p53^{-/-} (both provided by Prof. Bert Vogelstein, Johns Hopkins University, Baltimore in 2012), Caco-2, DLD-1, HT29, RKO, SW48, SW480, and LS174T (all obtained from the Institute of Toxicology, University Medical Center Mainz between 2012 and 2015). Cells were reauthenticated by the p53 status, their differential response to genotoxic anticancer drugs such as 5-FU and IT (see Table 1) as well as their typical cell morphology. The primary patient-derived cell lines HROC60 and HROC278 were established as described previously (18). Cells were grown in corresponding medium (DMEM: HCT116, RKO, DLD-1; RPMI: SW48, HT29, SW480; IMDM: LS174T; DMEM/Ham F-12 1:1: HROC60, HROC278; MEM: Caco-2) supplemented with 10% fetal calf serum and 1% penicillin/streptomycin. Colorectal cancer cells were routinely maintained in culture for 20–25 passages. Media and supplements were obtained from Gibco Life Technologies or Pan-Biotech. Nontransformed HCEC (1CT) were kindly provided by Prof. Jerry W. Shay (Department of Cell Biology, UT Southwestern Medical Center, Dallas) in 2015 and reauthenticated by their p53 status and their typical cell morphology. Cells were isolated from normal human colonic biopsies and immortalized by CDK4- and hTERT-transfection as described (19). HCEC were grown in a nitrogen incubator with reduced oxygen levels (7% O₂) and 5% CO₂ at 37°C in 4:1 DMEM GlutaMax/Medium 199 (Thermo Fisher Scientific) with supplements as reported previously (20). HCEC were usually cultured for 8–10 passages at maximum. Cell lines were *mycoplasma* negative as routinely demonstrated by PCR using the VenorGem Classic kit (Minerva Biolabs) and immunofluorescence microscopy with nuclear staining.

Table 1. Cytotoxicity screening in a panel of colorectal cancer cell lines based on IC₅₀ values.

IC ₅₀ (μmol/L)	Devimistat	5-FU	IT
<i>MSI/p53-wild-type</i>			
HCT116	167	4	6
HCT116-p53 ^{-/-}	151	n.d.	n.d.
LS174T	184	4	2
RKO	164	32	11
SW48	175	64	56
DLD-1	155	4	52
<i>MSS/p53-mutant</i>			
Caco-2	183	186	67
HT29	163	20	23
SW480	187	63	91
<i>Patient-derived</i>			
HROC278	190	172	17
HROC60	211	1,190	53
<i>Noncancerous</i>			
HCEC	286	31	6

Note: Indicated cell lines were incubated with increasing concentrations of devimistat or the cytostatic drugs 5-FU and IT for 72 hours followed by measurement of the cell viability using the ATP assay ($n = 3$). IC₅₀ values were determined as described in Materials and Methods. MSS: microsatellite stable; MSI: microsatellite instable; HCEC: human colonic epithelial cells; n.d. not determined.

Transient transfection with siRNA

Knockdown of Bim was performed using siGENOME SMARTpool siRNA obtained from Dharmacon. Nonsense, scrambled RNA served as control. Transfections were conducted as reported (20), and successful knockdown was confirmed by western blot analysis as detailed below.

Drugs and drug treatment

Devimistat (CPI-613; Hycultec GmbH) was dissolved in dimethylsulfoxide (DMSO) and stock solutions (125 mmol/L) were stored at –20°C. 5-FU (medac) and IT (Fresenius Kabi) were obtained from the pharmacy of the University Medical Center Mainz and prepared as solution in 0.9% saline solution stored at –20°C. In the combination regimen, cytostatic drug treatment was performed 2 hours after treatment with devimistat.

Isolation of RNA and quantitative real-time PCR

Preparation of total RNA, transcription into cDNA, and quantitative gene-expression analysis by real-time PCR was performed as described (21) using the primers listed in Supplementary Table S1. In three independent experiments, qPCR was conducted in technical duplicates with a CFX96 Real-Time PCR Detection System (Bio-Rad). The subsequent analysis was performed using CFX Manager Software. Nontranscribed controls were included in each run. Gene-expression levels were normalized to *GAPDH* as well as *ACTB*, and the solvent control was set to one.

Preparation of cell and tissue extracts

Protein extracts were generated from either cell culture experiments or xenograft mouse studies (22). Whole-cell lysis was performed in RIPA buffer containing 25 mmol/L Tris-HCl pH 8.0, 2 mmol/L EDTA, 150 mmol/L NaCl, 1% NP-40, 0.5% Na-deoxycholate, 0.1% SDS supplemented with cOmplete protease inhibitor cocktail (Roche Diagnostics), 1 mmol/L Na₃VO₄, 2 mmol/L NaF, and 1 mmol/L

Arnold et al.

PMSF for 15 minutes on ice, followed by sonication and centrifugation. Protein extracts of tumor xenografts were obtained by homogenization of snap-frozen isolated tumor tissue in RIPA buffer with slight modifications. Clarified extracts were determined for their protein content using the Bradford assay.

SDS-PAGE and immunoblot analysis

Western blot analysis was essentially conducted as described previously (23), and proteins were detected using a c300 chemiluminescence imager (Azure Biosystems). The used primary and secondary antibodies are detailed in Supplementary Table S2.

In-cell western analysis

The In-Cell Western (ICW) analysis of γ H2AX as DNA strand break marker was performed as previously described (24). Samples were analyzed using an Odyssey Infrared Imaging Scanner (LI-COR Biosciences) by simultaneous measurement of γ H2AX and DNA staining. Statistical analysis was performed using Image Studio Lite (Version 5.2; LI-COR Biosciences) by determining the x-fold increase in γ H2AX signal normalized to the DNA content per well in relation to the control.

Measurement of ROS formation

Quantitative analysis of ROS levels was performed using the probe CM-H₂DCFDA (Invitrogen) as described (25). Staining was performed for 30 minutes at 37°C in the dark in phenol red- and serum-free medium, and samples were measured by flow cytometry using a BD Canto II and BD FACS Diva software 6.0 (BD Biosciences).

Assessment of DNA damage using the Comet assay

The alkaline Comet assay and the Fpg-modified alkaline Comet assay were essentially performed as described (26). Samples were analyzed by microscopy, and at least 50 cells per sample were scored using Comet IV software (Perceptive Instruments Ltd.). Olive tail moment (OTM) was used for the quantification of DNA damage.

MitoTracker staining and confocal microscopy

MitoTracker Orange CMTMRos (Thermo Fisher Scientific) staining was used to visualize the relative amount of intact mitochondria. Cells were seeded on cover slips and treated as indicated. Upon the desired incubation time, cells were stained using 250 nmol/L MitoTracker for 15 minutes and then fixed with 4% paraformaldehyde. Following mounting using VectaShield with DAPI (Vector Labs), cells were analyzed using a Zeiss Axio Observer 7 microscope equipped with an LSM900 confocal laser scanner (Zeiss) as reported (24). Images were processed using ZEN software (Zeiss) and ImageJ software (NIH).

Cell death measurement

Cell death induction was measured using Annexin V/PI staining and flow-cytometric analysis as reported (27). Cells were incubated as indicated, harvested, and washed with PBS. Cells were then stained with Annexin V (Miltenyi Biotec) for 15 minutes on ice in binding buffer (5% dye; 10 mmol/L HEPES pH 7.4, 140 mmol/L NaCl, 2.5 mmol/L CaCl₂, and 0.1% BSA) followed by the addition of propidium iodide (2% dye in binding buffer). Cells were analyzed on a BD Canto II and the corresponding BD FACS Diva software 6.0 (BD Biosciences), which was used for gating of living cells (Annexin V/PI double negative), early apoptotic cells (Annexin V-positive, PI-negative), and late apoptotic/necrotic cells (Annexin V/PI double positive).

Analysis of cell-cycle distribution

Cell-cycle distribution was assessed as reported previously (28). Cells were treated and incubated for various time periods as indicated. Cells were then harvested, washed with PBS, and incubated in 80% ethanol at -20°C overnight. Cells were washed with PBS, incubated with RNase A (Sigma) for 1 hour, and stained by propidium iodide (Sigma). Finally, cells were analyzed by flow cytometry using a BD Canto II and the corresponding BD FACS Diva software 6.0 (BD Biosciences).

Measurement of cell viability and assessment of synergism

Cell viability was determined by the CellTiter-Glo Luminescent Cell Viability Assay Kit (Promega). According to the manufacturer's protocol, cells were seeded in white 96-well plates, treated as indicated, and incubated for 72 hours. The medium was then exchanged for medium containing 50% CellTiter-Glo Luminescent Solution and analyzed with the luminometer Fluoroskan Ascent FL (Thermo Scientific). In order to determine the combination index (CI) by the Chou-Talalay method (29), experiments were performed as explained previously using CompuSyn software (CompuSyn Inc.; ref. 30). Simultaneously, Combeneft analysis was undertaken as described elsewhere (31).

Assessment of mitochondrial membrane potential

Mitochondrial membrane potential was analyzed using the dye JC-1 (5',6,6'-tetrachloro-1,1',3,3'-tetraethyl-benzamidazolylcarbocyanine iodide; Sigma) as reported (27). Valinomycin served as positive control. Staining was performed according to the manufacturer's protocol of the Mitochondrial Staining Kit (Sigma). Monomeric cytosolic JC-1 in the cytoplasm exhibits green fluorescence emission (530 nm), whereas aggregated JC-1 in intact mitochondria exhibits red fluorescence emission (585 nm). This is monitored by flow cytometry using a BD Canto II and BD FACS Diva software 6.0 (BD Biosciences).

Assessment of metabolic function using the Seahorse Mito stress test kit

Mitochondrial dysfunction of colorectal cancer cells upon treatment with devimistat was assessed in Seahorse XF96 Cell Culture Microplates (Agilent). In brief, medium was replaced with Seahorse assay medium (glucose-free DMEM supplemented with 2 mmol/L glutamine, 1 mmol/L pyruvate, and 25 mmol/L glucose) at the day of measurement. Oxygen consumption rate (OCR) was measured with Seahorse XF396 Analyzer (Agilent). Mitochondrial ATP production was defined as the difference between basal OCR reading and the OCR following the injection of 2 μ mol/L oligomycin. Maximal respiration was defined as the difference in OCR after injection of 1 μ mol/L CCCP, which uncouples the electron transport, and OCR after injection of a mixture of 2.5 μ mol/L rotenone/antimycin A (Anti A), inhibiting complex I and III.

Analysis of normal intestinal organoids and tumor organoids

Murine intestinal organoids and tumor organoids were generated and maintained as described previously (20, 32). Viability of organoids following treatment with increasing devimistat concentrations was assessed using the MTS assay and absorbance measurements in a Sirius HT reader (MWG Biotech). Solvent-treated organoids were defined as 100% viable. Furthermore, organoids were analyzed for morphologic changes and cell death induction using PI/Hoechst 33342 costaining and live-cell microscopy as reported (33).

Downloaded from <http://aacrjournals.org/med/article-pdf/11/1/100/3017002/100.pdf> by guest on 27 February 2024

Colorectal cancer xenograft mouse model

Male Balb/c^{nu/nu} mice were purchased from Janvier Laboratories and maintained at 25°C and 65% humidified atmosphere at the animal facility of the University Medical Center Mainz or the Justus Liebig University Gießen. Mice were housed at a 12 hours day and night cycle with food and drinking water supply *ad libitum*. Following acclimatization, mice were inoculated subcutaneously with either HCT116 or HT29 cells (5×10^6 and 10^6 cells/flank) into the right and left flank each as reported previously (34). After 7 days of xenograft tumor growth, animals were randomized into four treatment groups and received tumor therapy for up to four consecutive weeks. Animals received i.p. injections with either devimistat (25 mg/kg bw, twice per week, dissolved in 1 mol/L triethanolamine, injected with 5% dextrose in water) or IT (40 mg/kg bw, once per week, dissolved in and injected with 0.9% NaCl) or the combination of both or the corresponding vehicle control. Three times per week, body weight was monitored and tumor diameters (length, width, and volume) were measured using a sliding caliper. At the end of the experiments, animals were sacrificed by cervical dislocation. Tumor xenografts were isolated, snap-frozen in liquid nitrogen, and stored at -80°C until further analysis.

Study approval for experiments using animals

All animal experiments were approved by the government of Hesse or Rhineland-Palatinate and the Animal Care and Use Committee at the JLU Gießen and the JGU Mainz. All animal studies were performed according to German federal law and the guidelines for the protection of animals.

Statistical analysis

Experiments were performed independently at least three times, except otherwise stated. Results from representative experiments are shown. Values underwent Grubb test to exclude outliers and are displayed as mean + standard error of the mean (SEM) using the GraphPad Prism 8.0 Software (GraphPad Software Inc.). Statistical analysis (Student *t* test, log-rank test, two-way-ANOVA) was performed as indicated in figure legends, and statistical significance was defined as $P < 0.05$.

Data availability

The data generated in this study are available within the article and its supplementary data files.

Results**Devimistat kills colorectal cancer cells independent of their molecular subtype**

Initially, we screened a panel of colorectal cancer cell lines including patient-derived short-term cultures for their sensitivity toward devimistat and established anticancer drugs used in colorectal cancer therapy, 5-FU and IT (Table 1). The molecular colorectal cancer subtypes and genetic features clearly affected the cytotoxicity of both 5-FU and IT, which were generally more potent in colorectal cancer cells with microsatellite instability (MSI) and wild-type p53. In contrast, microsatellite stable (MSS) colorectal cancer cells with mutated p53 displayed higher IC₅₀ values and were thus more resistant. Patient-derived short-term cultures (HROC60, HROC278) exhibit a high resistance particularly to 5-FU treatment. Interestingly, devimistat showed comparable toxicity in all tested colorectal cancer cells independent of the molecular subtype. Furthermore, nonmalignant HCECs were less vulnerable to devimistat, whereas 5-FU and IT caused strong toxicity. In contrast to HCEC, the viability of both

HT29 and HCT116 colorectal cancer cells was strongly reduced upon treatment with the same devimistat concentration (Supplementary Fig. S1A).

In order to analyze the impact of p53 on cytotoxicity induced by devimistat, isogenic p53-proficient and -deficient HCT116 cells were used and exposed to devimistat. Our findings clearly showed a p53-independent cytotoxicity of devimistat (Fig. 1A). Further experiments provided evidence that devimistat exerts its cytotoxicity not only in proliferating colorectal cancer cells, but also in colorectal cancer cells pretreated with 5-FU or IT (Fig. 1B; Supplementary Fig. S1B and S1C). In opposition to that, both anticancer drugs lost their cytotoxic effects in arrested colorectal cancer cells rechallenged with the drugs. Flow cytometry-based cell-cycle analysis in HCT116 and HT29 cells revealed a reduction of cells in S- and G₂-M-phase and an induction of cells in sub-G₁, which was more prominent in HCT116 cells (Fig. 1C; Supplementary Fig. S1D–S1F). In line with these findings, devimistat caused cell death as shown by Annexin V/PI staining (Fig. 1D; Supplementary Fig. S1G). Finally, the cytotoxicity of devimistat was analyzed in murine intestinal organoids and intestinal tumoroids. Devimistat had almost no effects on normal intestinal organoids as attested by immunofluorescence microscopy and MTS viability assay (Fig. 1E and F). In contrast, devimistat caused a concentration-dependent decrease in viability together with severe morphologic changes and cell death in tumoroids (Fig. 1G and H). Taken together, devimistat was cytotoxic in a plethora of colorectal cancer cell lines with similar potency independent of the molecular colorectal cancer subtype as well as in intestinal tumoroids. Importantly, devimistat showed moderate to low toxicity in normal HCEC as well as normal intestinal organoids, and was active in pretreated and arrested cells, making it an attractive drug candidate for colorectal cancer therapy.

Devimistat disrupts mitochondrial function in colorectal cancer cells

Because devimistat was reported to target enzymes involved in the mitochondrial TCA cycle and energy metabolism, metabolic measurements of OCRs were carried out in HCT116 and HT29 cells. Using the Cell Mito Stress Test kit (Seahorse assay) with oligomycin, CCCP and a combination of rotenone (Rot) and antimycin A (Anti A), oxidative phosphorylation (OXPHOS) was analyzed in the presence of increasing devimistat concentrations. Although 100 μmol/L devimistat had no effect on oxygen consumption rate, 150 μmol/L devimistat strongly impaired basal (oligomycin), ATP production-related (CCCP) and maximal (Rot/Anti A) respiration in both colorectal cancer cell lines (Fig. 2A and B; Supplementary Fig. S2A and S2B). This was preceded by a dose-dependent burst of ROS triggered by devimistat, which was shown by H₂DCFDA staining and also observed under hypoxic conditions (Fig. 2C and D; Supplementary Fig. S2C and S2D). Concomitantly, changes in mitochondrial membrane potential (MMP) were assessed by JC-1 dye. This staining revealed an elevated number of cells with JC-1 monomers upon devimistat treatment and, thus, indicated loss of MMP (Fig. 2E and F). A similar effect was observed with the positive control rotenone and with the ionophore valinomycin, which is known to depolarize mitochondria (Fig. 2E and F). As a next step, mitochondrial integrity was analyzed using MitoTracker Orange staining and confocal microscopy. This dye only accumulates in mitochondria with intact MMP and thus directly reflects intact mitochondria (35). Devimistat treatment caused a reduction of intact mitochondria in HCT116 cells, which was slightly more pronounced in cells exposed

Arnold et al.

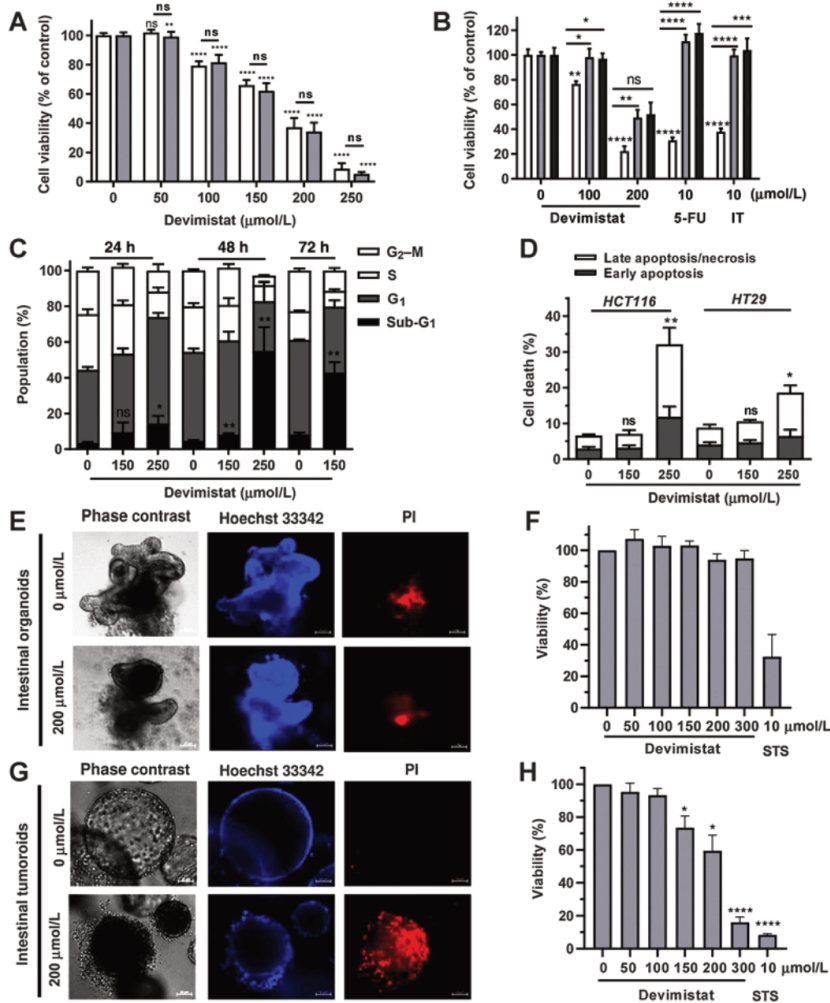


Figure 1. Impaired cell viability and cell death induction by devimistat in colorectal cancer (CRC) cells and intestinal tumoroids. **A**, Isogenic HCT116 cells with either wild-type p53 (white bars) or p53 knockout (gray bars) were treated with devimistat (for 72 hours), and viability was assessed using ATP assays ($n = 5$). **B**, Proliferating (white bars) and nonproliferating (cells chronically treated with 5-FU are depicted in gray and cells chronically treated with IT are depicted in dark-gray bars) HCT116 cells were exposed to devimistat or rechallenged with 5-FU and IT. Viability was measured as described in **A** ($n = 3$). **C**, HCT116 cells were treated with increasing doses of devimistat for up to 72 hours, and cell-cycle distribution was determined by PI staining and flow cytometry ($n \geq 3$). **D**, Cell death induction after 48 hours in HCT116 and HT29 cells exposed to devimistat followed by Annexin V/PI staining and flow cytometry ($n \geq 3$). **E**, Normal intestinal organoids were challenged with devimistat or solvent control for 72 hours followed by Hoechst 33342/PI staining and immunofluorescence microscopy. Representative images are shown. Scale bar: 50 μm . **F**, Viability of intestinal organoids upon treatment with increasing concentrations of devimistat or the positive control staurosporine (STS) determined by MTS assay. **G**, Intestinal tumoroids were treated as described in **E**, stained with Hoechst 33342/PI, and analyzed by immunofluorescence microscopy. Scale bar, 50 μm . **H**, Viability of intestinal tumoroids treated as described in **F** and analyzed by MTS assay. Data, mean + SEM ($n \geq 3$; except for STS in normal organoids: $n = 2$). ns: $P > 0.05$; *, $P < 0.05$; **, $P < 0.01$; ***, $P < 0.001$; ****, $P < 0.0001$; t test.

to the mitochondrial complex I inhibitor rotenone (Fig. 2G and H). In summary, devimistat increases ROS generation and disrupts MMP in colorectal cancer cell lines, thereby leading to mitochondrial dysfunction and impairment of OXPHOS.

Devimistat acts cytotoxic in colorectal cancer cells without causing DNA damage

Next, we wished to know whether devimistat is genotoxic similar to the established anticancer drugs 5-FU and IT. To this end, HCT116

Downloaded from <http://ascrjournals.org/ncdr/article-pdf/21/1/100/3017002/100.pdf> by guest on 27 February 2024

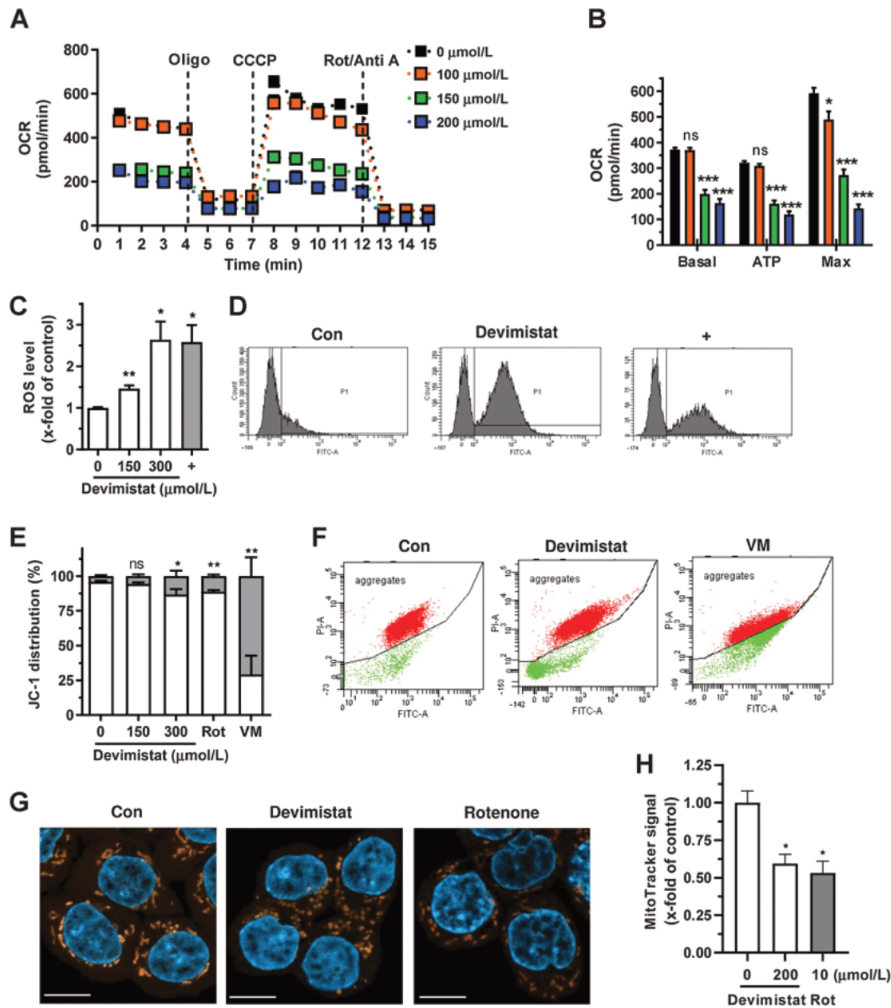


Figure 2. Devimistat triggered disruption of mitochondrial integrity and function in colorectal cancer cells. **A**, HCT116 cells were incubated with increasing doses of devimistat for 24 hours. OCR was determined with Seahorse metabolic analyzer. OCR was measured basally and after the addition of mitochondrial inhibitors oligomycin (Oligo), CCCP, and rotenone/antimycin A (Rot/Anti A; $n \geq 3$). **B**, Basal, ATP-coupled and maximal respiration as determined in **A**. **C** and **D**, ROS level in HCT116 cells after incubation with devimistat for 2 hours. ROS formation was assessed by H_2DCFDA staining and flow cytometry. tBOOH (200 $\mu\text{mol/L}$; 20 minutes) was included as positive control. Representative histograms are shown ($n = 3$). **E** and **F**, Loss of MMP in HCT116 cells after 1 hour of devimistat treatment was measured using JC-1 staining. The respiratory complex I-inhibitor rotenone (Rot; 1 $\mu\text{mol/L}$; 24 hours) and ionophore valinomycin (VM) served as positive controls. Formation of JC-1 aggregates (red) versus monomers (green) was quantified by flow cytometry. Representative dot blots are shown ($n \geq 3$). **G** and **H**, HCT116 cells were incubated with either 200 $\mu\text{mol/L}$ devimistat, solvent control, or rotenone (10 $\mu\text{mol/L}$) for 24 hours and stained for vital mitochondria using MitoTracker Orange dye. Cells were then analyzed by confocal microscopy. Representative images are displayed. Nuclear staining with DAPI is depicted in blue, whereas MitoTracker staining is visualized in orange. Size bar, 10 μm . Data, mean \pm SEM ($n = 3$). ns; $P > 0.05$; *, $P < 0.05$; **, $P < 0.01$; ***, $P < 0.001$; ****, $P < 0.0001$; t test.

cells were incubated with increasing concentrations of devimistat, and the DNA damage marker phosphorylated histone 2AX (γH2AX) was studied by ICW analysis. No γH2AX formation was detected after devimistat treatment, whereas 5-FU clearly increased γH2AX levels (Fig. 3A; Supplementary Fig. S3A). Furthermore, an alkaline Comet assay was performed, which reveals apurinic/aprimidinic (AP) sites,

DNA single-strand breaks and DNA double-strand breaks. However, no DNA damage formation was observed following devimistat treatment (Fig. 3B; Supplementary Fig. S3B). These experiments were repeated in HT29 cells, confirming lack of genotoxicity for devimistat (Supplementary Fig. S3C–S3F). Because we observed ROS formation by devimistat treatment (compare Fig. 2C), we also

Arnold et al.

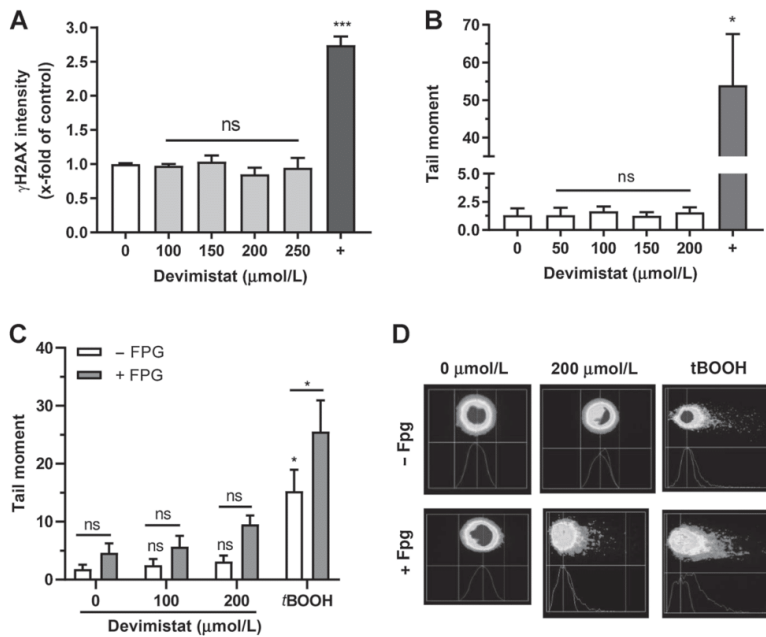


Figure 3. Lack of genotoxicity after devimistat treatment. **A**, HCT116 cells were incubated with increasing concentrations of devimistat for 24 hours and subjected to ICW analysis of the DNA damage marker γ H2AX. Incubation with 10 μ mol/L 5-FU served as positive control. **B**, HCT116 cells were treated as described in **A**. Subsequently, DNA strand break formation was assessed by the alkaline Comet assay. Incubation with 200 μ mol/L tBOOH was used as positive control. **C**, HCT116 cells were treated as stated in **A**, and oxidative DNA lesions were revealed using the Fpg-modified alkaline Comet assay. Incubation with 200 μ mol/L tBOOH for 30 minutes was used as positive control. **D**, Representative photographs of cells obtained by the Fpg-modified alkaline Comet assay in HCT116 cells. All data, mean \pm SEM ($n = 3$). ns: $P > 0.05$; *, $P < 0.05$; ***, $P < 0.001$; t test.

used a Fpg-modified Comet assay that allows for the detection of oxidative DNA damage. Devimistat caused a moderate, but not statistically significant, increase at the highest concentration tested (200 μ mol/L; **Fig. 3C and D**). The positive control tBOOH induced both DNA strand breaks and oxidative DNA damage as revealed by the Fpg-modified Comet assay (**Fig. 3C and D**). In conclusion, our experiments demonstrated a nongenotoxic mode of action for devimistat, which is an important advantage over genotoxic anticancer drugs in terms of damage to healthy tissue.

Devimistat synergizes with anticancer drugs in colorectal cancer cell lines by increasing cell death induction in a Bim-dependent manner

Due to its nongenotoxic mitochondria-targeted mode of action, we hypothesized that devimistat should prove valuable in combination regimens with the DNA-damaging anticancer drugs 5-FU and IT. Therefore, mono- and combination treatments were performed in HCT116 cells, and viability was assessed by ATP assays. CIs were calculated according to the Chou-Talalay method (29), revealing a clear synergism of devimistat with both anticancer drugs (Supplementary Table S3). In order to determine the optimal concentration for combination therapy, a wide range of concentrations was tested followed by Combeneft modeling. This analysis also demonstrated synergy for devimistat at a concentration between 150 and 200 μ mol/L with nearly all tested concentrations of 5-FU and IT (**Fig. 4A**). The same set of experiments was conducted in HT29 cells. Although Chou-Talalay analysis displayed clear synergism for devimistat with 5-FU and a moderate antagonism for its combination with IT, Combeneft modeling revealed synergistic effects for all combination regimens (Supplementary Table S3; Supplementary Fig. S4A).

Subsequently, we wanted to detail the mechanisms underlying the synergism between devimistat and the genotoxic anticancer drugs.

HCT116 cells were exposed to devimistat, 5-FU, and IT or combinations thereof followed by cell death analysis with Annexin V/PI staining. As expected, all single treatments caused cell death to a certain degree (**Fig. 4B**; Supplementary Fig. S4B). However, the combination of devimistat with either 5-FU or IT strongly increased cell death in a synergistic manner (**Fig. 4B**). Cell death induction was also moderately augmented in HT29 cells treated with the combination regimens as compared with the single treatments (Supplementary Fig. S4C and S4D). Next, the expression levels of antiapoptotic and proapoptotic genes in HCT116 cells were determined by qPCR. Interestingly, the combination devimistat/5-FU as well as the combination devimistat/IT resulted in decreased expression of the antiapoptotic genes *Bcl-X_L* and *Survivin* (**Fig. 4C**). Proapoptotic gene expression was induced by the genotoxic anticancer drugs 5-FU and IT, but was hardly modulated by addition of devimistat except for *FASR* expression levels that were augmented in the combination devimistat/IT (Supplementary Fig. S5A and S5B). Interestingly, we observed that devimistat in a combination regimen with 5-FU or IT strongly increased Bim protein levels in HCT116 cells (**Fig. 4D**), although no effects were revealed on gene-expression level (Supplementary Fig. S5A). A similar upregulation of Bim protein was also detected in HT29 cells in the combination treatments (Supplementary Fig. S5C). Using p53-proficient and -deficient HCT116 cells, we found that Bim induction was even higher in cells without p53 as demonstrated by western blot analysis (**Fig. 4E and F**). It should also be noted that devimistat reduced basal p53 levels and blocked IT-triggered p53 accumulation in p53-proficient HCT116 cells (**Fig. 4E**; Supplementary Fig. S5D). To detail the contribution of Bim to the observed synergism, a siRNA-mediated knockdown was performed in HCT116 cells and confirmed by western blot analysis upon treatment with the drugs or combination for 48 hours (**Fig. 4G**). At the same time, cell death induction was analyzed by Annexin V/PI staining, showing a

Downloaded from <http://aacrjournals.org/ncr/article-pdf/21/1/100/3017002/100.pdf> by guest on 27 February 2024

Synergism of Devimistat (CPI-613) in Colorectal Cancer Chemotherapy

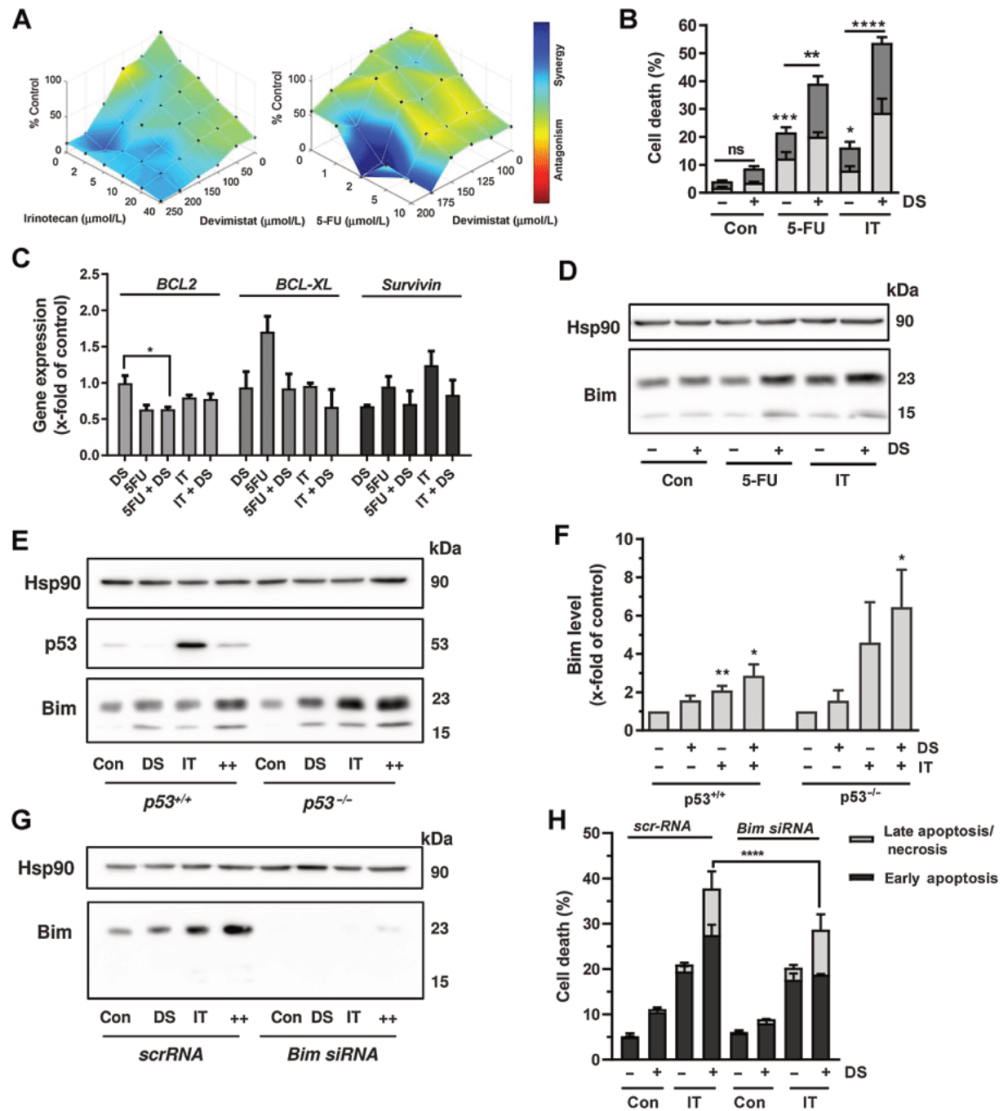


Figure 4.

Synergism of devimistat with anticancer drugs in colorectal cancer (CRC) cells and role of Bim. **A**, The 3D diagrams show Combeneft analysis of the combination regimens 5-FU + devimistat and IT + devimistat in HCT116 cells using cell viability data after 72 hours of incubation as indicated. Arithmetically averaged data of three independent experiments were used for analysis. **B**, HCT116 cells were treated as indicated (10 $\mu\text{mol/L}$ 5-FU, 20 $\mu\text{mol/L}$ IT, and 200 $\mu\text{mol/L}$ devimistat: DS) for 48 hours. Cell death analysis was then performed by Annexin V/PI staining and flow cytometry ($n \geq 3$). ns: $P > 0.05$; **, $P < 0.01$; ****, $P < 0.0001$; two-way-ANOVA. **C**, Expression levels of antiapoptotic genes in HCT116 cells treated as described in **B** for 24 hours. Gene expression was assessed by quantitative real-time PCR ($n = 3$). ns: $P > 0.05$ is not shown; *, $P < 0.05$. **D**, Protein expression of proapoptotic Bim in HCT116 cells treated as described in **B** for 24 hours. Whole-cell lysates were analyzed by SDS-PAGE followed by western blot detection of Bim. Hsp90 served as loading control. A representative western blot is shown. **E**, p53 level and its impact on Bim following single or combination treatment. HCT116 cells were exposed to IT, devimistat, or the combination regimen as described in **D**. A representative western blot analysis of p53, Bim, and the loading control Hsp90 is shown. **F**, Quantitative evaluation of western blot analysis. Data, mean + SEM ($n = 3$). ns: $P > 0.05$ is not shown; *, $P < 0.05$; **, $P < 0.01$, t test. **G**, siRNA-mediated knockdown of Bim in HCT116 cells followed by treatment with devimistat, IT, or the combination (++) for 48 hours. Cells were transfected with scrambled RNA (scrRNA) as control. Western blot detection of Bim and Hsp90 as loading control. **H**, Impact of Bim knockdown on cell death induction upon treatment with devimistat, IT, or the combination regimen as described under **G**. Cell death analysis was performed by Annexin V/PI staining and flow cytometry ($n \geq 3$). ns: $P > 0.05$ is not shown; ****, $P < 0.0001$; two-way ANOVA.

Arnold et al.

significantly reduced cell death level in the devimistat/IT combination regimen upon Bim knockdown (Fig. 4H). Finally, the impact of the combination regimens on the expression of cyclins and important CDK-cyclin inhibitors was analyzed. The experiments revealed a strong reduction of *CCNB1* (*cyclin B1*) and *CCNH* (*cyclin H*) expression in all combinations as well as a suppression of *CCND1* (*cyclin D1*) and *CCND2* (*cyclin D2*) in the regimen with IT and devimistat (Supplementary Fig. S5E and S5F). The expression levels of the CDK-cyclin inhibitors *p14*, *p16*, and *p21* were unaffected by the combination treatment (Supplementary Fig. S5G). Taken together, our data demonstrate that devimistat synergizes with IT and 5-FU in colorectal cancer cells mainly by increasing cell death induction, which is mediated by induction of the BH3-only protein Bim.

Devimistat synergizes with IT in colorectal cancer xenograft models *in vivo*

Finally, these results were translated into an *in vivo* setting with two different colorectal cancer xenograft mouse models focusing on the promising combination of devimistat and IT. To this end, Balb/c^{nu/nu} animals were inoculated subcutaneously with either HCT116 or HT29 cells, were randomized into four groups (control, devimistat, IT and devimistat/IT) and treated as depicted in Fig. 5A. In HCT116 xenografts, single treatment with devimistat or IT suppressed tumor growth (Fig. 5B), resulting in a significant increase in survival rates (Fig. 5C). Intriguingly, the strongest inhibition of tumor growth was observed in animals receiving the combination devimistat/IT (Fig. 5B). In agreement with this finding, this regimen displayed the best overall survival rates (Fig. 5C). In HT29 xenografts, both devimistat and IT retarded tumor growth on their own (Fig. 5D). The best tumor growth suppression was achieved with the combination regimen (Fig. 5D), although the growth retardation was not as strong as in HCT116 cells. Remarkably, only the devimistat/IT combination resulted in significantly increased overall survival (Fig. 5E). It should further be mentioned that devimistat single treatment exhibited no general toxicity as reflected by normal weight gain comparable to the control group (Supplementary Fig. S6A and B). IT displayed moderate toxicity starting after 14 days of therapy, which was, however, not further increased by the addition of devimistat in the combination regimen (Supplementary Fig. S6A and B). Finally, the DNA damage markers p53 and γ H2AX as well as the BH3-only protein Bim were assessed in tumor homogenates using western blot analysis. IT treatment caused p53 induction and γ H2AX formation in both colorectal cancer xenograft models, which was suppressed in the combination regimen particularly in HCT116 xenografts (Fig. 5F; Supplementary Fig. S6C and S6D, and S6F). Furthermore, both devimistat and IT treatment increased Bim levels, which was potentiated in the combination regimen especially in HCT116 xenografts (Fig. 5G; Supplementary Fig. S6C and S6E). In conclusion, these findings provide evidence that devimistat also synergizes with IT in colorectal cancer *in vivo*, resulting in better therapy response and improved overall survival. Notably, the combination therapy was not associated with a higher toxicity than the single treatments, but caused even reduced DNA damage levels and triggered Bim induction in tumor xenograft tissue. The key pathways involved in the synergism between devimistat and the anticancer drugs are summarized in a model shown in Fig. 5H.

Discussion

This study demonstrates that the mitochondrial targeted drug devimistat is cytotoxic with similar efficacy in a broad panel of established colorectal cancer cell lines and patient-derived short-

term cultures independent of their genetic and epigenetic alterations. This is a clear advantage over the mother compound LA, which is also active in various colorectal cancer cell lines, but displays IC₅₀ values differing up to 10-fold (8, 27). 5-FU is the gold standard in colorectal cancer chemotherapy, whose activity is linked to the mismatch-repair (MMR) status. Patients with MMR-deficient tumors and high MSI did not show a benefit from adjuvant 5-FU chemotherapy (36), which was confirmed in MMR-deficient colorectal cancer cells exposed to 5-FU (37). Genetic features also determine the response and adverse effects induced by SN-38, the active metabolite of IT (38). Colorectal cancer patients with a deficiency in uridine diphosphate glucuronosyltransferase 1A1 exhibit insufficient hepatic glucuronidation and subsequent elimination of SN-38, thereby causing severe side effects after high IT doses (39). In contrast, neither MSI nor chromosomal instability affected the susceptibility of colorectal cancer cells toward devimistat. Furthermore, the devimistat-triggered cytotoxicity is independent of p53 as revealed by our studies in isogenic HCT116 cell lines. This is an important finding, because p53 mutations occur frequently in human cancer cells and affect their sensitivity toward DNA-damaging chemotherapeutics, as illustrated by an increased resistance of p53-deficient colorectal cancer cells to 5-FU (30, 40).

Our cytotoxicity data further show that nonmalignant HCEC are less susceptible toward the cytotoxic effects of devimistat, whereas the genotoxic anticancer drugs 5-FU and IT exerted a similar degree of cytotoxicity in colorectal cancer cells and HCEC. In support of these findings, devimistat killed intestinal tumoroids in a concentration-dependent manner, but hardly affected the viability of normal intestinal organoids. The reduced cytotoxicity in noncancerous cells was also observed in normal lung, breast, and kidney cells, which were all more resistant toward devimistat than the respective tumor cell lines (9). This tumor-selective mode of action is very likely attributable to differences in the metabolism between normal and cancer cells as highlighted recently (10). Nevertheless, further studies are required to elucidate the precise molecular mechanisms. Another asset of devimistat is the fact that devimistat is able to eliminate colorectal cancer cells independent of ongoing cell proliferation as attested by our experiments with 5-FU or IT arrested colorectal cancer cells. Although devimistat was still active in this setting, treatment with 5-FU or IT displayed no cytotoxicity at all. This fits to the notion that the antimetabolite 5-FU and topoisomerase I poisons like IT require cancer cell proliferation to exert their cytotoxicity (38, 41).

Furthermore, we were able to show that devimistat targets mitochondria and strongly impairs OXPHOS in colorectal cancer cell lines, which is preceded by ROS formation and decreased MMP. This is in agreement with other studies performed in H460 lung cancer cells, in which devimistat caused a loss of MMP (9) and a mitochondrial ROS burst with oxidation of the mitochondrial peroxiredoxin 3 isoform (11). The underlying mechanism by which the non-redox active devimistat promotes ROS formation is not fully understood, but was attributed to the E3 dihydrolipoamide dehydrogenase subunit of KGDH as primary source (11). A concentration-dependent inhibition of mitochondrial respiration was also detected in leukemia cell lines (42), which were even more susceptible than the colorectal cancer cell lines tested herein. Our genotoxicity assays conducted with devimistat in two colorectal cancer cell lines displayed lack of genotoxicity, except for a moderate, but statistically insignificant increase in oxidative DNA damage at high concentrations (i.e., 200 μ mol/L devimistat). This might be a consequence of the early ROS burst triggered by devimistat and the compromised mitochondria, resulting in nuclear DNA damage. However, this genotoxic effect is rather small

Downloaded from <http://aacrjournals.org/> on 11/03/2021 10:00:30 AM by guest on 27 February 2024

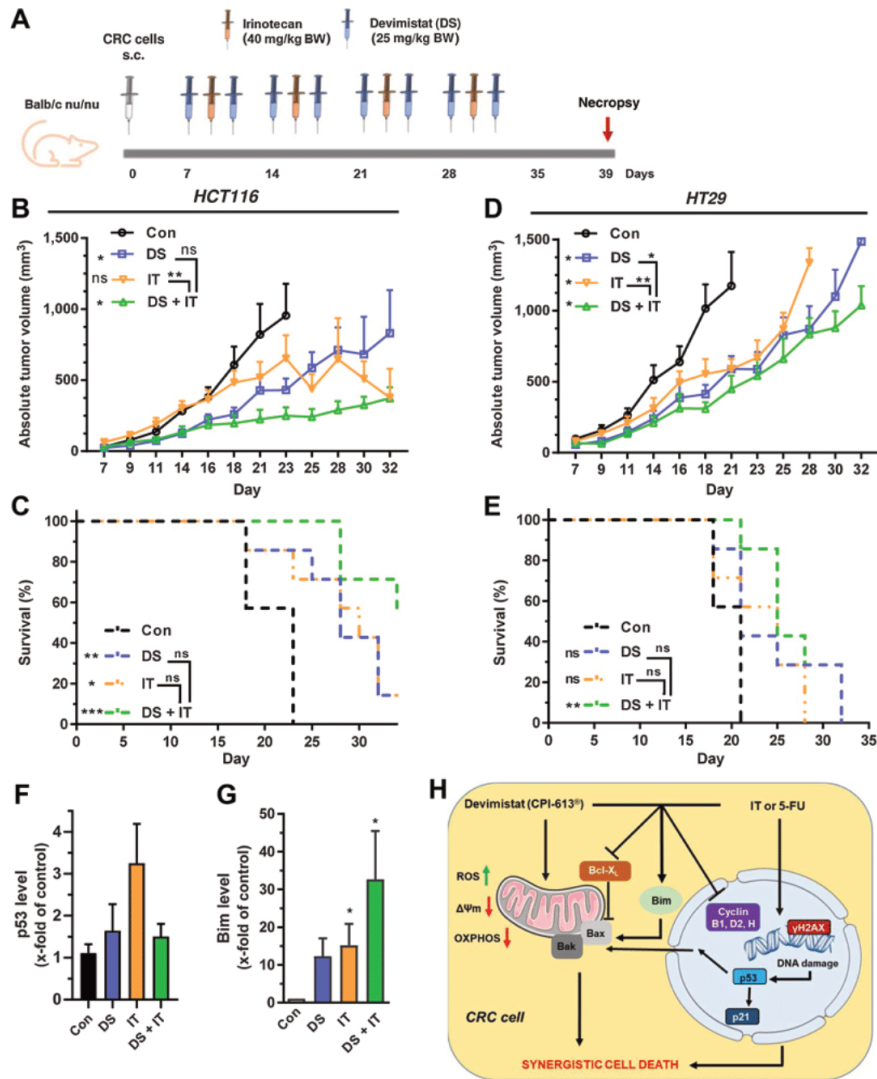


Figure 5.

Therapeutic efficacy and synergism of devimistat and IT in colorectal cancer xenograft mouse models. **A**, Experimental setup of xenograft experiments in male Balb/*c*^{nu/nu} animals. Mice were inoculated subcutaneously with colorectal cancer cells into both flanks and tumors were allowed to develop for 7 days. Animals were then grouped (*n* = 7/group with two tumors/animal) and either received mock treatment, devimistat (25 mg/kg BW, 2×/week), IT (40 mg/kg BW, 1×/week), or devimistat + IT. **B**, Growth curve with HCT116 xenografts depicting the absolute tumor volume. Tumor volume was determined every second day using a digital caliper. **C**, Kaplan–Meier curve illustrates survival of animals in the HCT116 xenograft experiment. ns: *P* > 0.05; *, *P* < 0.01; **, *P* < 0.01; ***, *P* < 0.001 (log-rank test). **D**, Growth curve with HT29 xenografts depicting the absolute tumor volume. Tumor volume was determined every second day using a digital caliper. **E**, Kaplan–Meier curve illustrates survival of animals in the HT29 xenograft experiment. ns: *P* > 0.05; **, *P* < 0.01 (log-rank test). **F** and **G**, Snap frozen tumor segments were lysed, subjected to SDS-PAGE and western blot analysis. Shown are densitometric evaluations for western blot analysis of p53 and Bim in HCT116 xenograft tumors (*n* = 4). Data, mean + SEM. ns: *P* > 0.05 is not shown; *, *P* < 0.01; *t* test. **H**, Model of synergistic cell death induction by devimistat and the anticancer drugs 5-FU and IT in colorectal cancer cells. Devimistat promotes ROS formation followed by a decrease in the MMP ($\Delta\psi_m$) and impaired oxidative phosphorylation, thereby preferentially killing colorectal cancer cells and murine colorectal cancer organoids. IT and 5-FU induced DNA damage as detected by γ H2AX formation and activation of the p53 tumor suppressor protein, leading to cell-cycle arrest via p21 and cell death. Combination therapy causes synergistic cell death with upregulation of Bim as a proapoptotic key factor as demonstrated by genetic knockdown experiments. Apart from that, combination therapy resulted in a repression of antiapoptotic genes (e.g., *Bcl-X_L*) and cyclins required for cell-cycle progression. The synergistic effects of devimistat and IT were validated *in vivo* using two colorectal cancer xenograft models, resulting in significantly retarded tumor growth and increased survival. This figure was created using Servier Medical Art templates, which are licensed under a Creative Commons Attribution 3.0 Unported License; <https://smart.servier.com>.

Downloaded from <http://ascrjournals.org/inarticle-pdf/11/100/3017002/100.pdf> by guest on 27 February 2024

Arnold et al.

compared with the potent DNA-damaging properties of 5-FU or IT, as attested in the γ H2AX ICW. A similar lack of genotoxicity was previously reported for the mother compound LA (27).

Based upon their different mode of actions, we hypothesized that the combination of the metabolic disruptor devimistat with the genotoxic agents 5-FU and IT will result in synergistic colorectal cancer cell death. The synergism of the combination regimens was demonstrated in colorectal cancer cells by both Chou-Talalay analysis and Combeneft analysis. Increased apoptotic cell death was identified as a major mechanism for the observed synergism. In the combination regimen with 5-FU or IT, devimistat caused a downregulation of the antiapoptotic genes *Bcl-X_L* and *Survivin*. Targeting *Survivin* by small-molecule inhibitors has recently been shown to sensitize p53-mutated colorectal cancer cells to IT treatment (43), highlighting *Survivin* as critical target in colorectal cancer. High expression levels of *Bcl-X_L* are known to contribute to the resistance of colorectal cancer cells towards 5-FU treatment (44). Furthermore, our study revealed a pronounced upregulation of the proapoptotic protein *Bim* in combination regimens of 5-FU/IT with devimistat. This was not only observed in colorectal cancer cells but also found in tumor xenograft tissue. siRNA-mediated downregulation of *Bim* significantly reduced the cell death induction by devimistat and IT, thereby highlighting its important function for the observed synergism. *Bim* is a BH3-only protein that antagonizes antiapoptotic proteins of the *Bcl2* family, such as *Bcl-2* and *Mcl-1*, and thereby promotes mitochondrial apoptosis (45). Because no changes in gene expression were detected in our experiments, the observed upregulation of *Bim* is likely attributable to its posttranslational regulation. Phosphorylation of *Bim* by JNK and p38 MAPK is known to prevent *Bim* degradation and promote its proapoptotic activity (45). Interestingly, JNK-mediated *Bim* activation was shown in liver cancer cells after exposure to the antineoplastic agent doxorubicin, which was potentiated by combined treatment with the death ligand TRAIL (46). Also in glioblastoma cells, JNK/c-Jun—mediated induction of *Bim* enhanced apoptosis triggered by the alkylating anticancer drugs temozolomide and nimustine (47).

Moreover, we found a pronounced downregulation of different cyclins, especially *cyclin B1*, *cyclin H1*, and *cyclin D1/D2*, in colorectal cancer cells challenged with the combination regimen. While *Cyclin B1* is involved in G₂-M transition, *Cyclin D1* and *D2* regulate the progression from G₁ to S-phase (48). *Cyclin H* is part of the CDK-activating kinase, which activates CDKs, including CDK4 and CDK6, to promote cell-cycle progression and is involved in transcription as subunit of TFIIF (49). The reduced gene expression levels of certain *cyclins* in the combination group therefore suggest an impaired cell-cycle progression. Interestingly, a previous study conducted in pancreatic cancer cells reported a devimistat-triggered downregulation of several cell-cycle regulating genes, including *cyclin B1*, *cyclin D3*, and *cyclin E1* (50).

Finally, the antitumor activity of devimistat was demonstrated in two different human colorectal cancer xenograft mouse models (HCT116—MSI; HT29—MSS). This extends the findings of a previous study, which reported growth inhibition of human lung cancer xenografts by devimistat (9). In a human pancreatic cancer xenograft model, devimistat was found to be even more potent than the antimetabolite gemcitabine, which is the mainstay in pancreatic cancer chemotherapy (50). In the present work, the therapeutic effects of devimistat were comparable to that of IT and clearly prolonged survival. With regard to its antitumor activity, devimistat

is also superior to that of the parental compound LA, which weakly retarded growth of HCT116 tumor xenografts (34). Importantly, we showed that devimistat synergizes with IT in both colorectal cancer xenografts, resulting in prolonged survival and enhanced therapeutic efficacy. Notably, this is the first preclinical study revealing a synergism between the mitochondrial disruptor devimistat and a genotoxic anticancer drug *in vivo*. In view of these positive results, clinical studies evaluating the benefit of devimistat in combination with anticancer drugs commonly used in colorectal cancer chemotherapy, such as 5-FU, IT, or oxaliplatin, are eagerly awaited. There is already an ongoing phase I study dealing with devimistat in combination with 5-FU for the treatment of patients with metastatic colorectal cancer (NCT02232152), which will be completed in the next year.

In conclusion, our study showed that devimistat is a promising building block in colorectal cancer chemotherapy and synergizes with antineoplastic agents *in vitro* and *in vivo*. By targeting mitochondrial metabolism in colorectal cancer cells independent of their genetic and epigenetic aberrations, devimistat complements the genotoxic mode of action of 5-FU and IT. This represents a novel and efficient combination strategy to fight colorectal cancer, which is still a fatal disease for many patients.

Authors' Disclosures

M. Huber reports grants from DFG during the conduct of the study. J. Fahrner reports grants from Wilhelm Sander Foundation and German Research Foundation during the conduct of the study. No disclosures were reported by the other authors.

Authors' Contributions

C. Arnold: Conceptualization, formal analysis, validation, investigation, visualization, methodology, writing—original draft, writing—review and editing. P. Demuth: Formal analysis, validation, investigation, methodology, writing—original draft, writing—review and editing. N. Seiwert: Methodology, writing—review and editing. S. Wittmann: Formal analysis, investigation, methodology, writing—review and editing. K. Boengler: Methodology, writing—review and editing. B. Rasenberger: Formal analysis and investigation. M. Christmann: Formal analysis, validation, methodology, writing—review and editing. M. Huber: Formal analysis, validation, methodology, writing—review and editing. T. Brunner: Resources, methodology, writing—review and editing. M. Linnebacher: Methodology, writing—review and editing. J. Fahrner: Conceptualization, formal analysis, supervision, funding acquisition, validation, visualization, writing—original draft, writing—review and editing.

Acknowledgments

J. Fahrner was supported by the Wilhelm Sander Foundation (grant numbers 2016.039.1 and 2016.039.2) and the German Research Foundation (DFG; INST 248/331-1 FUGG). M. Christmann received funding from the DFG (SFB 1361, project-ID 393547839, subproject 05). M. Huber was supported by the DFG (HU1824/5-2, HU1824/7-1, HU1824/9-1). We thank Svenja Stroh and Georg Nagel (both Department of Toxicology, University Medical Center Mainz, Germany) as well as Beate von Derschau (Rudolf Buchheim Institute of Pharmacology, Justus Liebig University Giessen, Germany) for excellent technical assistance and Dennis Vogel (Institute for Medical Microbiology and Hospital Hygiene, University of Marburg, Germany) for performing Seahorse measurements. We are grateful to Prof. Bert Vogelstein (John Hopkins University, Baltimore) for providing HCT116 cells and to Prof. Jerry W. Shay (University of Texas Southwestern Medical Center, Dallas) for providing HCEC. Fpg enzyme was a kind gift of Prof. Bernd Epe (University of Mainz, Germany).

The costs of publication of this article were defrayed in part by the payment of page charges. This article must therefore be hereby marked *advertisement* in accordance with 18 U.S.C. Section 1734 solely to indicate this fact.

Received May 2, 2021; revised September 22, 2021; accepted November 3, 2021; published first November 8, 2021.

References

1. Arnold M, Sierra M, Laversanne M, Soerjomataram I, Jemal A, Bray F. Global patterns and trends in colorectal cancer incidence and mortality. *Gut* 2016;66:683–91.
2. Siegel RL, Torre LA, Soerjomataram I, Hayes RB, Bray F, Weber TK, et al. Global patterns and trends in colorectal cancer incidence in young adults. *Gut* 2019;68:2179–85.
3. Seiwert N, Heylmann D, Hasselwander S, Fahrner J. Mechanism of colorectal carcinogenesis triggered by heme iron from red meat. *Biochim Biophys Acta Rev Cancer* 2020;1873:188334.
4. Lauby-Secretan B, Scoccianti C, Loomis D, Grosse Y, Bianchini F, Straif K. Body fatness and cancer—viewpoint of the IARC working group. *N Engl J Med* 2016;375:794–98.
5. Keum N, Giovannucci E. Global burden of colorectal cancer: emerging trends, risk factors and prevention strategies. *Nat Rev Gastroenterol Hepatol* 2019;16:713–32.
6. Kuipers EJ, Grady WM, Lieberman D, Seufferlein T, Sung JJ, Boelens PG, et al. Colorectal cancer. *Nat Rev Dis Primers* 2015;1:15065.
7. Xie YH, Chen YX, Fang JY. Comprehensive review of targeted therapy for colorectal cancer. *Signal Transduct Target Ther* 2020;5:22.
8. Dörsam B, Fahrner J. The disulfide compound α -lipoic acid and its derivatives: a novel class of anticancer agents targeting mitochondria. *Cancer Lett* 2016;371:12–19.
9. Zachar Z, Marecek J, Maturó C, Gupta S, Stuart SD, Howell K, et al. Non-redox-active lipoate derivatives disrupt cancer cell mitochondrial metabolism and are potent anticancer agents in vivo. *J Mol Med* 2011;89:1137–48.
10. Neitzel C, Demuth P, Wittmann S, Fahrner J. Targeting altered energy metabolism in colorectal cancer: oncogenic reprogramming, the central role of the TCA cycle and therapeutic opportunities. *Cancers* 2020;12:1731.
11. Stuart SD, Schauble A, Gupta S, Kennedy AD, Keppler BR, Bingham PM, et al. A strategically designed small molecule attacks alpha-ketoglutarate dehydrogenase in tumor cells through a redox process. *Cancer Metab* 2014;2:4.
12. Gao L, Xu Z, Huang Z, Tang Y, Yang D, Huang J, et al. CPI-613 rewires lipid metabolism to enhance pancreatic cancer apoptosis via the AMPK-ACC signaling. *J Exp Clin Cancer Res* 2020;39:73.
13. Oppermann H, Schnabel L, Meixensberger J, Gaunitz F. Pyruvate attenuates the anti-neoplastic effect of carnosine independently from oxidative phosphorylation. *Oncotarget* 2016;7:85848–60.
14. Pardee T, DeFord-Watts L, Peronto E, Levitan D, Hurd D, Kridel S, et al. Evaluation of the first-in-class antimetabolic agent CPI-613 in hematologic malignancies. *J Clin Oncol* 2012;30:6524–24.
15. Philip PA, Buyse ME, Alistar AT, Rocha Lima CM, Luther S, Pardee TS, et al. A phase III open-label trial to evaluate efficacy and safety of CPI-613 plus modified FOLFIRINOX (mFFX) versus FOLFIRINOX (FFX) in patients with metastatic adenocarcinoma of the pancreas. *Future Oncol* 2019;15:3189–96.
16. Alistar A, Morris BB, Desnoyer R, Klepin HD, Hosseinzadeh K, Clark C, et al. Safety and tolerability of the first-in-class agent CPI-613 in combination with modified FOLFIRINOX in patients with metastatic pancreatic cancer: a single-center, open-label, dose-escalation, phase I trial. *Lancet Oncol* 2017;18:770–78.
17. Pardee TS, Anderson RG, Pladna KM, Isom S, Ghiraldeli LP, Miller LD, et al. A phase I study of CPI-613 in combination with high-dose cytarabine and mitoxantrone for relapsed or refractory acute myeloid leukemia. *Clin Cancer Res* 2018;24:2060–73.
18. Mullins CS, Micheel B, Matschos S, Leuchter M, Burtin F, Krohn M, et al. Integrated biobanking and tumor model establishment of human colorectal carcinoma provides excellent tools for preclinical research. *Cancers* 2019;11:1520.
19. Roig AI, Eskiocak U, Hight SK, Kim SB, Delgado O, Souza RF, et al. Immortalized epithelial cells derived from human colon biopsies express stem cell markers and differentiate in vitro. *Gastroenterology* 2010;138:1012–21.
20. Seiwert N, Wecklein S, Demuth P, Hasselwander S, Kemper TA, Schwerdtle T, et al. Heme oxygenase 1 protects human colonocytes against ROS formation, oxidative DNA damage and cytotoxicity induced by heme iron, but not inorganic iron. *Cell Death Dis* 2020;11:787.
21. Christmann M, Boisseau C, Kitzinger R, Berac C, Allmann S, Sommer T, et al. Adaptive upregulation of DNA repair genes following benzo(a)pyrene diol epoxide protects against cell death at the expense of mutations. *Nucleic Acids Res* 2016;44:10727–43.
22. Fahrner J, Frisch J, Nagel G, Kraus A, Dörsam B, Thomas AD, et al. DNA repair by MGMT, but not AAG, causes a threshold in alkylation-induced colorectal carcinogenesis. *Carcinogenesis* 2015;36:1235–44.
23. Fahrner J, Schweitzer B, Fiedler K, Langer T, Gierschik P, Barth H. C2-streptavidin mediates the delivery of biotin-conjugated tumor suppressor protein p53 into tumor cells. *Bioconjug Chem* 2013;24:595–603.
24. Seiwert N, Neitzel C, Stroh S, Frisan T, Audebert M, Toulany M, et al. AKT2 suppresses pro-survival autophagy triggered by DNA double-strand breaks in colorectal cancer cells. *Cell Death Dis* 2017;8:e3019.
25. Dörsam B, Wu CF, Efferth T, Kaina B, Fahrner J. The eucalyptus oil ingredient 1,8-cineol induces oxidative DNA damage. *Arch Toxicol* 2015;89:797–805.
26. Fahrner J, Huelsenbeck J, Jaurich H, Dörsam B, Frisan T, Eich M, et al. Cytolethal distending toxin (CDT) is a radiomimetic agent and induces persistent levels of DNA double-strand breaks in human fibroblasts. *DNA Repair* 2014;18:31–43.
27. Dörsam B, Göder A, Seiwert N, Kaina B, Fahrner J. Lipoic acid induces p53-independent cell death in colorectal cancer cells and potentiates the cytotoxicity of 5-fluorouracil. *Arch Toxicol* 2015;89:1829–46.
28. Mimmler M, Peter S, Kraus A, Stroh S, Nikolova T, Seiwert N, et al. DNA damage response curtails detrimental replication stress and chromosomal instability induced by the dietary carcinogen PhIP. *Nucleic Acids Res* 2016;44:10259–76.
29. Chou TC. Drug combination studies and their synergy quantification using the Chou-Talalay method. *Cancer Res* 2010;70:440–6.
30. Neitzel C, Seiwert N, Göder A, Diehl E, Weber C, Nagel G, et al. Lipoic acid synergizes with anti-neoplastic drugs in colorectal cancer by targeting p53 for proteasomal degradation. *Cells* 2019;8:794.
31. Di Veroli GY, Fornari C, Wang D, Mollard S, Bramhall JL, Richards FM, et al. Combeneft: an interactive platform for the analysis and visualization of drug combinations. *Bioinformatics* 2016;32:2866–8.
32. Ripani P, Delp J, Bode K, Delgado ME, Dietrich L, Betzler VM, et al. Thiazolidines promote G1 cell cycle arrest in colorectal cancer cells by targeting the mitochondrial respiratory chain. *Oncogene* 2020;39:2345–57.
33. Jiso A, Demuth P, Bachowsky M, Haas M, Seiwert N, Heylmann D, et al. Natural merosequiterpenes activate the DNA damage response via DNA strand break formation and trigger apoptotic cell death in p53-Wild-type and mutant colorectal cancer. *Cancers* 2021;13:3282.
34. Göder A, Nagel G, Kraus A, Dörsam B, Seiwert N, Kaina B, et al. Lipoic acid inhibits the DNA repair protein O6-methylguanine-DNA methyltransferase (MGMT) and triggers its depletion in colorectal cancer cells with concomitant autophagy induction. *Carcinogenesis* 2015;36:817–31.
35. Chazotte B. Labeling mitochondria with MitoTracker dyes. *Cold Spring Harb Protoc* 2011;2011:990–2.
36. Sargent DJ, Marsoni S, Monges G, Thibodeau SN, Labianca R, Hamilton SR, et al. Defective mismatch repair as a predictive marker for lack of efficacy of fluorouracil-based adjuvant therapy in colon cancer. *J Clin Oncol* 2010;28:3219–26.
37. Carethers JM, Chauhan DP, Fink D, Nebel S, Bresalier RS, Howell SB, et al. Mismatch repair proficiency and in vitro response to 5-fluorouracil. *Gastroenterology* 1999;117:123–31.
38. Tomicic MT, Kaina B. Topoisomerase degradation, DSB repair, p53 and IAPs in cancer cell resistance to camptothecin-like topoisomerase I inhibitors. *Biochim Biophys Acta* 2013;1835:11–27.
39. Innocenti F, Undevia SD, Iyer L, Chen PX, Das S, Kocherginsky M, et al. Genetic variants in the UDP-glucuronosyltransferase 1A1 gene predict the risk of severe neutropenia of irinotecan. *J Clin Oncol* 2004;22:1382–8.
40. Bunz F, Hwang PM, Torrance C, Waldman T, Zhang Y, Dillehay L, et al. Disruption of p53 in human cancer cells alters the responses to therapeutic agents. *J Clin Invest* 1999;104:263–9.
41. Longley DB, Harkin DP, Johnston PG. 5-fluorouracil: mechanisms of action and clinical strategies. *Nat Rev Cancer* 2003;3:330–8.
42. Pardee TS, Lee K, Luddy J, Maturó C, Rodriguez R, Isom S, et al. A phase I study of the first-in-class antimetabolic agent, CPI-613, in patients with advanced hematologic malignancies. *Clin Cancer Res* 2014;20:5255–64.
43. Steigerwald C, Rasenberger B, Christmann M, Tomicic MT. Sensitization of colorectal cancer cells to irinotecan by the Survivin inhibitor LLP3 depends on XAF1 proficiency in the context of mutated p53. *Arch Toxicol* 2018;92:2645–48.
44. Violette S, Poulain L, Dussault E, Pepin D, Faussat AM, Chambaz J, et al. Resistance of colon cancer cells to long-term 5-fluorouracil exposure is correlated to the relative level of Bcl-2 and Bcl-X(L) in addition to Bax and p53 status. *Int J Cancer* 2002;98:498–504.
45. Sionov RV, Vlahopoulos SA, Granot Z. Regulation of Bim in Health and Disease. *Oncotarget* 2015;6:23058–134.

Arnold et al.

46. Schneider-Jakob S, Corazza N, Badmann A, Sidler D, Stuber-Roos R, Keogh A, et al. Synergistic induction of cell death in liver tumor cells by TRAIL and chemotherapeutic drugs via the BH3-only proteins Bim and Bid. *Cell Death Dis* 2010;1:e86.
47. Tomicic MT, Meise R, Aasland D, Berte N, Kitzinger R, Kramer OH, et al. Apoptosis induced by temozolomide and nimustine in glioblastoma cells is supported by JNK/c-Jun-mediated induction of the BH3-only protein BIM. *Oncotarget* 2015;6:33755–68.
48. Roskoski R, Jr. Cyclin-dependent protein serine/threonine kinase inhibitors as anticancer drugs. *Pharmacol Res* 2019;139:471–88.
49. Sava GP, Fan H, Coombes RC, Buluwela L, Ali S. CDK7 inhibitors as anticancer drugs. *Cancer Metastasis Rev* 2020;39:805–23.
50. Lee KC, Maturro C, Perera CN, Luddy J, Rodriguez R, Shorr R. Translational assessment of mitochondrial dysfunction of pancreatic cancer from *in vitro* gene microarray and animal efficacy studies, to early clinical studies, via the novel tumor-specific anti-mitochondrial agent, CPI-613. *Ann Transl Med* 2014;2:91.

SUPPLEMENTARY MATERIAL

The mitochondrial disruptor devimistat (CPI-613[®]) synergizes with genotoxic anticancer drugs in colorectal cancer therapy in a Bim-dependent manner

Carina Arnold^{1,2,3,‡}, Philipp Demuth^{1,‡}, Nina Seiwert^{1,2,3}, Simon Wittmann¹, Kerstin Boengler⁴, Birgit Rasenberger³, Markus Christmann³, Magdalena Huber⁵, Thomas Brunner⁶, Michael Linnebacher⁷, Jörg Fahrner^{1,2,3}

¹ Division of Food Chemistry and Toxicology, Department of Chemistry, Technical University of Kaiserslautern, 67663 Kaiserslautern, Germany

² Rudolf Buchheim Institute of Pharmacology, Justus Liebig University Giessen, 35392 Giessen, Germany

³ Department of Toxicology, University Medical Center, 55131 Mainz, Germany

⁴ Institute for Physiology, Faculty of Medicine, Justus Liebig University Giessen, 35392 Giessen, Germany

⁵ Institute for Medical Microbiology and Hospital Hygiene, University of Marburg, 35037 Marburg, Germany

⁶ Biochemical Pharmacology, Department of Biology, University of Konstanz, 78464 Konstanz, Germany

⁷ Department of General Surgery, Molecular Oncology and Immunotherapy, Rostock University Medical Center, 18057 Rostock, Germany

‡ These authors contributed equally to this work

CORRESPONDENCE:

Jörg Fahrner, PhD, Division of Food Chemistry and Toxicology, Department of Chemistry, Technical University of Kaiserslautern, Erwin-Schroedinger-Str. 52, D-67663 Kaiserslautern, Germany. Phone: + 49 631/2052974; e-mail: fahrer@chemie.uni-kl.de

Supplementary Figures

Figure S1

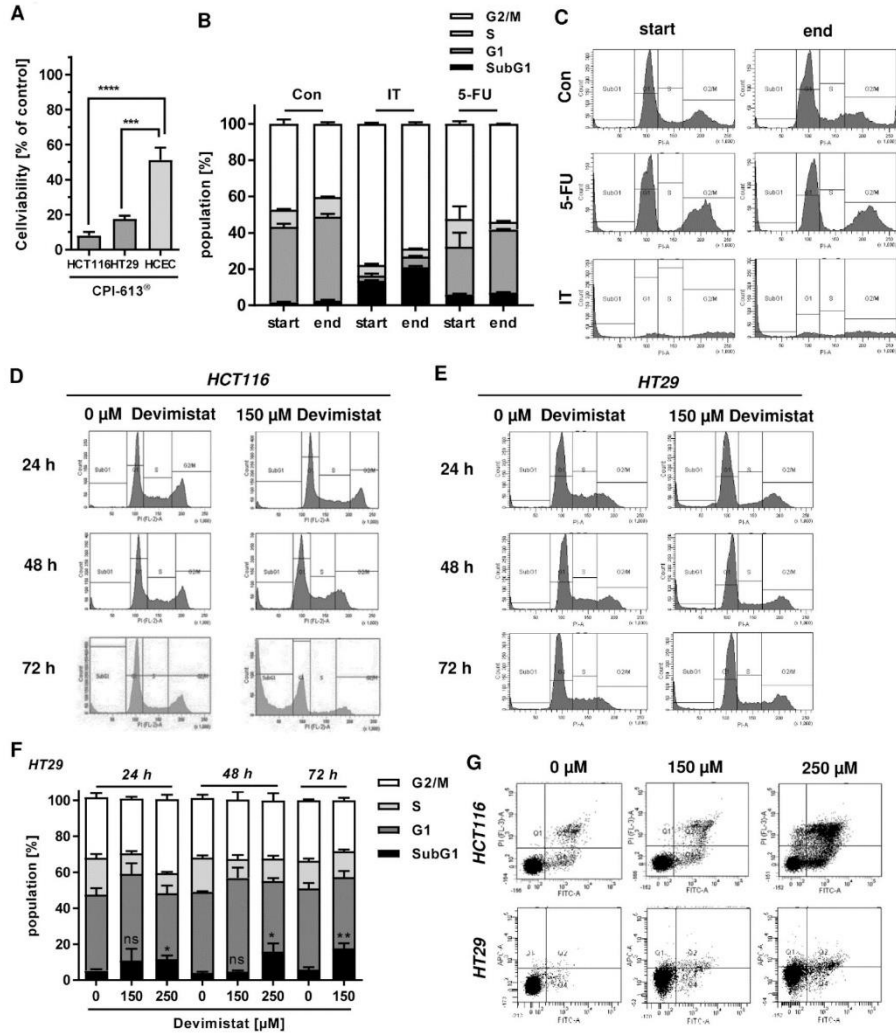


Figure S1: Cytotoxicity of devimistat in HCEC, HCT116 and HT29 cells (A) HCT116 and HT29 CRC cells as well as human colonic epithelial cells (HCEC) were exposed to 200 μM devimistat for 72 h and viability was determined using the ATP assay. Data are shown as mean + SEM ($n \geq 3$). $***p < 0.001$, $****p < 0.0001$; t-test (B) Flow cytometry based analysis of cell cycle distribution in HCT116 cells chronically treated with 5-FU and IT at the

beginning (start) and at the end (end) of the ATP assay as described in Figure 1 (n=3). **(C)** Representative histograms of **(B)**. **(D)** and **(E)** HCT116 and HT29 cells were exposed to increasing doses of devimistat for up to 72 h and cell cycle distribution was determined by PI staining and flow cytometry. Representative histograms are shown. **(F)** Quantitative evaluation of cell cycle distribution in HT29 cells exposed to increasing concentrations of devimistat for up to 72 h. Data are presented as mean + SEM (n≥3). ns: p>0.05, *p<0.05, **p<0.01; t-test. **(G)** Cell death induction after 48 h in HCT116 and HT29 cells exposed to devimistat followed by AnnexinV/PI staining and flow cytometry. Representative dot plots are shown.

Figure S2

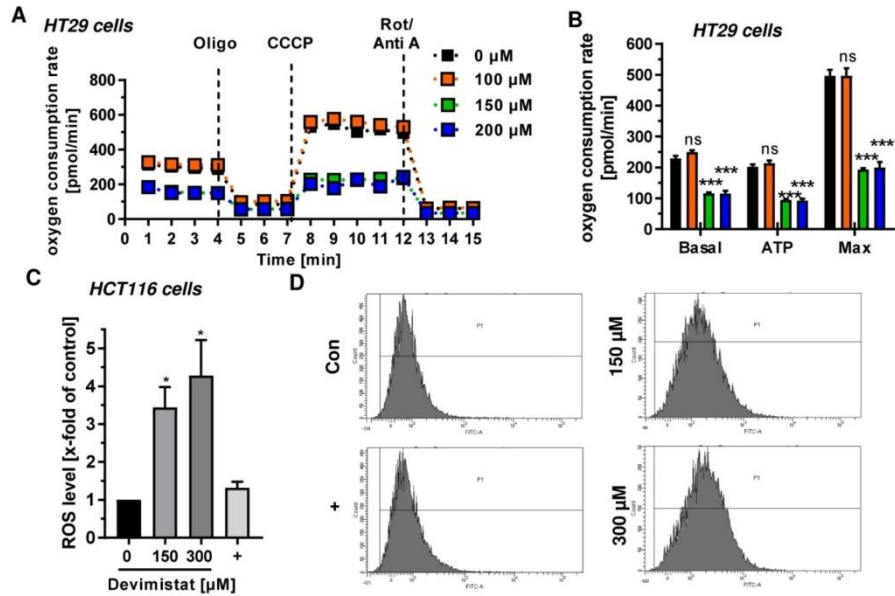


Figure S2: Devimistat triggered disruption of mitochondrial function in CRC cells. (A) HT29 cells were incubated with increasing doses of devimistat for 24 h. Oxygen consumption rate (OCR) was determined with Seahorse metabolic analyser. OCR was measured basally and after the addition of mitochondrial inhibitors Oligomycin (Oligo), CCCP and Rotenone/Antimycin A (Rot/Anti A) (n≥3). **(B)** Basal, ATP-coupled and maximal respiration as determined in A. **(C)** and **(D)** ROS level in HCT116 cells after incubation with devimistat for 2 h under hypoxic conditions (7 % O₂). ROS formation was assessed by H₂DCFDA staining and flow cytometry. tBOOH (200 μM; 20 min) was included as positive control. Representative histograms are shown. Data in A – C are presented as mean + SEM. ns: p>0.05, *p<0.05, ***p<0.001; t-test.

Figure S3

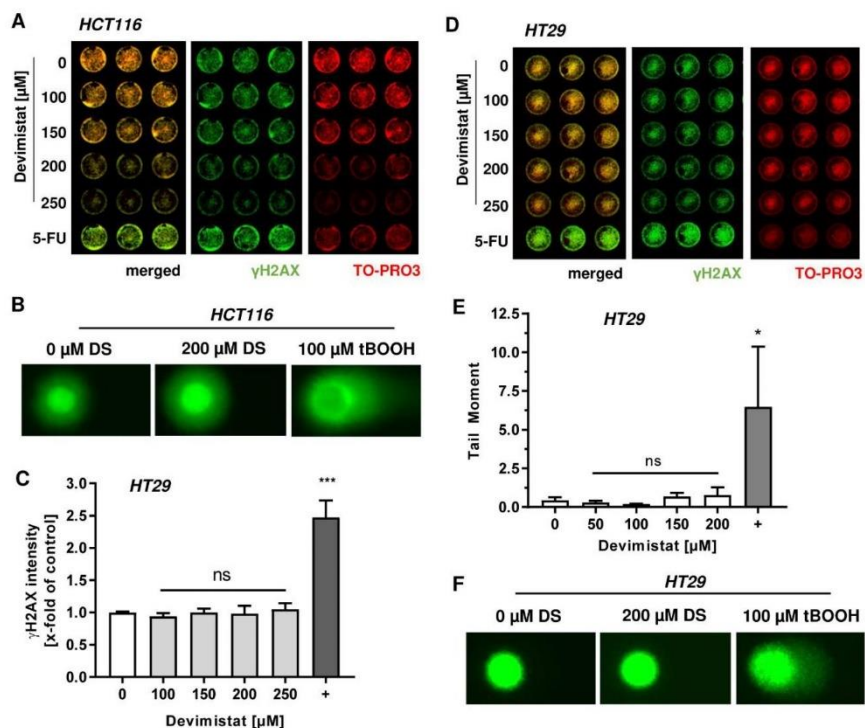


Figure S3: Lack of genotoxicity in CRC cells after devimistat treatment. (A) Representative In Cell Western images from HCT116 cells exposed to devimistat or 5-FU. (B) Representative pictures of the alkaline Comet assay conducted in HCT116 cells after treatment with devimistat (DS) or tBOOH. (C) HT29 cells were incubated with increasing concentrations of devimistat for 24 h and subjected to In Cell Western analysis of the DNA damage marker γH2AX . Incubation with 10 μM 5-FU served as positive control (+). (D) Representative In Cell Western images from HT29 cells. (E) HT29 cells were treated as described in (C). Subsequently, DNA strand break formation was assessed by the alkaline Comet assay. Incubation with 200 μM tBOOH was used as positive control (+). (F) Representative pictures of the alkaline Comet assay conducted in HT29 cells after treatment with devimistat (DS) or tBOOH. Data in C and E are presented as mean + SEM (n=3). ns: $p > 0.05$, * $p < 0.05$, *** $p < 0.001$; t-test.

Figure S4

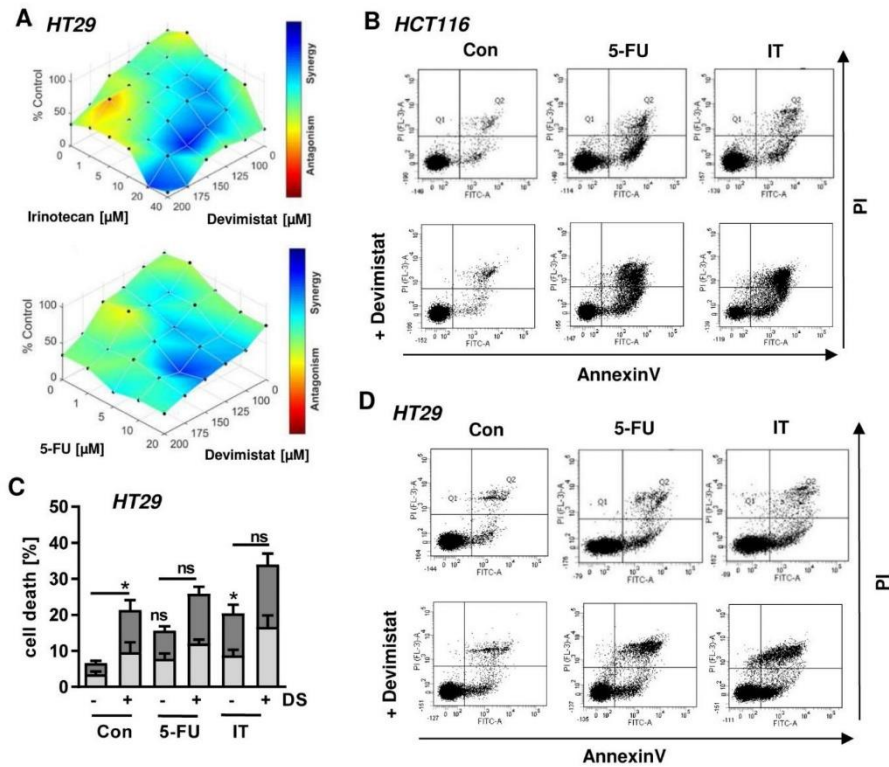


Figure S4: Synergism of devimistat with anticancer drugs in HT29 and HCT116 CRC cells. (A) The 3D-diagrams show Combeneft analysis of the combination regimens 5-FU + devimistat and irinoitecan (IT) + devimistat in HT29 cells using cell viability data after 72 h of incubation as indicated. Arithmetically averaged data of three independent experiments were used for analysis. (B) HCT116 cells were treated as indicated (10 μ M 5-FU, 20 μ M IT, 200 μ M devimistat [DS]) for 48 h. Cell death analysis was performed by Annexin V/PI staining and flow cytometry ($n \geq 3$). Representative dot plots are shown. (C) HT29 cells were treated as indicated (10 μ M 5-FU, 20 μ M IT, 200 μ M DS) for 48 h. Cell death analysis was performed by Annexin V/PI staining and flow cytometry ($n \geq 3$). ns: $p > 0.05$, * $p < 0.05$; 2-way-ANOVA. (D) Representative dot plots in HT29 cells treated as described in (C).

Figure S5

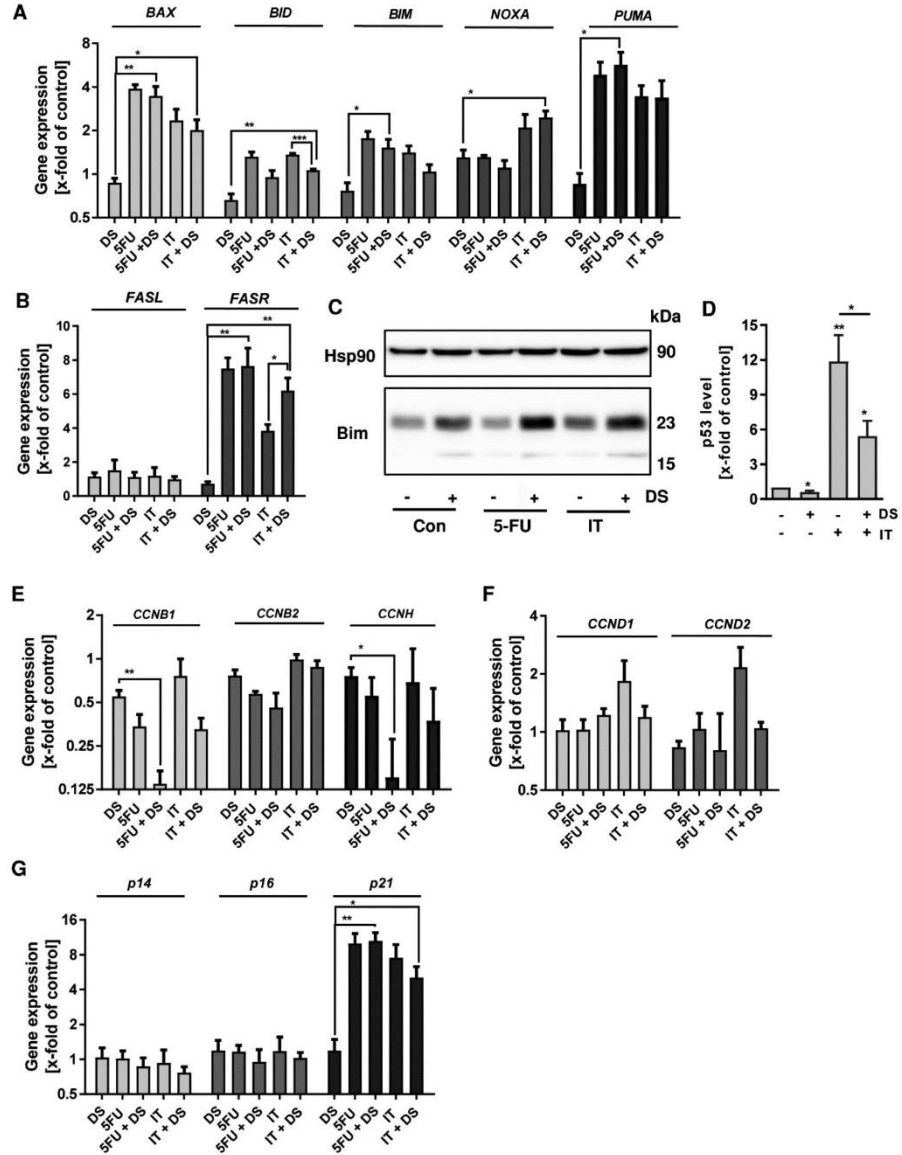


Figure S5: Effects of devimistat combination therapy on cell death induction and gene expression levels in CRC cells. (A) and (B) Expression levels of pro-apoptotic genes in HCT116 cells treated as indicated (10 μ M 5-FU, 20 μ M irinotecan [IT], 200 μ M devimistat [DS]) for 24 h. Gene expression was assessed by quantitative Real-Time PCR

(n=3). **(C)** Protein expression of pro-apoptotic Bim in HT29 cells treated as indicated (10 μ M 5-FU, 20 μ M IT, 200 μ M DS) for 24 h. Whole cell lysates were analysed by SDS-PAGE followed by western blot detection of Bim. Hsp90 served as loading control. A representative western blot is shown. **(D)** p53 level in HCT116 cells following single or combination treatment. Cells were exposed to 20 μ M IT, 200 μ M DS or the combination regimen for 24 h. Quantitative evaluation of p53 western blot analysis (n=3). **(E) - (G)** Gene expression levels of cyclins and cyclin-dependent kinase inhibitors in HCT116 cells treated as described in A for 24 h. Gene expression was determined by quantitative Real-Time PCR (n=3). Data in A, B, D – G are presented as mean + SEM. ns: $p > 0.05$ is not shown, * $p < 0.05$, ** $p < 0.01$, *** $p < 0.001$; t-test.

Figure S6

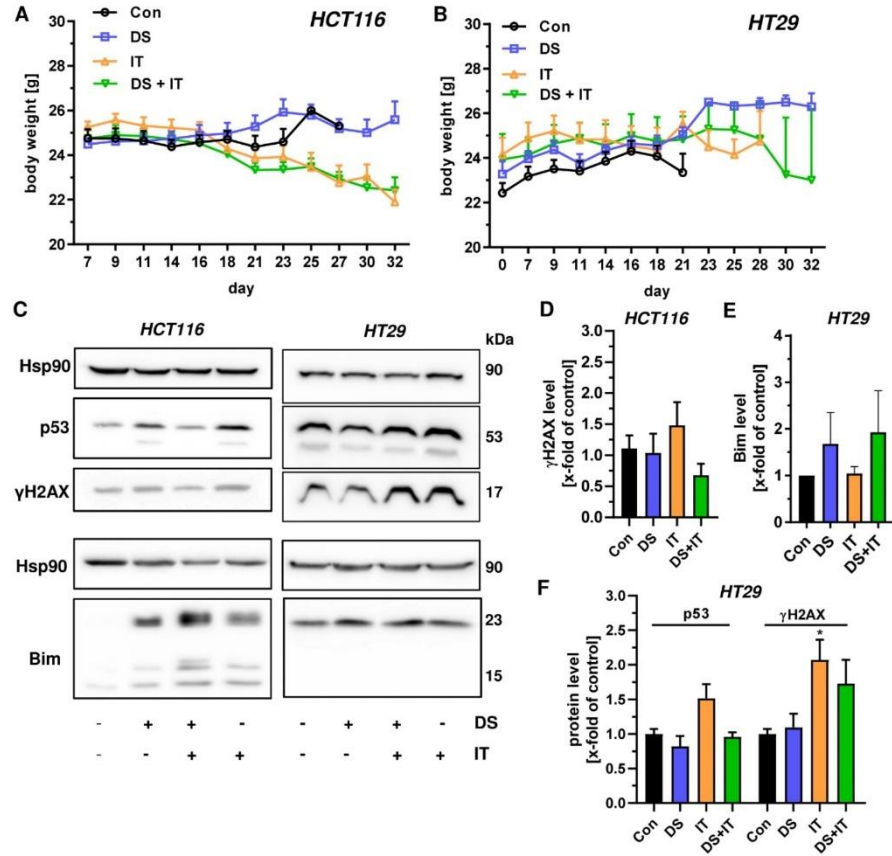


Figure S6: General toxicity as well as impact on DNA damage response markers and Bim in CRC xenograft mouse models treated with devimistat and IT. (A) and (B) Body weight gain curves of animals during xenograft experiments. Mice were inoculated subcutaneously with CRC cells into both flanks and tumours were allowed to develop for 7 days. Animals were then grouped (n=7/group with two tumours/animal) and either received mock treatment, devimistat [DS] (25 mg/kg BW, 2x/week), IT (40 mg/kg BW, 1x/week) or devimistat [DS] + IT. **(C)** Analysis of DNA damage response markers and the BH3-only protein Bim in tumour xenografts. Snap frozen tumour segments were lysed, subjected to SDS-PAGE and Western Blot analysis. Shown are representative western blots for p53, γH2AX, Bim and the loading control Hsp90 in HCT116 and HT29 xenograft tumours. **(D) –**

(F) Quantitative evaluation of Western Blots in HCT116 and HT29 cells (n=4 for HCT116, n=3 for HT29). Data are depicted as mean + SEM. Ns: p>0.05 is not shown, *p<0.05, t-test.

Supplementary Tables

Table S1: Primers used for qPCR

qPCR target	Forward Primer (5'-3')	Reverse primer (5'- 3')
ACTB	TGGCATCCACGAACTACC	GTGTTGGCGTACAGGTCTT
BAX	CAGAAGGCACTAATCAAG	ATCAGATGTGGTCTATAATG
BCL2	TTCAGAGACAGCCAGGAGAAA	AGTACCTGAACCGGCACCT
BCL-x _L	AAGCGTAGACAAGGAGAT	TAGGTGGTCATTCAGGTAA
BID	GTGTGGATGATATGAAGGC	GAAGACAGGCTGGAAGATA
BIM	CCAATGGCAAAGCAACCTTCTG	CTGTCAATGCATTCTCCACACC
CCNB1	CATAGTTAGTTCCATCAGGTATT	CCTTCGGAGAGCATCTAA
CCNB2	GGAGACTCTGTACATGTGCGT	AGAGCAGAGCAGTAATCCCA
CCND1	CATCTACACCGACAACCTCCATCC	GAGGCGGTAGTAGGACAGGAAGT
CCNE1	ATTAACCAATCCAGAAGAAT	GCAAATAGAGAGGAAGTC
CCNH	TAAGTTGCTGTATAAGAAGT	AATGTATCTAGTCCTCAGT
FASL	GGGATGTTTCAGCTCTTCCA	TAAATGGGCCACTTTCTCTCA
FASR	AGAACTTGGAAAGGCCTGCAT	CTGGTTCATCCCCATTGACT
GAPDH	CATGAGAAGTATGACAACAG	ATGAGTCCTTCCACGAT
NOXA	ACACGGTGGACGTCCTGT	ACGAAGCACTTGGGGAAGAT
p14	CCCTCGTGCTGATGCTACTG	CATCATGACCTGGTCTTCTAGGAA
p16	GGAGCAGCATGGAGCCTTC	CATCATCATGACCTGGATCG
p21	TACATCTTCTGCCTTAGT	TCTTAGGAACCTCTCATT
PUMA	GACGACCTCAACGCACAGTA	CTGGGTAAGGCAGGAGTC
Survivin	ATGACTTGTGTGTGATGA	GTTTGTGCTATTCTGTGAA

Table S2: Antibodies used in this study

Antibody	Catalog No.	Provider
Anti-Bim, rabbit monoclonal	2933	Cell Signaling Technology, Danvers, Massachusetts, USA
Anti-p53 (DO-1), monoclonal mouse	sc-126	Santa Cruz Biotechnology, Heidelberg, Germany
Anti-Hsp90 (F8), monoclonal mouse	sc-13119	Santa Cruz Biotechnology, Heidelberg, Germany
Anti-γH2AX, monoclonal rabbit	ab81299	Abcam, Cambridge, UK
Mouse IgGκ binding protein HRP	sc-516102	Santa Cruz Biotechnology, Heidelberg, Germany
Goat-anti-Rabbit-HRP	7074S	Cell Signaling Technology, Danvers, Massachusetts, USA
Goat-anti-Mouse-HRP	sc-2005	Santa Cruz Biotechnology, Heidelberg, Deutschland
Goat-anti-Rabbit-HRP	sc-2004	Santa Cruz Biotechnology, Heidelberg, Germany

Table S3: Combination Indices (CI) for devimistat with standard chemotherapeutics IT and 5-FU in CRC cell lines. Calculation with the Chou Talalay method based on cell viability data obtained by ATP assays after 72 h of incubation using the constant ratio approach (n=3).

CI	Devimistat
<i>HCT116</i>	
IT	0.39 (+++)
5-FU	0.87 (+)
<i>HT29</i>	
IT	1.31 (--)
5-FU	0.65 (+++)

3.2. Natural Merosesquiterpenes Activate the DNA Damage Response via DNA Strand Break Formation and Trigger Apoptotic Cell Death in p53-Wild-Type and Mutant Colorectal Cancer

Publication II

Apisada Jiso, Philipp Demuth, Madeleine Bachowsky, Manuel Haas, Nina Seiwert, Daniel Heylmann, Birgit Rasenberger, Markus Christmann, Lea Dietrich, Thomas Brunner, Riyanti, Till Schäberle, Anuchit Plubrukarn, Jörg Fahrer

Publication II, of which I am second author, was prepared in an international cooperation with 13 coauthors. The tested merosesquiterpenes were provided by the Department of Pharmacognosy and Pharmaceutical Botany at the Prince of Songkla University in Hat-Yai, Thailand and were subsequently characterized at the Fraunhofer Institute for Molecular Biology and Applied Ecology (IME) at the Branch for Bioresources in Giessen. I was involved in methodology, validation, formal analysis and investigation as well as visualization, review and editing of the original draft. In regard to experiments, I performed the western blot analysis of Bim, measurement of intracellular ROS after treatment with merosesquiterpenes, flow cytometry-based cell death measurement, and quantification of γ H2AX by confocal microscopy. Additionally, I investigated the effects of selected merosesquiterpenes in murine tumor organoids.

This publication appeared in the peer-reviewed journal *Cancers* (Volume 13) in June 2021.

Jiso, A., Demuth, P., Bachowsky, M., Haas, M., Seiwert, N., Heylmann, D., Rasenberger, B., Christmann, M., Dietrich, L., Brunner, T., Riyanti, Schäberle, T.F., Plubrukarn, A., Fahrer, J., 2021a. Natural Merosesquiterpenes Activate the DNA Damage Response via DNA Strand Break Formation and Trigger Apoptotic Cell Death in p53-Wild-Type and Mutant Colorectal Cancer. *Cancers* (Basel) 13, 3282.

DOI: <https://doi.org/10.3390/cancers13133282>



Article

Natural Merosesquiterpenes Activate the DNA Damage Response via DNA Strand Break Formation and Trigger Apoptotic Cell Death in p53-Wild-Type and Mutant Colorectal Cancer

Apisada Jiso ^{1,2}, Philipp Demuth ¹, Madeleine Bachowsky ¹, Manuel Haas ¹, Nina Seiwert ¹, Daniel Heylmann ³, Birgit Rasenberger ⁴, Markus Christmann ⁴, Lea Dietrich ⁵, Thomas Brunner ⁵, Riyanti ^{6,7}, Till F. Schäberle ^{6,8}, Anuchit Plubrukarn ² and Jörg Fahrer ^{1,3,*}

¹ Division of Food Chemistry and Toxicology, Department of Chemistry, Technical University of Kaiserslautern, 67663 Kaiserslautern, Germany; jiso.apisada@gmail.com (A.J.); pdemuth@rhrk.uni-kl.de (P.D.); madele.bach@online.de (M.B.); manhaas@rhrk.uni-kl.de (M.H.); seiwert@rhrk.uni-kl.de (N.S.)

² Department of Pharmacognosy and Pharmaceutical Botany, Faculty of Pharmaceutical Sciences, Prince of Songkla University, Hat-Yai, Songkhla 90112, Thailand; anuchit.pl@psu.ac.th

³ Rudolf Buchheim Institute of Pharmacology, Justus Liebig University Giessen, 35392 Giessen, Germany; Daniel.Heylmann@pharma.med.uni-giessen.de

⁴ Institute of Toxicology, University Medical Center Mainz, 55131 Mainz, Germany; rasebi00@uni-mainz.de (B.R.); mchristm@uni-mainz.de (M.C.)

⁵ Biochemical Pharmacology, Department of Biology, University of Konstanz, 78464 Konstanz, Germany; lea.dietrich@uni-konstanz.de (L.D.); thomas.brunner@uni-konstanz.de (T.B.)

⁶ Institute for Insect Biotechnology, Justus-Liebig-University Giessen, 35392 Giessen, Germany; Riyanti@bio.uni-giessen.de (R.); Till.F.Schaeberle@agr.uni-giessen.de (T.F.S.)

⁷ Faculty of Fisheries and Marine Science, Jenderal Soedirman University, Purwokerto 53122, Indonesia

⁸ Fraunhofer Institute for Molecular Biology and Applied Ecology (IME), Branch for Bioresources, 35392 Giessen, Germany

* Correspondence: fahrer@chemie.uni-kl.de; Tel.: +49-6312052974



Citation: Jiso, A.; Demuth, P.; Bachowsky, M.; Haas, M.; Seiwert, N.; Heylmann, D.; Rasenberger, B.; Christmann, M.; Dietrich, L.; Brunner, T.; et al. Natural Merosesquiterpenes Activate the DNA Damage Response via DNA Strand Break Formation and Trigger Apoptotic Cell Death in p53-Wild-Type and Mutant Colorectal Cancer. *Cancers* **2021**, *13*, 3282. <https://doi.org/10.3390/cancers13133282>

Academic Editor:
Fortunato Ciardiello

Received: 18 May 2021
Accepted: 27 June 2021
Published: 30 June 2021

Publisher's Note: MDPI stays neutral with regard to jurisdictional claims in published maps and institutional affiliations.



Copyright: © 2021 by the authors. Licensee MDPI, Basel, Switzerland. This article is an open access article distributed under the terms and conditions of the Creative Commons Attribution (CC BY) license (<https://creativecommons.org/licenses/by/4.0/>).

Simple Summary: Bowel cancer is a serious disease, which affects many people worldwide. Unfortunately, the disease is often diagnosed in an advanced stage, which impairs the chance of survival. Furthermore, resistance to therapy occurs frequently. Thus, novel therapeutic approaches are required to improve cancer therapy. Here, we studied whether merosesquiterpenes might be useful for cancer treatment. These compounds occur in marine sponges and were isolated by our group. We were able to identify three compounds with potent cytotoxic activity in different cell lines established from human large bowel cancer. Our experiments provided evidence that the compounds cause DNA damage and trigger cell death, so-called mitochondrial apoptosis, which was attested in cancer cells with expression of wild-type and mutated p53 tumor suppressor. Finally, we show that merosesquiterpenes also kill intestinal tumor organoids, an ex vivo model of large bowel cancer.

Abstract: Colorectal cancer (CRC) is a frequently occurring malignant disease with still low survival rates, highlighting the need for novel therapeutics. Merosesquiterpenes are secondary metabolites from marine sponges, which might be useful as antitumor agents. To address this issue, we made use of a compound library comprising 11 isolated merosesquiterpenes. The most cytotoxic compounds were smenospongine > ilimaquinone ≈ dactylospontriol, as shown in different human CRC cell lines. Alkaline Comet assays and γ H2AX immunofluorescence microscopy demonstrated DNA strand break formation in CRC cells. Western blot analysis revealed an activation of the DNA damage response with CHK1 phosphorylation, stabilization of p53 and p21, which occurred both in CRC cells with p53 knockout and in p53-mutated CRC cells. This resulted in cell cycle arrest followed by a strong increase in the subG1 population, indicative of apoptosis, and typical morphological alterations. In consistency, cell death measurements showed apoptosis following exposure to merosesquiterpenes. Gene expression studies and analysis of caspase cleavage revealed mitochondrial apoptosis via *BAX*, *BIM*, and caspase-9 as the main cell death pathway. Interestingly, the compounds were equally effective in p53-wild-type and p53-mutant CRC cells. Finally, the cytotoxic activity of the merosesquiterpenes was corroborated in intestinal tumor organoids, emphasizing their potential for CRC chemotherapy.

Keywords: colorectal cancer; chemotherapy; tumor suppressor p53; apoptosis; natural compounds; DNA damage

1. Introduction

Marine sponges are an important source of a plethora of bioactive natural compounds [1]. Merosesquiterpenes belong to these secondary metabolites produced by marine sponges, which were reported to display various biological activities including anti-inflammatory and antibacterial properties [1]. Ilimaquinone (IQ) is a well-studied member of this class. There is increasing evidence that IQ also exerts antiproliferative and/or cytotoxic effects as attested by its growth inhibition of prostate, liver, lung, and pancreatic cancer cells [2]. More recently, IQ was reported to induce apoptosis in oral squamous cell carcinoma, which was attenuated by transient knockdown of the tumor suppressor p53 [3]. In another study, IQ was shown to promote TRAIL-induced cell death in colorectal cancer (CRC) cells via upregulation of TRAIL death receptor expression, which was associated with moderate induction of reactive oxygen species (ROS) [4]. Increased mitochondrial ROS levels were also observed in lung cancer cells exposed to IQ, leading to apoptosis induction [5]. Moreover, it was reported that IQ causes the accumulation of p53 in two CRC cell lines and can induce cell death on its own [6]. Very recently, IQ has been identified as an activator of the DNA damage response (DDR) within a large screen consisting of 296 natural compounds [7]. Consistent with this finding, IQ was toxic in pancreatic cancer cells without anticancer drug treatment [7]. Smenospongine (SP) is a structurally related compound, which was hardly studied with regard to its putative cytotoxic effects in cancer cells until now. It was shown that SP inhibits the growth of different leukemia cell lines and increases the subG1 population, indicative of apoptosis [8]. A more recent study provided evidence that SP eliminates breast cancer stem cells by activating p38 and AMPK-signaling pathways [9]. Collectively, these studies suggest that merosesquiterpenes may have the potential to kill cancer cells and could offer a novel therapeutic option in the treatment of CRC.

CRC is a frequently occurring malignant disease, which is causally linked to various genetic, lifestyle, and dietary risk factors [10–12]. CRC incidence and mortality are increasing in younger people under 50 years of age, particularly in Europe and the United States [13,14]. The treatment of CRC involves surgical resection, chemotherapy, radiation, and, in metastatic disease, targeted therapies [15]. Despite recent progress in CRC therapy, patients with the advanced and metastatic disease still face low 5-year survival rates, highlighting the need for novel therapeutics. These promising therapeutic strategies include inhibitors of tumor cell metabolism such as α -lipoic acid and others [16,17], natural or synthetic small molecules targeting oncogenic signaling mediated by mTOR, AKT, or STAT3 [18], and inhibitors of the DDR [19].

To address this issue, we made use of a compound library comprising 11 naturally occurring merosesquiterpenes. First, the identity and purity of all isolated compounds were characterized by NMR spectroscopy. A cytotoxicity screening was conducted in three CRC cell lines with wild-type p53 (HCT116, RKO) or mutated p53 (HT29), allowing for the calculation of IC₅₀ values. As a next step, the formation of DNA damage and ROS production was evaluated by the alkaline Comet assay, immunofluorescence microscopy, and flow cytometry using the most promising compounds. Activation of the DDR and effects on cell cycle progression were assessed by Western blot analysis and flow cytometry. Furthermore, cell death induction and apoptosis triggered by selected merosesquiterpenes were studied by flow cytometry, Western blot detection, quantitative PCR, and microscopy. The role of p53 was addressed by using isogenic p53 knockout cells and p53 knockdown by siRNA. Finally, the results were translated into a murine tumor organoid model using viability assays, phase-contrast, and fluorescence microscopy.

2. Materials and Methods

2.1. Compounds

The meros sesquiterpenes used in this study (Figure 1) were isolated from the sponges *Haliclona* sp. (smenospongine) [20] and *Verongula rigida* (smenospongine, smenospongiarine, smenospongidine, ilimaquinone, 5-epi-ilimaquinone, quintaquinone, cyclosporgiaquinone-1, smenodiol, dactylospontriol, and 3-farnesyl-2-hydroxy-5-methoxyquinone) [21], as described. All tested compounds were directly used with no additional purification steps. The structures were reauthenticated using spectroscopic analysis, particularly NMR spectroscopy. The spectral data were identical to those reported previously [20–29]. The NMR spectrum of each tested compound revealed almost no signals of impurity. The compounds were stored at $-20\text{ }^{\circ}\text{C}$ until experiments were carried out. Please see Supporting Information for the isolation and ^1H NMR spectral data (Figures S1–S11). The anticancer drug 5-fluorouracil (5-FU) was from Medac (Wedel, Germany) and provided by the pharmacy of the University Medical Center Mainz.

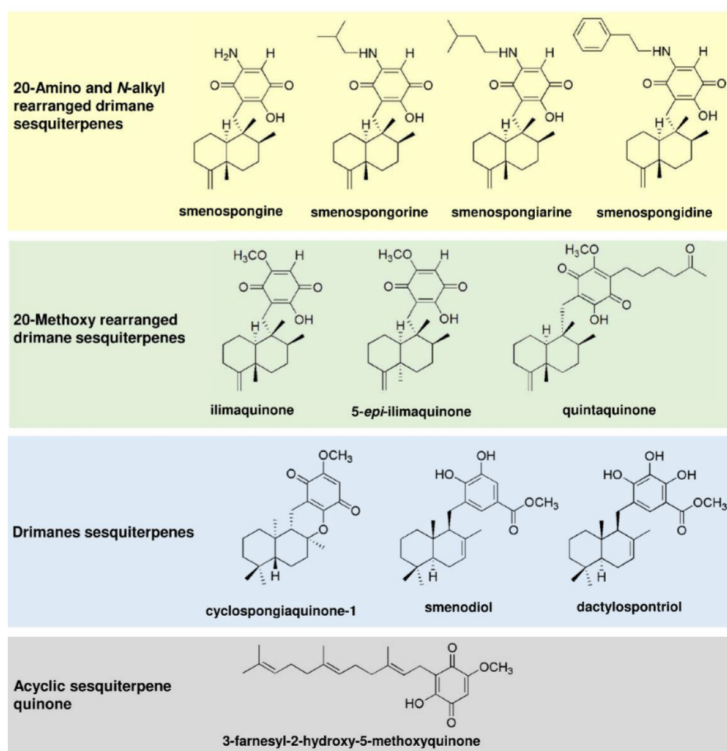


Figure 1. Chemical structures of meros sesquiterpenes used in this study.

2.2. Cell Culture and Treatments

The human CRC cell line HCT116 and isogenic p53-deficient HCT116 cells were provided by Dr. Bert Vogelstein (John Hopkins University, Baltimore, MD, USA). HT29 and RKO cells were provided by the Institute of Toxicology, University Medical Center Mainz, Germany. HCT116 and RKO cells were maintained in DMEM and HT29 cells in RPMI1640 medium supplemented with 10% fetal calf serum and 1% penicillin/streptomycin at 37° C in a humidified atmosphere of 5% CO₂. Media and supplements were obtained from Gibco Life Technologies (Darmstadt, Germany) and PanBiotech (Aidenbach, Germany). All cell lines were mycoplasma negative, as confirmed by routine PCR testing. The meroseresquiterpenes were dissolved in DMSO as a 10 mM stock solution and added to the culture medium reaching a final concentration from 0–100 µM. DMSO served as solvent control (0 µM). Cells were exposed to the compounds for up to 72 h, as indicated.

2.3. Transient Transfection with siRNA

Knockdown of p53 was performed using siGENOME SMARTpool siRNA bought from Dharmacon (Lafayette, CO, USA). Non-sense, scrambled RNA, also purchased at Dharmacon, was used as control. Transfections were carried out, as reported previously [30]. Briefly, HT29 cells were transfected with 20 nM siRNA using Lipofectamine™ RNAiMAX (Thermo Fisher Scientific, Darmstadt, Germany) for 24 h before exposure to ilimaquinone for 48 h. Successful knockdown of p53 was verified by Western blot analysis.

2.4. Preparation of Cell Lysates

Whole-cell extracts were generated as described [31]. After treatment for 48 h, cells were harvested, and whole-cell lysis was performed using a buffer containing 25 mM Tris-HCl pH 8.0, 5 mM EDTA, 1 mM DTT, 0.5 M NaCl supplemented with cOmplete™ protease inhibitor cocktail (Roche Diagnostics, Mannheim, Germany). After incubation for 15 min at 4 °C on a rotating platform, extracts were clarified by centrifugation (10 min, 10,000 × g) and protein content was determined using Bradford assay.

Blue extracts were prepared as published elsewhere [32]. Briefly, cells were treated with the compounds for 24 h, as indicated and harvested in 1 × Lämmli loading buffer.

2.5. SDS-PAGE and Immunoblot Analysis

Western blot analysis was essentially performed as described [33]. Equal protein amounts were separated by SDS-PAGE, followed by wet blot transfer onto a nitrocellulose membrane (PerkinElmer, Rodgau, Germany). Membranes were blocked with 5% nonfat dry milk in TBS/0.1% Tween-20 (TBS-T) for 1 h at RT. Subsequently, primary antibody incubation was carried out overnight at 4° C, followed by three washing steps in TBS/0.1% Tween-20. Membranes were then incubated with appropriate secondary antibodies for at least 1 h at RT. After three washing steps in TBS-T, proteins were detected with Western Lightning® Plus-ECL (PerkinElmer, Rodgau, Germany) using a c300 chemiluminescence imager (azure biosystems, Dublin, CA, USA).

2.6. Antibodies

The following primary antibodies were used: Hsp90α/β (F8, mouse monoclonal; Santa Cruz Biotechnology, Dallas, TX, USA, no. sc-13119), p53 (DO-1, mouse monoclonal; Santa Cruz, no. sc-126), p21 (C-19, rabbit polyclonal; Santa Cruz, no. sc-397), γH2AX (Ser139, rabbit monoclonal; Abcam, Cambridge, United Kingdom, no. ab81299), cleaved caspase-3 (rabbit monoclonal, Cell Signaling Technology, Danvers, MA, USA, no. 9661) and cleaved caspase-9 (rabbit monoclonal, Cell Signaling Technology, no. 7237), phospho-CHEK1 (Ser345; rabbit monoclonal; Cell Signaling Technology, no. 2348), Bim (rabbit monoclonal, Cell Signaling Technology, no. 2933). Secondary antibodies conjugated with horseradish-peroxidase were purchased from Santa Cruz (anti-mouse, no. K2818) and Cell Signaling Technology (anti-rabbit, no. 7074).

2.7. Isolation of RNA, cDNA Synthesis, and Quantitative Real-Time PCR (qPCR)

Gene expression analysis was performed as described [34]. Total RNA was isolated using the NucleoSpin® RNA Kit (Macherey-Nagel, Düren, Germany), and concentrations were determined using a NanoDrop™ 2000 spectrophotometer (Thermo Scientific, Waltham, MA, USA). 0.5 µg of total RNA was transcribed into cDNA using the Verso cDNA Synthesis Kit (Thermo Scientific, Dreieich, Germany). qPCR was performed with the SensiMix™SYBR Green and Fluorescein Kit (Bioline, London, UK) and the CFX96™ Real-Time PCR Detection System (Biorad, München, Germany), with the primers detailed below (Table 1). In all three experiments, qPCR was conducted using biological and technical triplicates. The analysis was performed using CFX Manager™ Software (BioRad, Hercules, CA, USA). Non-transcribed controls were included in each run. Finally, the expression of genes of interest was normalized to GAPDH and ACTB. The solvent control was set to one.

Table 1. Primers used for qPCR analysis.

qPCR Target	Forward Primer (5'-3')	Reverse Primer (5'-3')
ACTB	TGGCATCCACGAAACTACC	GTGTTGGCGTACAGGTCTT
BAX	CAGAAGGCATAATCAAG	ATCAGATGTGGTCTATAATG
BCL2	TTCAGAGACAGCCAGGAGAAA	AGTACCTGAACCGGCACCT
BCL-X _L	AAGCGTAGACAAGGAGAT	TAGGTGGTCATTACAGGTAA
BID	GTGTGGATGATATGAAGGC	GAAGACAGGCTGGAAGATA
BIM	CCAAATGGCAAAGCAACCTTCTG	CTGTCAATGCATTCTCCACACC
clAP1	TTCCAGGTCCTCGTATCA	CCGGCGGGAAAGTTGAATA
clAP2	TCACTCCCAGACTCTTTCCA	CCCCGTGTTCTACAAGTGTC
FASL	GGGATGTTTCAGCTCTTCCA	TAAATGGGCCACTTTCCTCA
FASR	TTATCTGATGTTGACTTGAGTAA	GGCTTCATTGACACCATT
GAPDH	CATGAGAAGTATGACAACAG	ATGAGTCCTTCCACGAT
MDM2	ATCTTGATGCTGGTGTA	AGGCTATAATCTTCTGAGTC
NOXA	TCTTCGGTCACTACACAAC	CCAACAGGAACACATTGAAT
p21	ACCATGTGAGAACCGGCTGGG	TGGGCGGATTAGGGCTTC
PUMA	TAAGGATGGAAAGTGTAG	TTCAGTTTCTCAITGTTAC
Survivin	ATGACTTGTGTGTATGA	GTTTGTGCTATTCTGTGAA

2.8. Measurement of ROS Formation

HCT116 cells grown in 6-well plates were exposed to smenospongine and ilimaquinone at the desired concentration for 24 h. As positive control, cells were treated with 200 µM H₂O₂ in PBS for 20 min. ROS generation was essentially determined as reported [35]. Cells were washed twice with PBS and loaded with CM-H₂DCFDA (Life Technologies, Darmstadt, Germany) in phenol red- and serum-free medium for 30 min. The cells were washed with PBS, detached by Trypsin/EDTA treatment, and collected by centrifugation. Finally, the cell pellets were resuspended in PBS, analyzed using a FACSCanto II flow cytometer (BD Biosciences, Heidelberg, Germany), and evaluated using FACSDiva software 6.0 (BD Biosciences).

2.9. Alkaline Comet Assay

HCT116 cells grown in 6-well plates were exposed to smenospongine and ilimaquinone for 24 h, as indicated. Etoposide (10 µM) served as positive control. Formation of DNA strand breaks and AP sites was assessed using the alkaline Comet assay as reported [36], with a cell lysis step (50 min), followed by alkaline DNA unwinding step (20 min) prior to electrophoresis under alkaline conditions. Following DNA staining with propidium iodide, samples were analyzed by using an Axioskop 2 fluorescence microscope (Zeiss, Jena, Germany). In total, 50 cells per slide were scored using the Comet Assay IV software (Perceptive Instruments, Bury St Edmunds, UK).

2.10. Cell Cycle Analysis

Cell cycle distribution was studied as described previously [37]. Briefly, CRC cells were exposed to the compounds as indicated for 24 h and 48 h, respectively. Attached and detached cells were collected. Cell pellets were washed with ice-cold PBS, followed by a precipitation step with ethanol overnight at $-20\text{ }^{\circ}\text{C}$. Subsequently, cell pellets were resuspended in PBS containing RNase A ($20\text{ }\mu\text{g}/\text{mL}$; Sigma, Deisenhofen, Germany) and incubated for one hour. Finally, propidium iodide (PI; Sigma) was added in a final concentration of $10\text{ }\mu\text{g}/\text{mL}$, and cells were analyzed using a FACSCanto II flow cytometer (BD Biosciences, Heidelberg, Germany). Cell cycle distribution was assessed with FACSDiva software 6.0 (BD Biosciences).

2.11. Cell Death Analysis

Cell death induction was studied by AnnexinV-FITC and PI staining as reported [38]. In short, CRC cells were exposed to the compounds for 48 h, as indicated. Attached and detached cells were harvested following Trypsin/EDTA digestion by centrifugation, washed in PBS, and resuspended in binding buffer (10 mM HEPES pH 7.4, 140 mM NaCl, 2.5 mM CaCl_2 , 0.1% BSA) containing AnnexinV-FITC (Miltenyi Biotec, Bergisch Gladbach, Germany). After incubation on ice for 15 min, a binding buffer containing PI ($50\text{ }\mu\text{g}/\text{mL}$) was added, and samples were subject to flow cytometry using a FACSCanto II (BD Biosciences). Gating of living cells (Annexin V/PI double negative), early apoptotic cells (Annexin V-positive, PI-negative), and late apoptotic/necrotic cells (Annexin V/PI-double positive) and data evaluation was performed with FACSDiva software 6.0 (BD Biosciences).

2.12. Cell Viability Assay and Determination of IC_{50} Values

To analyze the effects of the compounds on cell viability, CRC cells were grown in white 96-well plates overnight and incubated with increasing concentrations for 72 h, as indicated. Cell viability was then assessed with Cell Titer-Glo[®] Luminescent Cell Viability Assay (Promega, Mannheim, Germany) according to the manufacturer's instructions using a Fluoroskan[™] FL 96-well plate reader (Thermo Fisher, Dreieich, Germany). IC_{50} -values were determined by GraphPad Prism 7.0 software as reported previously [39]. To this end, concentrations were transformed into the log scale, plotted against the cell viability and the curve was fitted by nonlinear regression with variable slope, providing the IC_{50} values.

2.13. Analysis of Cell Morphology

CRC cells were treated with the compounds as indicated for up to 48 h. Cell morphology was monitored with a Leica DMi1 microscope equipped with an MC170 camera (Leica, Wetzlar, Germany). Images were acquired with LAS EZ software 3.4.0 (Leica).

2.14. Cultivation of Murine Tumor Organoids and Assessment of Viability

Murine tumor organoids were grown in 3D culture using Cultrex[®] basement membrane extract (BME) (R&D Systems, Inc., Minneapolis, MN, USA) and maintained as described previously [40]. Tumor organoids were collected by removing the culture medium and adding $500\text{ }\mu\text{L}$ of cold DMEM. The BME was destroyed with a pipette tip and tumor organoids were collected in a 15 mL tube. After centrifugation at 100 g for 5 min and removal of the supernatant, 5 mL TrypLE was added, and tumor organoids were digested at $37\text{ }^{\circ}\text{C}$ for 10 min . TrypLE was inactivated by adding 10 mL of DMEM and cells were again centrifuged at 100 g for 5 min . Cells were resuspended in 1 mL basal organoid culture medium, consisting of advanced DMEM/F12, 10 mM HEPES, $100\text{ U}/\text{mL}$ penicillin, $100\text{ mg}/\text{mL}$ streptomycin, $20\text{ mg}/\text{mL}$ nystatin, 1 mM N-acetyl cysteine (all from Sigma, Schnellendorf, Germany), 0.1% BSA (Carl Roth, Karlsruhe, Germany), 2 mM L-glutamine, $1\times$ B27 supplement, $1\times$ N2 supplement (all from Life Technologies, Darmstadt, Germany). Using a 96 well plate, 2.4×10^3 cells were seeded per well by applying $8\text{ }\mu\text{L}$ droplets of a 1:4 mixture of basal culture medium and BME. After polymerization for 30 min , $80\text{ }\mu\text{L}$

of complete culture medium were added, consisting of basal organoid culture medium supplemented with 50 ng/mL murine EGF, 100 ng/mL murine Noggin (all from Peprotech, Hamburg, Germany), 10 mM Nicotinamide, 500 nM A83-01 (all from Sigma, Schnelldorf, Germany), 10 μ M Y-27632 (MedChemExpress, Monmouth Junction, NJ, USA) and mR-Spondin-1 conditioned medium in a final concentration of 20% (*v/v*). Subsequently, tumor organoids were cultivated at 37 °C and 5% CO₂ for 72 h. After exchanging the culture medium, tumor organoids were exposed to smenospongine and ilimaquinone in the desired concentrations as well as 5-FU as the positive control for another 72 h.

Tumor organoid viability was determined by the MTS assay as described [30]. After discarding the medium, 80 μ L basal organoid culture medium containing 75 μ g/mL MTT were added and tumor organoids were incubated for 1 h at 37 °C. BME was solubilized by adding 20 μ L of 10% SDS solution to each well and incubating for 30 min at 37 °C. Absorbance was measured using a microplate reader at 490 nm. Background absorbance was estimated by measuring tumor organoids without added MTT and subtracted from all values. Solvent treated organoids were defined as 100% viable.

2.15. Immunofluorescence Microscopy of CRC Cells and Tumor Organoids

HCT116 cells grown on coverslips were treated with smenospongine and ilimaquinone as indicated and incubated for 24 h. γ H2AX foci formation was analyzed by immunofluorescence microscopy as described elsewhere [32]. After fixation with paraformaldehyde and methanol, cells were blocked in PBS containing 5% BSA and 0.3% Triton X-100 for 1 h. Subsequently, the samples were incubated with a primary antibody directed against γ H2AX (diluted 1:1000; see Section 2.6.) for 1 h. After several washing steps, incubation with a secondary antibody conjugated with Alexa Fluor 488 (1:400; Life Technologies, Darmstadt, Germany) was performed for 1 h. Finally, the samples were mounted using Vectashield[®] containing DAPI (VectorLabs, Burlingame, CA, USA). Analysis was carried out with a Zeiss Axio Observer 7 microscope equipped with an Axiocam 305 mono (Carl Zeiss Microscopy, Jena, Germany). Images were acquired and processed with ZEN software (Carl Zeiss Microscopy, Jena, Germany).

Tumor organoids were seeded in 96-well plates and cultivated, as mentioned above. Tumor organoids were then treated with smenospongine and ilimaquinone in the desired concentrations as well as 5-FU as the positive control for 72 h. Microscopic determination of cell death in tumor organoids was performed by PI/ Hoechst 33342 co-staining, as described elsewhere [41]. Briefly, the organoid culture medium was removed after treatment and PBS containing PI and Hoechst 33342 at a final concentration of 10 μ g/mL each was added for 30 min. The staining solution was exchanged for basal organoid culture medium before analysis by fluorescence microscopy, as described in the last paragraph.

2.16. Statistics

Experiments were performed independently three times, except otherwise stated. Representative experiments are displayed. Values are presented as means + standard error of the means (SEM) using GraphPad Prism 7.0 software. Statistical analysis was performed using a two-sided Student's *t*-test and statistical significance was defined as $p < 0.05$.

3. Results

3.1. Cytotoxicity Screening of Merositerpenes in Human CRC Cell Lines

First, 11 merositerpenes (Figure 1) were analyzed with regard to their cytotoxic potential in 3 colorectal cancer (CRC) cell models, displaying either microsatellite instability (HCT116, RKO) or chromosomal instability (HT29) [42]. Smenospongine (SP) caused a concentration-dependent reduction in cell viability, which was most pronounced in HCT116 cells, followed by HT29 and RKO cells (Figure 2A). Ilimaquinone (IQ) was somewhat less potent than SP and displayed the highest cytotoxicity in HT29 cells (Figure 2B). Dactylospontriol (DS) was most effective in HCT116 cells and exerted similar cytotoxicity in RKO and HT29 cells (Figure 2C). The calculated IC₅₀ values ranged from 8 μ M to 44 μ M

for these three compounds in all CRC cell lines (Table 2). The other compounds tested revealed either weaker cytotoxicity throughout the CRC cell lines (e.g., smenospongiorine and smenodiol) or only showed moderate efficacy in HCT116 cells and were therefore excluded from the analysis in RKO and HT29 cells. Two compounds (smenospongiorine and 3-farnesyl-2-hydroxy-5-methoxyquinone) showed a lack of cytotoxicity in HCT116 cells and were therefore not considered further (Table 2). Taken together, SP, IQ, and DS were identified as the most promising merosessquiterpenes in our initial cytotoxicity screening.

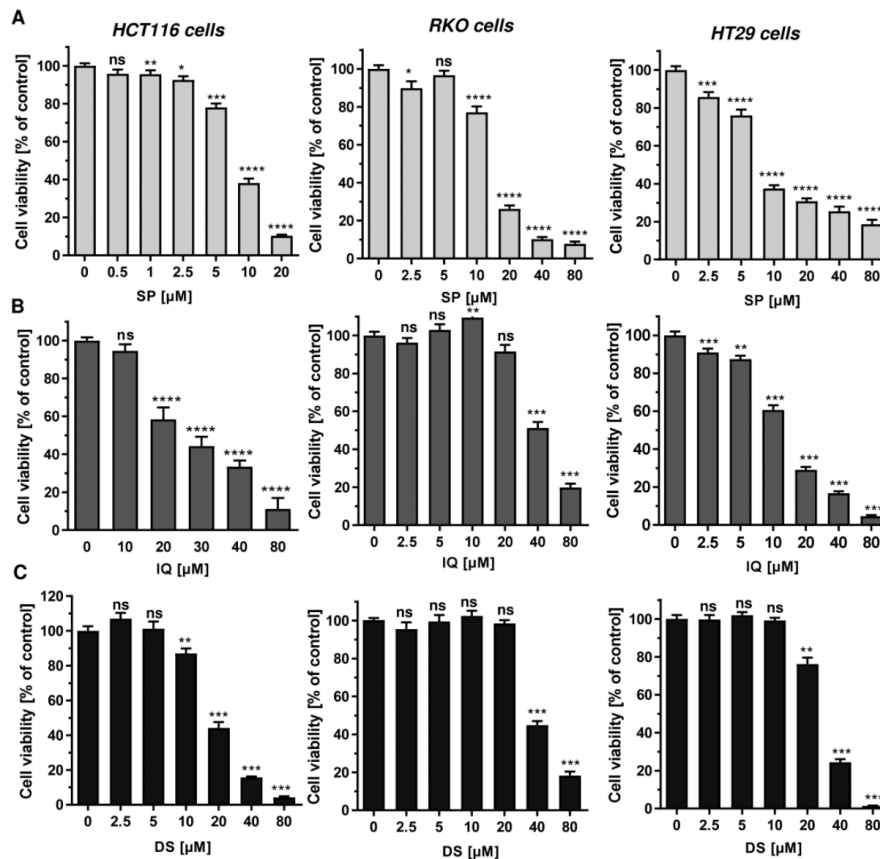


Figure 2. Cytotoxicity of selected merosessquiterpenes in CRC cell lines: (A–C) CRC cells (HCT116, RKO, HT29) were treated with increasing concentration of SP (panel A), IQ (panel B) and DS (panel C) for 72 h. Viability was determined using a luminescent ATP test. Data are presented as mean + SEM ($n = 3$). Not significant (ns): $p > 0.05$; * $p < 0.05$; ** $p < 0.01$; *** $p < 0.001$; **** $p < 0.0001$.

Table 2. IC₅₀ values of merosesquiterpenes analyzed in three CRC cell models.

Compound	HCT116	RKO	HT29
smenospongine	8 μ M	15 μ M	10 μ M
smenospongiorine	39 μ M	58 μ M	37 μ M
smenospongiarine	-	n.d.	n.d.
smenospongidine	80 μ M	n.d.	n.d.
ilimaquinone	27 μ M	43 μ M	13 μ M
5-epi-ilimaquinone	47 μ M	n.d.	n.d.
quintaquinone	80 μ M	n.d.	n.d.
cyclosponiaquinone-1	79 μ M	n.d.	n.d.
smenodiol	31 μ M	66 μ M	42 μ M
dactylospontriol	19 μ M	40 μ M	29 μ M
3-farnesyl-2-hydroxy-5-methoxyquinone	-	n.d.	n.d.

n.d. = not determined.

3.2. Activation of the DNA Damage Response and Impact on Cell Cycle Progression

Next, we studied whether the merosesquiterpenes cause DNA damage and trigger the DNA damage response (DDR). To this end, we used HCT116 cells with wild-type p53 protein and HT29 cells that express p53 with a hot spot mutation in the DNA binding domain [43]. First, DNA strand break formation was analyzed using the alkaline Comet assay, which detects DNA strand breaks and alkali labile sites. A concentration-dependent increase in DNA damage levels was observed after treatment with both SP and IQ (Figure 3A,B). These findings were substantiated by immunofluorescence microscopy of phosphorylated histone 2AX (γ H2AX), a well-established marker for DNA strand breaks that was induced by both merosesquiterpenes (Figure 3C). Western blot analysis revealed a concentration-dependent increase of γ H2AX after SP and DS exposure in HCT116 cells after 24 h (Figure 3D). Furthermore, phosphorylation of the checkpoint kinase 1 (CHK1) was detected (Figures 3D and A1C), also reflecting DDR activation. Consistent with this finding, a simultaneous accumulation of p53 and its downstream target p21 was observed. Interestingly, these effects were even more pronounced than that of the positive control 5-FU, an antimetabolite used for CRC chemotherapy. Similar findings were obtained in p53-mutated HT29 cells, except for CHK1 phosphorylation that was rather unaffected after 24 h (Figure 3B). Furthermore, ROS formation was measured in CRC cells after 24 h, revealing increased ROS levels following treatment with high concentrations of SP and IQ (Figure A1A,B).

Since p53 controls cell cycle progression via p21, the cell cycle distribution was analyzed in both CRC cell lines following treatment with merosesquiterpenes for 24 h. In both CRC cell lines, SP and DS reduced cell density and/or promoted cell rounding, as shown by microscopy (Figure 4A). In HCT116 cells, SP caused an accumulation of cells in the G2-M phase at low concentration, while a high concentration resulted in decreased S-phase population and higher G1 population (Figure 4B,D). DS displayed similar effects at low concentration but increased subG1 at high concentration, the latter being indicative of apoptotic cell death (Figure 4C,E). In HT29 cells, SP at high concentration caused a G1 arrest with a decreased number of cells in the S-phase (Figure A2A,C), whereas DS moderately induced subG1 population (Figure A2B,D).

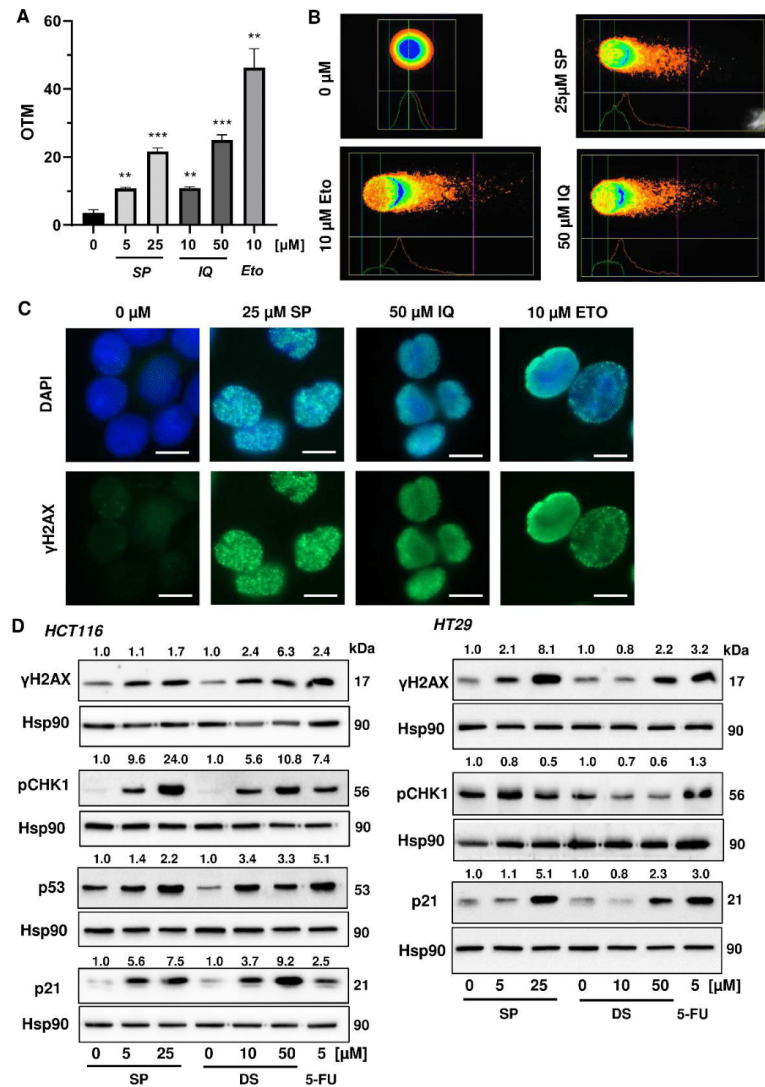


Figure 3. Induction of DNA strand breaks and DNA damage response in CRC cells after treatment with merosquiterpenes: (A) HCT116 cells were treated with SP or IQ as indicated for 24 h. The anticancer drug etoposide was included as positive control. DNA strand break induction was determined by the alkaline Comet assay. Data are presented as mean + SEM ($n = 3$). ** $p < 0.01$, *** $p < 0.001$; (B) representative images of Comet assay shown in A; (C) HCT116 cells were treated as described in (A). Formation of the DNA damage marker γ H2AX was visualized by immunofluorescence microscopy. Nuclei are depicted in blue, while γ H2AX is shown in green. Representative pictures are displayed. Scale bar: 10 μ m; (D) HCT116 cells were treated with SP or IQ, as indicated, for 24 h. The anticancer drug 5-FU was included as positive control. Samples were analyzed by SDS-PAGE and Western Blot detection of γ H2AX, p-CHK1, p53, and p21. Hsp90 served as loading control. Representative blots are shown together with the densitometry evaluation.

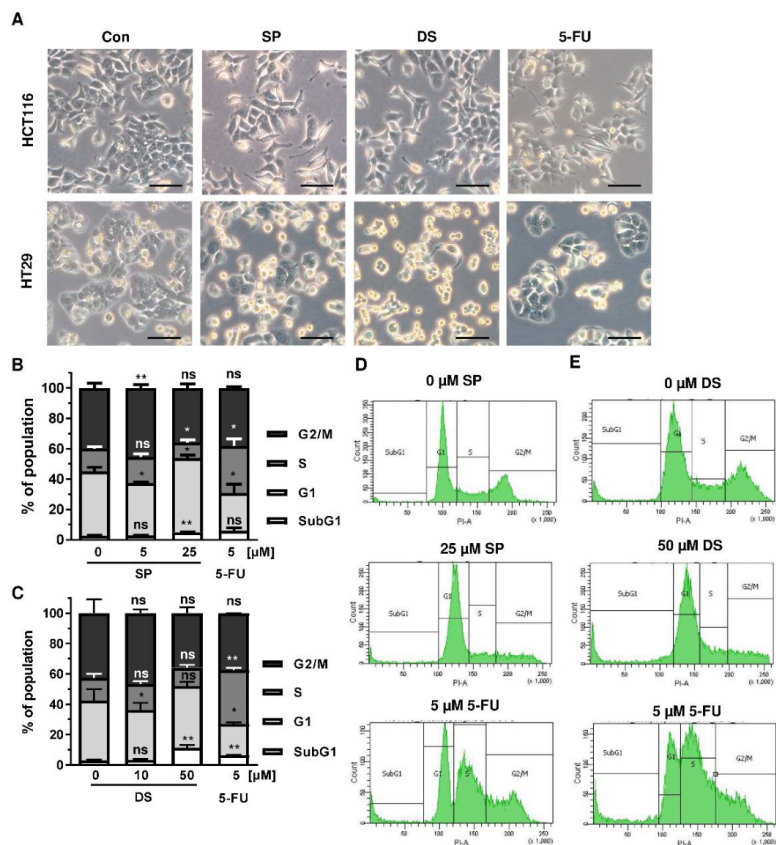


Figure 4. Effects on morphology and cell cycle distribution in CRC cells after treatment with merosquiterpenes: (A) HCT116 and HT29 cells were incubated with solvent control, 25 μM SP, 50 μM DS and 5 μM 5-FU for 24 h. Cell morphology was observed by light microscopy. Representative pictures are shown. Scale bar: 25 μm; (B,C) cell cycle analysis in HCT116 cells challenged with increasing concentrations of SP (B) and DS (C), respectively, for 24 h, and 5-FU served as positive control. Data are given as mean + SEM ($n \geq 3$). Not significant (ns): $p > 0.05$; * $p < 0.05$; ** $p < 0.01$; (D,E) representative histograms of cell cycle analysis shown in (B,C).

We then analyzed how prolonged exposure to SP and DS over 48 h affects morphology and cell cycle distribution in HCT116 and HT29 cells. Microscopy revealed drastic morphological changes with increased cell rounding and detachment of cells, strongly suggesting cell death induction (Figure 5A). In agreement with these observations, SP and DS caused a huge increase of the subG1 population in HCT116 cells at high concentrations (Figure 5B–E), which was also detected in HT29 cells (Figure A3A–D). Treatment with lower concentrations of both compounds induced a pronounced G2-M arrest in the tested CRC cell lines. Interestingly, the positive control 5-FU exerted also potent cytotoxic effects in HCT116 cells (Figure 5), whereas 5-FU had little impact on HT29 cells, as attested by lack of subG1 (Figure A3).

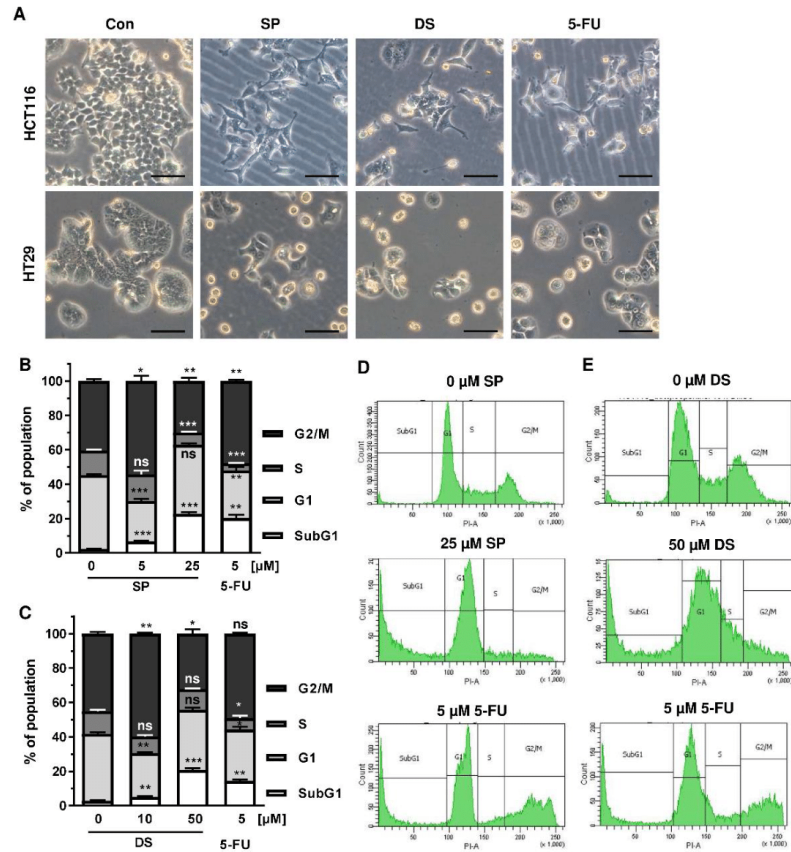


Figure 5. Morphological changes and cell death induction by merosquiterpenes in CRC cells: (A) HCT116 and HT29 cells were incubated with solvent control, 25 μM SP, 50 μM DS and 5 μM 5-FU for 48 h. Cell morphology was observed by light microscopy. Representative pictures are shown. Scale bar: 25 μm; (B,C) cell cycle analysis in HCT116 cells treated with increasing concentrations of SP (B) and DS (C), respectively, for 48 h, and 5-FU served as positive control. Data are given as mean + SEM ($n \geq 3$). Not significant (ns): $p > 0.05$; * $p < 0.05$; ** $p < 0.01$; *** $p < 0.001$; (D,E) representative histograms of cell cycle analysis performed in (B,C).

In conclusion, our results demonstrated that merosquiterpenes cause DNA strand breaks, activate the CHK1-p53-p21 mediated DDR, affect cell cycle progression in p53-mutant and p53-wild-type cells, and increase the subG1 population indicative of cell death.

3.3. Cell Death Induction by Merosquiterpenequinones and Impact of p53

In order to investigate the cell death mechanism and the role of p53, we made use of isogenic HCT116 cells proficient and deficient for p53 (HCT116-p53^{+/+} vs. HCT116-p53^{-/-}). Both cell lines were exposed to increasing concentrations of smenospongine for 48 h, and cell death was analyzed by Annexin V/PI staining. SP induced both early apoptosis and late apoptosis/necrosis, which was significantly reduced in HCT116 p53 k.o. cells (Figure 6A,B). However, a marked increase in dead cells (i.e., only PI positive) was observed in HCT116-p53^{-/-} cells after treatment with SP at high concentration. In addition, 5-FU triggered cell death in a p53-dependant manner in HCT116 cells as expected,

whereas the p53 status did not affect cell killing by etoposide (Figure A4A,B). Microscopic inspection revealed a similar ratio of round and detached cells in both isogenic HCT116 cell lines but a somewhat higher cell density in p53 k.o. cells (Figure A4C).

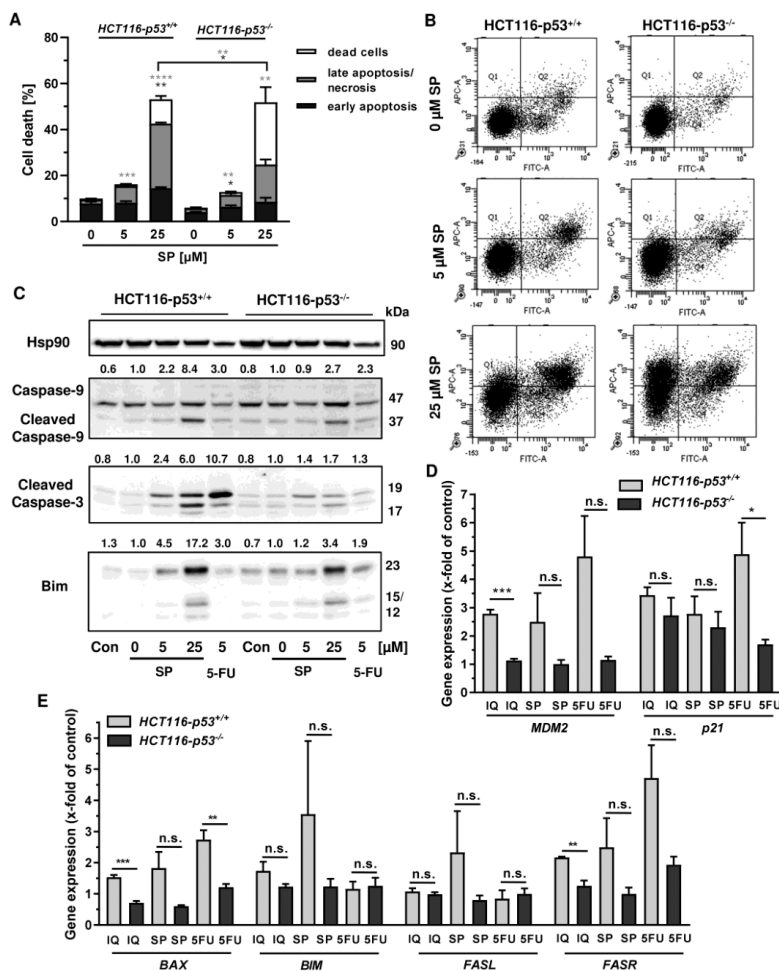


Figure 6. Impact of p53 status on merosquiterpenes triggered cell death in CRC cells: (A) isogenic HCT116-p53^{+/+} and HCT116-p53^{-/-} cells were exposed to increasing concentrations of SP for 48 h. Cell death induction was assessed by Annexin V-FITC/PI staining and flow cytometry. Data are shown as mean + SEM (n = 3). Not significant (ns): p > 0.05; * p < 0.05; ** p < 0.01; *** p < 0.001; **** p < 0.0001; (B) representative dot plots of (A); (C) isogenic HCT116 cell lines differing in their p53 status were exposed to increasing concentration of SP for 48 h. 5-FU was included as positive control and untreated cells as the corresponding negative control. Samples were subject to SDS-PAGE, followed by Western blot analysis of cleaved caspase-3, cleaved caspase-9, and Bim. Hsp90 was included as the loading control. Representative blots are shown including the densitometric evaluation; (D) expression levels of *MDM2* and *p21* in p53-proficient and -deficient HCT116 cells treated with 50 μM IQ, 25 μM SP and 5 μM 5-FU for 24 h. Gene expression was assessed by qPCR (n = 3); (E) expression levels of proapoptotic genes (*BAX*, *BIM*, *FASL*, *FASR*) in HCT116 cells differing in their p53-status treated as described in (D). Gene expression was assessed by qPCR (n = 3). Not significant (ns): p > 0.05; * p < 0.05; ** p < 0.01; *** p < 0.001.

Since both Annexin/PI staining and analysis of cell cycle distribution indicated apoptosis induction by SP, the cleavage of the caspase-3 and caspase-9 was assessed by Western blot detection. The experiments demonstrated a concentration-dependent cleavage of both caspases upon SP treatment, which was strongly attenuated in p53-deficient HCT116 cells, particularly for caspase-9 (Figure 6C). Similar to this finding, caspase-9 cleavage by 5-FU treatment was completely blocked in HCT116 p53 k.o. cells (Figure 6C). IQ also caused caspase-9 and caspase-3 cleavage, which was much more prominent in HCT116 cells with p53 expression (Figure A5A). Furthermore, the proapoptotic BH3-only protein Bim was analyzed, revealing a concentration-dependent increase in HCT116 p53 WT cells upon both SP and IQ treatment (Figures 6C and A5A). This effect was strongly attenuated in HCT116 p53 k.o. cells. Interestingly, the p53 status had no impact on Bim levels after challenge with 5-FU, which were found moderately elevated in both isogenic HCT116 cell lines (Figures 6C and A5A).

The impact of p53 on the mode of cell death triggered by merosquiterpenes was further studied by gene expression analysis using qPCR. The p53 negative feedback regulator *MDM2* was induced in HCT116-p53^{+/+} cells by both SP and IQ, as well as the positive control 5-FU, which was completely abolished in p53 k.o. cells (Figure 6D). Furthermore, the cell cycle regulator *p21* was substantially upregulated by all test compounds. Interestingly, this effect was strongly repressed in HCT116-p53^{-/-} cells after 5-FU incubation but was almost as strong after treatment with both merosquiterpenes (Figure 6D). Both SP and IQ induced the expression of the proapoptotic genes *BAX*, *BIM*, *FASL*, and *FASR*, with higher levels in p53-proficient HCT116 cells (Figure 6E). Other proapoptotic genes such as *BID*, *NOXA*, and *PUMA* were hardly influenced by SP and IQ (Figure A5B). Antiapoptotic genes including *cIAP1*, *BCL2*, and *BCL-XL* were only slightly regulated, which occurred to a similar extent in both isogenic HCT116 cell lines (Figure A5C,D). Only *cIAP2* was found to be upregulated in p53-proficient HCT116 cells, which was reduced in p53 k.o. cells. The expression of *survivin* was repressed by all test compounds in a p53-independent manner (Figure A5C). In summary, our findings showed that merosquiterpenes induce apoptosis in a p53-dependent manner in HCT116 cells, which involved mainly the intrinsic mitochondrial pathway via the Bim–Bax–caspase-9–caspase-3 axis. Intriguingly, SP and IQ caused similar cell death rates independent of the p53 status despite reduced apoptosis induction in the absence of p53 (see Figure 6A).

3.4. Influence of Mutant p53 on Cell Death Induction

Given that p53 is frequently mutated in CRC, we wanted to know whether mutant p53 affects the sensitivity of CRC cells towards merosquiterpene treatment. First, Annexin V/PI-staining was performed in p53-mutated HT29 cells and showed induction of apoptotic and necrotic cell death by SP and IQ after 48 h (Figure 7A,B). Western blot analysis revealed caspase-9 and caspase-3 cleavage following treatment with SP and IQ, which was also observed upon exposure to 5-FU (Figure 7C). Furthermore, both merosquiterpenes caused induction of the proapoptotic protein Bim (Figure 7C). In order to characterize the role of mutant p53, a siRNA-mediated p53 knockdown was carried out in HT29 cells. As shown before, IQ caused substantial levels of cell death similar to the 5-FU treatment (Figure 7D,E). In contrast to HCT116 cells, downregulation of p53 had no impact on cell death induction triggered by IQ in HT29 cells (Figure 7D,E). Moreover, 5-FU-dependent cell death only slightly decreased upon p53 downregulation, which also contrasts with the results obtained in isogenic HCT116 cells (see Figure A4). Taken together, these findings provide evidence that merosquiterpenes eliminate CRC cells independent of mutant p53 expression via apoptosis.

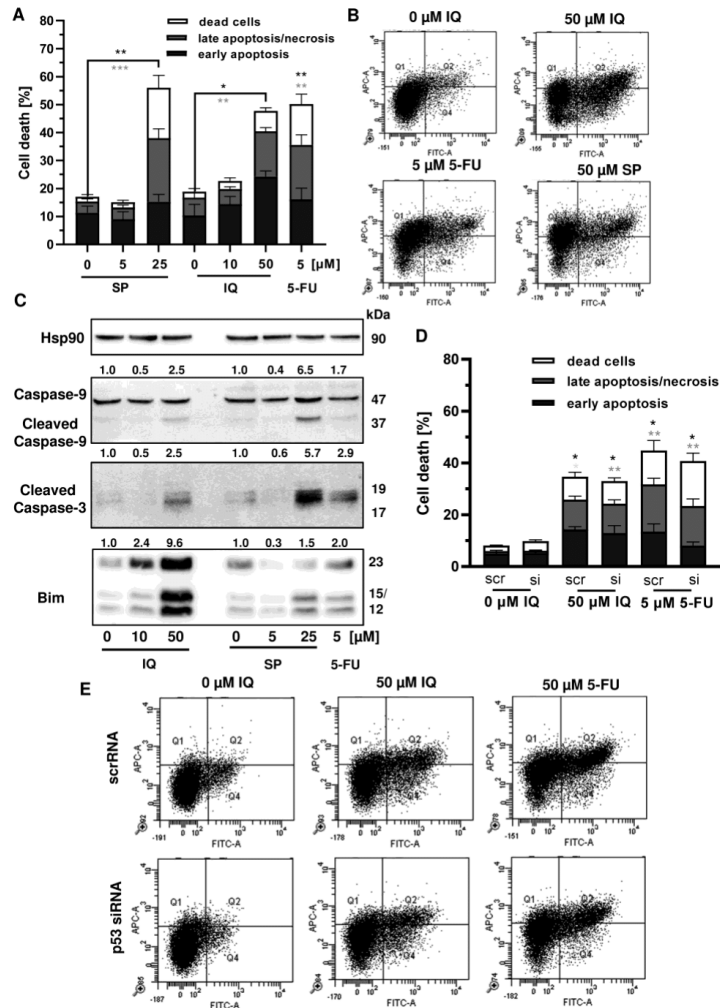


Figure 7. Cell death induction by merosquiterpenes in p53-mutant CRC cells: (A) HT29 cells were incubated with increasing concentrations of SP or IQ, and 5-FU was included as positive control. Cell death induction was assessed by Annexin V-FITC/PI staining and flow cytometry. Data are depicted as mean + SEM ($n = 5$). Not significant (ns): $p > 0.05$; * $p < 0.05$; ** $p < 0.01$; *** $p < 0.001$; (B) representative dot plots of (A); (C) HT29 cells were exposed to increasing concentrations of IQ or SP for 48 h, and 5-FU was included as positive control. Samples were separated by SDS-PAGE, followed by Western blot analysis of cleaved caspase-3, cleaved caspase-9, and Bim. Hsp90 served as loading control. Representative blots are shown including the densitometric evaluation; (D) knockdown of p53 in HT29 cells. The cells were transfected with p53 siRNA or scrambled RNA, followed by treatment with 50 μM IQ and 5 μM 5-FU. Cell death induction was analyzed as described in panel A. Data are given as mean + SEM ($n = 3$). Not significant (ns): $p > 0.05$; * $p < 0.05$; ** $p < 0.01$; (E) representative dot plots of (D).

3.5. Therapeutic Efficacy of Meresquiterpenquinone in Murine Tumor Organoids

Finally, we translated our findings to a murine tumor organoid model. Tumor organoids were exposed to increasing concentrations of SP and IQ for up to 72 h, and 5-FU was included as the positive control. While low concentrations of the meresquiterpenes had no impact on tumor organoid morphology and viability, higher concentrations caused substantial morphological alterations already after 24 h, culminating in complete disruption of tumor organoids after 72 h (Figure 8A, top vs. bottom panel).

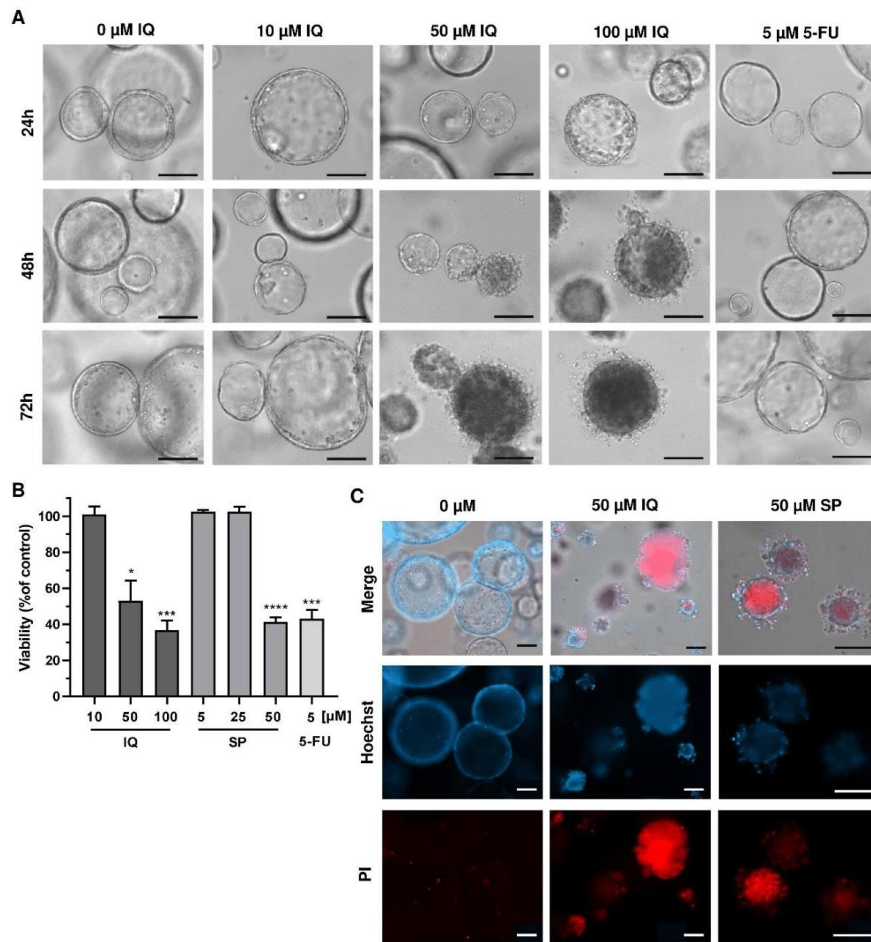


Figure 8. Effects of meresquiterpenes on intestinal tumor organoids: (A) tumor organoids were treated with increasing concentrations of IQ, SP, 5-FU, or the solvent control and incubated for up to 72 h. Representative images of organoid morphology are shown. Scale bar: 100 μm; (B) organoid viability upon treatment as described in A determined by MTT assay. Data are given as mean + SEM ($n \geq 3$). * $p < 0.05$; *** $p < 0.001$; **** $p < 0.0001$. (C) cell death staining in tumor organoids exposed to the indicated compounds for 72 h. Representative immunofluorescence pictures are depicted. Scale bar: 100 μm.

This correlated very well with the concentration-dependent decrease in tumor organoid viability as determined by the MTT assay (Figure 8B). In support of these findings, tumor organoids were highly positive for the cell death marker PI after treatment with IQ and SP, which was visualized by fluorescence microscopy (Figure 8C). In summary, these experiments showed that merosquiterpenes not only caused cell death in established CRC cell lines but also efficiently kill tumor organoids. The major findings of this study have been summarized in a scheme shown in Figure 9.

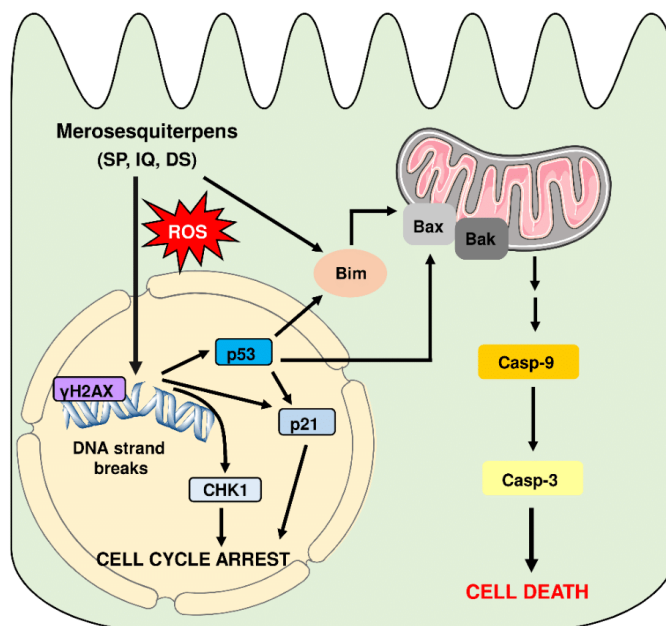


Figure 9. Model of cell death induction triggered by genotoxic merosquiterpenes and involved key players. Merosquiterpenes cause DNA strand break formation in CRC cells with a concomitant ROS production. This results in the activation of the DNA damage response, as attested by γ H2AX formation, CHK1 phosphorylation, and accumulation of p53 and p21. Notably, p21 induction is also observed in p53-mutant CRC cells after exposure to merosquiterpenes. Activation of p21 and CHK1 causes initial cell cycle arrest. In CRC cells with expression of WT p53, the tumor suppressor protein activates a cell death program by upregulation of Bax, FasR, and Bim as the main proapoptotic factors, as demonstrated in isogenic p53 knockout cells. This finally results in mitochondrial apoptosis via caspase-9 and caspase-3 in p53 WT CRC cells after treatment with merosquiterpenes. Interestingly, induction of the cell cycle regulator p21 occurs independently of the p53 status, as attested in CRC cells with mutant p53 and p53 knockout. Another important finding is that Bim induction and mitochondrial cell death are also executed in p53-mutated CRC cells after treatment with merosquiterpenes. This figure was created using Servier Medical Art templates, which are licensed under a Creative Commons Attribution 3.0 Unported License; <https://smart.servier.com>, accessed on 18 May 2021.

4. Discussion

In this study, the therapeutic potential of numerous merosquiterpenes was evaluated in CRC cell lines and tumor organoids. The most promising compounds were SP, IQ, and DS, with potent cytotoxic activities in the μ M range. The cytotoxicity was influenced by the chemical structure, particularly the side chains. With regard to the

20-Amino and *N*-alkyl rearranged drimane sesquiterpenes, an unsubstituted amino group (i.e., SP) was responsible for the high cytotoxic activity, while an amino group substituted with an alkyl- or aromatic side chain reduced cytotoxicity. This also holds true for the sesquiterpenes with a 20-Methoxy rearranged drimane skeleton, i.e., IQ was more potent than its oxohexyl-substituted derivative quintaquinone. Interestingly, the compound 3-farnesyl- 2-hydroxy-5-methoxyquinone with an open chain configuration was completely inactive, suggesting a toxicity mechanism beyond ROS generation by the (hydro)quinone structure (see paragraph below). Another factor potentially modulating the cytotoxicity of merosesquiterpenes is the enzyme NQO1 (NAD(P)H:quinone oxidoreductase 1), which catalyzes the conversion of quinones to hydroquinones [44]. This is usually considered a detoxification step but could also give rise to reactive hydroquinones. These can undergo redox cycling with the subsequent formation of electrophilic species and ROS. Thus, the expression levels of NQO1 found in cancer cells and tissues should affect their sensitivity towards merosesquiterpenes. In support of this view, inhibition of NQO1 in PC3 prostate cancer cells reduced the cytotoxic effects of IQ [45].

The growth arrest and cell death induction by merosesquiterpenes were preceded by the formation of DNA strand breaks with potent activation of the DDR, as attested by alkaline Comet assays, γ H2AX formation, CHK1 phosphorylation, and p53 accumulation. Together, these genotoxicity markers demonstrate that merosesquiterpenes cause DNA damage. One plausible mechanism could involve the generation of ROS by merosesquiterpenes due to redox cycling mediated by their hydroquinone structure. In line with this notion, IQ has recently been reported to promote mitochondrial ROS production in A549 lung cancer cells [5] and to increase ROS levels in HCT116 CRC cells [4]. We were able to confirm ROS generation after treatment of HCT116 cells with high concentrations of IQ and SP, which was most prominent after 24 h. However, no effects on ROS levels were observed at lower concentrations despite clear genotoxicity, as evidenced by induction of DNA strand breaks, γ H2AX formation, and DDR activation. This suggests that ROS formation is likely not the main trigger of DNA damage detected after treatment with merosesquiterpenes. Furthermore, it is conceivable that the compounds might interfere with enzymes regulating DNA topology and/or directly interact with DNA, thereby causing DNA damage. In line with the latter, an *in vitro* study using plasmid DNA indicated DNA cleavage by the hydroquinone species [45]. This is also in agreement with the finding that an open-chain sesquiterpene quinone displays no cytotoxicity despite being capable of redox cycling.

The merosesquiterpenes caused cell cycle arrest in G1 and/or G2/M phase, depending on the concentrations and incubation periods in CRC cells. Consistent with this finding, phosphorylation of CHK1 and upregulation of p21 were detected. CHK1 is involved in the regulation of cell cycle checkpoints in S, G2, and M-phase [46], while p21, as a CDK inhibitor, halts G1/S transition and G2/M transition [47]. Interestingly, p21 induction by merosesquiterpenes also occurred in the absence of p53 and in p53-mutated cells, strongly suggesting a p53-independent regulation of p21. Indeed, several p53-independent pathways controlling p21 gene expression were described [47], including the recently identified zinc finger protein ZNF84 upon genotoxic stress [48]. Treatment of CRC cells with higher concentrations of the merosesquiterpenes caused a significant increase in subG1 levels, indicative of apoptotic cell death, which was seen already after 24 h. Further cell death measurements, detection of caspase cleavage, and analysis of proapoptotic and antiapoptotic gene expression clearly demonstrated apoptosis induction in the CRC cell models. Our findings (caspase-9 and caspase-3 cleavage, upregulation of *BAX* and *BIM*) indicate mitochondrial apoptosis as a major cell death pathway. This was clearly dependent on p53 in CRC cells with the expression of WT p53 but also occurred in CRC cells with a hot spot mutation in p53. This is an important aspect since p53 is inactivated in the vast majority of human CRC cell lines and in more than 40% of human sporadic CRC cases [49,50]. Interestingly, the observed upregulation of the proapoptotic BH3-only protein Bim occurred not only in CRC cells with p53 WT expression but to a similar extent

also in p53-mutated CRC cells, as shown by Western blot analysis. Bim can stimulate apoptosis by directly activating Bax and Bak, as well as by antagonizing antiapoptotic Bcl-2 proteins [51]. It is further worth mentioning that the selected merosessquiterpenes kill CRC cells and also display comparable cytotoxicity in tumor organoids, as shown herein. Aberrant activation of the WNT signaling pathway is a hallmark of sporadic and hereditary CRC [52]. This is primarily caused by mutations of the APC tumor suppressor gene, which regulates the degradation of the key effector molecule β -catenin [52]. Interestingly, IQ was shown to suppress the WNT/ β -catenin signaling pathway in multiple myeloma cells via downregulation of β -catenin levels [53]. Thus, the deregulated WNT signaling in CRC cells might represent an additional target of merosessquiterpenes.

Another contributor to cell death induction by merosessquiterpenes might be endoplasmic reticulum (ER) stress. It was reported that IQ causes the upregulation of C/EBP homologous protein (CHOP), also denoted as DNA damage-inducible gene 153 (GADD153), in prostate cancer cells [2]. CHOP is known to be activated by ER stress and DNA damage [54]. Furthermore, CHOP can induce mitochondrial apoptosis via upregulation of the BH3-only proteins Puma and Bim [54], the latter of which was also found in our experiments. Interestingly, another study indicated IQ-dependent upregulation of CHOP in HCT116 cells via ERK and MAPK signaling, which depended on ROS formation [4]. These effects could therefore contribute to the mitochondrial apoptosis observed in our CRC cell models following exposure to the different merosessquiterpenes.

To date, little information is available on the pharmacokinetics and the potential toxicity profile of merosessquiterpenes in vivo. With regard to pharmacokinetics, a recent study performed in rats reported an oral bioavailability of 45% after administration of 10 mg IQ/kg body weight (b.w.) [55]. The maximum plasma concentration determined for single oral administration was 0.94 $\mu\text{g/mL}$, which corresponds to approximately three μM . Further experiments with i.v. injection of only 2 mg IQ/kg b.w. revealed an area under the curve (AUC) of 1.46 $\mu\text{g} \times \text{h/mL}$, as compared to an AUC of 3.39 $\mu\text{g} \times \text{h/mL}$, after oral administration of 10 mg/kg b.w. This suggests that i.v. injection of 10–20 mg IQ/kg b.w. yields plasma concentrations of approximately 6–12 μM . Given that SP and DS display similar pharmacokinetics, plasma concentrations with cytotoxic activity in CRC cells could thus be reached in vivo. Nevertheless, basic animal studies incorporating dose–response curves and comparing different routes of administration are clearly required. This holds also true for preclinical toxicity studies to obtain detailed information on the safety profile of the compounds, which will ultimately determine their applicability and therapeutic range. Finally, it is tempting to speculate that the merosessquiterpenes identified in this study may synergize with established anticancer drugs used in CRC therapy, as has been previously demonstrated for the combination of the natural disulfide compound LA with 5-FU or doxorubicin [34,39].

5. Conclusions

Taken together, we identified three natural merosessquiterpenes with potent cytotoxic activity in different human CRC cell lines independent of their p53 status. The underlying mechanism involved DNA strand break formation and activation of the DNA damage response, followed by cell cycle arrest and mitochondrial apoptotic cell death. Importantly, these findings were corroborated in murine intestinal tumor organoids, suggesting merosessquiterpenes as promising building blocks in CRC chemotherapy.

Supplementary Materials: The following are available online at <https://www.mdpi.com/article/10.3390/cancers13133282/s1>, Supplementary Material and Methods: isolation and characterization of merosoterpenes, Figure S1: ¹H-NMR of smenospongine (400 MHz, CD₃OD), Figure S2: ¹H-NMR of smenospongine (500 MHz, C₆D₆), Figure S3: ¹H-NMR of smenospongine (500 MHz, C₆D₆), Figure S4: ¹H-NMR of smenospongine (500 MHz, C₆D₆), Figure S5: ¹H-NMR of ilimaquinone (500 MHz, C₆D₆), Figure S6: ¹H-NMR of 5-*epi*-ilimaquinone (500 MHz, C₆D₆), Figure S7: ¹H NMR of quintaquinone (500 MHz, C₆D₆), Figure S8: ¹H-NMR of cyclospingiaquinone-1 (500 MHz, C₆D₆), Figure S9: ¹H-NMR of smenodiol (500 MHz, C₆D₆), ¹H-NMR of dactylospontriol (500 MHz, C₆D₆), Figure S10: ¹H-NMR of dactylospontriol (500 MHz, C₆D₆), Figure S11: ¹H-NMR of 3-farnesyl-2-hydroxy-5-methoxyquinone (500 MHz, C₆D₆), Figure S12: uncropped western blot images of HCT116 cells shown in Figure 3D, Figure S13: uncropped western blot images of HT29 cells shown in Figure 3D, Figure S14: uncropped western blot images of HCT116 cells and HT29 cells displayed in Figures 6C and 7C, Figure S15: uncropped western blot images of HCT116 cells displayed in Figure A5A.

Author Contributions: Conceptualization, J.F.; methodology, M.H., N.S., P.D., L.D., T.B. and M.C.; validation, A.J., M.B., P.D. and J.F.; formal analysis, A.J., M.B., P.D., M.H., D.H. and M.C.; investigation, A.J., M.B., P.D., M.H., N.S., D.H. and B.R.; resources, L.D., T.B., R., T.F.S. and A.P.; writing—original draft preparation, J.F., A.P. and T.F.S.; writing—review and editing, J.F., A.J., M.B., P.D., M.H., N.S., D.H., B.R., M.C., T.B., R., T.F.S. and A.P.; visualization, A.J., M.B., P.D. and J.F.; supervision, J.F.; project administration, J.F.; funding acquisition, J.F., T.F.S. and A.P. All authors have read and agreed to the published version of the manuscript.

Funding: This research was partially supported by Wilhelm Sander Foundation, Grant Number 2016.039.2 (to J.F.). A.J. was supported by a grant from the Royal Golden Jubilee PhD Program (PHD/0094/2556). T.F.S. and A.P. were supported by the German Federal Ministry of Education and Research (BMBF) Grant Number 01DP17037. R. received a PhD fellowship from the Indonesia Endowment Fund for Education (LPDP), Grant Number 20160222305487.

Institutional Review Board Statement: Not applicable.

Informed Consent Statement: Not applicable.

Data Availability Statement: All datasets were included in the main text and in Appendix A. Raw datasets are available from the corresponding author upon reasonable request.

Acknowledgments: The authors thank Beate von Derschau (Rudolf Buchheim Institute of Pharmacology, Justus Liebig University Giessen) for excellent technical assistance. We are grateful to Bert Vogelstein (John Hopkins University, Baltimore, USA) for providing HCT116-p53^{+/+} and HCT116-p53^{-/-} cells.

Conflicts of Interest: The authors declare no conflict of interest.

Appendix A

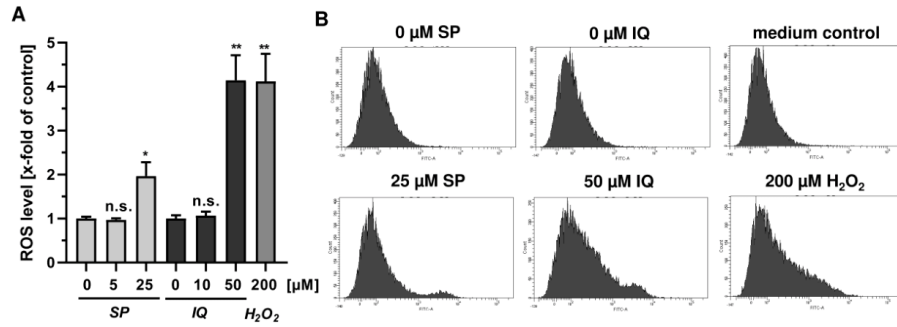


Figure A1. Effects of merosquiterpenes on cellular ROS production and DNA damage response in CRC cells after 24 h: (A) flow-cytometry-based measurements of ROS formation in HCT116 cells challenged with increasing concentrations of SP and IQ, respectively. H₂O₂ was included as positive control. Data are given as mean + SEM (*n* = 4). Not significant (ns): *p* > 0.05; * *p* < 0.05; ** *p* < 0.01; (B) representative histograms of ROS analysis shown in (A).

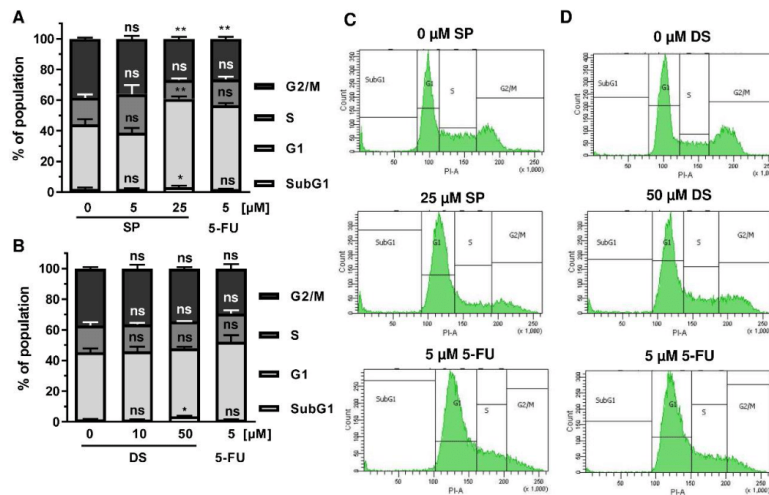


Figure A2. Effect of merosquiterpenes on cell cycle distribution in HT29 cells after 24 h: (A,B) cell cycle analysis in HT29 cells challenged with increasing concentrations of SP (A) and DS (B), respectively, for 24 h, and 5-FU served as positive control. Data are given as mean + SEM (*n* = 4). Not significant (ns): *p* > 0.05; * *p* < 0.05; ** *p* < 0.01; (C,D) representative histograms of cell cycle analysis shown in (A,B).

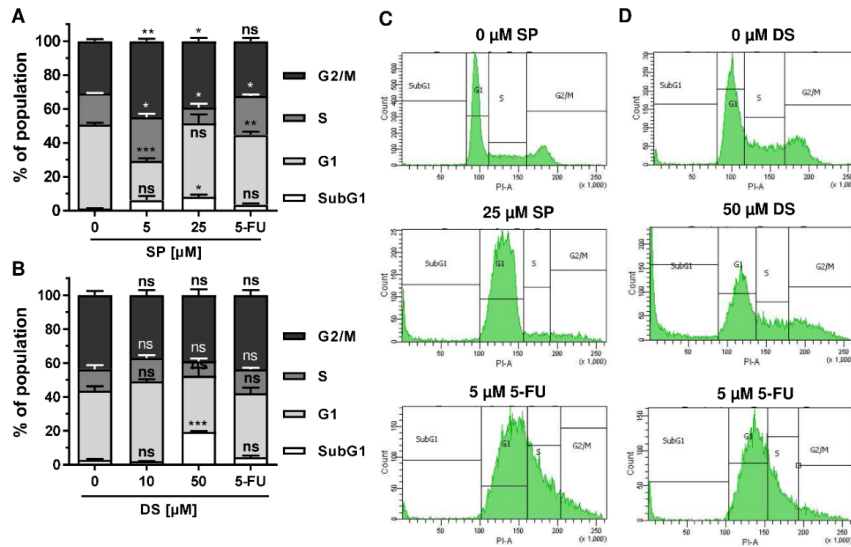


Figure A3. Effect of merosquiterpenes on cell cycle distribution in HT29 cells after 48 h: (A,B) cell cycle analysis in HT29 cells treated with increasing concentrations of SP (A) and DS (B), respectively, for 48 h, and 5-FU served as positive control. Data are given as mean + SEM ($n = 4$). Not significant (ns): $p > 0.05$; * $p < 0.05$; ** $p < 0.01$; *** $p < 0.001$; (C,D) representative histograms of cell cycle analysis performed in (A,B).

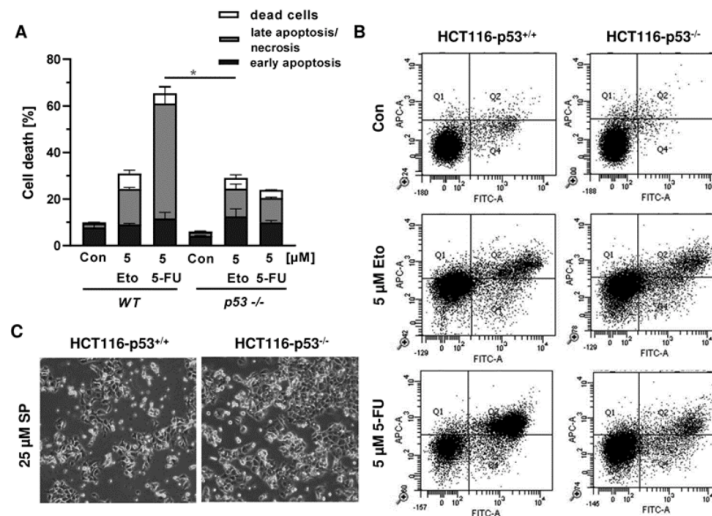


Figure A4. Impact of p53 status on anticancer drug triggered cell death in CRC cells: (A) isogenic HCT116-p53^{+/+} and HCT116-p53^{-/-} cells were exposed to 5 μM 5-FU and 5 μM Etoposide (Eto) for 48 h. Cell death induction was assessed by Annexin V-FITC/PI staining and flow cytometry. Data are shown as mean + SEM ($n = 3$). Not significant (ns): $p > 0.05$; * $p < 0.05$; ** $p < 0.01$; (B) representative dot plots of measurements performed in (A). (C) Morphological changes in HCT116-p53^{+/+} and HCT116-p53^{-/-} cells challenged with 25 μM SP for 48 h.

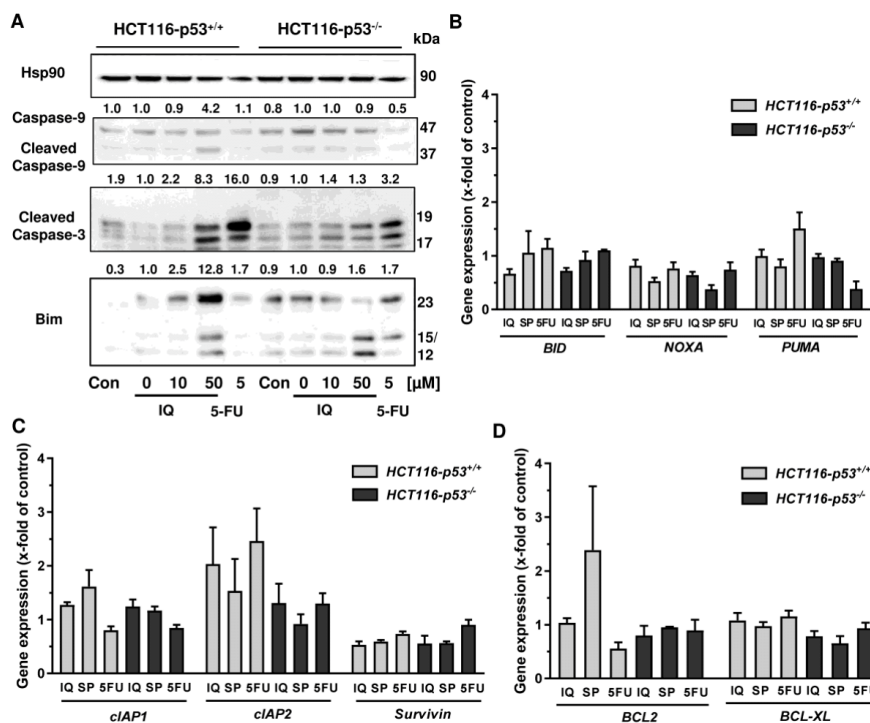


Figure A5. Impact of p53 status on caspase cleavage, proapoptotic and antiapoptotic gene expression in CRC cells upon merosquinone treatment: (A) isogenic HCT116 cell lines differing in their p53 status were exposed to increasing concentration of IQ for 48 h, and 5-FU was included as positive control and untreated cells as the corresponding negative control. Samples were subject to SDS-PAGE, followed by Western blot analysis of cleaved caspase-3, cleaved caspase-9, and Bim. Hsp90 was used as loading control. Representative blots are shown including densitometric evaluation; (B) expression levels of the proapoptotic genes *BID*, *NOXA*, and *PUMA* in p53-proficient and -deficient HCT116 cells treated with 50 μM IQ, 25 μM SP and 5 μM 5-FU for 24 h. Gene expression was assessed by qPCR ($n = 3$); (C) expression levels of the antiapoptotic genes *cIAP1*, *cIAP2*, and *Survivin* determined, as described in A; (D) expression levels of the antiapoptotic genes *BCL2* and *BCL-XL* determined as described in A.

References

- Maximo, P.; Ferreira, L.M.; Branco, P.; Lima, P.; Lourenco, A. The Role of Spongia sp. in the Discovery of Marine Lead Compounds. *Mar. Drugs* **2016**, *14*, 139. [[CrossRef](#)] [[PubMed](#)]
- Lu, P.H.; Chueh, S.C.; Kung, F.L.; Pan, S.L.; Shen, Y.C.; Guh, J.H. Ilimaquinone, a marine sponge metabolite, displays anticancer activity via GADD153-mediated pathway. *Eur. J. Pharmacol.* **2007**, *556*, 45–54. [[CrossRef](#)]
- Lin, C.W.; Bai, L.Y.; Su, J.H.; Chiu, C.F.; Lin, W.Y.; Huang, W.T.; Shih, M.C.; Huang, Y.T.; Hu, J.L.; Weng, J.R. Ilimaquinone Induces Apoptosis and Autophagy in Human Oral Squamous Cell Carcinoma Cells. *Biomedicines* **2020**, *8*, 296. [[CrossRef](#)] [[PubMed](#)]
- Do, M.T.; Na, M.; Kim, H.G.; Khanal, T.; Choi, J.H.; Jin, S.W.; Oh, S.H.; Hwang, I.H.; Chung, Y.C.; Kim, H.S.; et al. Ilimaquinone induces death receptor expression and sensitizes human colon cancer cells to TRAIL-induced apoptosis through activation of ROS-ERK/p38 MAPK-CHOP signaling pathways. *Food Chem. Toxicol.* **2014**, *71*, 51–59. [[CrossRef](#)] [[PubMed](#)]
- Kwak, C.H.; Jin, L.; Han, J.H.; Han, C.W.; Kim, E.; Cho, M.; Chung, T.W.; Bae, S.J.; Jang, S.B.; Ha, K.T. Ilimaquinone Induces the Apoptotic Cell Death of Cancer Cells by Reducing Pyruvate Dehydrogenase Kinase 1 Activity. *Int. J. Mol. Sci.* **2020**, *21*, 6021. [[CrossRef](#)] [[PubMed](#)]

6. Lee, H.Y.; Chung, K.J.; Hwang, I.H.; Gwak, J.; Park, S.; Ju, B.G.; Yun, E.; Kim, D.E.; Chung, Y.H.; Na, M.; et al. Activation of p53 with ilimaquinone and ethylsmenoquinone, marine sponge metabolites, induces apoptosis and autophagy in colon cancer cells. *Mar. Drugs* **2015**, *13*, 543–557. [[CrossRef](#)]
7. Van Stuijvenberg, J.; Proksch, P.; Fritz, G. Targeting the DNA damage response (DDR) by natural compounds. *Bioorg. Med. Chem.* **2020**, *28*, 115279. [[CrossRef](#)] [[PubMed](#)]
8. Kong, D.; Aoki, S.; Sowa, Y.; Sakai, T.; Kobayashi, M. Smenospongine, a sesquiterpene aminoquinone from a marine sponge, induces G1 arrest or apoptosis in different leukemia cells. *Mar. Drugs* **2008**, *6*, 480–488. [[CrossRef](#)]
9. Tang, J.; Wu, W.; Yang, F.; Liu, L.; Yang, Z.; Liu, L.; Tang, W.; Sun, F.; Lin, H. Marine sponge-derived smenospongine preferentially eliminates breast cancer stem-like cells via p38/AMPKalpha pathways. *Cancer Med.* **2018**, *7*, 3965–3976. [[CrossRef](#)]
10. Keum, N.; Giovannucci, E. Global burden of colorectal cancer: Emerging trends, risk factors and prevention strategies. *Nat. Rev. Gastroenterol. Hepatol.* **2019**, *16*, 713–732. [[CrossRef](#)]
11. Murphy, N.; Moreno, V.; Hughes, D.J.; Vodicka, L.; Vodicka, P.; Aglago, E.K.; Gunter, M.J.; Jenab, M. Lifestyle and dietary environmental factors in colorectal cancer susceptibility. *Mol. Asp. Med.* **2019**, *69*, 2–9. [[CrossRef](#)]
12. Seiwert, N.; Heylmann, D.; Hasselwander, S.; Fahrer, J. Mechanism of colorectal carcinogenesis triggered by heme iron from red meat. *Biochim. Biophys. Acta Rev. Cancer* **2020**, *1873*, 188334. [[CrossRef](#)]
13. Vuik, F.E.; Nieuwenburg, S.A.; Bardou, M.; Lansdorp-Vogelaar, I.; Dinis-Ribeiro, M.; Bento, M.J.; Zadnik, V.; Pellise, M.; Esteban, L.; Kaminski, M.F.; et al. Increasing incidence of colorectal cancer in young adults in Europe over the last 25 years. *Gut* **2019**, *68*, 1820–1826. [[CrossRef](#)] [[PubMed](#)]
14. Siegel, R.L.; Miller, K.D.; Goding Sauer, A.; Fedewa, S.A.; Butterly, L.F.; Anderson, J.C.; Cercek, A.; Smith, R.A.; Jemal, A. Colorectal cancer statistics, 2020. *CA Cancer J. Clin.* **2020**, *70*, 145–164. [[CrossRef](#)] [[PubMed](#)]
15. Kuipers, E.J.; Grady, W.M.; Lieberman, D.; Seufferlein, T.; Sung, J.J.; Boelens, P.G.; van de Velde, C.J.; Watanabe, T. Colorectal cancer. *Nat. Rev. Dis. Primers* **2015**, *1*, 15065. [[CrossRef](#)] [[PubMed](#)]
16. Dörsam, B.; Fahrer, J. The disulfide compound alpha-lipoic acid and its derivatives: A novel class of anticancer agents targeting mitochondria. *Cancer Lett.* **2016**, *371*, 12–19. [[CrossRef](#)]
17. Neitzel, C.; Demuth, P.; Wittmann, S.; Fahrer, J. Targeting Altered Energy Metabolism in Colorectal Cancer: Oncogenic Reprogramming, the Central Role of the TCA Cycle and Therapeutic Opportunities. *Cancers* **2020**, *12*, 1731. [[CrossRef](#)]
18. Xie, Y.H.; Chen, Y.X.; Fang, J.Y. Comprehensive review of targeted therapy for colorectal cancer. *Signal Transduct. Target. Ther.* **2020**, *5*, 22. [[CrossRef](#)]
19. Mauri, G.; Arena, S.; Siena, S.; Bardelli, A.; Sartore-Bianchi, A. The DNA damage response pathway as a land of therapeutic opportunities for colorectal cancer. *Ann. Oncol.* **2020**, *31*, 1135–1147. [[CrossRef](#)]
20. Balansa, W.; Mettall, U.; Wuisan, Z.G.; Plubrukarn, A.; Ijong, F.G.; Liu, Y.; Schaberle, T.F. A New Sesquiterpenoid Aminoquinone from an Indonesian Marine Sponge. *Mar. Drugs* **2019**, *17*, 158. [[CrossRef](#)]
21. Jiso, A.; Kittiwisut, S.; Chantakul, R.; Yuenyongsawad, S.; Putchakarn, S.; Schaberle, T.F.; Temkitthaworn, P.; Ingkaninan, K.; Chaithirayanon, K.; Plubrukarn, A. Quinone, a Merosequinone, a Merosequinone from the Yellow Sponge *Verongula cf. rigida* Esper. *J. Nat. Prod.* **2020**, *83*, 532–536. [[CrossRef](#)]
22. Kazlauskas, R.; Murphy, P.; Warren, R.; Wells, R.; Blount, J. New quinones from a dictyoceratid sponge. *Aust. J. Chem.* **1978**, *31*, 2685–2697. [[CrossRef](#)]
23. Luibrand, R.T.; Erdman, T.R.; Vollmer, J.J.; Scheuer, P.J.; Finer, J.; Clardy, J. Ilimaquinone, a sesquiterpenoid quinone from a marine sponge. *Tetrahedron* **1979**, *35*, 609–612. [[CrossRef](#)]
24. Carte, B.; Rose, C.B.; Faulkner, D.J. 5-Epi-Ilimaquinone, a metabolite of the sponge *Fenestraspongia* sp. *J. Org. Chem.* **1985**, *50*, 2785–2787. [[CrossRef](#)]
25. Kondracki, M.-L.; Guyot, M. Smenospongine: A cytotoxic and antimicrobial aminoquinone isolated from *Smenospongia* sp. *Tetrahedron Lett.* **1987**, *28*, 5815–5818. [[CrossRef](#)]
26. Kondracki, M.-L.; Guyot, M. Biologically active quinone and hydroquinone sesquiterpenoids from the sponge *smenospongia* sp. *Tetrahedron* **1989**, *45*, 1995–2004. [[CrossRef](#)]
27. Kushlan, D.M.; Faulkner, D.J.; Parkanyi, L.; Clardy, J. Metabolites of the Palauan sponge *dactylospongia* sp. *Tetrahedron* **1989**, *45*, 3307–3312. [[CrossRef](#)]
28. Venkateswarlu, Y.; Faulkner, D.J.; Steiner, J.L.R.; Corcoran, E.; Clardy, J. Smenochromenes, unusual macrocyclic sesquiterpene hydroquinone derivatives from a Seychelles sponge of the genus *Smenospongia*. *J. Org. Chem.* **1991**, *56*, 6271–6274. [[CrossRef](#)]
29. Rodriguez, J.; Quiñoá, E.; Riguera, R.; Peters, B.M.; Abrell, L.M.; Crews, P. The structures and stereochemistry of cytotoxic sesquiterpene quinones from *Dactylospongia elegans*. *Tetrahedron* **1992**, *48*, 6667–6680. [[CrossRef](#)]
30. Seiwert, N.; Wecklein, S.; Demuth, P.; Hasselwander, S.; Kemper, T.A.; Schwerdtle, T.; Brunner, T.; Fahrer, J. Heme oxygenase 1 protects human colonocytes against ROS formation, oxidative DNA damage and cytotoxicity induced by heme iron, but not inorganic iron. *Cell Death Dis.* **2020**, *11*, 787. [[CrossRef](#)]
31. Göder, A.; Nagel, G.; Kraus, A.; Dörsam, B.; Seiwert, N.; Kaina, B.; Fahrer, J. Lipoic acid inhibits the DNA repair protein O6-methylguanine-DNA methyltransferase (MGMT) and triggers its depletion in colorectal cancer cells with concomitant autophagy induction. *Carcinogenesis* **2015**, *36*, 817–831. [[CrossRef](#)]

32. Fahrner, J.; Huelsenbeck, J.; Jaurich, H.; Dörsam, B.; Frisan, T.; Eich, M.; Roos, W.P.; Kaina, B.; Fritz, G. Cytotoxic distending toxin (CDT) is a radiomimetic agent and induces persistent levels of DNA double-strand breaks in human fibroblasts. *DNA Repair* **2014**, *18*, 31–43. [[CrossRef](#)]
33. Fahrner, J.; Schweitzer, B.; Fiedler, K.; Langer, T.; Gierschik, P.; Barth, H. C2-streptavidin mediates the delivery of biotin-conjugated tumor suppressor protein p53 into tumor cells. *Bioconjug. Chem.* **2013**, *24*, 595–603. [[CrossRef](#)] [[PubMed](#)]
34. Neitzel, C.; Seiwert, N.; Göder, A.; Diehl, E.; Weber, C.; Nagel, G.; Stroh, S.; Rasenberger, B.; Christmann, M.; Fahrner, J. Lipoic Acid Synergizes with Antineoplastic Drugs in Colorectal Cancer by Targeting p53 for Proteasomal Degradation. *Cells* **2019**, *8*, 794. [[CrossRef](#)] [[PubMed](#)]
35. Dörsam, B.; Wu, C.F.; Efferth, T.; Kaina, B.; Fahrner, J. The eucalyptus oil ingredient 1,8-cineol induces oxidative DNA damage. *Arch. Toxicol.* **2015**, *89*, 797–805. [[CrossRef](#)] [[PubMed](#)]
36. Dörsam, B.; Seiwert, N.; Foersch, S.; Stroh, S.; Nagel, G.; Begaliew, D.; Diehl, E.; Kraus, A.; McKeague, M.; Minneker, V.; et al. PARP-1 protects against colorectal tumor induction, but promotes inflammation-driven colorectal tumor progression. *Proc. Natl. Acad. Sci. USA* **2018**, *115*, E4061–E4070. [[CrossRef](#)]
37. Mimmeler, M.; Peter, S.; Kraus, A.; Stroh, S.; Nikolova, T.; Seiwert, N.; Hasselwander, S.; Neitzel, C.; Haub, J.; Monien, B.H.; et al. DNA damage response curtails detrimental replication stress and chromosomal instability induced by the dietary carcinogen PhIP. *Nucleic Acids Res.* **2016**, *44*, 10259–10276. [[CrossRef](#)] [[PubMed](#)]
38. Seiwert, N.; Neitzel, C.; Stroh, S.; Frisan, T.; Audebert, M.; Toulany, M.; Kaina, B.; Fahrner, J. AKT2 suppresses pro-survival autophagy triggered by DNA double-strand breaks in colorectal cancer cells. *Cell Death Dis.* **2017**, *8*, e3019. [[CrossRef](#)]
39. Dörsam, B.; Göder, A.; Seiwert, N.; Kaina, B.; Fahrner, J. Lipoic acid induces p53-independent cell death in colorectal cancer cells and potentiates the cytotoxicity of 5-fluorouracil. *Arch. Toxicol.* **2015**, *89*, 1829–1846. [[CrossRef](#)]
40. Ripani, P.; Delp, J.; Bode, K.; Delgado, M.E.; Dietrich, L.; Betzler, V.M.; Yan, N.; von Scheven, G.; Mayer, T.U.; Leist, M.; et al. Thiazolidines promote G1 cell cycle arrest in colorectal cancer cells by targeting the mitochondrial respiratory chain. *Oncogene* **2020**, *39*, 2345–2357. [[CrossRef](#)]
41. Bode, K.J.; Mueller, S.; Schweinlin, M.; Metzger, M.; Brunner, T. A fast and simple fluorometric method to detect cell death in 3D intestinal organoids. *Biotechniques* **2019**, *67*, 23–28. [[CrossRef](#)]
42. Ahmed, D.; Eide, P.W.; Eilertsen, I.A.; Danielsen, S.A.; Eknaes, M.; Hektoen, M.; Lind, G.E.; Lothe, R.A. Epigenetic and genetic features of 24 colon cancer cell lines. *Oncogenesis* **2013**, *2*, e71. [[CrossRef](#)]
43. Rodrigues, N.R.; Rowan, A.; Smith, M.E.; Kerr, I.B.; Bodmer, W.F.; Gannon, J.V.; Lane, D.P. p53 mutations in colorectal cancer. *Proc. Natl. Acad. Sci. USA* **1990**, *87*, 7555–7559. [[CrossRef](#)]
44. Ross, D.; Siegel, D. The diverse functionality of NQO1 and its roles in redox control. *Redox Biol.* **2021**, *41*, 101950. [[CrossRef](#)]
45. Jiso, A.; Yurasakpong, L.; Janta, S.; Chaithirayanon, K.; Plubrukarn, A. Exerting DNA Damaging Effects of the Ilimaquinones through the Active Hydroquinone Species. *Sci. Pharm.* **2021**, *89*, 26. [[CrossRef](#)]
46. Zhang, Y.; Hunter, T. Roles of Chk1 in cell biology and cancer therapy. *Int. J. Cancer* **2014**, *134*, 1013–1023. [[CrossRef](#)]
47. Karimian, A.; Ahmadi, Y.; Yousefi, B. Multiple functions of p21 in cell cycle, apoptosis and transcriptional regulation after DNA damage. *DNA Repair* **2016**, *42*, 63–71. [[CrossRef](#)] [[PubMed](#)]
48. Strzeszewska-Potyrala, A.; Staniak, K.; Czarnicka-Herok, J.; Rafiej, M.-R.; Herok, M.; Mosieniak, G.; Krijgsveld, J.; Sikora, E. Chromatin-Directed Proteomics Identifies ZNF84 as a p53-Independent Regulator of p21 in Genotoxic Stress Response. *Cancers* **2021**, *13*, 2115. [[CrossRef](#)]
49. Liu, Y.; Bodmer, W.F. Analysis of P53 mutations and their expression in 56 colorectal cancer cell lines. *Proc. Natl. Acad. Sci. USA* **2006**, *103*, 976–981. [[CrossRef](#)]
50. Olivier, M.; Hollstein, M.; Hainaut, P. TP53 mutations in human cancers: Origins, consequences, and clinical use. *Cold Spring Harb. Perspect. Biol.* **2010**, *2*, a001008. [[CrossRef](#)]
51. Sionov, R.V.; Vlahopoulos, S.A.; Granot, Z. Regulation of Bim in Health and Disease. *Oncotarget* **2015**, *6*, 23058–23134. [[CrossRef](#)] [[PubMed](#)]
52. Markowitz, S.D.; Bertagnolli, M.M. Molecular origins of cancer: Molecular basis of colorectal cancer. *N. Engl. J. Med.* **2009**, *361*, 2449–2460. [[CrossRef](#)] [[PubMed](#)]
53. Park, S.; Yun, E.; Hwang, I.H.; Yoon, S.; Kim, D.-E.; Kim, J.S.; Na, M.; Song, G.-Y.; Oh, S. Ilimaquinone and Ethylsmenoquinone, Marine Sponge Metabolites, Suppress the Proliferation of Multiple Myeloma Cells by Down-Regulating the Level of β -Catenin. *Mar. Drugs* **2014**, *12*, 3231–3244. [[CrossRef](#)]
54. Yang, Y.; Liu, L.; Naik, I.; Braunstein, Z.; Zhong, J.; Ren, B. Transcription Factor C/EBP Homologous Protein in Health and Diseases. *Front. Immunol.* **2017**, *8*, 1612. [[CrossRef](#)] [[PubMed](#)]
55. Son, H.; Noh, K.; Park, I.; Na, M.; Oh, S.; Shin, B.S.; Kang, W. Stereo-Selective Pharmacokinetics of Ilimaquinone Epimers Extracted from a Marine Sponge in Rats. *Mar. Drugs* **2019**, *17*, 171. [[CrossRef](#)] [[PubMed](#)]



Supplementary Information

Natural Merosesquiterpenes Activate the DNA Damage Response via DNA Strand Break Formation and Trigger Apoptotic Cell Death in p53-Wild-type and Mutant Colorectal Cancer

Apisada Jiso, Philipp Demuth, Madeleine Bachowsky, Manuel Haas, Nina Seiwert, Daniel Heylmann, Birgit Rasenberger, Markus Christmann, Lea Dietrich, Thomas Brunner, Riyanti, Till F. Schäberle, Anuchit Plubrukarn, and Jörg Fahrner

Supplementary Material & Methods

Isolation and characterization of Merosesquiterpenes

Merosesquiterpenes were obtained from two sponge species, an Indonesian *Haliclona* sp. BL-3, as well as a Thai *Verongula* cf. *rigida* Esper.

Smenospongine was isolated before from sponge *Dactylospongia elegans* collected from Towo'e Beach Tahuna Bay, Sangihe Islands. For reisolation of smenospongine, the sponges *Haliclona* sp. BL-3, collected from Batulewehe's coral reef Sangihe Island, was used. Therefore, the *Haliclona* specimen was extracted with MeOH (shake at 140 rpm, 30 °C, overnight). Upon removal of the solvent to dryness, the extract was purified using an HPLC system (Shimadzu Deutschland GmbH, Duisburg, Germany) equipped with a reverse-phase column (EC Gravity C18, 250 × 10 mm) and eluted with a gradient 6:4 MeCN/H₂O + 0.01% TFA to 8.5:1.5 MeCN/H₂O + 0.01% TFA, over 55 min, flow rate 3.0 mL/min, yielding five fractions (M1-M5). Fraction M3 was purified by reverse-phase HPLC column (gradient 55:45 MeCN/H₂O + 0.01% TFA to 8:2 MeCN/H₂O + 0.01% TFA, over 75 min, flow rate 3.0 mL/min) to yield **smenospongine** (2.2 mg).

The sponge *Verongula* cf. *rigida* Esper was collected from Koh Ha Islets, Krabi Province, Thailand, in two separate expeditions—one in 2010, and the other in 2014. The specimen from the 2010 expedition (1.8 kg, wet weight) was extracted with 1:1 MeOH/EtOAc (2.5 L) and EtOAc (3 × 2.5 L). The extract (23 g) was partitioned with hexane, CH₂Cl₂, and *n*-BuOH, respectively. An aliquot of the hexane extract (2.6 g) was chromatographed over a Sephadex LH-20 column (MeOH) and an HPLC system (Waters 1525 binary solvent delivery system with Waters 2998 photodiode array detector, a Rheodyne 7125 injection port, and performed with Empower 3 software) using a reverse-phase column (C-18, Phenomenex®, 250 × 10 mm, 10 μm) with a 9:1 MeCN/water (2.0 mL/min) to yield **dactylospontriol** (6 mg). Another aliquot of the hexane extract (11.7 g) was separated over a Sephadex LH-20 (EtOAc), SiO₂ (98:2 CH₂Cl₂/MeOH), and a SiO₂ HPLC columns (VertiSep GES Silica, 250×10 mm, 10 μm; 85:15 hexane/EtOAc, 2.0 mL/min) to yield **3-farnesyl-2-hydroxy-5-methoxyquinone** (6.4 mg).

The sponge specimen from the 2014 expedition (325 g, dry weight) was exhaustively extracted with hexane (5 × 3 L), CH₂Cl₂ (4 × 3 L), and MeOH (4 × 3 L). An aliquot of the hexane extract (3 g) was isolated with a SiO₂ (gradient 100:0 – 0:100 hexane/EtOAc) and Sephadex LH-20 columns (4:1 MeOH/EtOAc), yielding six pooled fractions (H1–H6). Fraction H4 was separated over AgNO₃-impregnated SiO₂ column (4:1 hexane/EtOAc) to yield **ilimaquinone** (300 mg) and **5-epi-ilimaquinone** (81 mg). Fraction H5 was isolated with a SiO₂ (8.5:1.5 hexane/CHCl₃ + 1 % v/v acetic acid), reverse-phase C-18 solid phase extraction (CH₃CN), and reverse-phase HPLC columns (C-18, Mightysil RP-18 GII, 250 × 4.6 mm, 5 μm; 8.5:1.5 MeCN/water, 1.0 mL/min) to yield **quintaquinone** (1.4 mg). Another aliquot of the hexane extract (2 g) was chromatographed over a SiO₂ (gradient 100:0–0:100

hexane/EtOAc) and Sephadex LH-20 columns (4:1 MeOH/EtOAc) to yield six fractions (HH1–HH6). Fraction HH4 was chromatographed over reverse-phase C-18 solid phase extraction (CH₃CN) and separated with a reverse-phase HPLC column (8.5:1.5 CH₃CN/water, 1.0 mL/min) to yield **smenospongoringine** (1.5 mg), **smenospongiarine** (1.2 mg), and **smenospongidine** (0.8 mg). Fraction HH5 was isolated using a reverse-phase column (7:3 CH₃CN/water, 1.0 mL/min) to yield **cyclosporgiaquinone-1** (4.4 mg) and **smenodiol** (9 mg).

Smenospongine. ¹H-NMR (CD₃OD, 400 MHz) δ 5.51 (1H, s, H-19), 4.43 (2H, brs, H2-11), 2.47 (1H, d, *J* = 13.7 Hz, H-15a), 2.41 (1H, d, *J* = 13.7 Hz, H-15b), 2.34 (1H, ddd, *J* = 13.7, 4.3, 2.7 Hz, H-3ax), 2.15 (1H, brd, *J* = 12.7 Hz, H-1eq), 2.05 (1H, brd, *J* = 13.7, 4.5 Hz, H-3eq), 1.95 (1H, m, H-2eq), 1.52 (1H, m, H-6eq), 1.43 (1H, m, H-1ax), 1.40 (1H, m, H-2ax), 1.39 (1H, m, H-8), 1.34 (3H, m, H-6ax, H2-7), 1.06 (3H, s, H3-12), 1.01 (1H, brd, *J* = 11.5 Hz, H-10), 0.98 (3H, d, *J* = 6.4 Hz, H3-13), 0.84 (3H, s, H3-14); HRESI-LCMS *m/z* 344.2218 [M+H]⁺ (calcd for C₂₁H₂₉NO₃ 344.2220).

Smenospongoringine. ¹H-NMR (C₆D₆, 500 MHz) δ 6.02 (1H, brs, -NH), 5.17 (1H, s, H-19), 4.60 (1H, dd, *J* = 1.6, 1.6 Hz, H-11a), 4.56 (1H, dd, *J* = 1.6, 1.6 Hz, H-11b), 2.66 (1H, d, *J* = 13.8 Hz, H-15a), 2.57 (1H, d, *J* = 13.8 Hz, H-15b), 2.38 (1H, ddd, *J* = 12.4, 5.3, 2.2 Hz, H-1eq), 2.35 (1H, ddd, *J* = 13.7, 13.7, 5.3 Hz, H-3ax), 2.17 (1H, ddd, *J* = 13.7, 2.4, 2.4 Hz, H-3eq), 2.03 (2H, H2-22), 1.97 (1H, ddd, *J* = 11.5, 5.3, 2.4 Hz, H-2eq), 1.55 (1H, ddd, *J* = 12.4, 8.9, 2.9 Hz, H-6eq), 1.45 (1H, ddd, *J* = 12.4, 9.7, 2.4 Hz, H-1ax), 1.44 (1H, ddd, *J* = 11.5, 5.3, 2.4 Hz, H-2ax), 1.43 (1H, ddq, *J* = 12.4, 10.0, 5.8 Hz, H-8), 1.40 (3H, overlapped, H-6ax, H2-7), 1.20 (3H, d, *J* = 5.8 Hz, H3-13), 1.12 (1H, ddd, *J* = 13.5, 6.8, 6.8 Hz, H-23), 1.06 (3H, s, H3-12), 1.04 (1H, dd, *J* = 9.7, 2.2 Hz, H-10), 0.89 (3H, s, H3-14), 0.45 (6H, d, *J* = 6.0 Hz, H3-24, H3-25); HRESIMS *m/z* 398.2702 [M-H]⁻ (calcd for C₂₅H₃₆NO₃, 398.2686).

Smenospongiarine. ¹H-NMR (C₆D₆, 500 MHz) δ 5.87 (1H, brs, -NH), 5.17 (1H, s, H-19), 4.60 (1H, dd, *J* = 1.6, 1.6 Hz, H-11a), 4.56 (1H, d, *J* = 1.6 Hz, H-11b), 2.68 (1H, d, *J* = 13.8 Hz, H-15a), 2.58 (1H, d, *J* = 13.8 Hz, H-15b), 2.38 (1H, overlapped, H-3ax), 2.37 (1H, overlapped, H-1eq), 2.19 (2H, H2-22), 2.16 (1H, dd, *J* = 13.7, 5.9 Hz, H-3eq), 1.95 (1H, ddd, *J* = 12.3, 6.0, 3.8 Hz, H-2eq), 1.53 (1H, dd, *J* = 13.5, 4.5 Hz, H-6eq), 1.44 (1H, overlapped, H-2ax), 1.43 (2H, overlapped, H-1ax, H-6ax), 1.42 (1H, dd, *J* = 5.7, 3.1 Hz, H-8), 1.40 (2H, H2-7), 1.21 (3H, d, *J* = 5.8 Hz, H3-13), 1.06 (3H, s, H3-12), 1.06 (1H, overlapped, H-24), 1.04 (1H, dd, *J* = 11.1, 1.8 Hz, H-10), 0.90 (3H, s, H3-14), 0.68 (2H, H2-23), 0.55 (6H, d, *J* = 6.6 Hz, H3-25, H3-26); HRESIMS *m/z* 412.2856 [M-H]⁻ (calcd for C₂₆H₃₈NO₃, 412.2842).

Smenospongidine. ¹H-NMR (C₆D₆, 500 MHz) δ 7.08 (2H, brd, *J* = 7.9 Hz, H-25, H-29), 7.05 (1H, brd, *J* = 7.5 Hz, H-27), 6.74 (2H, brd, *J* = 7.3 Hz, H-26, H-28), 5.91 (1H, brs, -NH), 5.12 (1H, s, H-19), 4.61 (1H, dd, *J* = 1.6, 1.6 Hz, H-11a), 4.57 (1H, brs, H-11b), 2.64 (1H, d, *J* = 13.8 Hz, H-15a), 2.53 (1H, d, *J* = 13.8 Hz, H-15b), 2.40 (2H, H2-22), 2.36 (1H, ddd, *J* = 13.7, 13.7, 7.1 Hz, H-3ax), 2.33 (1H, brd, *J* = 12.6 Hz, H-1eq), 2.19 (1H, brd, *J* = 13.7 Hz, H-3eq), 2.04 (2H, H2-23), 1.94 (1H, ddd, *J* = 12.7, 5.9, 2.4 Hz, H-2eq), 1.55 (1H, dd, *J* = 13.5, 2.9 Hz, H-6eq), 1.46 (1H, overlapped, H-1ax), 1.42 (3H, overlapped, H-2ax, H2-7), 1.41 (1H, dd, *J* = 5.7, 3.1 Hz, H-8), 1.40 (1H, overlapped, H-6ax), 1.17 (3H, d, *J* = 5.4 Hz, H3-13), 1.06 (3H, s, H-14, H3-12), 1.03 (1H, dd, *J* = 11.7, 2.2 Hz, H-10), 0.88 (3H, s, H3-14); HRESIMS *m/z* 448.2846 [M+H]⁺ (calcd for C₂₉H₃₈NO₃, 448.2842).

Ilimaquinone. ¹H-NMR (C₆D₆, 500 MHz) δ 7.37 (1H, s, 17-OH), 5.08 (1H, s, H-19), 4.58 (1H, dd, *J* = 1.6, 1.6 Hz, H-11a), 4.55 (1H, dd, *J* = 1.6, 1.6 Hz, H-11b), 2.68 (1H, d, *J* = 13.7 Hz, H-15a), 2.64 (3H, s, 20-OCH₃), 2.55 (1H, d, *J* = 13.7 Hz, H-15b), 2.35 (1H, dddd, *J* = 13.5, 11.5, 5.5, 1.6 Hz, H-3ax), 2.32 (1H, brdd, *J* = 11.5, 2.2 Hz, H-1eq), 2.13 (1H, dddd, *J* = 13.5, 4.5, 2.2, 2.2 Hz, H-3eq), 1.93 (1H, brddd, *J* = 11.7, 5.5, 2.2 Hz, H-2eq), 1.53 (1H, ddd, *J* = 11.8, 3.1, 3.1 Hz, H-6eq), 1.44 (1H, dddd, *J* = 11.5, 11.5, 11.3, 2.2 Hz, H-1ax), 1.43 (1H, dddd, *J* = 11.7, 11.5, 2.2, 2.2 Hz, H-2ax), 1.40 (1H, ddd, *J* = 11.8, 2.4, 2.4 Hz, H-6ax), 1.38 (1H, brdd, *J* = 5.8, 1.7 Hz, H-8), 1.36 (2H, H2-7), 1.16 (3H, d, *J* = 5.8 Hz, H3-13), 1.03 (3H, s, H3-12), 0.98 (1H, dd, *J* = 11.3, 2.2 Hz, H-10), 0.86 (3H, s, H3-14); HRESIMS *m/z* 381.2025 [M+Na]⁺ (calcd for C₂₂H₃₀O₄Na, 381.2034).

5-Epi-ilimaquinone. $^1\text{H-NMR}$ (C_6D_6 , 500 MHz) δ 7.36 (1H, s, 17-OH), 5.19 (1H, s, H-19), 4.81 (1H, dd, $J = 1.7, 1.7$ Hz, H-S-13 11a), 4.78 (1H, dd, $J = 1.7, 1.7$ Hz, H-11b), 2.72 (1H, d, $J = 13.6$ Hz, H-15a), 2.70 (3H, s, 20-OCH₃), 2.60 (1H, d, $J = 13.6$ Hz, H-15b), 2.43 (1H, dddd, $J = 13.9, 13.5, 6.4, 1.7$ Hz, H-3ax), 2.34 (1H, brdd, $J = 15.4, 4.3$ Hz, H-1eq), 2.12 (1H, dd, $J = 13.9, 5.5$ Hz, H-3eq), 2.05 (1H, ddd, $J = 13.9, 3.2, 3.2$ Hz, H-6eq), 1.96 (1H, dddd, $J = 15.4, 14.6, 6.4, 6.4$ Hz, H-1ax), 1.83 (1H, dddd, $J = 13.5, 13.5, 5.5, 5.5$ Hz, H-2eq), 1.64 (1H, dddd, $J = 13.5, 13.5, 11.7, 2.3$ Hz, H-2ax), 1.61 (1H, ddd, $J = 13.4, 6.4, 3.2$ Hz, H-7eq), 1.37 (1H, ddd, $J = 6.4, 6.4, 3.5$ Hz, H-8), 1.36 (1H, dd, $J = 6.4, 4.3$ Hz, H-10), 1.22 (1H, dddd, $J = 13.4, 7.7, 3.5, 3.2$ Hz, H-7ax), 1.12 (3H, d, $J = 6.4$ Hz, H3-13), 1.10 (1H, ddd, $J = 13.9, 7.7, 3.5$ Hz, H-6ax), 1.10 (3H, s, H3-12), 1.00 (3H, s, H3-14); HRESIMS m/z 381.2047 $[\text{M}+\text{Na}]^+$ (calcd for $\text{C}_{22}\text{H}_{30}\text{O}_4\text{Na}$, 381.2034).

Quintaquinone. $^1\text{H-NMR}$ (C_6D_6 , 500 MHz) δ 4.59 (1H, dd, $J = 1.6, 1.6$ Hz, H-11a), 4.55 (1H, brs, H-11b), 3.78 (3H, s, 20-OCH₃), 2.66 (1H, d, $J = 13.6$ Hz, H-15a), 2.51 (1H, d, $J = 13.6$ Hz, H-15b), 2.35 (1H, dddd, $J = 11.5, 11.2, 3.2, 1.6$ Hz, H-3ax), 2.30 (2H, H2-22), 2.28 (1H, ddd, $J = 11.2, 3.5, 1.8$ Hz, H-1eq), 2.14 (1H, dd, $J = 11.5, 2.2$ Hz, H-3eq), 1.93 (1H, ddd, $J = 11.2, 3.2, 2.2$ Hz, H-2eq), 1.86 (2H, t, $J = 7.3$ Hz, H2-25), 1.61 (3H, s, H3-27), 1.55 (1H, brdd, $J = 10.9, 2.6$ Hz, H-6eq), 1.45 (3H, ddd, $J = 11.2, 11.2, 2.2$ Hz, H-1ax, H2-24), 1.42 (2H, ddd, $J = 10.9, 10.9, 2.6$ Hz, H-6ax, H-7eq), 1.40 (1H, dddd, $J = 11.2, 11.2, 3.5, 2.2$ Hz, H-2ax), 1.35 (1H, overlapped, H-7ax), 1.32 (1H, dq, $J = 12.2, 6.0$ Hz, H-8), 1.26 (2H, H2-23), 1.13 (3H, d, $J = 6.0$ Hz, H3-13), 1.04 (3H, s, H3-12), 0.96 (1H, dd, $J = 11.2, 1.8$ Hz, H-10), 0.86 (3H, s, H3-14); HRESIMS m/z 479.2763 $[\text{M}+\text{Na}]^+$ (calcd for $\text{C}_{28}\text{H}_{40}\text{O}_5\text{Na}$, 479.2763).

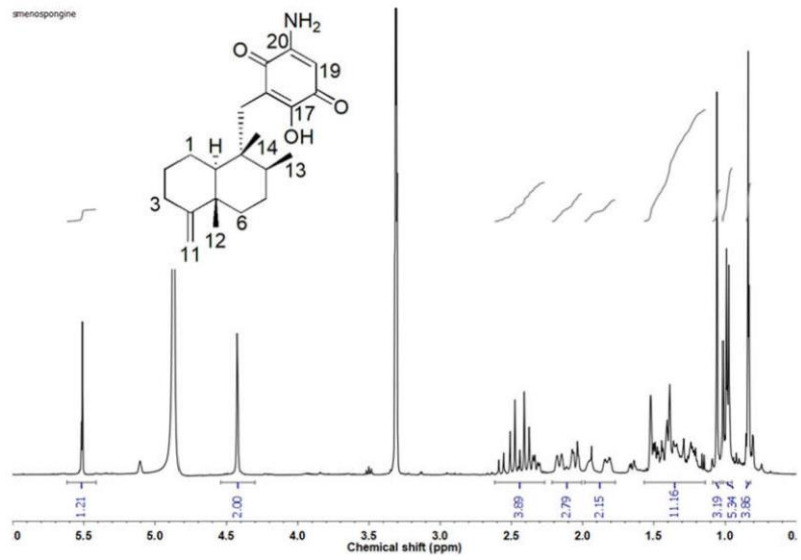
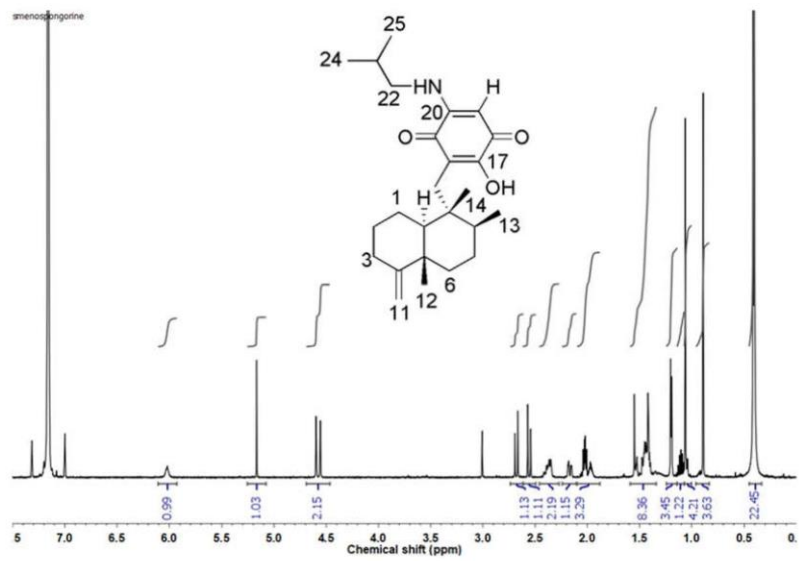
Cyclospingiaquinone-1. $^1\text{H-NMR}$ (C_6D_6 , 500 MHz) δ 5.41 (1H, s, H-19), 2.88 (3H, s, 20-OCH₃), 2.45 (1H, dd, $J = 18, 4.7$ Hz, H-15a), 1.97 (1H, ddd, $J = 12.7, 3.3, 3.3$ Hz, H-7eq), 1.91 (1H, dd, $J = 18, 12.9$ Hz, H-15b), 1.57 (1H, ddd, $J = 12.7, 12.7, 4.4$ Hz, H-7ax), 1.37 (1H, ddd, $J = 13.8, 7.1, 3.6$ Hz, H-2eq), 1.32 (1H, ddd, $J = 12.8, 7.2, 3.4$ Hz, H-1eq), 1.27 (1H, ddd, $J = 13.1, 4.3, 2.9$ Hz, H-6eq), 1.25 (1H, ddd, $J = 13.9, 5.2, 3.2$ Hz, H-3eq), 1.22 (1H, ddd, $J = 13.1, 7.1, 3.5$ Hz, H-6ax), 1.07 (1H, dd, $J = 12.9, 4.7$ Hz, H-9), 0.97 (1H, ddd, $J = 13.9, 13.9, 3.8$ Hz, H-3ax), 0.90 (1H, ddd, $J = 13.8, 13.8, 3.4$ Hz, H-2ax), 0.90 (3H, s, H3-13), 0.74 (3H, s, H3-12), 0.66 (3H, s, H3-11), 0.62 (1H, dd, $J = 12.4, 2.2$ Hz, H-5), 0.54 (1H, ddd, $J = 12.8, 3.3, 3.3$ Hz, H-1ax), 0.49 (3H, s, H3-14); ESIMS m/z 381.2037 $[\text{M}+\text{Na}]^+$ (calcd for $\text{C}_{22}\text{H}_{30}\text{O}_4\text{Na}$, 381.2034).

Smenodiol. $^1\text{H-NMR}$ (C_6D_6 , 500 MHz) δ 7.96 (1H, brs, H-17), 7.41 (1H, brs, H-19), 5.77 (1H, brs, 21-OH), 5.41 (1H, brs, H-7), 5.01 (1H, brs, 20-OH), 3.51 (3H, s, 22-OCH₃), 2.89 (1H, dd, $J = 15.4, 9.4$ Hz, H-15a), 2.69 (1H, dd, $J = 15.4, 2.5$ Hz, H-15b), 2.56 (1H, brd, $J = 9.4$ Hz, H-9), 1.94 (1H, brd, $J = 13.0$ Hz, H-6eq), 1.86 (2H, overlapped, H-1eq, H-6ax), 1.64 (3H, dd, $J = 2.2, 1.2$ Hz, H3-13), 1.47 (1H, ddd, $J = 13.0, 3.3, 3.3$ Hz, H-2eq), 1.35 (2H, ddd, $J = 13.0, 5.6, 3.3$ Hz, H-2ax, H-3eq), 1.20 (1H, dd, $J = 11.8, 5.1$ Hz, H-5), 1.12 (1H, ddd, $J = 13.0, 10.1, 3.3$ Hz, H-1ax), 1.10 (1H, ddd, $J = 13.0, 10.1, 3.3$ Hz, H-3ax), 0.90 (3H, s, H3-14), 0.86 (3H, s, H3-11), 0.83 (3H, s, H3-12); HRESIMS m/z 373.2369 $[\text{M}+\text{H}]^+$ (calcd for $\text{C}_{23}\text{H}_{33}\text{O}_4$, 373.2370).

Dactylospontriol. $^1\text{H-NMR}$ (C_6D_6 , 500 MHz) δ 11.29 (1H, s, 19-OH), 7.55 (1H, s, H-17), 5.78 (1H, s, 20-OH), 5.42 (1H, s, H-7), 3.31 (3H, s, 22-OCH₃), 2.82 (1H, d, $J = 15.5$ Hz, H-15a), 2.65 (1H, dd, $J = 15.5, 9.6$ Hz, H-15b), 2.51 (1H, brs, H-9), 1.94 (1H, overlapped, H-6eq), 1.87 (1H, overlapped, H-6ax), 1.85 (1H, overlapped, H-1eq), 1.66 (3H, s, H3-13), 1.48 (1H, overlapped, H-2eq), 1.35 (1H, overlapped, H-2ax), 1.33 (1H, overlapped, H-3eq), 1.21 (1H, dd, $J = 11.7, 5.0$ Hz, H-5), 1.08 (1H, overlapped, H-1ax), 1.05 (1H, overlapped, H-3ax), 0.89 (3H, s, H3-14), 0.85 (3H, s, H3-11), 0.82 (3H, s, H3-12); EIMS m/z (% relative intensity): 388 ($[\text{M}]^+$, 36), 197 (100), 164 (40).

3-Farnesyl-2-hydroxy-5-methoxyquinone. $^1\text{H-NMR}$ (C_6D_6 , 500 MHz) δ 5.48 (1H, tq, $J = 7.1, 1.2$ Hz, H-2'), 5.22 (2H, tq, $J = 6.9, 1.4$ Hz, H-6', H-10'), 5.13 (1H, s, H-6), 3.30 (2H, d, $J = 7.1$ Hz, H2-1'), 2.72 (3H, s, 5-OCH₃), 2.15 (2H, overlapped, H2-5'), 2.14 (2H, overlapped, H2-9'), 2.04 (2H, overlapped, H2-4'), 2.03 (2H, overlapped, H2-8'), 1.82 (3H, brs, 3'-CH₃), 1.67 (3H, d, $J = 1.10$ Hz, H3-12'), 1.55 (3H, s, 7'-CH₃), 1.54 (3H, s, 11'-CH₃); HRESIMS m/z 359.2211 $[\text{M}+\text{H}]^+$ (calcd for $\text{C}_{22}\text{H}_{31}\text{O}_4$, 359.2214).

Supplementary Figures

Figure S1. $^1\text{H-NMR}$ of smenospongine (400 MHz, CD_3OD).Figure S2. $^1\text{H-NMR}$ of smenospongine (500 MHz, C_6D_6).

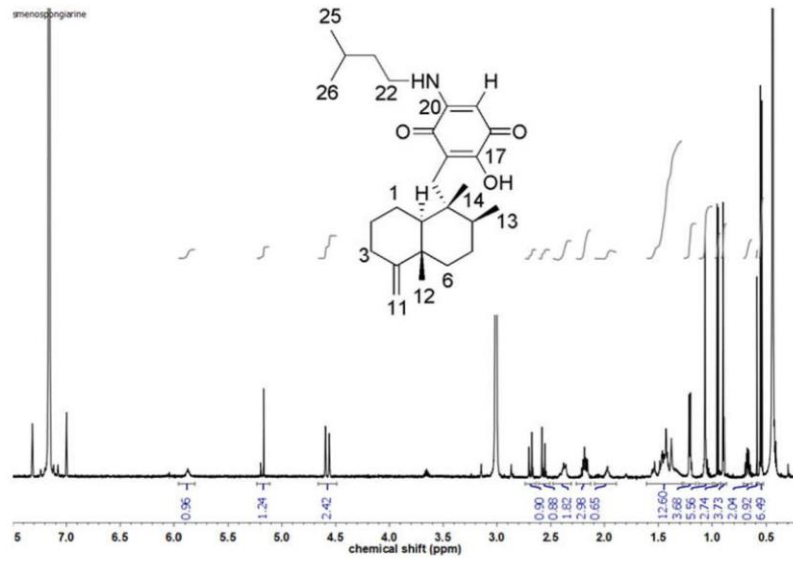


Figure S3. ¹H-NMR of smenospongine (500 MHz, C₆D₆).

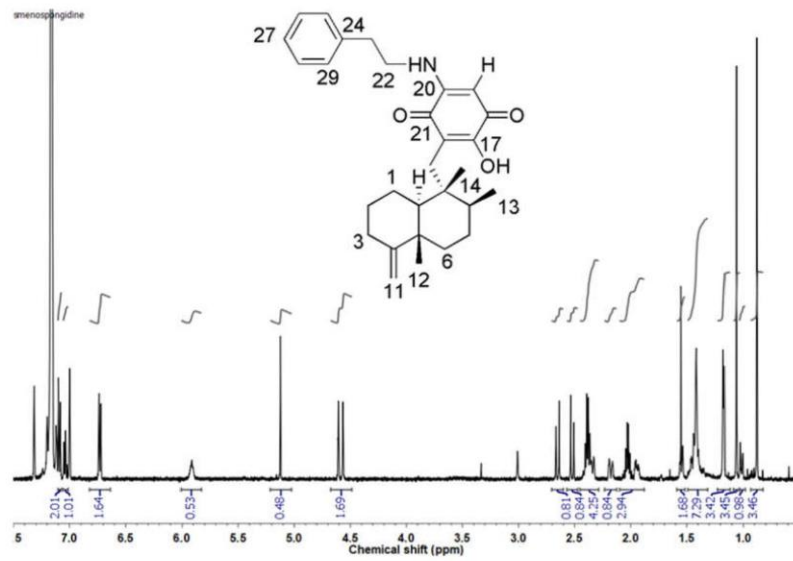


Figure S4. ¹H-NMR of smenospondine (500 MHz, C₆D₆).

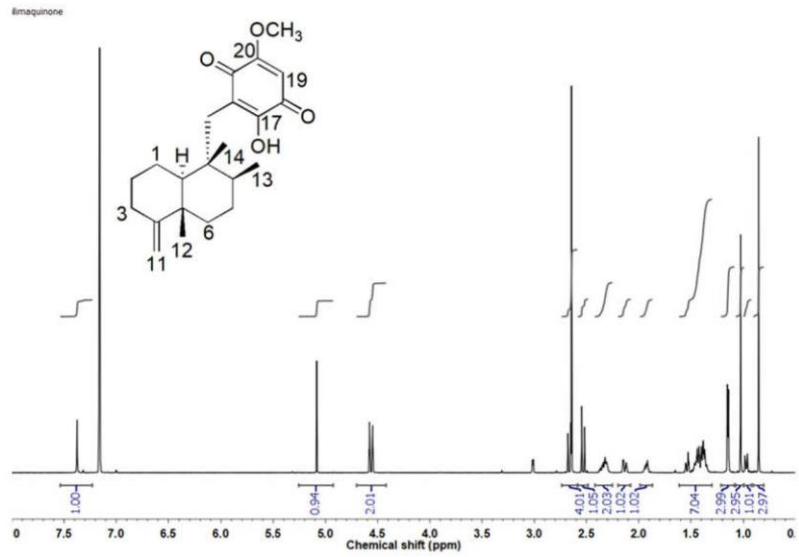


Figure S5. $^1\text{H-NMR}$ of ilimaquinone (500 MHz, C_6D_6).

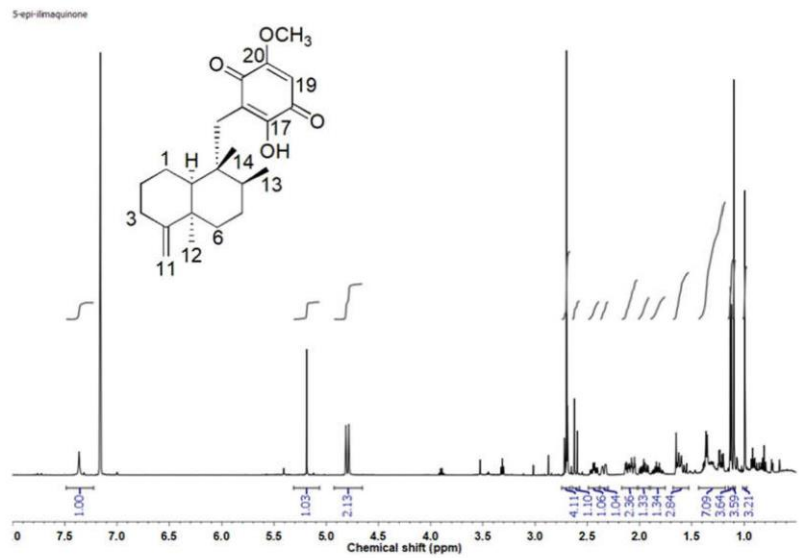


Figure S6. $^1\text{H-NMR}$ of 5-*epi*-ilimaquinone (500 MHz, C_6D_6).

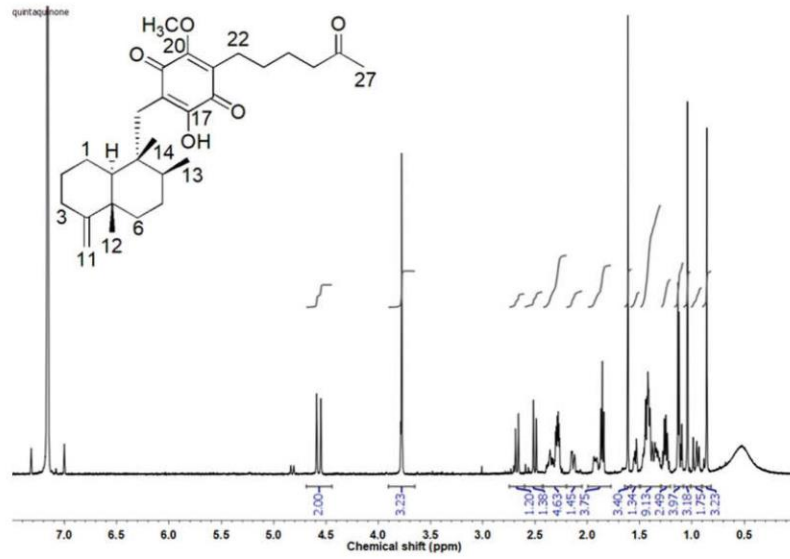


Figure S7. ¹H-NMR of quintaquinone (500 MHz, C₆D₆).

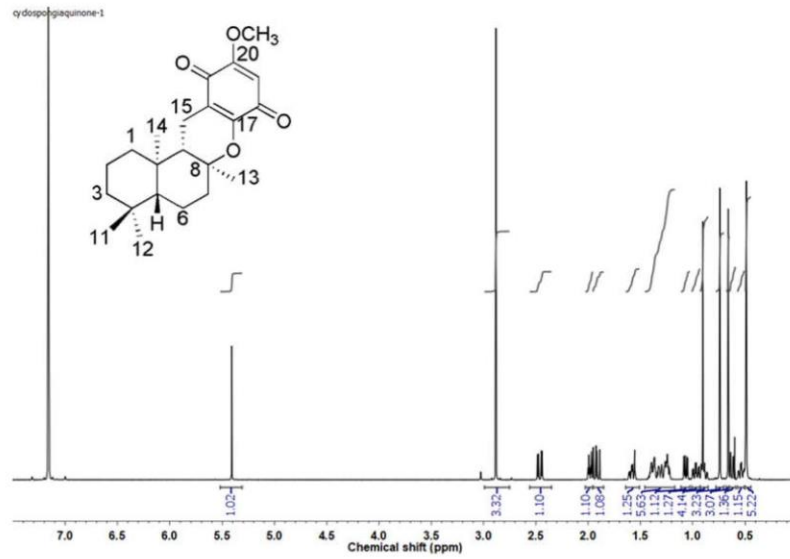


Figure S8. ¹H-NMR of cyclospogoniaquinone-1 (500 MHz, C₆D₆).

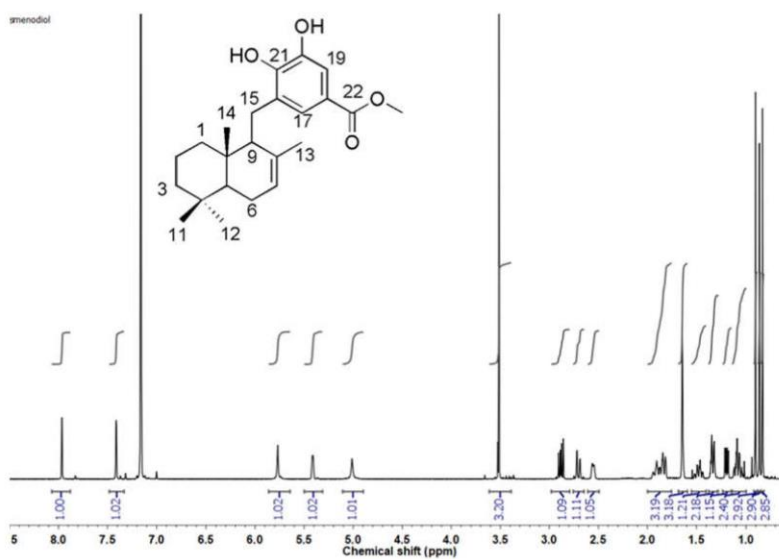


Figure S9. ¹H-NMR of smenodiol (500 MHz, C₆D₆).

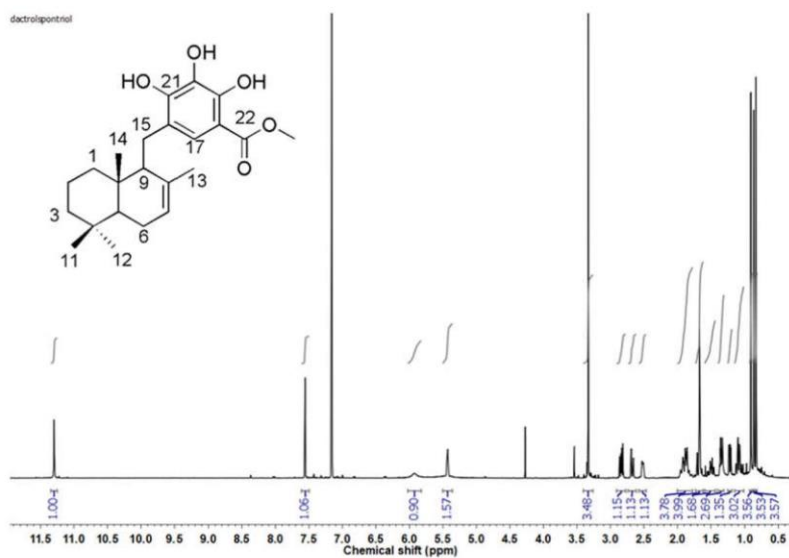


Figure S10. ¹H-NMR of dactylospontriol (500 MHz, C₆D₆).

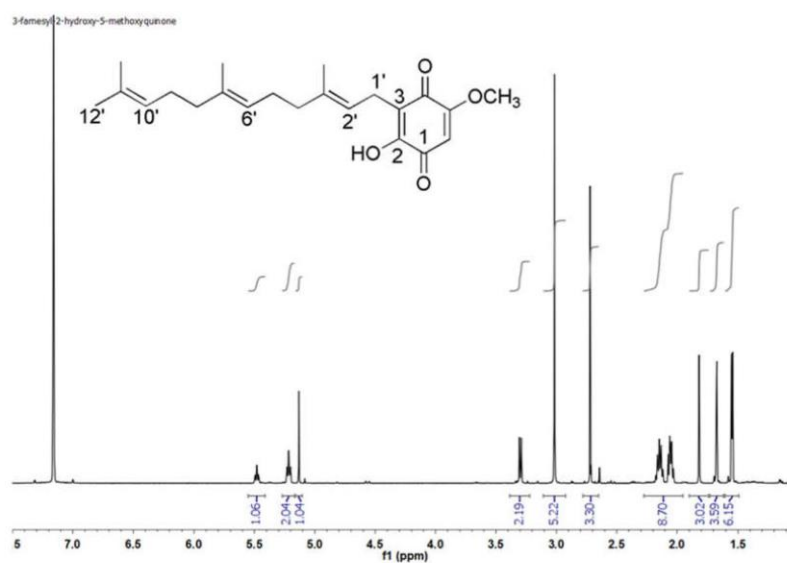


Figure S12

Western blots HCT116 cells, Fig. 3D

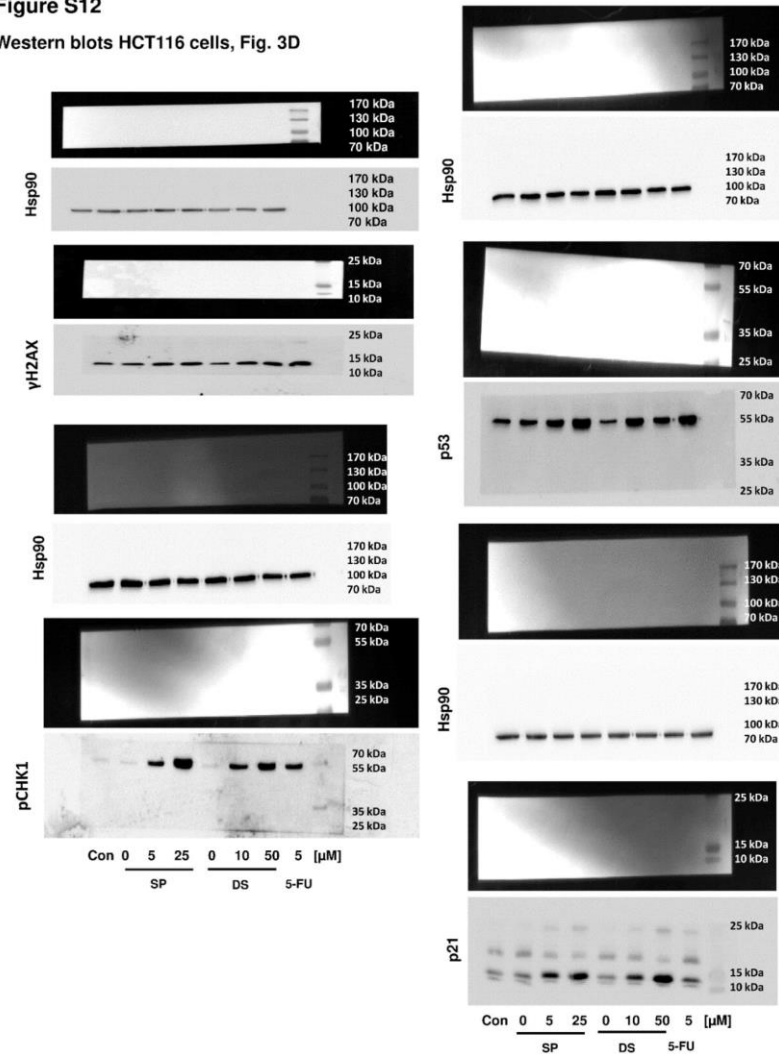


Figure S13

Western blots HT29 cells, Fig. 3D

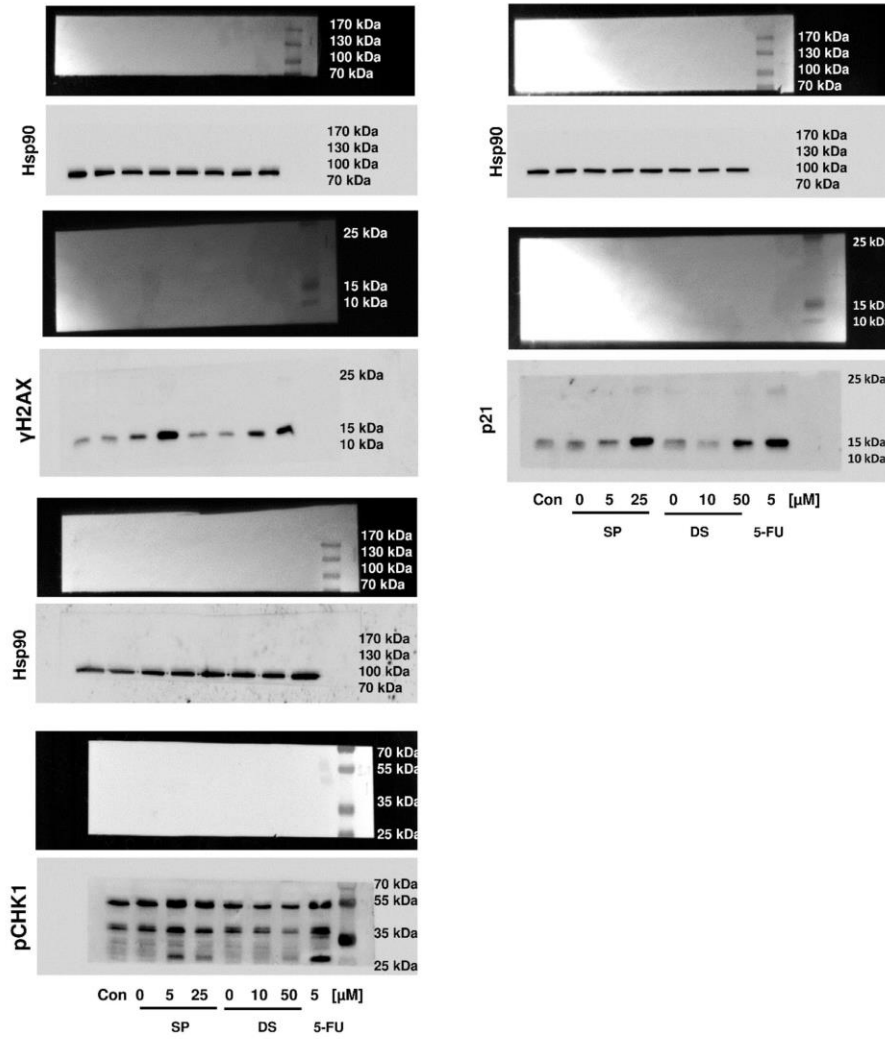


Figure S14

Western blots HCT116 cells, Fig. 6C and HT29 cells, Fig. 7C

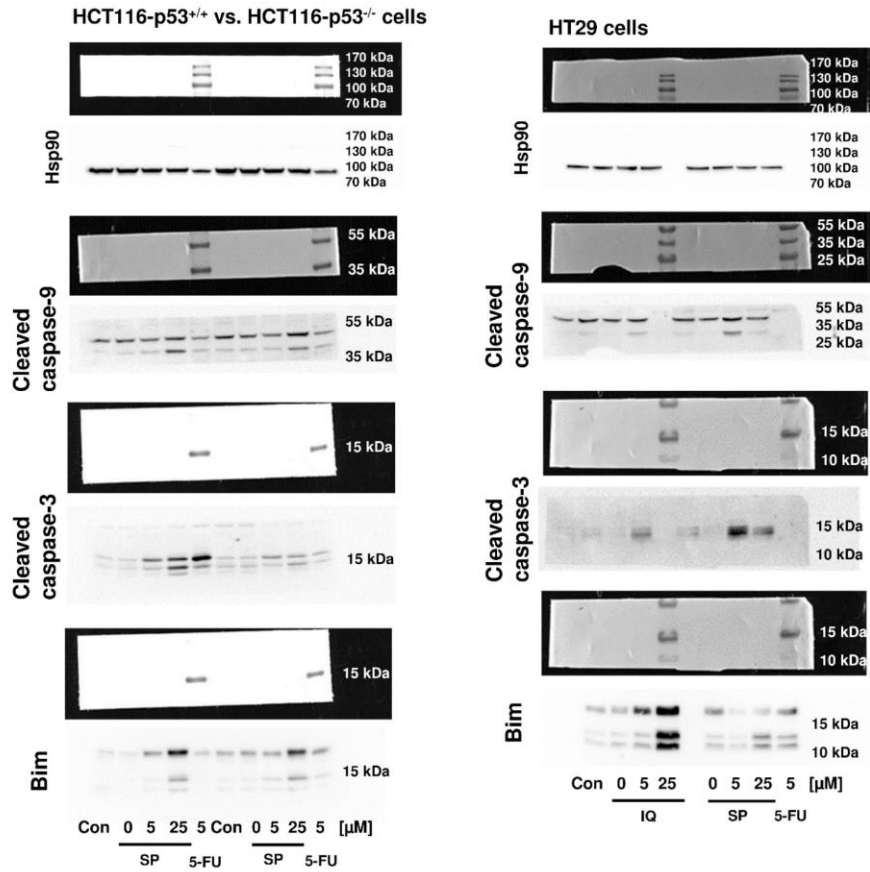
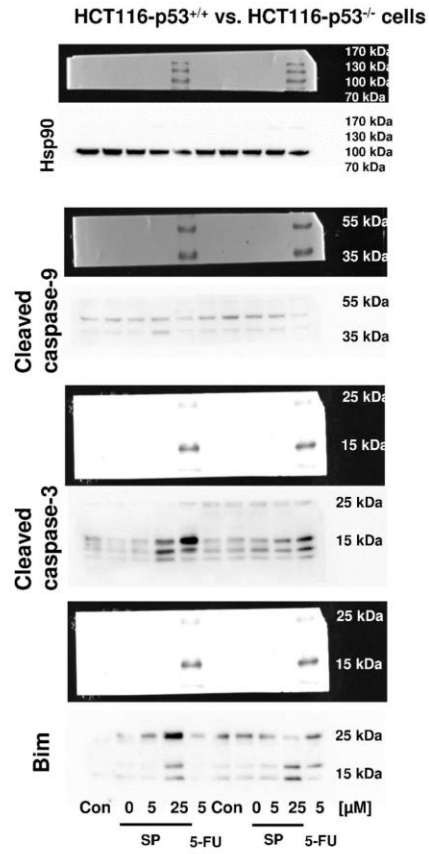


Figure S15

Western blots HCT116 cells, Fig. A5A



3.3. Targeting PARP-1 and DNA Damage Response Defects in Colorectal Cancer Chemotherapy with Established and Novel PARP Inhibitors

Publication III

Philipp Demuth, Lea Thibol, Anna Lemsch, Felix Potlitz, Lukas Schulig, Christoph Grathwol, Georg Manolikakes, Dennis Schade, Vassilis Roukos, Andreas Link, Jörg Fahrer

First, I would like to expand on my participation in this publication and the collaborations that enabled this work. Publication III, of which I am first author, was prepared in cooperation with 10 coauthors. The manuscript has been submitted to an international peer reviewed journal and is currently under review. The test substances were provided by the Institute of Biological and Chemical Systems - Functional Molecular Systems (IBCS-FMS), at the Karlsruhe Institute of Technology (KIT) in Eggenstein-Leopoldshafen, Germany. During the creation of this publication, I took part in the formal analysis, validation, investigation and methodology as well as visualization, writing of the original draft and its subsequent review and editing. The experiments I conducted for this publication included the enzymatic PARP-1 inhibitor screening assay as well as the subsequent microscopy-based quantification of PARylation in HCT116 cells after treatment with four selected inhibitor candidates (X17613, X17618, X17620 & X17621). In addition, I performed the cytotoxicity assessment of olaparib, veliparib and the two novel inhibitor candidates (X17613 & X17618) in combination with established cytostatic drugs (IT, OXA and 5-FU) in HCT116 WT and BRCA2^{-/-} cells. I conducted the western blot-based quantification of PARP-1 trapping in response to two selected inhibitor candidates (X17613 & X17618) and the positive control olaparib in HCT116 cells. Furthermore, I measured the induction of γH2AX in response to X17613, IT and the combination treatment in HCT116 WT and BRCA2^{-/-} cells by western blot analysis.

This publication appeared in the peer-reviewed journal *Cancers* (Volume 16) in October 2024.

Demuth, P., Thibol, L., Lemsch, A., Potlitz, F., Schulig, L., Grathwol, C., Manolikakes, G., Schade, D., Roukos, V., Link, A., & Fahrer, J. (2024). Targeting PARP-1 and DNA Damage Response Defects in Colorectal Cancer Chemotherapy with Established and Novel PARP Inhibitors. *Cancers*, 16(20), 3441.

DOI: <https://doi.org/10.3390/cancers16203441>



Article

Targeting PARP-1 and DNA Damage Response Defects in Colorectal Cancer Chemotherapy with Established and Novel PARP Inhibitors

Philipp Demuth ¹, Lea Thibol ¹, Anna Lemsch ¹, Felix Potlitz ², Lukas Schulig ², Christoph Grathwol ³, Georg Manolikakes ⁴, Dennis Schade ⁵, Vassilis Roukos ⁶, Andreas Link ² and Jörg Fahrner ^{1,*}

¹ Department of Chemistry, Division of Food Chemistry and Toxicology, RPTU Kaiserslautern-Landau, 67663 Kaiserslautern, Germany; pdemuth@rptu.de (P.D.); thibol@rptu.de (L.T.); anna.lemsch@gmx.de (A.L.)

² Department of Pharmaceutical and Medicinal Chemistry, Institute of Pharmacy, University of Greifswald, 17489 Greifswald, Germany; felix.potlitz@gmail.com (F.P.); lukas.schulig@uni-greifswald.de (L.S.); link@uni-greifswald.de (A.L.)

³ Institute of Biological and Chemical Systems—Functional Molecular Systems (IBCS-FMS), Karlsruhe Institute of Technology (KIT), 76344 Eggenstein-Leopoldshafen, Germany; christoph.grathwol@kit.edu

⁴ Department of Chemistry, RPTU Kaiserslautern-Landau, 67663 Kaiserslautern, Germany; manolikakes@chemie.uni-kl.de

⁵ Department of Pharmaceutical and Medicinal Chemistry, Institute of Pharmacy, Christian-Albrechts-University of Kiel, 24118 Kiel, Germany; schade@pharmazie.uni-kiel.de

⁶ Institute of Molecular Biology, 55128 Mainz, Germany; v.roukos@imb-mainz.de

* Correspondence: fahrner@chemie.uni-kl.de; Tel.: + 49-631-205-2974



Citation: Demuth, P.; Thibol, L.; Lemsch, A.; Potlitz, F.; Schulig, L.; Grathwol, C.; Manolikakes, G.; Schade, D.; Roukos, V.; Link, A.; et al. Targeting PARP-1 and DNA Damage Response Defects in Colorectal Cancer Chemotherapy with Established and Novel PARP Inhibitors. *Cancers* **2024**, *16*, 3441. <https://doi.org/10.3390/cancers16203441>

Academic Editors: Gabriella D'Orazi and Mara Cirone

Received: 28 August 2024

Revised: 28 September 2024

Accepted: 7 October 2024

Published: 10 October 2024



Copyright: © 2024 by the authors. Licensee MDPI, Basel, Switzerland. This article is an open access article distributed under the terms and conditions of the Creative Commons Attribution (CC BY) license (<https://creativecommons.org/licenses/by/4.0/>).

Simple Summary: Inhibition of the DNA repair protein PARP-1 is a promising concept in cancer therapy. More recently, PARP-1 has been revealed as a possible target in colorectal cancer, which is the second leading cause of cancer-related death worldwide. In this work, we screened a compound library to identify novel PARP inhibitors with low cytotoxicity and tested their efficacy in colorectal cancer cell models with and without defects in the DNA damage response. Furthermore, we evaluated whether the putative PARP inhibitors synergize with chemotherapeutic drugs used in the clinics to treat colorectal cancer patients. Using various experimental approaches, we were able to identify two promising molecules with potent PARP inhibition in colorectal cancer cells without causing cytotoxicity on their own. Moreover, the novel PARP inhibitors sensitized colorectal cancer cells to the anticancer drug irinotecan dependent on homologous recombination deficiency. Remarkably, the clinically approved PARP inhibitor olaparib displayed the strongest synergistic effects, but it was also cytotoxic as a single agent in wildtype colorectal cancer cells. The novel PARP inhibitors might, therefore, be useful for a combination therapy with irinotecan to avoid overlapping toxicity on healthy tissue such as bone marrow, which warrants further preclinical studies.

Abstract: The DNA repair protein PARP-1 emerged as a valuable target in the treatment of tumor entities with deficiencies of *BRCA1/2*, such as breast cancer. More recently, the application of PARP inhibitors (PARPi) such as olaparib has been expanded to other cancer entities including colorectal cancer (CRC). We previously demonstrated that PARP-1 is overexpressed in human CRC and promotes CRC progression in a mouse model. However, acquired resistance to PARPi and cytotoxicity-mediated adverse effects limit their clinical applicability. Here, we detailed the role of PARP-1 as a therapeutic target in CRC and studied the efficacy of novel PARPi compounds in wildtype (WT) and DNA repair-deficient CRC cell lines together with the chemotherapeutics irinotecan (IT), 5-fluorouracil (5-FU), and oxaliplatin (OXA). Based on the ComPlat molecule archive, we identified novel PARPi candidates by molecular docking experiments *in silico*, which were then confirmed by *in vitro* PARP activity measurements. Two promising candidates (X17613 and X17618) also showed potent PARP-1 inhibition in a CRC cell-based assay. In contrast to olaparib, the PARPi candidates caused no PARP-1 trapping and, consistently, were not or only weakly cytotoxic in WT CRC cells and their BRCA2- or ATR-deficient counterparts. Importantly, both PARPi candidates did not affect the viability of nonmalignant human colonic epithelial cells. While both olaparib and

veliparib increased the sensitivity of WT CRC cells towards IT, no synergism was observed for X17613 and X17618. Finally, we provided evidence that all PARPi (olaparib > veliparib > X17613 > X17618) synergize with chemotherapeutic drugs (IT > OXA) in a BRCA2-dependent manner in CRC cells, whereas ATR deficiency had only a minor impact. Collectively, our study identified novel lead structures with potent PARP-1 inhibitory activity in CRC cells but low cytotoxicity due to the lack of PARP-1 trapping, which synergized with IT in homologous recombination deficiency.

Keywords: PARP-1; colorectal cancer; synthetic lethality; DNA damage response; chemotherapy

1. Introduction

Despite ongoing progress in the development of new approaches for CRC therapy, the five-year survival rate is still low, making it the second leading cause of cancer-related death worldwide [1]. An increasing incidence was observed primarily among younger age groups, which was attributed to changing lifestyle, medication, and environmental factors [2]. Current treatment of advanced CRC is based on surgery and chemotherapy with the DNA damage-inducing drugs irinotecan (IT), oxaliplatin (OXA) and 5-fluorouracil (5-FU), which are combined in several chemotherapy regimens [3]. Both the development of resistance during prolonged application and systemic toxicity limit the efficacy of currently used therapeutics [4].

Colorectal carcinogenesis is associated with (epi)genetic alterations of DNA repair. In hereditary CRC, mutations of DNA mismatch repair (MMR) genes such as *MLH1* and *MSH2* give rise to microsatellite instability (MSI) [5]. The MMR gene *MLH1* can also be epigenetically inactivated in sporadic CRC together with other genes, which is referred to as a CpG island methylator phenotype (CIMP) and results in MSI as well [5]. In contrast, the vast majority of sporadic CRC cases (up to 90%) arise through the chromosomal instability pathway (CIN), which is characterized by microsatellite stability (MSS) [6]. Furthermore, sporadic CRC formation is frequently accompanied by epigenetic inactivation of *MGMT* involved in the repair of DNA alkylation damage [7]. Mutations of *BRCA2* required for homologous recombination (HR)-mediated DNA repair occur rarely but were observed predominantly in young patients [8]. However, they have not been causally linked to an increased CRC susceptibility, unlike *BRCA1* mutations [9]. Interestingly, a more comprehensive study revealed that around 14% of all CRC cases exhibit HR deficiency (HRD) [10].

DNA damage induction represents the primary mechanism of anticancer drugs used in CRC treatment [11]. A fundamental component of the DNA damage response (DDR) is the enzyme poly (ADP-ribose) polymerase 1 (PARP-1) [12,13]. After binding to DNA strand breaks, PARP-1 is activated and catalyzes the post-translational formation of poly ADP-ribose (PAR) on various acceptor proteins, associated with DNA repair, histone modification, or cell cycle progression [13,14]. We found that PARP-1 is overexpressed in human CRC tissue, correlating with disease progression [15]. Using a CRC mouse model, we further demonstrated that PARP-1 protects against colorectal tumor induction, whereas it promoted colorectal tumor progression driven by intestinal inflammation [15]. These findings highlight the potential benefit arising from pharmacological PARP inhibition in CRC.

In recent years, several PARP inhibitors (PARPi) have been clinically approved for the treatment of ovarian and breast cancer [12,16]. The PARPi olaparib, rucaparib, and niraparib were shown to induce synthetic lethality in tumors deficient in *BRCA1/2* [17]. The application of PARPi is currently expanded beyond *BRCA1/2* deficiency to malignancies with other defects in HR and extensive testing may identify patient populations that benefit from PARPi treatment [18,19]. This includes defects of the apical DDR kinases ATM and ATR, as well as *RAD51* involved in HR [20]. Mutations of *MRE11*, which is important for the detection of DNA double-strand breaks (DSBs), were reported to occur in CRC with

MSI [21] and lead to higher cytotoxicity of PARPi in vitro [22] but not in patients receiving monotherapy [23]. Deficiency of ATM, which is observed in up to 10% of CRC cases, is accompanied by sensitivity towards olaparib, especially in the absence of wildtype (WT) p53 [24]. Although the anticancer effects of PARPi generally rely on mutations in DDR genes, multiple lines of evidence suggest a synergistic effect of PARPi and conventional chemotherapy also in tumors without genetic alterations of DNA repair [12,25]. Molecular susceptibilities beyond HRD have been identified in CRC [19]. Increased sensitivity towards the PARP inhibitor olaparib was found in patient-derived HROC278-Met cells containing a *BRAF* mutation [26]. Furthermore, *KRAS* mutant intrahepatic cholangiocarcinoma cells were shown to be highly sensitive to PARP inhibition [27], which might also hold true for *KRAS* mutated CRC. Despite these promising results from preclinical and clinical studies, the application of PARPi in cancer therapy is limited due to the development of PARPi resistance and adverse effects such as bone marrow toxicity, fatigue, and gastrointestinal toxicity [28,29].

In view of the emerging role of PARP-1 as a therapeutic target in CRC and the limitations observed for established PARPi, we aimed to identify PARPi with novel scaffolds and lower toxicity, in order to test their activity in MSI and MSS CRC cell lines without or with DDR defects. By in silico analysis, a set of 12 possible PARP inhibitors was identified and tested with a recombinant PARP-1 enzyme activity assay. The four most potent compounds were then used in an immunofluorescence-based PARP-1 activity assay applying human CRC cells. After identifying the two most potent inhibitors, their potential to cause PARP-1 trapping and their cytotoxicity was investigated in CRC cells proficient or deficient for PARP-1, BRCA2, and ATR and compared to human colonic epithelial cells (HCEC). Furthermore, the putative synergism with the chemotherapeutics IT, OXA, and 5-FU was investigated in CRC cell models with and without the DDR defects.

2. Material and Methods

2.1. Test Compounds

Synthesis of test compounds X17613, X17618, X17620, and X17621, and analysis by ESI mass spectrometry and NMR spectroscopy were conducted as described in SI material and methods. ¹H and ¹³C-NMR spectra are shown in Supplementary Figures S1–S8. The test compounds X17608, X17610, X17611, X17616, X4739, X5157, X9563, and X12750 were kindly provided by ComPlat (KIT, Karlsruhe, Germany).

2.2. Molecular Docking

The virtual screening was calculated and analyzed using Schrödinger release 2020-4 (Schrödinger, LLC, New York, NY, USA, 2021). All protein structures (RCSB PDB: 4PJT [30], 7AAC, 7AAD [31]) were prepared using the Protein Preparation Wizard [32] by adding hydrogen atoms, assigning OPLS3e force field parameters [33], and replacing missing side chains or loops with Prime [34], followed by H-bond assignment optimization and restraint minimization. Before molecular docking, all compounds of the ComPlat library were prepared with LigPrep to predict possible protonation states and configurations. The hydrogen bonds to either G863 or S904 were set as constraints for Glide grid generation. Next, molecular docking with flexible ligands and rigid protein conformation was performed with Glide SP scoring [35]. Finally, the binding poses were visually inspected and re-scored with Glide XP to obtain the binding free energy values [36].

2.3. PARP Inhibitor Assay

Twelve compounds were screened regarding their ability to inhibit PARP-1 enzyme activity in vitro. Therefore, we utilized a chemiluminescence-based PARP-1 assay kit (BPS Bioscience, San Diego, CA, USA) and performed two independent experiments according to the manufacturer's instructions. Briefly, non-transparent 96-well plates were coated with histones overnight. Substances were tested in duplicates, applying concentrations of 0.001, 0.01, 0.1, 1, 10, and 100 µM. Olaparib and veliparib in concentrations of 5 and

50 nM served as positive controls. After adding activated DNA and biotinylated NAD⁺, the ADP-ribosylation reaction was initiated by the addition of PARP-1 enzyme and incubated at RT for 1 h. Quantification of biotinylated PAR was conducted by using Streptavidin-HRP and subsequent ECL-based detection of chemiluminescence, applying a Spark[®] multiplate reader (Tecan, Crailsheim, Germany). The lowest applied concentration was set to 100% and IC₅₀ values were calculated by nonlinear regression using GraphPad Prism 9.0 Software (GraphPad Software Inc., Boston, MA, USA).

2.4. Cell Culture and Treatments

Genetically engineered HCT116 PARP-1^{+/+} and HCT116 PARP-1^{-/-} were generated in 2017 by CRISPR-based targeting as described elsewhere [15]. Wildtype HCT116 cells were obtained from the Core Cell Center (John Hopkins University, Baltimore, MD, USA) in 2012, while HCT116 BRCA2^{-/-} cells were kindly provided by Dr. Carlos Caldas in 2017 (University of Cambridge, Cambridge, UK) [37]. Parental DLD-1 ATR^{+/+} and DLD-1 ATR^{s/s} cells were generated by Dr. Fred Bunz (John Hopkins University, Baltimore, USA) [38] and obtained in 2018. Caco-2 cells were obtained from CLS Cell Lines Service (Eppelheim, Germany) in 2012. Non-transformed human colonic epithelial cells (HCEC; 1CT) were established by Dr. Jerry W. Shay (UT Southwestern Medical Center, Dallas, TX, USA) [39] and kindly provided in 2015. Cells lines were re-authenticated by p53, PARP-1, ATR, and BRCA2 immunoblotting, by their characteristic differential response to genotoxic agents and their typical cell morphology. HCT116, HCT116 BRCA2^{-/-}, DLD-1 ATR^{+/+} and DLD-1 ATR^{s/s} cells were maintained in DMEM, whereas HCT116 PARP-1^{+/+} and HCT116 PARP-1^{-/-} cells were maintained in RPMI1640 containing 10% FCS and 1% penicillin/streptomycin in a humidified atmosphere at 37 °C and 5% CO₂. Caco-2 cells were cultured in MEM with 10% FCS, 1% penicillin/streptomycin, and nonessential amino acids. HCECs were grown in a nitrogen incubator with reduced oxygen levels (7% O₂) and 5% CO₂ at 37 °C in DMEM GlutaMax/Medium 199 (4:1) with supplements as reported previously [40]. The media and supplements were obtained from PAN-Biotech (Aidenbach, Germany) and Thermo Fisher Scientific (Darmstadt, Germany). Cell culture was frequently tested for contamination with mycoplasma by PCR using the Venor[®] GeM Classic kit (Minerva Biolabs, Berlin, Germany) and immunofluorescence microscopy with nuclear staining. The PARP inhibitors olaparib and veliparib were from MedChemExpress and bought at Hycultec (Beutelsbach, Germany). The PARP inhibitors as well as the test compounds were dissolved in DMSO as 10 mM stock solution and used in cell culture experiments in a final concentration range from 0 to 50 μM. DMSO, in a concentration equivalent to the highest inhibitor concentration used, served as a negative control (0 μM). Cells were exposed for 1 h for the quantification of PARP-1 trapping or 2 h for assessing the inhibitory potential by confocal fluorescence microscopy. PARP activity was either induced by methyl methanesulfonate (MMS) cotreatment (1 mM) for 1 h (PARP trapping) or by treatment with H₂O₂ (1 mM) for 5 min subsequent to inhibitor incubation. The chemotherapeutic drugs 5-FU, IT, and OXA (all from MedChemExpress and purchased at Hycultec, Beutelsbach, Germany) were dissolved in water or DMSO as 75 mM, 34 mM, and 10 mM stock solution, respectively, and used as indicated. If the PARPi treatment was conducted in combination with cytostatic drugs for 24 h (γH2AX Western blot analysis) or 72 h (cytotoxicity testing), the PARPi was added 2 h prior.

2.5. Cytotoxicity Testing of PARP Inhibitors

To assess the cytotoxicity of newly developed PARP inhibitors, cells were cultivated in translucent 96-well plates overnight and treated with PARP inhibitors or cytostatic drugs for 72 h. For the assessment of synergistic activity, cells were pretreated with the inhibitors for 2 h, before the inhibitor or cytostatic drug was added. Cell viability was assessed by the resazurin reduction assay (RRA) as described previously [41], and fluorescence was measured using a Spark[®] Multi-well reader (Tecan, Crailsheim, Germany). IC₅₀ values were calculated using GraphPad Prism 9.0 software (GraphPad Software Inc., Boston, MA,

USA). To this end, concentrations were transformed into the log scale, plotted against the cell viability and the curve was fitted by nonlinear regression with variable slope, providing the IC₅₀ values.

2.6. PAR Immunofluorescence Analysis

The activity of potential PARP inhibitors was tested in a cell model using immunofluorescence-based detection of PAR essentially as reported previously [15]. HCT116 cells were seeded in Ibidi 12-well chamber slides and cultivated until they reached 70% confluence. Induction of PARylation was achieved by adding 1 mM H₂O₂ in PBS/1 mM MgCl₂ for 5 min at 37 °C. Cells were washed with PBS/1 mM MgCl₂ and fixed by adding 4% PFA at RT. After 20 min, cells were washed with PBS/100 mM glycine for 1 min and permeabilized with PBS/0.3% Triton X-100 for 3 min. Blocking of the cells was conducted by adding PBS/0.05% Tween containing 5% powdered milk for 1 h at RT. Immunofluorescence staining of PAR was performed by either adding a PAR antibody clone 10H or pan-ADP-ribose binding reagent (Sigma-Aldrich, Saint Louis, MO, USA) diluted 1:300 in PBS/0.05% Tween containing 5% powdered milk overnight at 4 °C. Cells were washed and an Alexa488-coupled secondary antibody was added for 1 h at RT. The slides were mounted with VectaShield containing DAPI and analyzed by confocal microscopy using a Zeiss Axio Observer 7 microscope (Oberkochen, Germany) equipped with a 63× oil objective (Plan-Apochromat 63×/1.40 DIC M27) and a LSM900 confocal laser scanner (Zeiss, Oberkochen, Germany). Images were analyzed using Zeiss Zen software version 3.4 and ImageJ v1.53t (NIH, Bethesda, MD, USA). Briefly, nuclei were identified based on the DAPI signal and marked as regions of interest (ROI). Subsequently, the mean PAR signal in the identified ROI was quantified in each image and exported for further analysis. For the individual experiments, the mean PAR intensity was averaged for each treatment group and the control was set to 100%. Only images with a minimum of 4 cells were included in the analysis and at least 5 images were assessed per treatment group. The experiments were conducted in at least 3 biological replicates. To derive IC₅₀ concentrations, relative PAR levels of the experiments were transferred to GraphPad Prism 9.0 Software (GraphPad Software Inc., Boston, MA, USA) for a nonlinear regression analysis applying a three-parameter model.

2.7. Chromatin Retention Assay and Western Blot Analysis

Quantification of chromatin-trapped PARP-1 was performed as described elsewhere [42]. Briefly, HCT116 cells were harvested, and pellets were lysed in buffer containing 150 mM KCl, 2.5 mM MgCl₂, 50 mM HEPES pH 7.8, 5 mM EDTA pH 8, 3 mM dithiothreitol (DTT), 10% glycerol, 0.5% Triton X-100, and freshly added protease inhibitor cocktail (Roche) for 15 min on ice. The chromatin-bound protein fraction was isolated by centrifugation at 4 °C for 15 min and 16,000× g. After transferring the soluble fraction, the chromatin-containing pellet was washed twice in lysis buffer and sonicated for 3 min. The soluble and chromatin fractions were mixed with self-made 5× Laemmli buffer (200 mM TRIS pH 6.8, 40% glycerol, 8% SDS, 4% β-mercaptoethanol, 0.08% Bromphenol Blue) and incubated at 95 °C for 10 min. Samples were then separated by SDS-PAGE followed by Western blot analysis essentially as described previously [43]. For the analysis of γH2AX, cells were directly harvested in 1× Laemmli buffer, incubated at 95 °C for 5 min, and subjected to SDS-PAGE and subsequent Western blot analysis [44]. The following primary antibodies were used: anti-PARP-1 (#GTX112864, Genetex, Irvine, CA, USA), anti-Histone H3 (#GTX122148, Genetex), anti-heat shock protein (Hsp90) α/β (#sc-13119, Santa Cruz Biotechnology, Heidelberg, Germany), anti-γ-H2AX (#ab81299, Abcam, Cambridge, UK). The following secondary antibodies were used: anti-rabbit IgG-HRP (#7074, Cell Signaling Technology, Danvers, MA, USA) and m-IgGκ binding protein-HRP (#sc-516102, Santa Cruz Biotechnology). The proteins of interest were detected using a c300 chemiluminescence imager (Azure Biosystems, Dublin, CA, USA). Densitometric image analysis was conducted by applying the software AzureSpot version 2.0.062 (Azure Biosystems, USA). The signal

intensity (e.g., PARP-1 or γ H2AX) of each lane was quantified and subsequently normalized to the respective loading control as indicated in the figure legends, which was analyzed in each experiment. Finally, the normalized signal intensity of each treatment group was expressed relative to the negative control and transferred to GraphPad Prism 9.0 Software (GraphPad Software Inc., Boston, MA, USA) for statistical analysis (see Section 2.8).

2.8. Statistics

Experiments were performed independently at least three times, except otherwise stated. Results from representative experiments are depicted. Values underwent Grubbs' test to exclude outliers and are displayed as mean \pm standard error of the mean (SEM) using the GraphPad Prism 9.0 Software (GraphPad Software Inc., Boston, MA, USA). Statistical analysis was performed using a two-sided Student's *t*-test and statistical significance was defined as $p < 0.05$.

3. Results

3.1. Identification of Putative PARPi Using Molecular Docking Studies

We devised a focused library of 3,4-bifunctionalized and -bridged indoles that fill an underrepresented chemical space within the vast number of reported indole derivatives as privileged scaffolds in drug discovery. From *in silico* screening of this focused in-house library within the whole ComPlat archive with more than 18,000 molecules, four compounds were identified with similar docking scores and binding poses compared to the well-established PARP inhibitors veliparib and olaparib (Figure 1(A1,A2)). *In silico* analysis revealed that the most active compound, X17613 with the carboxylic acid hydrazide motif, forms key interactions with G863, S904, and Y907 (Figure 1(A3)), while hydrogen bonding to the carbonyl oxygen atom of G863 is not mandatory. The derivatives X17618, X17620, and X17621, nevertheless, suggested PARP-1 binding affinity *in silico*, albeit lower, while alkylation of the amide of, e.g., X17611 would lead to a clash with the backbone carbonyl oxygen atom of G863 (Appendix A, Figure A1(A1)). Furthermore, a binding mode allowing hydrogen bonding to G863 or S904 could be identified for almost no compound substituted at this position. Hence, for compound X17610, we obtained a completely different binding mode, where the indole NH could interact with D766, and the hydrogen bond to S904 is formed via the morpholine oxygen atom (Appendix A, Figure A1(A2)). Therefore, we tested this compound despite a shallow scoring value to evaluate the possibility of other binding modes. Although X17608 is structurally similar to veliparib, the docking score is significantly reduced due to an intramolecular clash in a similar binding mode (Appendix A, Figure A1(A3)). All chiral compounds were tested as racemates, and no favored binding modes for the individual enantiomers could be identified by molecular docking (Figure 1(A4–A9)). To sum up, *in silico* studies revealed X17613 as the compound with the highest PARP-1 binding affinity, followed by the derivatives X17618, X17620, and X17621 (for chemical structures see Figure 1B and Appendix A, Figure A1B).

3.2. Activity Screening of PARP Inhibitors

After the molecular docking studies, twelve selected compounds were tested with regard to their potential to inhibit PARP-1 in a chemiluminescent PARP-1 screening assay kit. Five test compounds led to a concentration-dependent decrease in PARylation catalyzed by PARP-1, whereas the other seven compounds had no or only little effect on PARP-1 activity (Figure 2A and Appendix A, Figure A2B). The calculated IC_{50} values varied between 41 nM for the most potent compound X17613 and 9.2 μ M for the compound X17616 with the lowest inhibitory potency. In general, these IC_{50} values are higher than the inhibitory activity observed for the positive controls olaparib and veliparib (Appendix A, Figure A2A), which are in the low nM range (1.6 nM and 4 nM, respectively). Applied in a concentration of 5 nM, olaparib and veliparib reduced PARP-1 activity to approximately 25% and 50% of the negative control, respectively. The most potent compounds X17613, X17618, X17620, and X17621 were selected for further testing in a cell-based screening of PARP-1 activity

(see below). Overall, the determined IC₅₀ values of the tested compounds correlated well with the Glide XP scoring values of the determined docking poses from virtual screening (Figure 1A, and Appendix A, Figure A1A).

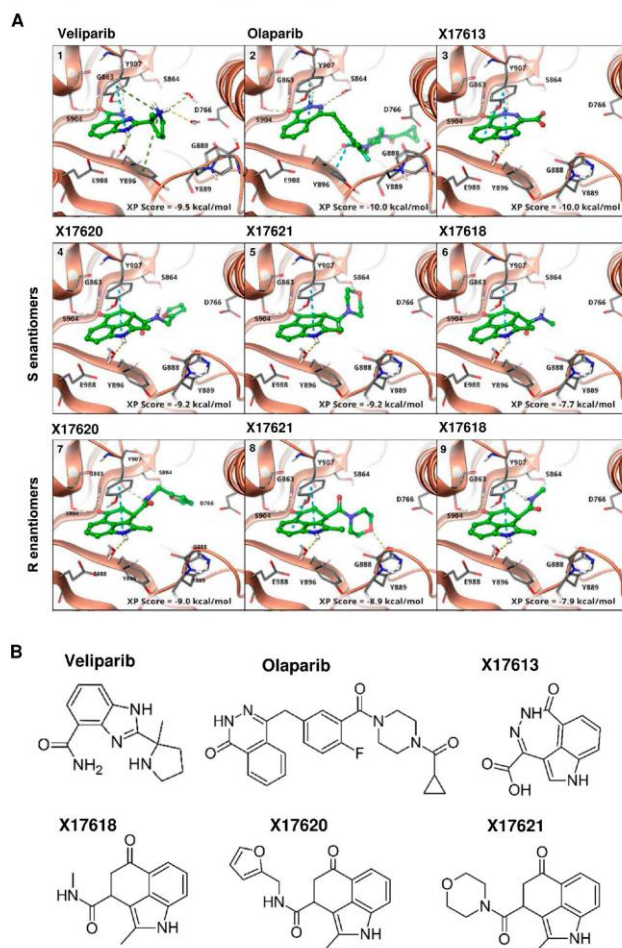


Figure 1. (A) Binding modes of veliparib (1), PDB: 7AAC), olaparib ((2), PDB: 7AAD), and selected compounds from virtual screening ((3–9), PDB: 4PJT) to PARP-1. The binding to either G863 or S904, as also found for veliparib, was used as a constraint in docking. All active compounds are able to form this bond and adopt a similar binding mode. Through the indole NH, there is an interaction with E988 by a bridging water molecule. No preference between the binding modes of the S-(4–6) or R-enantiomers (7–9) is observed, while the scoring values also differ only slightly. (B) Chemical structure of the most active compounds X17613, X17618, X17620, and X17621, according to in vitro screening and the two established PARPi veliparib and olaparib.

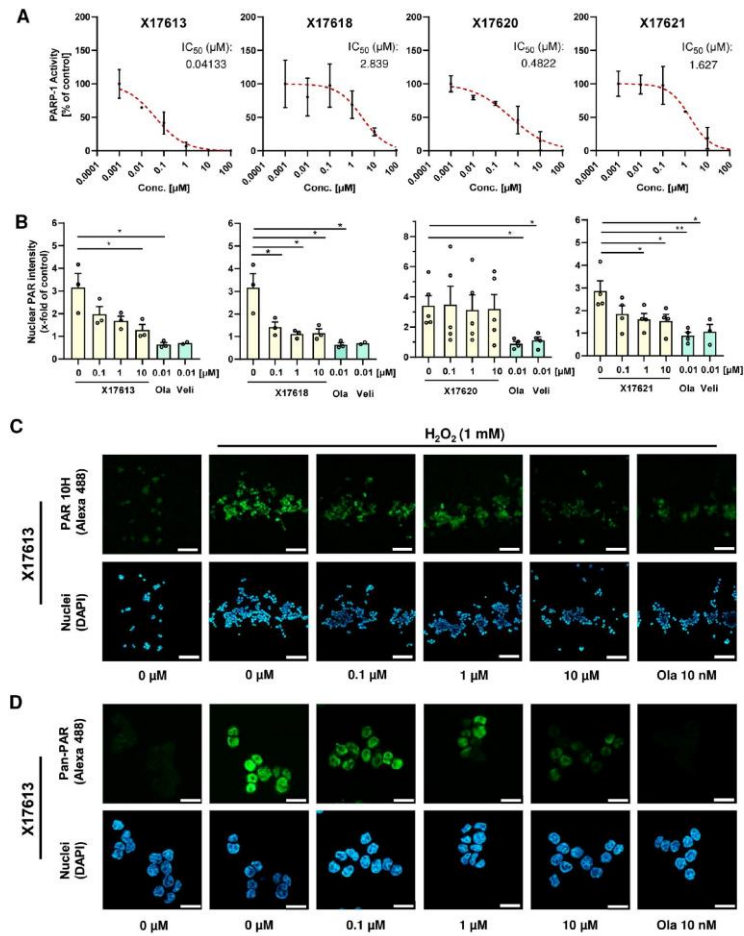


Figure 2. (A) Concentration–response curves of four potential PARP-1 inhibitors with the highest activity in the PARP-1 screening assay kit. All concentrations were tested in duplicates. IC₅₀ values were derived using a nonlinear regression model in GraphPad Prism 9 (*n* = 2). (B) Investigation of PARP inhibition by X17613, X17618, X17620, and X17621 in HCT116 cells. Cells were challenged with 1 mM H₂O₂ for 5 min and pretreated or not with the indicated compounds for 2 h. PAR synthesis was identified by confocal IF microscopy using the PAR 10H antibody. The signal intensity of five images per concentration was evaluated by ImageJ (*n* ≥ 3). (C) Representative confocal microscopy images at 100× magnification after PAR staining in HCT116 cells treated with the indicated concentrations of X17613 for 2 h with or without subsequent PARP activation by H₂O₂ treatment for 5 min. Scale bar: 100 μm. (D) Confocal microscopy images at 630× magnification after pan-PAR staining in HCT116 cells treated according to (C). Scale bar: 20 μm. Data are presented as mean ± SEM. * *p* < 0.01, ** *p* < 0.01; *t*-test.

3.3. Effect of Selected Test Compounds on PAR Formation in HCT116 Cells

Further assessment of the PARPi activity of the four most potent compounds X17613, X17618, X17620, and X17621 was conducted in HCT116 CRC cells (Figure 2B). The inhibitory potential of the compounds on H₂O₂-induced PAR formation was measured by PAR antibody staining and subsequent analysis by confocal fluorescence microscopy (Figures 2C and A3A). A significant decrease in the PAR signal was observed for the inhibitors X17613, X17618, and X17621 already at a concentration of 100 nM. In contrast to that, the compound X17620 showed no effect on PAR formation in the cell-based assay even at a concentration of 10 μ M (Figure 2B). Unlike the inhibitors X17613 and X17618, the compound X17621 did not entirely inhibit PAR formation at the highest concentration. As a positive control, 10 nM olaparib was included, which completely blocked PAR formation (Figure 2B,C). Since the applied 10H PAR-Antibody detects PAR in a chain length-dependent manner with preferential binding to PAR polymers consisting of more than 20 monomers [45], we also conducted immunostaining with the pan-ADP-ribose binding reagent using the same protocol. Fluorescence microscopy revealed comparable results to the 10H clone PAR antibody (Figure 2D and Appendix A, Figure A3B). Taken together, the three compounds X17613, X17618, and X17621 showed a similar potency for cellular PARP inhibition following DNA damage induction by H₂O₂ with IC₅₀ values between 5 and 35 nM (Figure 2B and Appendix A, Figure A3C). In contrast to the PARPi studies with recombinant PARP-1 enzyme, X17620 was not active in the cell model and, thus, was excluded from further testing.

3.4. PARP-1 Trapping and Cytotoxicity of PARP Inhibitors

In the next step, we focused on X17613 and X17618 with the highest *in vitro* and *in cellulo* PARPi activity and analyzed their potential to cause PARP-1 trapping. To this end, chromatin isolation was performed in MSI HCT116 cells after PARP activation by exposure to the alkylating agent MMS for 1 h with or without an inhibitor. The results showed that only olaparib caused a substantial increase in chromatin-bound PARP-1 (Figure 3A). No enrichment of PARP-1 in the chromatin fraction was observed after treatment with X17613 or X17618, indicating that PARP-1 trapping is not induced by these inhibitors at the used concentrations. The same set of experiments was repeated in MSS Caco-2 cells, revealing comparable results. Olaparib caused strong PARP-1 trapping, whereas no effects were detected after treatment with X17613 and X17618 (Figure 3B). Since the ability of PARPi to trap PARP-1 is associated with their cytotoxic potential and side effects *in vivo*, we assessed the viability in HCT116 cells depending on PARP-1. Prior to that experiment, Western blot analysis was used to validate the lack of PARP-1 protein expression in HCT116 PARP-1^{-/-} cells, while HCT116 PARP-1^{+/+} control cells displayed PARP-1 expression as expected (Appendix A, Figure A4A). Neither X17613 nor X17618 decreased cell viability in HCT116 cells, irrespective of the PARP-1 status (Figure 3C). Veliparib displayed only mild cytotoxicity at the highest test concentration. In contrast to that, olaparib decreased viability in HCT116 cells in a concentration-dependent manner, which was much more pronounced in cells expressing PARP-1 (Figure 3C). Moreover, the effects of the established and novel PARPi on the viability of MSS Caco-2 cells were determined. X17618 had no impact on cell viability at all, while veliparib and X17613 showed little cytotoxicity at the highest test concentration (Figure 3D). In line with the findings in HCT116 cells, olaparib treatment resulted in a concentration-dependent reduction in Caco-2 viability (Figure 3D). Finally, we evaluated the cytotoxic potential of PARPi in human colonic epithelial cells (HCEC), which were established from human healthy colon biopsies. While olaparib caused a moderate decline in viability at the highest concentration, the other PARPi (veliparib, X17613, and X17618) had no effect on HCEC (Appendix A, Figure A4B). Taken together, the novel PARPi X17613 and X17618 did not trap PARP-1 and, similar to veliparib, induced no cytotoxicity in two different CRC cell models (MSI and MSS) and HCEC (Table 1). Olaparib in turn caused substantial PARP-1 trapping and was cytotoxic in CRC cells in a PARP-1-dependent manner.

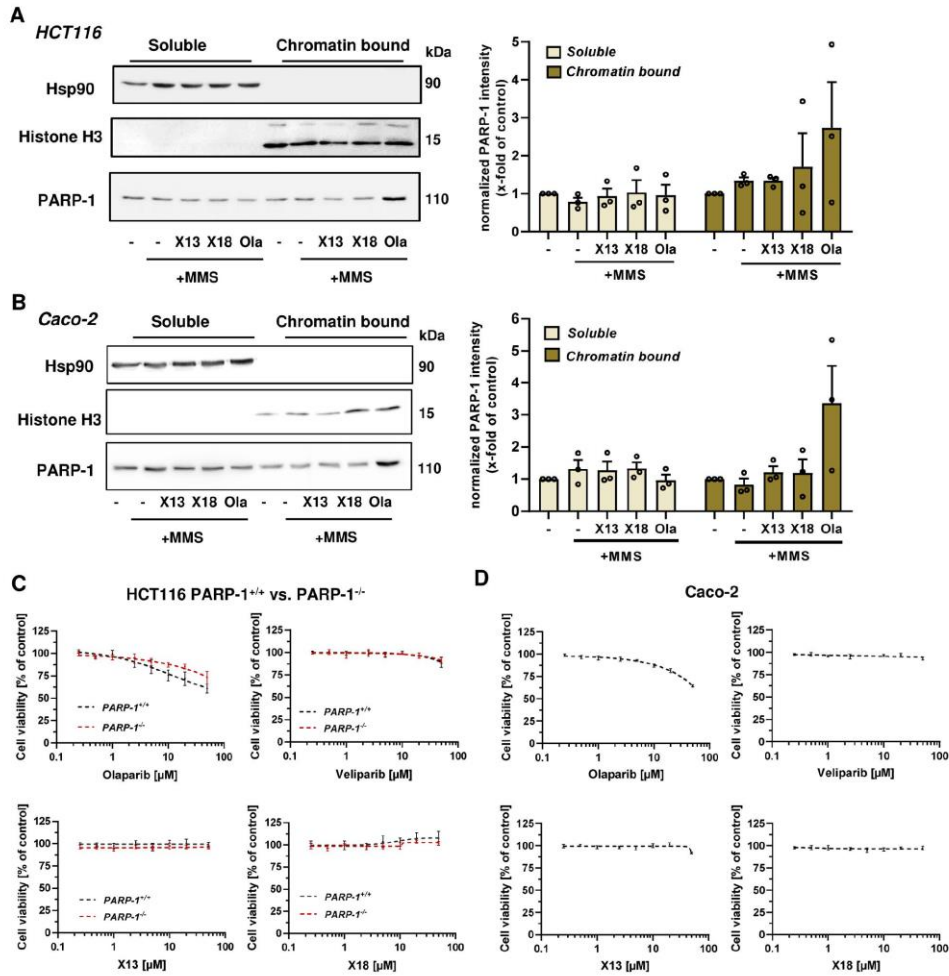


Figure 3. (A,B) Analysis of PARP-1 trapping in HCT116 and Caco-2 cells. Immunoblot detection of PARP-1 after pre-treatment with X17613, X17618, and olaparib followed by MMS exposure for 1 h and chromatin isolation. The cytosolic marker Hsp90 and the chromatin marker Histone H3 served as respective loading controls. Representative Western blot images and densitometric evaluation are shown ($n = 3$). Data are shown as mean + SEM. (C) Cell viability determined by the resazurin reduction assay (RRA) in HCT116 PARP-1^{-/-} and HCT116 PARP-1^{+/+} cells after PARPi treatment for 72 h. A nonlinear regression curve fit was conducted using GraphPad Prism 9 ($n \geq 3$). (D) Viability in Caco-2 cells after exposure to PARPi as indicated. ($n = 3$). All data are shown as mean +/− SEM.

Table 1. IC₅₀-values [μM] of established PARP inhibitors (olaparib and veliparib), two PARP inhibitor candidates (X17613 and X17618) and chemotherapeutic drugs in CRC cells with or without DDR defects. “-” indicates that IC₅₀ values could not be determined due to insufficient or lack of cytotoxicity.

	X17613	X17618	Olaparib	Veliparib	IT	5-FU	OXA
HCT116 WT	-	-	8.40	-	1.28	0.50	1.19
HCT116 BRCA2 ^{-/-}	-	-	0.46	7.45	0.16	0.34	0.25
HCT116 PARP1 ^{+/+}	-	-	11.21	-	0.93	0.24	0.71
HCT116 PARP1 ^{-/-}	-	-	-	-	0.35	0.15	0.28
DLD-1 WT	-	-	5.88	-	4.19	0.35	8.77
DLD-1 ATR ^{s/s}	-	-	1.99	-	2.99	0.22	9.08
Caco-2	-	-	-	-	66.52	-	11.18
HCEC	-	-	-	-	2.95	26.23	40.71

3.5. Cytotoxicity of PARPi Depending on the Cellular BRCA2 and ATR Status

To investigate the impact of the cellular DDR on the cytotoxicity of PARP inhibitors, we used genetically engineered CRC cell models proficient or deficient for *BRCA2* and *ATR*, respectively. Cell models were re-authenticated using Western blot analysis, which confirmed a lack of *BRCA2* and *ATR* protein expression in the respective knockout model (Appendix A, Figure A4). Cytotoxicity testing revealed no impact of X17613 and X17618 on viability in HCT116 WT cells, whereas both compounds decreased viability in HCT116 BRCA2^{-/-} cells by about 25% at the highest test concentration of 50 μM (Figure 4A). High cytotoxicity in the low micromolar concentration range was observed in HCT116 BRCA2^{-/-} cells incubated with olaparib or veliparib. The determined IC₅₀ values in BRCA2-deficient HCT116 cells were 18-times lower for olaparib and 5-times lower for veliparib in comparison to HCT116 WT cells (Table 1). Further experiments in DLD-1 WT and DLD-1 ATR^{s/s} cells showed no effects of X17613 and X17618, irrespective of the ATR status (Figure 4B). Veliparib caused a concentration-dependent decrease in viability in both cell models, but concentration-response data did not allow for deriving IC₅₀ values. Olaparib showed the strongest cytotoxic effects of all tested PARPi, which was affected by the ATR status. DLD-1 ATR^{s/s} cells displayed a 3-fold higher sensitivity for olaparib than DLD-1 WT cells, as revealed by the respective IC₅₀ values (Table 1). In summary, BRCA2 deficiency potentiated the sensitivity of CRC cells towards all tested PARPi (Olaparib » veliparib > X17613 ≈ X17618), while ATR deficiency only increased sensitivity towards olaparib.

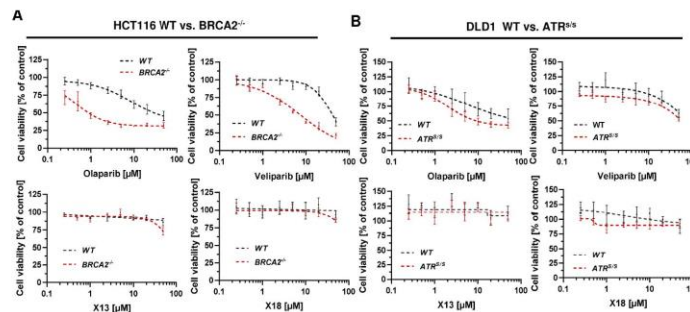


Figure 4. (A) Toxicity of PARPi in HCT116 cells depending on BRCA2 status. HCT116 WT and HCT116 BRCA2^{-/-} cells were incubated with PARPi for 72 h and viability was assessed using the resazurin reduction assay (RRA). Nonlinear regression curve fit was conducted using GraphPad Prism 9 (*n* ≥ 3). (B) Toxicity of PARPi in DLD-1 cells depending on ATR status. DLD-1 WT and DLD-1 ATR^{s/s} cells were incubated with PARPi for 72 h and viability was assessed using the RRA. Nonlinear regression curve fit was conducted using GraphPad Prism 9 (*n* ≥ 3). Data are depicted as mean ± SEM.

3.6. Combination of PARPi and Clinically Relevant Chemotherapeutic Drugs in CRC Cells

To investigate a putative synergism with anticancer drugs, IC₅₀ values of IT, 5-FU, and OXA were first determined in all cell models (Appendix A, Figure A5). In HCT116 cells, the toxicity of IT and OXA were dependent on the molecular subtype. In comparison to HCT116 WT cells, HCT116 BRCA2^{-/-} was revealed to be more sensitive with an IC₅₀ value 8-times lower for IT and 5-times lower for OXA, while no such difference was observed for 5-FU (Appendix A, Figure A5A and Table 1). The PARP-1 status also impacted the sensitivity of HCT116 cells to IT and OXA with 2.5–3-fold higher sensitivity in PARP-1^{-/-} cells, while the cytotoxicity of 5-FU was less affected (Appendix A, Figure A5B and Table 1). Experiments in DLD-1 cells showed little influence of ATR on cytotoxicity, as reflected by a 1.4-times lower IC₅₀ value for IT and a 1.6-times lower IC₅₀ value for 5-FU in DLD-1 ATR^{S/S} cells (Appendix A, Figure A5C and Table 1). The cytotoxic effects of OXA were independent of ATR. In Caco-2 cells, the cytotoxicity of the anticancer drugs was generally lower than in HCT116 or DLD-1 cells (Figure A5D and Table 1). Furthermore, nonmalignant HCEC were tested, which displayed similar sensitivity for IT but lower cytotoxicity for 5-FU and OXA than the CRC cell lines (Appendix A, Figure A5E).

Subsequently, combined treatment of PARPi and DNA damage-inducing anticancer drugs was performed. We observed a significant decrease in cell viability compared to mono-treatment with cytostatics for olaparib and veliparib in HCT116 PARP-1^{+/+}, whereas in HCT116 PARP-1^{-/-} olaparib and veliparib did not sensitize to the anticancer drugs (Figure 5A). The novel compounds X17613 and X17618 did not affect the cytotoxicity of the anticancer drugs (Figure 5B and Appendix A, Figure A6A). In Caco-2, both olaparib and veliparib moderately increased the cytotoxicity of IT, which was, however, not statistically significant (Figure 5C).

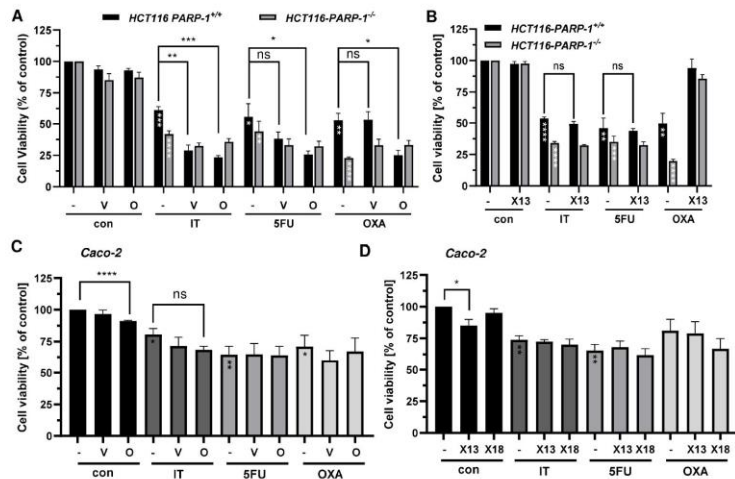


Figure 5. (A) Viability in HCT116 PARP-1^{-/-} and HCT116 PARP-1^{+/+} cells after treatment with PARPi olaparib or veliparib in combination with chemotherapeutic drugs irinotecan (IT, 0.5 μM), 5-fluorouracil (5-FU, 0.25 μM), and oxaliplatin (OXA, 0.5 μM) for 72 h ($n \geq 3$). (B) Viability in HCT116 PARP-1^{-/-} and HCT116 PARP-1^{+/+} cells after treatment with PARPi X17613 in combination with chemotherapeutic drugs for 72 h. Data ($n \geq 3$) are given as mean \pm SEM. (C,D) Viability in Caco-2 cells after treatment with PARPi in combination with chemotherapeutic drugs irinotecan (IT, 10 μM), 5-fluorouracil (5-FU, 5 μM), and oxaliplatin (OXA, 1 μM). Data ($n = 3$) are shown as mean \pm SEM. ns: $p > 0.05$, * $p < 0.01$, ** $p < 0.01$, *** $p < 0.001$, **** $p < 0.0001$; *t*-test.

No effects were observed for the combination treatment with the cytostatic drugs 5-FU and OXA. In line with the findings in HCT116 cells, no sensitization towards the anticancer drugs was detected upon incubation with X17613 and X17618 (Figure 5D). Collectively, these results showed an increased sensitivity of CRC cells (HCT116 > Caco-2) towards IT after treatment with olaparib and veliparib, while X17613 and X17618 had no synergistic effect. Furthermore, our data highlighted the relevance of PARP-1 expression for the cytotoxicity of both IT and OXA.

3.7. Impact of BRCA2 and ATR on the Potential Synergism of PARPi and Chemotherapeutics

Finally, we studied how the DDR status (BRCA2 and ATR) affects the therapeutic efficacy of a combination regimen consisting of PARPi and chemotherapeutics. Olaparib synergized with IT and OXA in a BRCA2-dependent manner (Figure 6A). Veliparib also increased the sensitivity to IT and OXA in a BRCA2-deficient background, which was generally not as strong as for olaparib. For the novel compounds, an additional cytotoxic effect was observed for the combination treatment with IT in HCT116 BRCA2^{-/-} cells but not with the other anticancer drugs (Figures 6B and A6B). Consistently, bright field microscopy revealed morphological changes such as cell rounding and detachment in BRCA2-deficient HCT116 cells treated with X17613 and IT, indicative of cell death (Figure 6C).

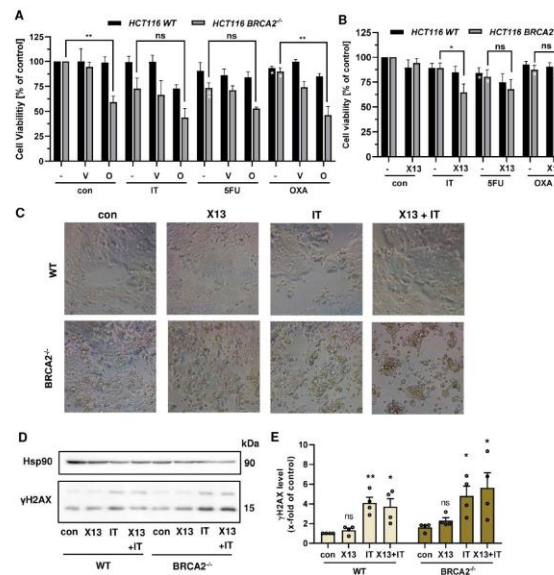


Figure 6. (A) Viability in HCT116 WT and HCT116 BRCA2^{-/-} cells after treatment with PARPi olaparib or veliparib in combination with chemotherapeutic drugs (IT, 0.25 μM), 5-fluorouracil (5-FU, 0.1 μM), and oxaliplatin (OXA, 0.25 μM) for 72 h (n ≥ 3). (B) Viability in HCT116 WT and HCT116 BRCA2^{-/-} cells after treatment with PARPi X17613 in combination with chemotherapeutic drugs (IT, 0.25 μM), 5-fluorouracil (5-FU, 0.1 μM), and oxaliplatin (OXA, 0.25 μM) for 72 h (n ≥ 3). (C) Representative brightfield microscopic images at 20X magnification of HCT116 WT and HCT116 BRCA2^{-/-} cells after treatment with X17613 (50 μM), IT (0.25 μM), or a combination of both for 24 h. (D,E) γH2AX formation in HCT116 WT and BRCA2^{-/-} cells after treatment as described in (C). Representative Western blot images and densitometric evaluation are shown (n = 4). Hsp90 served as loading control. All data are given as mean + SEM. ns: p > 0.05, * p < 0.01, ** p < 0.01; t-test.

In order to investigate whether this effect is attributable to an increased DSB formation, we performed Western blot analysis of phosphorylated H2AX (γ H2AX) as a well-established DSB marker [46]. To this end, HCT116 WT and BRCA2-deficient cells were pretreated with X17613 for 2 h and subsequently co-treated with IT for an additional 24 h. No significant increase in γ H2AX was observed in HCT116 WT cells upon treatment with X17613 alone (Figure 6D,E). The genotoxic drug IT led to a significant induction of γ H2AX as compared to the control. However, no significant further increase was detected after co-treatment as compared to IT mono-treatment. It should be noted that IT caused slightly higher γ H2AX levels in BRCA2^{-/-} cells, which were further augmented in the presence of X17613 (Figure 6D,E), and that similar results were obtained for X17618 (Appendix A, Figure A6C). Further experiments in DLD-1 WT and DLD-1 ATR^{S/S} cells revealed little impact of the ATR status on the sensitivity of CRC cells towards a combination of PARPi and chemotherapeutic drugs (Appendix A, Figure A7A,B). Taken together, these findings provided evidence that PARPi (olaparib > veliparib > X17613 > X17618) and chemotherapeutic drugs (IT > OXA) synergize in a BRCA2-dependent manner in CRC cells.

4. Discussion

Our work addresses the role of PARP-1 as a target for chemotherapeutic intervention in both MSI and MSS CRC by applying novel PARP inhibitors to overcome PARPi resistance and reduce cytotoxicity-mediated adverse effects. Therefore, we analyzed an array of indole-based compounds by *in silico* screening regarding their ability to inhibit PARP-1 activity in a molecular docking model and used the compounds for *in vitro* testing by applying a cell-free assay based on recombinant PARP-1. The four substances with the lowest IC₅₀ value and, thus, highest PARPi activity *in vitro*, X17613, X17618, X17620, and X17621, were also identified *in silico* to have the highest binding affinity to the active center of PARP-1. Interestingly, the compound, X17613, with the highest inhibitory activity contains a cyclic carboxylic acid hydrazide motif (i.e., a dihydrodiazepinone, [cd]-fused to indole). Among PARPi developed so far, a similar core structure can only be found in pamiparib, which is currently tested clinically for the treatment of brain tumors, since improved penetration across the blood–brain barrier was demonstrated [47]. Compared to X17613, olaparib and veliparib share key interactions with the amino acid residues G863, S904, and Y907 but contain an additional side chain that interacts with Y896 and D766, presumably leading to a higher potency. Further chemical modification of the lead compound X17613 might, thus, result in higher inhibitory activity. In a recent study, the side chain modification of veliparib was shown to drastically increase its PARP trapping activity due to allosteric retention, independent of enzymatic inhibition [48]. However, one should keep in mind that this will very likely also cause higher toxicity in healthy tissue, since the capability for PARP trapping closely correlates with PARPi toxicity [49].

Applying a CRC cell-based assay, the inhibitory activity of the four compounds was assessed by PAR staining and confocal microscopy. We detected a marked inhibition of H₂O₂-dependent PAR generation by X17613 and X17618, albeit at higher concentrations as compared to the positive control olaparib. The reduced activity of X17620 in the cell-based assay, despite potent inhibition of recombinant PARP-1, could be attributable to an efficient cellular efflux. Certain PARPi (e.g., olaparib) are known substrates for P-glycoprotein, which is an efflux transporter responsible for the resistance of cancers to numerous drugs, whereas other PARPi (e.g., veliparib) are not excreted [50].

We then assessed the ability of the novel PARPi to cause PARP-1 trapping in HCT116 and Caco-2 cells, which represent CRC cell models with MSI and MSS, respectively [51]. While olaparib induced substantial PARP-1 trapping, X17613 and X17618 showed no effects in both CRC cell models. Zandarashvili and colleagues dissected the molecular mechanisms that determine PARPi-dependent trapping of PARP-1 [48]. Catalytic inhibition of PARP-1 prevents automodification-dependent release, and, therefore, depends on the IC₅₀ of the PARPi. Simultaneously, PARPi can influence PARP-1 allostery, which either promotes the release or retention of the enzyme, depending on its structure [48]. Veliparib

was shown to have an allosteric pro-release effect, which olaparib is lacking [48]. It is conceivable that X17613 and X17618 also display an allosteric pro-release effect, which together with their lower PARPi activity compared to olaparib might explain the observed lack of PARP-1 trapping.

Interestingly, monotreatment with the compounds X17613 and X17618 as well as veliparib failed to induce cytotoxicity in HCT116 PARP-1^{+/+} and PARP-1^{-/-} cells. These three compounds were also not cytotoxic in nonmalignant HCEC. Only olaparib led to a decrease in viability in HCT116 PARP-1^{+/+} cells, and to a lesser degree also in HCT116 PARP-1^{-/-} cells, indicating the importance of PARP-1 trapping for cytotoxicity in cells without genetic susceptibility. It should be mentioned that mutations of PARP-1, which impair its DNA binding affinity and, thus, reduce cytotoxic PARP trapping, were observed in tumors with acquired PARPi-resistance, underlining the role of PARP trapping in a clinical setting [52]. As mentioned above, olaparib also decreased the viability in PARP-1 deficient HCT116 cells. This is likely attributable to the effects of olaparib on other PARPs, particularly PARP-2, which is inhibited with similar potency as PARP-1 (IC₅₀ 56 nM vs. 13 nM) [53] and is trapped on DNA by olaparib via an allosteric pro-retention effect [54]. Furthermore, this could be explained by potential off-target effects of PARPi. Rucaparib and niraparib were, for example, shown to modulate cellular kinases *in vitro* at higher nanomolar concentrations [53,55].

In HCT116 BRCA2^{-/-} cells, which were used as a model for synthetic lethality by PARPi, the low cytotoxicity of X17613 and X17618, despite PARP-1 inhibition, might be caused by an insufficient inhibitor potency. While olaparib and veliparib restrained recombinant PARP-1 activity in low nM concentrations, a significant reduction in HCT116 BRCA2^{-/-} cell viability by these two PARPi could only be observed at around 100-fold higher concentrations. Since inhibition of recombinant PARP-1 by X17613 and X17618 occurs with 10–100-fold less potency as compared to olaparib and veliparib, equally higher doses should be necessary to induce cytotoxicity and might, therefore, not have been detected in our assays.

Nevertheless, the inhibitor X17613 led to a significant reduction in viability in HCT116 BRCA2^{-/-} cells in combination with the established cytostatic drug IT. These results show that the occurrence of HR deficiency renders CRC cells susceptible towards dual inhibition of TOP-1 and PARP-1, also in the absence of PARP-1 trapping. BRCA2 mutations in CRC are rare, occurring with a prevalence of around 1% [56], but were shown to be associated with an early onset of the disease [9]. Inhibition of PARP-1 could improve CRC chemotherapy beyond defects of BRCA1/2, leading to synergistic cytotoxicity in tumor cells. This was illustrated by siRNA-mediated knockdown of the HR-mediator RAD51 in colon cancer cells, which potentiated the cytotoxicity of olaparib monotreatment and in combination with SN38 [57]. Our study revealed a marked decrease in CRC cell viability due to co-treatment with olaparib or veliparib and the DNA-damaging agent IT. These results are in accordance with an earlier study conducted in human prostate cancer and glioblastoma cells, revealing synergistic effects of both PARPi with the TOP-1 inhibitor camptothecin [58]. The synergism between PARPi and TOP-1 inhibitors was further demonstrated using a HCT116 xenograft model, in which a combination regimen of IT and rucaparib strongly reduced tumor growth *in vivo* [59]. Furthermore, combinations of PARPi with inhibitors of ATR could provide a therapeutic approach for the treatment of tumors with or without HR deficiencies in the future, as shown in ovarian cancer models [60].

Interestingly, a comparison of HCT116 PARP-1^{-/-} and PARP-1^{+/+} revealed a higher cytotoxicity of the agents IT and OXA in the absence of PARP-1, highlighting its pivotal role in DNA repair and replication stress response. Consistent with this finding, we could detect a synergistic activity of olaparib with IT and OXA, but not with 5-FU in HCT116 PARP-1^{+/+} cells. These effects were generally also observed in DLD-1 cells, whereas in Caco-2 cells PARPi had little impact on the cytotoxic activity of the anticancer drugs. Applying different cancer cell lines, Murai et al. observed that enzymatic PARP inhibition is sufficient for synergistic effects by combination therapy with TOP-1 Inhibitors (see above), while PARP

trapping is necessary for alkylating agents such as temozolomide [58]. We were able to confirm these results for CRC cells, showing that veliparib, which lacks PARP trapping activity, fails to induce cytotoxicity in combination with OXA, in contrast to olaparib. While inhibitor-induced PARP trapping is the main contributor to cytotoxicity in a monotherapy regimen, these observations imply that enzymatic inhibition is sufficient for the synergistic effect in combination with IT. This could allow for the application of better-tolerated PARPi in a combination treatment regimen. Hopkins et al. revealed PARP-1 trapping to be the primary mechanism of PARPi cytotoxicity towards healthy bone marrow cells [49]. This side effect was also found to limit the efficacy of olaparib for CRC treatment in a clinical study by further amplification of the adverse effects of chemotherapeutic drugs in a combination regimen [23]. It might, therefore, be worth considering the application of PARPi with attenuated PARP trapping activity in combination with TOP-1 inhibitors to reduce dose-limiting toxicity (DLT). This is an important clinical aspect since TOP-1 inhibitors, like IT, also cause myelosuppression as DLT. Genetic variants of the phase II gene *UDP-glucuronosyltransferase 1A1 (UGT1A1)* were clearly linked to severe myelosuppression and neutropenia [61]. Diarrhea represents the other most common DLT in response to IT administration. This can occur rapidly within the first hours or in a delayed manner after 24 h, representing a very serious and potentially life-threatening situation [62]. Indeed, the combination of PARPi with the TOP-1 inhibitors IT and topotecan for the treatment of patients with solid tumors was illustrated as challenging due to the severe myelosuppression and diarrhea. However, our new PARPi compounds with little cytotoxicity due to the lack of PARP trapping might be a promising alternative for the combination therapy with TOP-1 inhibitors. Furthermore, it was proposed to switch the combination therapy regimen to a gapped schedule, which avoids the overlapping toxicity of PARPi and TOP-1 inhibitors in normal healthy tissue such as bone marrow [62]. Another possibility in this regard might be the use of indenoisoquinolines, which are TOP-1 inhibitors structurally unrelated to camptothecin and irinotecan [63]. DLD-1 cells with *BRCA2* deficiency were hypersensitive towards these compounds, which further synergized with olaparib *in vitro* and *in vivo* [63].

Moreover, PARPi and other DDR inhibitors such as ATRi have also great potential as radiosensitizers, which is of particular interest for the treatment of rectal cancer [64]. Radiotherapy represents an important treatment modality for rectal cancer, typically performed in combination with chemotherapy in a peri- or postoperative setting depending on the tumor and nodes stages [65]. Using cell culture models and an *in vivo* xenograft mouse model, olaparib was shown to sensitize CRC cells (i.e., HCT116 and SW480) towards radiotherapy in a XRCC2-dependent manner [66]. Furthermore, the PARPi talazoparib synergized with radiotherapy in CRC cells with both wild-type BRAF (i.e., DLD-1) and mutant BRAF (i.e., RKO), while olaparib had lower synergistic effects [67]. In addition to those preclinical studies, a phase 1b clinical study was conducted in patients with locally advanced rectal cancer. This investigated the safety and tolerability of veliparib in combination with chemoradiotherapy (CRT), consisting of the orally available 5-FU prodrug capecitabine and fractionated radiotherapy [68]. Interestingly, the results provided first evidence that veliparib could potentiate the antitumor activity of CRT [68]. It is, therefore, tempting to speculate that our novel identified PARPi X17613 and X17618 may also sensitize CRC cells towards radiotherapy or radiotherapy combined with IT, which warrants future preclinical studies. There are completed clinical studies showing a lack of PARPi efficacy, in which CRC patients were not stratified according to their PARP-1 expression beforehand [23,69]. Routine assessment of PARP-1 expression in CRC biopsies is, therefore, strongly recommended to identify patients who might benefit from PARPi combination therapy, while patients with low PARP-1 expression might be suitable for application of other DDR inhibitors, with ATR [70] and RAD51 [71] as promising targets. More recently, a composite biomarker approach has been described to predict responses to ATR inhibitors. This is based upon the detection of basal pSer33-RPA32 levels, RAD51 foci, ATM, and RAD51C expression in formalin-fixed paraffin-embedded colorectal tumor samples or

derived preclinical models [72]. It is obvious to complement this set of biomarkers by PARP-1 expression in order to select the tailored cancer therapy regimen.

5. Conclusions

In summary, our study identified novel PARPi lead structures with potent PARP-1 inhibitory activity in CRC cells but low cytotoxicity in wildtype CRC cells and no adverse effects on normal HCEC due to lack of PARP trapping. The most promising compound, X17613, synergized with the anticancer drug and TOP-1 inhibitor IT in a BRCA2-dependent manner, which can be transferred to other settings with HRD. In support of this view, a very recent study provided evidence that PARP inhibition, rather than PARP trapping, is sufficient for killing cancer cells with HRD [73].

Supplementary Materials: The following supporting information can be downloaded at: <https://www.mdpi.com/article/10.3390/cancers16203441/s1>, Supplementary Material and Methods: synthesis of test compounds. Scheme S1: Synthesis of compound 4; Scheme S2: Synthesis of compounds 10a–c. Figure S1: ¹H-NMR of 1-oxo-2,6-dihydro-1H-[1,2]diazepino [4,5,6-cd]indole-4-carboxylic acid (X17613); Figure S2: ¹³C-NMR of 1-oxo-2,6-dihydro-1H-[1,2]diazepino [4,5,6-cd]indole-4-carboxylic acid (X17613); Figure S3: ¹H-NMR of N,2-dimethyl-5-oxo-1,3,4,5-tetrahydrobenzo[cd]indole-3-carboxamide (X17618); Figure S4: ¹³C-NMR of N,2-dimethyl-5-oxo-1,3,4,5-tetrahydrobenzo[cd]indole-3-carboxamide (X17618); Figure S5: ¹H-NMR of N-(furan-2-ylmethyl)-2-methyl-5-oxo-1,3,4,5-tetrahydrobenzo[cd]indole-3-carboxamide (X17620); Figure S6: ¹³C-NMR of N-(furan-2-ylmethyl)-2-methyl-5-oxo-1,3,4,5-tetrahydrobenzo[cd]indole-3-carboxamide (X17620); Figure S7: ¹H-NMR of 2-methyl-3-(morpholine-4-carbonyl)-3,4-dihydrobenzo[cd]indol-5(1H)-one (X17621); Figure S8: ¹³C-NMR of 2-methyl-3-(morpholine-4-carbonyl)-3,4-dihydrobenzo[cd]indol-5(1H)-one (10c) (X17621); Figure S9: Uncropped Western blot images of HCT116 cells shown in Figure 3A (#1) and two independent repetitions (#2 and #3); Figure S10: Uncropped Western blot images of Caco-2 cells shown in Figure 3B (#1) and two independent repetitions (#2 and #3); Figure S11: Uncropped Western blot images of HCT116 WT and BRCA2^{-/-} cells shown in Figure 6C (#1) and three independent repetitions (#2–#4); Figure S12: Uncropped Western blot images of HCT116 WT, HCT116 BRCA2^{-/-}, HCT116-PARP1^{+/+}, HCT116 PARP-1^{-/-}, DLD-1 WT and DLD-1 ATR^{s/s} cells shown in Figure A5; Figure S13: Uncropped Western blot images of HCT116 WT and BRCA2^{-/-} cells shown in Figure A6C (#1) and three independent repetitions (#2–#4).

Author Contributions: Conceptualization: D.S., A.L. (Andreas Link) and J.F. Methodology: P.D., F.P., L.S., A.L. (Andreas Link), V.R. and J.F. Validation: P.D., L.S. and J.F. Formal analysis: P.D., A.L. (Anna Lemsch), L.T., F.P. and L.S. Investigation: P.D., A.L. (Anna Lemsch), L.T., F.P. and L.S. Resources: C.G., G.M., A.L. (Andreas Link) and V.R. Writing—original draft preparation: P.D. and J.F. Writing—review and editing: P.D., A.L. (Anna Lemsch), L.T., F.P., L.S., C.G., G.M., D.S., V.R., A.L. (Andreas Link) and J.F. Visualization, P.D., A.L. (Anna Lemsch), L.S. and J.F. Supervision: J.F. Project administration: J.F. Funding acquisition: A.L. (Andreas Link) and J.F. All authors have read and agreed to the published version of the manuscript.

Funding: This work was supported by the German Research Foundation (INST 248/331-1 FUGG and INST 292/161-1 FUGG) and by the Wilhelm Sander Foundation, grant number 2016.039.2.

Institutional Review Board Statement: Not applicable.

Informed Consent Statement: Not applicable.

Data Availability Statement: The data generated during this study were included in the article and its supplementary files. All data on the synthesis and analysis of the main compounds X17613, X17618, X17620, and X17621 are also available via the Chemotion repository (<https://www.chemotion-repository.net/>) and can be accessed via the following DOI: https://dx.doi.org/10.14272/collection/CWG_2024-02-14 (accessed on 14 February 2024) [74].

Acknowledgments: We thank Alexander Bürkle (University of Konstanz, Germany) for the kind gift of 10H antibody. We acknowledge the DFG-core facility Molecule Archive (DFG project number: 284178167) for the management and provision of the compounds for screening and for providing all test compounds. We are grateful to Carlos Caldas (University of Cambridge, Cambridge, UK) for providing HCT116 BRCA2^{-/-} cells, Fred Bunz (John Hopkins University, Baltimore, USA) for

providing DLD-1 ATR^{+/+} and DLD-1 ATR^{S/S} cells and Jerry W. Shay (UT Southwestern Medical Center, Dallas, USA) for providing HCEC.

Conflicts of Interest: The authors declare no potential conflicts of interest.

Appendix A

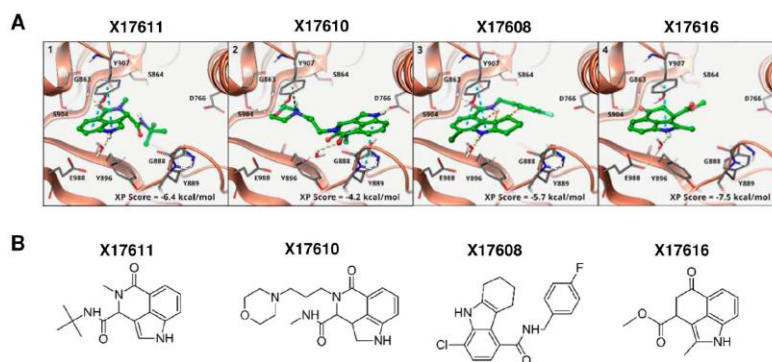


Figure A1. (A) Binding modes of selected compounds from virtual screening ((1–4), PDB: 4PJT) to PARP-1. The binding to either G863 or S904 was used as a constraint in docking. All active compounds are able to form this bond and adopt a similar binding mode (compare Figure 1A). The three compounds X17611, X17610, and X17608 (1–3) serve as a verification of the binding mode since the constraints can only be fulfilled with significant losses in the binding free energy due to unfavorable inter- and intramolecular interactions. X17616 (4) is similar to X17618 (Figure 1A), but cannot form a potential hydrogen bond due to the lack of the amide function. (B) Chemical structure of the compounds X17611, X17610, X17608 and X17616.

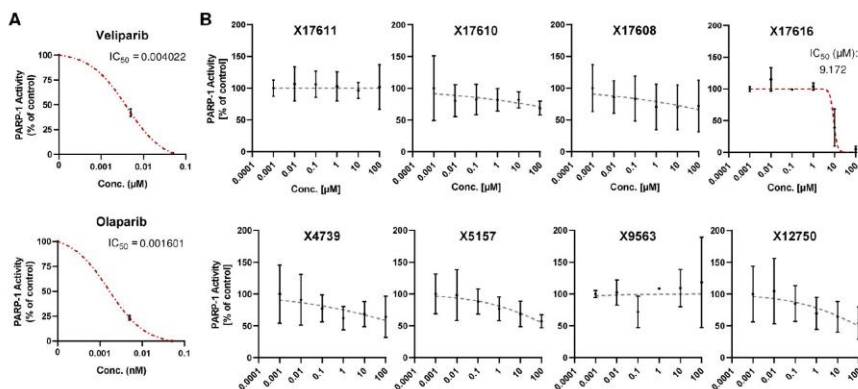


Figure A2. (A,B) Concentration response curve of established PARP inhibitors veliparib and olaparib (A) and eight potential PARP inhibitors (B) with low or no activity in the PARP-1 screening assay kit. All concentrations were tested in duplicates. IC₅₀ values were derived using a nonlinear regression model in GraphPad Prism 9 (*n* = 2).

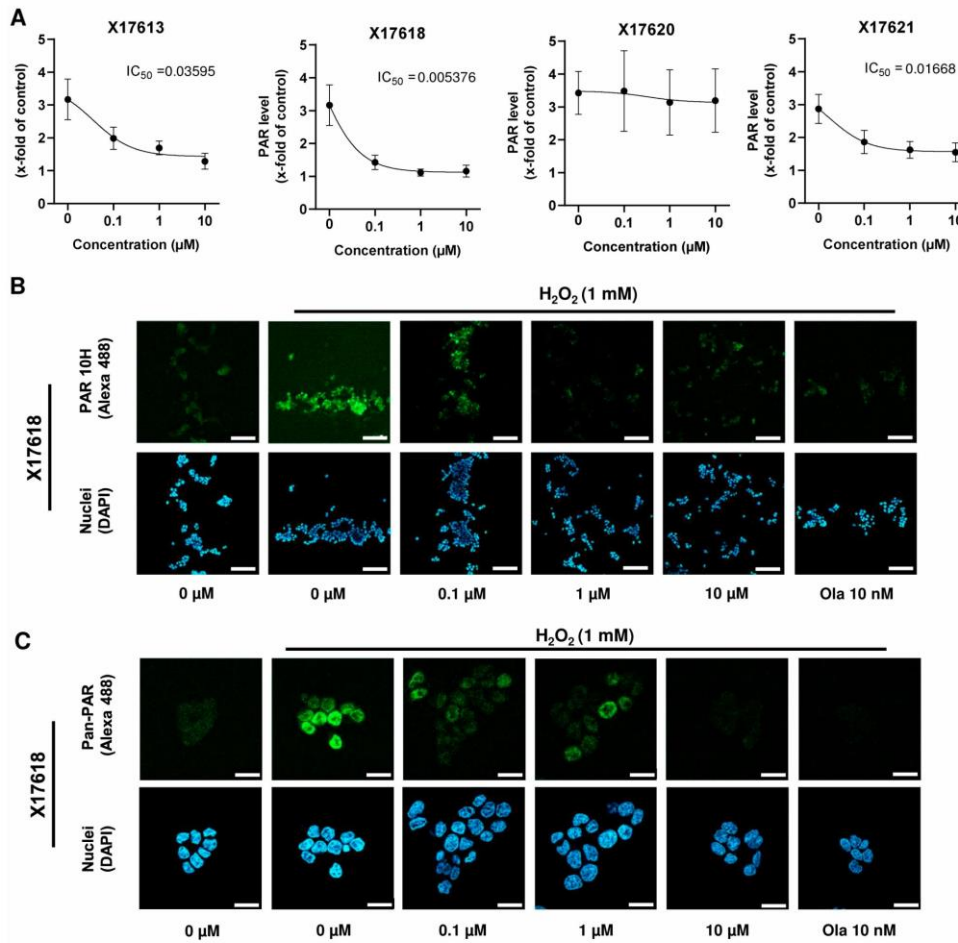


Figure A3. (A) Concentration-response curves of 4 potential PARP-1 inhibitors (X17613, X17618, X17620 and X17621) assessed in HCT116 cells as described in Figure 2B ($n = 3$). IC_{50} values were derived using a nonlinear regression model in GraphPad Prism 9. (B) Representative confocal microscopy images at 100 \times magnification after PAR staining in HCT116 cells treated with the indicated concentrations of X17618 for 2 h with or without subsequent PARP induction by H₂O₂ treatment for 5 min. Scale bar: 100 μ m. (C) Confocal microscopy images at 630 \times magnification after pan-PAR staining in HCT116 treated as described in B. Scale bar: 20 μ m.

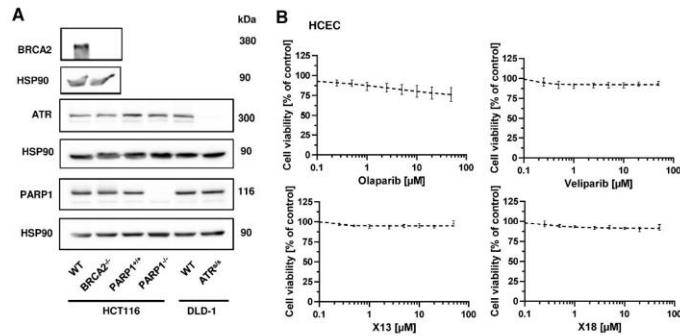


Figure A4. (A) Western Blot analysis of PARP-1, BRCA2 and ATR expression in HCT116 WT, HCT116 BRCA2^{-/-}, HCT116 PARP-1^{+/+}, HCT116 PARP-1^{-/-}, DLD-1 WT and DLD-1 ATR^{s/s} cells. HSP90 served as loading control. (B) Toxicity of PARPi in human colonic epithelial cells (HCEC). Cells were incubated with PARPi for 72 h and viability was assessed using the RRA. Nonlinear regression curve fit was conducted using GraphPad Prism 9 ($n \geq 3$).

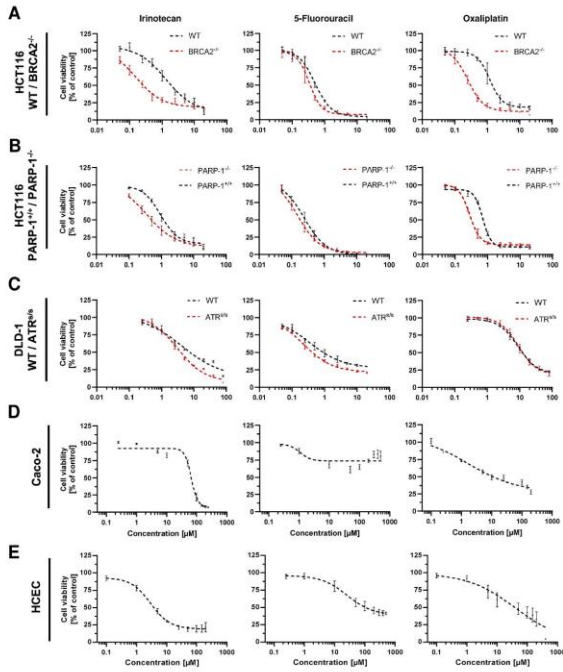


Figure A5. Cell viability of (A) HCT116 WT and HCT116 BRCA2^{-/-}, (B) HCT116 PARP-1^{+/+} and HCT116 PARP-1^{-/-}, (C) DLD-1 WT and DLD-1 ATR^{s/s}, (D) Caco-2 cells and (E) HCEC after monotreatment with cytostatic drugs IT, 5-FU and OXA for 72 h. Nonlinear regression curve fit was conducted using GraphPad Prism 9 ($n \geq 3$).

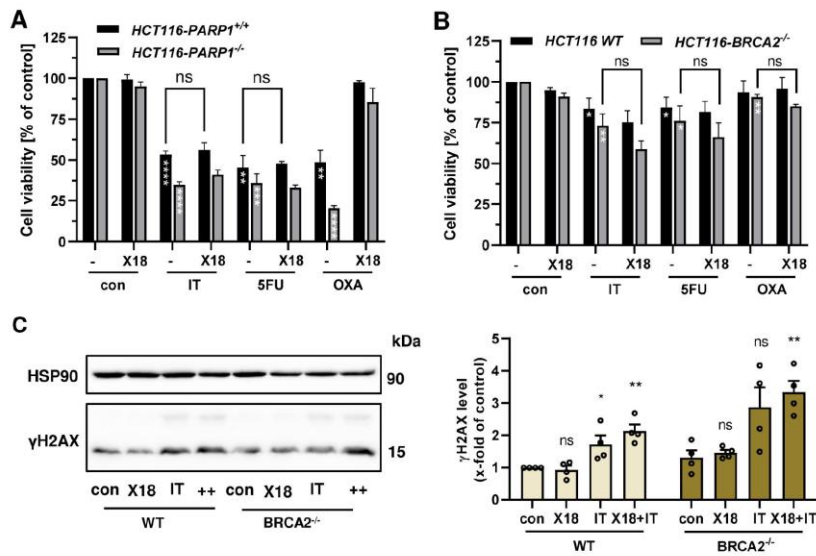


Figure A6. (A) Viability of HCT116 PARP-1^{-/-} and HCT116 PARP-1^{+/+} cells after treatment with PARPi X17618 in combination with chemotherapeutic drugs irinotecan (IT, 0.5 μM), 5-fluorouracil (5-FU, 0.25 μM) and oxaliplatin (OXA, 0.5 μM) for 72 h ($n \geq 3$) (B) Viability of HCT116 WT and HCT116 BRCA2^{-/-} cells after treatment with PARPi X17618 in combination with chemotherapeutic drugs irinotecan (IT, 0.25 μM), 5-fluorouracil (5-FU, 0.1 μM) and oxaliplatin (OXA, 0.25 μM) for 72 h ($n \geq 3$). (C) γ H2AX formation in HCT116 WT and BRCA2^{-/-} cells after treatment with X17618 (50 μM), IT (0.25 μM) or a combination of both for 24 h. Representative Western blot images and densitometric evaluation are shown ($n = 4$). All data are presented as mean \pm SEM. ns: $p > 0.05$, * $p < 0.01$, ** $p < 0.01$, *** $p < 0.001$, **** $p < 0.0001$; t -test.

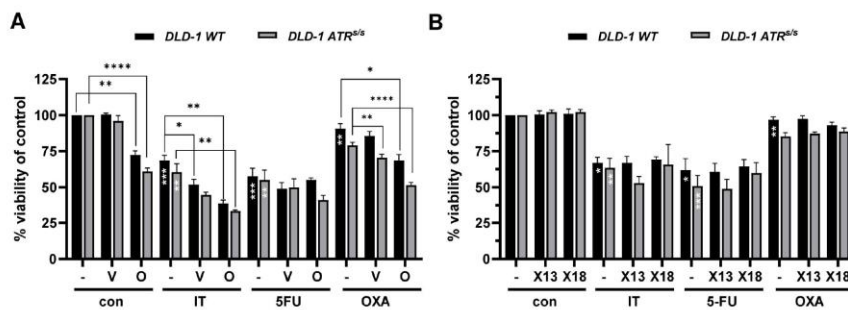


Figure A7. (A) Viability of DLD-1 WT and DLD-1 ATR^{s/s} cells after treatment with PARPi olaparib or veliparib in combination with chemotherapeutic drugs (IT, 2.5 μM), 5-fluorouracil (5-FU, 0.1 μM) and oxaliplatin (OXA, 5 μM) for 72 h ($n \geq 3$). (B) Viability of DLD-1 WT and DLD-1 ATR^{s/s} cells after treatment with PARPi X17613 and X17618 in combination with chemotherapeutic drugs (IT, 2.5 μM), 5-fluorouracil (5-FU, 0.1 μM) and oxaliplatin (OXA, 5 μM) for 72 h ($n \geq 3$). Data are shown as mean \pm SEM. * $p < 0.01$, ** $p < 0.01$, *** $p < 0.001$, **** $p < 0.0001$; t -test.

References

1. Favoriti, P.; Carbone, G.; Greco, M.; Pirozzi, F.; Pirozzi, R.E.M.; Corcione, F. Worldwide burden of colorectal cancer: A review. *Updates Surg.* **2016**, *68*, 7–11. [\[CrossRef\]](#)
2. Spaander, M.C.W.; Zauber, A.G.; Syngal, S.; Blaser, M.J.; Sung, J.J.; You, Y.N.; Kuipers, E.J. Young-onset colorectal cancer. *Nat. Rev. Dis. Prim.* **2023**, *9*, 21. [\[CrossRef\]](#)
3. Biller, L.H.; Schrag, D. Diagnosis and Treatment of Metastatic Colorectal Cancer: A Review. *JAMA* **2021**, *325*, 669–685. [\[CrossRef\]](#)
4. Hammond, W.A.; Swaika, A.; Mody, K. Pharmacologic resistance in colorectal cancer: A review. *Ther. Adv. Med. Oncol.* **2016**, *8*, 57–84. [\[CrossRef\]](#)
5. Boland, C.R.; Goel, A. Microsatellite instability in colorectal cancer. *Gastroenterology* **2010**, *138*, 2073–2087.e3. [\[CrossRef\]](#)
6. Keum, N.; Giovannucci, E. Global burden of colorectal cancer: Emerging trends, risk factors and prevention strategies. *Nat. Rev. Gastroenterol. Hepatol.* **2019**, *16*, 713–732. [\[CrossRef\]](#)
7. Fahrer, J.; Kaina, B. O6-methylguanine-DNA methyltransferase in the defense against N-nitroso compounds and colorectal cancer. *Carcinogenesis* **2013**, *34*, 2435–2442. [\[CrossRef\]](#)
8. Degrolard-Courcet, E.; Sokolowska, J.; Padeano, M.-M.; Guiu, S.; Bronner, M.; Chery, C.; Coron, F.; Lepage, C.; Chapusot, C.; Loustalot, C.; et al. Development of primary early-onset colorectal cancers due to biallelic mutations of the FANCD1/BRCA2 gene. *Eur. J. Hum. Genet.* **2014**, *22*, 979–987. [\[CrossRef\]](#)
9. Phelan, C.M.; Iqbal, J.; Lynch, H.T.; Lubinski, J.; Gronwald, J.; Moller, P.; Ghadirian, P.; Foulkes, W.D.; Armel, S.; Eisen, A.; et al. Incidence of colorectal cancer in BRCA1 and BRCA2 mutation carriers: Results from a follow-up study. *Br. J. Cancer* **2014**, *110*, 530–534. [\[CrossRef\]](#)
10. Moretto, R.; Elliott, A.; Zhang, J.; Arai, H.; Germani, M.M.; Conca, V.; Xiu, J.; Stafford, P.; Oberley, M.; Abraham, J.; et al. Homologous Recombination Deficiency Alterations in Colorectal Cancer: Clinical, Molecular, and Prognostic Implications. *J. Natl. Cancer Inst.* **2022**, *114*, 271–279. [\[CrossRef\]](#)
11. Gustavsson, B.; Carlsson, G.; Machover, D.; Petrelli, N.; Roth, A.; Schmoll, H.-J.; Tveit, K.-M.; Gibson, F. A Review of the Evolution of Systemic Chemotherapy in the Management of Colorectal Cancer. *Clin. Color. Cancer* **2015**, *14*, 1–10. [\[CrossRef\]](#)
12. Mangerich, A.; Burkle, A. How to kill tumor cells with inhibitors of poly(ADP-ribose)ylation. *Int. J. Cancer* **2011**, *128*, 251–265. [\[CrossRef\]](#)
13. Martín-Hernández, K.; Rodríguez-Vargas, J.M.; Schreiber, V.; Dantzer, F. Expanding functions of ADP-ribosylation in the maintenance of genome integrity. *Semin. Cell Dev. Biol.* **2017**, *63*, 92–101. [\[CrossRef\]](#)
14. Gibson, B.A.; Kraus, W.L. New insights into the molecular and cellular functions of poly(ADP-ribose) and PARPs. *Nat. Rev. Mol. Cell Biol.* **2012**, *13*, 411–424. [\[CrossRef\]](#)
15. Dörsam, B.; Seiwert, N.; Foersch, S.; Stroh, S.; Nagel, G.; Begaliew, D.; Diehl, E.; Kraus, A.; McKeague, M.; Minneker, V.; et al. PARP-1 protects against colorectal tumor induction, but promotes inflammation-driven colorectal tumor progression. *Proc. Natl. Acad. Sci. USA* **2018**, *115*, E4061–E4070. [\[CrossRef\]](#)
16. Mateo, J.; Lord, C.J.; Serra, V.; Tutt, A.; Balmaña, J.; Castroviejo-Bermejo, M.; Cruz, C.; Oaknin, A.; Kaye, S.B.; de Bono, J.S. A decade of clinical development of PARP inhibitors in perspective. *Ann. Oncol.* **2019**, *30*, 1437–1447. [\[CrossRef\]](#)
17. Cortesi, L.; Rugo, H.S.; Jackisch, C. An Overview of PARP Inhibitors for the Treatment of Breast Cancer. *Target. Oncol.* **2021**, *16*, 255–282. [\[CrossRef\]](#)
18. Paulet, L.; Trecourt, A.; Leary, A.; Peron, J.; Descotes, F.; Devouassoux-Shisheboran, M.; Leroy, K.; You, B.; Lopez, J. Cracking the homologous recombination deficiency code: How to identify responders to PARP inhibitors. *Eur. J. Cancer* **2022**, *166*, 87–99. [\[CrossRef\]](#)
19. Reilly, N.M.; Novara, L.; Di Nicolantonio, F.; Bardelli, A. Exploiting DNA repair defects in colorectal cancer. *Mol. Oncol.* **2019**, *13*, 681–700. [\[CrossRef\]](#)
20. Pilié, P.G.; Gay, C.M.; Byers, L.A.; O'Connor, M.J.; Yap, T.A. PARP Inhibitors: Extending Benefit Beyond BRCA-Mutant Cancers. *Clin. Cancer Res.* **2019**, *25*, 3759–3771. [\[CrossRef\]](#)
21. Giannini, G.; Ristori, E.; Cerignoli, F.; Rinaldi, C.; Zani, M.; Viel, A.; Ottini, L.; Crescenzi, M.; Martinotti, S.; Bignami, M.; et al. Human MRE11 is inactivated in mismatch repair-deficient cancers. *EMBO Rep.* **2002**, *3*, 248–254. [\[CrossRef\]](#)
22. Vilar, E.; Bartnik, C.M.; Stenzel, S.L.; Raskin, L.; Ahn, J.; Moreno, V.; Mukherjee, B.; Iniesta, M.D.; Morgan, M.A.; Rennert, G.; et al. MRE11 Deficiency Increases Sensitivity to Poly(ADP-ribose) Polymerase Inhibition in Microsatellite Unstable Colorectal Cancers. *Cancer Res.* **2011**, *71*, 2632–2642. [\[CrossRef\]](#)
23. Leichman, L.; Groshen, S.; O'Neil, B.H.; Messersmith, W.; Berlin, J.; Chan, E.; Leichman, C.G.; Cohen, S.J.; Cohen, D.; Lenz, H.-J.; et al. Phase II Study of Olaparib (AZD-2281) after Standard Systemic Therapies for Disseminated Colorectal Cancer. *Oncologist* **2016**, *21*, 172–177. [\[CrossRef\]](#)
24. Wang, C.; Jette, N.; Moussienko, D.; Bebb, D.G.; Lees-Miller, S.P. ATM-Deficient Colorectal Cancer Cells Are Sensitive to the PARP Inhibitor Olaparib. *Transl. Oncol.* **2017**, *10*, 190–196. [\[CrossRef\]](#)
25. Curtin, N.J.; Szabo, C. Poly(ADP-ribose) polymerase inhibition: Past, present and future. *Nat. Rev. Drug Discov.* **2020**, *19*, 711–736. [\[CrossRef\]](#)
26. Arena, S.; Corti, G.; Durinikova, E.; Montone, M.; Reilly, N.M.; Russo, M.; Lorenzato, A.; Arcella, P.; Lazzari, L.; Rospo, G.; et al. A Subset of Colorectal Cancers with Cross-Sensitivity to Olaparib and Oxaliplatin. *Clin. Cancer Res.* **2020**, *26*, 1372–1384. [\[CrossRef\]](#)

27. Keggenhoff, F.L.; Castven, D.; Becker, D.; Stojkovic, S.; Castven, J.; Zimpel, C.; Straub, B.K.; Gerber, T.; Langer, H.; Hahnel, P.; et al. PARP-1 selectively impairs KRAS-driven phenotypic and molecular features in intrahepatic cholangiocarcinoma. *Gut* **2024**, *73*, 1712–1724. [[CrossRef](#)]
28. LaFargue, C.J.; Dal Molin, G.Z.; Sood, A.K.; Coleman, R.L. Exploring and comparing adverse events between PARP inhibitors. *Lancet Oncol.* **2019**, *20*, e15–e28. [[CrossRef](#)]
29. Rose, M.; Burgess, J.T.; O'Byrne, K.; Richard, D.J.; Bolderson, E. PARP Inhibitors: Clinical Relevance, Mechanisms of Action and Tumor Resistance. *Front. Cell Dev. Biol.* **2020**, *8*, 564601. [[CrossRef](#)]
30. Aoyagi-Scharber, M.; Gardberg, A.S.; Yip, B.K.; Wang, B.; Shen, Y.; Fitzpatrick, P.A. Structural basis for the inhibition of poly(ADP-ribose) polymerases 1 and 2 by BMN 673, a potent inhibitor derived from dihydropyridophthalazinone. *Acta Crystallogr. Sect. F Struct. Biol. Commun.* **2014**, *70*, 1143–1149. [[CrossRef](#)]
31. Ogden, T.E.H.; Yang, J.-C.; Schimpl, M.; Easton, L.E.; Underwood, E.; Rawlins, P.B.; McCauley, M.M.; Langelier, M.-F.; Pascal, J.M.; Embrey, K.J.; et al. Dynamics of the HD regulatory subdomain of PARP-1; substrate access and allostery in PARP activation and inhibition. *Nucleic Acids Res.* **2021**, *49*, 2266–2288. [[CrossRef](#)]
32. Sastry, G.M.; Adzhigirey, M.; Day, T.; Annabhimoju, R.; Sherman, W. Protein and ligand preparation: Parameters, protocols, and influence on virtual screening enrichments. *J. Comput.-Aided Mol. Des.* **2013**, *27*, 221–234. [[CrossRef](#)]
33. Roos, K.; Wu, C.; Damm, W.; Reboul, M.; Stevenson, J.M.; Lu, C.; Dahlgren, M.K.; Mondal, S.; Chen, W.; Wang, L.; et al. OPLS3e: Extending Force Field Coverage for Drug-Like Small Molecules. *J. Chem. Theory Comput.* **2019**, *15*, 1863–1874. [[CrossRef](#)]
34. Jacobson, M.P.; Friesner, R.A.; Xiang, Z.; Honig, B. On the Role of the Crystal Environment in Determining Protein Side-chain Conformations. *J. Mol. Biol.* **2002**, *320*, 597–608. [[CrossRef](#)]
35. Friesner, R.A.; Banks, J.L.; Murphy, R.B.; Halgren, T.A.; Klicic, J.J.; Mainz, D.T.; Repasky, M.P.; Knoll, E.H.; Shelley, M.; Perry, J.K.; et al. Glide: A New Approach for Rapid, Accurate Docking and Scoring. 1. Method and Assessment of Docking Accuracy. *J. Med. Chem.* **2004**, *47*, 1739–1749. [[CrossRef](#)]
36. Friesner, R.A.; Murphy, R.B.; Repasky, M.P.; Frye, L.L.; Greenwood, J.R.; Halgren, T.A.; Sanschagrin, P.C.; Mainz, D.T. Extra Precision Glide: Docking and Scoring Incorporating a Model of Hydrophobic Enclosure for Protein-Ligand Complexes. *J. Med. Chem.* **2006**, *49*, 6177–6196. [[CrossRef](#)]
37. Xu, H.; Xian, J.; Vire, E.; McKinney, S.; Wei, V.; Wong, J.; Tong, R.; Kouzarides, T.; Caldas, C.; Aparicio, S. Up-regulation of the interferon-related genes in BRCA2 knockout epithelial cells. *J. Pathol.* **2014**, *234*, 386–397. [[CrossRef](#)]
38. Hurley, P.J.; Wilsker, D.; Bunz, F. Human cancer cells require ATR for cell cycle progression following exposure to ionizing radiation. *Oncogene* **2007**, *26*, 2535–2542. [[CrossRef](#)]
39. Roig, A.I.; Eskiciak, U.; Hight, S.K.; Kim, S.B.; Delgado, O.; Souza, R.F.; Spechler, S.J.; Wright, W.E.; Shay, J.W. Immortalized epithelial cells derived from human colon biopsies express stem cell markers and differentiate in vitro. *Gastroenterology* **2010**, *138*, 1012–1021.e5. [[CrossRef](#)]
40. Seiwert, N.; Wecklein, S.; Demuth, P.; Hasselwander, S.; Kemper, T.A.; Schwerdtle, T.; Brunner, T.; Fahrner, J. Heme oxygenase 1 protects human colonocytes against ROS formation, oxidative DNA damage and cytotoxicity induced by heme iron, but not inorganic iron. *Cell Death Dis.* **2020**, *11*, 787. [[CrossRef](#)]
41. Carlsson, M.J.; Vollmer, A.S.; Demuth, P.; Heylmann, D.; Reich, D.; Quarz, C.; Rasenberger, B.; Nikolova, T.; Hofmann, T.G.; Christmann, M.; et al. p53 triggers mitochondrial apoptosis following DNA damage-dependent replication stress by the hepatotoxin methyleugenol. *Cell Death Dis.* **2022**, *13*, 1009. [[CrossRef](#)] [[PubMed](#)]
42. Demin, A.A.; Hirota, K.; Tsuda, M.; Adamowicz, M.; Hailstone, R.; Brazina, J.; Gittens, W.; Kalasova, I.; Shao, Z.; Zha, S.; et al. XRCC1 prevents toxic PARP1 trapping during DNA base excision repair. *Mol. Cell* **2021**, *81*, 3018–3030.e5. [[CrossRef](#)] [[PubMed](#)]
43. Mimmler, M.; Peter, S.; Kraus, A.; Stroh, S.; Nikolova, T.; Seiwert, N.; Hasselwander, S.; Neitzel, C.; Haub, J.; Monien, B.H.; et al. DNA damage response curtails detrimental replication stress and chromosomal instability induced by the dietary carcinogen PhIP. *Nucleic Acids Res.* **2016**, *44*, 10259–10276. [[CrossRef](#)] [[PubMed](#)]
44. Fahrner, J.; Huelsenbeck, J.; Jaurich, H.; Dorsam, B.; Frisan, T.; Eich, M.; Roos, W.P.; Kaina, B.; Fritz, G. Cytotoxic distending toxin (CDT) is a radiomimetic agent and induces persistent levels of DNA double-strand breaks in human fibroblasts. *DNA Repair* **2014**, *18*, 31–43. [[CrossRef](#)] [[PubMed](#)]
45. Haince, J.F.; Poirier, G.G.; Kirkland, J.B. Nonisotopic methods for determination of poly(ADP-ribose) levels and detection of poly(ADP-ribose) polymerase. *Curr. Protoc. Cell Biol.* **2004**, *21*, Unit18.7. [[CrossRef](#)] [[PubMed](#)]
46. Sharma, A.; Singh, K.; Almasan, A. Histone H2AX phosphorylation: A marker for DNA damage. *Methods Mol. Biol.* **2012**, *920*, 613–626. [[CrossRef](#)]
47. Xiong, Y.; Guo, Y.; Liu, Y.; Wang, H.; Gong, W.; Liu, Y.; Wang, X.; Gao, Y.; Yu, F.; Su, D.; et al. Pamiparib is a potent and selective PARP inhibitor with unique potential for the treatment of brain tumor. *Neoplasia* **2020**, *22*, 431–440. [[CrossRef](#)]
48. Zandarashvili, L.; Langelier, M.-F.; Velagapudi, U.K.; Hancock, M.A.; Steffen, J.D.; Billur, R.; Hannan, Z.M.; Wicks, A.J.; Krastev, D.B.; Pettitt, S.J.; et al. Structural basis for allosteric PARP-1 retention on DNA breaks. *Science* **2020**, *368*, eaax6367. [[CrossRef](#)]
49. Hopkins, T.A.; Ainsworth, W.B.; Ellis, P.A.; Donawho, C.K.; DiGiammarino, E.L.; Panchal, S.C.; Abraham, V.C.; Algire, M.A.; Shi, Y.; Olson, A.M.; et al. PARP1 Trapping by PARP Inhibitors Drives Cytotoxicity in Both Cancer Cells and Healthy Bone Marrow. *Mol. Cancer Res.* **2019**, *17*, 409–419. [[CrossRef](#)]
50. Lawlor, D.; Martin, P.; Busschots, S.; Thery, J.; O'Leary, J.J.; Hennessy, B.T.; Stordal, B. PARP Inhibitors as P-glycoprotein Substrates. *J. Pharm. Sci.* **2014**, *103*, 1913–1920. [[CrossRef](#)]

51. Arnold, C.; Demuth, P.; Seiwert, N.; Wittmann, S.; Boengler, K.; Rasenberger, B.; Christmann, M.; Huber, M.; Brunner, T.; Linnebacher, M.; et al. The Mitochondrial Disruptor Devimistat (CPI-613) Synergizes with Genotoxic Anticancer Drugs in Colorectal Cancer Therapy in a Bim-Dependent Manner. *Mol. Cancer Ther.* **2022**, *21*, 100–112. [[CrossRef](#)]
52. Pettitt, S.J.; Krastev, D.B.; Brandsma, I.; Dréan, A.; Song, F.; Aleksandrov, R.; Harrell, M.I.; Menon, M.; Brough, R.; Campbell, J.; et al. Genome-wide and high-density CRISPR-Cas9 screens identify point mutations in PARP1 causing PARP inhibitor resistance. *Nat. Commun.* **2018**, *9*, 1849. [[CrossRef](#)]
53. Sandhu, D.; Antolin, A.A.; Cox, A.R.; Jones, A.M. Identification of different side effects between PARP inhibitors and their polypharmacological multi-target rationale. *Br. J. Clin. Pharmacol.* **2022**, *88*, 742–752. [[CrossRef](#)]
54. Langelier, M.F.; Lin, X.; Zha, S.; Pascal, J.M. Clinical PARP inhibitors allosterically induce PARP2 retention on DNA. *Sci. Adv.* **2023**, *9*, eadf7175. [[CrossRef](#)]
55. Antolin, A.A.; Ameratunga, M.; Banerji, U.; Clarke, P.A.; Workman, P.; Al-Lazikani, B. The kinase polypharmacology landscape of clinical PARP inhibitors. *Sci. Rep.* **2020**, *10*, 2585. [[CrossRef](#)]
56. Yurgelun, M.B.; Kulke, M.H.; Fuchs, C.S.; Allen, B.A.; Uno, H.; Hornick, J.L.; Ukaegbu, C.I.; Brais, L.K.; McNamara, P.G.; Mayer, R.J.; et al. Cancer Susceptibility Gene Mutations in Individuals With Colorectal Cancer. *J. Clin. Oncol.* **2017**, *35*, 1086–1095. [[CrossRef](#)]
57. Tahara, M.; Inoue, T.; Sato, F.; Miyakura, Y.; Horie, H.; Yasuda, Y.; Fujii, H.; Kotake, K.; Sugano, K. The Use of Olaparib (AZD2281) Potentiates SN-38 Cytotoxicity in Colon Cancer Cells by Indirect Inhibition of Rad51-Mediated Repair of DNA Double-Strand Breaks. *Mol. Cancer Ther.* **2014**, *13*, 1170–1180. [[CrossRef](#)]
58. Murai, J.; Zhang, Y.; Morris, J.; Ji, J.; Takeda, S.; Doroshow, J.H.; Pommier, Y.G. Rationale for PARP inhibitors in combination therapy with camptothecins or temozolomide based on PARP trapping versus catalytic inhibition. *J. Pharmacol. Exp. Ther.* **2014**, *349*, 408–416. [[CrossRef](#)]
59. Augustine, T.; Maitra, R.; Zhang, J.; Nayak, J.; Goel, S. Sensitization of colorectal cancer to irinotecan therapy by PARP inhibitor rucaparib. *Investig. New Drugs* **2019**, *37*, 948–960. [[CrossRef](#)]
60. Kim, H.; Xu, H.; George, E.; Hallberg, D.; Kumar, S.; Jagannathan, V.; Medvedev, S.; Kinose, Y.; Devins, K.; Verma, P.; et al. Combining PARP with ATR inhibition overcomes PARP inhibitor and platinum resistance in ovarian cancer models. *Nat. Commun.* **2020**, *11*, 3726. [[CrossRef](#)]
61. Innocenti, F.; Undevia, S.D.; Iyer, L.; Chen, P.X.; Das, S.; Kocherginsky, M.; Karrison, T.; Janisch, L.; Ramirez, J.; Rudin, C.M.; et al. Genetic variants in the UDP-glucuronosyltransferase 1A1 gene predict the risk of severe neutropenia of irinotecan. *J. Clin. Oncol.* **2004**, *22*, 1382–1388. [[CrossRef](#)]
62. Thomas, A.; Pommier, Y. Targeting Topoisomerase I in the Era of Precision Medicine. *Clin. Cancer Res. Off. J. Am. Assoc. Cancer Res.* **2019**, *25*, 6581–6589. [[CrossRef](#)]
63. Marzi, L.; Szabova, L.; Gordon, M.; Weaver Ohler, Z.; Sharan, S.K.; Beshiri, M.L.; Etemadi, M.; Murai, J.; Kelly, K.; Pommier, Y. The Indenoisoquinoline TOP1 Inhibitors Selectively Target Homologous Recombination-Deficient and Schlafen 11-Positive Cancer Cells and Synergize with Olaparib. *Clin. Cancer Res. Off. J. Am. Assoc. Cancer Res.* **2019**, *25*, 6206–6216. [[CrossRef](#)]
64. Deng, S.; Vlatkovic, T.; Li, M.; Zhan, T.; Veldwijk, M.R.; Herskind, C. Targeting the DNA Damage Response and DNA Repair Pathways to Enhance Radiosensitivity in Colorectal Cancer. *Cancers* **2022**, *14*, 4874. [[CrossRef](#)]
65. Glynn-Jones, R.; Wyrwicz, L.; Tiret, E.; Brown, G.; Rodel, C.; Cervantes, A.; Arnold, D.; Committee, E.G. Rectal cancer: ESMO Clinical Practice Guidelines for diagnosis, treatment and follow-up. *Ann. Oncol. Off. J. Eur. Soc. Med. Oncol.* **2017**, *28*, iv22–iv40. [[CrossRef](#)] [[PubMed](#)]
66. Qin, C.; Ji, Z.; Zhai, E.; Xu, K.; Zhang, Y.; Li, Q.; Jing, H.; Wang, X.; Song, X. PARP inhibitor olaparib enhances the efficacy of radiotherapy on XRCC2-deficient colorectal cancer cells. *Cell Death Dis.* **2022**, *13*, 505. [[CrossRef](#)]
67. Carter, R.; Cheraghchi-Bashi, A.; Westhorpe, A.; Yu, S.; Shanneik, Y.; Seraia, E.; Ouaret, D.; Inoue, Y.; Koch, C.; Wilding, J.; et al. Identification of anticancer drugs to radiosensitize BRAF-wild-type and mutant colorectal cancer. *Cancer Biol. Med.* **2019**, *16*, 234–246. [[CrossRef](#)]
68. Czito, B.G.; Deming, D.A.; Jameson, G.S.; Mulcahy, M.F.; Vaghefi, H.; Dudley, M.W.; Holen, K.D.; DeLuca, A.; Mittapalli, R.K.; Munasinghe, W.; et al. Safety and tolerability of veliparib combined with capecitabine plus radiotherapy in patients with locally advanced rectal cancer: A phase 1b study. *Lancet Gastroenterol. Hepatol.* **2017**, *2*, 418–426. [[CrossRef](#)]
69. Gorbunova, V.; Beck, J.T.; Hofheinz, R.-D.; Garcia-Alfonso, P.; Nechaeva, M.; Cubillo Gracian, A.; Mangel, L.; Elez Fernandez, E.; Deming, D.A.; Ramanathan, R.K.; et al. A phase 2 randomised study of veliparib plus FOLFIRI±bevacizumab versus placebo plus FOLFIRI±bevacizumab in metastatic colorectal cancer. *Br. J. Cancer* **2019**, *120*, 183–189. [[CrossRef](#)]
70. Combès, E.; Andrade, A.F.; Tosi, D.; Michaud, H.-A.; Coquel, F.; Garambois, V.; Desigaud, D.; Jarlier, M.; Coquelle, A.; Pasero, P.; et al. Inhibition of Ataxia-Telangiectasia Mutated and RAD3-Related (ATR) Overcomes Oxaliplatin Resistance and Promotes Antitumor Immunity in Colorectal Cancer. *Cancer Res.* **2019**, *79*, 2933–2946. [[CrossRef](#)]
71. Shkundina, I.S.; Gall, A.A.; Dick, A.; Cocklin, S.; Mazin, A.V. New RAD51 Inhibitors to Target Homologous Recombination in Human Cells. *Genes* **2021**, *12*, 920. [[CrossRef](#)] [[PubMed](#)]
72. Durinikova, E.; Reilly, N.M.; Buzo, K.; Mariella, E.; Chila, R.; Lorenzato, A.; Dias, J.M.L.; Grasso, G.; Pisati, F.; Lamba, S.; et al. Targeting the DNA Damage Response Pathways and Replication Stress in Colorectal Cancer. *Clin. Cancer Res. Off. J. Am. Assoc. Cancer Res.* **2022**, *28*, 3874–3889. [[CrossRef](#)] [[PubMed](#)]

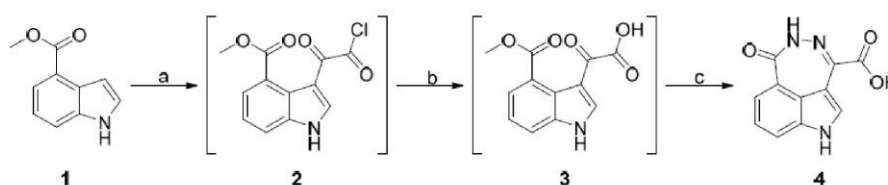
73. Petropoulos, M.; Karamichali, A.; Rossetti, G.G.; Freudenmann, A.; Iacovino, L.G.; Dionellis, V.S.; Sotiriou, S.K.; Halazonetis, T.D. Transcription-replication conflicts underlie sensitivity to PARP inhibitors. *Nature* **2024**, *628*, 433–441. [CrossRef] [PubMed]
74. Potlitz, F.; Link, A. Chemotion Repository 2024. Available online: https://dx.doi.org/10.14272/collection/CWG_2024-02-14 (accessed on 14 February 2024).

Disclaimer/Publisher's Note: The statements, opinions and data contained in all publications are solely those of the individual author(s) and contributor(s) and not of MDPI and/or the editor(s). MDPI and/or the editor(s) disclaim responsibility for any injury to people or property resulting from any ideas, methods, instructions or products referred to in the content.

SUPPORTING INFORMATION – MATERIAL AND METHODS

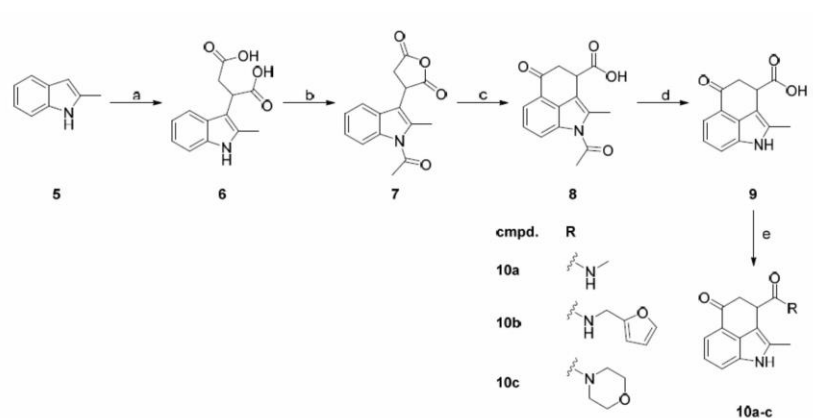
Synthesis of test compounds

Synthesis of test compound **4** (X17613, s. scheme 1) was conducted as described below. The reaction sequence started with the acylation of the starting material methyl 1*H*-indole-4-carboxylate (**1**) by treatment with oxalyl chloride in the cold to achieve acylation of the indole heterocycle in the 3-position. The resulting 3-(2-chloro-2-oxo-acetyl)oxy-indole derivative **2** was then subjected to hydrolysis of the acyl chloride motif by addition of water (in THF) to yield the free 2-oxoacetic acid **3** at ambient temperature. Due to the almost quantitative character of most reactions in this cascade and the high reactivity of key intermediates, isolation and analytical characterization of these intermediates was omitted, as reported for similar structural motifs [1,2]. During the final step, cyclization of **3** to **4** was achieved by means of reacting the substrate **3** with aqueous hydrazine hydrate solution in the presence of acetic acid. Following this procedure, compound **4** (X17613) could be isolated as a yellow amorphous solid with a yield of 76% over three steps (S. Scheme S1).



Scheme S1. Synthesis of compound **4**. Reagents and conditions: (a) oxalyl chloride, DEE, 0–20 °C, 12 h; (b) H₂O, THF, 20 °C, 2 h; (c) N₂H₄ × H₂O, CH₃COOH, MeOH, 20 °C, 18 h, 76% (over three steps).

Compounds **10a-c** (X17618, X17620, X17621) were synthesized from their respective carboxylic acid and amine precursors via HATU/DIPEA-assisted amide coupling reactions. The corresponding 1,3,4,5-tetrahydrobenzo[*cd*]indole-derived carboxylic acid **9** was prepared by adapting a procedure from Böhshagen et al. (s. Scheme S2) [3]. Thus, the starting material 2-methylindole (**5**) was reacted with maleic acid to yield the intermediate succinic acid derivative **6**, which was dehydrated in the next step using prop-1-en-2-yl acetate and *p*-toluenesulfonic acid as the catalyst. Due to the ability of prop-1-en-2-yl acetate to act as an acetylating agent, the N-atom of the indole nucleus was acetylated as a side reaction, which did, however, not pose any problems regarding the following steps. Formation of the tricyclic carboxylic acid **8** was achieved via intramolecular Friedel–Crafts acylation using dry aluminum chloride in 1,2-dichloroethane with excellent yields. Removal of the accidentally introduced *N*-acetyl group of **8** proceeded smoothly by alkaline hydrolysis, followed by precipitation of the carboxylic acid **9**. With the key intermediate **9** thus prepared, derivatization to amides like **10** by reacting it with various amines proved to be fairly straightforward. Standard amide coupling reagents HATU and DIPEA in DMF were utilized to achieve this goal. The reaction times could be shortened significantly by reacting the mixture in a microwave reactor at elevated temperatures (18 h at 20 °C vs. 10 min at 140 °C and microwave irradiation).



Scheme S2. Synthesis of compounds **10a-c**. Reagents and conditions: (a) maleic acid, 120 °C, 1 h, 83%; (b) prop-1-en-2-yl acetate, TsOH, 20–120 °C, 61%; (c) AlCl₃, DCE, 50 °C, 94%; (d) NaOH, H₂O, 75 °C, 87%; (e) R₁NHR₂, HATU, DIPEA, DMF, 140 °C, 10 min, μ -wave irradiation, 35–56%.

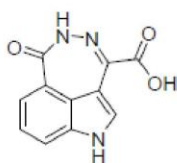
Experimental Section

General Remarks

All starting materials, reagents, and solvents were commercially available and purchased from Sigma-Aldrich, VWR, abcr, or Carl Roth. Unless otherwise stated, starting materials were used as provided. Melting points were determined using a BÜCHI Melting Point M-565 device. Analytical thin-layer chromatography was performed using silica gel 60 F254 aluminum plates supplied by Merck; visualization was accomplished with UV light. Microwave-assisted syntheses were carried out in a Monowave 400 reactor manufactured by Anton Paar in suitable glass vessels while monitoring and controlling the temperature with the integrated infrared sensor. Preparative column chromatography was carried out with an Interchim puriFlash XS 520Plus system and the corresponding 25 g silica gel cartridges available from Interchim (30-SI-HP). NMR analysis was run on a Bruker Avance III instrument at 400 MHz (¹H) and 101 MHz (¹³C), using DMSO-*d*₆ as the solvent. Chemical shifts are given in relation to the internal standard tetramethylsilane and reported as parts per million (ppm). MIR analyses were performed on an ALPHA-FT-IR device from Bruker Optics equipped with a diamond ATR accessory unit. High-resolution (HR) accurate mass (AM)-MS analyses were performed either on a Bruker MAXIS LC-QTOF-MS or a Bruker compact LC-qTOF-MS run with ESI ionization.

Synthesis

1. -Oxo-2,6-dihydro-1H-[1,2]diazepino[4,5,6-cd]indole-4-carboxylic acid (**4**) (X17613)



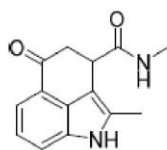
Synthetic procedure modified from Ferraris et al. and Webber et al. [1,2]. To a round-bottom flask were added methyl 1*H*-indole-4-carboxylate (**1**, 3.50 g, 20.00 mmol, 1.00 eq) and 100 mL diethyl ether. To the suspension, oxalyl chloride (3.05 g, 2.06 mL, 24.00 mmol, 1.20 eq) was added dropwise via an addition funnel. After stirring at 20 °C for 12 h, the solvent was evaporated, and the residue resuspended in 75 mL of tetrahydrofuran, followed by the addition of water (1.80 mL, 1.80 g, 100.00 mmol, 5.00 eq). After stirring at 20 °C for 2 h, the solvent was evaporated. The residue was resuspended in methanol (12 mL) and glacial acetic acid (1.72 mL, 1.80 g, 30.00 mmol, 1.50 eq) and an aqueous solution of hydrazine hydrate (3.8 mL, equals 3.00 g of hydrazine hydrate, 60.00 mmol, 2.00 eq) were added. The mixture was stirred at 20 °C for 18 h. The precipitate was separated via vacuum filtration, washed multiple times with water, and dried under reduced pressure, yielding **4** as a yellow amorphous solid (3.50 g, 76%).

$R_f = 0.62$ (15% acetic acid and 15% water in *n*-butanol); mp: 226.8°C; ¹H-NMR (400 MHz, DMSO-*d*₆): δ (ppm) = 7.05-7.16 (m, 1H), 7.41-7.61 (m, 2H), 7.89 (s, 1H), 10.00 (s, 1H), 11.89 (s, 1H); ¹³C-NMR (101 MHz, DMSO-*d*₆): δ (ppm) = 110.9, 116.1, 120.5, 121.9, 123.4, 127.2, 128.1, 128.6, 135.9, 165.2, 167.9; IR (ATR): $\tilde{\nu} = 3222$ (m, ν_{N-H}), 3098 (m, ν_{O-H}), 1669 (s, $\nu_{C=O}$); ESI-HRAM-MS (*m/z*): calcd. for [C₁₁H₇N₃O₃ + H]⁺ 230.0560, found 230.0559.

Additional information on the chemical synthesis is available via the Chemotion repository: <https://dx.doi.org/10.14272/reaction/SA-FUHFF-UHFFFADPSC-DRRJDSUMVPRFOC-UHFFFAOYSA-N.2>

Additional information on the analysis of the target compound is available via the Chemotion repository: <https://dx.doi.org/10.14272/DRRJDSUMVPRFOC-UHFFFAOYSA-N.2>

N,2-Dimethyl-5-oxo-1,3,4,5-tetrahydrobenzo[*cd*]indole-3-carboxamide (**10a**) (X17618)



To a G10 microwave reaction vial were added **9** (114 mg, 0.50 mmol, 1.00 eq), methylamine hydrochloride (34 mg, 0.50 mmol, 1.00 eq), HATU (380 mg, 1.00 mmol, 2.00 eq), DIPEA (610 μ L, 452 mg, 3.50 mmol, 7.00 eq), and dry DMF (4.0 mL). The vial was flushed with argon and the mixture was heated in a microwave reactor at 140 °C for 10 min. It was poured into water and extracted multiple times with ethyl acetate. The combined organic phases were washed with diluted hydrochloric acid (1M) and saturated aqueous sodium chloride solution. The product was isolated via column chromatography using an *n*-hexane/ethyl acetate gradient, yielding an amorphous yellow solid (35 mg, 35%).

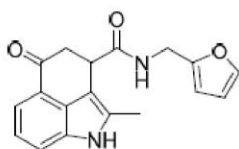
$R_f = 0.27$ (50% ethyl acetate in *n*-hexane); mp: 248.3°C (decomp.); ¹H-NMR (400 MHz, DMSO-*d*₆): δ (ppm) = 2.39 (s, 3H), 2.56 (d, $J = 4.6$ Hz, 3H), 2.73 (dd, $J = 16.0$ Hz, $J = 3.9$ Hz, 1H), 2.85 (dd, $J = 16.0$ Hz, $J = 6.6$ Hz, 1H), 4.04 (dd, $J = 6.6$ Hz, $J = 3.9$ Hz, 1H), 7.07-7.12 (m, 1H), 7.28 (dd, $J = 7.4$ Hz, $J = 0.6$ Hz, 1H), 7.45 (dd, $J = 7.9$ Hz, $J = 0.6$ Hz, 1H), 7.97 (d, $J = 4.6$ Hz, 1H), 11.07 (s, 1H); ¹³C-NMR (101 MHz, DMSO-*d*₆): δ (ppm) = 11.6, 25.6, 39.5, 42.3, 105.1, 113.7, 114.9, 120.6, 124.0, 132.8, 132.8, 134.0, 172.9, 196.0; IR (ATR): $\tilde{\nu} = 3317$ (m, ν_{N-H}), 2916 (w, ν_{C-H}), 1640 (s, $\nu_{C=O}$); ESI-HRAM-MS (*m/z*): calcd. for [C₂₈H₂₈N₄O₃ + H]⁺ ([2M+H]⁺) 485.2183, found 485.2201.

Additional information on the chemical synthesis is available via the Chemotion repository:

<https://dx.doi.org/10.14272/reaction/SA-FUHFF-UHFFFADPSC-QJYPGCPJNL-UHFFFADPSC-NUHFF-NUHFF-NUHFF-ZZZ>

Additional information on the analysis of the target compound is available via the Chemotion repository: <https://dx.doi.org/10.14272/QIYPGCPINLNOJT-UHFFFAOYSA-N.1>

N-(Furan-2-ylmethyl)-2-methyl-5-oxo-1,3,4,5-tetrahydrobenzo[cd]indole-3-carboxamide (10b)(X17620)



To a G10 microwave reaction vial were added **9** (172 mg, 0.75 mmol, 1.00 eq), furfurylamine (66 μ L, 73 mg, 0.75 mmol, 1.00 eq), HATU (570 mg, 1.50 mmol, 2.00 eq), DIPEA (653 μ L, 485 mg, 3.75 mmol, 5.00 eq), and dry DMF (4.0 mL). The vial was flushed with argon and the mixture was heated in a microwave reactor at 140 $^{\circ}$ C for 10 min. It was poured into water and extracted multiple times with ethyl acetate. The combined organic phases were washed with diluted hydrochloric acid (1M) and saturated aqueous sodium chloride solution. The product was isolated via column chromatography using an *n*-hexane/ethyl acetate gradient, yielding an amorphous yellow solid (130 mg, 56%).

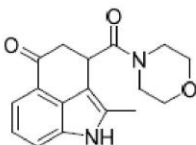
R_f = 0.53 (50% ethyl acetate in *n*-hexane); mp: 193.4 $^{\circ}$ C; 1 H-NMR (400 MHz, DMSO- d_6): δ (ppm) = 2.35 (s, 3H), 2.72 (dd, J = 16.0 Hz, J = 3.7 Hz, 1H), 2.88 (dd, J = 16.0 Hz, J = 6.7 Hz, 1H), 4.13 (dd, J = 6.7 Hz, J = 3.7 Hz, 1H), 4.20 (dd, J = 15.6 Hz, J = 5.8 Hz, 1H), 4.26 (dd, J = 15.6 Hz, J = 4.7 Hz, 1H), 6.18 (dd, J = 3.2 Hz, J = 0.7 Hz, 1H), 6.38 (dd, J = 3.2 Hz, J = 1.9 Hz, 1H), 7.10 (t, J = 7.6 Hz, 1H), 7.28 (dd, J = 7.3 Hz, J = 0.5 Hz, 1H), 7.45 (dd, J = 7.3 Hz, J = 0.5 Hz, 1H), 7.57 (dd, J = 1.8 Hz, J = 0.8 Hz, 1H), 8.55 (t, J = 5.6 Hz, 1H), 11.06 (s, 1H); 13 C-NMR (101 MHz, DMSO- d_6): δ (ppm) = 11.5, 35.5, 39.4, 42.1, 104.9, 106.7, 110.4, 113.7, 114.9, 120.6, 123.9, 132.8, 132.9, 134.0, 142.1, 152.1, 172.4, 195.9; IR (ATR): ν = 3307 (m, $\nu_{\text{N-H}}$), 1630 (s, $\nu_{\text{C=O}}$); ESI-HRAM-MS (m/z): calcd. for $[\text{C}_{18}\text{H}_{16}\text{N}_2\text{O}_3 + \text{H}]^+$ 331.1053, found 331.1053.

Additional information on the chemical synthesis is available via the Chemotion repository:

<https://dx.doi.org/10.14272/reaction/SA-FUHFF-UHFFADPSC-QIROZZVNYL-UHFFADPSC-NUHFF-NUHFF-NUHFF-ZZZ>

Additional information on the analysis of the target compound is available via the Chemotion repository: <https://dx.doi.org/10.14272/QIROZZVNYLUVGF-UHFFFAOYSA-N.1>

2-Methyl-3-(morpholine-4-carbonyl)-3,4-dihydrobenzo[cd]indol-5(1H)-one (10c)(X17621)



To a G10 microwave reaction vial were added **9** (172 mg, 0.75 mmol, 1.00 eq), morpholine (65 μ L, 0.75 mmol, 1.00 eq), HATU (570 mg, 1.00 mmol, 2.00 eq), DIPEA (653 μ L, 485 mg, 3.75 mmol, 5.00 eq), and dry DMF (4.0 mL). The vial was flushed with argon

and the mixture was heated in a microwave reactor at 140 °C for 10 min. It was poured into water and extracted multiple times with ethyl acetate. The combined organic phases were washed with diluted hydrochloric acid (1N) and saturated aqueous sodium chloride solution. The product was isolated via column chromatography using an *n*-hexane/ethyl acetate gradient, yielding an amorphous orange solid (83 mg, 37%).

R_f = 0.61 (50% ethyl acetate in *n*-hexane); mp: >300 °C; $^1\text{H-NMR}$ (400 MHz, DMSO- d_6): δ (ppm)=2.37 (s, 3H), 2.69 (dd, J = 15.8 Hz, J = 4.2 Hz, 1H), 2.83 (dd, J = 15.8 Hz, J = 6.2 Hz, 1H), 3.22-3.59 (m, 8H), 4.77 (dd, J = 5.9 Hz, J = 4.2 Hz, 1H), 7.10 (t, J = 7.6 Hz, 1H), 7.26-7.31 (m, 1H), 7.44 (d, J = 7.6 Hz, 1H), 11.06 (s, 1H); $^{13}\text{C-NMR}$ (101 MHz, DMSO- d_6): δ (ppm)=12.2, 34.4, 42.7, 46.3, 66.3, 105.3, 113.7, 114.9, 120.6, 124.2, 132.2, 132.9, 134.0, 171.7, 195.9; IR (ATR): $\tilde{\nu}$ = 3238 (m, $\nu_{\text{N-H}}$), 2856 (w, $\nu_{\text{C-H}}$), 1661 (s, $\nu_{\text{C=O}}$); ESI-HRAM-MS (m/z): calcd. for $[\text{C}_{17}\text{H}_{18}\text{N}_2\text{O}_3 + \text{H}]^+$ 321.1204, found 321.1204.

Additional information on the chemical synthesis is available via the Chemotion repository:

<https://dx.doi.org/10.14272/reaction/SA-FUHFF-UHFFFADPSC-AHZDMNVTLQ-UHFFFADPSC-NUHFF-NUHFF-NUHFF-ZZZ>

Additional information on the analysis of the target compound is available via the Chemotion repository: <https://dx.doi.org/10.14272/AHZDMNVTLOOTLN-UHFFFAOYSA-N.1>

References

1. Ferraris, D.V., Li, J.H., Kalish, V.J., Zhang, J. Benzoazepine and benzodiazepine derivatives and their use as parp inhibitors. Patent WO0244183 (A2), 6 June 2002.
2. Webber, S.E., Canan, K.S.S., Tikhe, J., Thoresen, L.H. Tricyclic Inhibitors of Poly(ADP-ribose)polymerases. Patent WO0042040 (A1), 20 July 2000.
3. Böshagen, H., Rosentreter, U., Perzborn, E., Fiedler, V. Tetrahydro-1-benzo-(c,d)- indolpropionsäure-sulfonamide. Patent DE3826371 (A1), 8 February 1990.

SUPPORTING INFORMATION – FIGURES AND FIGURE LEGENDS

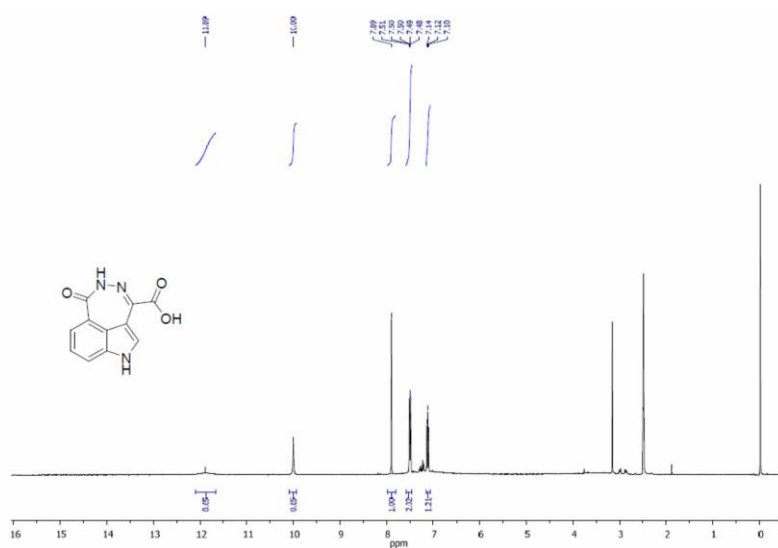


Figure S1. ¹H-NMR spectrum of 1-oxo-2,6-dihydro-1H-[1,2]diazepino[4,5,6-cd]indole-4-carboxylic acid (4) (X17613).

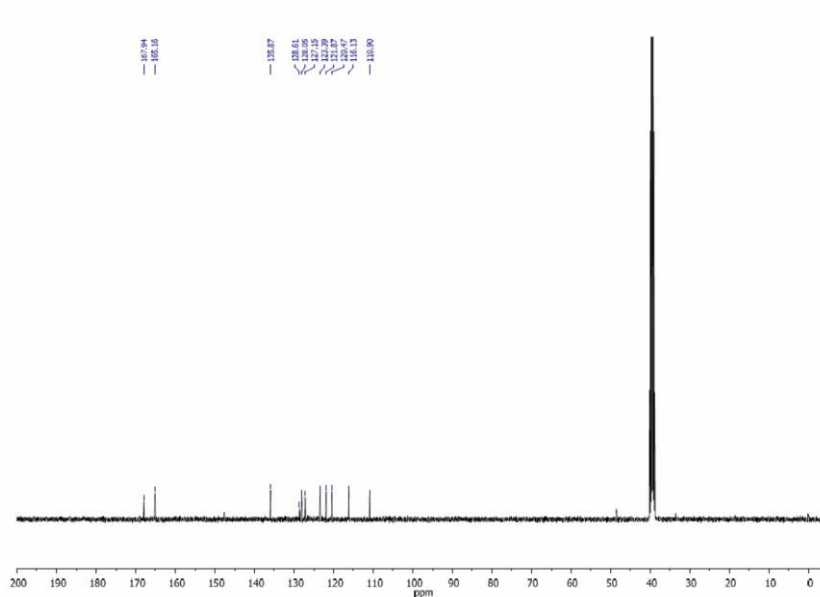


Figure S2. ¹³C-NMR spectrum of compound 1-oxo-2,6-dihydro-1H-[1,2]diazepino[4,5,6-cd]indole-4-carboxylic acid (4) (X17613).

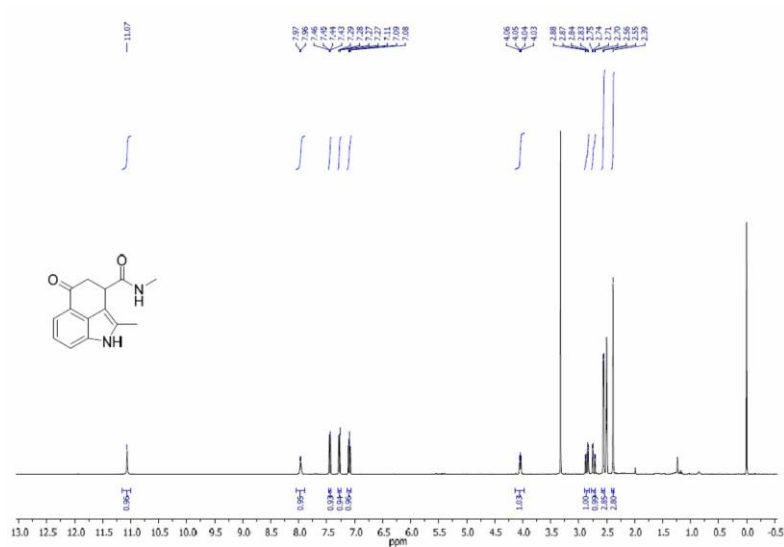


Figure S3. ¹H-NMR spectrum of *N*,2-dimethyl-5-oxo-1,3,4,5-tetrahydrobenzo[*cd*]indole-3-carboxamide (**10a**) (X17618).

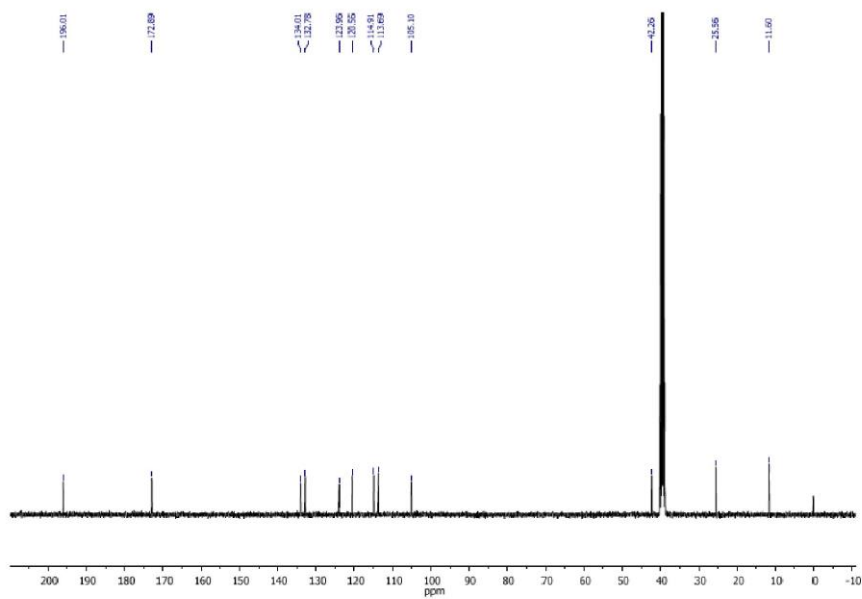


Figure S4. ¹³C-NMR spectrum of *N*,2-dimethyl-5-oxo-1,3,4,5-tetrahydrobenzo[*cd*]indole-3-carboxamide (**10a**) (X17618).

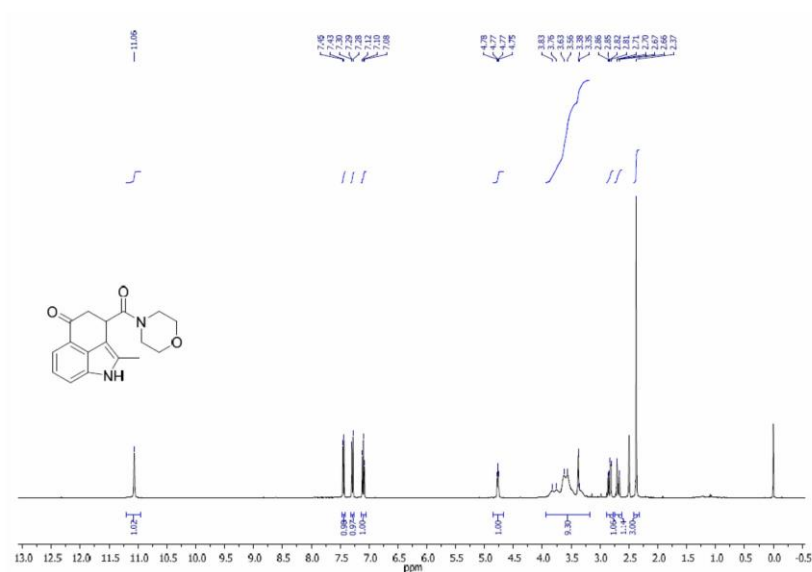


Figure S7. $^1\text{H-NMR}$ spectrum of 2-methyl-3-(morpholine-4-carbonyl)-3,4-dihydrobenzo[cd]indol-5(1H)-one (10c) (X17621).

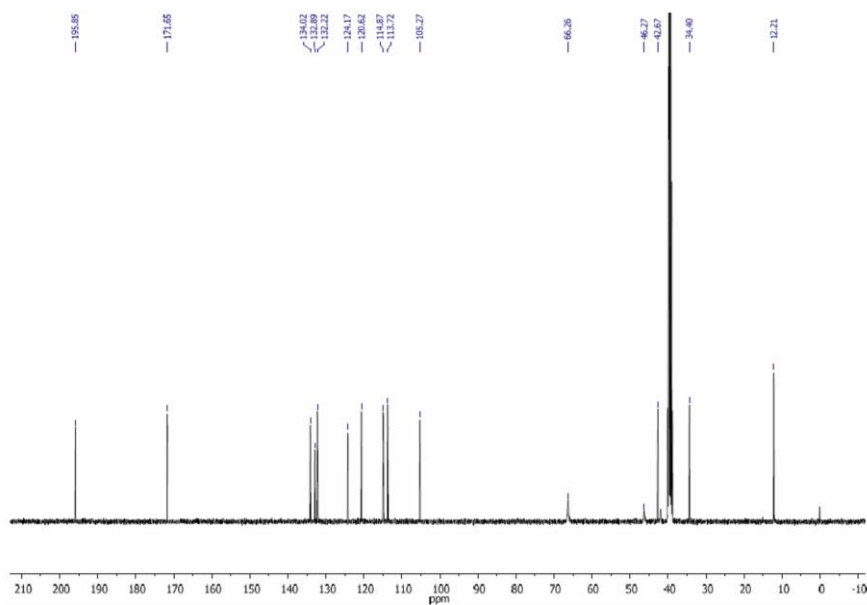


Figure S8. $^{13}\text{C-NMR}$ spectrum of 2-methyl-3-(morpholine-4-carbonyl)-3,4-dihydrobenzo[cd]indol-5(1H)-one (10c) (X17621).

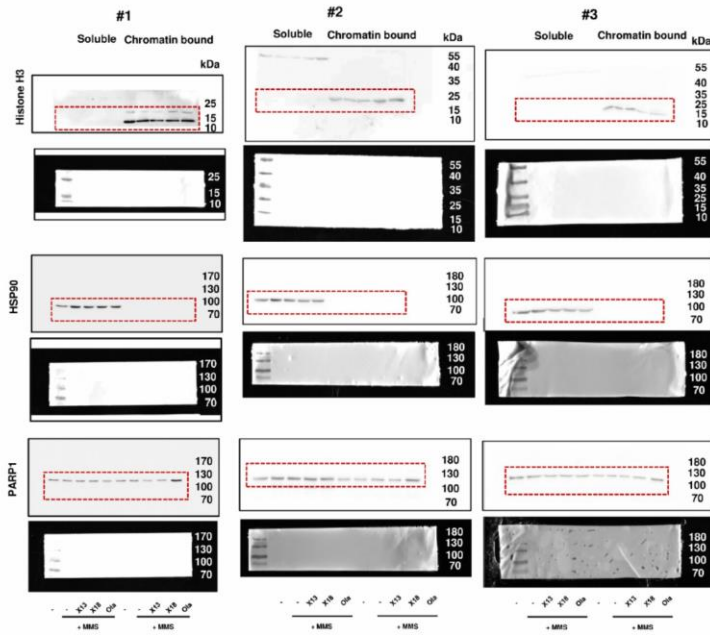


Figure S9. Uncropped Western blot images of HCT116 cells shown in Figure 3A (#1) and two independent repetitions (#2 and #3).

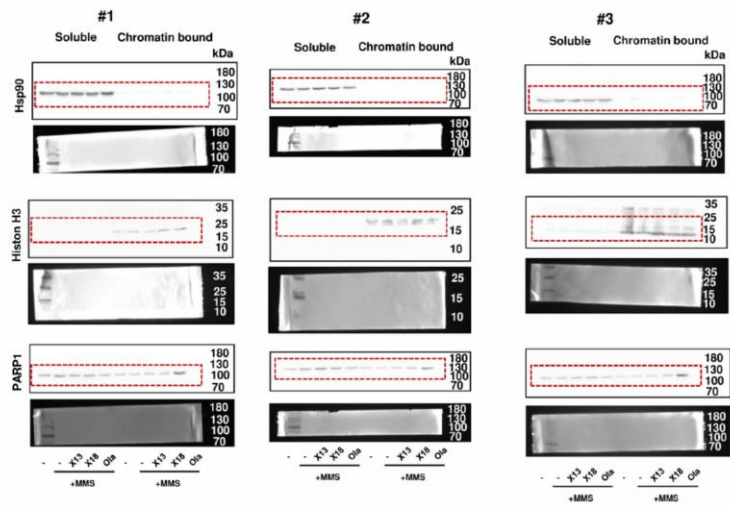


Figure S10. Uncropped Western blot images of Caco-2 cells shown in Figure 3B (#1) and two independent repetitions (#2 and #3).

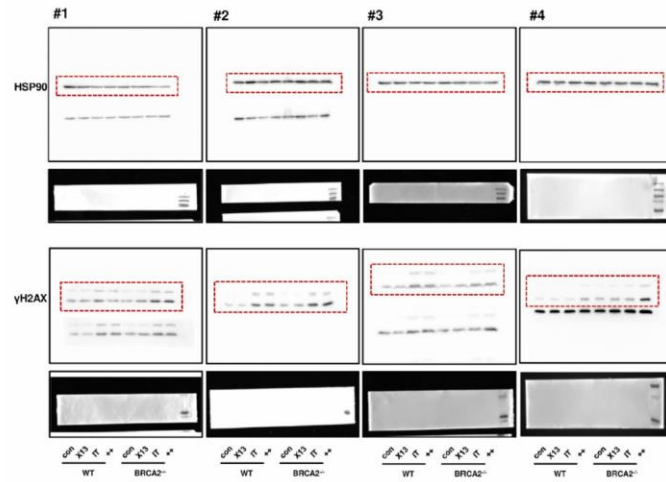


Figure S11. Uncropped Western blot images of HCT116 WT and BRCA2^{-/-} cells shown in Figure 6C (#1) and three independent repetitions (#2–4).

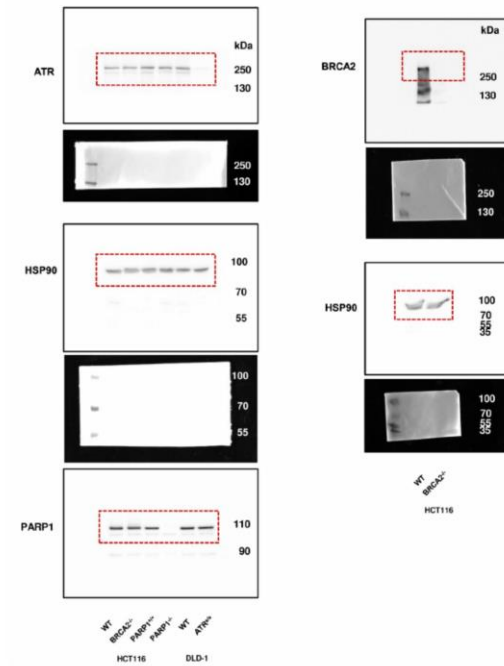


Figure S12. Uncropped Western blot images of HCT116 WT, HCT116 BRCA2^{-/-}, HCT116-PARP1^{+/+}, HCT116-PARP1^{-/-}, DLD-1 WT, and DLD1 ATR^{s/s} cells shown in Figure A5.

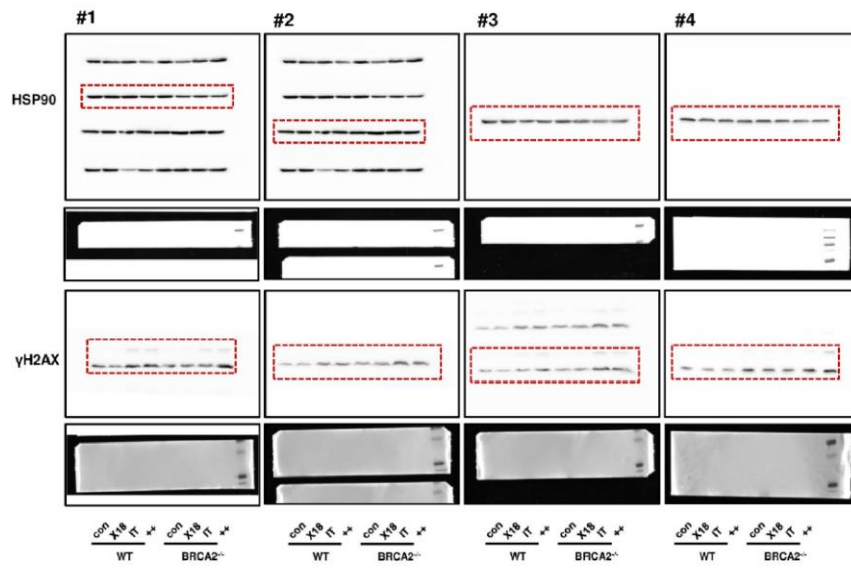


Figure S13. Uncropped Western blot images of HCT116 WT and BRCA2^{-/-} cells shown in Figure A6C (#1) and three independent repetitions (#2–4).

4. Summary of Results

4.1. Publication I: The Mitochondrial Disruptor Devimistat (CPI-613) Synergizes with Genotoxic Anticancer Drugs in Colorectal Cancer Therapy in a Bim-Dependent Manner

In publication I, the antitumorigenic activity of the metabolic inhibitor devimistat was investigated *in vitro*, applying CRC cell lines as well as murine primary intestinal organoids and tumor organoids, and *in vivo* utilizing a xenograft tumor model. First, cytotoxicity was assessed in a panel of 11 MSS and MSI CRC cell lines with varying mutational subtypes as well as non-malignant human colon epithelial cells (HCEC) to derive IC₅₀ values as an indicator of sensitivity. In contrast to its mother compound α -lipoic acid, only minor differences regarding sensitivity could be detected for devimistat depending on the molecular subtype and p53 status as IC₅₀ values varied between 164 μ M and 211 μ M. Non-malignant HCEC cells showed the lowest sensitivity with an IC₅₀ value of 286 μ M, indicating a cancer cell specific mode of action. In the next step, cytotoxicity of devimistat in murine primary organoids and tumor organoids was compared to further investigate a potential cancer cell specificity in a 3D cell culture model. At the highest tested concentration of 300 μ M, a dose dependent decrease of tumor organoid viability to 20% of the control and an increase of dead cells were observed, as shown by MTS cell viability assay and Hoechst 33342/PI costaining. No decrease of cell viability or induction of cytotoxicity occurred in non-malignant intestinal primary organoids, as the viability remained above 90% at 300 μ M and the proportion of PI-positive cells remained unchanged.

Since devimistat inhibits the TCA cycle enzymes PDH and KGDH, mitochondrial integrity, metabolic capacity and induction of ROS were investigated in HCT116 and HT29 cells. Applying a Seahorse™ XF metabolic analyzer, the OCR was quantified and a significant inhibition of the basal, ATP-coupled and maximal respiration rate was observed in response to devimistat concentrations of 150 μ M and 200 μ M. In parallel, vital mitochondria were stained using MitoTracker® Orange and a reduced signal and altered morphology were observed by confocal microscopy after treatment with 200 μ M devimistat. Additionally, 2',7'-Dichlorofluorescein diacetate (H₂DCFDA) staining and subsequent analysis by flow cytometry revealed significant induction of ROS after treatment with 150 μ M and 300 μ M devimistat for 2 h in HCT116 cells.

γ H2AX was quantified by In Cell western analysis to identify whether devimistat treatment results in the formation of DNA damage. Additionally, the alkaline Comet assay was applied to assess DNA strand breaks. Neither an induction of γ H2AX nor an

increase in tail moment could be identified at concentrations of up to 250 μM . Subsequently, the formamidopyrimidine DNA glycosylase (Fpg)-modified alkaline Comet assay was utilized to assess whether the devimistat-dependent formation of ROS results in oxidative DNA lesions. The addition of Fpg led to a moderate but not significant induction of tail moment at a devimistat concentration of 200 μM , indicating a non-genotoxic mechanism of action for the metabolic inhibitor.

In the next step, the activity of devimistat in combination with established chemotherapeutic drugs IT and 5-FU was investigated by performing Chou-Talalay analysis and subsequent Combenefit modelling of ATP-based cytotoxicity data after mono- and cotreatment of HCT116 and HT29 cells. Synergistic cancer cell killing by devimistat with IT and 5-FU was detected in both cell lines and 200 μM devimistat in combination with 10 μM 5-FU or 20 μM IT were identified as the most active. Subsequently, the underlying mechanisms of the observed synergism were further investigated by applying qPCR analysis of a panel of cell death markers as well as western blot analysis. An increased cell death induction due to downregulation of anti-apoptotic proteins and accumulation of the proapoptotic protein Bim were identified as a key actor for the synergy. As further demonstrated by siRNA-mediated genetic knockdown experiments, the additional cytotoxicity induced by devimistat cotreatment diminished in the absence of Bim.

Finally, devimistat (25 mg/kg BW) was applied in combination with IT (40 mg/kg BW) in a xenograft mouse model, using human HCT116 and HT29 cells. Compared to IT-monotreatment, cotreatment with devimistat led to a significantly prolonged survival and reduced tumor growth, demonstrating an increased therapeutic efficacy. In agreement with the *in vitro* results, a significant induction of Bim protein levels and a prevention of IT-induced p53 accumulation were detected in xenograft tumor lysates of the cotreatment groups.

In summary, the mitochondrial metabolism was identified as a crucial target of devimistat in CRC cells, resulting in cancer specific cell death induction independent of genetic or epigenetic alterations. Our study demonstrated *in vitro* and *in vivo* synergy of devimistat with established antineoplastic drugs dependent on the pro-apoptotic protein Bim, rendering it a potential candidate for future CRC treatment regimen.

4.2. Publication II: Natural Merosesquiterpenes Activate the DNA Damage Response via DNA Strand Break Formation and Trigger Apoptotic Cell Death in p53-Wild-Type and Mutant Colorectal Cancer

In publication II, the antitumor activity of a panel of 11 merosesquiterpenes isolated from marine sponges was investigated in the three CRC cell lines HCT116, RKO and HT29 to evaluate their potential applicability as novel anticancer agents. Three compounds with pronounced cytotoxic activity were identified, namely ilimaquinone (IQ) smenospongine (SM) and dactylospontriol (DS), with IC₅₀ values of 27 μM, 8 μM and 19 μM in HCT116 cells. SP and IQ in concentrations of 25 μM and 50 μM, respectively, led to DNA strand break formation, detected by the alkaline Comet assay and IF-microscopy after γH2AX staining. In accordance, upregulation of the DDR was observed, including phosphorylation of the checkpoint kinase Chk1, accumulation of p21 in HT29 cells and additional accumulation of p53 in HCT116 cells. As measured by using flow cytometry and the fluorescence probe H₂DCFDA after 24 h, SP and IQ led to a 2-fold and 4-fold induction of ROS, respectively.

Subsequently, cell cycle progression was analyzed and a pronounced induction of the sub-G₁ population was detected after treatment with DS and SP for 48 h, indicative of apoptotic cell death. Necrotic and apoptotic induction of cell death were observed by Annexin-V/PI staining and flow cytometry in HT29 and HCT116 cells after treatment with IQ and SP, comparable to the effects of the positive control 5-FU. In parallel, western blot analysis revealed upregulation of proapoptotic Bim, cleaved caspase-3 and cleaved caspase-9 as markers of the mitochondrial apoptosis pathway. By applying HCT116 p53^{-/-} cells, it could be shown that this pathway was attenuated but remained active in the absence of p53. Interestingly, total cell death rate analyzed by Annexin-V/PI staining was comparable in both HCT116 WT and p53^{-/-} cells. Additionally, qPCR analysis was performed to assess the expression of proteins involved in the intrinsic and extrinsic apoptosis pathway and detected accumulation of p21 in HCT116 p53^{-/-} cells. Finally, the cytotoxicity of SP and IQ was assessed in murine tumor organoids and a significant reduction of cell viability to below 40% of the control as well as pronounced induction of PI uptake were detected in response to merosesquiterpene treatment.

Our study revealed p53-dependent and -independent induction of apoptotic and necrotic cell death in CRC cells and murine CRC tumor organoids via induction of ROS and DNA damage. Additional research will be necessary to further elucidate the underlying mechanism of DNA damage induction and confirm the relevance of these findings *in vivo*.

4.3. Publication III: Targeting PARP-1 and DNA Damage Response Defects in Colorectal Cancer Chemotherapy with Established and Novel PARP Inhibitors

Publication III focused on the role of DNA repair enzyme PARP-1 in colorectal cancer as a target for chemotherapeutic intervention by applying novel PARP-1 inhibitors. First, a library of novel 3,4-bifunctionalized and -bridged indole compounds was screened regarding the ability to inhibit PARP-1 *in silico*. The compounds with the highest calculated binding affinities were applied in an *in vitro* assay kit to quantify the potential to inhibit recombinant PARP-1 in a cell free system by deriving IC₅₀ values for enzymatic inhibition. The four compounds with the highest activity, referred to as X17613, X17618, X17620 and X17621, showed IC₅₀ values ranging between 41 nM and 2.84 μM.

Subsequently, these compounds were applied in a CRC cell based *in vitro* assay to measure inhibition of H₂O₂-induced PAR generation by applying confocal immunofluorescence microscopy. Since a marked inhibition of PARylation due to treatment with X17613 and X17618 could be detected in HCT116 cells in concentrations of 0.1 μM and higher, the cytotoxicity was assessed in a monotreatment setup and in combination with established CRC chemotherapeutics IT, 5-FU and OXA. To this end, HCT116 PARP-1^{+/+} and HCT116 PARP-1^{-/-} cells were applied to assess the role of PARP-1 for PARPi cytotoxicity. Additionally, the MSS cell line Caco-2 was used and the sensitivities of HCT116 BRCA2^{-/-} with HCT116 WT cells as well as DLD-1 ATR^{s/s} with DLD-1 WT cells as models for HR deficiency were compared. In parallel, the cytotoxicity of the established PARP-1 inhibitors olaparib and veliparib was identified in all mentioned cell models.

Among the cell lines tested, cytotoxicity of X17613 and X17618 as monotreatment was detected in the highest concentration of 50 μM in HCT116 BRCA2^{-/-} cells, with a reduction of cell viability to around 75% of the control. In comparison, olaparib caused a dose dependent decrease of cell viability in all tested cell lines with IC₅₀ values varying between 0.5 μM and 11.2 μM. Olaparib showed higher cytotoxicity in HCT116 PARP-1^{+/+} cells compared to HCT116 PARP-1^{-/-} cells, indicating the significance of PARP trapping, while no such difference could be detected for veliparib. HCT116 BRCA2^{-/-} cells showed a considerably higher sensitivity to both olaparib and veliparib monotreatment compared to HCT116 WT cells, with viability values below 30% of the control at the highest concentration of 50 μM. The same could be observed for DLD-1 ATR^{s/s} cells compared to DLD-1 WT cells, albeit to a lesser extent. Subsequently, the combination treatment with IT, 5-FU and OXA was investigated to identify potential synergism with PARP inhibitors. A significant decrease was only observed after cotreatment with 50 μM

X17613 and 0.25 μ M IT in HCT116 BRCA2^{-/-} cells, with a reduction from 90% to approximately 60% viability. In the next step, the role of DNA damage induction for the activity of X17613 and X17618 was investigated and therefore γ H2AX was quantified by western blot analysis in HCT116 BRCA2^{-/-} and HCT116 WT cells but no further increase of IT-induced γ H2AX levels due to X17613 or X17618 cotreatment was measured. To clarify the role of PARP trapping, chromatin isolation after treatment with the alkylating agent methyl methane sulfonate (MMS) and cotreatment with X17613, X17618 or olaparib was performed. Pronounced trapping of PARP-1 with a 2.5-fold induction of chromatin-bound PARP-1 was detected due to olaparib treatment but not due to treatment with X17613 and X17618.

In summary, the novel compound X17613 was identified as a potent inhibitor of PARP-1 that does not induce PARP trapping. An increased cytotoxicity of IT in combination with X17613 was detected in HCT116 BRCA2^{-/-} cells, rendering it a potential lead structure for the development of future PARP inhibitors. Our results indicate that novel PARPi without PARP trapping potential could be applied in combination with TOP1 inhibitors for the treatment of HR-deficient CRC tumors.

5. Summarizing Discussion

Despite ongoing advances in the development of new therapeutic approaches, the 5-year survival rate for metastatic CRC is still low. As detailed in Chapter 1.1.2., the current therapeutic array of pharmacological approaches is primarily comprised of genotoxic agents, growth factor inhibitors and biologicals. This work aimed to assess three different novel approaches for the treatment of CRC with a focus on the pharmacological mechanisms, the impact of molecular CRC subtypes and the combination with established chemotherapy.

First, the therapeutic potential of devimistat was analyzed, a first-in-class drug that targets the TCA cycle, thereby inducing metabolic inhibition and selective cell death of cancer cells. The role of the mitochondria as a target of devimistat, the mechanism of cytotoxicity and the selectivity for malignant cells were elucidated. The synergism with established CRC therapeutics was investigated with a focus on proapoptotic protein Bim *in vitro* and *in vivo*. Second, the potential of merosesquiterpenes was investigated, a group of bioactive chemical compounds found in marine sponges that revealed to be cytotoxic in several cancer cell lines. Our study aimed to evaluate the applicability of selected compounds as cytostatic agents to provide new options in future chemotherapy. The cytotoxicity of a panel of 11 merosesquiterpenes was analyzed, considering the impact of different molecular subtypes with a focus on the tumor suppressor p53. Furthermore, the underlying mechanism of cell death induction was investigated, emphasizing the role of DNA damage induction. Third, the inhibition of PARP was examined as an approach which is already applied in the treatment of several tumor entities and of potential benefit in the chemotherapy of CRC. An *in silico* and *in vitro* screening of 12 novel chemical structures was conducted to identify candidates for the development of new PARP inhibitors. The impact of DNA repair deficiencies in CRC cells on the activity of PARPi applied as monotreatment or in combination with established cytostatic drugs was assessed.

5.1. Publication I: The Mitochondrial Disruptor Devimistat (CPI-613) Synergizes with Genotoxic Anticancer Drugs in Colorectal Cancer Therapy in a Bim-Dependent Manner

The prognosis of advanced and metastatic CRC is still grim, despite the application of subtype-specific treatment regimen that combine genotoxic and cytostatic agents as well as targeted therapy based on monoclonal antibodies and small molecule inhibitors. Driven by a better understanding of the underlying biological pathways and molecular

mechanisms, the altered metabolism of tumor cells has emerged as a potential target in various cancer entities. Devimistat, a non-redox active derivative of α -lipoic acid, which is thoroughly discussed in Chapter 1.2.4., represents a clinically applied metabolic inhibitor in cancer treatment and currently has approval by the FDA as an orphan drug for the therapy of peripheral T cell lymphoma, soft tissue clear cell sarcoma and biliary tract cancer.

Our first study focused on the potential of devimistat in the treatment of CRC, either as a standalone drug or in combination with established chemotherapy. Devimistat targets the altered metabolism of CRC cells by inhibition of the mitochondrial enzymes PDH and KGDH. Our study addressed several features of devimistat, which could indicate a potential benefit of its application in CRC chemotherapy: I) The mechanism of action with a focus on the mitochondria as a cellular target. II) The selectivity for malignant cells and the role of molecular alterations in cancer cells for devimistat sensitivity. III) The mechanism of cell death induction and the potential to induce DNA damage. IV) The synergy of devimistat with genotoxic chemotherapeutic drugs IT and 5-FU *in vitro* and *in vivo*. In the following chapter, these aspects are detailed and discussed in the context of existing literature.

5.1.1. Devimistat targets the mitochondria of CRC cells

Being a non-redox active derivative of the cofactor α -lipoic acid, devimistat impairs the mitochondrial function of cancer cells, as investigated by several publications (Stuart et al., 2014; Zachar et al., 2011). Applying the SeaHorse™ XF analyzer and using a MitoStress Test Kit, our study demonstrated that devimistat dose-dependently impairs basal, ATP-dependent and maximal mitochondrial respiration capacity in CRC cells (Arnold et al., 2022). While a concentration of 100 μ M had no effect compared to the control, 150 μ M and 250 μ M led to a significant reduction of all three parameters after treatment for a duration of 24 h. In accordance, MitoTracker™ staining revealed reduction of intact mitochondria and structural alterations at a concentration of 200 μ M for 24 h. These observations were preceded by reduced MMP (300 μ M) and increased levels of ROS (150 μ M), observed after short term treatment for 1 h and 2 h, respectively.

The results are in accordance with published observations. Inhibition of KGDH by devimistat was found to result in a ROS-burst dependent on the enzymatic E3-subunit in H460 lung cancer cells after prolonged incubation for 16 h (Stuart et al., 2014). Applying transmission electron microscopy, morphological alterations of mitochondria and a reduction of cristae junctions were observed, following a devimistat treatment for 45 min at 200 μ M in pancreatic cancer cells (Gao et al., 2020). Prolonged treatment for 7 days

resulted in an attenuation of the MMP, whereas the total number of mitochondria remained unchanged in porcine fibroblasts (Mordhorst et al., 2019). Pardee et al. revealed a decrease of the mitochondrial OCR as an indicator of TCA cycle impairment in response to devimistat treatment in leukemia cells (Pardee et al., 2018b). In response to devimistat-induced TCA cycle inhibition, concentration of intermediates malate, fumarate, succinate and citrate diminished while anaplerotic inputs alanine, aspartate and glutamine accumulated (Stuart et al., 2014). Our results confirmed the devimistat-dependent induction of ROS and mitochondrial dysfunction for CRC cells and detailed for the first time impairment of basal, ATP-dependent and maximal mitochondrial respiration capacity (Arnold et al., 2022). In summary, devimistat targets the altered tumor metabolism as an important factor of malignancy in CRC.

5.1.2. Devimistat induces selective cell death in CRC cells and organoids

Devimistat led to the induction of cell death in a set of various established and patient-derived CRC cell lines. As oncogenes and tumor suppressors regulate several aspects of the tumor cell metabolism, different tumor cells rely on glycolysis, OXPHOS or glutaminolysis to varying degrees, which might therefore affect sensitivity to devimistat. The applied cell lines covered a diverse set of mutational subtypes regarding their p53, MSI, BRAF and KRAS status. Cytotoxicity of devimistat was not influenced by the p53 status, as revealed by isogenic p53-wild type and -deficient HCT116 cells. Mutations of the p53 pathway are common in colorectal tumors, resulting in resistance towards frequently applied anticancer drugs (Stiewe and Haran, 2018). In addition, activity of wild type p53 prevents metabolic alterations in CRC by downregulation of aerobic glycolysis and maintaining OXPHOS, as described in Chapter 1.2., which constitutes an integral aspect of its tumor-suppressor function (Li et al., 2012).

In contrast to 5-FU and IT, devimistat induced cell death in proliferating and non-proliferating cells, indicating a cell cycle independent mode of action. In accordance, several studies described that cell cycle phase, mutations of tumor suppressors (p53) and oncogenes (KRAS) did not affect cytotoxicity of devimistat (Pardee et al., 2018b; Zachar et al., 2011). In contrast to its mother compound LA and despite the described molecular diversity, the cytotoxicity of devimistat was uniform across the tested tumor cell line panel with an average IC₅₀ value of 175 µM. Accordingly, cytotoxicity screening by Zachar et al. in a diverse set of cell lines originating from multiple malignancies identified IC₅₀ values between 100 µM and 250 µM, while in another study by Gao et al. median IC₅₀ value calculated in pancreatic cancer cell lines was 200 µM (Zachar et al., 2011).

A cancer cell specific activity of devimistat was revealed by comparing cytotoxicity in non-malignant HCEC cells and several colorectal cancer cell lines. Furthermore, primary murine intestinal organoids were applied for cytotoxicity assessment in comparison to murine tumor organoids and no decline in cell viability was observed, even at high devimistat concentrations of 300 μ M, adding further proof to a tumor selective activity. While our study as well as preceding research articles identified selectivity in 2D cell line models, 3D cultured intestinal organoids can provide a closer representation of the *in vivo* situation. A comprehensive study by Grabinger and colleagues identified a 10-30 times higher sensitivity of murine intestinal organoids to 5-FU compared to the cell lines Caco-2 and MC38 as surrogates for non-malignant intestinal epithelium, thereby showing a higher correlation to the *in vivo* effects observed in mice (Grabinger et al., 2014).

Noteworthy, the protocol applied for crypt organoid isolation and cultivation resembles the one used in our study. Transcriptome analysis of *ex vivo* cultured intestinal primary organoids in comparison to *in vivo* intestinal tissue revealed changes in the expression of genes related to immune response and lipid metabolism, associated with the lack of cell-extrinsic immune communication and *in vitro* culturing conditions. Nevertheless, general intrinsic transcriptional programs, including compartment-related features are well preserved *ex vivo*, indicating applicability for our purpose (Lu et al., 2021). Furthermore, the application of patient-derived organoids could help to elucidate the significance of specific genetic and epigenetic alterations for the therapeutic efficacy of devimistat.

A tumor specific activity of devimistat has been described in preceding publications, but not much is known about the underlying mechanisms. Stuart et al. identified a redox-dependent autoregulation process of KGDH in cancer cell lines, which is disturbed by a devimistat-induced ROS burst (Stuart et al., 2014). In tumor cells, redox blockage at the dihydrolipoyl S-succinyltransferase (E2) subunit of KGDH and glutathionylation at lipoate residues result in down-modulation of KGDH activity by devimistat, while no such effect was observed in non-malignant cells (Stuart et al., 2014). In addition, devimistat targets carbon entry into the TCA cycle by activating the enzyme PDK, which downregulates PDH activity by lipoate-responsive phosphorylation of its E1 α subunit as further detailed in Chapter 1.2.4.1. Isoforms PDK1 and PDK3 are upregulated in tumors due to activation of the HIF1 α pathway (Lu et al., 2008; McFate et al., 2008), resulting in an altered response of PDH towards devimistat in tumor cells (Zachar et al., 2011). Methylation-dependent induction of PDK4 has been observed in CRC and inhibition led to downregulation of cell migration and invasion as well as induction of apoptosis (Leclerc et al., 2017).

In addition to specific alterations described for the enzymes PDH and KGDH, which render cancer cells sensitive towards devimistat treatment, general alterations of the tumor metabolism also contribute to the effects of mitochondrial disruption. Nevertheless, further research regarding the metabolic foundation is necessary to fully understand the underlying molecular mechanisms. *In vitro* metabolome analysis of malignant and non-malignant cells could be a promising tool to elucidate quantitative changes of the complex metabolic networks in response to devimistat treatment.

5.1.3. Synergism of devimistat with genotoxic chemotherapeutics

Combination treatment is frequently conducted in CRC therapy and typically involves genotoxic and cytostatic drugs as well as specific growth factor receptor inhibitors (Morris et al., 2023). Benefits include enhanced therapeutic efficacy and reduced side effects, often achieved by the possibility to reduce the necessary single drug doses. In addition, the combination of different drugs covers the heterogeneity of tumor cell types, circumvents the development of resistances and impairs metastasis formation (Giantonio et al., 2007; Vogel et al., 2017).

Based on the distinct mode of action of the metabolic inhibitor devimistat in comparison to established cytostatic drugs IT and 5-FU, their potential to induce synergistic cytotoxicity was further investigated in cancer cell lines. Chou-Talalay analysis and Combeneft analysis were performed based on cytotoxicity data as an approach to quantify the synergism of devimistat with 5-FU and IT in HCT116 and HT29 cells and identify dose combinations with the highest cytotoxic efficacy.

An enhanced induction of apoptotic cell death was identified as the underlying mechanism and further detailed by qPCR and western blot analysis of the corresponding pathways: Devimistat cotreatment resulted in downregulation of the antiapoptotic proteins Bcl_{XL} and survivin. Upregulation of survivin has been identified during colorectal carcinogenesis and increased with worsening tumor grade (Hernandez et al., 2011). Survivin was shown to antagonize the cytotoxic activity of IT in CRC cells, underlining its biological significance in chemotherapy-induced cell death and application of novel small molecule inhibitors targeting survivin was shown to sensitize p53-mutant CRC to IT (Rauch et al., 2018; Steigerwald et al., 2018). Contrasting the antiapoptotic proteins Bcl-2 and Mcl, Bcl_{XL} expression was directly linked to the chemotherapy outcome in CRC patients and revealed to be crucial as an oncogenic driver in the adenoma-to-carcinoma sequence (Ramesh et al., 2021; Scherr et al., 2016).

As described in our study, devimistat synergized with chemotherapeutic drugs IT and 5-FU in a Bim-dependent manner, resulting in a decrease of tumor cell viability and tumor

growth rate *in vitro* and *in vivo*. Interestingly, no increase of Bim gene expression was observed but instead a strong accumulation of Bim protein could be detected, which indicates the involvement of a post-translational mechanism. Jun-kinase (JNK) has been described to prevent Bim degradation, resulting in accumulation of Bim and subsequent Bax-dependent apoptosis (Lei and Davis, 2003). In response to cellular stressors, JNK phosphorylates the dynein light chain 1 (DLC) binding motif of the Bim_L and Bim_{EL} isoforms, inducing sequestration of their latent forms from dynein motor complexes (Lei and Davis, 2003). Brockmann et al. observed JNK-mediated Bim phosphorylation and subsequent stabilization after treatment with thiazolomides in CRC cell lines, which resulted in sensitization to chemotherapeutic drug cisplatin (Brockmann et al., 2015). Since Bim protein levels were analyzed by western blot analysis of whole cell lysates in our study, it is debatable if a release of Bim from cytoskeleton-associated dynein complexes would result in an increase of detectable Bim protein levels.

Proteasomal degradation of Bim_{EL} induced by ERK1/2-dependent phosphorylation is another possible pathway that alters Bim protein levels independent of gene transcription (Ley et al., 2003) and the significance of ERK1/2-mediated phosphorylation of Ser-55/65/73 for Bim degradation has been elucidated *in vivo* (Hübner et al., 2008). The downregulation of Bim levels due to hyperactivated ERK1/2 signaling was shown to be associated with a phenomenon termed oncogene addiction in lung cancer. Application of ERK1/2 inhibitors resulted in increased cell death, underlining the role of Bim as a mediator between survival signaling networks and the mitochondrion-dependent apoptotic program (Bean et al., 2013). In a subset of CRC cells, the overexpression of COX2 induced elevated levels of PGE₂, which led to activation of the RAF-MEK-ERK1/2 pathway, promoting Bim phosphorylation and thereby its proteasomal degradation to avoid apoptosis (Greenhough et al., 2010). In accordance, for *BRAF*-V600E-mutated CRC cell lines, addiction to ERK1/2 signaling was described to repress Bim-dependent apoptosis and growth factor independent survival (Wickenden et al., 2008). Mutations of *BRAF*-V600E, as an early event in the serrated pathway of tumorigenesis, can be found in 15% of sporadic CRC tumors and are frequently associated with the CpG island methylator phenotype and microsatellite instability (Bond and Whitehall, 2018). As accumulation of Bim was identified as a critical step in the antitumor activity of devimistat in our study, additional research regarding the role of ERK1/2 and JNK could further elucidate the mechanism of cell death induction.

In a recent study Sun and colleagues observed that regorafenib, a multi-kinase inhibitor that is frequently applied in the third-line therapy of CRC, induces intrinsic apoptosis via Bim. Mechanistically, following regorafenib treatment, expression of PI3K is downregulated, leading to AKT-dephosphorylation and translocation of FOXO3a from

the nucleus to the cytosol, which results in upregulated Bim expression and thus mitochondrial apoptosis (Sun et al., 2023). A similar mechanism of AKT inhibition, leading to nuclear translocation of FOXO3a and thereby induction of Bim and subsequent cell death has also been described for CRC cells after treatment with selenite (Luo et al., 2013) and for hepatocellular carcinoma after treatment with idelalisib (Yue and Sun, 2018). Analysis of the clinical prognostic impact of Bim, Puma (p53 upregulated modulator of apoptosis) and Noxa expression in human CRC patients revealed that Bim expression was significantly associated with a higher overall survival and longer disease-free survival adjusted for tumor stage, histologic grade, age, and treatment, underlining its function as a tumor suppressor (Sinicrope et al., 2008). These observations underline the significance of our findings regarding the role of Bim for the synergy of devimistat and IT.

In addition to the accumulation of Bim, metabolic inhibition by devimistat is also likely to directly interfere with DDR induced by IT treatment. Several studies have shown an upregulation of oxidative metabolism as a result of DNA damage to provide energy for DDR pathways (Sobanski et al., 2021). In parallel, the DDR kinase ATM was found to activate the PPP by inducing glucose-6-phosphate dehydrogenase (G6PD) via phosphorylation of HSP (heat shock protein) 27 in the presence of DSBs, thereby stimulating production of NADPH to fuel DNA repair (Cosentino et al., 2011). In breast cancer cells, upregulation of MYC and MCL1 was observed as a mechanism of chemotherapy resistance that promoted mitochondrial OXPHOS and enrichment of CSCs, mediated by transcription factor HIF1 α (Lee et al., 2017). By interfering with cellular metabolic pathways due to a dual inhibition of PDH and KGDH, devimistat might impair energy dependent DNA repair pathways, resulting in an increase of cell death. Interestingly, no upregulation of p53 was observed due to combined treatment with devimistat and IT, but instead a pronounced downregulation occurred.

A potential mechanism could be an intracellular accumulation of α KG, which has been shown to inhibit DNA repair pathways and resolution of DNA double-strand breaks (DSBs) due to an epigenetic mechanism (Efimova et al., 2016). Marx and colleagues recently described a pronounced upregulation of the metabolism in CRC cells induced by IT treatment, characterized by enhanced glycolysis, oxygen consumption rate (OCR) and mitochondrial electron transport chain activation (Marx et al., 2022). Interestingly, these effects were more pronounced in p53 WT cells. However, no differences in the sensitivity of p53-proficient and -deficient HCT116 cells regarding IT treatment could be detected in combination with devimistat (Arnold et al., 2022), underlining that the relevance of p53 for the activity of devimistat is yet to be understood.

Cotreatment of CRC cells with devimistat in combination with IT or 5-FU resulted in a pronounced downregulation of the expression of several cyclins, including cyclin B1, cyclin H1 and cyclin D1/2, suggesting an impaired cell cycle progression. While progression from the G₁ to S-phase is regulated by cyclin D1 and D2, cyclin B1 enables the G₂/M transition and cyclin H1 is part of the CDK-activating kinase which promotes cell cycle progression by CDK4 and CDK6 activation (Roskoski, 2019b; Sava et al., 2020). These observations indicate impairment of cell cycle progression, induced by additional treatment with devimistat, providing an additional antiproliferative effect beyond cell death induction. In accordance with our findings, Lee et al. observed downregulated expression of multiple cell cycle regulating genes when investigating the effects of devimistat in pancreatic cancer cells, including *CCNB1*, *CCND3* and *CCNE1* (Lee et al., 2014).

As an approach to verify our results *in vivo*, a mouse xenograft model utilizing MSI (HCT116) and MSS (HT29) CRC cell lines was applied to assess the efficacy of devimistat as monotreatment and in combination with IT. A pronounced antitumor activity of devimistat monotreatment was observed, indicated by prolonged survival and reduced tumor growth rate as well as additional improvement in the combination treatment groups of both CRC xenografts. These findings confirm the results of several studies that applied mouse xenograft models of lung, ovarian and pancreatic cancer to assess antitumorigenic activity of devimistat in a preclinical setting at a comparable dose level of 25 mg/kg BW (Bellio et al., 2019; Lee et al., 2014; Zachar et al., 2011).

Remarkably, our study is the first to reveal synergistic activity of devimistat with an established chemotherapeutic drug *in vivo*, despite ongoing efforts to integrate devimistat as a building block in the chemotherapy of solid tumors in various clinical trials (Rocha Lima et al., 2019; Philip et al., 2019). In accordance with our *in vitro* findings, a pronounced upregulation of Bim protein level in response to devimistat treatment and a significant increase after cotreatment with IT in xenograft tumor lysates were observed. These findings underline the *in vivo* relevance of the proapoptotic protein Bim for the antitumorigenic activity of devimistat. Interestingly, Park et al. observed enhanced activation of Bim in tumor lysates of murine xenograft models after treatment with the DNA damage inducing drug doxorubicin in combination with the antimitochondrial agent gamitrinib, mediated through activation of JNK (H.-K. Park et al., 2014). Since the two drugs mechanistically resemble the agents used in our study, a comparable mode of action might be responsible for the synergistic activity. Despite a higher antitumorigenic activity, no increase of toxicity of the combined treatment regimen *in vivo* was observed. This indicates that the combination of IT and devimistat did not result in unexpected adversities or aggravated adverse side effects occurring in the single treatment

regimens. Correspondingly, it has been reported that the combination of antitumorigenic drugs covering disparate cellular targets can provide increased therapeutic efficacy without risking additional adverse effects (Al-Lazikani et al., 2012).

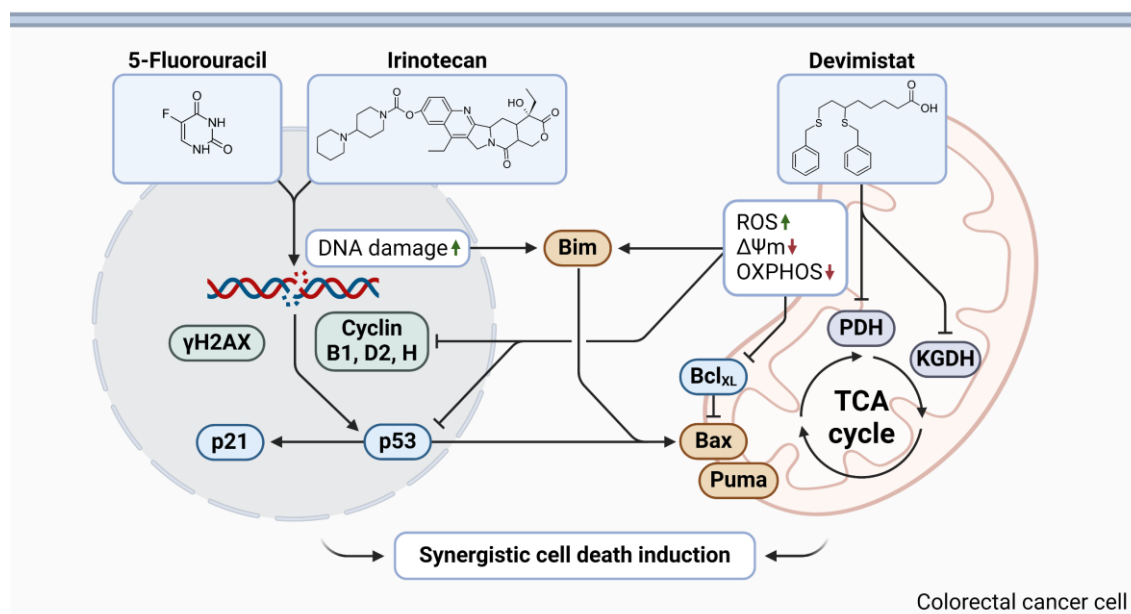


Figure 11: Mechanistic overview summarizing the synergism of devimistat with anticancer drugs IT and 5-FU in colorectal cancer cells. Devimistat induces inhibition of the mitochondrial enzymes PDH and KGDH, thereby promoting ROS formation and subsequently attenuating oxidative phosphorylation and mitochondrial membrane potential ($\Delta\Psi_m$). The DNA damage triggered by IT and 5-FU causes accumulation of p53, p21-dependent cell cycle arrest and apoptotic cell death. In addition, expression of proapoptotic BH3-only proteins Bax and Puma as well as of the antiapoptotic Bcl-2 protein Bcl_{XL} is induced. Synergistic cell death is caused by combined treatment with accumulation of Bim as a key factor, as demonstrated by genetic knockdown. Furthermore, reduced expression of antiapoptotic proteins (Bcl_{XL} and survivin) as well as cell cycle regulators (cyclin B1, D2 and H) was observed. (Created with BioRender)

Our studies elucidated the potential benefit of devimistat in combination with established chemotherapeutic drugs IT and 5-FU in CRC therapy while at the same time shedding light on possible limitations and resistance mechanisms. Devimistat induced synergistic activity in combination with the DNA damage inducing drugs IT and 5-FU in a Bim-dependent manner. Although this mechanism could increase the clinical efficacy of CRC chemotherapy, additional studies are necessary to exclude the possibility that non-malignant cells are also harmed, leading to a higher incidence of adverse side effects. While devimistat itself already exerts a dual mechanism of action by inhibiting PDH and KGDH, two important enzymes of the TCA cycle, application of additional metabolic inhibitors is discussed to further restrict energy and nutrient supply of tumors (Bingham and Zachar, 2023).

Four general pharmacological aspects of devimistat were identified to evaluate its potential as a building block in CRC chemotherapy: I) Devimistat targets mitochondria and impairs mitochondrial function II) Devimistat induces cell death irrespective of the mutational subtype with a higher activity in malignant cells compared to non-malignant cells. III) Devimistat induces apoptotic and necrotic cell death without exerting genotoxic activity IV) Devimistat synergizes with genotoxic chemotherapeutics 5-FU and IT *in vitro* and *in vivo*. In essence, our findings confirmed mitochondrial disruption as a main mechanism of action for devimistat in CRC that results in cancer cell specific cell death induction, independent of the molecular subtype. Detailed insight into the mitochondrial apoptosis pathway as the underlying mechanism of cell death induction was provided and the pro-apoptotic protein Bim was identified as a key actor for the synergy of devimistat with IT and 5-FU *in vitro* and *in vivo*.

5.2. Publication II: Natural Merosesquiterpenes Activate the DNA Damage Response via DNA Strand Break Formation and Trigger Apoptotic Cell Death in p53-Wild-Type and Mutant Colorectal Cancer

While various targeted therapy approaches have been successfully applied for CRC therapy in recent years, including monoclonal antibodies and small molecule inhibitors, genotoxic cytostatic drugs still represent the foundation of most treatment regimens. Merosesquiterpenes are secondary metabolites produced by marine sponges that exhibit a variety of bioactive properties, as detailed in Chapter 1.1.3. In a variety of cancer cell lines, cytotoxic and antiproliferative effects have been reported in response to different merosesquiterpenes, indicating therapeutic potential. With the objective to identify novel substances with cytostatic antitumor activity, the cytotoxicity of 11 different merosesquiterpenes isolated from marine sponges was compared in three CRC cell lines (Jiso et al., 2021a).

5.2.1. Cell death induction by merosesquiterpenes in CRC cells

Among the 11 tested merosesquiterpenes, SP, IQ and DS revealed to be the most promising compounds, indicated by IC_{50} values in the low μ M range among the three tested cell lines. Comparing the activity of the tested compounds, structural determinants of cytotoxicity could be identified: Among the 20-amino and *N*-alkyl rearranged drimane sesquiterpenes, an unsubstituted amino-group (SP) was correlated with a high cytotoxicity, while substitutions with alkyls or aromatic side chains reduced activity. Correspondingly, the 20-methoxy rearranged drimane sesquiterpene IQ showed a higher cytotoxicity than its oxohexyl-substituted derivative quinquinaquinone.

Our study revealed a pronounced induction of apoptotic and necrotic cell death by merosesquiterpenes IQ and SP in CRC cell lines and murine tumor organoids. Formation of DNA strand breaks, as shown by the alkaline Comet assay and γ H2AX formation, led to activation of the DDR, with phosphorylation of Chk1 and accumulation of p53. In summary, these direct genotoxicity markers and the distinct cellular response illustrate that merosesquiterpenes induce DNA damage *in vitro*. A potential mechanism involved in the genotoxicity and cytotoxicity of merosesquiterpenes is the generation of ROS due to redox cycling mediated by their hydroquinone structure. In support of this hypothesis, induction of mitochondrial ROS by IQ was observed in lung cancer cells (Kwak et al., 2020) and a general increase of cellular ROS has been detected in colon cancer cells (Do et al., 2014). In human oral squamous carcinoma cells, IQ-dependent induction of ROS was partially rescued by pretreatment with antioxidants *N*-acetylcysteine (NAC) and GSH (Lin et al., 2020).

The enzyme NAD(P)H-quinone oxidoreductase 1 (NQO1), which catalyzes the detoxification of quinones to hydroquinones, might further facilitate ROS production by merosesquiterpenes. Generation of reactive hydroquinones, which undergo redox cycling, can lead to generation of electrophilic species and production of ROS. Accordingly, inhibition of NQO1 in prostate cancer cells abrogated the cytotoxic effects of IQ (Jiso et al., 2021b). Interestingly, overexpression of NQO1 has been observed in various types of cancer including CRC and is exploited using chemotherapeutic drugs that are metabolically activated by the enzyme, including mitomycin C (Oh and Park, 2015). In accordance, mitomycin C, a chemotherapeutic agent with a heterocyclic quinone structure showed increased antitumor activity in an *in vivo* model of colon cancer after dietary induction of NQO1 (Begleiter et al., 2004). Since no data about the activity of merosesquiterpenes in non-malignant cells is available, these observations can provide indication of a tumor specific cytotoxicity of IQ and SP. Additional research using human colon epithelial cells (HCEC) and murine primary organoids as a surrogate for healthy tissue could identify a potential specificity of merosesquiterpenes for malignant cells. Induction of DNA damage and activation of the DDR by merosesquiterpenes IQ and SP occurred in low concentrations that did not increase H₂DCFDA signal, suggesting a mechanism beyond ROS production. Possible hypotheses might be an interaction with enzymes involved in the repair or maintenance of the DNA as well as direct interaction with DNA. Cleavage of plasmid-DNA by the active hydroquinone species of IQ has recently been demonstrated *in vitro*, indicating the involvement of a direct mechanism (Jiso et al., 2021b). In accordance, open chain merosesquiterpene 3-farnesyl-2-hydroxy-5-methoxyquinone showed no cytotoxic activity despite exhibiting a hydroquinone structure capable of redox cycling.

While low concentrations of merosquiterpenes SP and DS induced significant G₂/M arrest after treatment for 48 h in HCT116 and HT29 cells, high concentrations led to a pronounced increase of the sub G₁ population. Correspondingly, western blot analysis revealed phosphorylation of the kinase Chk1, a key regulator of the S-phase, the G₂/M-transition and part of the DDR (Li et al., 2012; Zhang and Hunter, 2014). Single stranded DNA recruits replication protein A (RPA), which together with ATRIP and TOPBP1 subsequently activates ATR and Chk1 to inhibit progression of the cell cycle, allowing for DNA repair or induction of apoptosis (Gupta et al., 2022).

In parallel, upregulation of p21, a CDK inhibitor that prevents G₁/S and G₂/M transition, was observed, thereby inducing cell cycle arrest in response to DNA damage (Li et al., 2012). Despite being a direct transcriptional target of p53, accumulation of p21 occurred also in its absence, as demonstrated in p53-mutant HT29 and p53-deficient HCT116 cells, indicating a p53-independent mechanism. The zinc finger protein ZNF84 has recently been described as a critical mediator of p21 expression upon genotoxic stress in the absence of p53, as observed in p53-deficient HCT116 cells (Strzeszewska-Potyrała et al., 2021). As a critical regulator of *CDKN1A* gene expression, knockdown of ZNF84 lowered the genotoxic burden caused by doxorubicin (Strzeszewska-Potyrała et al., 2021). In addition, other p53-independent mechanisms have been described, including direct transcriptional induction by the variant BRCA1a, which underlines the complex role of p21 for cell cycle regulation, apoptosis and senescence (Karimian et al., 2016).

5.2.2. The Role of p53 for the cell death induction by merosquiterpenes

In response to higher concentrations of SP and DS, a pronounced upregulation of the sub-G₁ population was measured after only 24 h, indicating induction of the apoptotic cell death pathway. Quantification of caspase-3 and caspase-9 cleavage as well as proapoptotic Bim by western blot analysis further supported this observation. The cell death mechanism after treatment with SP was subsequently investigated via Annexin-V/PI costaining and flow cytometry analysis. A similar total cell death rate was observed, but a significantly higher proportion of apoptotic cells in HCT116 WT cells compared to higher proportion of necrotic cells in HCT116 p53^{-/-} cells. In accordance, the induction of caspase-3 cleavage was substantially stronger in the presence of WT p53, underlining the role of p53 for the intrinsic mitochondrial apoptosis pathway. Gene expression analysis of pro- and antiapoptotic genes revealed mitochondrial apoptosis as a major cell death pathway induced by merosquiterpenes, which was clearly dependent on WT p53 status but also occurred in p53-mutant HT29 cells. Nevertheless, induction of proapoptotic BH-3 only protein Bim revealed to be comparably strong in both, HCT116 WT

and p53^{-/-} cells indicating a role for p53-independent cell death induction by merosesquiterpenes. Bim antagonizes antiapoptotic Bcl-2 proteins and functions as a direct activator of the pro-apoptotic effector proteins Bax and Bak, which induce pore-formation and thereby MOMP, resulting in cytochrome C release and apoptosis (Sionov et al., 2015).

As the intracellular equilibrium of pro- and antiapoptotic members of the Bcl-2 family needs to be finely tuned, regulation of intracellular Bim levels occurs on the transcriptional, translational and post-translational level. Downregulation of Bim has been described in approximately 40% of human colorectal carcinomas *in vivo* and is associated with worsened therapy outcome, rendering it a potential target in cancer therapy (Greenhough et al., 2010). A recent study by Wang et al. identified Bim as a mediator of cell death independent of p53 in the presence of severe DNA damage stress in models of prostate cancer, glioblastoma, and osteosarcoma (Wang et al., 2022). This finding is of particular interest, since mutations of p53 are frequently observed in sporadic CRC and have been linked to worse clinical outcome and therapy resistance (Goh et al., 1995; Olivier et al., 2010).

In addition to the described cellular effects, endoplasmic reticulum (ER) stress might depict another component of the cytotoxicity induced by merosesquiterpenes. With an integral role in the quality control of the cellular protein homeostasis, the ER activates an adaptive stress response when unfolded or misfolded proteins accumulate, referred to as unfolded protein response (UPR), which leads to rectifiable or persistent ER stress (Chen et al., 2023). When prolonged and unresolved ER stress occurs, the UPR can trigger proapoptotic signaling, including activation of JNK, upregulation of C/EBP homologous protein (CHOP) and mitochondrial apoptosis (Hetz et al., 2020). As demonstrated in HCT116 cells, IQ treatment led to ROS-dependent induction of CHOP, which was mediated by ERK and MAPK signaling (Do et al., 2014). In line with this observation, upregulated expression and nuclear translocation of CHOP (also denoted as DNA damage inducible gene 153 or GADD153) have been observed in response to IQ treatment in the prostate cancer cell line PC-3, leading to G₁ cell cycle arrest and apoptosis (Lu et al., 2007). CHOP is activated by ER stress and DNA damage and has been described to promote the mitochondrial apoptosis pathway via upregulation of the BH3-only proteins Bim and Puma (Yang et al., 2017).

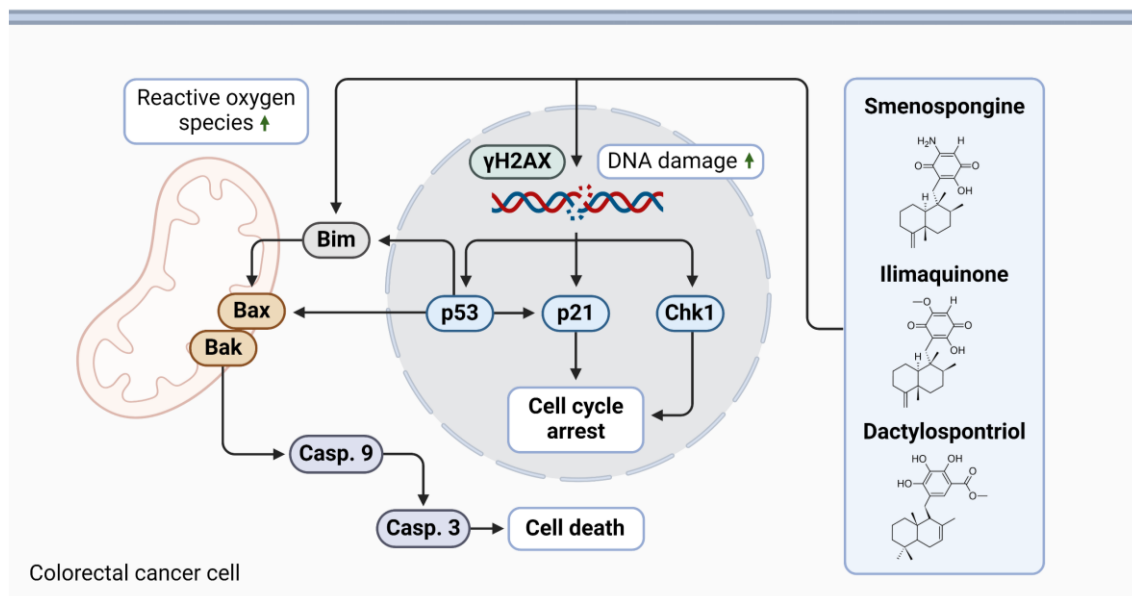


Figure 12: Mechanistic model of the merosessquiterpene-induced cell death pathway. Initially, merosessquiterpenes trigger simultaneous generation of ROS and the formation of DNA strand breaks, culminating in the induction of the DDR as demonstrated by phosphorylation of H2AX and Chk1 as well as p53-dependent and -independent accumulation of p21. In consequence, cell cycle arrest is induced by p21 and phosphorylated Chk1. At the same time, activation of WT p53 initiates the mitochondrial apoptosis pathway, characterized by upregulation of Bim and Bax as well as subsequent cleavage of caspase-9 and caspase-3. Remarkably, accumulation of Bim and induction of apoptotic cell death also occur in isogenic p53 knockout and p53-mutated cells, implying the involvement of additional cellular stress response mechanisms. (Created with BioRender)

Finally, the antitumorigenic potential of merosessquiterpenes SP and IQ was demonstrated in tumor organoids derived from *APC*-deficient mice, as shown by distinct morphological alterations, uptake of PI and reduced conversion of MTS. Organoids derived from colorectal tumor tissue can provide a better representation of the cellular diversity and tumor-specific drug responses *ex vivo* as compared to regular cell lines in 2D culture (Bode et al., 2019). Mutations or deficiencies of the tumor suppressor gene *APC* are the leading causes for overactivation of the Wnt signaling pathway, a key characteristic of sporadic and hereditary CRC (Markowitz and Bertagnolli, 2009). As part of the so-called destruction complex, APC induces degradation of the transcriptional coactivator β -catenin, a key component of the Wnt signaling pathway, by targeting it for ubiquitination and subsequent proteasomal digestion (Zhang and Shay, 2017). In multiple myeloma cells, IQ has been shown to attenuate the Wnt signaling pathway and downregulate β -catenin accumulation, leading to reduced expression of the proteins cyclin D1 and c-MYC (S. Park et al., 2014). Correspondingly, merosessquiterpenes might interfere with the deregulated Wnt signaling of CRC cells, thereby providing an additional mechanism of anti-tumorigenicity.

Based on the observed effects, a mouse xenograft model could elucidate the *in vivo* antitumor activity of the tested merosesquiterpenes as a next step. The availability of data regarding the *in vivo* bioactivity of the merosesquiterpenes IQ, DS and SP is limited. Applying a rat *in vivo* model, a recently published study investigated the pharmacokinetics of IQ and its stereo-isomer epi-IQ following intravenous and oral administration (Son et al., 2019). An area under the curve (AUC) of 3.39 $\mu\text{g h/mL}$ was determined after administration of a single oral dose of 10 mg/kg BW, which corresponds to an oral bioavailability of 46%. As a maximum plasma concentration 0.94 $\mu\text{g/mL}$ IQ was observed, which converts to 3.4 μM , and the half-life $t_{1/2}$ of the compound was identified at 1.2 h. Subsequent experiments performing i.v. injection of 2 mg/kg BW IQ determined an AUC of 1.46 $\mu\text{g h/mL}$. Under the assumption that an injection of 20 mg/kg BW IQ results in proportionately higher plasma concentrations, therapeutic concentrations necessary for antitumor activity might be reached *in vivo*.

Further studies regarding the pharmacokinetics of merosesquiterpenes will be necessary to assess that hypothesis, especially for SP and DS, given that these compounds showed the highest potency *in vitro*. To date, no data regarding the *in vivo* activity of IQ, DS and SP is published but structurally related synthetic merosesquiterpenes exhibiting a similar quinone backbone have been tested in a breast cancer mouse xenograft model (Carrasco et al., 2014). Oral doses of 5, 10 and 15 mg/kg BW led to significant reduction of xenograft growth in C57BL/6 mice after 42 days, but no dose dependency was detected. In general, good tolerance to the compound was reported with no signs of toxicity, including absence of hair loss and diarrhea. Detailed information about the *in vivo* safety profile of IQ, DS and SP will be necessary to evaluate their applicability for cancer treatment and calculate their therapeutic index, which is the ratio between efficacy and toxicity.

In summary, our study demonstrated pronounced cytotoxicity of the merosesquiterpenes IQ, SP and DS in CRC cell lines with mutant, deficient and wild type *TP53*. Formation of DNA strand breaks and activation of the DNA damage response as well as subsequent cell cycle arrest and activation of the mitochondrial apoptosis pathway were identified as underlying mechanisms. Finally, our results were confirmed applying murine intestinal tumor organoids. In summary, merosesquiterpenes are promising lead candidates for the development of novel cytostatic drugs in CRC therapy. As a next step, application of IQ, SP and DS in a murine CRC model could provide information about their therapeutic efficacy and the *in vivo* relevance of the observed mechanisms.

5.3. Publication III: Targeting PARP-1 and DNA Damage Response Defects in Colorectal Cancer Chemotherapy with Established and Novel PARP Inhibitors

Components of the DNA damage response are frequently altered in cancer, either due to mutations or epigenetic downregulation (Arai et al., 2021). As a result, genomic instability occurs as a common feature of tumors and a driver of malignancy, allowing for uncontrolled proliferation, dedifferentiation and metastasis, but also leading to susceptibility to treatments which induce DNA damage, including radiotherapy and various chemotherapeutic drugs (Walther et al., 2008). For more than a decade, PARPi have been applied in the treatment of ovarian and breast cancer, which frequently exhibit hereditary deficiencies of the HR factors *BRCA1* and *BRCA2* (Lord and Ashworth, 2008). The mechanism of inhibitor-induced PARP-1 trapping was elucidated more recently, resulting in new applications beyond the concept of synthetic lethality (Murai et al., 2012; Xue et al., 2022). Several studies suggested PARP-1 as a promising target in CRC subtypes with defective DNA repair (Arena et al., 2020; Durinikova et al., 2022; Mauri et al., 2020) and novel approaches could allow for the functional assessment of the DNA repair capacity in tumor specimen (Lee et al., 2023). Furthermore, application of PARPi has been shown to improve the efficacy of DNA damage inducing chemotherapeutic agents in HR-proficient types of cancer (D.-S. Kim et al., 2021). The synergy with established cytostatic drugs was identified as a possible opportunity to exploit vulnerabilities of CRC due to mutations or epigenetic downregulation of HR mediators (Abu-Sanad et al., 2015; Augustine et al., 2019; Wang et al., 2017).

In order to extend previous work regarding the dual role of PARP-1 in CRC initiation and progression (Dörsam et al., 2018), our study focused on PARP-1 as a potential target in CRC chemotherapy. Therefore, an *in silico* screening of novel indole compounds regarding the potential to inhibit PARP-1 was performed. Subsequently, the 12 most active compounds identified were applied in an *in vitro* cell free assay to quantify enzymatic inhibition of PARP-1-dependent PARylation. The four compounds with the lowest IC₅₀ values were applied for a cell-based screening to assess inhibition of PARylation in CRC cells. Cytotoxicity testing of the two most active compounds as well as the clinically applied PARPi olaparib and veliparib as monotreatment or in combination with chemotherapeutic drugs IT, OXA or 5-FU was performed in isogenic CRC cell line pairs to evaluate the significance of defective PARP-1, BRCA2 and ATR. Finally, the ability of the two novel PARPi to induce trapping of PARP-1 was tested in MSI HCT116 cells and MSS Caco-2 cells and the induction of DNA double-strand breaks was measured by γ H2AX quantification in wild type and *BRCA2*-deficient HCT116 cells.

5.3.1. Identification of novel PARP inhibitors for CRC treatment by *in silico* and *in vitro* testing

Proceeding from their first successful integration in the therapy of breast, ovarian and prostate cancer, the repertoire of PARPi gets constantly refined (Mateo et al., 2019). Currently, several novel PARPi are developed to exhibit desirable properties for certain applications including penetration of the blood-brain barrier for the treatment of brain tumors or increased PARP trapping capacity and are tested in non-clinical and clinical trials (Wang et al., 2020; Xiong et al., 2020). An *in silico* screening of a library of 3,4-bifunctionalized and -bridged indoles was performed to identify lead structures for novel PARPi and identified 12 compounds with a potentially high PARP-1 binding affinity. Four of those compounds, referred to as X17613, X17618, X17620 and X17621, were identified *in vitro* to induce pronounced enzymatic inhibition of recombinant PARP-1 in a cell free assay with IC₅₀ values ranging between 41 nM and 2.84 μM. In comparison, an IC₅₀ value of 5 nM for enzymatic inhibition of PARP-1 has been described for olaparib and veliparib (Oplustil O'Connor et al., 2016), demonstrating a comparable activity of our most active compound X17613. Intriguingly, X17613 contains a cyclic carboxylic acid hydrazide (i.e., dihydro-azepindolone), a structural motif found in the novel PARPi pamiparib that showed improved blood-brain barrier penetration and is applied in first clinical studies for the treatment of brain tumors (Xiong et al., 2020). *In silico* modelling revealed that X17613 interacts with G863-, S904-, and Y907-residues of PARP-1 in a similar manner as described for olaparib and veliparib, but lacks interaction with Y896 and D766, resulting in a lower binding affinity and therefore lower potency.

Applying chromatin isolation experiments, X17613 and X17618 were demonstrated to lack the ability to induce PARP-1 trapping in the cell lines HCT116 and Caco-2 and correspondingly show limited cytotoxicity as a monotherapy. The ability of PARPi to induce chromatin trapping of PARP-1 is an integral factor for the induction of cytotoxicity in cancer cells in the absence of synthetic lethality (Murai et al., 2014). In accordance, higher cytotoxicity of olaparib was observed in HCT116, Caco-2 and DLD-1 WT cell lines compared to veliparib. Olaparib has been described to induce pronounced PARP-1 trapping, while veliparib does so to a much lesser extent (Hopkins et al., 2015). Additional modification of the lead structure of X17613 could further refine its inhibitory capacity and improve its PARP trapping activity due to allosteric retention, as previously demonstrated for veliparib (Zandarashvili et al., 2020). Nevertheless, it is important to note, that PARP-trapping is also the main driver for the side effects of PARPi (Hopkins et al., 2019, 2015). Furthermore, certain combination-treatment regimens might benefit from the application of PARPi with low PARP-trapping activity to minimize side effects.

5.3.2. Role of PARP-1 expression for activity of PARPi monotreatment

Remarkably, the novel compounds X17613 and X17618 as well as veliparib induced no decrease of cell viability in HCT116 PARP-1^{+/+} and PARP-1^{-/-} cells. In contrast, olaparib revealed to be cytotoxic in both isogenic cell lines, albeit to a lesser extent in HCT116 PARP-1^{-/-} cells, underlining the significance of PARP-1 trapping for the activity of PARPi in cells lacking genetic susceptibility. Acquired resistance to PARPi in a clinical setting is frequently attributed to mutations which enable a reduced DNA binding affinity of PARP-1, underlining the significance of PARP trapping for the efficacy of PARPi monotherapy (Pettitt et al., 2018). Sufficient PARP-1 expression is necessary to exert the cytotoxic activity of PARP-1 trapping induced by PARPi, resulting in insensitivity in the absence of PARP-1 as first demonstrated in a PARP-1-deficient *in vitro* model (Murai et al., 2012). As outlined in Chapter 1.3.2.3., several clinical studies, which revealed insufficient efficacy of PARPi in CRC, did not assess PARP-1 status beforehand to stratify accordingly (Gorbunova et al., 2019; Leichman et al., 2016). Applying routine quantification of PARP-1 expression in CRC tumor biopsies could help to identify patients which benefit from an addition of PARPi to chemotherapy regimen in the future. To date, several publications have assessed the PARP-1 status in CRC patients. A high concentration of nuclear PARP-1 was detected by immunohistochemistry in 63.3% of tumor specimen in a set of 60 CRC patients (Abdelrahman et al., 2020). PARP-1 mRNA overexpression was identified in 70.3% of 91 CRC tumors and correlated with disease progression (Nosho et al., 2006). In parallel, Bianchi et al. showed that high PARPi expression and PARylation activity are associated with the *in vivo* response of patient-derived xenografts to olaparib treatment, independent of HR deficiencies (Bianchi et al., 2019). These results indicate that the assessment of PARP-1 expression might be crucial in the patient selection for clinical studies regarding the application of PARPi for CRC treatment. Patients with tumors that lack PARP-1 expression and are therefore not eligible for PARPi therapy might benefit from inhibitors of the HR DNA repair pathway, as further discussed in Chapter 5.3.3.

A recently published study analyzed PARP-1 and p53 in a set of 201 CRC patients and linked low expression to reduced overall and disease free survival in the presence of mutated p53, while this difference was not statistically significant for the subset of tumors expressing WT p53 (Puentes-Pardo et al., 2023). Since low PARP-1 expression has been linked to high genomic instability in non-malignant and cancer cells, this observation might reflect the detrimental consequences of this molecular subtype in CRC (Bièche et al., 1996; Bürkle, 2001). In line with this hypothesis, significant upregulation of PARP-1 expression was shown in MSI-high CRC tumor specimen compared with MSS counterparts (Jarrar et al., 2019). Contrasting the MSI subtype, which generally predicts

good clinical outcome in CRC, the genomic instability observed in MSS tumors is associated with a worsened prognosis, as shown by a meta-analysis of 10,126 CRC patients (Walther et al., 2008). Low PARP-1 expression has been linked to poor prognosis in other cancer entities, including pancreatic, breast and gastric cancer, but the underlying mechanism has not been elucidated so far (Aiad et al., 2015; Klauschen et al., 2012; Park et al., 2022). Further research will be necessary to identify if a mechanistical link exists between PARP-1 expression and prognosis or if the observations are a consequence of the described correlation of PARP-1 expression and genomic instability.

5.3.3. Cytotoxicity of PARPi as monotreatment and in combination with chemotherapeutic drugs in CRC

Despite pronounced inhibition of PARP-1-dependent PARylation in HCT116 cells at concentrations of 0.1 μM and higher, X17613 and X1718 monotreatment did not induce cytotoxicity in the tested cell lines. Only in HCT116 BRCA2^{-/-} cells, a decrease of cell viability to approximately 75% of the control was observed in response to 50 μM X17613, indicating a weak but specific cytotoxic activity. An explanation for the low cytotoxicity observed despite pronounced inhibition of PARP-1 could be an insufficient concentration of X17613. While olaparib inhibited PARP-1 in concentrations of the low nanomolar range, cytotoxicity was only observed in concentrations nearly 10,000-fold higher. If the same applies to X17613, a top concentration of 50 μM might have been too low. In addition, X17613 and X17618 might be potential substrates of active transporters that facilitate cellular efflux of the compounds, thereby lowering intracellular concentration. P-glycoprotein, an efflux transporter that enables tumor resistance to chemotherapeutic drugs, has been shown to excrete olaparib, whereas veliparib and paliparib are not translocated (Lawlor et al., 2014).

Pharmacokinetic studies of olaparib after therapeutic administration of an oral dose of 400 mg twice a day revealed a steady state plasma concentration of 5.7-9.1 $\mu\text{g/ml}$ which corresponds to 13.1-21.0 μM (Bruin et al., 2022). In our study, IC₅₀ values for the cytotoxicity of olaparib varied between 0.5 μM and 11.2 μM in the tested cell lines, depending on the genetic deficiencies, demonstrating that pharmacologically active concentrations for CRC therapy are reached in patients. Interestingly, olaparib was demonstrated to induce cytotoxicity in HCT116 PARP-1^{-/-} cells despite the absence of its main cellular target. This observation implies that the interaction with other cellular components contributes to the cytotoxicity of olaparib. PARP-2, PARP-3, PARP-4 as well as tankyrase 1 and 2 have been described as the most sensitive targets beyond PARP-1 with IC₅₀ values in the low micromolar range (Antolin et al., 2020). Furthermore, off-

target inhibition of other cellular kinases, including DYRK1A, PIM3, H6PD, DCK and CDK16, was described for clinically applied PARPi and is associated with potential side effects (Antolín and Mestres, 2014; Knezevic et al., 2016).

Furthermore, the potential of X17613, X17618 and olaparib to induce PARP trapping was assessed as an important determinant of PARPi cytotoxicity by applying HCT116 and Caco-2 cells as models for MSI and MSS CRC, respectively. Pronounced PARP-1 trapping was observed due to olaparib treatment in both CRC models but no effects for the two novel inhibitors. The mechanism of PARPi-induced trapping of PARP-1 is determined by two separate mechanisms. The automodification of PARP-1, which is necessary for its release, is prevented by its catalytic inhibition and thereby dependent on the IC₅₀ value of the PARPi (Pommier et al., 2016). In parallel, PARPi may induce allosteric alteration of PARP-1, thereby either promoting its retention or release (Kanev et al., 2024; Zandarashvili et al., 2020). While veliparib and olaparib have a comparable IC₅₀ for the enzymatic inhibition of PARP-1, veliparib was observed to exert an allosteric pro-release effect which olaparib is lacking, resulting in markedly different monotreatment cytotoxicity in cells without genetic susceptibility. Correspondingly, X17613 and X17618 might also have an allosteric pro-release activity, which, combined with a lower inhibitory activity, result in a lack of PARP-1 trapping.

As described above, cytotoxic PARP trapping has been identified as a driver of the antitumor efficacy for PARPi monotherapy (Pommier et al., 2016). Simultaneously, trapping of PARP-1 was found to be a main contributor to off-target activity, which is associated with severe side effects (Hopkins et al., 2019, 2015). The application in combined therapy regimen with certain chemotherapeutic drugs could allow for the usage of PARPi with a low PARP trapping potential, as described in several studies: While synergistic effects with chemotherapeutic drug temozolomide required PARP trapping activity (Murai et al., 2016), enzymatic inhibition is sufficient for combination treatment with TOP1 inhibitors, including IT and its active metabolite SN-38 (Abu-Sanad et al., 2015; Augustine et al., 2019; Genter Williams et al., 2015). Our study was able to confirm this observation *in vitro*. While veliparib induced no further decrease of cell viability in combination with OXA, it enhanced the cytotoxicity of IT to a degree that is comparable to olaparib. Several phase I and II clinical studies regarding the efficacy of PARPi for the treatment of CRC either as monotreatment or in combination with established therapy regimen are currently carried out or have already been finished (Table 3). Combination therapy has been described to result in dose limiting side effects, regularly involving hematological conditions. In particular, cytotoxic PARP-1 trapping by olaparib has been identified as an amplifier of the adverse effects induced by cytostatic drugs in the combination treatment of CRC, resulting in a limited overall therapeutic

efficacy (Leichman et al., 2016). Therefore, a potential approach to avoid dose limiting side effects in combination therapy regimen could be the application of PARPi lacking PARP trapping activity.

A recently published study by Petropoulos and colleagues demonstrated that in an HR-deficiency setting enzymatic inhibition without PARP-1 trapping is sufficient to induce synthetic lethality in tumor cells (Petropoulos et al., 2024). Applying a HR-deficiency model of the CRC cell line DLD-1, induction of synthetic lethality by four different PARPi revealed a high correlation with enzymatic PARP-1 inhibition but no correlation with PARP-1 trapping potential (Petropoulos et al., 2024). Several studies demonstrated that trapping of PARP-1 is a direct consequence of its enzymatic inhibition, which leads to the concurrent attenuation of its auto-modification and the reduced binding of DDR mediators, thereby attenuating its release and promoting its rebinding (Gopal et al., 2024; Pommier et al., 2016). Recent work revealed an additional allosteric mechanism, which affects PARP trapping and can be achieved by distinct structural modifications (Kanev et al., 2024; Zandarashvili et al., 2020). This might allow for the development of PARP inhibitors that exert strong enzymatic inhibition of PARP-1 and low PARP trapping activity for application in combination with TOP1 inhibitors to amplify chemotherapeutic efficacy while minimizing potential side effects.

Furthermore, new diagnostic approaches could provide the basis for an application in the treatment of tumors not targeted by PARPi so far. By conducting fluorescence imaging, Lee et al. realized real-time identification of functional HR deficiency in tumor specimen, providing a potential tool to identify patients who could benefit from PARPi treatment (Lee et al., 2023). Interestingly, a higher susceptibility of HR-deficient CRC cells compared to ovarian or triple negative breast cancer cells was revealed, underlining the potential of PARPi in CRC chemotherapy (Lee et al., 2023). While PARPi are currently used in the treatment of cancers with defects of DNA repair leading to synthetic lethality, development of novel inhibitors of DDR pathways might provide potential options for combination therapy of tumors without genetic susceptibility in the future. In 2017, The United States FDA approved application of PARPi niraparib for the treatment of recurrent gynecologic cancers with sensitivity to platinum-based chemotherapy, independent of HR status (Sisay and Edessa, 2017). Inhibitors of ATR are currently tested clinically and first phase I trials in combination with PARPi are carried out. Simultaneously, an increasing number of genetic markers is identified that help to identify sensitivity of tumors towards ATRi/PARPi combination treatment and could thereby guide clinical application in the future (Zimmermann et al., 2022).

The development of PARPi resistances in tumors might provide an additional field of application for ATRi, as revealed by several studies applying *in vitro* tumor models (Kim et al., 2020; Murai et al., 2016; Yazinski et al., 2017). Resistance mechanisms towards PARPi that can be overcome by ATRi treatment differ between tumor types. In small lung cancer cells, inactivation of SLFN11, a protein that induces permanent replication inhibition, was associated with resistance towards PARPi talazoparib. Since cells deficient in functional SLFN11 protein rely on ATR activation for their survival during PARPi treatment, application of ATRi could negate this resistance mechanism (Murai et al., 2016). Remarkably, sensitivity towards TOP1 inhibitor IT was also associated with *SLFN11* status in CRC (Tian et al., 2014). In ovarian cancer, increased activity of the ATR-Chk1 axis is observed in tumors with acquired PARPi resistance and associated with ATRi sensitivity (Kim et al., 2020). ATR was found to facilitate BRCA1-independent loading of RAD51 on stalled replication forks and DNA double-strand breaks, resulting in reduced sensitivity to PARPi in *BRCA1*-deficient ovarian cancer cells. Targeting ATR dependence by applying ATRi was found to overcome PARPi resistance (Yazinski et al., 2017). Furthermore, coapplication of the ATRi ceralasertib significantly improved the efficacy of PARPi olaparib in an *in vivo* mouse model applying ATM-deficient, patient-derived xenografts (Lloyd et al., 2020). Analyzing a panel of 112 CRC cell lines, Durinikova and colleagues identified the basal levels of phospho-RPA32 and RAD51 foci as well as the expression of ATM and RAD51C as critical predictors for the response to ATR inhibitors (Durinikova et al., 2022).

5.3.4. Combining devimistat and PARPi in CRC treatment

Despite the involvement of PARP-1 in several metabolic processes, little is known about combinational treatment of PARPi and metabolic inhibitors. PARP-1 represents a major NAD⁺-consuming enzyme, modulating the intracellular energy supply and inducing a metabolic shift from glycolysis to oxidative phosphorylation in the presence of DNA damage (Murata et al., 2019). Contrasting these results in the absence of DNA damage, deletion or inhibition of PARP-1 was shown to increase intracellular NAD⁺ content and thereby SIRT1 activity *in vivo*, resulting in upregulated oxidative metabolism (Bai et al., 2011). Interestingly, Andrabi and colleagues revealed PAR-dependent inhibition of the enzyme HK that was associated with downregulation of glycolysis, independent of cellular NAD⁺ levels. Simultaneously, PARP-dependent reduction of mitochondrial function, including mitochondrial OCR and reserve respiratory capacity, have been observed, occurring before cellular NAD⁺ levels are depleted (Andrabi et al., 2014).

Defects of HR in cancer cells have been associated with an upregulation of oxidative metabolism to provide ATP and NAD⁺ for PARP-dependent DNA repair (Lahiguera et

al., 2020). At the same time, deletions of mitochondrial DNA (mtDNA), which frequently occur in different types of cancer, are linked to a downregulation of BRCA2 due to the activation of AKT, resulting in chromosomal instability and an increase in DNA double-strand breaks (Arbini et al., 2013). This non-hereditary *BRCA2* deficiency leads to sensitivity towards PARPi, suggesting novel routes of synthetic lethality, which could be achieved by pharmacologically targeting the mitochondria of tumor cells. Our study demonstrated downregulation of mitochondrial activity and alterations of mitochondrial structure due to devimistat treatment (Arnold et al., 2022). Mitochondrial inhibition with metformin or rotenone combined with a supply of pyruvate led to resistance against olaparib due to upregulation of glycolysis (Lahiguera et al., 2020). In response to the PARPi olaparib, upregulation of the stem cell markers CD133 and CD117 was observed in ovarian cancer cells, resulting in an increase of tumorigenicity and induction of CSC. Intriguingly, pretreatment with devimistat was found to inhibit the PARPi-induced formation of CSC in ovarian cancer, presumably by targeting CSC dependency on oxidative phosphorylation (Bellio et al., 2019). In summary, these results suggest a potential synergistic activity of PARPi with metabolic inhibition by devimistat in CRC. So far, no *in vitro* or *in vivo* studies regarding the effects of a combination treatment with PARPi and devimistat have been published, indicating a potential area for further research.

6. Conclusion and Outlook

6.1. Conclusion

The following research was focused on three potential vulnerabilities that were identified in CRC: the altered metabolism of tumor cells, the induction of DNA damage dependent cell death and deregulated DNA repair mechanisms which can be exploited to induce synthetic lethality. Several aspects of these novel therapeutic approaches were elucidated, including identification of new lead structures, synergy with established chemotherapeutic drugs and the effects of common CRC mutations on sensitivity, as a guidance for a potential future application in CRC therapy.

The first area of focus was the metabolic inhibition by the mitochondrial inhibitor devimistat. Our publication elucidated the significance of mitochondria as a target of devimistat in CRC. The known mode of action of devimistat, based on the disruption of cellular energy metabolism, was confirmed in the context of CRC by measurement of mitochondrial membrane potential, oxygen consumption rate, ROS production and mitochondrial integrity. Subsequently, devimistat demonstrated to induce apoptotic and necrotic cell death in an array of CRC cancer cell lines with diverse molecular subtypes and revealed to lack genotoxic activity. The pathways involved on the gene and protein level were further detailed and a tumor cell specific mechanism was revealed, as shown by lower sensitivity of non-malignant cells and primary organoids. A synergistic activity of devimistat with established chemotherapeutic drugs IT and 5-FU was demonstrated, the most active concentrations for a combined treatment were calculated and the proapoptotic protein Bim was identified as a key factor for the combination effects. Application of a xenograft mouse model confirmed the results *in vivo* and showed prolonged survival and reduced tumor growth rate, demonstrating that devimistat could improve therapy outcome of CRC treatment in combination with conventional cytostatic drugs in the future. Currently, first phase I and II clinical trials for the application in CRC treatment are conducted and results are anticipated soon. Additional data regarding the metabolic effects of devimistat in non-malignant and malignant cells will be important for the further understanding of its tumor cell specificity and the mechanism responsible for Bim accumulation.

In the second step, the applicability of marine sponge toxins as novel lead structures for chemotherapeutic drugs was investigated. Three promising compounds were identified in a panel of 11 merosesquiterpenes, namely ilimaquinone, dactylospontriol and smenospongine, which caused cell death in three CRC cell lines with different molecular subtypes. The induction of DNA damage by ROS-dependent and -independent

mechanisms and the subsequent activation of apoptotic cell death were revealed as the corresponding modes of action. The role of p53 for the activity of merosesquiterpenes was further detailed by applying isogenic p53 wild-type and knockout cell lines as well as a p53-mutant cell line, since this tumor suppressor is frequently altered in CRC. Merosesquiterpenes could therefore provide lead structures for novel cytostatic drugs, which might help to circumnavigate the development of resistances and provide an improved therapeutic outcome. Further work regarding the specificity for malignant cells as well as the mechanism of DNA damage induction will be necessary to further advance the application of merosesquiterpenes.

Finally, the role of the DNA repair protein PARP-1 in CRC was examined. The *in silico* and *in vitro* screening of a library of 3,4-bifunctionalized and -bridged indole compounds revealed a novel candidate for PARP inhibitor development, referred to as X17613, which showed marked inhibition of PARP-dependent PARylation in nanomolar concentrations. The compound X17613 does not induce PARP trapping in MSS and MSI CRC cell lines, as demonstrated by chromatin isolation and subsequent PARP-1 western blot analysis, and correspondingly showed limited cytotoxicity as single treatment. Nevertheless, X17613 led to a reduced viability in combination with the TOP1 inhibitor IT in HCT116 BRCA^{-/-} cells as a model for HR deficiency. Subsequently, the potential synergy of established PARP inhibitors olaparib and veliparib with cytostatic drugs IT, 5-FU and OXA was quantified in genetically altered CRC cell lines, deficient in DNA repair proteins: A further reduction of cell viability was detected due to cotreatment of olaparib with IT and OXA as well as veliparib with IT, underlining the potential of PARPi for combination treatment of CRC. Our results indicate that the application of PARPi with limited PARP trapping capacity, including veliparib and the novel compound X17613, in combination with TOP1 inhibitors could provide an option to improve therapeutic efficacy without aggravating potential side effects. Further research regarding the role of DDR alterations in CRC for PARPi sensitivity can help to identify patient subpopulations which benefit from the coapplication of PARPi and provide information about meaningful combination regimen with established antineoplastic drugs.

In summary, this work contributed to the future application of novel therapeutic approaches in the treatment of CRC by providing information on the underlying molecular mechanisms to better understand possible synergisms and molecular determinants of sensitivity.

6.2. Outlook: Metabolic Inhibition by Devimistat Modulates Intracellular Signaling Pathways Associated with Metastasis and Metabolism

The ability of tumor cells to migrate and invade surrounding tissue is frequently increased as part of the malignant progression of CRC and enables development of metastases. To date, no targeted approach is available to impair these processes, rendering tumor metastasis a main driver of CRC mortality (Dillekås et al., 2019). Migration and invasion are highly energy-dependent processes, which are often fueled by specific metabolic alterations, including upregulation of glycolysis and OXPHOS. At the same time, several metabolic intermediates interfere with cellular signaling pathways that modulate migration and invasion of tumor cells (Wei et al., 2020).

In first experiments, the effects of devimistat on epithelial-to-mesenchymal transition (EMT), migration and invasion of CRC cells were investigated, as these mechanisms are fundamental for tumor metastasis. In preceding experiments, a wound healing assay has been applied to demonstrate the anti-migratory effects of devimistat in HCT116 and HT29 cells (Neitzel, 2021). Further experiments confirmed these observations for the CRC cell line RKO, underlining the attenuation tumor cell migration due to the metabolic inhibition by devimistat (Fig. 13A). Furthermore, HROC cell line pairs, which are short-term cultures derived from the primary tumor and the corresponding metastasis of the same patient, were applied to compare their sensitivities to devimistat, IT and 5-FU (Fig.13B). Since various metabolic alterations have been described to occur during the metastatic process (Wei et al., 2020), potential changes in the sensitivity against devimistat-induced cytotoxicity were quantified. While the metastasis-derived cells showed a slightly higher sensitivity to devimistat in the HROC147 and HROC300 cell line pairs, indicated by a lower IC₅₀ value, the HROC348-Met cells revealed to be less sensitive compared to HROC348 cells (Fig. 13B). Overall, no marked differences could be identified, demonstrating a sufficient activity of devimistat in metastasis-derived cells.

In the next step, the role of TGF- β -dependent EMT for the effects of devimistat on the migration and invasion of CRC cells was investigated. Preceding experiments had revealed a downregulation of the mesenchymal marker N-cadherin, while E-cadherin expression as an epithelial marker remained unchanged in response to devimistat (Neitzel, 2021). To further detail the underlying mechanisms, the effects of devimistat on TGF- β -dependent Smad2 signaling were investigated. Pretreatment of HCT116 and HT29 cells with devimistat for 8 h led to a dose dependent downregulation of the phosphorylation and nuclear translocation of Smad2 induced by short duration TGF- β exposure, which was measured by immunofluorescence and western blot analysis after cell fractionation (Fig. 14A).

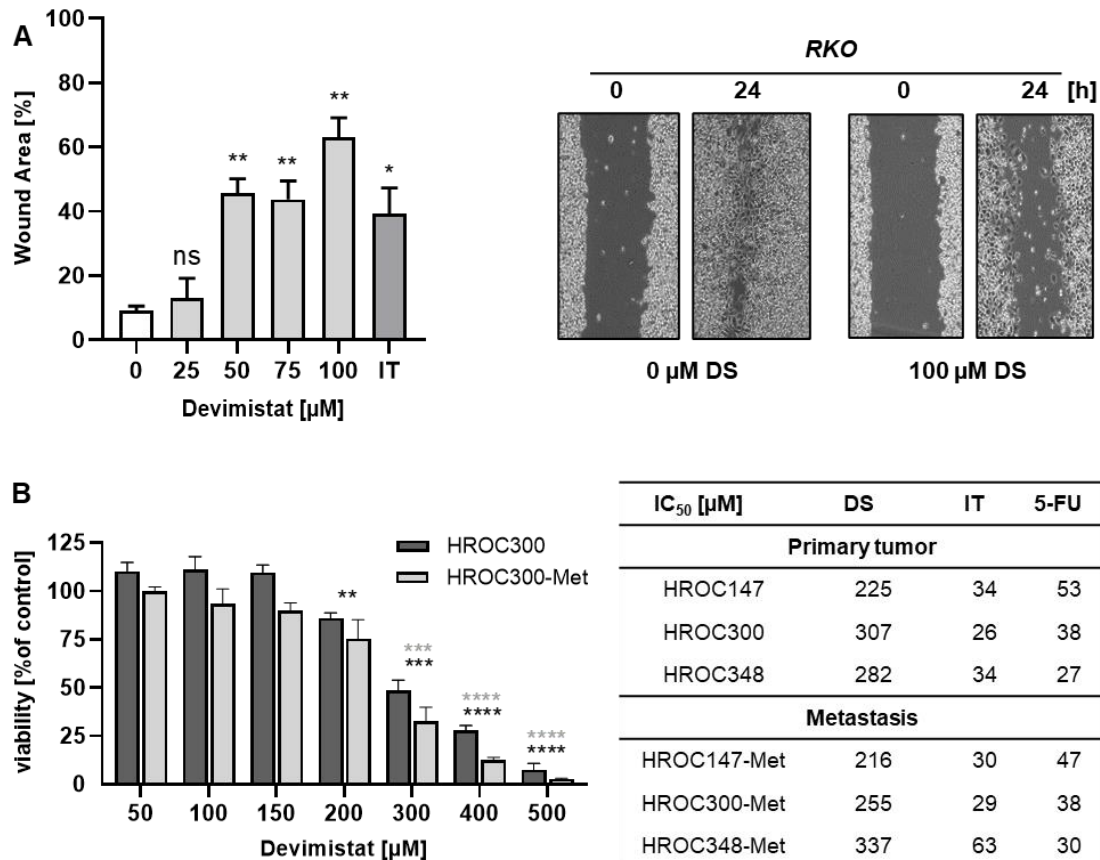


Figure 13: Devimistat attenuates the migration of tumor cells and is equally active in primary tumor- and metastasis-derived cell lines. (A) RKO cells were applied in a wound healing assay and treated with increasing concentrations of devimistat (DS) over a period of 24 h in medium with reduced FCS content. 5-FU in a concentration of 5 µM served as a control for a representative antineoplastic drug. Representative microscopic images at the beginning of the experiment and after 24 h are shown. Data presented are mean + SEM (n≥3). ns: p>0.05, * p<0.05, ** p<0.01, *** p<0.001, **** p<0.0001; t-test

In accordance with these findings, expression of the transcription factor ZEB1, a transcriptional target of the Smad2 complex, revealed to be downregulated in response to devimistat pretreatment (Fig. 14B). In tumor cells, nuclear pSmad2 functions as a master regulator of EMT, inducing the expression of other transcription factors including ZEB1, Snail and Slug, which subsequently modulate phenotypic alterations leading to EMT. Expression of the downstream target ZEB1 was detected after prolonged TGF-β treatment as well as impairment of its expression in response to devimistat treatment, confirming the functionality of Smad2 signaling in HCT116 and HT29 cells.

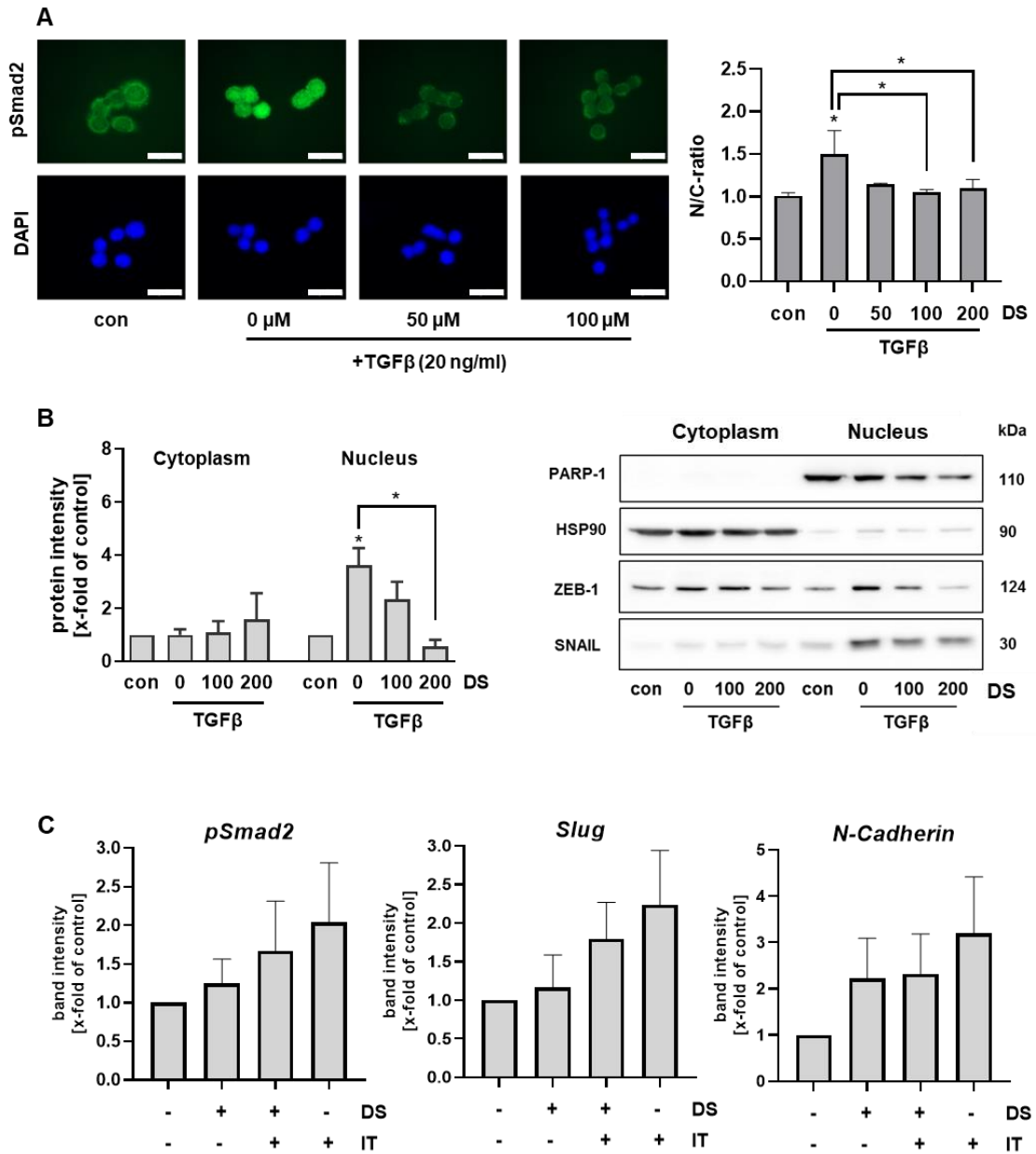


Figure 14: Devimistat downregulates the nuclear translocation of pSmad2 and the expression of EMT transcription factor ZEB1. (A) HCT116 cells were treated with devimistat in increasing concentrations for 8 h before TGF- β (20 ng/ml) was added for 30 min. After fixation, pSmad2 and nuclei were stained and microscopic images were acquired (Scale bar: 30. The pSmad2 intensity in nuclei and cytoplasm was quantified using ImageJ. Pretreatment with devimistat significantly ($p < 0.05$) attenuated the nuclear translocation and accumulation of pSmad2 induced by TGF- β . (B) HCT116 cells were treated with devimistat in increasing concentrations for 8 h before TGF- β (20 ng/ml) was added for 24 h. The nucleic and cytoplasmic fractions of the cells were derived and expression levels of ZEB1 and Snail were quantified by western blot analysis. Devimistat pretreatment significantly ($p > 0.05$) reduced the nuclear translocation and accumulation of ZEB1 induced by TGF- β . (C) Western blot analysis of pSmad2, Slug and N-Cadherin in HCT116 xenograft tumor lysates. Data presented are mean + SEM ($n \geq 3$). ns: $p > 0.05$, * $p < 0.05$; t-test.

Since TGF- β signaling exerts tumor-suppressive functions in early stages of CRC development, the corresponding pathway is frequently subject to various mutations which attenuate the proapoptotic activity while EMT-inducing functionality is maintained. This transformation can result in a tumor-promoting activity of TGF- β signaling in advanced CRC, rendering this pathway a possible target for therapy. Expression of EMT markers N-cadherin, E-cadherin, Snail, Slug and pSmad2 was investigated in HCT116 and HT29 xenograft tumor lysates. IT monotreatment induced expression of EMT markers while cotreatment with devimistat led to a consistent but non-significant decrease of the IT-dependent induction, indicating activity on EMT-related pathways *in vivo* (Fig. 14C).

So far, the effects of devimistat on tumor cell migration and invasion have not been subject to scientific studies. Interestingly, the prevention of breast-cancer associated lung metastases in an orthotopic mouse model has been reported due to treatment with KGDH inhibitor S-2-[(2,6-dichlorobenzoyl) amino] succinic acid (AA6). Mechanistically, metabolic inhibition by AA6 induced accumulation of α KG, leading to upregulated activity of the KG-dependent epigenetic enzymes TETs and subsequent repression of ZEB1 expression (Atlante et al., 2018). Accordingly, α KG has been shown to reduce low-glutamine-induced stemness and attenuated Wnt-hyperactivation in CRC by inducing DNA hypomethylation (Tran et al., 2020). A comparable mechanism of interference with the cellular signaling by TCA cycle intermediates might apply in the case of devimistat. Stuart et al. described significant downregulation of the metabolites fumarate, succinate, citrate and malate as well as accumulation of glutamine, aspartate and alanine in response to devimistat treatment for 2 h (240 μ M), although α KG levels were too low for detection (Stuart et al., 2014). Intriguingly, fumarate accumulation has been described to induce EMT in renal cancer by downregulating TET-dependent demethylation of anti-metastatic mRNA miRNA200 which inhibits expression of the pro-metastatic transcription factors ZEB1 and Snail, as outlined in Figure 6 (Sciacovelli et al., 2016). In summary, our research showed for the first time that novel TCA cycle inhibitor devimistat inhibits migration and invasion of CRC cells and modulates the TGF- β signaling pathway *in vitro* and *in vivo*. Additional experiments will be necessary to further elucidate how the metabolic inhibition by devimistat attenuates TGF- β signaling and to clarify the relevance of TCA cycle intermediates for the cellular effects of devimistat.

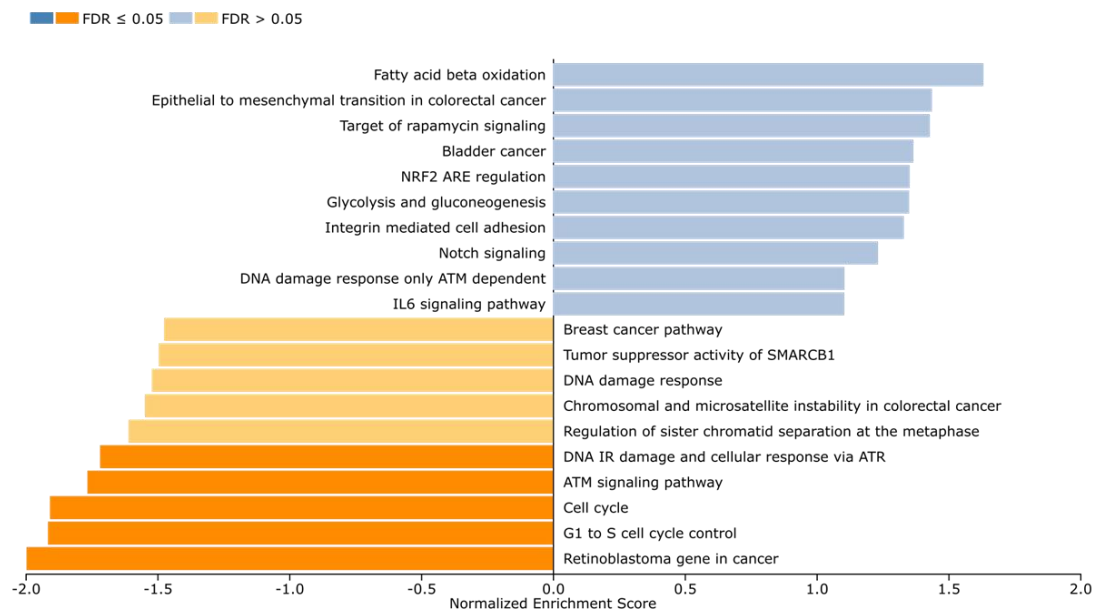
In the next step, proteomics analysis was applied to acquire a comprehensive understanding of the signaling pathways which are altered in response to devimistat treatment providing a potential basis for future research. For this reason, HCT116 cells were treated with devimistat in concentrations of 100 μ M and 200 μ M for 24 h and the cellular proteins were isolated and purified. Subsequently, mass spectrometry was

conducted in the laboratory of Dr. Markus Räsche at the RPTU Kaiserslautern to quantitatively profile the corresponding changes of cellular protein levels on the global level in response to devimistat. High content proteomics analysis and subsequent gene set enrichment analysis revealed several deregulated pathways in response to treatment with devimistat. In general, proteomics analysis revealed three major cellular responses in the CRC cell line HCT116 to devimistat treatment for 24 h: Reprogramming of metabolic pathways, downregulation of DNA damage repair and attenuation of cell cycle progression.

As revealed by proteomics-based analysis of treatment-induced changes in cellular protein levels, the CRC cell line HCT116 adapts to prolonged TCA cycle inhibition by devimistat with several alterations of its cellular metabolism. Gene set enrichment analysis and subsequent pathway analysis revealed significant upregulation of catabolic pathways including fatty acid catabolism and amino acid catabolism, presumably facilitating survival of the CRC cell line. A deregulation of monocarboxylic acid metabolic processes was observed, marked by a pronounced increase of the expression of acetyl-CoA synthetase short-chain family member 2 (ACSS2) and the adjacent enzymes phosphoenolpyruvate carboxykinase 2 (PCK2) and pyruvate carboxylase (PC). Under nutrient deprived conditions, ACSS2 utilizes acetate to catalyze the synthesis of acetyl-CoA in an ATP-dependent manner, thereby supplying tumor growth. Upregulated expression under metabolic stress, in particular hypoxia and low-serum culture conditions, was observed to be dependent on HIF1 α and SREBP2 signaling (Schug et al., 2015). Induction of ACSS2 expression was reported as a major mechanism of devimistat resistance in AML cell lines, while application of an ACSS2 inhibitor significantly restored sensitivity (Anderson et al., 2023). Upregulation of PCK2 was observed as another adaptive response to the metabolic inhibition by devimistat. The enzyme PCK2 catalyzes the production of phosphoenolpyruvate (PEP) from glutamine under glucose-deprived conditions to fuel biosynthetic pathways normally supplied by glucose (Vincent et al., 2015).

Induction of the enzyme PC was identified as an additional response of the tumor cells to treatment with devimistat. By catalyzing the irreversible carboxylation of pyruvate to oxaloacetate, PC replenishes the TCA cycle with this anaplerotic reaction, thereby allowing for tumor cells to grow under low-glutamine conditions (Cheng et al., 2011). In response to PDH inhibition by devimistat, PC might enable the utilization of pyruvate in the TCA cycle by providing an alternative point of entry, thereby promoting tumor cell survival.

A Gene Set Enrichment Analysis: Devimistat 0 μ m vs 200 μ m
(WikiPathways Cancer)



B Differential Gene Expression: Devimistat 0 μ m vs 200 μ m

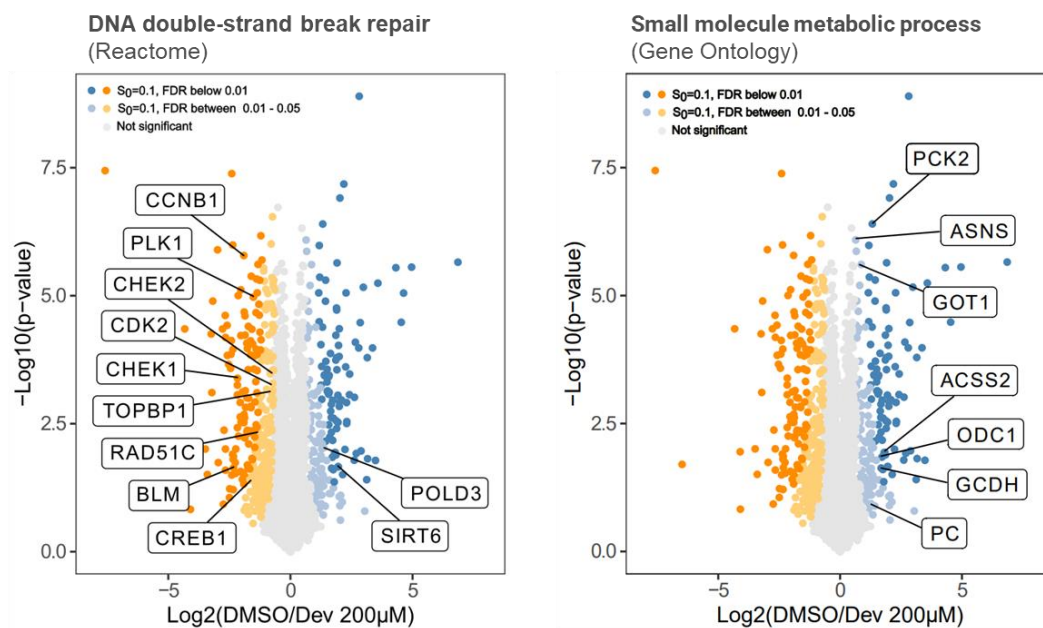


Figure 15: Gene set enrichment and differential expression analysis based on proteomic changes in response to devimistat treatment. (A) Colorectal cancer cells (HCT116) were treated for 24 h with devimistat in a concentration of 200 μ M following an LC/MS-based proteome analysis. Gene set enrichment analysis was conducted using WebGestalt (WEB-based Gene Set Analysis Toolkit) based on the WikiPathways cancer functional database. Weighted set cover was applied for redundancy removal and a minimum number of 5 and maximum number of 5000 analytes per category were used while 1000 permutations were conducted. (B) Differential expression analysis of the same dataset for genes involved in DNA double-strand break repair and small molecule metabolic process.

The upregulated expression of these three enzymes, ACSS2, PCK2 and PC, likely counterbalances the effects of devimistat to a certain degree, representing a possible resistance mechanism. Additional studies will be necessary to evaluate the clinical relevance of these findings as well as the possibility for an additional pharmacological intervention. While the plasticity of the tumor metabolism has been studied thoroughly (Bergers and Fendt, 2021), little is known about metabolic adaptations to small molecule inhibitors in a clinical setting.

These findings could help to identify possible resistance mechanisms, which occur in CRC cells in response to metabolic inhibition by devimistat and might therefore explain the limited efficacy of devimistat monotherapy in clinical trials (Pardee et al., 2018a). Bingham and Zachar have recently outlined how alterations in the lipid catabolism occur after therapeutic intervention in carcinoma cells, thereby enabling treatment resistance (Bingham and Zachar, 2023). Upregulation of lipid catabolism by peroxisomal fatty acid β -oxidation in response to devimistat has been described as a potential adaptive mechanism of carcinoma cells to circumnavigate energy depletion (Rivas et al., 2022). Intriguingly, an upregulation of enzymes critical for peroxisomal fatty acid β -oxidation was observed in response to devimistat treatment: The peroxisomal acetyl-CoA oxidase 1 (ACOX1), peroxisomal targeting signal 1 receptor (PTS1R) encoded by the gene *PEX5* and propionyl-CoA carboxylase (PCCA) showed a significant increase in response to 200 μ M devimistat. ACOX1 catalyzes the rate-limiting oxidation of acyl-CoA to enoyl-CoA during peroxisomal fatty acid β -oxidation with a preference for long or very long straight-chain fatty acids (Q. Zhang et al., 2023). A recent study reported low expression of ACOX1 in human CRC tumor tissue and described reduction of patient-derived xenograft growth following ACOX1 overexpression, indicating a tumor suppressor function. Mechanistically, ACOX1 reduces intracellular levels of palmitic acid, which acts as an oncometabolite by inducing stabilization of β -catenin to promote CRC progression (Q. Zhang et al., 2023). The PTS1R recognizes and transports peroxisomal matrix proteins in the cytosol, thereby playing a central role in peroxisome biogenesis in response to different stressors (Wang and Subramani, 2017). PCCA catalyzes the carboxylation of propionyl-CoA, produced in the catabolism of cholesterol, valine, odd chain fatty acids, methionine, isoleucine and threonine, to methylmalonyl-CoA. This anaplerotic reaction replenishes the TCA cycle, as methylmalonyl-CoA is ultimately transformed to succinyl-CoA (Wongkittichote et al., 2017). In addition, a pronounced downregulation of phospholipase C (PLCG1) was observed, an enzyme that catalyzes the cleavage of phosphatidylinositol 4,5-bisphosphate to produce diacylglycerol (DAG) and inositol triphosphate (IP3) as second messengers, thereby playing a key role in cell migration and invasion.

In addition to alterations of metabolic pathways, the gene set enrichment analysis revealed pronounced downregulation of the pathway responsible for the regulation of mitotic division, cell cycle progression and DNA repair. Among the key proteins downregulated, Cyclin B1 (CCNB1), the serine/threonine-protein kinase polo-like kinase 1 (PLK1) and CDK2 were found, which is in good accordance with our previous results, revealing inhibition of cell cycle progression and downregulation of CCNB1 on gene expression level (Arnold et al., 2022), as well as results published by other groups (Lee et al., 2014). The complex interplay of cellular metabolism and cell cycle regulation was recently detailed by Diehl et al (Diehl et al., 2023). Fueling the high cellular energy demand during G₂/M progression, CCNB1 activates mitochondrial respiration by phosphorylating respiratory chain complex 1 (Wang et al., 2014). At the same time, inhibition of mitochondrial ATP synthesis by the inhibitor oligomycin attenuates CCNB1 expression at non-cytotoxic concentrations (Xiong et al., 2012).

Devimistat led to a downregulation of the DNA damage response and the ATM signaling pathway. Key proteins, which showed a pronounced downregulation, are the DNA topoisomerase II binding protein (TOPBP) 1, Chk1, Chk2 and Rad51C. As one of five RAD51 paralogs, the Rad51C protein is required for an efficient DSB repair by homologous recombination (HR) and its depletion significantly attenuates HR frequency (Chun et al., 2013). The expression of RAD51 is associated with chemoresistance against DNA damage inducing antineoplastic drugs (Hoppe et al., 2021; Ohba et al., 2014) and has thus been discussed as a potential biomarker for DNA repair capacity in solid malignancies (Gachechiladze et al., 2017). Furthermore, a significant decrease of checkpoint kinase Chk1 and Chk2 protein levels were observed in response to devimistat. Overexpression of Chk1 is associated with resistance against DNA damage inducing drugs in AML, which was abrogated by ATR inhibition (David et al., 2016). Accordingly, Chk1 inhibitor rabusertib sensitized CRC organoids against genotoxic stress, underlining the significance of Chk1 for the chemoresistance of solid tumors (Franco et al., 2021). In parallel, activation of Chk2 is a critical step in the development of oxaliplatin-resistance in CRC, as demonstrated by IHC-based analysis of patient-derived tumor biopsies. Application of the Chk2 inhibitor BML-277 or genetic knockdown of Chk2 reversed oxaliplatin-resistance in CRC cells, underlining the potential of Chk2 as a target in combination with genotoxic chemotherapeutics (Hsieh et al., 2022). In summary, the synergistic activity of devimistat with IT and 5-FU, which was observed in our recently published study (Arnold et al., 2022), could to a certain extent be associated with the downregulation of proteins involved in the DNA damage response, including RAD51C, Chk1, Chk2.

Finally, devimistat induced upregulated protein levels of SIRT6, a histone deacetylase that regulates aerobic glycolysis in cancer cells and was thus denoted as a potential tumor suppressor in CRC (Sebastián et al., 2012). Mechanistically, SIRT6 attenuates HIF1 α signaling by deacetylating Histone 3K9 (H3K9) at HIF1 α target gene promoters, resulting in reduced glucose uptake and downregulated expression of glycolytic genes (Zhong et al., 2010). In addition, SIRT6 was observed to bind and deacetylate nuclear pyruvate kinase PKM2, a glycolytic enzyme with non-metabolic oncogenic functions (Bhardwaj and Das, 2016). SIRT6 was observed to be downregulated in CRC tumor specimen and expression positively correlated with patient survival which was attributed to the induction of Bax-dependent mitochondrial apoptosis pathway by SIRT6 (Zhang et al., 2019). In response to palmitic acid treatment, induction of fatty acid β -oxidation was revealed to be mediated by SIRT6 in colon cancer cells, leading to upregulated expression of corresponding genes (Gao et al., 2019). Liu et al. reported inhibition of cell proliferation and G₀/G₁ cell cycle arrest mediated by repression of CDC25A in colorectal CSCs after reintroducing SIRT6 expression (Liu et al., 2018). In summary, upregulated SIRT6 expression is linked to a favorable outcome with regards to metabolism and cell cycle progression in CRC.

In summary, cellular processes related to cell division and DNA damage repair showed a significant downregulation, indicating concordance with our previous results. Synergism of devimistat and cytostatic anticancer drugs IT and 5-FU was accompanied by reduced levels of p53, indicative of an impaired DDR (Arnold et al., 2022; Neitzel, 2021). Additionally, devimistat monotreatment led to downregulated expression of cyclins and cyclin-dependent kinases as well as cell cycle arrest. Therefore, proteomics analysis in HCT116 cells further supports our hypothesis of devimistat as a building block in CRC therapy in combination with established treatment regimen based on cytostatic drugs. By attenuating DNA damage response and DNA repair mechanisms, which are upregulated in proliferating CRC cells, devimistat amplifies the cytotoxicity of IT and 5-FU. These first results provided a detailed insight into the diverse changes of cellular signaling which are induced by devimistat on the proteome level. Additional experiments could confirm these observations in additional CRC cell lines and apply this method to further analyze the synergy of devimistat with genotoxic anticancer drugs.

7. References

- Abbotts, R., Wilson, D.M., 2017. Coordination of DNA Single Strand Break Repair. *Free Radic. Biol. Med.* 107, 228–244. <https://doi.org/10.1016/j.freeradbiomed.2016.11.039>
- Abdelrahman, A.E., Ibrahim, D.A., El-Azony, A., Alnagar, A.A., Ibrahim, A., 2020. ERCC1, PARP-1, and AQP1 as predictive biomarkers in colon cancer patients receiving adjuvant chemotherapy. *Cancer Biomark.* 27, 251–264. <https://doi.org/10.3233/CBM-190994>
- Abkevich, V., Timms, K.M., Hennessy, B.T., Potter, J., Carey, M.S., Meyer, L.A., Smith-McCune, K., Broaddus, R., Lu, K.H., Chen, J., Tran, T.V., Williams, D., Iliev, D., Jammulapati, S., FitzGerald, L.M., Krivak, T., DeLoia, J.A., Gutin, A., Mills, G.B., Lanchbury, J.S., 2012. Patterns of genomic loss of heterozygosity predict homologous recombination repair defects in epithelial ovarian cancer. *Br. J. Cancer* 107, 1776–1782. <https://doi.org/10.1038/bjc.2012.451>
- Abu-Sanad, A., Wang, Y., Hasheminasab, F., Panasci, J., Noe, A., Rosca, L., Davidson, D., Sharif-Askari, B., Amrein, L., Aloyz, R., Panasci, L., 2015. Simultaneous inhibition of ATR and PARP sensitizes colon cancer cell lines to irinotecan. *Front. Pharmacol.* 6.
- Acar, V., Fernandez, F.L.C., Buscariolo, F.F., Novais, A.A., Pereira, R.A.M., Zuccari, D.A.P. de C., 2021. Immunohistochemical Evaluation of PARP and Caspase-3 as Prognostic Markers in Prostate Carcinomas. *Clin. Med. Res.* 19, 183–191. <https://doi.org/10.3121/cmr.2021.1607>
- Agani, F., Jiang, B.-H., 2013. Oxygen-independent Regulation of HIF-1: Novel Involvement of PI3K/ AKT/mTOR Pathway in Cancer. *Curr. Cancer Drug Targets* 13, 245–251.
- Ahrabi, S., Sarkar, S., Pfister, S.X., Pirovano, G., Higgins, G.S., Porter, A.C.G., Humphrey, T.C., 2016. A role for human homologous recombination factors in suppressing microhomology-mediated end joining. *Nucleic Acids Res.* 44, 5743–5757. <https://doi.org/10.1093/nar/gkw326>
- Aiad, H.A., Kandil, M.A.H., El-Tahmody, M.A., Abulkheir, I.L., Abulkasem, F.M., Elmansori, A.A., Aleskandarany, M.A., 2015. The prognostic and predictive significance of PARP-1 in locally advanced breast cancer of Egyptian patients receiving neoadjuvant chemotherapy. *Appl. Immunohistochem. Mol. Morphol. AIMM* 23, 571–579. <https://doi.org/10.1097/PAI.000000000000124>
- Alistar, A., Morris, B.B., Desnoyer, R., Klepin, H.D., Hosseinzadeh, K., Clark, C., Cameron, A., Leyendecker, J., D'Agostino, R., Topaloglu, U., Boteju, L.W., Boteju, A.R., Shorr, R., Zachar, Z., Bingham, P.M., Ahmed, T., Crane, S., Shah, R., Migliano, J.J., Pardee, T.S., Miller, L., Hawkins, G., Jin, G., Zhang, W., Pasche, B., 2017. Safety and tolerability of the first-in-class agent CPI-613 in combination with modified FOLFIRINOX in patients with metastatic pancreatic cancer: a single-centre, open-label, dose-escalation, phase 1 trial. *Lancet Oncol.* 18, 770–778. [https://doi.org/10.1016/S1470-2045\(17\)30314-5](https://doi.org/10.1016/S1470-2045(17)30314-5)
- Al-Lazikani, B., Banerji, U., Workman, P., 2012. Combinatorial drug therapy for cancer in the post-genomic era. *Nat. Biotechnol.* 30, 679–692. <https://doi.org/10.1038/nbt.2284>
- Altmeyer, M., Neelsen, K.J., Teloni, F., Pozdnyakova, I., Pellegrino, S., Grøfte, M., Rask, M.-B.D., Streicher, W., Jungmichel, S., Nielsen, M.L., Lukas, J., 2015. Liquid demixing of intrinsically disordered proteins is seeded by poly(ADP-ribose). *Nat. Commun.* 6, 8088. <https://doi.org/10.1038/ncomms9088>
- Alvarez-Manzaneda, E., Chahboun, R., Alvarez, E., Fernández, A., Alvarez-Manzaneda, R., Haidour, A., Ramos, J.M., Akhaouzan, A., 2011. First enantiospecific synthesis of marine sesquiterpene quinol akaol A. *Chem. Commun.* 48, 606–608. <https://doi.org/10.1039/C1CC14608D>
- Amendola, C.R., Mahaffey, J.P., Parker, S.J., Ahearn, I.M., Chen, W.-C., Zhou, M., Court, H., Shi, J., Mendoza, S.L., Morten, M.J., Rothenberg, E., Gottlieb, E., Wadghiri, Y.Z., Possemato, R., Hubbard, S.R., Balmain, A., Kimmelman, A.C., Phillips, M.R., 2019. KRAS4A directly regulates hexokinase 1. *Nature* 576, 482–486. <https://doi.org/10.1038/s41586-019-1832-9>

References

- Anderson, E.M., Zhang, J., Russell, G., Bowline, I.G., Thyagarajan, B., Li, D., Ma, L., Anderson, E.R., Murea, M., 2019. A Single-Center Retrospective Study of Acute Kidney Injury Incidence in Patients With Advanced Malignancies Treated With Antimitochondrial Targeted Drug. *Kidney Int. Rep.* 4, 310–320. <https://doi.org/10.1016/j.ekir.2018.10.021>
- Anderson, N.M., Mucka, P., Kern, J.G., Feng, H., 2018. The emerging role and targetability of the TCA cycle in cancer metabolism. *Protein Cell* 9, 216–237. <https://doi.org/10.1007/s13238-017-0451-1>
- Anderson, R., Pladna, K.M., Schramm, N.J., Wheeler, F.B., Kridel, S., Pardee, T.S., 2023. Pyruvate Dehydrogenase Inhibition Leads to Decreased Glycolysis, Increased Reliance on Gluconeogenesis and Alternative Sources of Acetyl-CoA in Acute Myeloid Leukemia. *Cancers* 15, 484. <https://doi.org/10.3390/cancers15020484>
- Andrabi, S.A., Umanah, G.K.E., Chang, C., Stevens, D.A., Karuppagounder, S.S., Gagné, J.-P., Poirier, G.G., Dawson, V.L., Dawson, T.M., 2014. Poly(ADP-ribose) polymerase-dependent energy depletion occurs through inhibition of glycolysis. *Proc. Natl. Acad. Sci.* 111, 10209–10214. <https://doi.org/10.1073/pnas.1405158111>
- André, T., Boni, C., Navarro, M., Tabernero, J., Hickish, T., Topham, C., Bonetti, A., Clingan, P., Bridgewater, J., Rivera, F., de Gramont, A., 2009. Improved overall survival with oxaliplatin, fluorouracil, and leucovorin as adjuvant treatment in stage II or III colon cancer in the MOSAIC trial. *J. Clin. Oncol. Off. J. Am. Soc. Clin. Oncol.* 27, 3109–3116. <https://doi.org/10.1200/JCO.2008.20.6771>
- André, T., Shiu, K.-K., Kim, T.W., Jensen, B.V., Jensen, L.H., Punt, C., Smith, D., Garcia-Carbonero, R., Benavides, M., Gibbs, P., de la Fouchardiere, C., Rivera, F., Elez, E., Bendell, J., Le, D.T., Yoshino, T., Van Cutsem, E., Yang, P., Farooqui, M.Z.H., Marinello, P., Diaz, L.A., 2020. Pembrolizumab in Microsatellite-Instability-High Advanced Colorectal Cancer. *N. Engl. J. Med.* 383, 2207–2218. <https://doi.org/10.1056/NEJMoa2017699>
- Antolin, A.A., Ameratunga, M., Banerji, U., Clarke, P.A., Workman, P., Al-Lazikani, B., 2020. The kinase polypharmacology landscape of clinical PARP inhibitors. *Sci. Rep.* 10, 2585. <https://doi.org/10.1038/s41598-020-59074-4>
- Antolín, A.A., Mestres, J., 2014. Linking off-target kinase pharmacology to the differential cellular effects observed among PARP inhibitors. *Oncotarget* 5, 3023–3028.
- Applegate, M.A.B., Humphries, K.M., Szweda, L.I., 2008. Reversible inhibition of alpha-ketoglutarate dehydrogenase by hydrogen peroxide: glutathionylation and protection of lipoic acid. *Biochemistry* 47, 473–478. <https://doi.org/10.1021/bi7017464>
- Arai, H., Battaglin, F., Wang, J., Lo, J.H., Soni, S., Zhang, W., Lenz, H.-J., 2019. Molecular insight of regorafenib treatment for colorectal cancer. *Cancer Treat. Rev.* 81, 101912. <https://doi.org/10.1016/j.ctrv.2019.101912>
- Arai, H., Elliott, A., Xiu, J., Wang, J., Battaglin, F., Kawanishi, N., Soni, S., Zhang, W., Millstein, J., Sohal, D., Goldberg, R.M., Hall, M.J., Scott, A.J., Khushman, M., Hwang, J.J., Lou, E., Weinberg, B.A., Marshall, J.L., Lockhart, A.C., Stafford, P., Zhang, J., Moretto, R., Cremolini, C., Korn, W.M., Lenz, H.-J., 2021. The Landscape of Alterations in DNA Damage Response Pathways in Colorectal Cancer. *Clin. Cancer Res. Off. J. Am. Assoc. Cancer Res.* 27, 3234–3242. <https://doi.org/10.1158/1078-0432.CCR-20-3635>
- Arai, S., Varkaris, A., Nouri, M., Chen, S., Xie, L., Balk, S.P., 2020. MARCH5 mediates NOXA-dependent MCL1 degradation driven by kinase inhibitors and integrated stress response activation. *eLife* 9, e54954. <https://doi.org/10.7554/eLife.54954>
- Arango, D., Wilson, A.J., Shi, Q., Corner, G.A., Arañes, M.J., Nicholas, C., Lesser, M., Mariadason, J.M., Augenlicht, L.H., 2004. Molecular mechanisms of action and prediction of response to oxaliplatin in colorectal cancer cells. *Br. J. Cancer* 91, 1931–1946. <https://doi.org/10.1038/sj.bjc.6602215>
- Arbini, A.A., Guerra, F., Greco, M., Marra, E., Gandee, L., Xiao, G., Lotan, Y., Gasparre, G., Hsieh, J.-T., Moro, L., 2013. Mitochondrial DNA depletion sensitizes cancer cells to PARP inhibitors by translational and post-translational repression of BRCA2. *Oncogenesis* 2, e82–e82. <https://doi.org/10.1038/oncsis.2013.45>

- Arena, S., Corti, G., Durinikova, E., Montone, M., Reilly, N.M., Russo, M., Lorenzato, A., Arcella, P., Lazzari, L., Rospo, G., Pagani, M., Cancelliere, C., Negrino, C., Isella, C., Bartolini, A., Cassingena, A., Amatu, A., Mauri, G., Sartore-Bianchi, A., Mittica, G., Medico, E., Marsoni, S., Linnebacher, M., Abrignani, S., Siena, S., Di Nicolantonio, F., Bardelli, A., 2020. A Subset of Colorectal Cancers with Cross-Sensitivity to Olaparib and Oxaliplatin. *Clin. Cancer Res.* 26, 1372–1384. <https://doi.org/10.1158/1078-0432.CCR-19-2409>
- Argilés, G., Taberero, J., Labianca, R., Hochhauser, D., Salazar, R., Iveson, T., Laurent-Puig, P., Quirke, P., Yoshino, T., Taieb, J., Martinelli, E., Arnold, D., 2020. Localised colon cancer: ESMO Clinical Practice Guidelines for diagnosis, treatment and follow-up†. *Ann. Oncol.* 31, 1291–1305. <https://doi.org/10.1016/j.annonc.2020.06.022>
- Arnold, C., Demuth, P., Seiwert, N., Wittmann, S., Boengler, K., Rasenberger, B., Christmann, M., Huber, M., Brunner, T., Linnebacher, M., Fahrner, J., 2022. The Mitochondrial Disruptor Devimistat (CPI-613) Synergizes with Genotoxic Anticancer Drugs in Colorectal Cancer Therapy in a Bim-Dependent Manner. *Mol. Cancer Ther.* 21, 100–112. <https://doi.org/10.1158/1535-7163.MCT-21-0393>
- Arnold, D., Prager, G.W., Quintela, A., Stein, A., Moreno Vera, S., Mounedji, N., Taieb, J., 2018. Beyond second-line therapy in patients with metastatic colorectal cancer: a systematic review. *Ann. Oncol., Epigenetic modifiers as immunomodulatory therapies in solid tumours* 29, 835–856. <https://doi.org/10.1093/annonc/mdy038>
- Atalay, E.B., Kayali, H.A., 2022. The elevated D-2-hydroxyglutarate level found as a characteristic metabolic change of colon cancer in both in vitro and in vivo models. *Biochem. Biophys. Res. Commun.* 627, 191–199. <https://doi.org/10.1016/j.bbrc.2022.08.019>
- Atlante, S., Visintin, A., Marini, E., Savoia, M., Dianzani, C., Giorgis, M., Sürün, D., Maione, F., Schnütgen, F., Farsetti, A., Zeiher, A.M., Bertinaria, M., Giraudo, E., Spallotta, F., Cencioni, C., Gaetano, C., 2018. α -ketoglutarate dehydrogenase inhibition counteracts breast cancer-associated lung metastasis. *Cell Death Dis.* 9, 1–18. <https://doi.org/10.1038/s41419-018-0802-8>
- Augustine, T., Maitra, R., Zhang, J., Nayak, J., Goel, S., 2019. Sensitization of colorectal cancer to irinotecan therapy by PARP inhibitor rucaparib. *Invest. New Drugs* 37, 948–960. <https://doi.org/10.1007/s10637-018-00717-9>
- Azambuja, D. de B., e Gloria, H. de C., Montenegro, G. e S., Kalil, A.N., Hoffmann, J.-S., Leguisamo, N.M., Saffi, J., 2023. High Expression of MRE11A Is Associated with Shorter Survival and a Higher Risk of Death in CRC Patients. *Genes* 14, 1270. <https://doi.org/10.3390/genes14061270>
- Bai, P., Cantó, C., Oudart, H., Brunyánszki, A., Cen, Y., Thomas, C., Yamamoto, H., Huber, A., Kiss, B., Houtkooper, R.H., Schoonjans, K., Schreiber, V., Sauve, A.A., Menissier-de Murcia, J., Auwerx, J., 2011. PARP-1 Inhibition Increases Mitochondrial Metabolism through SIRT1 Activation. *Cell Metab.* 13, 461–468. <https://doi.org/10.1016/j.cmet.2011.03.004>
- Barkauskaite, E., Brassington, A., Tan, E.S., Warwicker, J., Dunstan, M.S., Banos, B., Lafite, P., Ahel, M., Mitchison, T.J., Ahel, I., Leys, D., 2013. Visualization of poly(ADP-ribose) bound to PARG reveals inherent balance between exo- and endo-glycohydrolase activities. *Nat. Commun.* 4, 2164. <https://doi.org/10.1038/ncomms3164>
- Bean, G.R., Ganesan, Y.T., Dong, Y., Takeda, S., Liu, H., Chan, P.M., Huang, Y., Chodosh, L.A., Zambetti, G.P., Hsieh, J.J.-D., Cheng, E.H.-Y., 2013. PUMA and BIM Are Required for Oncogene Inactivation–Induced Apoptosis. *Sci. Signal.* 6, ra20. <https://doi.org/10.1126/scisignal.2003483>
- Begleiter, A., Leith, M.K., Thliveris, J.A., Digby, T., 2004. Dietary induction of NQO1 increases the antitumour activity of mitomycin C in human colon tumours in vivo. *Br. J. Cancer* 91, 1624–1631. <https://doi.org/10.1038/sj.bjc.6602171>
- Beijers, A.J.M., Mols, F., Vreugdenhil, G., 2014. A systematic review on chronic oxaliplatin-induced peripheral neuropathy and the relation with oxaliplatin administration. *Support. Care Cancer* 22, 1999–2007. <https://doi.org/10.1007/s00520-014-2242-z>

References

- Bellio, C., DiGloria, C., Spriggs, D.R., Foster, R., Growdon, W.B., Rueda, B.R., 2019. The Metabolic Inhibitor CPI-613 Negates Treatment Enrichment of Ovarian Cancer Stem Cells. *Cancers* 11. <https://doi.org/10.3390/cancers11111678>
- Bellomo, C., Caja, L., Moustakas, A., 2016. Transforming growth factor β as regulator of cancer stemness and metastasis. *Br. J. Cancer* 115, 761–769. <https://doi.org/10.1038/bjc.2016.255>
- Bergers, G., Fendt, S.-M., 2021. The metabolism of cancer cells during metastasis. *Nat. Rev. Cancer* 21, 162–180. <https://doi.org/10.1038/s41568-020-00320-2>
- Bhamidipati, D., Haro-Silerio, J., Dumbrava, E.E., Fu, S., Hong, D.S., Karp, D.D., Naing, A., Pant, S., Piha-Paul, S.A., Rodon Ahnert, J., Tsimberidou, A.M., Johnson, A., Lee, M.S., Dasari, A., Raghav, K.P.S., Morris, V.K., Overman, M.J., Kopetz, S., Meric-Bernstam, F., Yap, T.A., 2024. Clinical characterization and therapeutic outcomes of patients (pts) with colorectal cancer (CRC) harboring somatic BRCA1/2 mutations. *J. Clin. Oncol.* 42, 134–134. https://doi.org/10.1200/JCO.2024.42.3_suppl.134
- Bhardwaj, A., Das, S., 2016. SIRT6 deacetylates PKM2 to suppress its nuclear localization and oncogenic functions. *Proc. Natl. Acad. Sci.* 113, E538–E547. <https://doi.org/10.1073/pnas.1520045113>
- Bhatt, A.P., Pellock, S.J., Biernat, K.A., Walton, W.G., Wallace, B.D., Creekmore, B.C., Letertre, M.M., Swann, J.R., Wilson, I.D., Roques, J.R., Darr, D.B., Bailey, S.T., Montgomery, S.A., Roach, J.M., Azcarate-Peril, M.A., Sartor, R.B., Gharaibeh, R.Z., Bultman, S.J., Redinbo, M.R., 2020. Targeted inhibition of gut bacterial β -glucuronidase activity enhances anticancer drug efficacy. *Proc. Natl. Acad. Sci. U. S. A.* 117, 7374–7381. <https://doi.org/10.1073/pnas.1918095117>
- Bianchi, A., Lopez, S., Altwerger, G., Bellone, S., Bonazzoli, E., Zammataro, L., Manzano, A., Manara, P., Perrone, E., Zeybek, B., Han, C., Menderes, G., Ratner, E., Silasi, D.-A., Huang, G.S., Azodi, M., Newberg, J.Y., Pavlick, D.C., Elvin, J., Frampton, G.M., Schwartz, P.E., Santin, A.D., 2019. PARP-1 activity (PAR) determines the sensitivity of cervical cancer to olaparib. *Gynecol. Oncol.* 155, 144–150. <https://doi.org/10.1016/j.ygyno.2019.08.010>
- Bièche, I., de Murcia, G., Lidereau, R., 1996. Poly(ADP-ribose) polymerase gene expression status and genomic instability in human breast cancer. *Clin. Cancer Res.* 2, 1163–1167.
- Bihl, M.P., Foerster, A., Lugli, A., Zlobec, I., 2012. Characterization of CDKN2A(p16) methylation and impact in colorectal cancer: systematic analysis using pyrosequencing. *J. Transl. Med.* 10, 173. <https://doi.org/10.1186/1479-5876-10-173>
- Bingham, P.M., Zachar, Z., 2023. Toward a Unifying Hypothesis for Redesigned Lipid Catabolism as a Clinical Target in Advanced, Treatment-Resistant Carcinomas. *Int. J. Mol. Sci.* 24, 14365. <https://doi.org/10.3390/ijms241814365>
- Blunt, J., Copp, B., A. Keyzers, R., G. Munro, M.H., R. Prinsep, M., 2015. Marine natural products. *Nat. Prod. Rep.* 32, 116–211. <https://doi.org/10.1039/C4NP00144C>
- Bocci, G., Barbara, C., Vannozzi, F., Di Paolo, A., Melosi, A., Barsanti, G., Allegrini, G., Falcone, A., Del Tacca, M., Danesi, R., 2006. A pharmacokinetic-based test to prevent severe 5-fluorouracil toxicity. *Clin. Pharmacol. Ther.* 80, 384–395. <https://doi.org/10.1016/j.clpt.2006.06.007>
- Bode, K.J., Mueller, S., Schweinlin, M., Metzger, M., Brunner, T., 2019. A fast and simple fluorometric method to detect cell death in 3D intestinal organoids. *BioTechniques* 67, 23–28. <https://doi.org/10.2144/btn-2019-0023>
- Bohanes, P., LaBonte, M.J., Lenz, H.-J., 2011. A Review of Excision Repair Cross-complementation Group 1 in Colorectal Cancer. *Clin. Colorectal Cancer* 10, 157–164. <https://doi.org/10.1016/j.clcc.2011.03.024>
- Boidot, R., Végran, F., Meulle, A., Breton, A.L., Dessy, C., Sonveaux, P., Lizard-Nacol, S., Feron, O., 2012. Regulation of Monocarboxylate Transporter MCT1 Expression by p53 Mediates Inward and Outward Lactate Fluxes in Tumors. *Cancer Res.* 72, 939–948. <https://doi.org/10.1158/0008-5472.CAN-11-2474>

- Bond, C.E., Whitehall, V.L.J., 2018. How the *BRAF* V600E Mutation Defines a Distinct Subgroup of Colorectal Cancer: Molecular and Clinical Implications. *Gastroenterol. Res. Pract.* 2018, e9250757. <https://doi.org/10.1155/2018/9250757>
- Brockmann, A., Bluwstein, A., Kögel, A., May, S., Marx, A., Tschan, M.P., Brunner, T., 2015. Thiazolides promote apoptosis in colorectal tumor cells via MAP kinase-induced Bim and Puma activation. *Cell Death Dis.* 6, e1778–e1778. <https://doi.org/10.1038/cddis.2015.137>
- Brown, R.E., Short, S.P., Williams, C.S., 2018. Colorectal Cancer and Metabolism. *Curr. Colorectal Cancer Rep.* 14, 226–241. <https://doi.org/10.1007/s11888-018-0420-y>
- Bruin, M.A.C., Sonke, G.S., Beijnen, J.H., Huitema, A.D.R., 2022. Pharmacokinetics and Pharmacodynamics of PARP Inhibitors in Oncology. *Clin. Pharmacokinet.* 61, 1649–1675. <https://doi.org/10.1007/s40262-022-01167-6>
- Bryant, H.E., Schultz, N., Thomas, H.D., Parker, K.M., Flower, D., Lopez, E., Kyle, S., Meuth, M., Curtin, N.J., Helleday, T., 2005. Specific killing of BRCA2-deficient tumours with inhibitors of poly(ADP-ribose) polymerase. *Nature* 434, 913–917. <https://doi.org/10.1038/nature03443>
- Bürkle, A., 2001. Poly(ADP-ribosyl)ation, a DNA damage-driven protein modification and regulator of genomic instability. *Cancer Lett.* 163, 1–5. [https://doi.org/10.1016/S0304-3835\(00\)00694-7](https://doi.org/10.1016/S0304-3835(00)00694-7)
- Buß, I., Hamacher, A., Sarin, N., Kassack, M.U., Kalayda, G.V., 2018. Relevance of copper transporter 1 and organic cation transporters 1-3 for oxaliplatin uptake and drug resistance in colorectal cancer cells. *Met. Integr. Biometal Sci.* 10, 414–425. <https://doi.org/10.1039/c7mt00334j>
- Cairns, R.A., Mak, T.W., 2013. Oncogenic isocitrate dehydrogenase mutations: mechanisms, models, and clinical opportunities. *Cancer Discov.* 3, 730–741. <https://doi.org/10.1158/2159-8290.CD-13-0083>
- Calon, A., Espinet, E., Palomo-Ponce, S., Tauriello, D.V.F., Iglesias, M., Céspedes, M.V., Sevillano, M., Nadal, C., Jung, P., Zhang, X.H.-F., Byrom, D., Riera, A., Rossell, D., Mangués, R., Massagué, J., Sancho, E., Batlle, E., 2012. Dependency of Colorectal Cancer on a TGF- β -Driven Program in Stromal Cells for Metastasis Initiation. *Cancer Cell* 22, 571–584. <https://doi.org/10.1016/j.ccr.2012.08.013>
- Calon, A., Lonardo, E., Berenguer-Llergo, A., Espinet, E., Hernando-Momblona, X., Iglesias, M., Sevillano, M., Palomo-Ponce, S., Tauriello, D.V.F., Byrom, D., Cortina, C., Morral, C., Barceló, C., Tosi, S., Riera, A., Attolini, C.S.-O., Rossell, D., Sancho, E., Batlle, E., 2015. Stromal gene expression defines poor-prognosis subtypes in colorectal cancer. *Nat. Genet.* 47, 320–329. <https://doi.org/10.1038/ng.3225>
- Cannan, W.J., Pederson, D.S., 2016. Mechanisms and Consequences of Double-strand DNA Break Formation in Chromatin. *J. Cell. Physiol.* 231, 3–14. <https://doi.org/10.1002/jcp.25048>
- Cao, D., Hou, M., Guan, Y., Jiang, M., Yang, Y., Gou, H., 2009. Expression of HIF-1 α and VEGF in colorectal cancer: association with clinical outcomes and prognostic implications. *BMC Cancer* 9, 432. <https://doi.org/10.1186/1471-2407-9-432>
- Carr, P.R., Weigl, K., Jansen, L., Walter, V., Erben, V., Chang-Claude, J., Brenner, H., Hoffmeister, M., 2018. Healthy Lifestyle Factors Associated With Lower Risk of Colorectal Cancer Irrespective of Genetic Risk. *Gastroenterology* 155, 1805-1815.e5. <https://doi.org/10.1053/j.gastro.2018.08.044>
- Carrasco, E., Álvarez, P.J., Melguizo, C., Prados, J., Álvarez-Manzaneda, E., Chahboun, R., Messouri, I., Vázquez-Vázquez, M.I., Aránega, A., Rodríguez-Serrano, F., 2014. Novel merosesquiterpene exerts a potent antitumor activity against breast cancer cells in vitro and in vivo. *Eur. J. Med. Chem.* 79, 1–12. <https://doi.org/10.1016/j.ejmech.2014.03.071>
- Ceccaldi, R., Liu, J.C., Amunugama, R., Hajdu, I., Primack, B., Petalcorin, M.I.R., O'Connor, K.W., Konstantinopoulos, P.A., Elledge, S.J., Boulton, S.J., Yusufzai, T., D'Andrea, A.D., 2015. Homologous-recombination-deficient tumours are dependent on Pol θ -mediated repair. *Nature* 518, 258–262. <https://doi.org/10.1038/nature14184>

References

- Ceccaldi, R., Rondinelli, B., D'Andrea, A.D., 2016. Repair Pathway Choices and Consequences at the Double-Strand Break. *Trends Cell Biol.* 26, 52–64. <https://doi.org/10.1016/j.tcb.2015.07.009>
- Cervantes, A., Adam, R., Roselló, S., Arnold, D., Normanno, N., Taïeb, J., Seligmann, J., Baere, T.D., Osterlund, P., Yoshino, T., Martinelli, E., 2023. Metastatic colorectal cancer: ESMO Clinical Practice Guideline for diagnosis, treatment and follow-up☆. *Ann. Oncol.* 34, 10–32. <https://doi.org/10.1016/j.annonc.2022.10.003>
- Chekulayev, V., Mado, K., Shevchuk, I., Koit, A., Kaldma, A., Klepinin, A., Timohhina, N., Tepp, K., Kandashvili, M., Ounpuu, L., Heck, K., Truu, L., Planken, A., Valvere, V., Kaambre, T., 2015. Metabolic remodeling in human colorectal cancer and surrounding tissues: alterations in regulation of mitochondrial respiration and metabolic fluxes. *Biochem. Biophys. Rep.* 4, 111–125. <https://doi.org/10.1016/j.bbrep.2015.08.020>
- Chen, E.X., Jonker, D.J., Siu, L.L., McKeever, K., Keller, D., Wells, J., Hagerman, L., Seymour, L., 2016. A Phase I study of olaparib and irinotecan in patients with colorectal cancer: Canadian Cancer Trials Group IND 187. *Invest. New Drugs* 34, 450–457. <https://doi.org/10.1007/s10637-016-0351-x>
- Chen, X., Shi, C., He, M., Xiong, S., Xia, X., 2023. Endoplasmic reticulum stress: molecular mechanism and therapeutic targets. *Signal Transduct. Target. Ther.* 8, 1–40. <https://doi.org/10.1038/s41392-023-01570-w>
- Cheng, T., Sudderth, J., Yang, C., Mullen, A.R., Jin, E.S., Matés, J.M., DeBerardinis, R.J., 2011. Pyruvate carboxylase is required for glutamine-independent growth of tumor cells. *Proc. Natl. Acad. Sci.* 108, 8674–8679. <https://doi.org/10.1073/pnas.1016627108>
- Chow, J.P.H., Man, W.Y., Mao, M., Chen, H., Cheung, F., Nicholls, J., Tsao, S.W., Li Lung, M., Poon, R.Y.C., 2013. PARP1 Is Overexpressed in Nasopharyngeal Carcinoma and Its Inhibition Enhances Radiotherapy. *Mol. Cancer Ther.* 12, 2517–2528. <https://doi.org/10.1158/1535-7163.MCT-13-0010>
- Christensen, S., Van der Roest, B., Besselink, N., Janssen, R., Boymans, S., Martens, J.W.M., Yaspo, M.-L., Priestley, P., Kuijk, E., Cuppen, E., Van Hoeck, A., 2019. 5-Fluorouracil treatment induces characteristic T>G mutations in human cancer. *Nat. Commun.* 10, 4571. <https://doi.org/10.1038/s41467-019-12594-8>
- Chu, X.-Y., Kato, Y., Ueda, K., Suzuki, H., Niinuma, K., Tyson, C.A., Weizer, V., Dabbs, J.E., Froehlich, R., Green, C.E., Sugiyama, Y., 1998. Biliary Excretion Mechanism of CPT-11 and Its Metabolites in Humans: Involvement of Primary Active Transporters1. *Cancer Res.* 58, 5137–5143.
- Chun, J., Buechelmaier, E.S., Powell, S.N., 2013. Rad51 Paralog Complexes BCDX2 and CX3 Act at Different Stages in the BRCA1-BRCA2-Dependent Homologous Recombination Pathway. *Mol. Cell. Biol.* 33, 387–395. <https://doi.org/10.1128/MCB.00465-12>
- Chun, S.Y., Johnson, C., Washburn, J.G., Cruz-Correa, M.R., Dang, D.T., Dang, L.H., 2010. Oncogenic KRAS modulates mitochondrial metabolism in human colon cancer cells by inducing HIF-1 α and HIF-2 α target genes. *Mol. Cancer* 9, 293. <https://doi.org/10.1186/1476-4598-9-293>
- Colvin, H., Nishida, N., Konno, M., Haraguchi, N., Takahashi, H., Nishimura, J., Hata, T., Kawamoto, K., Asai, A., Tsunekuni, K., Koseki, J., Mizushima, T., Satoh, T., Doki, Y., Mori, M., Ishii, H., 2016. Oncometabolite D-2-Hydroxyglurate Directly Induces Epithelial-Mesenchymal Transition and is Associated with Distant Metastasis in Colorectal Cancer. *Sci. Rep.* 6, 1–11. <https://doi.org/10.1038/srep36289>
- Compton, C.C., Greene, F.L., 2004. The Staging of Colorectal Cancer: 2004 and Beyond. *CA. Cancer J. Clin.* 54, 295–308. <https://doi.org/10.3322/canjclin.54.6.295>
- Conroy, T., Bosset, J.-F., Etienne, P.-L., Rio, E., François, É., Mesgouez-Nebout, N., Vendrely, V., Artignan, X., Bouché, O., Gargot, D., Boige, V., Bonichon-Lamichhane, N., Louvet, C., Morand, C., Fouchardièrre, C. de la, Lamfichekh, N., Juzyna, B., Jouffroy-Zeller, C., Rullier, E., Marchal, F., Gourgou, S., Castan, F., Borg, C., Etienne, P.-L., Rio, E., Mesgouez-Nebout, N., François, É., Vendrely, V., Conroy, T., Artignan, X., Bouché, O., Gargot, D., Boige, V., Bonichon-Lamichhane, N., Louvet, C., Morand, C., Fouchardièrre, C. de la, Ronchin, P., Seitz, J.-F., Corbinais, S., Maillard, E., Noirclerc, M., Hajbi, F.E., Ronchin, P.,

- Villing, A.-L., Bécouarn, Y., Sang, L.F.F.L.K., Artru, P., Bachet, J.-B., Hocine, F., Ligeza-Poisson, C., Vautravers, C., Abdelghani, M.B., Aparicio, T., Desot, E., Marquis, I., 2021. Neoadjuvant chemotherapy with FOLFIRINOX and preoperative chemoradiotherapy for patients with locally advanced rectal cancer (UNICANCER-PRODIGE 23): a multicentre, randomised, open-label, phase 3 trial. *Lancet Oncol.* 22, 702–715. [https://doi.org/10.1016/S1470-2045\(21\)00079-6](https://doi.org/10.1016/S1470-2045(21)00079-6)
- Contractor, T., Harris, C.R., 2012. p53 Negatively Regulates Transcription of the Pyruvate Dehydrogenase Kinase Pdk2. *Cancer Res.* 72, 560–567. <https://doi.org/10.1158/0008-5472.CAN-11-1215>
- Cosentino, C., Grieco, D., Costanzo, V., 2011. ATM activates the pentose phosphate pathway promoting anti-oxidant defence and DNA repair. *EMBO J.* 30, 546–555. <https://doi.org/10.1038/emboj.2010.330>
- Crosas-Molist, E., Samain, R., Kohlhammer, L., Orgaz, J.L., George, S.L., Maiques, O., Barcelo, J., Sanz-Moreno, V., 2022. Rho GTPase signaling in cancer progression and dissemination. *Physiol. Rev.* 102, 455–510. <https://doi.org/10.1152/physrev.00045.2020>
- Cuezva, J.M., Krajewska, M., de Heredia, M.L., Krajewski, S., Santamaría, G., Kim, H., Zapata, J.M., Marusawa, H., Chamorro, M., Reed, J.C., 2002. The Bioenergetic Signature of Cancer: A Marker of Tumor Progression¹. *Cancer Res.* 62, 6674–6681.
- Cunningham, D., Humblet, Y., Siena, S., Khayat, D., Bleiberg, H., Santoro, A., Bets, D., Mueser, M., Harstrick, A., Verslype, C., Chau, I., Van Cutsem, E., 2004. Cetuximab Monotherapy and Cetuximab plus Irinotecan in Irinotecan-Refractory Metastatic Colorectal Cancer. *N. Engl. J. Med.* 351, 337–345. <https://doi.org/10.1056/NEJMoa033025>
- Cunningham, J.M., Christensen, E.R., Tester, D.J., Kim, C.Y., Roche, P.C., Burgart, L.J., Thibodeau, S.N., 1998. Hypermethylation of the hMLH1 promoter in colon cancer with microsatellite instability. *Cancer Res.* 58, 3455–3460.
- Curtin, N.J., Szabo, C., 2020. Poly(ADP-ribose) polymerase inhibition: past, present and future. *Nat. Rev. Drug Discov.* 19, 711–736. <https://doi.org/10.1038/s41573-020-0076-6>
- Cvitkovic, E., 1998. A historical perspective on oxaliplatin: rethinking the role of platinum compounds and learning from near misses. *Semin. Oncol.* 25, 1–3.
- Dang, C.V., O'Donnell, K.A., Zeller, K.I., Nguyen, T., Osthus, R.C., Li, F., 2006. The c-Myc target gene network. *Semin. Cancer Biol.* 16, 253–264. <https://doi.org/10.1016/j.semcancer.2006.07.014>
- Danielsen, S.A., Eide, P.W., Nesbakken, A., Guren, T., Leithe, E., Lothe, R.A., 2015. Portrait of the PI3K/AKT pathway in colorectal cancer. *Biochim. Biophys. Acta BBA - Rev. Cancer* 1855, 104–121. <https://doi.org/10.1016/j.bbcan.2014.09.008>
- Danzi, F., Pacchiana, R., Mafficini, A., Scupoli, M.T., Scarpa, A., Donadelli, M., Fiore, A., 2023. To metabolomics and beyond: a technological portfolio to investigate cancer metabolism. *Signal Transduct. Target. Ther.* 8, 1–22. <https://doi.org/10.1038/s41392-023-01380-0>
- Das, B.B., Huang, S.N., Murai, J., Rehman, I., Amé, J.-C., Sengupta, S., Das, S.K., Majumdar, P., Zhang, H., Biard, D., Majumder, H.K., Schreiber, V., Pommier, Y., 2014. PARP1–TDP1 coupling for the repair of topoisomerase I–induced DNA damage. *Nucleic Acids Res.* 42, 4435–4449. <https://doi.org/10.1093/nar/gku088>
- David, B., Wolfender, J.-L., Dias, D.A., 2015. The pharmaceutical industry and natural products: historical status and new trends. *Phytochem. Rev.* 14, 299–315. <https://doi.org/10.1007/s11101-014-9367-z>
- David, L., Fernandez-Vidal, A., Bertoli, S., Grgurevic, S., Lepage, B., Deshaies, D., Prade, N., Cartel, M., Larrue, C., Sarry, J.-E., Delabesse, E., Cazaux, C., Didier, C., Récher, C., Manenti, S., Hoffmann, J.-S., 2016. CHK1 as a therapeutic target to bypass chemoresistance in AML. *Sci. Signal.* 9, ra90–ra90. <https://doi.org/10.1126/scisignal.aac9704>
- de Streef, G., Bertrand, C., Chalon, N., Liénart, S., Bricard, O., Lecomte, S., Devreux, J., Gaignage, M., De Boeck, G., Mariën, L., Van De Walle, I., van der Woning, B., Saunders, M., de Haard, H., Vermeersch, E., Maes, W., Deckmyn, H., Coulie, P.G., van Baren, N., Lucas, S., 2020. Selective inhibition of TGF- β 1 produced by GARP-expressing Tregs

References

- overcomes resistance to PD-1/PD-L1 blockade in cancer. *Nat. Commun.* 11, 4545. <https://doi.org/10.1038/s41467-020-17811-3>
- de With, M., van Doorn, L., Kloet, E., van Veggel, A., Matic, M., de Neijs, M.J., Oomen - de Hoop, E., van Meerten, E., van Schaik, R.H.N., Mathijssen, R.H.J., Bins, S., 2023. Irinotecan-Induced Toxicity: A Pharmacogenetic Study Beyond UGT1A1. *Clin. Pharmacokinet.* 62, 1589–1597. <https://doi.org/10.1007/s40262-023-01279-7>
- Demain, A.L., Vaishnav, P., 2011. Natural products for cancer chemotherapy. *Microb. Biotechnol.* 4, 687–699. <https://doi.org/10.1111/j.1751-7915.2010.00221.x>
- Denise, C., Paoli, P., Calvani, M., Taddei, M.L., Giannoni, E., Kopetz, S., Kazmi, S.M.A., Pia, M.M., Pettazoni, P., Sacco, E., Caselli, A., Vanoni, M., Landriscina, M., Cirri, P., Chiarugi, P., 2015. 5-Fluorouracil resistant colon cancer cells are addicted to OXPPOS to survive and enhance stem-like traits. *Oncotarget* 6, 41706–41721.
- Denkert, C., Budczies, J., Weichert, W., Wohlgemuth, G., Scholz, M., Kind, T., Niesporek, S., Noske, A., Buckendahl, A., Dietel, M., Fiehn, O., 2008. Metabolite profiling of human colon carcinoma – deregulation of TCA cycle and amino acid turnover. *Mol. Cancer* 7, 72. <https://doi.org/10.1186/1476-4598-7-72>
- Deshwar, A., Margonis, G.A., Andreatos, N., Barbon, C., Wang, J., Buettner, S., Wagner, D., Sasaki, K., Beer, A., Løes, I.M., Pikoulis, E., Damaskos, C., Garpis, N., Kamphues, K., He, J., Kaczirek, K., Poultides, G., Lønning, P.E., Mischinger, H.J., Aucejo, F.N., Kreis, M.E., Wolfgang, C.L., Weiss, M.J., 2018. Double KRAS and BRAF Mutations in Surgically Treated Colorectal Cancer Liver Metastases: An International, Multi-institutional Case Series. *Anticancer Res.* 38, 2891–2895.
- Dias, M.P., Moser, S.C., Ganesan, S., Jonkers, J., 2021. Understanding and overcoming resistance to PARP inhibitors in cancer therapy. *Nat. Rev. Clin. Oncol.* 18, 773–791. <https://doi.org/10.1038/s41571-021-00532-x>
- Diasio, R.B., Harris, B.E., 1989. Clinical pharmacology of 5-fluorouracil. *Clin. Pharmacokinet.* 16, 215–237. <https://doi.org/10.2165/00003088-198916040-00002>
- Diehl, F.F., Sapp, K.M., Heiden, M.G.V., 2023. The bidirectional relationship between metabolism and cell cycle control. *Trends Cell Biol.* 0. <https://doi.org/10.1016/j.tcb.2023.05.012>
- Dillekås, H., Rogers, M.S., Straume, O., 2019. Are 90% of deaths from cancer caused by metastases? *Cancer Med.* 8, 5574–5576. <https://doi.org/10.1002/cam4.2474>
- Do, M.T., Na, M., Kim, H.G., Khanal, T., Choi, J.H., Jin, S.W., Oh, S.H., Hwang, I.H., Chung, Y.C., Kim, H.S., Jeong, T.C., Jeong, H.G., 2014. Ilimaquinone induces death receptor expression and sensitizes human colon cancer cells to TRAIL-induced apoptosis through activation of ROS-ERK/p38 MAPK-CHOP signaling pathways. *Food Chem. Toxicol. Int. J. Publ. Br. Ind. Biol. Res. Assoc.* 71, 51–59. <https://doi.org/10.1016/j.fct.2014.06.001>
- Domagala, P., Huzarski, T., Lubinski, J., Gugala, K., Domagala, W., 2011. PARP-1 expression in breast cancer including BRCA1-associated, triple negative and basal-like tumors: possible implications for PARP-1 inhibitor therapy. *Breast Cancer Res. Treat.* 127, 861–869. <https://doi.org/10.1007/s10549-011-1441-2>
- Dörsam, B., Seiwert, N., Foersch, S., Stroh, S., Nagel, G., Begaliew, D., Diehl, E., Kraus, A., McKeague, M., Minneker, V., Roukos, V., Reißig, S., Waisman, A., Moehler, M., Stier, A., Mangerich, A., Dantzer, F., Kaina, B., Fahrner, J., 2018. PARP-1 protects against colorectal tumor induction, but promotes inflammation-driven colorectal tumor progression. *Proc. Natl. Acad. Sci. U. S. A.* 115, E4061–E4070. <https://doi.org/10.1073/pnas.1712345115>
- Durinkova, E., Reilly, N.M., Buzo, K., Mariella, E., Chilà, R., Lorenzato, A., Dias, J.M.L., Grasso, G., Pisati, F., Lamba, S., Corti, G., Degasperis, A., Cancelliere, C., Mauri, G., Andrei, P., Linnebacher, M., Marsoni, S., Siena, S., Sartore-Bianchi, A., Nik-Zainal, S., Di Nicolantonio, F., Bardelli, A., Arena, S., 2022. Targeting the DNA Damage Response Pathways and Replication Stress in Colorectal Cancer. *Clin. Cancer Res.* 28, 3874–3889. <https://doi.org/10.1158/1078-0432.CCR-22-0875>
- Durkacz, B.W., Omidij, O., Gray, D.A., Shall, S., 1980. (ADP-ribose)_n participates in DNA excision repair. *Nature* 283, 593–596. <https://doi.org/10.1038/283593a0>

References

- Durko, L., Malecka-Panas, E., 2014. Lifestyle Modifications and Colorectal Cancer. *Curr. Colorectal Cancer Rep.* 10, 45–54. <https://doi.org/10.1007/s11888-013-0203-4>
- Dziaman, T., Ludwiczak, H., Ciesla, J.M., Banaszkiwicz, Z., Winczura, A., Chmielarczyk, M., Wisniewska, E., Marszalek, A., Tudek, B., Olinski, R., 2014. PARP-1 Expression is Increased in Colon Adenoma and Carcinoma and Correlates with OGG1. *PLOS ONE* 9, e115558. <https://doi.org/10.1371/journal.pone.0115558>
- Efimova, E.V., Takahashi, S., Shamsi, N.A., Wu, D., Labay, E., Ulanovskaya, O.A., Weichselbaum, R.R., Kozmin, S.A., Kron, S.J., 2016. Linking Cancer Metabolism to DNA Repair and Accelerated Senescence. *Mol. Cancer Res.* 14, 173–184. <https://doi.org/10.1158/1541-7786.MCR-15-0263>
- Egawa, Y., Saigo, C., Kito, Y., Moriki, T., Takeuchi, T., 2018. Therapeutic potential of CPI-613 for targeting tumorous mitochondrial energy metabolism and inhibiting autophagy in clear cell sarcoma. *PLoS One* 13, e0198940. <https://doi.org/10.1371/journal.pone.0198940>
- Eng, C., 2009. Toxic effects and their management: daily clinical challenges in the treatment of colorectal cancer. *Nat. Rev. Clin. Oncol.* 6, 207–218. <https://doi.org/10.1038/nrclinonc.2009.16>
- Eniafe, J., Jiang, S., 2021. The functional roles of TCA cycle metabolites in cancer. *Oncogene* 40, 3351–3363. <https://doi.org/10.1038/s41388-020-01639-8>
- Erez, N., Milyavsky, M., Eilam, R., Shats, I., Goldfinger, N., Rotter, V., 2003. Expression of Prolyl-Hydroxylase-1 (PHD1/EGLN2) Suppresses Hypoxia Inducible Factor-1 α Activation and Inhibits Tumor Growth. *Cancer Res.* 63, 8777–8783.
- Essack, M., Bajic, V.B., Archer, J.A.C., 2011. Recently Confirmed Apoptosis-Inducing Lead Compounds Isolated from Marine Sponge of Potential Relevance in Cancer Treatment. *Mar. Drugs* 9, 1580–1606. <https://doi.org/10.3390/md9091580>
- Fatokun, A.A., Dawson, V.L., Dawson, T.M., 2014. Parthanatos: mitochondrial-linked mechanisms and therapeutic opportunities. *Br. J. Pharmacol.* 171, 2000–2016. <https://doi.org/10.1111/bph.12416>
- Feng, S., Xiong, L., Ji, Z., Cheng, W., Yang, H., 2011. Correlation between increased copy number of mitochondrial DNA and clinicopathological stage in colorectal cancer. *Oncol. Lett.* 2, 899–903. <https://doi.org/10.3892/ol.2011.322>
- Fessler, E., Drost, J., van Hooff, S.R., Linnekamp, J.F., Wang, X., Jansen, M., De Sousa E Melo, F., Prasetyanti, P.R., IJspeert, J.E., Franitza, M., Nürnberg, P., van Noesel, C.J., Dekker, E., Vermeulen, L., Clevers, H., Medema, J.P., 2016. TGF β signaling directs serrated adenomas to the mesenchymal colorectal cancer subtype. *EMBO Mol. Med.* 8, 745–760. <https://doi.org/10.15252/emmm.201606184>
- Fidler, I.J., 2003. The pathogenesis of cancer metastasis: the “seed and soil” hypothesis revisited. *Nat. Rev. Cancer* 3, 453–458. <https://doi.org/10.1038/nrc1098>
- Forsythe, J.A., Jiang, B.-H., Iyer, N.V., Agani, F., Leung, S.W., Koos, R.D., Semenza, G.L., 1996. Activation of Vascular Endothelial Growth Factor Gene Transcription by Hypoxia-Inducible Factor 1. *Mol. Cell. Biol.* 16, 4604–4613.
- Franco, S.D., Parrino, B., Gaggianesi, M., Pantina, V.D., Bianca, P., Nicotra, A., Mangiapane, L.R., Iacono, M.L., Ganduscio, G., Veschi, V., Brancato, O.R., Glaviano, A., Turdo, A., Pillitteri, I., Colarossi, L., Cascioferro, S., Carbone, D., Pecoraro, C., Fiori, M.E., Maria, R.D., Todaro, M., Screpanti, I., Cirrincione, G., Diana, P., Stassi, G., 2021. CHK1 inhibitor sensitizes resistant colorectal cancer stem cells to nortopsentin. *iScience* 24. <https://doi.org/10.1016/j.isci.2021.102664>
- Fronik, P., Gutmann, M., Vician, P., Stojanovic, M., Kastner, A., Heffeter, P., Pirker, C., Keppler, B.K., Berger, W., Kowol, C.R., 2022. A platinum(IV) prodrug strategy to overcome glutathione-based oxaliplatin resistance. *Commun. Chem.* 5, 1–13. <https://doi.org/10.1038/s42004-022-00661-z>
- Fruman, D.A., Chiu, H., Hopkins, B.D., Bagrodia, S., Cantley, L.C., Abraham, R.T., 2017. The PI3K Pathway in Human Disease. *Cell* 170, 605–635. <https://doi.org/10.1016/j.cell.2017.07.029>

References

- Fu, Y., Yu, J., Li, F., Ge, S., 2022. Oncometabolites drive tumorigenesis by enhancing protein acylation: from chromosomal remodelling to nonhistone modification. *J. Exp. Clin. Cancer Res.* 41, 144. <https://doi.org/10.1186/s13046-022-02338-w>
- Fujita, K., Kubota, Y., Ishida, H., Sasaki, Y., 2015. Irinotecan, a key chemotherapeutic drug for metastatic colorectal cancer. *World J. Gastroenterol.* 21, 12234–12248. <https://doi.org/10.3748/wjg.v21.i43.12234>
- Fuloria, N.K., Raheja, R.K., Shah, K.H., Oza, M.J., Kulkarni, Y.A., Subramaniyan, V., Sekar, M., Fuloria, S., 2022. Biological activities of meroterpenoids isolated from different sources. *Front. Pharmacol.* 13, 830103. <https://doi.org/10.3389/fphar.2022.830103>
- Gachechiladze, M., Škarda, J., Soltermann, A., Joerger, M., 2017. RAD51 as a potential surrogate marker for DNA repair capacity in solid malignancies. *Int. J. Cancer* 141, 1286–1294. <https://doi.org/10.1002/ijc.30764>
- Gaglio, D., Metallo, C.M., Gameiro, P.A., Hiller, K., Danna, L.S., Balestrieri, C., Alberghina, L., Stephanopoulos, G., Chiaradonna, F., 2011. Oncogenic K-Ras decouples glucose and glutamine metabolism to support cancer cell growth. *Mol. Syst. Biol.* 7, 523. <https://doi.org/10.1038/msb.2011.56>
- Ganapathy, V., Ge, R., Grazioli, A., Xie, W., Banach-Petrosky, W., Kang, Y., Lonning, S., McPherson, J., Yingling, J.M., Biswas, S., Mundy, G.R., Reiss, M., 2010. Targeting the Transforming Growth Factor- β pathway inhibits human basal-like breast cancer metastasis. *Mol. Cancer* 9, 122. <https://doi.org/10.1186/1476-4598-9-122>
- Gao, L., Xu, Z., Huang, Z., Tang, Y., Yang, D., Huang, J., He, L., Liu, M., Chen, Z., Teng, Y., 2020. CPI-613 rewires lipid metabolism to enhance pancreatic cancer apoptosis via the AMPK-ACC signaling. *J. Exp. Clin. Cancer Res.* 39, 73. <https://doi.org/10.1186/s13046-020-01579-x>
- Gao, P., Tchernyshyov, I., Chang, T.-C., Lee, Y.-S., Kita, K., Ochi, T., Zeller, K.I., Marzo, A.M., van Eyk, J.E., Mendell, J.T., Dang, C.V., 2009. c-Myc suppression of miR-23a/b enhances mitochondrial glutaminase expression and glutamine metabolism. *Nature* 458, 762–765. <https://doi.org/10.1038/nature07823>
- Gao, T., Li, M., Mu, G., Hou, T., Zhu, W.-G., Yang, Y., 2019. PKC ζ Phosphorylates SIRT6 to Mediate Fatty Acid β -Oxidation in Colon Cancer Cells. *Neoplasia* 21, 61–73. <https://doi.org/10.1016/j.neo.2018.11.008>
- Garcia, M.R., Steinbauer, B., Srivastava, K., Singhal, M., Mattijssen, F., Maida, A., Christian, S., Hess-Stumpp, H., Augustin, H.G., Müller-Decker, K., Nawroth, P.P., Herzig, S., Diaz, M.B., 2017. Acetyl-CoA Carboxylase 1-Dependent Protein Acetylation Controls Breast Cancer Metastasis and Recurrence. *Cell Metab.* 26, 842-855.e5. <https://doi.org/10.1016/j.cmet.2017.09.018>
- García-Foncillas, J., Sunakawa, Y., Aderka, D., Wainberg, Z., Ronga, P., Witzler, P., Stintzing, S., 2019. Distinguishing Features of Cetuximab and Panitumumab in Colorectal Cancer and Other Solid Tumors. *Front. Oncol.* 9. <https://doi.org/10.3389/fonc.2019.00849>
- Gargalionis, A.N., Piperi, C., Adamopoulos, C., Papavassiliou, A.G., 2012. Histone modifications as a pathogenic mechanism of colorectal tumorigenesis. *Int. J. Biochem. Cell Biol.* 44, 1276–1289. <https://doi.org/10.1016/j.biocel.2012.05.002>
- Gaude, E., Frezza, C., 2016. Tissue-specific and convergent metabolic transformation of cancer correlates with metastatic potential and patient survival. *Nat. Commun.* 7, 13041. <https://doi.org/10.1038/ncomms13041>
- Gay, L.J., Mitrou, P.N., Keen, J., Bowman, R., Naguib, A., Cooke, J., Kuhnle, G.G., Burns, P.A., Luben, R., Lentjes, M., Khaw, K.-T., Ball, R.Y., Ibrahim, A.E., Arends, M.J., 2012. Dietary, lifestyle and clinicopathological factors associated with APC mutations and promoter methylation in colorectal cancers from the EPIC-Norfolk study. *J. Pathol.* 228, 405–415. <https://doi.org/10.1002/path.4085>
- Gemignani, F., Moreno, V., Landi, S., Moullan, N., Chabrier, A., Gutiérrez-Enríquez, S., Hall, J., Guino, E., Peinado, M.A., Capella, G., Canzian, F., 2004. A TP53 polymorphism is associated with increased risk of colorectal cancer and with reduced levels of TP53 mRNA. *Oncogene* 23, 1954–1956. <https://doi.org/10.1038/sj.onc.1207305>

- Genther Williams, S.M., Kuznicki, A.M., Andrade, P., Dolinski, B.M., Elbi, C., O'Hagan, R.C., Toniatti, C., 2015. Treatment with the PARP inhibitor, niraparib, sensitizes colorectal cancer cell lines to irinotecan regardless of MSI/MSS status. *Cancer Cell Int.* 15, 14. <https://doi.org/10.1186/s12935-015-0162-8>
- Giantonio, B.J., Catalano, P.J., Meropol, N.J., O'Dwyer, P.J., Mitchell, E.P., Alberts, S.R., Schwartz, M.A., Benson, A.B., Eastern Cooperative Oncology Group Study E3200, 2007. Bevacizumab in combination with oxaliplatin, fluorouracil, and leucovorin (FOLFOX4) for previously treated metastatic colorectal cancer: results from the Eastern Cooperative Oncology Group Study E3200. *J. Clin. Oncol. Off. J. Am. Soc. Clin. Oncol.* 25, 1539–1544. <https://doi.org/10.1200/JCO.2006.09.6305>
- Gibbs-Seymour, I., Fontana, P., Rack, J.G.M., Ahel, I., 2016. HPF1/C4orf27 Is a PARP-1-Interacting Protein that Regulates PARP-1 ADP-Ribosylation Activity. *Mol. Cell* 62, 432–442. <https://doi.org/10.1016/j.molcel.2016.03.008>
- Gibson, B.A., Kraus, W.L., 2012. New insights into the molecular and cellular functions of poly(ADP-ribose) and PARPs. *Nat. Rev. Mol. Cell Biol.* 13, 411–424. <https://doi.org/10.1038/nrm3376>
- Gibson, F.S., Gupta, D., Shorr, R., Rodriguez, R., 2011. An Efficient, Economical Synthesis of the Novel Anti-tumor Agent CPI-613. *Org. Process Res. Dev.* 15, 855–857. <https://doi.org/10.1021/op200091t>
- Glynne-Jones, R., Anyamene, N., Moran, B., Harrison, M., 2012. Neoadjuvant chemotherapy in MRI-staged high-risk rectal cancer in addition to or as an alternative to preoperative chemoradiation? *Ann. Oncol.* 23, 2517–2526. <https://doi.org/10.1093/annonc/mds010>
- Goel, H.L., Mercurio, A.M., 2013. VEGF targets the tumour cell. *Nat. Rev. Cancer* 13, 871–882. <https://doi.org/10.1038/nrc3627>
- Goh, H.-S., Yao, J., Smith, D.R., 1995. p53 Point Mutation and Survival in Colorectal Cancer Patients. *Cancer Res.* 55, 5217–5221.
- Gopal, A.A., Fernandez, B., Delano, J., Weissleder, R., Dubach, J.M., 2024. PARP trapping is governed by the PARP inhibitor dissociation rate constant. *Cell Chem. Biol.* 31, 1373–1382.e10. <https://doi.org/10.1016/j.chembiol.2023.12.019>
- Gorbunova, V., Beck, J.T., Hofheinz, R.-D., Garcia-Alfonso, P., Nechaeva, M., Cubillo Gracian, A., Mangel, L., Elez Fernandez, E., Deming, D.A., Ramanathan, R.K., Torres, A.H., Sullivan, D., Luo, Y., Berlin, J.D., 2019. A phase 2 randomised study of veliparib plus FOLFIRI±bevacizumab versus placebo plus FOLFIRI±bevacizumab in metastatic colorectal cancer. *Br. J. Cancer* 120, 183–189. <https://doi.org/10.1038/s41416-018-0343-z>
- Gourdier, I., Del Rio, M., Crabbé, L., Candeil, L., Copois, V., Ychou, M., Auffray, C., Martineau, P., Mechti, N., Pommier, Y., Pau, B., 2002. Drug specific resistance to oxaliplatin is associated with apoptosis defect in a cellular model of colon carcinoma. *FEBS Lett.* 529, 232–236. [https://doi.org/10.1016/s0014-5793\(02\)03347-1](https://doi.org/10.1016/s0014-5793(02)03347-1)
- Grabinger, T., Luks, L., Kostadinova, F., Zimmerlin, C., Medema, J.P., Leist, M., Brunner, T., 2014. Ex vivo culture of intestinal crypt organoids as a model system for assessing cell death induction in intestinal epithelial cells and enteropathy. *Cell Death Dis.* 5, e1228–e1228. <https://doi.org/10.1038/cddis.2014.183>
- Grady, W.M., 2003. Genetic testing for high-risk colon cancer patients. *Gastroenterology* 124, 1574–1594. [https://doi.org/10.1016/s0016-5085\(03\)00376-7](https://doi.org/10.1016/s0016-5085(03)00376-7)
- Graham, M.A., Lockwood, G.F., Greenslade, D., Brienza, S., Bayssas, M., Gamelin, E., 2000. Clinical pharmacokinetics of oxaliplatin: a critical review. *Clin. Cancer Res. Off. J. Am. Assoc. Cancer Res.* 6, 1205–1218.
- Grassian, A.R., Lin, F., Barrett, R., Liu, Y., Jiang, W., Korpai, M., Astley, H., Gitterman, D., Henley, T., Howes, R., Levell, J., Korn, J.M., Pagliarini, R., 2012. Isocitrate Dehydrogenase (IDH) Mutations Promote a Reversible ZEB1/MicroRNA (miR)-200-dependent Epithelial-Mesenchymal Transition (EMT)*. *J. Biol. Chem.* 287, 42180–42194. <https://doi.org/10.1074/jbc.M112.417832>
- Greenhough, A., Wallam, C.A., Hicks, D.J., Moorghen, M., Williams, A.C., Paraskeva, C., 2010. The proapoptotic BH3-only protein Bim is downregulated in a subset of colorectal cancers

- and is repressed by antiapoptotic COX-2/PGE2 signalling in colorectal adenoma cells. *Oncogene* 29, 3398–3410. <https://doi.org/10.1038/onc.2010.94>
- Grothey, A., Cutsem, E.V., Sobrero, A., Siena, S., Falcone, A., Ychou, M., Humblet, Y., Bouché, O., Mineur, L., Barone, C., Adenis, A., Tabernero, J., Yoshino, T., Lenz, H.-J., Goldberg, R.M., Sargent, D.J., Cihon, F., Cupit, L., Wagner, A., Laurent, D., 2013. Regorafenib monotherapy for previously treated metastatic colorectal cancer (CORRECT): an international, multicentre, randomised, placebo-controlled, phase 3 trial. *The Lancet* 381, 303–312. [https://doi.org/10.1016/S0140-6736\(12\)61900-X](https://doi.org/10.1016/S0140-6736(12)61900-X)
- Grothey, A., Goldberg, R.M., 2004. A review of oxaliplatin and its clinical use in colorectal cancer. *Expert Opin. Pharmacother.* 5, 2159–2170. <https://doi.org/10.1517/14656566.5.10.2159>
- Grothey, A., Sobrero, A.F., Shields, A.F., Yoshino, T., Paul, J., Taieb, J., Souglakos, J., Shi, Q., Kerr, R., Labianca, R., Meyerhardt, J.A., Vernerey, D., Yamanaka, T., Boukovinas, I., Meyers, J.P., Renfro, L.A., Niedzwiecki, D., Watanabe, T., Torri, V., Saunders, M., Sargent, D.J., Andre, T., Iveson, T., 2018. Duration of Adjuvant Chemotherapy for Stage III Colon Cancer. *N. Engl. J. Med.* 378, 1177–1188. <https://doi.org/10.1056/NEJMoa1713709>
- Guglielmi, A.P., Sobrero, A.F., 2007. Second-Line Therapy for Advanced Colorectal Cancer. *Gastrointest. Cancer Res. GCR* 1, 57–63.
- Guinney, J., Dienstmann, R., Wang, X., de Reyniès, A., Schlicker, A., Soneson, C., Marisa, L., Roepman, P., Nyamundanda, G., Angelino, P., Bot, B.M., Morris, J.S., Simon, I.M., Gerster, S., Fessler, E., De Sousa E Melo, F., Missiaglia, E., Ramay, H., Barras, D., Homicsko, K., Maru, D., Manyam, G.C., Broom, B., Boige, V., Perez-Villamil, B., Laderas, T., Salazar, R., Gray, J.W., Hanahan, D., Tabernero, J., Bernardis, R., Friend, S.H., Laurent-Puig, P., Medema, J.P., Sadanandam, A., Wessels, L., Delorenzi, M., Kopetz, S., Vermeulen, L., Tejpar, S., 2015. The consensus molecular subtypes of colorectal cancer. *Nat. Med.* 21, 1350–1356. <https://doi.org/10.1038/nm.3967>
- Gupta, N., Huang, T.-T., Horibata, S., Lee, J.-M., 2022. Cell cycle checkpoints and beyond: Exploiting the ATR/CHK1/WEE1 pathway for the treatment of PARP inhibitor-resistant cancer. *Pharmacol. Res.* 178, 106162. <https://doi.org/10.1016/j.phrs.2022.106162>
- Hala, D., Faulkner, P., He, K., Kamalanathan, M., Brink, M., Simons, K., Apaydin, M., Hernout, B., Petersen, L.H., Ivanov, I., Qian, X., 2021. An integrated in vivo and in silico analysis of the metabolism disrupting effects of CPI-613 on embryo-larval zebrafish (*Danio rerio*). *Comp. Biochem. Physiol. Part C Toxicol. Pharmacol.* 248, 109084. <https://doi.org/10.1016/j.cbpc.2021.109084>
- Hall, J.M., Lee, M.K., Newman, B., Morrow, J.E., Anderson, L.A., Huey, B., King, M.-C., 1990. Linkage of Early-Onset Familial Breast Cancer to Chromosome 17q21. *Science* 250, 1684–1689. <https://doi.org/10.1126/science.2270482>
- Haller, D.G., 2000. Safety of oxaliplatin in the treatment of colorectal cancer. *Oncol. Williston Park* 14, 15–20.
- Haller, D.G., Tabernero, J., Maroun, J., de Braud, F., Price, T., Van Cutsem, E., Hill, M., Gilberg, F., Rittweger, K., Schmoll, H.-J., 2011. Capecitabine plus oxaliplatin compared with fluorouracil and folinic acid as adjuvant therapy for stage III colon cancer. *J. Clin. Oncol. Off. J. Am. Soc. Clin. Oncol.* 29, 1465–1471. <https://doi.org/10.1200/JCO.2010.33.6297>
- Han, J., Jackson, D., Holm, J., Turner, K., Ashcraft, P., Wang, X., Cook, B., Arning, E., Genta, R.M., Venuprasad, K., Souza, R.F., Sweetman, L., Theiss, A.L., 2018. Elevated d-2-hydroxyglutarate during colitis drives progression to colorectal cancer. *Proc. Natl. Acad. Sci. U. S. A.* 115, 1057–1062. <https://doi.org/10.1073/pnas.1712625115>
- Hanahan, D., 2022. Hallmarks of Cancer: New Dimensions. *Cancer Discov.* 12, 31–46. <https://doi.org/10.1158/2159-8290.CD-21-1059>
- Hankey, W., Frankel, W.L., Groden, J., 2018. Functions of the APC tumor suppressor protein dependent and independent of canonical WNT signaling: Implications for therapeutic targeting. *Cancer Metastasis Rev.* 37, 159–172. <https://doi.org/10.1007/s10555-017-9725-6>

- Hao, Y., Baker, D., ten Dijke, P., 2019. TGF- β -Mediated Epithelial-Mesenchymal Transition and Cancer Metastasis. *Int. J. Mol. Sci.* 20, 2767. <https://doi.org/10.3390/ijms20112767>
- Hao, Y., Samuels, Y., Li, Q., Krokowski, D., Guan, B.-J., Wang, C., Jin, Z., Dong, B., Cao, B., Feng, X., Xiang, M., Xu, C., Fink, S., Meropol, N.J., Xu, Y., Conlon, R.A., Markowitz, S., Kinzler, K.W., Velculescu, V.E., Brunengraber, H., Willis, J.E., LaFramboise, T., Hatzoglou, M., Zhang, G.-F., Vogelstein, B., Wang, Z., 2016. Oncogenic PIK3CA mutations reprogram glutamine metabolism in colorectal cancer. *Nat. Commun.* 7, 1–13. <https://doi.org/10.1038/ncomms11971>
- Hatch, S.B., Swift, L.P., Caporali, S., Carter, R., Hill, E.J., MacGregor, T.P., D'Atri, S., Middleton, M.R., McHugh, P.J., Sharma, R.A., 2014. XPF protein levels determine sensitivity of malignant melanoma cells to oxaliplatin chemotherapy: suitability as a biomarker for patient selection. *Int. J. Cancer* 134, 1495–1503. <https://doi.org/10.1002/ijc.28454>
- He, T.C., Sparks, A.B., Rago, C., Hermeking, H., Zawel, L., da Costa, L.T., Morin, P.J., Vogelstein, B., Kinzler, K.W., 1998. Identification of c-MYC as a target of the APC pathway. *Science* 281, 1509–1512. <https://doi.org/10.1126/science.281.5382.1509>
- Heeke, A.L., Pishvaian, M.J., Lynce, F., Xiu, J., Brody, J.R., Chen, W.-J., Baker, T.M., Marshall, J.L., Isaacs, C., 2018. Prevalence of Homologous Recombination-Related Gene Mutations Across Multiple Cancer Types. *JCO Precis. Oncol.* 1–13. <https://doi.org/10.1200/PO.17.00286>
- Heidelberger, C., Chaudhuri, N.K., Danneberg, P., Mooren, D., Griesbach, L., Duschinsky, R., Schnitzer, R.J., Plevin, E., Scheiner, J., 1957. Fluorinated Pyrimidines, A New Class of Tumour-Inhibitory Compounds. *Nature* 179, 663–666. <https://doi.org/10.1038/179663a0>
- Herbertz, S., Sawyer, J.S., Stauber, A.J., Gueorguieva, I., Driscoll, K.E., Estrem, S.T., Cleverly, A.L., Desai, D., Guba, S.C., Benhadji, K.A., Slapak, C.A., Lahn, M.M., 2015. Clinical development of galunisertib (LY2157299 monohydrate), a small molecule inhibitor of transforming growth factor-beta signaling pathway. *Drug Des. Devel. Ther.* 9, 4479–4499. <https://doi.org/10.2147/DDDT.S86621>
- Hernandez, J.M., Farma, J.M., Coppola, D., Hakam, A., Fulp, W.J., Chen, D.-T., Siegel, E.M., Yeatman, T.J., Shibata, D., 2011. Expression of the Antiapoptotic Protein Survivin in Colon Cancer. *Clin. Colorectal Cancer* 10, 188–193. <https://doi.org/10.1016/j.clcc.2011.03.014>
- Hetz, C., Zhang, K., Kaufman, R.J., 2020. Mechanism, regulation and functions of the unfolded protein response. *Nat. Rev. Mol. Cell Biol.* 21, 421–438. <https://doi.org/10.1038/s41580-020-0250-z>
- Hewish, M., Lord, C.J., Martin, S.A., Cunningham, D., Ashworth, A., 2010. Mismatch repair deficient colorectal cancer in the era of personalized treatment. *Nat. Rev. Clin. Oncol.* 7, 197–208. <https://doi.org/10.1038/nrclinonc.2010.18>
- Hopkins, T.A., Ainsworth, W.B., Ellis, P.A., Donawho, C.K., DiGiammarino, E.L., Panchal, S.C., Abraham, V.C., Algire, M.A., Shi, Y., Olson, A.M., Johnson, E.F., Wilsbacher, J.L., Maag, D., 2019. PARP1 Trapping by PARP Inhibitors Drives Cytotoxicity in Both Cancer Cells and Healthy Bone Marrow. *Mol. Cancer Res.* 17, 409–419. <https://doi.org/10.1158/1541-7786.MCR-18-0138>
- Hopkins, T.A., Shi, Y., Rodriguez, L.E., Solomon, L.R., Donawho, C.K., DiGiammarino, E.L., Panchal, S.C., Wilsbacher, J.L., Gao, W., Olson, A.M., Stolarik, D.F., Osterling, D.J., Johnson, E.F., Maag, D., 2015. Mechanistic Dissection of PARP1 Trapping and the Impact on In Vivo Tolerability and Efficacy of PARP Inhibitors. *Mol. Cancer Res.* 13, 1465–1477. <https://doi.org/10.1158/1541-7786.MCR-15-0191-T>
- Hoppe, M.M., Jaynes, P., Wardyn, J.D., Upadhyayula, S.S., Tan, T.Z., Lie, S., Lim, D.G.Z., Pang, B.N.K., Lim, S., P S Yeong, J., Karnezis, A., Chiu, D.S., Leung, S., Huntsman, D.G., Sedukhina, A.S., Sato, K., Topp, M.D., Scott, C.L., Choi, H., Patel, N.R., Brown, R., Kaye, S.B., Pitt, J.J., Tan, D.S.P., Jeyasekharan, A.D., 2021. Quantitative imaging of RAD51 expression as a marker of platinum resistance in ovarian cancer. *EMBO Mol. Med.* 13, e13366. <https://doi.org/10.15252/emmm.202013366>

- Hoppe, M.M., Sundar, R., Tan, D.S.P., Jeyasekharan, A.D., 2018. Biomarkers for Homologous Recombination Deficiency in Cancer. *JNCI J. Natl. Cancer Inst.* 110, 704–713. <https://doi.org/10.1093/jnci/djy085>
- Hou, J.-Y., Cao, J., Gao, L.-J., Zhang, F.-P., Shen, J., Zhou, L., Shi, J.-Y., Feng, Y.-L., Yan, Z., Wang, D.-P., Cao, J.-M., 2021. Upregulation of α enolase (ENO1) crotonylation in colorectal cancer and its promoting effect on cancer cell metastasis. *Biochem. Biophys. Res. Commun.* 578, 77–83. <https://doi.org/10.1016/j.bbrc.2021.09.027>
- Howell, S.B., Safaei, R., Larson, C.A., Sailor, M.J., 2010. Copper transporters and the cellular pharmacology of the platinum-containing cancer drugs. *Mol. Pharmacol.* 77, 887–894. <https://doi.org/10.1124/mol.109.063172>
- Hruba, L., Das, V., Hajduch, M., Dzubak, P., 2023. Nucleoside-based anticancer drugs: Mechanism of action and drug resistance. *Biochem. Pharmacol.* 215, 115741. <https://doi.org/10.1016/j.bcp.2023.115741>
- Hsieh, C.-C., Hsu, S.-H., Lin, C.-Y., Liaw, H.-J., Li, T.-W., Jiang, K.-Y., Chiang, N.-J., Chen, S.-H., Lin, B.-W., Chen, P.-C., Chan, R.-H., Lin, P.-C., Yeh, Y.-M., Shen, C.-H., 2022. CHK2 activation contributes to the development of oxaliplatin resistance in colorectal cancer. *Br. J. Cancer* 127, 1615–1628. <https://doi.org/10.1038/s41416-022-01946-9>
- Hu, J., Locasale, J.W., Bielas, J.H., O'Sullivan, J., Sheahan, K., Cantley, L.C., Heiden, M.G.V., Vitkup, D., 2013. Heterogeneity of tumor-induced gene expression changes in the human metabolic network. *Nat. Biotechnol.* 31, 522–529. <https://doi.org/10.1038/nbt.2530>
- Huang, F., Zhang, Q., Ma, H., Lv, Q., Zhang, T., 2014. Expression of glutaminase is upregulated in colorectal cancer and of clinical significance. *Int. J. Clin. Exp. Pathol.* 7, 1093–1100.
- Huang, J., Tseng, L.-H., Parini, V., Lokhandwala, P.M., Pallavajjala, A., Rodriguez, E., Xian, R., Chen, L., Gocke, C.D., Eshleman, J.R., Lin, M.-T., 2021. IDH1 and IDH2 Mutations in Colorectal Cancers. *Am. J. Clin. Pathol.* 156, 777–786. <https://doi.org/10.1093/ajcp/aqab023>
- Huang, Q., Chen, Z., Cheng, P., Jiang, Z., Wang, Z., Huang, Y., Yang, C., Pan, J., Qiu, F., Huang, J., 2019. LYRM2 directly regulates complex I activity to support tumor growth in colorectal cancer by oxidative phosphorylation. *Cancer Lett.* 455, 36–47. <https://doi.org/10.1016/j.canlet.2019.04.021>
- Hübner, A., Barrett, T., Flavell, R.A., Davis, R.J., 2008. Multi-site Phosphorylation Regulates Bim Stability and Apoptotic Activity. *Mol. Cell* 30, 415–425. <https://doi.org/10.1016/j.molcel.2008.03.025>
- Hurwitz, H., Fehrenbacher, L., Novotny, W., Cartwright, T., Hainsworth, J., Heim, W., Berlin, J., Baron, A., Griffing, S., Holmgren, E., Ferrara, N., Fyfe, G., Rogers, B., Ross, R., Kabbinavar, F., 2004. Bevacizumab plus Irinotecan, Fluorouracil, and Leucovorin for Metastatic Colorectal Cancer. *N. Engl. J. Med.* 350, 2335–2342. <https://doi.org/10.1056/NEJMoa032691>
- Hutton, J.E., Wang, X., Zimmerman, L.J., Slebos, R.J.C., Trenary, I.A., Young, J.D., Li, M., Liebler, D.C., 2016. Oncogenic KRAS and BRAF Drive Metabolic Reprogramming in Colorectal Cancer. *Mol. Cell. Proteomics* 15, 2924–2938. <https://doi.org/10.1074/mcp.M116.058925>
- Iacopetta, B., 2003. TP53 mutation in colorectal cancer. *Hum. Mutat.* 21, 271–276. <https://doi.org/10.1002/humu.10175>
- Inigo, M., Deja, S., Burgess, S.C., 2021. Ins and Outs of the TCA Cycle: The Central Role of Anaplerosis. *Annu. Rev. Nutr.* 41, 19–47. <https://doi.org/10.1146/annurev-nutr-120420-025558>
- Iwaizumi, M., Tseng-Rogenski, S., Carethers, J.M., 2011. DNA mismatch repair proficiency executing 5-fluorouracil cytotoxicity in colorectal cancer cells. *Cancer Biol. Ther.* <https://doi.org/10.4161/cbt.12.8.17169>
- Iwamoto, M., Kawada, K., Nakamoto, Y., Itatani, Y., Inamoto, S., Toda, K., Kimura, H., Sasazuki, T., Shirasawa, S., Okuyama, H., Inoue, M., Hasegawa, S., Togashi, K., Sakai, Y., 2014. Regulation of 18F-FDG accumulation in colorectal cancer cells with mutated

- KRAS. *J. Nucl. Med. Off. Publ. Soc. Nucl. Med.* 55, 2038–2044.
<https://doi.org/10.2967/jnumed.114.142927>
- Jarrar, A., Lotti, F., DeVecchio, J., Ferrandon, S., Gantt, G., Mace, A., Karagkounis, G., Orloff, M., Venere, M., Hitomi, M., Lathia, J., Rich, J.N., Kalady, M.F., 2019. Poly(ADP-Ribose) Polymerase Inhibition Sensitizes Colorectal Cancer-Initiating Cells to Chemotherapy. *Stem Cells* 37, 42–53. <https://doi.org/10.1002/stem.2929>
- Jasperson, K.W., Tuohy, T.M., Neklason, D.W., Burt, R.W., 2010. Hereditary and Familial Colon Cancer. *Gastroenterology, Colon Cancer: An Update and Future Directions* 138, 2044–2058. <https://doi.org/10.1053/j.gastro.2010.01.054>
- Jenkins, L.J., Luk, I.Y., Chionh, F., Tan, T., Needham, K., Ayton, J., Reehorst, C.M., Vukelic, N., Sieber, O.M., Mouradov, D., Gibbs, P., Williams, D.S., Tebbutt, N.C., Desai, J., Hollande, F., Dhillon, A.S., Lee, E.F., Merino, D., Fairlie, W.D., Mariadason, J.M., 2024. BCL-XL inhibitors enhance the apoptotic efficacy of BRAF inhibitors in BRAFV600E colorectal cancer. *Cell Death Dis.* 15, 1–9. <https://doi.org/10.1038/s41419-024-06478-z>
- Jia, Z., An, J., Liu, Z., Zhang, F., 2022. Non-Coding RNAs in Colorectal Cancer: Their Functions and Mechanisms. *Front. Oncol.* 12.
- Jiso, A., Demuth, P., Bachowsky, M., Haas, M., Seiwert, N., Heylmann, D., Rasenberger, B., Christmann, M., Dietrich, L., Brunner, T., Riyanti, Schäberle, T.F., Plubrukarn, A., Fahrner, J., 2021a. Natural Merosesquiterpenes Activate the DNA Damage Response via DNA Strand Break Formation and Trigger Apoptotic Cell Death in p53-Wild-Type and Mutant Colorectal Cancer. *Cancers* 13, 3282. <https://doi.org/10.3390/cancers13133282>
- Jiso, A., Yurasakpong, L., Janta, S., Chaithirayanon, K., Plubrukarn, A., 2021b. Exerting DNA Damaging Effects of the Ilimaquinones through the Active Hydroquinone Species. *Sci. Pharm.* 89, 26. <https://doi.org/10.3390/scipharm89020026>
- Jones, P.A., Baylin, S.B., 2007. The Epigenomics of Cancer. *Cell* 128, 683–692.
<https://doi.org/10.1016/j.cell.2007.01.029>
- Jonker, D.J., O’Callaghan, C.J., Karapetis, C.S., Zalcborg, J.R., Tu, D., Au, H.-J., Berry, S.R., Krahn, M., Price, T., Simes, R.J., Tebbutt, N.C., van Hazel, G., Wierzbiicki, R., Langer, C., Moore, M.J., 2007. Cetuximab for the Treatment of Colorectal Cancer. *N. Engl. J. Med.* 357, 2040–2048. <https://doi.org/10.1056/NEJMoa071834>
- Jonsson, P., Bandlamudi, C., Cheng, M.L., Srinivasan, P., Chavan, S.S., Friedman, N.D., Rosen, E.Y., Richards, A.L., Bouvier, N., Selcuklu, S.D., Bielski, C.M., Abida, W., Mandelker, D., Birsoy, O., Zhang, L., Zehir, A., Donoghue, M.T.A., Baselga, J., Offit, K., Scher, H.I., O’Reilly, E.M., Stadler, Z.K., Schultz, N., Socci, N.D., Viale, A., Ladanyi, M., Robson, M.E., Hyman, D.M., Berger, M.F., Solit, D.B., Taylor, B.S., 2019. Tumour lineage shapes BRCA-mediated phenotypes. *Nature* 571, 576–579.
<https://doi.org/10.1038/s41586-019-1382-1>
- Jossé, R., Martin, S.E., Guha, R., Ormanoglu, P., Pfister, T.D., Reaper, P.M., Barnes, C.S., Jones, J., Charlton, P., Pollard, J.R., Morris, J., Doroshov, J.H., Pommier, Y., 2014. ATR Inhibitors VE-821 and VX-970 Sensitize Cancer Cells to Topoisomerase I Inhibitors by Disabling DNA Replication Initiation and Fork Elongation Responses. *Cancer Res.* 74, 6968–6979. <https://doi.org/10.1158/0008-5472.CAN-13-3369>
- Joyce, J.A., Pollard, J.W., 2009. Microenvironmental regulation of metastasis. *Nat. Rev. Cancer* 9, 239–252. <https://doi.org/10.1038/nrc2618>
- Jubin, T., Kadam, A., Jariwala, M., Bhatt, S., Sutariya, S., Gani, A.R., Gautam, S., Begum, R., 2016. The PARP family: insights into functional aspects of poly (ADP-ribose) polymerase-1 in cell growth and survival. *Cell Prolif.* 49, 421–437. <https://doi.org/10.1111/cpr.12268>
- Jung, G., Hernández-Illán, E., Moreira, L., Balaguer, F., Goel, A., 2020. Epigenetics of colorectal cancer: biomarker and therapeutic potential. *Nat. Rev. Gastroenterol. Hepatol.* 17, 111–130. <https://doi.org/10.1038/s41575-019-0230-y>
- Kanev, P.-B., Varhoshkova, S., Georgieva, I., Lukarska, M., Kirova, D., Danovski, G., Stoyanov, S., Aleksandrov, R., 2024. A unified mechanism for PARP inhibitor-induced PARP1 chromatin retention at DNA damage sites in living cells. *Cell Rep.* 43.
<https://doi.org/10.1016/j.celrep.2024.114234>

- Kannarkatt, J., Joseph, J., Kurniali, P.C., Al-Janadi, A., Hrinczenko, B., 2017. Adjuvant Chemotherapy for Stage II Colon Cancer: A Clinical Dilemma. *J. Oncol. Pract.* 13, 233–241. <https://doi.org/10.1200/JOP.2016.017210>
- Karimian, A., Ahmadi, Y., Yousefi, B., 2016. Multiple functions of p21 in cell cycle, apoptosis and transcriptional regulation after DNA damage. *DNA Repair* 42, 63–71. <https://doi.org/10.1016/j.dnarep.2016.04.008>
- Kaundal, R.K., Shah, K.K., Sharma, S.S., 2006. Neuroprotective effects of NU1025, a PARP inhibitor in cerebral ischemia are mediated through reduction in NAD depletion and DNA fragmentation. *Life Sci.* 79, 2293–2302. <https://doi.org/10.1016/j.lfs.2006.07.034>
- Kauppinen, T.M., Chan, W.Y., Suh, S.W., Wiggins, A.K., Huang, E.J., Swanson, R.A., 2006. Direct phosphorylation and regulation of poly(ADP-ribose) polymerase-1 by extracellular signal-regulated kinases 1/2. *Proc. Natl. Acad. Sci. U. S. A.* 103, 7136–7141. <https://doi.org/10.1073/pnas.0508606103>
- Kerk, S.A., Papagiannakopoulos, T., Shah, Y.M., Lyssiotis, C.A., 2021. Metabolic networks in mutant KRAS-driven tumours: tissue specificities and the microenvironment. *Nat. Rev. Cancer* 21, 510–525. <https://doi.org/10.1038/s41568-021-00375-9>
- Keum, N., Giovannucci, E., 2019. Global burden of colorectal cancer: emerging trends, risk factors and prevention strategies. *Nat. Rev. Gastroenterol. Hepatol.* 16, 713–732. <https://doi.org/10.1038/s41575-019-0189-8>
- Khan, H.Y., Kamgar, M., Aboukameel, A., Bannoura, S., Chung, B.Y., Li, Y., Hallak, M.N.A., Philip, P.A., Tsai, S., Luther, S., Hall, W.A., Azmi, A.S., 2023. Targeting Cellular Metabolism With CPI-613 Sensitizes Pancreatic Cancer Cells to Radiation Therapy. *Adv. Radiat. Oncol.* 8, 101122. <https://doi.org/10.1016/j.adro.2022.101122>
- Kikuchi, H., Pino, M.S., Zeng, M., Shirasawa, S., Chung, D.C., 2009. Oncogenic KRAS and BRAF Differentially Regulate Hypoxia-Inducible Factor-1 α and -2 α in Colon Cancer. *Cancer Res.* 69, 8499–8506. <https://doi.org/10.1158/0008-5472.CAN-09-2213>
- Kim, D.-S., Camacho, C.V., Kraus, W.L., 2021. Alternate therapeutic pathways for PARP inhibitors and potential mechanisms of resistance. *Exp. Mol. Med.* 53, 42–51. <https://doi.org/10.1038/s12276-021-00557-3>
- Kim, H., George, E., Ragland, R., Rafail, S., Zhang, R., Krepler, C., Morgan, M., Herlyn, M., Brown, E., Simpkins, F., 2017. Targeting the ATR/CHK1 Axis with PARP Inhibition Results in Tumor Regression in BRCA-Mutant Ovarian Cancer Models. *Clin. Cancer Res. Off. J. Am. Assoc. Cancer Res.* 23, 3097–3108. <https://doi.org/10.1158/1078-0432.CCR-16-2273>
- Kim, H., Xu, H., George, E., Hallberg, D., Kumar, S., Jagannathan, V., Medvedev, S., Kinose, Y., Devins, K., Verma, P., Ly, K., Wang, Y., Greenberg, R.A., Schwartz, L., Johnson, N., Scharpf, R.B., Mills, G.B., Zhang, R., Velculescu, V.E., Brown, E.J., Simpkins, F., 2020. Combining PARP with ATR inhibition overcomes PARP inhibitor and platinum resistance in ovarian cancer models. *Nat. Commun.* 11, 3726. <https://doi.org/10.1038/s41467-020-17127-2>
- Kim, J.C., Bodmer, W.F., 2022. Genomic landscape of colorectal carcinogenesis. *J. Cancer Res. Clin. Oncol.* 148, 533–545. <https://doi.org/10.1007/s00432-021-03888-w>
- Kim, T.W., Lee, K.W., Ahn, J.B., Lee, J., Ryu, J., Oh, B., Ock, C.-Y., Hwang, S., Hahm, K.B., Kim, S.-J., Park, Y.S., 2021. Efficacy and safety of vactosertib and pembrolizumab combination in patients with previously treated microsatellite stable metastatic colorectal cancer. *J. Clin. Oncol.* 39, 3573–3573. https://doi.org/10.1200/JCO.2021.39.15_suppl.3573
- Kinoshita, T., Nakanishi, I., Warizaya, M., Iwashita, A., Kido, Y., Hattori, K., Fujii, T., 2004. Inhibitor-induced structural change of the active site of human poly(ADP-ribose) polymerase. *FEBS Lett.* 556, 43–46. [https://doi.org/10.1016/s0014-5793\(03\)01362-0](https://doi.org/10.1016/s0014-5793(03)01362-0)
- Klauschen, F., von Winterfeld, M., Stenzinger, A., Sinn, B.V., Budczies, J., Kamphues, C., Bahra, M., Wittschieber, D., Weichert, W., Striefler, J., Riess, H., Dietel, M., Denkert, C., 2012. High nuclear poly-(ADP-ribose)-polymerase expression is prognostic of improved survival in pancreatic cancer. *Histopathology* 61, 409–416. <https://doi.org/10.1111/j.1365-2559.2012.04225.x>

References

- Kline, C.L.B., Schiccitano, A., Zhu, J., Beachler, C., Sheikh, H., Harvey, H.A., Mackley, H.B., McKenna, K., Staveley-O'Carroll, K., Poritz, L., Messaris, E., Stewart, D., Sivik, J., El-Deiry, W.S., 2014. Personalized Dosing via Pharmacokinetic Monitoring of 5-Fluorouracil Might Reduce Toxicity in Early- or Late-Stage Colorectal Cancer Patients Treated With Infusional 5-Fluorouracil-Based Chemotherapy Regimens. *Clin. Colorectal Cancer* 13, 119–126. <https://doi.org/10.1016/j.clcc.2013.11.001>
- Knezevic, C.E., Wright, G., Remsing Rix, L.L., Kim, W., Kuenzi, B.M., Luo, Y., Watters, J.M., Koomen, J.M., Haura, E.B., Monteiro, A.N., Radu, C., Lawrence, H.R., Rix, U., 2016. Proteome-wide Profiling of Clinical PARP Inhibitors Reveals Compound-Specific Secondary Targets. *Cell Chem. Biol.* 23, 1490–1503. <https://doi.org/10.1016/j.chembiol.2016.10.011>
- Kodama, M., Oshikawa, K., Shimizu, H., Yoshioka, S., Takahashi, M., Izumi, Y., Bamba, T., Tateishi, C., Tomonaga, T., Matsumoto, M., Nakayama, K.I., 2020. A shift in glutamine nitrogen metabolism contributes to the malignant progression of cancer. *Nat. Commun.* 11, 1320. <https://doi.org/10.1038/s41467-020-15136-9>
- Koh, D.W., Lawler, A.M., Poitras, M.F., Sasaki, M., Wattler, S., Nehls, M.C., Stöger, T., Poirier, G.G., Dawson, V.L., Dawson, T.M., 2004. Failure to degrade poly(ADP-ribose) causes increased sensitivity to cytotoxicity and early embryonic lethality. *Proc. Natl. Acad. Sci. U. S. A.* 101, 17699–17704. <https://doi.org/10.1073/pnas.0406182101>
- Koncošová, M., Vrzáčková, N., Křížová, I., Tomášová, P., Rimpelová, S., Dvořák, A., Vitek, L., Rumlová, M., Ruml, T., Zelenka, J., 2021. Inhibition of Mitochondrial Metabolism Leads to Selective Eradication of Cells Adapted to Acidic Microenvironment. *Int. J. Mol. Sci.* 22, 10790. <https://doi.org/10.3390/ijms221910790>
- Kong, D., Aoki, S., Sowa, Y., Sakai, T., Kobayashi, M., 2008. Smenospongine, a sesquiterpene aminoquinone from a marine sponge, induces G1 arrest or apoptosis in different leukemia cells. *Mar. Drugs* 6, 480–488. <https://doi.org/10.3390/md20080023>
- Koo, K.-M., Kim, C.-D., Kim, H., Cho, Y.-W., Suhito, I.R., Kim, T.-H., 2023. Extracellularly Detectable Electrochemical Signals of Living Cells Originate from Metabolic Reactions. *Adv. Sci.* 10, 2207084. <https://doi.org/10.1002/adv.202207084>
- Koopman, M., Kortman, G. a. M., Mekenkamp, L., Ligtenberg, M.J.L., Hoogerbrugge, N., Antonini, N.F., Punt, C.J.A., van Krieken, J.H.J.M., 2009. Deficient mismatch repair system in patients with sporadic advanced colorectal cancer. *Br. J. Cancer* 100, 266–273. <https://doi.org/10.1038/sj.bjc.6604867>
- Kopetz, S., Grothey, A., Yaeger, R., Cutsem, E.V., Desai, J., Yoshino, T., Wasan, H., Ciardiello, F., Loupakis, F., Hong, Y.S., Steeghs, N., Guren, T.K., Arkenau, H.-T., Garcia-Alfonso, P., Pfeiffer, P., Orlov, S., Lonardi, S., Elez, E., Kim, T.-W., Schellens, J.H.M., Guo, C., Krishnan, A., Dekervel, J., Morris, V., Ferrandiz, A.C., Tarpgaard, L.S., Braun, M., Gollerkeri, A., Keir, C., Maharry, K., Pickard, M., Christy-Bittel, J., Anderson, L., Sandor, V., Taberner, J., 2019. Encorafenib, Binimetinib, and Cetuximab in BRAF V600E-Mutated Colorectal Cancer. *N. Engl. J. Med.* 381, 1632–1643. <https://doi.org/10.1056/NEJMoa1908075>
- Kuebler, J.P., Wieand, H.S., O'Connell, M.J., Smith, R.E., Colangelo, L.H., Yothers, G., Petrelli, N.J., Findlay, M.P., Seay, T.E., Atkins, J.N., Zapas, J.L., Goodwin, J.W., Fehrenbacher, L., Ramanathan, R.K., Conley, B.A., Flynn, P.J., Soori, G., Colman, L.K., Levine, E.A., Lanier, K.S., Wolmark, N., 2007. Oxaliplatin Combined With Weekly Bolus Fluorouracil and Leucovorin As Surgical Adjuvant Chemotherapy for Stage II and III Colon Cancer: Results From NSABP C-07. *J. Clin. Oncol.* 25, 2198–2204. <https://doi.org/10.1200/JCO.2006.08.2974>
- Kuipers, E.J., Grady, W.M., Lieberman, D., Seufferlein, T., Sung, J.J., Boelens, P.G., van de Velde, C.J.H., Watanabe, T., 2015. Colorectal cancer. *Nat. Rev. Dis. Primer* 1, 15065. <https://doi.org/10.1038/nrdp.2015.65>
- Kumstel, S., Schreiber, T., Goldstein, L., Stenzel, J., Lindner, T., Joks, M., Zhang, X., Wendt, E.H.U., Schönrogge, M., Krause, B., Vollmar, B., Zechner, D., 2022. Targeting pancreatic cancer with combinatorial treatment of CPI-613 and inhibitors of lactate metabolism. *PLOS ONE* 17, e0266601. <https://doi.org/10.1371/journal.pone.0266601>

References

- Kun, E., Kirsten, E., Ordahl, C.P., 2002. Coenzymatic activity of randomly broken or intact double-stranded DNAs in auto and histone H1 trans-poly(ADP-ribosylation), catalyzed by poly(ADP-ribose) polymerase (PARP I). *J. Biol. Chem.* 277, 39066–39069. <https://doi.org/10.1074/jbc.C200410200>
- Kung, A.L., 2007. Practices and pitfalls of mouse cancer models in drug discovery. *Adv. Cancer Res.* 96, 191–212. [https://doi.org/10.1016/S0065-230X\(06\)96007-2](https://doi.org/10.1016/S0065-230X(06)96007-2)
- Kuo, C.-C., Wu, J.-Y., Wu, K.K., 2022. Cancer-derived extracellular succinate: a driver of cancer metastasis. *J. Biomed. Sci.* 29, 93. <https://doi.org/10.1186/s12929-022-00878-z>
- Kwak, C.-H., Jin, L., Han, J.H., Han, C.W., Kim, E., Cho, M., Chung, T.-W., Bae, S.-J., Jang, S.B., Ha, K.-T., 2020. Ilimaquinone Induces the Apoptotic Cell Death of Cancer Cells by Reducing Pyruvate Dehydrogenase Kinase 1 Activity. *Int. J. Mol. Sci.* 21, 6021. <https://doi.org/10.3390/ijms21176021>
- Kweekel, D.M., Gelderblom, H., Guchelaar, H.-J., 2005. Pharmacology of oxaliplatin and the use of pharmacogenomics to individualize therapy. *Cancer Treat. Rev.* 31, 90–105. <https://doi.org/10.1016/j.ctrv.2004.12.006>
- Lahiguera, Á., Hyroššová, P., Figueras, A., Garzón, D., Moreno, R., Soto-Cerrato, V., McNeish, I., Serra, V., Lazaro, C., Barretina, P., Brunet, J., Menéndez, J., Matias-Guiu, X., Vidal, A., Villanueva, A., Taylor-Harding, B., Tanaka, H., Orsulic, S., Junza, A., Yanes, O., Muñoz-Pinedo, C., Palomero, L., Pujana, M.À., Perales, J.C., Viñals, F., 2020. Tumors defective in homologous recombination rely on oxidative metabolism: relevance to treatments with PARP inhibitors. *EMBO Mol. Med.* 12, e11217. <https://doi.org/10.15252/emmm.201911217>
- Lampropoulos, P., Zizi-Sermpetzoglou, A., Rizos, S., Kostakis, A., Nikiteas, N., Papavassiliou, A.G., 2012. TGF-beta signalling in colon carcinogenesis. *Cancer Lett.* 314, 1–7. <https://doi.org/10.1016/j.canlet.2011.09.041>
- Lang, L., Wang, F., Ding, Z., Zhao, X., Loveless, R., Xie, J., Shay, C., Qiu, P., Ke, Y., Saba, N.F., Teng, Y., 2021. Blockade of glutamine-dependent cell survival augments antitumor efficacy of CPI-613 in head and neck cancer. *J. Exp. Clin. Cancer Res.* 40, 393. <https://doi.org/10.1186/s13046-021-02207-y>
- Langelier, M.-F., Planck, J.L., Roy, S., Pascal, J.M., 2011. Crystal structures of poly(ADP-ribose) polymerase-1 (PARP-1) zinc fingers bound to DNA: structural and functional insights into DNA-dependent PARP-1 activity. *J. Biol. Chem.* 286, 10690–10701. <https://doi.org/10.1074/jbc.M110.202507>
- Langelier, M.-F., Ruhl, D.D., Planck, J.L., Kraus, W.L., Pascal, J.M., 2010. The Zn³ domain of human poly(ADP-ribose) polymerase-1 (PARP-1) functions in both DNA-dependent poly(ADP-ribose) synthesis activity and chromatin compaction. *J. Biol. Chem.* 285, 18877–18887. <https://doi.org/10.1074/jbc.M110.105668>
- Langelier, M.-F., Zandarashvili, L., Aguiar, P.M., Black, B.E., Pascal, J.M., 2018. NAD⁺ analog reveals PARP-1 substrate-blocking mechanism and allosteric communication from catalytic center to DNA-binding domains. *Nat. Commun.* 9, 844. <https://doi.org/10.1038/s41467-018-03234-8>
- Langley, R.R., Fidler, I.J., 2011. The seed and soil hypothesis revisited--the role of tumor-stroma interactions in metastasis to different organs. *Int. J. Cancer* 128, 2527–2535. <https://doi.org/10.1002/ijc.26031>
- Latchman, J., Guastella, A., Tofthagen, C., 2014. 5-Fluorouracil toxicity and dihydropyrimidine dehydrogenase enzyme: implications for practice. *Clin. J. Oncol. Nurs.* 18, 581–585. <https://doi.org/10.1188/14.CJON.581-585>
- Lawlor, D., Martin, P., Busschots, S., Thery, J., O'Leary, J.J., Hennessy, B.T., Stordal, B., 2014. PARP Inhibitors as P-glycoprotein Substrates. *J. Pharm. Sci.* 103, 1913–1920. <https://doi.org/10.1002/jps.23952>
- Le Dung, Uram Jennifer N., Wang Hao, Bartlett Bjarne R., Kemberling Holly, Eyring Aleksandra D., Skora Andrew D., Lubner Brandon S., Azad Nilofer S., Laheru Dan, Biedrzycki Barbara, Donehower Ross C., Zaheer Atif, Fisher George A., Crocenzi Todd S., Lee James J., Duffy Steven M., Goldberg Richard M., de la Chapelle Albert, Koshiji Minoru, Bhajee Feriyil, Huebner Thomas, Hruban Ralph H., Wood Laura D., Cuka Nathan, Pardoll Drew M.,

References

- Papadopoulos Nickolas, Kinzler Kenneth W., Zhou Shibin, Cornish Toby C., Taube Janis M., Anders Robert A., Eshleman James R., Vogelstein Bert, Diaz Luis A., 2015. PD-1 Blockade in Tumors with Mismatch-Repair Deficiency. *N. Engl. J. Med.* 372, 2509–2520. <https://doi.org/10.1056/NEJMoa1500596>
- Leclerc, D., Pham, D.N.T., Lévesque, N., Truongcao, M., Foulkes, W.D., Sapienza, C., Rozen, R., 2017. Oncogenic role of PDK4 in human colon cancer cells. *Br. J. Cancer* 116, 930–936. <https://doi.org/10.1038/bjc.2017.38>
- Lee, C.-Y., Cheng, W.-F., Lin, P.-H., Chen, Y.-L., Huang, S.-H., Lei, K.-H., Chang, K.-Y., Ko, M.-Y., Chi, P., 2023. An activity-based functional test for identifying homologous recombination deficiencies across cancer types in real time. *Cell Rep. Med.* 4, 101247. <https://doi.org/10.1016/j.xcrm.2023.101247>
- Lee, H.-Y., Chung, K.J., Hwang, I.H., Gwak, J., Park, S., Ju, B.G., Yun, E., Kim, D.-E., Chung, Y.-H., Na, M., Song, G.-Y., Oh, S., 2015. Activation of p53 with Ilimaquinone and Ethylsmenoquinone, Marine Sponge Metabolites, Induces Apoptosis and Autophagy in Colon Cancer Cells. *Mar. Drugs* 13, 543–557. <https://doi.org/10.3390/md13010543>
- Lee, K., Giltmane, J.M., Balko, J.M., Schwarz, L.J., Guerrero-Zotano, A.L., Hutchinson, K.E., Nixon, M.J., Estrada, M.V., Sánchez, V., Sanders, M.E., Lee, T., Gómez, H., Lluch, A., Pérez-Fidalgo, J.A., Wolf, M.M., Andrejeva, G., Rathmell, J.C., Fesik, S.W., Arteaga, C.L., 2017. MYC and MCL1 Cooperatively Promote Chemotherapy-Resistant Breast Cancer Stem Cells via Regulation of Mitochondrial Oxidative Phosphorylation. *Cell Metab.* 26, 633–647.e7. <https://doi.org/10.1016/j.cmet.2017.09.009>
- Lee, K.C., Maturo, C., Perera, C.N., Luddy, J., Rodriguez, R., Shorr, R., 2014. Translational assessment of mitochondrial dysfunction of pancreatic cancer from in vitro gene microarray and animal efficacy studies, to early clinical studies, via the novel tumor-specific anti-mitochondrial agent, CPI-613. *Ann. Transl. Med.* 2, 91. <https://doi.org/10.3978/j.issn.2305-5839.2014.05.08>
- Lee, K.C., Shorr, R., Rodriguez, R., Maturo, C., Boteju, L.W., Sheldon, A., 2011. Formation and anti-tumor activity of uncommon in vitro and in vivo metabolites of CPI-613, a novel anti-tumor compound that selectively alters tumor energy metabolism. *Drug Metab. Lett.* 5, 163–182. <https://doi.org/10.2174/187231211796904991>
- Lee, M.S., Kopetz, S., 2022. Are Homologous Recombination Deficiency Mutations Relevant in Colorectal Cancer? *JNCI J. Natl. Cancer Inst.* 114, 176–178. <https://doi.org/10.1093/jnci/djab170>
- Lei, K., Davis, R.J., 2003. JNK phosphorylation of Bim-related members of the Bcl2 family induces Bax-dependent apoptosis. *Proc. Natl. Acad. Sci.* 100, 2432–2437. <https://doi.org/10.1073/pnas.0438011100>
- Leichman, L., Groshen, S., O'Neil, B.H., Messersmith, W., Berlin, J., Chan, E., Leichman, C.G., Cohen, S.J., Cohen, D., Lenz, H.-J., Gold, P., Boman, B., Fielding, A., Locker, G., Cason, R.C., Hamilton, S.R., Hochster, H.S., 2016. Phase II Study of Olaparib (AZD-2281) After Standard Systemic Therapies for Disseminated Colorectal Cancer. *The Oncologist* 21, 172–177. <https://doi.org/10.1634/theoncologist.2015-0319>
- Lenz, H.-J.J., Cutsem, E.V., Limon, M.L., Wong, K.Y., Hendlisch, A., Aglietta, M., Garcia-Alfonso, P., Neyns, B., Luppi, G., Cardin, D., Dragovich, T., Shah, U., Atasoy, A., Postema, R., Boyd, Z., Ledezine, J.-M., Overman, M., Lonardi, S., 2018. Durable clinical benefit with nivolumab (NIVO) plus low-dose ipilimumab (IPI) as first-line therapy in microsatellite instability-high/mismatch repair deficient (MSI-H/dMMR) metastatic colorectal cancer (mCRC). *Ann. Oncol.* 29, viii714. <https://doi.org/10.1093/annonc/mdy424.019>
- Leoz, M.L., Carballal, S., Moreira, L., Ocaña, T., Balaguer, F., 2015. The genetic basis of familial adenomatous polyposis and its implications for clinical practice and risk management. *Appl. Clin. Genet.* 8, 95–107. <https://doi.org/10.2147/TACG.S51484>
- Lévi, F., Metzger, G., Massari, C., Milano, G., 2000. Oxaliplatin: pharmacokinetics and chronopharmacological aspects. *Clin. Pharmacokinet.* 38, 1–21. <https://doi.org/10.2165/00003088-200038010-00001>
- Ley, R., Balmano, K., Hadfield, K., Weston, C., Cook, S.J., 2003. Activation of the ERK1/2 signaling pathway promotes phosphorylation and proteasome-dependent degradation of

- the BH3-only protein, *Bim*. *J. Biol. Chem.* 278, 18811–18816. <https://doi.org/10.1074/jbc.M301010200>
- Li, B., Mi, J., Yuan, Q., 2024. Fatty acid metabolism-related enzymes in colorectal cancer metastasis: from biological function to molecular mechanism. *Cell Death Discov.* 10, 1–9. <https://doi.org/10.1038/s41420-024-02126-9>
- Li, H., Lu, S., Chen, Y., Zheng, L., Chen, L., Ding, H., Ding, J., Lou, D., Liu, F., Zheng, B., 2019. AKT2 phosphorylation of hexokinase 2 at T473 promotes tumorigenesis and metastasis in colon cancer cells via NF- κ B, HIF1 α , MMP2, and MMP9 upregulation. *Cell. Signal.* 58, 99–110. <https://doi.org/10.1016/j.cellsig.2019.03.011>
- Li, T., Kon, N., Jiang, L., Tan, M., Ludwig, T., Zhao, Y., Baer, R., Gu, W., 2012. Tumor suppression in the absence of p53-mediated cell-cycle arrest, apoptosis, and senescence. *Cell* 149, 1269–1283. <https://doi.org/10.1016/j.cell.2012.04.026>
- Liang, T.-J., Wang, H.-X., Zheng, Y.-Y., Cao, Y.-Q., Wu, X., Zhou, X., Dong, S.-X., 2017. APC hypermethylation for early diagnosis of colorectal cancer: a meta-analysis and literature review. *Oncotarget* 8, 46468–46479. <https://doi.org/10.18632/oncotarget.17576>
- Liénart, S., Merceron, R., Vanderaa, C., Lambert, F., Colau, D., Stockis, J., van der Woning, B., De Haard, H., Saunders, M., Coulie, P.G., Savvides, S.N., Lucas, S., 2018. Structural basis of latent TGF- β 1 presentation and activation by GARP on human regulatory T cells. *Science* 362, 952–956. <https://doi.org/10.1126/science.aau2909>
- Lin, C.-W., Bai, L.-Y., Su, J.-H., Chiu, C.-F., Lin, W.-Y., Huang, W.-T., Shih, M.-C., Huang, Y.-T., Hu, J.-L., Weng, J.-R., 2020. Ilimaquinone Induces Apoptosis and Autophagy in Human Oral Squamous Cell Carcinoma Cells. *Biomedicines* 8, 296. <https://doi.org/10.3390/biomedicines8090296>
- Liu, B., Parsons, R., Papadopoulos, N., Nicolaidis, N.C., Lynch, H.T., Watson, P., Jass, J.R., Dunlop, M., Wyllie, A., Peltomäki, P., Chapeele, A.D.L., Hamilton, S.R., Vogelstein, B., Kinzler, K.W., 1996. Analysis of mismatch repair genes in hereditary non-polyposis colorectal cancer patients. *Nat. Med.* 2, 169–174. <https://doi.org/10.1038/nm0296-169>
- Liu, C., Vyas, A., Kassab, M.A., Singh, A.K., Yu, X., 2017. The role of poly ADP-ribosylation in the first wave of DNA damage response. *Nucleic Acids Res.* 45, 8129–8141. <https://doi.org/10.1093/nar/gkx565>
- Liu, C., Zhang, W., Wang, J., Si, T., Xing, W., 2021. Tumor-associated macrophage-derived transforming growth factor- β promotes colorectal cancer progression through HIF1-TRIB3 signaling. *Cancer Sci.* 112, 4198–4207. <https://doi.org/10.1111/cas.15101>
- Liu, G., Zhu, J., Yu, Menglei, Cai, C., Zhou, Y., Yu, Min, Fu, Z., Nguyen, C., Yang, B., Li, Y., Zhou, Q., Lin, Q., Ye, H., Ye, L., Zhao, X., Li, Z., Chen, R., Han, F., Tang, C., Zeng, B., 2015. Glutamate dehydrogenase is a novel prognostic marker and predicts metastases in colorectal cancer patients. *J. Transl. Med.* 13, 144. <https://doi.org/10.1186/s12967-015-0500-6>
- Liu, H., Liang, Z., Zhou, C., Zeng, Z., Wang, F., Hu, T., He, X., Wu, Xiaojian, Wu, Xianrui, Lan, P., 2021. Mutant KRAS triggers functional reprogramming of tumor-associated macrophages in colorectal cancer. *Signal Transduct. Target. Ther.* 6, 1–13. <https://doi.org/10.1038/s41392-021-00534-2>
- Liu, W., Wu, M., Du, H., Shi, X., Zhang, T., Li, J., 2018. SIRT6 inhibits colorectal cancer stem cell proliferation by targeting CDC25A. *Oncol. Lett.* 15, 5368–5374. <https://doi.org/10.3892/ol.2018.7989>
- Liu, Y., Zhang, Y., Zhao, Y., Gao, D., Xing, J., Liu, H., 2016. High PARP-1 expression is associated with tumor invasion and poor prognosis in gastric cancer. *Oncol. Lett.* 12, 3825–3835. <https://doi.org/10.3892/ol.2016.5169>
- Lloyd, R.L., Wijnhoven, P.W.G., Ramos-Montoya, A., Wilson, Z., Illuzzi, G., Falenta, K., Jones, G.N., James, N., Chabbert, C.D., Stott, J., Dean, E., Lau, A., Young, L.A., 2020. Combined PARP and ATR inhibition potentiates genome instability and cell death in ATM-deficient cancer cells. *Oncogene* 39, 4869–4883. <https://doi.org/10.1038/s41388-020-1328-y>
- Longley, D.B., Harkin, D.P., Johnston, P.G., 2003. 5-Fluorouracil: mechanisms of action and clinical strategies. *Nat. Rev. Cancer* 3, 330–338. <https://doi.org/10.1038/nrc1074>

References

- Lonskaya, I., Potaman, V.N., Shlyakhtenko, L.S., Oussatcheva, E.A., Lyubchenko, Y.L., Soldatenkov, V.A., 2005. Regulation of poly(ADP-ribose) polymerase-1 by DNA structure-specific binding. *J. Biol. Chem.* 280, 17076–17083. <https://doi.org/10.1074/jbc.M413483200>
- Lopez, A., Harada, K., Vasilakopoulou, M., Shanbhag, N., Ajani, J.A., 2019. Targeting Angiogenesis in Colorectal Carcinoma. *Drugs* 79, 63–74. <https://doi.org/10.1007/s40265-018-1037-9>
- Lord, C.J., Ashworth, A., 2017. PARP inhibitors: Synthetic lethality in the clinic. *Science* 355, 1152–1158. <https://doi.org/10.1126/science.aam7344>
- Lord, C.J., Ashworth, A., 2016. BRCAness revisited. *Nat. Rev. Cancer* 16, 110–120. <https://doi.org/10.1038/nrc.2015.21>
- Lord, C.J., Ashworth, A., 2008. Targeted therapy for cancer using PARP inhibitors. *Curr. Opin. Pharmacol., Cancer/Immunomodulation* 8, 363–369. <https://doi.org/10.1016/j.coph.2008.06.016>
- Lu, C.-W., Lin, S.-C., Chen, K.-F., Lai, Y.-Y., Tsai, S.-J., 2008. Induction of Pyruvate Dehydrogenase Kinase-3 by Hypoxia-inducible Factor-1 Promotes Metabolic Switch and Drug Resistance. *J. Biol. Chem.* 283, 28106–28114. <https://doi.org/10.1074/jbc.M803508200>
- Lu, J., Krepelova, A., Rasa, S.M.M., Annunziata, F., Husak, O., Adam, L., Nunna, S., Neri, F., 2021. Characterization of an in vitro 3D intestinal organoid model by using massive RNAseq-based transcriptome profiling. *Sci. Rep.* 11, 16668. <https://doi.org/10.1038/s41598-021-96321-8>
- Lu, P.-H., Chueh, S.-C., Kung, F.-L., Pan, S.-L., Shen, Y.-C., Guh, J.-H., 2007. Ilimaquinone, a marine sponge metabolite, displays anticancer activity via GADD153-mediated pathway. *Eur. J. Pharmacol.* 556, 45–54. <https://doi.org/10.1016/j.ejphar.2006.10.061>
- Luebeck, E.G., Moolgavkar, S.H., 2002. Multistage carcinogenesis and the incidence of colorectal cancer. *Proc. Natl. Acad. Sci.* 99, 15095–15100. <https://doi.org/10.1073/pnas.222118199>
- Luengo, A., Gui, D.Y., Heiden, M.G.V., 2017. Targeting Metabolism for Cancer Therapy. *Cell Chem. Biol.* 24, 1161–1180. <https://doi.org/10.1016/j.chembiol.2017.08.028>
- Lukashchuk, N., Armenia, J., Tobalina, L., Carr, T.H., Milenkova, T., Liu, Y.L., Penson, R.T., Robson, M.E., Harrington, E., 2022. BRCA reversion mutations mediated by microhomology-mediated end joining (MMEJ) as a mechanism of resistance to PARP inhibitors in ovarian and breast cancer. *J. Clin. Oncol.* 40, 5559–5559. https://doi.org/10.1200/JCO.2022.40.16_suppl.5559
- Luo, H., Yang, Y., Duan, J., Wu, P., Jiang, Q., Xu, C., 2013. PTEN-regulated AKT/FoxO3a/Bim signaling contributes to reactive oxygen species-mediated apoptosis in selenite-treated colorectal cancer cells. *Cell Death Dis.* 4, e481–e481. <https://doi.org/10.1038/cddis.2013.3>
- Majek, O., Gondos, A., Jansen, L., Emrich, K., Holleczeck, B., Katalinic, A., Nennecke, A., Eberle, A., Brenner, H., 2012. Survival from colorectal cancer in Germany in the early 21st century. *Br. J. Cancer* 106, 1875–1880. <https://doi.org/10.1038/bjc.2012.189>
- Mal, M., Koh, P.K., Cheah, P.Y., Chan, E.C.Y., 2012. Metabotyping of human colorectal cancer using two-dimensional gas chromatography mass spectrometry. *Anal. Bioanal. Chem.* 403, 483–493. <https://doi.org/10.1007/s00216-012-5870-5>
- Manzat Saplacan, R.M., Balacescu, L., Gherman, C., Chira, R.I., Craiu, A., Mircea, P.A., Lisencu, C., Balacescu, O., 2017. The Role of PDGFs and PDGFRs in Colorectal Cancer. *Mediators Inflamm.* 2017. <https://doi.org/10.1155/2017/4708076>
- Mao, T., Qin, F., Zhang, M., Li, Jing, Li, Jiankang, Lai, M., 2023. Elevated serum β -hydroxybutyrate, a circulating ketone metabolite, accelerates colorectal cancer proliferation and metastasis via ACAT1. *Oncogene* 42, 1889–1899. <https://doi.org/10.1038/s41388-023-02700-y>
- Mariano, G., Ricciardi, M.R., Trisciuglio, D., Zampieri, M., Ciccarone, F., Guastafierro, T., Calabrese, R., Valentini, E., Tafuri, A., Del Bufalo, D., Caiafa, P., Reale, A., 2015. PARP

References

- inhibitor ABT-888 affects response of MDA-MB-231 cells to doxorubicin treatment, targeting Snail expression. *Oncotarget* 6, 15008–15021.
- Marin-Hernandez, A., Gallardo-Perez, J.C., Ralph, S.J., Rodriguez-Enriquez, S., Moreno-Sanchez, R., 2009. HIF-1 α Modulates Energy Metabolism in Cancer Cells by Inducing Over-Expression of Specific Glycolytic Isoforms. *Mini Rev. Med. Chem.* 9, 1084–1101. <https://doi.org/10.2174/138955709788922610>
- Markowitz, S.D., Bertagnolli, M.M., 2009. Molecular origins of cancer: Molecular basis of colorectal cancer. *N. Engl. J. Med.* 361, 2449–2460. <https://doi.org/10.1056/NEJMra0804588>
- Martin, L.P., Hamilton, T.C., Schilder, R.J., 2008. Platinum Resistance: The Role of DNA Repair Pathways. *Clin. Cancer Res.* 14, 1291–1295. <https://doi.org/10.1158/1078-0432.CCR-07-2238>
- Martinez-Balibrea, E., Martínez-Cardús, A., Ginés, A., Ruiz de Porras, V., Moutinho, C., Layos, L., Manzano, J.L., Bugés, C., Bystrup, S., Esteller, M., Abad, A., 2015. Tumor-Related Molecular Mechanisms of Oxaliplatin Resistance. *Mol. Cancer Ther.* 14, 1767–1776. <https://doi.org/10.1158/1535-7163.MCT-14-0636>
- Martinez-Balibrea, E., Martínez-Cardús, A., Musulén, E., Ginés, A., Manzano, J.L., Aranda, E., Plasencia, C., Neamati, N., Abad, A., 2009. Increased levels of copper efflux transporter ATP7B are associated with poor outcome in colorectal cancer patients receiving oxaliplatin-based chemotherapy. *Int. J. Cancer* 124, 2905–2910. <https://doi.org/10.1002/ijc.24273>
- Martínez-Reyes, I., Chandel, N.S., 2021. Cancer metabolism: looking forward. *Nat. Rev. Cancer* 21, 669–680. <https://doi.org/10.1038/s41568-021-00378-6>
- Martínez-Reyes, I., Chandel, N.S., 2020. Mitochondrial TCA cycle metabolites control physiology and disease. *Nat. Commun.* 11, 1–11. <https://doi.org/10.1038/s41467-019-13668-3>
- Marx, C., Sonnemann, J., Maddocks, O.D.K., Marx-Blümel, L., Beyer, M., Hoelzer, D., Thierbach, R., Maletzki, C., Linnebacher, M., Heinzl, T., Krämer, O.H., 2022. Global metabolic alterations in colorectal cancer cells during irinotecan-induced DNA replication stress. *Cancer Metab.* 10, 10. <https://doi.org/10.1186/s40170-022-00286-9>
- Massagué, J., 2012. TGF β signalling in context. *Nat. Rev. Mol. Cell Biol.* 13, 616–630. <https://doi.org/10.1038/nrm3434>
- Mateo, J., Lord, C.J., Serra, V., Tutt, A., Balmaña, J., Castroviejo-Bermejo, M., Cruz, C., Oaknin, A., Kaye, S.B., de Bono, J.S., 2019. A decade of clinical development of PARP inhibitors in perspective. *Ann. Oncol.*, Suppressed immune microenvironment and repertoire in brain metastases from patients with resected NSCLC 30, 1437–1447. <https://doi.org/10.1093/annonc/mdz192>
- Mathijssen, R.H., van Alphen, R.J., Verweij, J., Loos, W.J., Nooter, K., Stoter, G., Sparreboom, A., 2001. Clinical pharmacokinetics and metabolism of irinotecan (CPT-11). *Clin. Cancer Res. Off. J. Am. Assoc. Cancer Res.* 7, 2182–2194.
- Matoba, S., Kang, J.-G., Patino, W.D., Wragg, A., Boehm, M., Gavrillova, O., Hurley, P.J., Bunz, F., Hwang, P.M., 2006. p53 Regulates Mitochondrial Respiration. *Science* 312, 1650–1653. <https://doi.org/10.1126/science.1126863>
- Matsuzaki, K., Kitano, C., Murata, M., Sekimoto, G., Yoshida, K., Uemura, Y., Seki, T., Taketani, S., Fujisawa, J., Okazaki, K., 2009. Smad2 and Smad3 Phosphorylated at Both Linker and COOH-Terminal Regions Transmit Malignant TGF- β Signal in Later Stages of Human Colorectal Cancer. *Cancer Res.* 69, 5321–5330. <https://doi.org/10.1158/0008-5472.CAN-08-4203>
- Matulonis, U.A., Monk, B.J., 2017. PARP inhibitor and chemotherapy combination trials for the treatment of advanced malignancies: does a development pathway forward exist? *Ann. Oncol.* 28, 443–447. <https://doi.org/10.1093/annonc/mdw697>
- Mauri, G., Arena, S., Siena, S., Bardelli, A., Sartore-Bianchi, A., 2020. The DNA damage response pathway as a land of therapeutic opportunities for colorectal cancer. *Ann. Oncol.* 31, 1135–1147. <https://doi.org/10.1016/j.annonc.2020.05.027>

- Mayer, A.M.S., Glaser, K.B., Cuevas, C., Jacobs, R.S., Kem, W., Little, R.D., McIntosh, J.M., Newman, D.J., Potts, B.C., Shuster, D.E., 2010. The odyssey of marine pharmaceuticals: a current pipeline perspective. *Trends Pharmacol. Sci.* 31, 255–265. <https://doi.org/10.1016/j.tips.2010.02.005>
- McFate, T., Mohyeldin, A., Lu, H., Thakar, J., Henriques, J., Halim, N.D., Wu, H., Schell, M.J., Tsang, T.M., Teahan, O., Zhou, S., Califano, J.A., Jeoung, N.H., Harris, R.A., Verma, A., 2008. Pyruvate dehydrogenase complex activity controls metabolic and malignant phenotype in cancer cells. *J. Biol. Chem.* 283, 22700–22708. <https://doi.org/10.1074/jbc.M801765200>
- McGranahan, N., Furness, A.J.S., Rosenthal, R., Ramskov, S., Lyngaa, R., Saini, S.K., Jamal-Hanjani, M., Wilson, G.A., Birkbak, N.J., Hiley, C.T., Watkins, T.B.K., Shafi, S., Murugaesu, N., Mitter, R., Akarca, A.U., Linares, J., Marafioti, T., Henry, J.Y., Van Allen, E.M., Miao, D., Schilling, B., Schadendorf, D., Garraway, L.A., Makarov, V., Rizvi, N.A., Snyder, A., Hellmann, M.D., Merghoub, T., Wolchok, J.D., Shukla, S.A., Wu, C.J., Peggs, K.S., Chan, T.A., Hadrup, S.R., Quezada, S.A., Swanton, C., 2016. Clonal neoantigens elicit T cell immunoreactivity and sensitivity to immune checkpoint blockade. *Science* 351, 1463–1469. <https://doi.org/10.1126/science.aaf1490>
- McQuade, R.M., Stojanovska, V., Bornstein, J.C., Nurgali, K., 2018. PARP inhibition in platinum-based chemotherapy: Chemopotential and neuroprotection. *Pharmacol. Res.* 137, 104–113. <https://doi.org/10.1016/j.phrs.2018.09.031>
- Melisi, D., Ishiyama, S., Sclabas, G.M., Fleming, J.B., Xia, Q., Tortora, G., Abbruzzese, J.L., Chiao, P.J., 2008. LY2109761, a novel transforming growth factor β receptor type I and type II dual inhibitor, as a therapeutic approach to suppressing pancreatic cancer metastasis. *Mol. Cancer Ther.* 7, 829–840. <https://doi.org/10.1158/1535-7163.MCT-07-0337>
- Melling, N., Grass, J., Reeh, M., Tachezy, M., Blessmann, M., Nickel, F., Hackert, T., Grupp, K., 2023. Decreased expression of prolyl hydroxylase 1 is associated with poor prognosis in colorectal cancers. *J. Cancer Res. Clin. Oncol.* 149, 7579–7585. <https://doi.org/10.1007/s00432-023-04717-y>
- Michels, J., Vitale, I., Galluzzi, L., Adam, J., Olaussen, K.A., Kepp, O., Senovilla, L., Talhaoui, I., Guegan, J., Enot, D.P., Talbot, M., Robin, A., Girard, P., Or ear, C., Lissa, D., Sukkurwala, A.Q., Garcia, P., Behnam-Motlagh, P., Kohno, K., Wu, G.S., Brenner, C., Dessen, P., Saparbaev, M., Soria, J.-C., Castedo, M., Kroemer, G., 2013. Cisplatin Resistance Associated with PARP Hyperactivation. *Cancer Res.* 73, 2271–2280. <https://doi.org/10.1158/0008-5472.CAN-12-3000>
- Min, W., Cortes, U., Herceg, Z., Tong, W.-M., Wang, Z.-Q., 2010. Deletion of the nuclear isoform of poly(ADP-ribose) glycohydrolase (PARG) reveals its function in DNA repair, genomic stability and tumorigenesis. *Carcinogenesis* 31, 2058–2065. <https://doi.org/10.1093/carcin/bgq205>
- Minami, H., Sai, K., Saeki, M., Saito, Y., Ozawa, S., Suzuki, K., Kaniwa, N., Sawada, J., Hamaguchi, T., Yamamoto, N., Shirao, K., Yamada, Y., Ohmatsu, H., Kubota, K., Yoshida, T., Ohtsu, A., Saijo, N., 2007. Irinotecan pharmacokinetics/pharmacodynamics and UGT1A genetic polymorphisms in Japanese: roles of UGT1A1*6 and *28. *Pharmacogenet. Genomics* 17, 497–504. <https://doi.org/10.1097/FPC.0b013e328014341f>
- Miyo, M., Konno, M., Nishida, N., Sueda, T., Noguchi, K., Matsui, H., Colvin, H., Kawamoto, K., Koseki, J., Haraguchi, N., Nishimura, J., Hata, T., Gotoh, N., Matsuda, F., Satoh, T., Mizushima, T., Shimizu, H., Doki, Y., Mori, M., Ishii, H., 2016. Metabolic Adaptation to Nutritional Stress in Human Colorectal Cancer. *Sci. Rep.* 6, 1–13. <https://doi.org/10.1038/srep38415>
- Mohan, A., Griffith, K.A., Wuchu, F., Zhen, D.B., Kumar-Sinha, C., Crysler, O., Hsiehchen, D., Enzler, T., Dippman, D., Gunchick, V., Achreja, A., Animasahun, O., Choppara, S., Nenwani, M., Chinnaiyan, A.M., Nagrath, D., Zalupski, M.M., Sahai, V., 2023. Devimistat in Combination with Gemcitabine and Cisplatin in Biliary Tract Cancer: Preclinical Evaluation and Phase Ib Multicenter Clinical Trial (BiIT-04). *Clin. Cancer Res.* OF1–OF7. <https://doi.org/10.1158/1078-0432.CCR-23-0036>

- Molnár, S., Beke, L., Méhes, G., Póka, R., 2020. The Prognostic Value of PARP Expression in High-Grade Epithelial Ovarian Cancer. *Pathol. Oncol. Res.* 26, 2549–2555. <https://doi.org/10.1007/s12253-020-00856-6>
- Mordhorst, B.R., Kerns, K.C., Schauflinger, M., Zigo, M., Murphy, S.L., Ross, R.M., Wells, K.D., Green, J.A., Sutovsky, P., Prather, R.S., 2019. Pharmacologic treatment with CPI-613 and PS48 decreases mitochondrial membrane potential and increases quantity of autolysosomes in porcine fibroblasts. *Sci. Rep.* 9, 1–11. <https://doi.org/10.1038/s41598-019-45850-4>
- Morris, V.K., Kennedy, E.B., Baxter, N.N., Benson, A.B., Cercek, A., Cho, M., Ciombor, K.K., Cremolini, C., Davis, A., Deming, D.A., Fakih, M.G., Gholami, S., Hong, T.S., Jaiyesimi, I., Klute, K., Lieu, C., Sanoff, H., Strickler, J.H., White, S., Willis, J.A., Eng, C., 2023. Treatment of Metastatic Colorectal Cancer: ASCO Guideline. *J. Clin. Oncol.* 41, 678–700. <https://doi.org/10.1200/JCO.22.01690>
- Murai, J., Feng, Y., Yu, G.K., Ru, Y., Tang, S.-W., Shen, Y., Pommier, Y., 2016. Resistance to PARP inhibitors by SLFN11 inactivation can be overcome by ATR inhibition. *Oncotarget* 7, 76534–76550. <https://doi.org/10.18632/oncotarget.12266>
- Murai, J., Huang, S.N., Das, B.B., Renaud, A., Zhang, Y., Doroshow, J.H., Ji, J., Takeda, S., Pommier, Y., 2012. Differential trapping of PARP1 and PARP2 by clinical PARP inhibitors. *Cancer Res.* 72, 5588–5599. <https://doi.org/10.1158/0008-5472.CAN-12-2753>
- Murai, J., Zhang, Y., Morris, J., Ji, J., Takeda, S., Doroshow, J.H., Pommier, Y., 2014. Rationale for poly(ADP-ribose) polymerase (PARP) inhibitors in combination therapy with camptothecins or temozolomide based on PARP trapping versus catalytic inhibition. *J. Pharmacol. Exp. Ther.* 349, 408–416. <https://doi.org/10.1124/jpet.113.210146>
- Murata, M.M., Kong, X., Moncada, E., Chen, Y., Imamura, H., Wang, P., Berns, M.W., Yokomori, K., Digman, M.A., 2019. NAD⁺ consumption by PARP1 in response to DNA damage triggers metabolic shift critical for damaged cell survival. *Mol. Biol. Cell* 30, 2584–2597. <https://doi.org/10.1091/mbc.E18-10-0650>
- Muvarak, N., Kelley, S., Robert, C., Baer, M.R., Perrotti, D., Gambacorti-Passerini, C., Civin, C., Scheibner, K., Rassool, F., 2015. c-MYC Generates Repair Errors via Increased Transcription of Alternative-NHEJ Factors, LIG3 and PARP1, in Tyrosine Kinase-activated Leukemias. *Mol. Cancer Res. MCR* 13, 699–712. <https://doi.org/10.1158/1541-7786.MCR-14-0422>
- Myint, K., Biswas, R., Li, Y., Jong, N., Jamieson, S., Liu, J., Han, C., Squire, C., Merien, F., Lu, J., Nakanishi, T., Tamai, I., McKeage, M., 2019. Identification of MRP2 as a targetable factor limiting oxaliplatin accumulation and response in gastrointestinal cancer. *Sci. Rep.* 9, 2245. <https://doi.org/10.1038/s41598-019-38667-8>
- Nagaraju, G.P., Bramhachari, P.V., Raghu, G., El-Rayes, B.F., 2015. Hypoxia inducible factor-1 α : Its role in colorectal carcinogenesis and metastasis. *Cancer Lett.* 366, 11–18. <https://doi.org/10.1016/j.canlet.2015.06.005>
- Naguib, A., Mitrou, P.N., Gay, L.J., Cooke, J.C., Luben, R.N., Ball, R.Y., McTaggart, A., Arends, M.J., Rodwell, S.A., 2010. Dietary, lifestyle and clinicopathological factors associated with BRAF and K-ras mutations arising in distinct subsets of colorectal cancers in the EPIC Norfolk study. *BMC Cancer* 10, 99. <https://doi.org/10.1186/1471-2407-10-99>
- Nakayama, T., Hirakawa, H., Shibata, K., Nazneen, A., Abe, K., Nagayasu, T., Taguchi, T., 2011. Expression of angiopoietin-like 4 (ANGPTL4) in human colorectal cancer: ANGPTL4 promotes venous invasion and distant metastasis. *Oncol. Rep.* 25, 929–935. <https://doi.org/10.3892/or.2011.1176>
- Neitzel, C., 2021. Synergism of Lipoates and Established Anticancer Drugs in Cell and Mouse Models of Colorectal Cancer. Technische Universität Kaiserslautern. <https://doi.org/10.26204/KLUEDO/6236>
- Neitzel, C., Demuth, P., Wittmann, S., Fahrner, J., 2020. Targeting Altered Energy Metabolism in Colorectal Cancer: Oncogenic Reprogramming, the Central Role of the TCA Cycle and Therapeutic Opportunities. *Cancers* 12, 1731. <https://doi.org/10.3390/cancers12071731>

- Neumann, J., Zeindl-Eberhart, E., Kirchner, T., Jung, A., 2009. Frequency and type of KRAS mutations in routine diagnostic analysis of metastatic colorectal cancer. *Pathol. - Res. Pract.* 205, 858–862. <https://doi.org/10.1016/j.prp.2009.07.010>
- Nguyen, D.X., Bos, P.D., Massagué, J., 2009. Metastasis: from dissemination to organ-specific colonization. *Nat. Rev. Cancer* 9, 274–284. <https://doi.org/10.1038/nrc2622>
- Nguyen, L., W. M. Martens, J., Van Hoeck, A., Cuppen, E., 2020. Pan-cancer landscape of homologous recombination deficiency. *Nat. Commun.* 11, 5584. <https://doi.org/10.1038/s41467-020-19406-4>
- Nguyen, L.H., Goel, A., Chung, D.C., 2020. Pathways of Colorectal Carcinogenesis. *Gastroenterology, Colorectal Cancer: Recent Advances & Future Challenges* 158, 291–302. <https://doi.org/10.1053/j.gastro.2019.08.059>
- Nosho, K., Yamamoto, H., Mikami, M., Taniguchi, H., Takahashi, T., Adachi, Y., Imamura, A., Imai, K., Shinomura, Y., 2006. Overexpression of poly(ADP-ribose) polymerase-1 (PARP-1) in the early stage of colorectal carcinogenesis. *Eur. J. Cancer Oxf. Engl.* 1990 42, 2374–2381. <https://doi.org/10.1016/j.ejca.2006.01.061>
- Obenauf, A.C., Massagué, J., 2015. Surviving at a Distance: Organ-Specific Metastasis. *Trends Cancer* 1, 76–91. <https://doi.org/10.1016/j.trecan.2015.07.009>
- Offermans, K., Jenniskens, J.C.A., Simons, C.C.J.M., Samarska, I., Fazzi, G.E., van der Meer, J.R.M., Smits, K.M., Schouten, L.J., Weijenberg, M.P., Grabsch, H.I., van den Brandt, P.A., 2023. Association between mutational subgroups, Warburg-subtypes, and survival in patients with colorectal cancer. *Cancer Med.* 12, 1137–1156. <https://doi.org/10.1002/cam4.4968>
- Oguri, T., Bessho, Y., Achiwa, H., Ozasa, H., Maeno, K., Maeda, H., Sato, S., Ueda, R., 2007. MRP8/ABCC11 directly confers resistance to 5-fluorouracil. *Mol. Cancer Ther.* 6, 122–127. <https://doi.org/10.1158/1535-7163.MCT-06-0529>
- Oh, E.-T., Park, H.J., 2015. Implications of NQO1 in cancer therapy. *BMB Rep.* 48, 609–617. <https://doi.org/10.5483/BMBRep.2015.48.11.190>
- Ohba, S., Mukherjee, J., See, W.L., Pieper, R.O., 2014. Mutant IDH1-Driven Cellular Transformation Increases RAD51-Mediated Homologous Recombination and Temozolomide Resistance. *Cancer Res.* 74, 4836–4844. <https://doi.org/10.1158/0008-5472.CAN-14-0924>
- Olivier, M., Hollstein, M., Hainaut, P., 2010. TP53 Mutations in Human Cancers: Origins, Consequences, and Clinical Use. *Cold Spring Harb. Perspect. Biol.* 2, a001008. <https://doi.org/10.1101/cshperspect.a001008>
- Ong, E.S., Zou, L., Li, S., Cheah, P.Y., Eu, K.W., Ong, C.N., 2010. Metabolic profiling in colorectal cancer reveals signature metabolic shifts during tumorigenesis. *Mol. Cell. Proteomics MCP.* <https://doi.org/10.1074/mcp.M900551-MCP200>
- Oplustil O'Connor, L., Rulten, S.L., Cranston, A.N., Odedra, R., Brown, H., Jaspers, J.E., Jones, L., Knights, C., Evers, B., Ting, A., Bradbury, R.H., Pajic, M., Rottenberg, S., Jonkers, J., Rudge, D., Martin, N.M.B., Caldecott, K.W., Lau, A., O'Connor, M.J., 2016. The PARP Inhibitor AZD2461 Provides Insights into the Role of PARP3 Inhibition for Both Synthetic Lethality and Tolerability with Chemotherapy in Preclinical Models. *Cancer Res.* 76, 6084–6094. <https://doi.org/10.1158/0008-5472.CAN-15-3240>
- Ordog, K., Horvath, O., Eros, K., Bruszt, K., Toth, S., Kovacs, D., Kalman, N., Radnai, B., Deres, L., Gallyas, F., Toth, K., Halmosi, R., 2021. Mitochondrial protective effects of PARP-inhibition in hypertension-induced myocardial remodeling and in stressed cardiomyocytes. *Life Sci.* 268, 118936. <https://doi.org/10.1016/j.lfs.2020.118936>
- Osovskaya, V., Koo, I.C., Kaldjian, E.P., Alvares, C., Sherman, B.M., 2010. Upregulation of Poly (ADP-Ribose) Polymerase-1 (PARP1) in Triple-Negative Breast Cancer and Other Primary Human Tumor Types. *Genes Cancer* 1, 812–821. <https://doi.org/10.1177/1947601910383418>
- Pandey, N., Black, B.E., 2021. Rapid Detection and Signaling of DNA Damage by PARP-1. *Trends Biochem. Sci.* 46, 744–757. <https://doi.org/10.1016/j.tibs.2021.01.014>

References

- Panieri, E., Santoro, M.M., 2016. ROS homeostasis and metabolism: a dangerous liason in cancer cells. *Cell Death Dis.* 7, e2253–e2253. <https://doi.org/10.1038/cddis.2016.105>
- Papandreou, I., Cairns, R.A., Fontana, L., Lim, A.L., Denko, N.C., 2006. HIF-1 mediates adaptation to hypoxia by actively downregulating mitochondrial oxygen consumption. *Cell Metab.* 3, 187–197. <https://doi.org/10.1016/j.cmet.2006.01.012>
- Pardee, T., Anderson, R.G., Pladna, K.M., Isom, S., Ghiraldeli, L.P., Miller, L.D., Chou, J.W., Jin, G., Zhang, W., Ellis, L.R., Berenzon, D., Howard, D.S., Hurd, D.D., Manuel, M., Dralle, S., Lyerly, S., Powell, B.L., 2018a. A Phase I Study of CPI-613 in Combination with High-Dose Cytarabine and Mitoxantrone for Relapsed or Refractory Acute Myeloid Leukemia. *Clin. Cancer Res. Off. J. Am. Assoc. Cancer Res.* 24, 2060–2073. <https://doi.org/10.1158/1078-0432.CCR-17-2282>
- Pardee, T., Isom, S., Ellis, L.R., Howard, D.S., Bhave, R., Manuel, M., Dralle, S., Lyerly, S., Powell, B.L., 2018b. Therapeutic Manipulation of Cancer Cell Metabolism with the Mitochondrial Metabolism Inhibitor Cpi-613 in Addition to Chemotherapy Abrogates the Adverse Prognostic Effect of Age in Relapsed and Refractory AML. *Blood* 132, 1355–1355. <https://doi.org/10.1182/blood-2018-99-118991>
- Pardee, T., Lee, K., Luddy, J., Maturo, C., Rodriguez, R., Isom, S., Miller, L.D., Stadelman, K.M., Levitan, D., Hurd, D., Ellis, L.R., Harrelson, R., Manuel, M., Dralle, S., Lyerly, S., Powell, B.L., 2014. A phase I study of the first-in-class antimetabolic agent, CPI-613, in patients with advanced hematologic malignancies. *Clin. Cancer Res. Off. J. Am. Assoc. Cancer Res.* 20, 5255–5264. <https://doi.org/10.1158/1078-0432.CCR-14-1019>
- Pardee, T., Powell, B.L., Larson, R.A., Maly, J., Keng, M., Foster, M., Choi, E.-J., Sill, H., Cluzeau, T., Jeyakumar, D., Frankfurt, O., Patel, P., Schuster, M., Koller, E., Costello, R., Platzbecker, U., Montesinos, P., Vives, S., Nazha, A., Cook, R., Vigil-Gonzales, C., Chantepie, S., Luther, S., Cortes, J., 2024. Devimistat plus chemotherapy vs chemotherapy alone for older relapsed or refractory patients with AML: results of the ARMADA trial. *Blood Neoplasia* 1, 100009. <https://doi.org/10.1016/j.bneo.2024.100009>
- Park, H.-K., Lee, J.-E., Lim, J., Jo, D.-E., Park, S.-A., Suh, P.-G., Kang, B.H., 2014. Combination treatment with doxorubicin and gamitrinib synergistically augments anticancer activity through enhanced activation of Bim. *BMC Cancer* 14, 431. <https://doi.org/10.1186/1471-2407-14-431>
- Park, S., Yun, E., Hwang, I.H., Yoon, S., Kim, D.-E., Kim, J.S., Na, M., Song, G.-Y., Oh, S., 2014. Ilimaquinone and ethylsmenquinone, marine sponge metabolites, suppress the proliferation of multiple myeloma cells by down-regulating the level of β -catenin. *Mar. Drugs* 12, 3231–3244. <https://doi.org/10.3390/md12063231>
- Park, S.E., Kim, H.S., Jung, E.-J., Suh, J.H., Min, H., Chi, K.-C., Kim, J.W., Park, J.-M., Hwang, I.G., 2022. Low PARP-1 expression level is an indicator of poor prognosis in patients with stage II and III gastric cancer. *J. Cancer* 13, 869–876. <https://doi.org/10.7150/jca.65145>
- Park, S.-Y., Lam, W., Cheng, Y., 2002. X-ray Repair Cross-Complementing Gene I Protein Plays an Important Role in Camptothecin Resistance. *Cancer Res.* 62, 459–465.
- Patterson-Fortin, J., D'Andrea, A.D., 2020. Exploiting the Microhomology-Mediated End-Joining Pathway in Cancer Therapy. *Cancer Res.* 80, 4593–4600. <https://doi.org/10.1158/0008-5472.CAN-20-1672>
- Paul, S., Chatterjee, S., Sinha, S., Dash, S.R., Pradhan, R., Das, B., Goutam, K., Kundu, C.N., 2023. Veliparib (ABT-888), a PARP inhibitor potentiates the cytotoxic activity of 5-fluorouracil by inhibiting MMR pathway through deregulation of MSH6 in colorectal cancer stem cells. *Expert Opin. Ther. Targets* 27, 999–1015. <https://doi.org/10.1080/14728222.2023.2266572>
- Petropoulos, M., Karamichali, A., Rossetti, G.G., Freudenmann, A., Iacovino, L.G., Dionellis, V.S., Sotiriou, S.K., Halazonetis, T.D., 2024. Transcription–replication conflicts underlie sensitivity to PARP inhibitors. *Nature* 628, 433–441. <https://doi.org/10.1038/s41586-024-07217-2>
- Pettersen, H.S., Visnes, T., Vågbø, C.B., Svaasand, E.K., Doseth, B., Slupphaug, G., Kavli, B., Krokan, H.E., 2011. UNG-initiated base excision repair is the major repair route for 5-

References

- fluorouracil in DNA, but 5-fluorouracil cytotoxicity depends mainly on RNA incorporation. *Nucleic Acids Res.* 39, 8430–8444. <https://doi.org/10.1093/nar/gkr563>
- Pettitt, S.J., Krastev, D.B., Brandsma, I., Dréan, A., Song, F., Aleksandrov, R., Harrell, M.I., Menon, M., Brough, R., Campbell, J., Frankum, J., Ranes, M., Pemberton, H.N., Rafiq, R., Fenwick, K., Swain, A., Guettler, S., Lee, J.-M., Swisher, E.M., Stoyanov, S., Yusa, K., Ashworth, A., Lord, C.J., 2018. Genome-wide and high-density CRISPR-Cas9 screens identify point mutations in PARP1 causing PARP inhibitor resistance. *Nat. Commun.* 9, 1849. <https://doi.org/10.1038/s41467-018-03917-2>
- Philip, P., Buyse, M.E., Alistar, A.T., Rocha Lima, C.M., Luther, S., Pardee, T.S., Van Cutsem, E., 2019. A Phase III open-label trial to evaluate efficacy and safety of CPI-613 plus modified FOLFIRINOX (mFFX) versus FOLFIRINOX (FFX) in patients with metastatic adenocarcinoma of the pancreas. *Future Oncol. Lond. Engl.* 15, 3189–3196. <https://doi.org/10.2217/fo-2019-0209>
- Phua, L.C., Mal, M., Koh, P.K., Cheah, P.Y., Chan, E.C.Y., Ho, H.K., 2013. Investigating the role of nucleoside transporters in the resistance of colorectal cancer to 5-fluorouracil therapy. *Cancer Chemother. Pharmacol.* 71, 817–823. <https://doi.org/10.1007/s00280-012-2054-0>
- Pino, M.S., Kikuchi, H., Zeng, M., Herraiz, M., Sperduti, I., Berger, D., Park, D., Iafrate, A.J., Zukerberg, L.R., Chung, D.C., 2010. Epithelial to Mesenchymal Transition Is Impaired in Colon Cancer Cells With Microsatellite Instability. *Gastroenterology* 138, 1406–1417. <https://doi.org/10.1053/j.gastro.2009.12.010>
- Pirozzi, C.J., Yan, H., 2021. The implications of IDH mutations for cancer development and therapy. *Nat. Rev. Clin. Oncol.* 18, 645–661. <https://doi.org/10.1038/s41571-021-00521-0>
- Plummer, R., Jones, C., Middleton, M., Wilson, R., Evans, J., Olsen, A., Curtin, N., Boddy, A., McHugh, P., Newell, D., Harris, A., Johnson, P., Steinfeldt, H., Dewji, R., Wang, D., Robson, L., Calvert, H., 2008. Phase I study of the poly(ADP-ribose) polymerase inhibitor, AG014699, in combination with temozolomide in patients with advanced solid tumors. *Clin. Cancer Res. Off. J. Am. Assoc. Cancer Res.* 14, 7917–7923. <https://doi.org/10.1158/1078-0432.CCR-08-1223>
- Pommier, Y., O'Connor, M.J., de Bono, J., 2016. Laying a trap to kill cancer cells: PARP inhibitors and their mechanisms of action. *Sci. Transl. Med.* 8, 362ps17. <https://doi.org/10.1126/scitranslmed.aaf9246>
- Puccini, A., Berger, M.D., Naseem, M., Tokunaga, R., Battaglin, F., Cao, S., Hanna, D.L., McSkane, M., Soni, S., Zhang, W., Lenz, H.-J., 2017. Colorectal cancer: epigenetic alterations and their clinical implications. *Biochim. Biophys. Acta BBA - Rev. Cancer* 1868, 439–448. <https://doi.org/10.1016/j.bbcan.2017.09.003>
- Puentes-Pardo, J.D., Moreno-SanJuan, S., Casado, J., Escudero-Feliu, J., López-Pérez, D., Sánchez-Uceta, P., González-Novoa, P., Gálvez, J., Carazo, Á., León, J., 2023. PARP-1 Expression Influences Cancer Stem Cell Phenotype in Colorectal Cancer Depending on p53. *Int. J. Mol. Sci.* 24, 4787. <https://doi.org/10.3390/ijms24054787>
- Qiao, C., Huang, W., Chen, J., Feng, W., Zhang, T., Wang, Y., Liu, D., Ji, X., Xie, M., Sun, M., Fan, D., Wu, K., Xia, L., 2021. IGF1-mediated HOXA13 overexpression promotes colorectal cancer metastasis through upregulating ACLY and IGF1R. *Cell Death Dis.* 12, 1–18. <https://doi.org/10.1038/s41419-021-03833-2>
- Qin, C., Ji, Z., Zhai, E., Xu, K., Zhang, Y., Li, Q., Jing, H., Wang, X., Song, X., 2022. PARP inhibitor olaparib enhances the efficacy of radiotherapy on XRCC2-deficient colorectal cancer cells. *Cell Death Dis.* 13, 1–8. <https://doi.org/10.1038/s41419-022-04967-7>
- Ramesh, P., Lannagan, T.R.M., Jackstadt, R., Atencia Taboada, L., Lansu, N., Wirapati, P., van Hooff, S.R., Dekker, D., Pritchard, J., Kirov, A.B., van Neerven, S.M., Tejpar, S., Kops, G.J.P.L., Sansom, O.J., Medema, J.P., 2021. BCL-XL is crucial for progression through the adenoma-to-carcinoma sequence of colorectal cancer. *Cell Death Differ.* 28, 3282–3296. <https://doi.org/10.1038/s41418-021-00816-w>
- Ramesh, V., Brabletz, T., Ceppi, P., 2020. Targeting EMT in Cancer with Repurposed Metabolic Inhibitors. *Trends Cancer* 6, 942–950. <https://doi.org/10.1016/j.trecan.2020.06.005>

References

- Rasheed, S., Harris, A.L., Tekkis, P.P., Turley, H., Silver, A., McDonald, P.J., Talbot, I.C., Glynn-Jones, R., Northover, J.M.A., Guenther, T., 2009. Hypoxia-inducible factor-1alpha and -2alpha are expressed in most rectal cancers but only hypoxia-inducible factor-1alpha is associated with prognosis. *Br. J. Cancer* 100, 1666–1673. <https://doi.org/10.1038/sj.bjc.6605026>
- Rauch, A., Carlstedt, A., Emmerich, C., Mustafa, A.-H.M., Göder, A., Knauer, S.K., Linnebacher, M., Heinzel, T., Krämer, O.H., 2018. Survivin antagonizes chemotherapy-induced cell death of colorectal cancer cells. *Oncotarget* 9, 27835–27850. <https://doi.org/10.18632/oncotarget.25600>
- Ray Chaudhuri, A., Callen, E., Ding, X., Gogola, E., Duarte, A.A., Lee, J.-E., Wong, N., Lafarga, V., Calvo, J.A., Panzarino, N.J., John, S., Day, A., Crespo, A.V., Shen, B., Starnes, L.M., Ruitter, J.R. de, Daniel, J.A., Konstantinopoulos, P.A., Cortez, D., Cantor, S.B., Fernandez-Capetillo, O., Ge, K., Jonkers, J., Rottenberg, S., Sharan, S.K., Nussenzweig, A., 2016. Replication fork stability confers chemoresistance in BRCA-deficient cells. *Nature* 535, 382–387. <https://doi.org/10.1038/nature18325>
- Ray Chaudhuri, A., Hashimoto, Y., Herrador, R., Neelsen, K.J., Fachinetti, D., Bermejo, R., Cocito, A., Costanzo, V., Lopes, M., 2012. Topoisomerase I poisoning results in PARP-mediated replication fork reversal. *Nat. Struct. Mol. Biol.* 19, 417–423. <https://doi.org/10.1038/nsmb.2258>
- Ray Chaudhuri, A., Nussenzweig, A., 2017. The multifaceted roles of PARP1 in DNA repair and chromatin remodelling. *Nat. Rev. Mol. Cell Biol.* 18, 610–621. <https://doi.org/10.1038/nrm.2017.53>
- Rebane-Klemm, E., Truu, L., Reinsalu, L., Puurand, M., Shevchuk, I., Chekulayev, V., Timohhina, N., Tepp, K., Bogovskaja, J., Afanasjev, V., Suurmaa, K., Valvere, V., Kaambre, T., 2020. Mitochondrial Respiration in KRAS and BRAF Mutated Colorectal Tumors and Polypos. *Cancers* 12. <https://doi.org/10.3390/cancers12040815>
- Reddy, V.B., Boteju, L., Boteju, A., Shen, L., Kassahun, K., Reddy, N., Sheldon, A., Luther, S., Hu, K., 2022. In Vitro and In Vivo Metabolism of a Novel Antimitochondrial Cancer Metabolism Agent, CPI-613, in Rat and Human. *Drug Metab. Dispos.* 50, 361–373. <https://doi.org/10.1124/dmd.121.000726>
- Ren, M., Yang, X., Bie, J., Wang, Z., Liu, M., Li, Y., Shao, G., Luo, J., 2020. Citrate synthase desuccinylation by SIRT5 promotes colon cancer cell proliferation and migration. *Biol. Chem.* 401, 1031–1039. <https://doi.org/10.1515/hsz-2020-0118>
- Riihimäki, M., Hemminki, A., Sundquist, J., Hemminki, K., 2016. Patterns of metastasis in colon and rectal cancer. *Sci. Rep.* 6, 29765. <https://doi.org/10.1038/srep29765>
- Rivas, M.O.G., Stuart, S.D., Thach, D., Dahan, M., Shorr, R., Zachar, Z., Bingham, P.M., 2022. Evidence for a novel, effective approach to targeting carcinoma catabolism exploiting the first-in-class, anti-cancer mitochondrial drug, CPI-613. *PLOS ONE* 17, e0269620. <https://doi.org/10.1371/journal.pone.0269620>
- Rocha Lima, C.M.S.P., Alistar, A.T., Desnoyers, R.J., Sorscher, S., Yacoub, G.H., Dressler, E.V.M., Pardee, T.S., Grant, S.C., Luther, S., Butler, D., Ogburn, O., Strickland, K., Pasche, B., 2019. A phase I clinical trial of fluorouracil (5-FU) + devimistat (CPI-613) combination in previously treated patients (pts) with metastatic colorectal cancer (MCR). *J. Clin. Oncol.* 37, e15054–e15054. https://doi.org/10.1200/JCO.2019.37.15_suppl.e15054
- Roskoski, R., 2019a. Small molecule inhibitors targeting the EGFR/ErbB family of protein-tyrosine kinases in human cancers. *Pharmacol. Res.* 139, 395–411. <https://doi.org/10.1016/j.phrs.2018.11.014>
- Roskoski, R., 2019b. Cyclin-dependent protein serine/threonine kinase inhibitors as anticancer drugs. *Pharmacol. Res.* 139, 471–488. <https://doi.org/10.1016/j.phrs.2018.11.035>
- Rösner, T., Kahle, S., Montenegro, F., Matlung, H.L., Jansen, J.H.M., Evers, M., Beurskens, F., Leusen, J.H.W., van den Berg, T.K., Valerius, T., 2019. Immune Effector Functions of Human IgG2 Antibodies against EGFR. *Mol. Cancer Ther.* 18, 75–88. <https://doi.org/10.1158/1535-7163.MCT-18-0341>

- Rottenberg, S., Disler, C., Perego, P., 2021. The rediscovery of platinum-based cancer therapy. *Nat. Rev. Cancer* 21, 37–50. <https://doi.org/10.1038/s41568-020-00308-y>
- Rouleau, M., Patel, A., Hendzel, M.J., Kaufmann, S.H., Poirier, G.G., 2010. PARP inhibition: PARP1 and beyond. *Nat. Rev. Cancer* 10, 293. <https://doi.org/10.1038/nrc2812>
- Sakai, W., Swisher, E.M., Karlan, B.Y., Agarwal, M.K., Higgins, J., Friedman, C., Villegas, E., Jacquemont, C., Farrugia, D.J., Couch, F.J., Urban, N., Taniguchi, T., 2008. Secondary mutations as a mechanism of cisplatin resistance in BRCA2-mutated cancers. *Nature* 451, 1116–1120. <https://doi.org/10.1038/nature06633>
- Salem, M., Wallace, C., Velegraki, M., Li, A., Ansa-Addo, E., Metelli, A., Kwon, H., Riesenber, B., Wu, B., Zhang, Y., Guglietta, S., Sun, S., Liu, B., Li, Z., 2019. GARP Dampens Cancer Immunity by Sustaining Function and Accumulation of Regulatory T Cells in the Colon. *Cancer Res.* 79, 1178. <https://doi.org/10.1158/0008-5472.CAN-18-2623>
- Sanz-Garcia, E., Argiles, G., Elez, E., Tabernero, J., 2017. BRAF mutant colorectal cancer: prognosis, treatment, and new perspectives. *Ann. Oncol.*, Availability, out-of-pocket costs and accessibility of anti-neoplastic medicines outside of Europe 28, 2648–2657. <https://doi.org/10.1093/annonc/mdx401>
- Sargent, D.J., Marsoni, S., Monges, G., Thibodeau, S.N., Labianca, R., Hamilton, S.R., French, A.J., Kabat, B., Foster, N.R., Torri, V., Ribic, C., Grothey, A., Moore, M., Zaniboni, A., Seitz, J.-F., Sinicropo, F., Gallinger, S., 2010. Defective mismatch repair as a predictive marker for lack of efficacy of fluorouracil-based adjuvant therapy in colon cancer. *J. Clin. Oncol. Off. J. Am. Soc. Clin. Oncol.* 28, 3219–3226. <https://doi.org/10.1200/JCO.2009.27.1825>
- Satoh, K., Yachida, S., Sugimoto, M., Oshima, M., Nakagawa, T., Akamoto, S., Tabata, S., Saitoh, K., Kato, K., Sato, S., Igarashi, K., Aizawa, Y., Kajino-Sakamoto, R., Kojima, Y., Fujishita, T., Enomoto, A., Hirayama, A., Ishikawa, T., Taketo, M.M., Kushida, Y., Haba, R., Okano, K., Tomita, M., Suzuki, Y., Fukuda, S., Aoki, M., Soga, T., 2017. Global metabolic reprogramming of colorectal cancer occurs at adenoma stage and is induced by MYC. *Proc. Natl. Acad. Sci.* 114, E7697–E7706. <https://doi.org/10.1073/pnas.1710366114>
- Satoh, M.S., Lindahl, T., 1992. Role of poly(ADP-ribose) formation in DNA repair. *Nature* 356, 356–358. <https://doi.org/10.1038/356356a0>
- Sava, G.P., Fan, H., Coombes, R.C., Buluwela, L., Ali, S., 2020. CDK7 inhibitors as anticancer drugs. *Cancer Metastasis Rev.* 39, 805–823. <https://doi.org/10.1007/s10555-020-09885-8>
- Saxton, R.A., Sabatini, D.M., 2017. mTOR Signaling in Growth, Metabolism, and Disease. *Cell* 168, 960–976. <https://doi.org/10.1016/j.cell.2017.02.004>
- Schell, J.C., Olson, K.A., Jiang, L., Hawkins, A.J., Van Vranken, J.G., Xie, J., Egnatchik, R.A., Earl, E.G., DeBerardinis, R.J., Rutter, J., 2014. A role for the mitochondrial pyruvate carrier as a repressor of the Warburg effect and colon cancer cell growth. *Mol. Cell* 56, 400–413. <https://doi.org/10.1016/j.molcel.2014.09.026>
- Scherr, A.-L., Gdynia, G., Salou, M., Radhakrishnan, P., Duglova, K., Heller, A., Keim, S., Kautz, N., Jassowicz, A., Elssner, C., He, Y.-W., Jaeger, D., Heikenwalder, M., Schneider, M., Weber, A., Roth, W., Schulze-Bergkamen, H., Koehler, B.C., 2016. Bcl-xL is an oncogenic driver in colorectal cancer. *Cell Death Dis.* 7, e2342–e2342. <https://doi.org/10.1038/cddis.2016.233>
- Schmutz, I., Timashev, L., Xie, W., Patel, D.J., de Lange, T., 2017. TRF2 binds branched DNA to safeguard telomere integrity. *Nat. Struct. Mol. Biol.* 24, 734–742. <https://doi.org/10.1038/nsmb.3451>
- Schrag, D., Weiser, M.R., Goodman, K.A., Goñen, M., Hollywood, E., Cercek, A., Reidy-Lagunes, D.L., Gollub, M.J., Shia, J., Guillem, J.G., Temple, L.K.F., Paty, P.B., Saltz, L.B., 2014. Neoadjuvant Chemotherapy Without Routine Use of Radiation Therapy for Patients With Locally Advanced Rectal Cancer: A Pilot Trial. *J. Clin. Oncol.* 32, 513–518. <https://doi.org/10.1200/JCO.2013.51.7904>
- Schug, Z.T., Peck, B., Jones, D.T., Zhang, Q., Grosskurth, S., Alam, I.S., Goodwin, L.M., Smethurst, E., Mason, S., Blyth, K., McGarry, L., James, D., Shanks, E., Kalna, G., Saunders, R.E., Jiang, M., Howell, M., Lassailly, F., Thin, M.Z., Spencer-Dene, B., Stamp,

- G., van den Broek, N.J.F., Mackay, G., Bulusu, V., Kamphorst, J.J., Tardito, S., Strachan, D., Harris, A.L., Aboagye, E.O., Critchlow, S.E., Wakelam, M.J.O., Schulze, A., Gottlieb, E., 2015. Acetyl-CoA Synthetase 2 Promotes Acetate Utilization and Maintains Cancer Cell Growth under Metabolic Stress. *Cancer Cell* 27, 57–71. <https://doi.org/10.1016/j.ccell.2014.12.002>
- Sciacovelli, M., Gonçalves, E., Johnson, T.I., Zecchini, V.R., da Costa, A.S.H., Gaude, E., Drubbel, A.V., Theobald, S.J., Abbo, S.R., Tran, M.G.B., Rajeeve, V., Cardaci, S., Foster, S., Yun, H., Cutillas, P., Warren, A., Gnanapragasam, V., Gottlieb, E., Franze, K., Huntly, B., Maher, E.R., Maxwell, P.H., Saez-Rodriguez, J., Frezza, C., 2016. Fumarate is an epigenetic modifier that elicits epithelial-to-mesenchymal transition. *Nature* 537, 544–547. <https://doi.org/10.1038/nature19353>
- Sebastián, C., Zwaans, B.M.M., Silberman, D.M., Gymrek, M., Goren, A., Zhong, L., Ram, O., Truelove, J., Guimaraes, A.R., Toiber, D., Cosentino, C., Greenson, J.K., MacDonald, A.I., McGlynn, L., Maxwell, F., Edwards, J., Giacosa, S., Guccione, E., Weissleder, R., Bernstein, B.E., Regev, A., Shiels, P.G., Lombard, D.B., Mostoslavsky, R., 2012. The Histone Deacetylase SIRT6 Is a Tumor Suppressor that Controls Cancer Metabolism. *Cell* 151, 1185–1199. <https://doi.org/10.1016/j.cell.2012.10.047>
- Seiwert, N., Heylmann, D., Hasselwander, S., Fahrner, J., 2020. Mechanism of colorectal carcinogenesis triggered by heme iron from red meat. *Biochim. Biophys. Acta BBA - Rev. Cancer* 1873, 188334. <https://doi.org/10.1016/j.bbcan.2019.188334>
- Seyedin, S.N., Hasibuzzaman, M.M., Pham, V., Petronek, M.S., Callaghan, C., Kalen, A.L., Mapuskar, K.A., Mott, S.L., Spitz, D.R., Allen, B.G., Caster, J.M., 2020. Combination Therapy with Radiation and PARP Inhibition Enhances Responsiveness to Anti-PD-1 Therapy in Colorectal Tumor Models. *Int. J. Radiat. Oncol., Radiation Therapy and the Immune Response* 108, 81–92. <https://doi.org/10.1016/j.ijrobp.2020.01.030>
- Seyfried, T.N., Arismendi-Morillo, G., Mukherjee, P., Chinopoulos, C., 2020. On the Origin of ATP Synthesis in Cancer. *iScience* 23, 101761. <https://doi.org/10.1016/j.isci.2020.101761>
- Sfeir, A., Symington, L.S., 2015. Microhomology-Mediated End Joining: A Back-up Survival Mechanism or Dedicated Pathway? *Trends Biochem. Sci.* 40, 701–714. <https://doi.org/10.1016/j.tibs.2015.08.006>
- Sharma, S., Javadekar, S.M., Pandey, M., Srivastava, M., Kumari, R., Raghavan, S.C., 2015. Homology and enzymatic requirements of microhomology-dependent alternative end joining. *Cell Death Dis.* 6, e1697. <https://doi.org/10.1038/cddis.2015.58>
- Shortt, J., Johnstone, R.W., 2012. Oncogenes in cell survival and cell death. *Cold Spring Harb. Perspect. Biol.* 4, a009829. <https://doi.org/10.1101/cshperspect.a009829>
- Siegel, R.L., Miller, K.D., Goding Sauer, A., Fedewa, S.A., Butterly, L.F., Anderson, J.C., Cercek, A., Smith, R.A., Jemal, A., 2020. Colorectal cancer statistics, 2020. *CA. Cancer J. Clin.* 70, 145–164. <https://doi.org/10.3322/caac.21601>
- Sinicrope, F.A., Rego, R.L., Okumura, K., Foster, N.R., O'Connell, M.J., Sargent, D.J., Windschitl, H.E., 2008. Prognostic Impact of Bim, Puma, and Noxa Expression in Human Colon Carcinomas. *Clin. Cancer Res.* 14, 5810–5818. <https://doi.org/10.1158/1078-0432.CCR-07-5202>
- Sionov, R.V., Vlahopoulos, S.A., Granot, Z., 2015. Regulation of Bim in Health and Disease. *Oncotarget* 6, 23058–23134.
- Sisay, M., Edessa, D., 2017. PARP inhibitors as potential therapeutic agents for various cancers: focus on niraparib and its first global approval for maintenance therapy of gynecologic cancers. *Gynecol. Oncol. Res. Pract.* 4, 18. <https://doi.org/10.1186/s40661-017-0055-8>
- Smeby, J., Kryeziu, K., Berg, K.C.G., Eilertsen, I.A., Eide, P.W., Johannessen, B., Guren, M.G., Nesbakken, A., Bruun, J., Lothe, R.A., Sveen, A., 2020. Molecular correlates of sensitivity to PARP inhibition beyond homologous recombination deficiency in pre-clinical models of colorectal cancer point to wild-type TP53 activity. *eBioMedicine* 59, 102923. <https://doi.org/10.1016/j.ebiom.2020.102923>

References

- Sobanski, T., Rose, M., Suraweera, A., O'Byrne, K., Richard, D.J., Bolderson, E., 2021. Cell Metabolism and DNA Repair Pathways: Implications for Cancer Therapy. *Front. Cell Dev. Biol.* 9.
- Son, H., Noh, K., Park, I., Na, M., Oh, S., Shin, B.S., Kang, W., 2019. Stereo-Selective Pharmacokinetics of Ilimaquinone Epimers Extracted from a Marine Sponge in Rats. *Mar. Drugs* 17, 171. <https://doi.org/10.3390/md17030171>
- Song, Z., Wei, B., Lu, C., Li, P., Chen, L., 2017. Glutaminase sustains cell survival via the regulation of glycolysis and glutaminolysis in colorectal cancer. *Oncol. Lett.* 14, 3117–3123. <https://doi.org/10.3892/ol.2017.6538>
- Sopik, V., Phelan, C., Cybulski, C., Narod, S.A., 2015. BRCA1 and BRCA2 mutations and the risk for colorectal cancer. *Clin. Genet.* 87, 411–418. <https://doi.org/10.1111/cge.12497>
- Sottoriva, A., Kang, H., Ma, Z., Graham, T.A., Salomon, M.P., Zhao, J., Marjoram, P., Siegmund, K., Press, M.F., Shibata, D., Curtis, C., 2015. A Big Bang model of human colorectal tumor growth. *Nat. Genet.* 47, 209–216. <https://doi.org/10.1038/ng.3214>
- Steigerwald, C., Rasenberger, B., Christmann, M., Tomicic, M.T., 2018. Sensitization of colorectal cancer cells to irinotecan by the Survivin inhibitor LLP3 depends on XAF1 proficiency in the context of mutated p53. *Arch. Toxicol.* 92, 2645–2648. <https://doi.org/10.1007/s00204-018-2240-x>
- Stiewe, T., Haran, T.E., 2018. How mutations shape p53 interactions with the genome to promote tumorigenesis and drug resistance. *Drug Resist. Updat.* 38, 27–43. <https://doi.org/10.1016/j.drug.2018.05.001>
- Stine, Z.E., Schug, Z.T., Salvino, J.M., Dang, C.V., 2022. Targeting cancer metabolism in the era of precision oncology. *Nat. Rev. Drug Discov.* 21, 141–162. <https://doi.org/10.1038/s41573-021-00339-6>
- Stoffel, E.M., Murphy, C.C., 2020. Epidemiology and Mechanisms of the Increasing Incidence of Colon and Rectal Cancers in Young Adults. *Gastroenterology, Colorectal Cancer: Recent Advances & Future Challenges* 158, 341–353. <https://doi.org/10.1053/j.gastro.2019.07.055>
- Stoppa-Lyonnet, D., 2016. The biological effects and clinical implications of BRCA mutations: where do we go from here? *Eur. J. Hum. Genet.* 24, S3–S9. <https://doi.org/10.1038/ejhg.2016.93>
- Strzeszewska-Potyrala, A., Staniak, K., Czarnecka-Herok, J., Rafiee, M.-R., Herok, M., Mosieniak, G., Krijgsveld, J., Sikora, E., 2021. Chromatin-Directed Proteomics Identifies ZNF84 as a p53-Independent Regulator of p21 in Genotoxic Stress Response. *Cancers* 13, 2115. <https://doi.org/10.3390/cancers13092115>
- Stuart, S.D., Schauble, A., Gupta, S., Kennedy, A.D., Keppler, B.R., Bingham, P.M., Zachar, Z., 2014. A strategically designed small molecule attacks alpha-ketoglutarate dehydrogenase in tumor cells through a redox process. *Cancer Metab.* 2, 4. <https://doi.org/10.1186/2049-3002-2-4>
- Sulzyc-Bielicka, V., Domagala, P., Hybiak, J., Majewicz-Broda, A., Safranow, K., Domagala, W., 2012. Colorectal cancers differ in respect of PARP-1 protein expression. *Pol. J. Pathol.* 63, 87–92.
- Sun, B., Chen, H., Wang, X., Chen, T., 2023. Regorafenib induces Bim-mediated intrinsic apoptosis by blocking AKT-mediated FOXO3a nuclear export. *Cell Death Discov.* 9, 1–11. <https://doi.org/10.1038/s41420-023-01338-9>
- Sun, X., Zhan, L., Chen, Y., Wang, G., He, L., Wang, Q., Zhou, F., Yang, F., Wu, J., Wu, Y., Xing, J., He, X., Huang, Q., 2018. Increased mtDNA copy number promotes cancer progression by enhancing mitochondrial oxidative phosphorylation in microsatellite-stable colorectal cancer. *Signal Transduct. Target. Ther.* 3, 1–9. <https://doi.org/10.1038/s41392-018-0011-z>
- Sung, H., Ferlay, J., Siegel, R.L., Laversanne, M., Soerjomataram, I., Jemal, A., Bray, F., 2021. Global Cancer Statistics 2020: GLOBOCAN Estimates of Incidence and Mortality Worldwide for 36 Cancers in 185 Countries. *CA. Cancer J. Clin.* 71, 209–249. <https://doi.org/10.3322/caac.21660>

- Tabata, S., Kojima, Y., Sakamoto, T., Igarashi, K., Umetsu, K., Ishikawa, T., Hirayama, A., Kajino-Sakamoto, R., Sakamoto, N., Yasumoto, K., Okano, K., Suzuki, Y., Yachida, S., Aoki, M., Soga, T., 2023. L-2hydroxyglutaric acid rewires amino acid metabolism in colorectal cancer via the mTOR-ATF4 axis. *Oncogene* 42, 1294–1307. <https://doi.org/10.1038/s41388-023-02632-7>
- Tabernero, J., Grothey, A., Van Cutsem, E., Yaeger, R., Wasan, H., Yoshino, T., Desai, J., Ciardiello, F., Loupakis, F., Hong, Y.S., Steeghs, N., Guren, T.K., Arkenau, H.-T., Garcia-Alfonso, P., Elez, E., Gollerkeri, A., Maharry, K., Christy-Bittel, J., Kopetz, S., 2021. Encorafenib Plus Cetuximab as a New Standard of Care for Previously Treated BRAF V600E–Mutant Metastatic Colorectal Cancer: Updated Survival Results and Subgroup Analyses from the BEACON Study. *J. Clin. Oncol.* 39, 273–284. <https://doi.org/10.1200/JCO.20.02088>
- Tabernero, J., Yoshino, T., Cohn, A.L., Obermannova, R., Bodoky, G., Garcia-Carbonero, R., Ciuleanu, T.-E., Portnoy, D.C., Cutsem, E.V., Grothey, A., Prausová, J., Garcia-Alfonso, P., Yamazaki, K., Clingan, P.R., Lonardi, S., Kim, T.W., Simms, L., Chang, S.-C., Nasroulah, F., 2015. Ramucirumab versus placebo in combination with second-line FOLFIRI in patients with metastatic colorectal carcinoma that progressed during or after first-line therapy with bevacizumab, oxaliplatin, and a fluoropyrimidine (RAISE): a randomised, double-blind, multicentre, phase 3 study. *Lancet Oncol.* 16, 499–508. [https://doi.org/10.1016/S1470-2045\(15\)70127-0](https://doi.org/10.1016/S1470-2045(15)70127-0)
- Tahara, M., Inoue, T., Sato, F., Miyakura, Y., Horie, H., Yasuda, Y., Fujii, H., Kotake, K., Sugano, K., 2014. The Use of Olaparib (AZD2281) Potentiates SN-38 Cytotoxicity in Colon Cancer Cells by Indirect Inhibition of Rad51-Mediated Repair of DNA Double-Strand Breaks. *Mol. Cancer Ther.* 13, 1170–1180. <https://doi.org/10.1158/1535-7163.MCT-13-0683>
- Tang, J., Wu, W., Yang, F., Liu, Liyun, Yang, Z., Liu, Li, Tang, W., Sun, F., Lin, H., 2018. Marine sponge-derived smenospongine preferentially eliminates breast cancer stem-like cells via p38/AMPK α pathways. *Cancer Med.* 7, 3965–3976. <https://doi.org/10.1002/cam4.1640>
- Tang, J., Yan, T., Bao, Y., Shen, C., Yu, C., Zhu, X., Tian, X., Guo, F., Liang, Q., Liu, Q., Zhong, M., Chen, J., Ge, Z., Li, X., Chen, X., Cui, Y., Chen, Y., Zou, W., Chen, H., Hong, J., Fang, J.-Y., 2019. LncRNA GLCC1 promotes colorectal carcinogenesis and glucose metabolism by stabilizing c-Myc. *Nat. Commun.* 10, 3499. <https://doi.org/10.1038/s41467-019-11447-8>
- Tarrado-Castellarnau, M., de Atauri, P., Cascante, M., 2016. Oncogenic regulation of tumor metabolic reprogramming. *Oncotarget* 7, 62726–62753. <https://doi.org/10.18632/oncotarget.10911>
- Thanki, K., Nicholls, M.E., Gajjar, A., Senagore, A.J., Qiu, S., Szabo, C., Hellmich, M.R., Chao, C., 2017. Consensus Molecular Subtypes of Colorectal Cancer and their Clinical Implications. *Int. Biol. Biomed. J.* 3, 105–111.
- Thiery, J.P., Acloque, H., Huang, R.Y.J., Nieto, M.A., 2009. Epithelial-Mesenchymal Transitions in Development and Disease. *Cell* 139, 871–890. <https://doi.org/10.1016/j.cell.2009.11.007>
- Thirion, P., Michiels, S., Pignon, J.P., Buyse, M., Braud, A.C., Carlson, R.W., O'Connell, M., Sargent, P., Piedbois, P., Meta-Analysis Group in Cancer, 2004. Modulation of fluorouracil by leucovorin in patients with advanced colorectal cancer: an updated meta-analysis. *J. Clin. Oncol. Off. J. Am. Soc. Clin. Oncol.* 22, 3766–3775. <https://doi.org/10.1200/JCO.2004.03.104>
- Thomas, A., Murai, J., Pommier, Y., 2018. The evolving landscape of predictive biomarkers of response to PARP inhibitors. *J. Clin. Invest.* 128, 1727–1730. <https://doi.org/10.1172/JCI120388>
- Thomas, A., Pommier, Y., 2019. Targeting Topoisomerase I in the Era of Precision Medicine. *Clin. Cancer Res.* 25, 6581–6589. <https://doi.org/10.1158/1078-0432.CCR-19-1089>
- Thorsell, A.-G., Ekblad, T., Karlberg, T., Löw, M., Pinto, A.F., Trésaugues, L., Moche, M., Cohen, M.S., Schüler, H., 2017. Structural Basis for Potency and Promiscuity in Poly(ADP-ribose) Polymerase (PARP) and Tankyrase Inhibitors. *J. Med. Chem.* 60, 1262–1271. <https://doi.org/10.1021/acs.jmedchem.6b00990>

References

- Tian, L., Song, S., Liu, X., Wang, Y., Xu, X., Hu, Y., Xu, J., 2014. Schlafen-11 sensitizes colorectal carcinoma cells to irinotecan. *Anticancer. Drugs* 25, 1175–1181. <https://doi.org/10.1097/CAD.0000000000000151>
- Tian, X.-H., Hong, L.-L., Jiao, W.-H., Lin, H.-W., 2023. Natural sesquiterpene quinone/quinols: chemistry, biological activity, and synthesis. *Nat. Prod. Rep.* 40, 718–749. <https://doi.org/10.1039/D2NP00045H>
- Tran, T.Q., Hanse, E.A., Habowski, A.N., Li, H., Ishak Gabra, M.B., Yang, Y., Lowman, X.H., Ooi, A.M., Liao, S.Y., Edwards, R.A., Waterman, M.L., Kong, M., 2020. α -Ketoglutarate attenuates Wnt signaling and drives differentiation in colorectal cancer. *Nat. Cancer* 1, 345–358. <https://doi.org/10.1038/s43018-020-0035-5>
- Tseng, C.-W., Kuo, W.-H., Chan, S.-H., Chan, H.-L., Chang, K.-J., Wang, L.-H., 2018. Transketolase Regulates the Metabolic Switch to Control Breast Cancer Cell Metastasis via the α -Ketoglutarate Signaling Pathway. *Cancer Res.* 78, 2799–2812. <https://doi.org/10.1158/0008-5472.CAN-17-2906>
- Tsuji, M., Kamano, S., Tsuji, S., Sawaoka, H., H'ori, M., DuBois, R.N., 1998. Cyclooxygenase Regulates Angiogenesis Induced by Colon Cancer Cells. *Cell* 93, 705–716.
- Tsushima, H., Ito, N., Tamura, S., Matsuda, Y., Inada, M., Yabuuchi, I., Imai, Y., Nagashima, R., Misawa, H., Takeda, H., Matsuzawa, Y., Kawata, S., 2001. Circulating Transforming Growth Factor β 1 as a Predictor of Liver Metastasis after Resection in Colorectal Cancer. *Clin. Cancer Res.* 7, 1258–1262.
- Turner, N., Tutt, A., Ashworth, A., 2004. Hallmarks of “BRCAness” in sporadic cancers. *Nat. Rev. Cancer* 4, 814–819. <https://doi.org/10.1038/nrc1457>
- Valle, L., Vilar, E., Tavtigian, S.V., Stoffel, E.M., 2019. Genetic predisposition to colorectal cancer: syndromes, genes, classification of genetic variants and implications for precision medicine. *J. Pathol.* 247, 574–588. <https://doi.org/10.1002/path.5229>
- van der Geest, L.G.M., Lam-Boer, J., Koopman, M., Verhoef, C., Elferink, M.A.G., de Wilt, J.H.W., 2015. Nationwide trends in incidence, treatment and survival of colorectal cancer patients with synchronous metastases. *Clin. Exp. Metastasis* 32, 457–465. <https://doi.org/10.1007/s10585-015-9719-0>
- van Osch, F.H.M., Voets, A.M., Schouten, L.J., Gottschalk, R.W.H., Simons, C.C.J.M., van Engeland, M., Lentjes, M.H.F.M., van den Brandt, P.A., Smeets, H.J.M., Weijnen, M.P., 2015. Mitochondrial DNA copy number in colorectal cancer: between tissue comparisons, clinicopathological characteristics and survival. *Carcinogenesis* 36, 1502–1510. <https://doi.org/10.1093/carcin/bgv151>
- van Stuijvenberg, J., Proksch, P., Fritz, G., 2020. Targeting the DNA damage response (DDR) by natural compounds. *Bioorg. Med. Chem.* 28, 115279. <https://doi.org/10.1016/j.bmc.2019.115279>
- Vaughn, C.P., ZoBell, S.D., Furtado, L.V., Baker, C.L., Samowitz, W.S., 2011. Frequency of KRAS, BRAF, and NRAS mutations in colorectal cancer. *Genes. Chromosomes Cancer* 50, 307–312. <https://doi.org/10.1002/gcc.20854>
- Vellinga, T.T., Borovski, T., de Boer, V.C.J., Fatrai, S., van Schelven, S., Trumpi, K., Verheem, A., Snoeren, N., Emmink, B.L., Koster, J., Rinkes, I.H.M.B., Kranenburg, O., 2015. SIRT1/PGC1 α -Dependent Increase in Oxidative Phosphorylation Supports Chemotherapy Resistance of Colon Cancer. *Clin. Cancer Res. Off. J. Am. Assoc. Cancer Res.* 21, 2870–2879. <https://doi.org/10.1158/1078-0432.CCR-14-2290>
- Venkitaraman, A.R., 2001. Functions of BRCA1 and BRCA2 in the biological response to DNA damage. *J. Cell Sci.* 114, 3591–3598. <https://doi.org/10.1242/jcs.114.20.3591>
- Vilar, E., Bartnik, C.M., Stenzel, S.L., Raskin, L., Ahn, J., Moreno, V., Mukherjee, B., Iniesta, M.D., Morgan, M.A., Rennert, G., Gruber, S.B., 2011. MRE11 Deficiency Increases Sensitivity to Poly(ADP-ribose) Polymerase Inhibition in Microsatellite Unstable Colorectal Cancers. *Cancer Res.* 71, 2632–2642. <https://doi.org/10.1158/0008-5472.CAN-10-1120>
- Vincent, E.E., Sergushichev, A., Griss, T., Gingras, M.-C., Samborska, B., Ntimbane, T., Coelho, P.P., Blagih, J., Raissi, T.C., Choinière, L., Bridon, G., Loginicheva, E., Flynn, B.R., Thomas, E.C., Tavaré, J.M., Avizonis, D., Pause, A., Elder, D.J.E., Artyomov, M.N.,

References

- Jones, R.G., 2015. Mitochondrial Phosphoenolpyruvate Carboxykinase Regulates Metabolic Adaptation and Enables Glucose-Independent Tumor Growth. *Mol. Cell* 60, 195–207. <https://doi.org/10.1016/j.molcel.2015.08.013>
- Vitiello, P.P., Cardone, C., Ciardiello, D., Belli, V., Matrone, N., Borrelli, C., Poliero, L., Falco, V.D., Giunta, E.F., Vitale, P., Zanaletti, N., Tirino, G., Troiani, T., Ciardiello, F., Martinelli, E., 2018. Combination treatment with the PARP inhibitor niraparib and chemotherapeutics in a preclinical model of KRAS/BRAF mutated colorectal cancer cell lines across the four consensus molecular subtypes. *Ann. Oncol.* 29, viii5. <https://doi.org/10.1093/annonc/mdy268.017>
- Vodenkova, S., Buchler, T., Cervena, K., Veskrnova, V., Vodicka, P., Vymetalkova, V., 2020. 5-fluorouracil and other fluoropyrimidines in colorectal cancer: Past, present and future. *Pharmacol. Ther.* 206, 107447. <https://doi.org/10.1016/j.pharmthera.2019.107447>
- Vogel, A., Hofheinz, R.D., Kubicka, S., Arnold, D., 2017. Treatment decisions in metastatic colorectal cancer – Beyond first and second line combination therapies. *Cancer Treat. Rev.* 59, 54–60. <https://doi.org/10.1016/j.ctrv.2017.04.007>
- Vogelstein, B., Fearon, E.R., Hamilton, S.R., Kern, S.E., Preisinger, A.C., Leppert, M., Smits, A.M.M., Bos, J.L., 1988. Genetic Alterations during Colorectal-Tumor Development. *N. Engl. J. Med.* 319, 525–532. <https://doi.org/10.1056/NEJM198809013190901>
- Waitkus, M.S., Diplas, B.H., Yan, H., 2018. Biological Role and Therapeutic Potential of IDH Mutations in Cancer. *Cancer Cell* 34, 186–195. <https://doi.org/10.1016/j.ccell.2018.04.011>
- Wakefield, L.M., Hill, C.S., 2013. Beyond TGF β : roles of other TGF β superfamily members in cancer. *Nat. Rev. Cancer* 13, 328–341. <https://doi.org/10.1038/nrc3500>
- Walko, C.M., Lindley, C., 2005. Capecitabine: a review. *Clin. Ther.* 27, 23–44. <https://doi.org/10.1016/j.clinthera.2005.01.005>
- Walther, A., Houlston, R., Tomlinson, I., 2008. Association between chromosomal instability and prognosis in colorectal cancer: a meta-analysis. *Gut* 57, 941–950. <https://doi.org/10.1136/gut.2007.135004>
- Wan, X., Li, Z.-G., Yingling, J.M., Yang, J., Starbuck, M.W., Ravoori, M.K., Kundra, V., Vazquez, E., Navone, N.M., 2012. Effect of transforming growth factor beta (TGF- β) receptor I kinase inhibitor on prostate cancer bone growth. *Bone* 50, 695–703. <https://doi.org/10.1016/j.bone.2011.11.022>
- Wang, C., Jette, N., Moussienko, D., Bebb, D.G., Lees-Miller, S.P., 2017. ATM-Deficient Colorectal Cancer Cells Are Sensitive to the PARP Inhibitor Olaparib. *Transl. Oncol.* 10, 190–196. <https://doi.org/10.1016/j.tranon.2017.01.007>
- Wang, H., Chen, Y., Wu, G., 2016a. SDHB deficiency promotes TGF β -mediated invasion and metastasis of colorectal cancer through transcriptional repression complex SNAIL1-SMAD3/4. *Transl. Oncol.* 9, 512–520. <https://doi.org/10.1016/j.tranon.2016.09.009>
- Wang, H., Liang, L., Fang, J.-Y., Xu, J., 2016b. Somatic gene copy number alterations in colorectal cancer: new quest for cancer drivers and biomarkers. *Oncogene* 35, 2011–2019. <https://doi.org/10.1038/onc.2015.304>
- Wang, H., Ren, B., Liu, Ye, Jiang, B., Guo, Y., Wei, M., Luo, L., Kuang, X., Qiu, M., Lv, L., Xu, H., Qi, R., Yan, H., Xu, D., Wang, Z., Huo, C.-X., Zhu, Y., Zhao, Y., Wu, Y., Qin, Z., Su, D., Tang, T., Wang, F., Sun, X., Feng, Y., Peng, H., Wang, X., Gao, Y., Liu, Yong, Gong, W., Yu, F., Liu, X., Wang, L., Zhou, C., 2020. Discovery of Pamiparib (BGB-290), a Potent and Selective Poly (ADP-ribose) Polymerase (PARP) Inhibitor in Clinical Development. *J. Med. Chem.* 63, 15541–15563. <https://doi.org/10.1021/acs.jmedchem.0c01346>
- Wang, W., Subramani, S., 2017. Role of PEX5 ubiquitination in maintaining peroxisome dynamics and homeostasis. *Cell Cycle* 16, 2037–2045. <https://doi.org/10.1080/15384101.2017.1376149>
- Wang, Y.-C., Wang, L.-T., Hung, T.I., Hong, Y.-R., Chen, C.-H., Ho, C.-J., Wang, C., 2022. Severe cellular stress drives apoptosis through a dual control mechanism independently of p53. *Cell Death Discov.* 8, 1–5. <https://doi.org/10.1038/s41420-022-01078-2>

References

- Wang, Z., Fan, M., Candas, D., Zhang, T.-Q., Qin, L., Eldridge, A., Wachsmann-Hogiu, S., Ahmed, K.M., Chromy, B.A., Nantajit, D., Duru, N., He, F., Chen, M., Finkel, T., Weinstein, L.S., Li, J.J., 2014. Cyclin B1/Cdk1 coordinates mitochondrial respiration for cell-cycle G2/M progression. *Dev. Cell* 29, 217–232. <https://doi.org/10.1016/j.devcel.2014.03.012>
- Ward, P.S., Thompson, C.B., 2012. Metabolic Reprogramming: A Cancer Hallmark Even Warburg Did Not Anticipate. *Cancer Cell* 21, 297–308. <https://doi.org/10.1016/j.ccr.2012.02.014>
- Wei, Q., Qian, Y., Yu, J., Wong, C.C., 2020. Metabolic rewiring in the promotion of cancer metastasis: mechanisms and therapeutic implications. *Oncogene* 39, 6139–6156. <https://doi.org/10.1038/s41388-020-01432-7>
- Wen, Y.-A., Xiong, X., Scott, T., Li, A.T., Wang, C., Weiss, H.L., Tan, L., Bradford, E., Fan, T.W.M., Chandel, N.S., Barrett, T.A., Gao, T., 2019. The mitochondrial retrograde signaling regulates Wnt signaling to promote tumorigenesis in colon cancer. *Cell Death Differ.* 26, 1955–1969. <https://doi.org/10.1038/s41418-018-0265-6>
- Wickenden, J.A., Jin, H., Johnson, M., Gillings, A.S., Newson, C., Austin, M., Chell, S.D., Balmanno, K., Pritchard, C.A., Cook, S.J., 2008. Colorectal cancer cells with the BRAFV600E mutation are addicted to the ERK1/2 pathway for growth factor-independent survival and repression of BIM. *Oncogene* 27, 7150–7161. <https://doi.org/10.1038/onc.2008.335>
- Wongkittichote, P., Ah Mew, N., Chapman, K.A., 2017. Propionyl-CoA carboxylase – A review. *Mol. Genet. Metab.* 122, 145–152. <https://doi.org/10.1016/j.ymgme.2017.10.002>
- Wu, W., Kong, Z., Duan, X., Zhu, H., Li, S., Zeng, S., Liang, Y., Iliakis, G., Gui, Z., Yang, D., 2013. Inhibition of PARP1 by small interfering RNA enhances docetaxel activity against human prostate cancer PC3 cells. *Biochem. Biophys. Res. Commun.* 442, 127–132. <https://doi.org/10.1016/j.bbrc.2013.11.027>
- Xie, Y.-H., Chen, Y.-X., Fang, J.-Y., 2020. Comprehensive review of targeted therapy for colorectal cancer. *Signal Transduct. Target. Ther.* 5, 1–30. <https://doi.org/10.1038/s41392-020-0116-z>
- Xiong, W., Jiao, Y., Huang, W., Ma, M., Yu, M., Cui, Q., Tan, D., 2012. Regulation of the cell cycle via mitochondrial gene expression and energy metabolism in HeLa cells. *Acta Biochim. Biophys. Sin.* 44, 347–358. <https://doi.org/10.1093/abbs/gms006>
- Xiong, Y., Guo, Y., Liu, Ye, Wang, H., Gong, W., Liu, Yong, Wang, X., Gao, Y., Yu, F., Su, D., Wang, F., Zhu, Y., Zhao, Y., Wu, Y., Qin, Z., Sun, X., Ren, B., Jiang, Bin, Jin, W., Shen, Z., Tang, Z., Song, X., Wang, L., Liu, X., Zhou, C., Jiang, Beibei, 2020. Pamiparib is a potent and selective PARP inhibitor with unique potential for the treatment of brain tumor. *Neoplasia* 22, 431–440. <https://doi.org/10.1016/j.neo.2020.06.009>
- Xu, F., Sun, Y., Yang, S.-Z., Zhou, T., Jhala, N., McDonald, J., Chen, Y., 2019. Cytoplasmic PARP-1 promotes pancreatic cancer tumorigenesis and resistance. *Int. J. Cancer* 145, 474–483. <https://doi.org/10.1002/ijc.32108>
- Xu, X., Li, J., Sun, X., Guo, Y., Chu, D., Wei, Li, Li, X., Yang, G., Liu, X., Yao, L., Zhang, J., Shen, L., 2015. Tumor suppressor NDRG2 inhibits glycolysis and glutaminolysis in colorectal cancer cells by repressing c-Myc expression. *Oncotarget* 6, 26161–26176.
- Xu, Y., Pasche, B., 2007. TGF- β signaling alterations and susceptibility to colorectal cancer. *Hum. Mol. Genet.* 16, R14–R20. <https://doi.org/10.1093/hmg/ddl486>
- Xue, H., Bhardwaj, A., Yin, Y., Fijen, C., Ephstein, A., Zhang, L., Ding, X., Pascal, J.M., VanArsdale, T.L., Rothenberg, E., 2022. A two-step mechanism governing PARP1-DNA retention by PARP inhibitors. *Sci. Adv.* 8, eabq0414. <https://doi.org/10.1126/sciadv.abq0414>
- Yagi, K., Akagi, K., Hayashi, H., Nagae, G., Tsuji, S., Isagawa, T., Midorikawa, Y., Nishimura, Y., Sakamoto, H., Seto, Y., Aburatani, H., Kaneda, A., 2010. Three DNA Methylation Epigenotypes in Human Colorectal Cancer. *Clin. Cancer Res.* 16, 21–33. <https://doi.org/10.1158/1078-0432.CCR-09-2006>

- Yamane, L., Scapulatempo-Neto, C., Reis, R.M., Guimarães, D.P., 2014. Serrated pathway in colorectal carcinogenesis. *World J. Gastroenterol. WJG* 20, 2634–2640. <https://doi.org/10.3748/wjg.v20.i10.2634>
- Yamazaki, T., Gunderson, A.J., Gilchrist, M., Whiteford, M., Kiely, M.X., Hayman, A., O'Brien, D., Ahmad, R., Manchio, J.V., Fox, N., McCarty, K., Phillips, M., Brosnan, E., Vaccaro, G., Li, R., Simon, M., Bernstein, E., McCormick, M., Yamasaki, L., Wu, Y., Drokin, A., Carnahan, T., To, Y., Redmond, W.L., Lee, B., Louie, J., Hansen, E., Solhjem, M.C., Cramer, J., Urba, W.J., Gough, M.J., Crittenden, M.R., Young, K.H., 2022. Galunisertib plus neoadjuvant chemoradiotherapy in patients with locally advanced rectal cancer: a single-arm, phase 2 trial. *Lancet Oncol.* 23, 1189–1200. [https://doi.org/10.1016/S1470-2045\(22\)00446-6](https://doi.org/10.1016/S1470-2045(22)00446-6)
- Yang, G., Liu, C., Chen, S.-H., Kassab, M.A., Hoff, J.D., Walter, N.G., Yu, X., 2018. Super-resolution imaging identifies PARP1 and the Ku complex acting as DNA double-strand break sensors. *Nucleic Acids Res.* 46, 3446–3457. <https://doi.org/10.1093/nar/gky088>
- Yang, M., Soga, T., Pollard, P.J., 2013. Oncometabolites: linking altered metabolism with cancer. *J. Clin. Invest.* 123, 3652–3658. <https://doi.org/10.1172/JCI67228>
- Yang, Y., Liu, L., Naik, I., Braunstein, Z., Zhong, J., Ren, B., 2017. Transcription Factor C/EBP Homologous Protein in Health and Diseases. *Front. Immunol.* 8, 1612. <https://doi.org/10.3389/fimmu.2017.01612>
- Yarom, N., Jonker, D.J., 2011. The Role of the Epidermal Growth Factor Receptor in the Mechanism and Treatment of Colorectal Cancer. *Discov. Med.* 11, 95–105.
- Yazinski, S.A., Comaills, V., Buisson, R., Genoie, M.-M., Nguyen, H.D., Ho, C.K., Todorova Kwan, T., Morris, R., Lauffer, S., Nussenzweig, A., Ramaswamy, S., Benes, C.H., Haber, D.A., Maheswaran, S., Birrer, M.J., Zou, L., 2017. ATR inhibition disrupts rewired homologous recombination and fork protection pathways in PARP inhibitor-resistant BRCA-deficient cancer cells. *Genes Dev.* 31, 318–332. <https://doi.org/10.1101/gad.290957.116>
- Yoo, B.H., Masson, O., Li, Y., Khan, I.A., Gowda, P.S., Rosen, K.V., 2015. Anoikis of colon carcinoma cells triggered by β -catenin loss can be enhanced by tumor necrosis factor receptor 1 antagonists. *Oncogene* 34, 4939–4951. <https://doi.org/10.1038/onc.2014.415>
- Yu, L., Chen, X., Wang, L., Chen, S., 2016. The sweet trap in tumors: aerobic glycolysis and potential targets for therapy. *Oncotarget* 7, 38908–38926. <https://doi.org/10.18632/oncotarget.7676>
- Yue, D., Sun, X., 2018. Idelalisib promotes Bim-dependent apoptosis through AKT/FoxO3a in hepatocellular carcinoma. *Cell Death Dis.* 9, 1–11. <https://doi.org/10.1038/s41419-018-0960-8>
- Zachar, Z., Marecek, J., Maturo, C., Gupta, S., Stuart, S.D., Howell, K., Schauble, A., Lem, J., Piramzadian, A., Karnik, S., Lee, K., Rodriguez, R., Shorr, R., Bingham, P.M., 2011. Non-redox-active lipolate derivatives disrupt cancer cell mitochondrial metabolism and are potent anticancer agents in vivo. *J. Mol. Med. Berl. Ger.* 89, 1137–1148. <https://doi.org/10.1007/s00109-011-0785-8>
- Zandarashvili, L., Langelier, M.-F., Velagapudi, U.K., Hancock, M.A., Steffen, J.D., Billur, R., Hannan, Z.M., Wicks, A.J., Krastev, D.B., Pettitt, S.J., Lord, C.J., Talele, T.T., Pascal, J.M., Black, B.E., 2020. Structural basis for allosteric PARP-1 retention on DNA breaks. *Science* 368, eaax6367. <https://doi.org/10.1126/science.aax6367>
- Zavadil, J., Böttinger, E.P., 2005. TGF- β and epithelial-to-mesenchymal transitions. *Oncogene* 24, 5764–5774. <https://doi.org/10.1038/sj.onc.1208927>
- Zawacka-Pankau, J., Grinkevich, V.V., Hünten, S., Nikulenkov, F., Gluch, A., Li, H., Enge, M., Kel, A., Selivanova, G., 2011. Inhibition of Glycolytic Enzymes Mediated by Pharmacologically Activated p53 TARGETING WARBURG EFFECT TO FIGHT CANCER. *J. Biol. Chem.* 286, 41600–41615. <https://doi.org/10.1074/jbc.M111.240812>
- Zeng, M., Kikuchi, H., Pino, M.S., Chung, D.C., 2010. Hypoxia Activates the K-Ras Proto-Oncogene to Stimulate Angiogenesis and Inhibit Apoptosis in Colon Cancer Cells. *PLOS ONE* 5, e10966. <https://doi.org/10.1371/journal.pone.0010966>

- Zhang, B., Halder, S.K., Zhang, S., Datta, P.K., 2009. Targeting transforming growth factor- β signaling in liver metastasis of colon cancer. *Cancer Lett.* 277, 114–120. <https://doi.org/10.1016/j.canlet.2008.11.035>
- Zhang, C., Lin, M., Wu, R., Wang, X., Yang, B., Levine, A.J., Hu, W., Feng, Z., 2011. Parkin, a p53 target gene, mediates the role of p53 in glucose metabolism and the Warburg effect. *Proc. Natl. Acad. Sci.* 108, 16259–16264. <https://doi.org/10.1073/pnas.1113884108>
- Zhang, C., Liu, J., Liang, Y., Wu, R., Zhao, Y., Hong, X., Lin, M., Yu, H., Liu, L., Levine, A.J., Hu, W., Feng, Z., 2013. Tumour-associated mutant p53 drives the Warburg effect. *Nat. Commun.* 4, 2935. <https://doi.org/10.1038/ncomms3935>
- Zhang, D., Wang, W., Xiang, B., Li, N., Huang, S., Zhou, W., Sun, Y., Wang, X., Ma, J., Li, G., Li, X., Shen, S., 2013. Reduced succinate dehydrogenase B expression is associated with growth and de-differentiation of colorectal cancer cells. *Tumor Biol.* 34, 2337–2347. <https://doi.org/10.1007/s13277-013-0781-4>
- Zhang, J., Zou, S., Fang, L., 2023. Metabolic reprogramming in colorectal cancer: regulatory networks and therapy. *Cell Biosci.* 13, 25. <https://doi.org/10.1186/s13578-023-00977-w>
- Zhang, L., Shay, J.W., 2017. Multiple Roles of APC and its Therapeutic Implications in Colorectal Cancer. *JNCI J. Natl. Cancer Inst.* 109, djw332. <https://doi.org/10.1093/jnci/djw332>
- Zhang, L., Xing, X., Meng, F., Wang, Y., Zhong, D., 2018. Oral fluoropyrimidine versus intravenous 5-fluorouracil for the treatment of advanced gastric and colorectal cancer: Meta-analysis. *J. Gastroenterol. Hepatol.* 33, 209–225. <https://doi.org/10.1111/jgh.13845>
- Zhang, Q., Yang, X., Wu, J., Ye, S., Gong, J., Cheng, W.M., Luo, Z., Yu, J., Liu, Y., Zeng, W., Liu, C., Xiong, Z., Chen, Y., He, Z., Lan, P., 2023. Reprogramming of palmitic acid induced by dephosphorylation of ACOX1 promotes β -catenin palmitoylation to drive colorectal cancer progression. *Cell Discov.* 9, 1–19. <https://doi.org/10.1038/s41421-022-00515-x>
- Zhang, Y., Hunter, T., 2014. Roles of Chk1 in Cell Biology and Cancer Therapy. *Int. J. Cancer J. Int. Cancer* 134, 10.1002/ijc.28226. <https://doi.org/10.1002/ijc.28226>
- Zhang, Y., Nie, L., Xu, K., Fu, Y., Zhong, J., Gu, K., Zhang, L., 2019. SIRT6, a novel direct transcriptional target of FoxO3a, mediates colon cancer therapy. *Theranostics* 9, 2380–2394. <https://doi.org/10.7150/thno.29724>
- Zhao, Y., Zhao, X., Chen, V., Feng, Y., Wang, L., Croniger, C., Conlon, R.A., Markowitz, S., Fearon, E., Puchowicz, M., Brunengraber, H., Hao, Y., Wang, Z., 2019. Colorectal cancers utilize glutamine as an anaplerotic substrate of the TCA cycle in vivo. *Sci. Rep.* 9, 1–9. <https://doi.org/10.1038/s41598-019-55718-2>
- Zhong, L., D'Urso, A., Toiber, D., Sebastian, C., Henry, R.E., Vadysirisack, D.D., Guimaraes, A., Marinelli, B., Wikstrom, J.D., Nir, T., Clish, C.B., Vaitheesvaran, B., Iliopoulos, O., Kurland, I., Dor, Y., Weissleder, R., Shirihai, O.S., Ellisen, L.W., Espinosa, J.M., Mostoslavsky, R., 2010. The histone deacetylase Sirt6 regulates glucose homeostasis via Hif1alpha. *Cell* 140, 280–293. <https://doi.org/10.1016/j.cell.2009.12.041>
- Zhou, H., Liu, Z., Wang, Y., Wen, X., Amador, E.H., Yuan, L., Ran, X., Xiong, L., Ran, Y., Chen, W., Wen, Y., 2022. Colorectal liver metastasis: molecular mechanism and interventional therapy. *Signal Transduct. Target. Ther.* 7, 1–25. <https://doi.org/10.1038/s41392-022-00922-2>
- Zhu, Y., Richardson, J.A., Parada, L.F., Graff, J.M., 1998. Smad3 Mutant Mice Develop Metastatic Colorectal Cancer. *Cell* 94, 703–714. [https://doi.org/10.1016/S0092-8674\(00\)81730-4](https://doi.org/10.1016/S0092-8674(00)81730-4)
- Zimmermann, M., Bernier, C., Kaiser, B., Fournier, S., Li, L., Desjardins, J., Skeldon, A., Rimkunas, V., Veloso, A., Young, J.T.F., Roulston, A., Zinda, M., 2022. Guiding ATR and PARP inhibitor combinations with chemogenomic screens. *Cell Rep.* 40. <https://doi.org/10.1016/j.celrep.2022.111081>

8. Acknowledgements

[Redacted text block 1]

[Redacted text block 2]

[Redacted text block 3]

[Redacted text block 4]

[Redacted text block 5]

[Redacted text block 6]

[Redacted text block 7]

[Redacted text block 8]

[Redacted text]

[Redacted text]

[Redacted text]

[Redacted text]

9. Curriculum Vitae

Personal Details

Name	Philipp Demuth
Date of Birth	████████
Place of Birth	Hachenburg

Academic Education and Engagements

Since 06/2023	BASF SE, Experimental Toxicology and Ecology Head of the Laboratory for the Development of New Approach Methods
01/2020 – 03/2023	Technical University Kaiserslautern, Department of Food Chemistry and Toxicology Experimental work on the Doctoral Thesis with the project title: “Application of the lipoic acid derivative CPI-613 in the treatment of colorectal cancer” supervised by Prof. Jörg Fahrer
Since 10/2021	Training for Expert Toxicologists (DGPT)
10/2015 – 10/2018	Technical University Kaiserslautern M.Sc. Toxicology
09/2012 – 09/2015	Johannes Gutenberg-University, Mainz B.Sc. Biology
08/2003 – 03/2012	Martin Butzer-Gymnasium, Dierdorf Allgemeine Hochschulreife

10. Publications

Neitzel, C.* **Demuth, P.***, Wittmann, S., Fahrer, J., 2020. Targeting Altered Energy Metabolism in Colorectal Cancer: Oncogenic Reprogramming, the Central Role of the TCA Cycle and Therapeutic Opportunities. *Cancers* 12, 1731.

<https://doi.org/10.3390/cancers12071731>

Seiwert, N., Wecklein, S., **Demuth, P.**, Hasselwander, S., Kemper, T.A., Schwerdtle, T., Brunner, T., Fahrer, J., 2020b. Heme oxygenase 1 protects human colonocytes against ROS formation, oxidative DNA damage and cytotoxicity induced by heme iron, but not inorganic iron. *Cell Death Dis* 11, 1–16.

<https://doi.org/10.1038/s41419-020-02950-8>

Jiso, A., **Demuth, P.**, Bachowsky, M., Haas, M., Seiwert, N., Heylmann, D., Rasenberger, B., Christmann, M., Dietrich, L., Brunner, T., Riyanti, Schäberle, T.F., Plubrukarn, A., Fahrer, J., 2021a. Natural Merosesquiterpenes Activate the DNA Damage Response via DNA Strand Break Formation and Trigger Apoptotic Cell Death in p53-Wild-Type and Mutant Colorectal Cancer. *Cancers* 13, 3282.

<https://doi.org/10.3390/cancers13133282>

Arnold, C.* **Demuth, P.***, Seiwert, N., Wittmann, S., Boengler, K., Rasenberger, B., Christmann, M., Huber, M., Brunner, T., Linnebacher, M., Fahrer, J., 2022. The Mitochondrial Disruptor Devimistat (CPI-613) Synergizes with Genotoxic Anticancer Drugs in Colorectal Cancer Therapy in a Bim-Dependent Manner. *Mol Cancer Ther* 21, 100–112.

<https://doi.org/10.1158/1535-7163.MCT-21-0393>

Carlsson, M.J., Vollmer, A.S., **Demuth, P.**, Heylmann, D., Reich, D., Quarz, C., Rasenberger, B., Nikolova, T., Hofmann, T.G., Christmann, M., Fuhlbrueck, J.A., Stegmüller, S., Richling, E., Cartus, A.T., Fahrer, J., 2022. p53 triggers mitochondrial apoptosis following DNA damage-dependent replication stress by the hepatotoxin methyleugenol. *Cell Death Dis* 13, 1009.

<https://doi.org/10.1038/s41419-022-05446-9>

Demuth, P., Thibol, L., Lemsch, A., Potlitz, F., Schulig, L., Grathwol, C., Manolikakes, G., Schade, D., Roukos, V., Link, A., Fahrer, J. 2024. Targeting PARP-1 and DNA Damage Response Defects in Colorectal Cancer Chemotherapy with Established and Novel PARP Inhibitors. *Cancers*, 16(20), 3441.

<https://doi.org/10.3390/cancers16203441>

*Shared first authorship

11. Conference Attendances

6th German Pharm-Tox Summit, Digital, March 1st – March 3rd, 2021, oral presentation (Synergism of the metabolic inhibitor CPI-613 and genotoxic chemotherapeutics in colorectal cancer therapy through a p53-independent mitochondrial apoptosis pathway)

7th GUM Young Scientist Workshop, Digital, March 17th, 2021, oral presentation (Metabolic inhibition by CPI-613 synergizes with DNA damage inducing chemotherapeutics in colorectal cancer therapy)

7th German Pharm-Tox Summit, Digital, March 7th – March 10th, 2022, oral presentation (Natural Merosesquiterpenes induce apoptotic cell death in p53-wild-type and mutant colorectal cancer via DNA strand break formation)

8th GUM Young Scientist Workshop, Würzburg, October 4th, 2022, oral presentation (Targeting colorectal cancer with the metabolic inhibitor Devimistat: Synergistic mechanism with genotoxic anticancer drugs and putative antimetastatic activity)

33rd GUM Meeting, Würzburg, October 5th - October 7th, 2022, poster presentation (Targeting colorectal cancer with the metabolic inhibitor Devimistat: Synergistic mechanism with genotoxic anticancer drugs and putative antimetastatic activity) **Award for best poster**

8th German Pharm-Tox Summit, Ulm, March 7th – March 10th, 2023, oral presentation (Metabolic inhibition by Devimistat in colorectal cancer treatment: Mechanism of synergy with genotoxic drugs and antimetastatic activity)